

# INTERNATIONAL WOMEN OF SUPRAMOLECULAR CHEMISTRY

EDITED BY: Jennifer Hiscock, Claudia Caltagirone, Anna McConnell,  
Cally Jo Elizabeth Haynes and Emily Draper  
PUBLISHED IN: Frontiers in Chemistry





# frontiers

## Frontiers eBook Copyright Statement

The copyright in the text of individual articles in this eBook is the property of their respective authors or their respective institutions or funders. The copyright in graphics and images within each article may be subject to copyright of other parties. In both cases this is subject to a license granted to Frontiers.

The compilation of articles constituting this eBook is the property of Frontiers.

Each article within this eBook, and the eBook itself, are published under the most recent version of the Creative Commons CC-BY licence.

The version current at the date of publication of this eBook is CC-BY 4.0. If the CC-BY licence is updated, the licence granted by Frontiers is automatically updated to the new version.

When exercising any right under the CC-BY licence, Frontiers must be attributed as the original publisher of the article or eBook, as applicable.

Authors have the responsibility of ensuring that any graphics or other materials which are the property of others may be included in the CC-BY licence, but this should be checked before relying on the CC-BY licence to reproduce those materials. Any copyright notices relating to those materials must be complied with.

Copyright and source acknowledgement notices may not be removed and must be displayed in any copy, derivative work or partial copy which includes the elements in question.

All copyright, and all rights therein, are protected by national and international copyright laws. The above represents a summary only. For further information please read Frontiers' Conditions for Website Use and Copyright Statement, and the applicable CC-BY licence.

ISSN 1664-8714

ISBN 978-2-88974-720-7

DOI 10.3389/978-2-88974-720-7

## About Frontiers

Frontiers is more than just an open-access publisher of scholarly articles: it is a pioneering approach to the world of academia, radically improving the way scholarly research is managed. The grand vision of Frontiers is a world where all people have an equal opportunity to seek, share and generate knowledge. Frontiers provides immediate and permanent online open access to all its publications, but this alone is not enough to realize our grand goals.

## Frontiers Journal Series

The Frontiers Journal Series is a multi-tier and interdisciplinary set of open-access, online journals, promising a paradigm shift from the current review, selection and dissemination processes in academic publishing. All Frontiers journals are driven by researchers for researchers; therefore, they constitute a service to the scholarly community. At the same time, the Frontiers Journal Series operates on a revolutionary invention, the tiered publishing system, initially addressing specific communities of scholars, and gradually climbing up to broader public understanding, thus serving the interests of the lay society, too.

## Dedication to Quality

Each Frontiers article is a landmark of the highest quality, thanks to genuinely collaborative interactions between authors and review editors, who include some of the world's best academicians. Research must be certified by peers before entering a stream of knowledge that may eventually reach the public - and shape society; therefore, Frontiers only applies the most rigorous and unbiased reviews.

Frontiers revolutionizes research publishing by freely delivering the most outstanding research, evaluated with no bias from both the academic and social point of view. By applying the most advanced information technologies, Frontiers is catapulting scholarly publishing into a new generation.

## What are Frontiers Research Topics?

Frontiers Research Topics are very popular trademarks of the Frontiers Journals Series: they are collections of at least ten articles, all centered on a particular subject. With their unique mix of varied contributions from Original Research to Review Articles, Frontiers Research Topics unify the most influential researchers, the latest key findings and historical advances in a hot research area! Find out more on how to host your own Frontiers Research Topic or contribute to one as an author by contacting the Frontiers Editorial Office: [frontiersin.org/about/contact](http://frontiersin.org/about/contact)

# INTERNATIONAL WOMEN OF SUPRAMOLECULAR CHEMISTRY

Topic Editors:

**Jennifer Hiscock**, University of Kent, United Kingdom

**Claudia Caltagirone**, University of Cagliari, Italy

**Anna McConnell**, University of Kiel, Germany

**Cally Jo Elizabeth Haynes**, University College London, United Kingdom

**Emily Draper**, University of Glasgow, United Kingdom

**Citation:** Hiscock, J., Caltagirone, C., McConnell, A., Haynes, C. J. E., Draper, E., eds. (2022). International Women of Supramolecular Chemistry.

Lausanne: Frontiers Media SA. doi: 10.3389/978-2-88974-720-7

# Table of Contents

- 04 Editorial: International Women of Supramolecular Chemistry**  
Claudia Caltagirone, Emily R. Draper, Jennifer S. Leigh, Cally J. E. Haynes, Jennifer R. Hiscock and Anna J. McConnell
- 07 Influence of Terminal Functionality on the Crystal Packing Behaviour and Cytotoxicity of Aromatic Oligoamides**  
Pierre Delfosse, Colin C. Seaton, Louise Male, Rianne M. Lord and Sarah J. Pike
- 15 Exploiting Peptide Self-Assembly for the Development of Minimalistic Viral Mimetics**  
Patrizia Janković, Iva Šantek, Ana Sofia Pina and Daniela Kalafatovic
- 26 Spiropyran-Based Drug Delivery Systems**  
Andrew Fagan, Michał Bartkowski and Silvia Giordani
- 45 Chaotropic and Kosmotropic Anions Regulate the Outcome of Enzyme-Mediated Dynamic Combinatorial Libraries of Cyclodextrins in Two Different Ways**  
Andreas Erichsen, Dennis Larsen and Sophie R. Beeren
- 53 The Importance of Spin State in Chiral Supramolecular Electronics**  
Ana M. Garcia, Gabriel Martínez and Amparo Ruiz-Carretero
- 62 Evolution of Supramolecular Systems Towards Next-Generation Biosensors**  
Sujeung Lim, Yuyao Kuang and Herdeline Ann M. Ardoña
- 83 Elucidation of Charge Contribution in Iridium-Chelated Hydrogen-Bonding Systems**  
Barbora Balónová and Barry A. Blight
- 89 Advances in the Supramolecular Chemistry of Tetracoordinate Boron-Containing Organic Molecules into Organogels and Mesogens**  
Sanchita Shah, Parvati Marandi and P. P. Neelakandan
- 99 Looking for Options to Sustainably Fixate Nitrogen. Are Molecular Metal Oxides Catalysts a Viable Avenue?**  
Rebeca González-Cabaleiro, Jake A. Thompson and Laia Vilà-Nadal
- 106 Self-Assembled Materials Incorporating Functional Porphyrins and Carbon Nanoplatfoms as Building Blocks for Photovoltaic Energy Applications**  
Boyang Mao, Benjamin Hodges, Craig Franklin, David G. Calatayud and Sofia I. Pascu
- 142 Enabling Technology for Supramolecular Chemistry**  
Katie Ollerton, Rebecca L. Greenaway and Anna G. Slater
- 150 Cyclohexanohemicucurbit[8]uril Inclusion Complexes With Heterocycles and Selective Extraction of Sulfur Compounds From Water**  
Tatsiana Shalima, Kamini A. Mishra, Sandra Kaabel, Lukas Ustrnul, Simona Bartkova, Kaia Tõnsuaadu, Ivo Heinmaa and Riina Aav
- 158 Removal of the Micropollutants Propranolol Hydrochloride and 2-Naphthol From Water by Pyridine-Functionalized Polymers**  
Qixuan Zheng, Daniel K. Unruh and Kristin M. Hutchins





# Editorial: International Women of Supramolecular Chemistry

Claudia Caltagirone<sup>1</sup>, Emily R. Draper<sup>2</sup>, Jennifer S. Leigh<sup>3\*</sup>, Cally J. E. Haynes<sup>4</sup>, Jennifer R. Hiscock<sup>5</sup> and Anna J. McConnell<sup>6</sup>

<sup>1</sup>Department of Chemical and Geological Science, University of Cagliari, Monserrato, Italy, <sup>2</sup>School of Chemistry, University of Glasgow, Glasgow, United Kingdom, <sup>3</sup>Centre for the Study of Higher Education, University of Kent, Canterbury, United Kingdom, <sup>4</sup>Department of Chemistry, University College London, London, United Kingdom, <sup>5</sup>School of Chemistry and Forensics, University of Kent, Canterbury, United Kingdom, <sup>6</sup>Otto Diels Institute of Organic Chemistry, Christian-Albrechts-Universität zu Kiel, Kiel, Germany

**Keywords:** supramolecular chemistry, women in chemistry, equality, diversity, inclusion

## Editorial on the Research Topic

### International Women of Supramolecular Chemistry

There is a need to address the lack of diversity in Chemistry (Urbina-Blanco et al., 2020). Despite dedicated programmes and outreach activities to attract individuals from minority backgrounds to initiate their academic studies in this area, at the most senior levels there remains an underrepresentation of minority and marginalised groups (RSC, 2018). People who have one or more protected EDI (Equality, Diversity, Inclusion) characteristic such as race, religion, disability, sexuality, or gender face more barriers to remain and to succeed within science.

The International Women In Supramolecular Chemistry (WISC) network, has taken a unique, area-specific approach that embeds EDI and creative social sciences to address the retention and progression of women and other marginalised groups (Caltagirone et al., 2021).

Our community-led approach to researching *with*, and **NOT on** scientists allows us to shape our offering to the community to specifically address its needs. In response to our first survey of the community, we created a mentoring programme, a series of webinars (in collaboration with vMASC—the Early Career arm of the Royal Society of Chemistry (RSC) Macrocyclic and Supramolecular Chemistry Special Interest Group), a series of virtual spaces where individuals of any gender could come together to find support (termed Community Clusters), and a Skills Workshop. These all sought to address the feelings of isolation and the progression gap shared by many respondents as they transitioned post-PhD to a post-doc/PDRA, fellowship, or related industrial position.

The mentoring programme run by WISC uses a model whereby small groups of up to five individuals at a similar career stage meet regularly with a mentor who is at least one career stage ahead of them. In the first 18 months over 90% of participants reported being satisfied with the programme and wishing to continue. This was an initiative that the supramolecular community asked WISC to initiate and is further known in literature to be particularly effective at supporting those who are marginalised (Laube and Crimmins, 2019).

The WISC collaboration with vMASC has been very successful, with seminars organised on topics such as careers outside of academia, science communication, and work-life balance attracting a wide audience across Europe, the United Kingdom, US, India, and Australia. In addition, vMASC provided the technical support to make the first WISC Skills Workshop (2021) a hybrid in person/virtual event, with over 200 registrations. One attendee said “*I liked the informative style, the small nature of the workshop group and the fact that almost everyone on site*”

## OPEN ACCESS

### Edited by:

Tony D. James,  
University of Bath, United Kingdom

### Reviewed by:

Sally Elisabeth Plush,  
University of South Australia, Australia

### \*Correspondence:

Jennifer S. Leigh  
j.s.leigh@kent.ac.uk

### Specialty section:

This article was submitted to  
Supramolecular Chemistry,  
a section of the journal  
Frontiers in Chemistry

**Received:** 13 January 2022

**Accepted:** 25 January 2022

**Published:** 28 February 2022

### Citation:

Caltagirone C, Draper ER, Leigh JS,  
Haynes CJ, Hiscock JR and  
McConnell AJ (2022) Editorial:  
International Women of  
Supramolecular Chemistry.  
Front. Chem. 10:854085.  
doi: 10.3389/fchem.2022.854085

*had the chance to participate (oral or 3 min poster presentation). I found the workshop to be extremely informative. I especially liked the way in which it encouraged the early career researchers to think outside the box.”*

WISC takes an intersectional approach to marginalisation, recognising that not all groups face the same barriers, and that those who have more than one protected characteristic face compounded barriers to reach their full potential. In response to this need, we initiated our virtual “Community Clusters” to provide safer spaces and dedicated support. The first cluster was the “Parenting Cluster” which aimed to support all people on a parenting journey—whether they were prospective parents, foster parents, adoptive parents, or step-parents. The second cluster was for disabled/neurodivergent/chronically ill people. This cluster provides a regular meeting space for people to talk and share experiences, and recently, gained RSC support for a project to envision future accessible labs. Our final cluster is the “first Gen Cluster” which will specifically look to support those who are first in their family into higher education within supramolecular chemistry.

WISC also undertakes high-quality qualitative research to capture the voices and stories of women and other marginalised groups.<sup>1</sup> We intentionally use a variety of creative and more traditional methods as part of an Embodied Inquiry (Leigh and Brown, 2021) that foregrounds lived experiences. During COVID-19 we triangulated a qualitative survey, a collaborative autoethnography, and reflective research group meetings to gather data on experiences both inside and outside the lab (Leigh et al., 2022). From these data we created a series of fictional vignettes to illustrate the lived experiences of women within supramolecular chemistry which will be published in the forthcoming book from Policy Press *Women in Supramolecular Chemistry: Collectively crafting the rhythms of our work and lives in STEM* (Leigh et al., 2022). Our current research includes looking at how creativity and communication can be improved within research teams led by women, and their role in developing leadership skills. We have associated outreach and Public Engagement projects, including a collaboration with Empowering Female Minds in STEM, (EFEMS, 2021) to increase the visibility of Black women in chemistry and science communication, and the National Association for Disabled Staff Networks STEMM Action Group to provide recommendations for funders and institutions to support disabled scientists.

This Special Issue, with articles showcasing the work of women in supramolecular chemistry, is part of our

commitment to action and change. Women face barriers at every stage of the publication process (RSC, 2019). Bringing their work together allows the supramolecular chemistry community an opportunity to see and value the ground-breaking science they are achieving despite the additional barriers they face just because of their gender. Bringing their work together allows the community to recognise and celebrate them. It will allow those coming through from undergraduate study to see that it is possible for women and other marginalised groups to succeed, and that there is a place for them.

WISC chooses not to “call out” instances of sexism or misogyny. Instead, we “call in” the community so that it can support its own (WISC, 2021). In this way we can create a supportive and inclusive environment which holistically enables the retention and progression of everyone—regardless of gender, race, disability, or any other characteristic. We need to continue the successful outreach that invites more diversity in chemists from undergraduate level upwards, and we need to support their retention and progression so that they can see that there is a clear path forward for everyone.

WISC has big aspirations and ambitions for the supramolecular community. We would like the model we have created and the work that we are doing to act as a framework for other area-specific networks and disciplines, reaching out to other marginalised communities. In order to do this, we need the community to be involved—so please get in touch via [www.womeninsuprachem.com](http://www.womeninsuprachem.com) if you:

- would like to be a mentor, or a mentee (or both)
- would like to be part of one of our virtual Community Clusters or help us to create a new one;
- would like to be part of our research, or to find out more about what we are doing to support women, disabled scientists, and the visibility of all women in science communication.

## AUTHOR CONTRIBUTIONS

JL led the writing of the editorial. JH, AM, CH, CC, ED, contributed equally to review and final preparation of this Editorial article.

<sup>1</sup>WISC believes that trans women are women. The use of other marginalised groups specifically includes other marginalised genders including trans men and non-binary people as well as those marginalised due to one or more other protected characteristic such as race, ethnicity, religion, sexuality, or disability

## REFERENCES

- Caltagirone, C., Draper, E. R., Hardie, M. J., Haynes, C. J. E., Hiscock, J. R., Jolliffe, K. A., et al. (2021). An Area-Specific, International Community-Led Approach to Understanding and Addressing Equality, Diversity, and Inclusion Issues within Supramolecular Chemistry. *Angew. Chem. Int. Ed.* 60, 11572–11579. doi:10.1002/anie.202015297
- EFeMS (2021). Empowering Female Minds in STEM: Showing African Women that Their Possibilities Are Endless. Available at: <https://www.empoweringfems.com> (Accessed July 16, 2021).
- Laube, H. (2019). in *Strategies for Resisting Sexism in the Academy: Higher Education, Gender and Intersectionality*. Editor G. Crimmins (Cham: Palgrave Macmillan), 95–113.
- Leigh, J., and Brown, N. (2021). *Embodied Inquiry: Research Methods*. London: Bloomsbury.
- Leigh, J. S., Hiscock, J. R., Haynes, C., McConnell, A., Kieffer, M., Draper, E., et al. (2022). *Women in Supramolecular Chemistry: Collectively Crafting the Rhythms of Our Work and Lives in STEM*. Bristol: Policy Press.
- Leigh, J. S., Hiscock, J. R., Koops, S., McConnell, A. J., Haynes, C. J. E., Caltagirone, C., et al. (2022). Managing Research Throughout COVID-19: Lived Experiences of Supramolecular Chemists. *Chem.* doi:10.1016/j.chempr.2022.01.001
- RSC (2018). *Diversity Landscape of the Chemical Sciences*. London: Royal Society of Chemistry.
- RSC (2019). *Is Publishing in the Chemical Sciences Gender Biased? Driving Change in Research Culture*. London: Royal Society of Chemistry.
- Urbina-Blanco, C. A., Jilani, S. Z., Speight, I. R., Bojdys, M. J., Friščić, T., Stoddart, J. F., et al. (2020). A Diverse View of Science to Catalyse Change. *Nat. Chem.* 12, 773–776. doi:10.1038/s41557-020-0529-x
- WISC (2021). *Chem. World*.

**Conflict of Interest:** The authors declare that the research was conducted in the absence of any commercial or financial relationships that could be construed as a potential conflict of interest.

**Publisher's Note:** All claims expressed in this article are solely those of the authors and do not necessarily represent those of their affiliated organizations, or those of the publisher, the editors and the reviewers. Any product that may be evaluated in this article, or claim that may be made by its manufacturer, is not guaranteed or endorsed by the publisher.

Copyright © 2022 Caltagirone, Draper, Leigh, Haynes, Hiscock and McConnell. This is an open-access article distributed under the terms of the Creative Commons Attribution License (CC BY). The use, distribution or reproduction in other forums is permitted, provided the original author(s) and the copyright owner(s) are credited and that the original publication in this journal is cited, in accordance with accepted academic practice. No use, distribution or reproduction is permitted which does not comply with these terms.



# Influence of Terminal Functionality on the Crystal Packing Behaviour and Cytotoxicity of Aromatic Oligoamides

Pierre Delfosse<sup>1</sup>, Colin C. Seaton<sup>1</sup>, Louise Male<sup>2</sup>, Rianne M. Lord<sup>1,3\*</sup> and Sarah J. Pike<sup>1,2\*</sup>

<sup>1</sup>School of Chemistry and Biosciences, University of Bradford, Bradford, United Kingdom, <sup>2</sup>School of Chemistry, University of Birmingham, Birmingham, United Kingdom, <sup>3</sup>School of Chemistry, University of East Anglia, Norwich Research Park, Norwich, United Kingdom

## OPEN ACCESS

### Edited by:

Jennifer Hiscock,  
University of Kent, United Kingdom

### Reviewed by:

Michelle Garrett,  
University of Kent, United Kingdom  
James Lewis,  
Imperial College London,  
United Kingdom  
Michael Ward,  
University of Warwick,  
United Kingdom

### \*Correspondence:

Rianne M. Lord  
r.lord@uea.ac.uk  
Sarah J. Pike  
s.j.pike@bham.ac.uk

### Specialty section:

This article was submitted to  
Supramolecular Chemistry,  
a section of the journal  
Frontiers in Chemistry

Received: 13 May 2021

Accepted: 10 June 2021

Published: 30 June 2021

### Citation:

Delfosse P, Seaton CC, Male L,  
Lord RM and Pike SJ (2021) Influence  
of Terminal Functionality on the Crystal  
Packing Behaviour and Cytotoxicity of  
Aromatic Oligoamides.  
Front. Chem. 9:709161.  
doi: 10.3389/fchem.2021.709161

The synthesis and characterization of three aromatic oligoamides, constructed from the same pyridyl carboxamide core but incorporating distinct end groups of acetyl (Ac) **1**, *tert*-butyloxycarbonyl (Boc) **2** and amine **3** is reported. Single crystal X-ray diffraction analysis of **1–3** and a dimethylsulfoxide (DMSO) solvate of **2** (**2**-DMSO), has identified the presence of a range of intra- and intermolecular interactions including N-H...N, N-H...O=C and N-H...O=S(CH<sub>3</sub>)<sub>2</sub> hydrogen-bonding interactions, C-H... $\pi$  interactions and off-set, face-to-face stacking  $\pi$ - $\pi$  interactions that support the variety of slipped stack, herringbone and cofacial crystal packing arrangements observed in **1–3**. Additionally, the cytotoxicity of this series of aromatic oligoamides was assessed against two human ovarian (A2780 and A2780cisR), two human breast (MCF-7 and MDA-MB-231) cancerous cell lines and one non-malignant human epithelial cell line (PNT-2), to investigate the influence of the terminal functionality of these aromatic oligoamides on their biological activity. The chemosensitivity results highlight that modification of the terminal group from Ac to Boc in **1** and **2** leads to a 3-fold increase in antiproliferative activity against the cisplatin-sensitive ovarian carcinoma cell line, A2780. The presence of the amine termini in **3** gave the only member of the series to display activity against the cisplatin-resistance ovarian carcinoma cell line, A2780cisR. Compound **2** is the lead candidate of this series, displaying high selectivity towards A2780 cancer cells when compared to non-malignant PNT-2 cells, with a selectivity index value >4.2. Importantly, this compound is more selective towards A2780 (*cf.* PNT-2) than the clinical platinum drugs oxaliplatin by > 2.6-fold and carboplatin by > 1.6-fold.

**Keywords:** aromatic oligoamides, cytotoxicity, crystallography, terminal group, breast and ovarian cancer

## INTRODUCTION

The rise of cancer cell resistance towards clinical anticancer drugs, combined with the poor selectivity they can demonstrate for cancers over non-malignant tissue and the occurrence of adverse side-effects, has driven the search for new compounds with increased antiproliferative activity and selectivity. (Mader et al., 1998; Winocur et al., 2006; Figaro et al., 2011; Tageja et al., 2011; Ward et al., 2021). Whilst there is a diverse array of anticancer agents currently used in the clinic, small organic molecules, for example, lenalidoamide and flutamide, represent an important group of chemotherapeutic agents. Aromatic oligoamides (Hamuro et al., 1994; Hamuro et al., 1996; Yuan et al., 2004; Yuan et al., 2005; Kortelainen et al., 2015) are a class of small organic

compounds that have been shown to possess potential anticancer activity (Tew et al., 2002; Ernst et al., 2003; Yin and Hamilton, 2005; Davis et al., 2007; Plante et al., 2009; Azzarito et al., 2012; Burslem et al., 2014; Jayatunga et al., 2014; Burslem et al., 2016) and have also been employed in a wide range of applications including catalysis, (Hegedus et al., 2019), sensing, (Yi et al., 2005; Bao et al., 2008; Yamato et al., 2009), materials chemistry (König et al., 2000; Garía et al., 2010) and crystal engineering. (Suhonen et al., 2016; Annala et al., 2017).

Systematic solid-state studies of aromatic oligoamides have identified that small structural variations in these molecules can have a profound influence on their conformational behavior and such studies can to help deepen our understanding of their structure-activity relationships (SARs). A crystallographic study of aromatic oligoamides by Nissinen and co-workers (Suhonen et al., 2012) showed that modification of the aromatic ring from benzene to pyridine results in marked changes in the folding behavior of these compounds resulting in the adoption of curved molecular structures. Gunnlaugsson and co-workers described a crystallographic analysis of a series of cytotoxic pyridine-based aromatic oligoamides, showing that they adopted curved molecular structures with a supramolecular arrangement that could potentially promote interaction with DNA. (Frimannsson et al., 2010). The pyridine-based aromatic oligoamides were identified as DNA-targeting supramolecular binders and displayed cytotoxicity against the drug-resistant chronic myeloid leukaemia, K562 cell line. Fletcher and co-workers determined SARs on a series of short chain aromatic oligoamides, highlighting that relaxation of the rigidity of the backbone of the scaffold lead to increased cytotoxicity. (Yap et al., 2012). The lead candidate of the series

displays low IC<sub>50</sub> values (1.1–4.3 μM) against the human colon carcinoma (DLD-1), mesothelioma (I45), lung carcinoma (A549), and human non-small cell lung carcinoma (H1299).

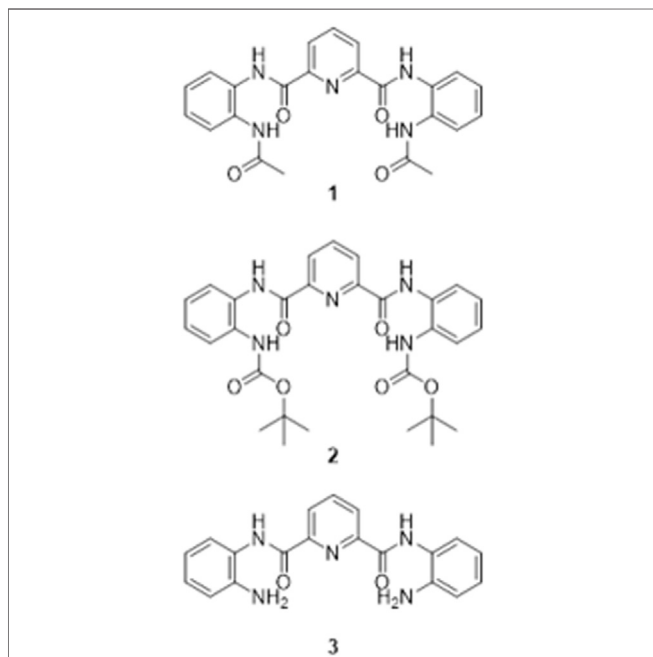
Gaining an understanding of the influence of the structure of an aromatic oligoamide on its biological activity is central to the development of new molecules within this class that have the potential to demonstrate improved cytotoxicity towards cancerous cells. To probe the influence of the terminal group on the solid-state structure and antiproliferative activity of these aromatic oligoamides, we undertook the synthesis, crystallographic analysis and cytotoxicity studies of three aromatic oligoamides based on the same pyridyl carboxamide core but including different end groups; acetyl (Ac) **1**, *tert*-butyloxycarbonyl (Boc) **2** and amine **3** (Figure 1). We report on the solid-state properties of **1–3** and solvatomorph **2**-DMSO, and employ single-crystal X-ray diffraction analysis to identify the presence of a range of non-covalent interactions which support the diverse crystal packing behavior of these aromatic oligoamides. We describe the influence of varying the terminal functionality in compounds **1–3** on their cytotoxicity against breast and ovarian cancer cell lines, and report the chemosensitivity studies against a non-malignant cell type. The results show that the most promising compound, a Boc-terminated aromatic oligoamide, is non-toxic towards non-malignant cells, unlike all cisplatin (CDDP), carboplatin (CARB) and oxaplatin (OXA), which all demonstrate high cytotoxicity.

## RESULTS AND DISCUSSION

Aromatic oligoamides, **1–3**, which all have the same pyridyl carboxamide core, but incorporate different terminal groups of Ac **1**, Boc **2** and NH<sub>2</sub> **3** (Figure 1) have been prepared according to known or modified literature procedures, (Annala et al., 2017; Suhonen et al., 2016; Suhonen et al., 2012) (Suhonen et al., 2012; Suhonen et al., 2016; Annala et al., 2017), and were all characterized by <sup>1</sup>H and <sup>13</sup>C{<sup>1</sup>H} NMR spectroscopy, melting point analysis, FTIR spectroscopy, high-resolution mass spectrometry and single crystal X-ray diffraction. The <sup>1</sup>H and <sup>13</sup>C NMR spectra of **1–3** indicate that these compounds are symmetrical, with the <sup>1</sup>H NMR spectra showing only one resonance for the NHs in the amide bonds of the terminal Ac and Boc group of **1** and **2** at δ 10.93 and δ 10.73 ppm respectively. Whilst the <sup>13</sup>C NMR spectrum of **3** displays only one resonance for the 2 C atoms in the carbonyl groups adjacent to the pyridine ring at δ 161.2 ppm (see Supporting Information). Electrospray ionization mass spectrometry identified the molecular ion peaks at *m/z* 432.1670 [M + H]<sup>+</sup> **1**, 548.2503 [M + H]<sup>+</sup> **2** and 348.1453 [M + H]<sup>+</sup> **3**.

### Crystallographic Studies

Single crystals suitable for X-ray diffraction were obtained for **1–3** and for a DMSO solvatomorph of **2** (**2**-DMSO). Table 1 summarizes selected crystallographic data for **1–3** and **2**-DMSO (for full crystallographic tables, see Supporting Information). X-ray diffraction analysis identified the nature of the non-covalent interactions present in the solid state for each of the studied aromatic oligoamides.



**FIGURE 1** | Short chain aromatic oligoamides **1–3** employed in this study.

**TABLE 1** | Selected crystallographic data for **1**, **2**, **2**-DMSO and **3**.

	<b>1</b>	<b>2</b>	<b>2</b> -DMSO	<b>3</b>
Empirical formula	C <sub>23</sub> H <sub>21</sub> N <sub>5</sub> O <sub>4</sub>	C <sub>29</sub> H <sub>33</sub> N <sub>5</sub> O <sub>6</sub>	C <sub>31</sub> H <sub>39</sub> N <sub>5</sub> O <sub>7</sub> S	C <sub>38</sub> H <sub>34</sub> N <sub>10</sub> O <sub>4</sub>
Formula weight	431.45	547.60	625.73	694.75
Crystal system	Monoclinic	Orthorhombic	Monoclinic	Monoclinic
Space group	<i>P</i> 2 <sub>1</sub> / <i>c</i>	<i>P</i> 2 <sub>1</sub> 2 <sub>1</sub> 2 <sub>1</sub>	<i>P</i> 2 <sub>1</sub> / <i>c</i>	<i>P</i> 2 <sub>1</sub> / <i>c</i>
<i>a</i> /Å	4.8617 (2)	9.9736 (7)	9.3413 (3)	16.114 (15)
<i>b</i> /Å	18.2381 (7)	14.9397 (11)	17.6116 (7)	13.297 (12)
<i>c</i> /Å	22.8681 (6)	19.4229 (15)	19.7290 (7)	17.625 (16)
$\alpha$ /°	90	90	90	90
$\beta$ /°	93.870 (3)	90	96.048 (2)	116.80 (2)
$\gamma$ /°	90	90	90	90
Volume/Å <sup>3</sup>	2023.05 (13)	2894.1 (4)	3227.7 (2)	3371 (5)
<i>Z</i>	4	4	4	4
Temperature/K	100.01	169.99	170.0	170.39
$\rho_{\text{calc}}$ g/cm <sup>3</sup>	1.417	1.257	1.288	1.369
$\mu$ /mm <sup>-1</sup>	0.823	0.089	0.153	0.093
<i>F</i> (000)	904.0	1160.0	1328.0	1456.0
Radiation	Cu K $\alpha$ ( $\lambda$ = 1.54184)	MoK $\alpha$ ( $\lambda$ = 0.71073)	MoK $\alpha$ ( $\lambda$ = 0.71073)	MoK $\alpha$ ( $\lambda$ = 0.71073)
2 $\theta$ range for data collection/°	7.75–145.704	4.91–56.9	4.754–66.276	2.832–55.33
Index ranges	–5 ≤ <i>h</i> ≤ 5, –22 ≤ <i>k</i> ≤ 15, –28 ≤ <i>l</i> ≤ 27	–13 ≤ <i>h</i> ≤ 13, –19 ≤ <i>k</i> ≤ 19, –26 ≤ <i>l</i> ≤ 25	–12 ≤ <i>h</i> ≤ 14, –27 ≤ <i>k</i> ≤ 26, –30 ≤ <i>l</i> ≤ 30	–19 ≤ <i>h</i> ≤ 20, –15 ≤ <i>k</i> ≤ 17, –22 ≤ <i>l</i> ≤ 22
Reflections collected	7,870	65,497	75,624	27,712
Independent reflections	3887 [ <i>R</i> <sub>int</sub> = 0.0202, <i>R</i> <sub>sigma</sub> = 0.0267]	7,098 [ <i>R</i> <sub>int</sub> = 0.1280, <i>R</i> <sub>sigma</sub> = 0.1249]	12,237 [ <i>R</i> <sub>int</sub> = 0.0829, <i>R</i> <sub>sigma</sub> = 0.0712]	7,712 [ <i>R</i> <sub>int</sub> = 0.1203, <i>R</i> <sub>sigma</sub> = 0.1340]
Data/restraints/parameters	3887/0/307	7,098/0/447	12,237/0/553	7,712/0/578
Goodness-of-fit on <i>F</i>	1.044	1.031	0.999	0.969
Final <i>R</i> indexes [ <i>I</i> ≥ 2 $\sigma$ ( <i>I</i> )]	<i>R</i> <sub>1</sub> = 0.0368, <i>wR</i> <sub>2</sub> = 0.0887	<i>R</i> <sub>1</sub> = 0.0596, <i>wR</i> <sub>2</sub> = 0.1058	<i>R</i> <sub>1</sub> = 0.0523, <i>wR</i> <sub>2</sub> = 0.1016	<i>R</i> <sub>1</sub> = 0.0947, <i>wR</i> <sub>2</sub> = 0.2264
Final <i>R</i> indexes [all data]	<i>R</i> <sub>1</sub> = 0.0446, <i>wR</i> <sub>2</sub> = 0.0932	<i>R</i> <sub>1</sub> = 0.1453, <i>wR</i> <sub>2</sub> = 0.1295	<i>R</i> <sub>1</sub> = 0.1143, <i>wR</i> <sub>2</sub> = 0.1221	<i>R</i> <sub>1</sub> = 0.2001, <i>wR</i> <sub>2</sub> = 0.3055
Largest diff. Peak/hole/e Å <sup>-3</sup>	0.22/–0.20	0.23/–0.27	0.36/–0.48	0.34/–0.39

**TABLE 2** | Cytotoxicity values (IC<sub>50</sub>/μM ± SD) for cisplatin (CDDP), oxaliplatin (OXA), carboplatin (CARB) and compounds **1–3** after a 96 h incubation period with human ovarian carcinomas (A2780, A2780cisR), human breast adenocarcinomas (MCF-7, MDA-MB-231) and non-malignant prostate cells (PNT-2).<sup>a</sup> Selective Index (SI) values when compared to PNT-2 are shown in parenthesis.

Compounds	IC <sub>50</sub> values (μM) ± SD				
	A2780	A2780cisR	MCF-7	MDA-MB-231	PNT-2
CDDP	1.3 ± 0.1 (6.4)	14 ± 1 (0.6)	1.5 ± 0.2 (5.6)	3.07 ± 0.02 (2.8)	8.5 ± 0.4
CARB	17 ± 1 (1.6)	>100 (0.3*)	>100 (0.3*)	33 ± 2 (0.8)	27 ± 2
OXA	0.505 ± 0.002 (2.6)	2.09 ± 0.03 (0.6)	2.6 ± 0.2 (0.5)	2.5 ± 0.6 (0.5)	1.3 ± 0.2
<b>1</b>	77 ± 5 (1.3*)	>100 (nd)	>100 (nd)	63 ± 4 (1.6*)	>100
<b>2</b>	24.0 ± 0.9 (4.2*)	>100 (nd)	84 ± 3 (1.2*)	69 ± 3 (1.4*)	>100
<b>3</b>	>100 (nd)	61 ± 2 (1.6*)	>100 (nd)	>100 (nd)	>100

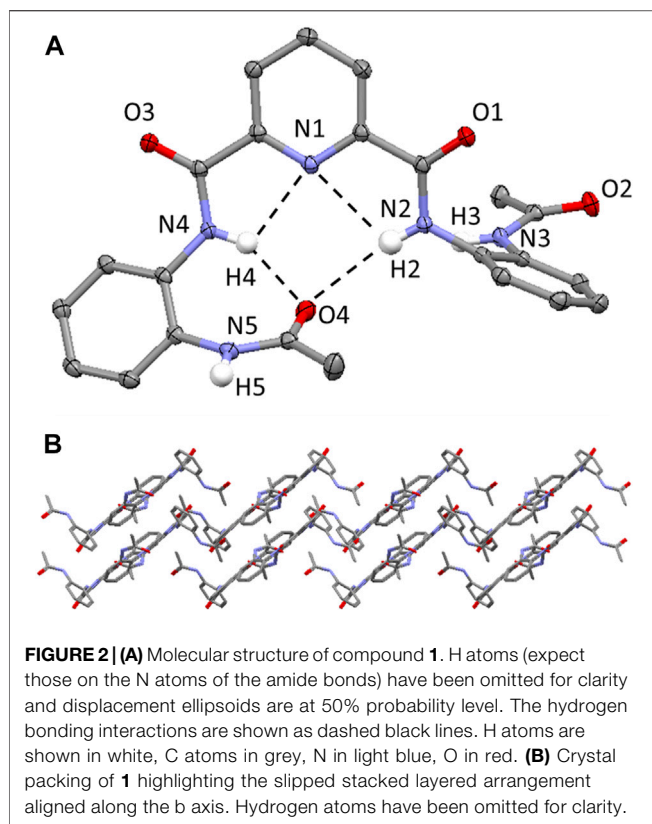
<sup>a</sup>All values are averages from duplicate technical repeats and triplicate experimental repeats. \* indicates the minimum SI value as at least one IC<sub>50</sub> value is >100 μM. n. d. (not determined) indicates the values where both IC<sub>50</sub> values are >100 μM.

## Crystallographic Analysis of **1**

Single crystals of **1** were grown by vapor diffusion of diethyl ether into a dimethylformamide solution at ambient temperature. **1** crystallizes in a monoclinic crystal system and solution refinement was performed in the *P*2<sub>1</sub>/*c* space group (Table 1). The molecular structure of **1** is shown in Figure 2A, with displacement ellipsoids placed at 50% probability level. **1** displays three sets of bifurcated intramolecular hydrogen-bonding interactions, firstly, involving the pyridyl N atom and the two NH's of the adjacent amide group (i.e., N (2/4)-H (2/4)···N (1) (2.6583(17)-3.2310(16) Å, Table 2) and, additionally, two

bifurcated interactions exist between each of the NH's of a central amide group and the adjacent pyridyl N atom and the O atom of the terminal amide group (N (2/4)-H (2/4A)···N (1) and N (2/4)-H (2/4A)···O (4) (1.97(2)-2.39(2) Å, Figure 2A). (Rozas et al., 1998) **1** displays a slipped stack crystal packing arrangement, (Yao et al., 2018), aligned along the *b* axis (Figure 2B), which is supported by two sets of intermolecular hydrogen-bonding interactions and one set of edge-to-face  $\pi$ - $\pi$  stacking interactions. One of the intermolecular hydrogen-bonding interactions is present between one of the NH's of an terminal Ac group and an O atom on the carbonyl of the central amide group (N (3)-H





(3A)⋯O (1) (1.99 (2) Å) and results in the formation of a hydrogen-bond chain orientated along the *c* axis (**Supplementary Figure S7**). The second intermolecular hydrogen-bonding interaction is present between one of the NH's of an terminal amide group and the O atom of the carbonyl group of the Ac capping group in an adjacent molecule (N (5)-H (5A)⋯O (2) (2.00 (2) Å, **Supplementary Figure S8**). **1** also displays an edge-to-face  $\pi$ - $\pi$  stacking interaction between the terminal 2-acylamino phenyl rings on neighboring molecules, further supporting the slipped stack crystal packing arrangement (**Supplementary Figure S9**). (Nishio, 2011).

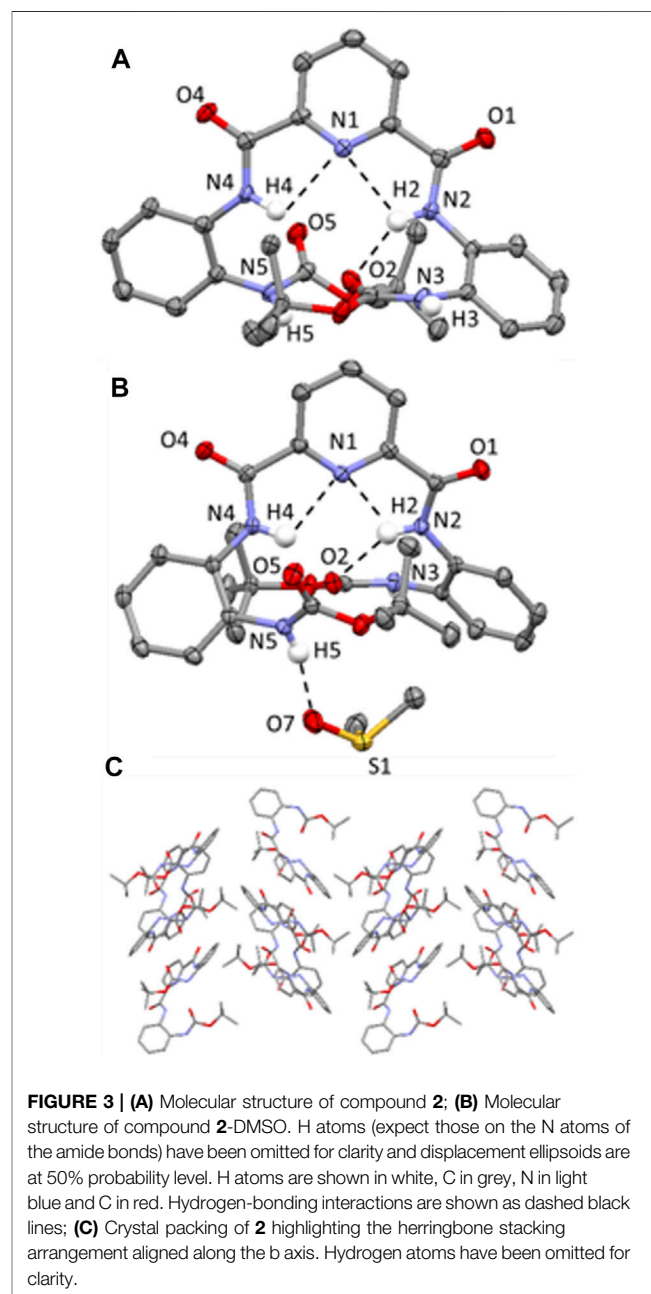
### Crystallographic Analysis of **2** and 2-DMSO

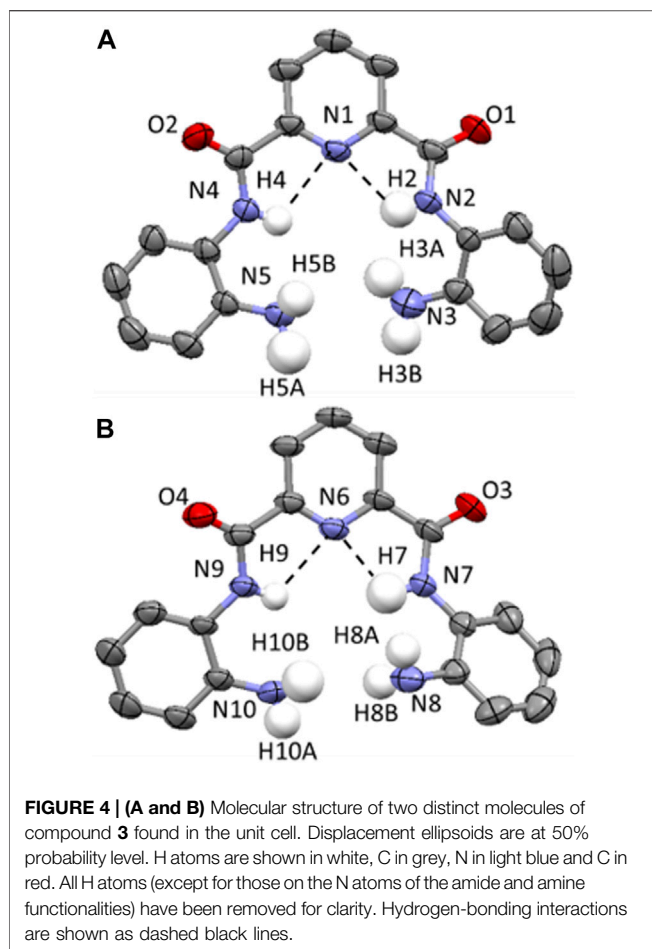
Single crystals of compound **2** and the dimethylsulfoxide (DMSO) solvate, **2**-DMSO, were grown from two different crystallization conditions at ambient temperature, firstly, through the slow evaporation of chloroform to give **2** and secondly, through the slow evaporation of a 9:1 chloroform: DMSO solvent mixture to generate **2**-DMSO. In the former conditions, **2** crystallizes in an orthorhombic crystal system and solution refinement was performed in the  $P2_12_12_1$  space group (**Table 1**) and in the latter conditions, **2** crystallizes, as the DMSO solvate, in a monoclinic crystal system and solution refinement was performed in the  $P2_1/c$  space group (**Table 1**).

The molecular structures of **2** and the **2**-DMSO solvate are shown in **Figure 3**, with displacement ellipsoids placed at 50% probability level. Both **2** and **2**-DMSO display two sets of

bifurcated intramolecular hydrogen bonding interactions, firstly, between the pyridyl N atom and the two NH's of the adjacent amide groups (N (2/4)-H (2/4A)⋯N (1) 2.34(4)-2.36(4) Å, **Figures 3A,B**) and, secondly, between one of the NH's in a central amide group and the adjacent pyridyl N atom and the O atom of the terminal amide group (N (2)-H (2A)⋯N (1) and N (2)-H (2)⋯O (2) (1.88(4)-2.36(4) Å, **Figures 3A,B**). (Arifuzzaman et al., 2013).

**2** adopts a herringbone crystal packing arrangement (Dhar et al., 2014) aligned along the *b* axis, shown in **Figure 3C**, and is supported by a range of different intermolecular non-covalent interactions including hydrogen-bonding interactions, edge-to-face  $\pi$ - $\pi$  stacking interactions and C-H (aryl)⋯ $\pi$  interactions.





Two distinct intermolecular N-H $\cdots$ O=C hydrogen-bonding interactions are observed in **2**, both of which are orientated along the *a* axis and involve the NH protons of the terminal Boc groups and the carbonyl O atoms on the pyridyl moiety of an adjacent molecule (i.e. N (3)-H (3) $\cdots$ O (4) = C and N (5)-H (5) $\cdots$ O (1) = C hydrogen bonding interactions, (2.03(4)-2.231(4) Å, **Supplementary Figure S12**). Additionally, there is an edge-to-face  $\pi$ - $\pi$  stacking interaction present between the terminal 2-*tert*-butylcarboxyaminophenyl rings on neighboring molecules (**Supplementary Figure S13**) and a C-H (aryl) $\cdots\pi$  interaction involving an H atom of the Boc group and a terminal 2-*tert*-butylcarboxyaminophenyl ring of an adjacent molecule (**Supplementary Figure S14**). (Tárkányi et al., 2008).

In the crystal packing of **2**-DMSO, there are two different types of intermolecular hydrogen-bonding interactions present; firstly, there is a N-H $\cdots$ O=C interaction between one of the NHs of a terminal Boc group and the O atom on the carbonyl group of a pyridyl amide group (N (3)-H (3) $\cdots$ O (4) = C, (2.012 (18) Å, **Supplementary Figure S17**) and, secondly, there is an intermolecular N-H $\cdots$ O=S(CH<sub>3</sub>)<sub>2</sub> hydrogen-bonding interaction present which involves one of the NH's of a terminal group moiety and the O atom of a DMSO solvent molecule (N (5)-H (5) $\cdots$ O (7) = S(CH<sub>3</sub>)<sub>2</sub>, (2.007 (19) Å, **Figure 3B**). (Arifuzzaman et al., 2013).

### Crystallographic Analysis of **3**

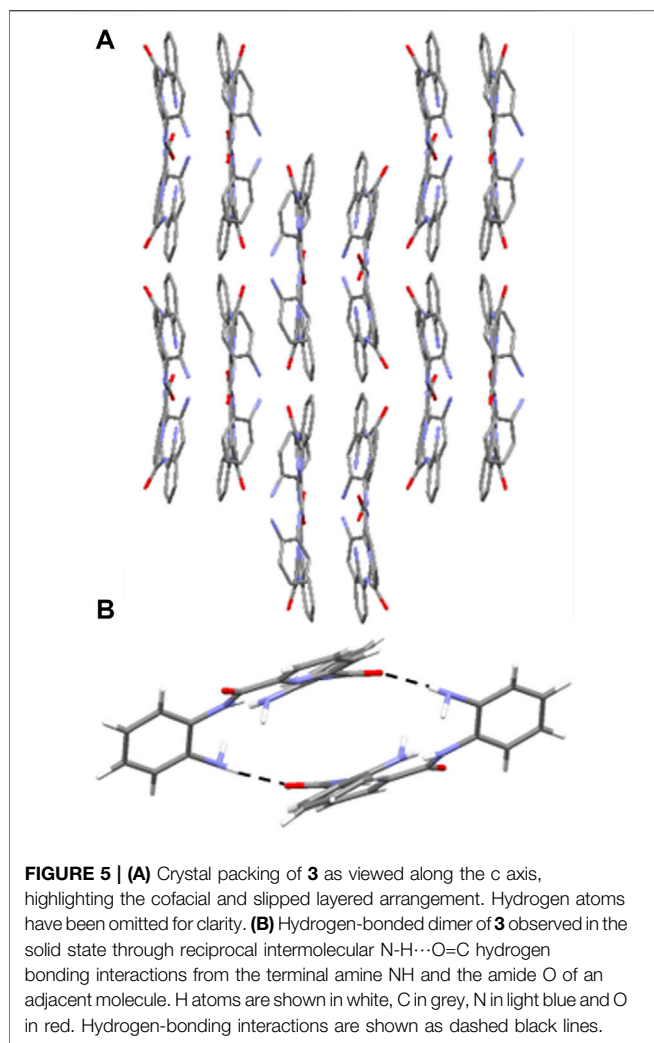
Single crystals of compound **3** were grown through the slow evaporation of chloroform at ambient temperature. **3** crystallizes in a monoclinic space group and solution refinement was performed in the *P*2<sub>1</sub>/*c* space group (**Table 1**). In the unit cell of **3**, there are two distinct molecules present and the molecular structure is shown in **Figure 4** with displacement ellipsoids placed at 50% probability level. Both molecules show the presence of a bifurcated intramolecular hydrogen-bonding interactions involving the pyridyl N atom and the adjacent amide NHs (N (2/4)-H (2/4) $\cdots$ N (1) and N (7/9)-H (7/9) $\cdots$ N (6), 2.08(5)-2.36 (4) Å, **Figure 4**). (Arifuzzaman et al., 2013).

**3** adopts a combination of cofacial and slipped stack layered crystal packing arrangement (Chang et al., 2008; Kobayashi et al., 2006) orientated along the *c* axis (**Figure 5A**) and this is supported by a series of intermolecular hydrogen-bonding interactions and parallel displaced  $\pi$ - $\pi$  stacking interactions. In **3**, there are three distinct sets of N-H $\cdots$ O=C intermolecular interactions including those observed between the NH of a terminal amine moiety in one molecule and the O atom of the carbonyl group in the amide group of an adjacent molecule (N (3)-H (3B) $\cdots$ O (2) 2.15 (7) Å (**Supplementary Figure S21**), N (8)-H (8A) $\cdots$ O (4) 2.06 (5) Å, (**Supplementary Figure S22**) and N (10)-H (10A) $\cdots$ O (3) 2.28 (4) Å (**Supplementary Figure S23**). The second of which adopts reciprocal intermolecular hydrogen-bonding interactions between two adjacent molecules, giving rise to the formation of a hydrogen-bonded dimer (**Figure 5B**). Additionally, there are two sets of intermolecular parallel displaced  $\pi$ - $\pi$  stacking interactions present which support the cofacial and slipped stacking crystal packing arrangement of **3** (**Supplementary Figure S24, 25**). (Egli et al., 2003).

### Chemosensitivity Studies

Cisplatin (**CDDP**), carboplatin (**CARB**) and oxaliplatin (**OXA**) and compounds **1–3** were screened for their cytotoxicity against human cell lines: cisplatin-sensitive ovarian carcinoma (A2780), cisplatin-resistant ovarian carcinoma (A2780cisR) and breast adenocarcinomas (MCF-7 and MDA-MB-231). The IC<sub>50</sub> values were obtained via the MTT assay after a 96 h incubation period of each compound with the cells at 37°C and 5% CO<sub>2</sub> (**Table 2**; **Figure 6**). The Ac-terminated compound **1** was found to be moderate to non-cytotoxic against all cell lines, with IC<sub>50</sub> values ranging from 63 ± 4 μM to >100 μM. Similarly, the Boc-terminated analogue **2** was found to be moderate to non-cytotoxic against A2780cisR, MCF-7 and MDA-MB-231. However, a significant increase in cytotoxicity is observed when comparing compounds **1** with **2** against A2780, with the potency of **2** increasing by up to 3-fold (77 ± 5 μM for **1** cf. 24 ± 0.9 μM for **2**). The amine-terminated compound **3** is non-toxic towards the breast adenocarcinomas cell lines (MCF-7 and MDA-MB-231), with IC<sub>50</sub> values greater than the tested threshold (>100 μM). Notably, **3** is non-toxic against the cisplatin-sensitive ovarian carcinoma A2780 but is the only one in the library which displays any level of antiproliferative activity against the cisplatin-resistant ovarian carcinoma cell line, A2780cisR, with a moderate IC<sub>50</sub> value of 61 ± 1 μM.

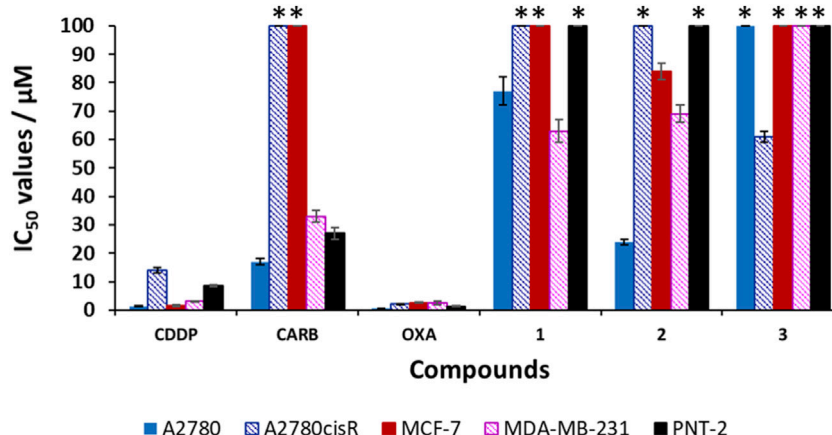




On analysis of these results no definite structure-activity relationship can be established but a general observation that the nature of the terminal group on these short aromatic oligoamides has a marked effect on determining their cytotoxicity against ovarian carcinomas (A2780 and A2780cisR) and breast adenocarcinomas (MCF-7 and MDA-MB-231). Results highlight the Boc-terminated compound **2** displays the highest activity, with moderate sensitivity against A2780 and the amine-terminated compound **3**, is the only compound to display any level of cytotoxicity against A2780cisR.

### Selectivity Index

CDDP, OXA, and CARB and compounds **1–3** were also screened against the non-malignant prostate cell line (immortalized with SV40), PNT-2, to determine any cancer cell selectivity. The results for CDDP, OXA, and CARB show that these clinical platinum drugs have high to moderately cytotoxicity towards PNT-2, with IC<sub>50</sub> values of 1.3 ± 0.2 μM (OXA), 8.5 ± 0.4 μM (CDDP) and 27 ± 2 μM (CARB). Unlike the clinical platinum drugs, compounds **1–3** are non-toxic towards PNT-2 (IC<sub>50</sub> values >100 μM). The selectivity index (SI) values were calculated for all the compounds, using the IC<sub>50</sub> values obtained against PNT-2 and dividing by the IC<sub>50</sub> value against the cancer cell line in parenthesis in Table 2). A SI value >1 indicates increased selectivity for the cancerous cell line over the non-malignant one, whilst a SI value <1 indicates the inverse (i.e., increased selectivity for the non-malignant cell line over the cancerous one). Compound **1** shows only slight increases in selectivity, with an SI > 1.3\* (*p* < 0.05, where \* indicates the minimum SI value due to the PNT-2 IC<sub>50</sub> value >100 μM, Table 2 footnote) for A2780.<sup>1</sup> However, an SI > 1.6\* (*p* < 0.05) for this compound against the triple negative breast cancer (TNBC) cell line, MDA-MB-231, is higher than those observed for the clinical platinum anticancer drugs OXA and CARB (of 0.5 and 0.8



**FIGURE 6 |** Cytotoxicity values (IC<sub>50</sub>/μM ± SD) for cisplatin (CDDP), carboplatin (CARB), oxaliplatin (OXA) and compounds **1–3** against human cell lines: ovarian carcinomas (A2780, A2780cisR), breast adenocarcinomas (MCF-7, MDA-MB-231) and non-malignant prostate (PNT-2). \* indicates that the IC<sub>50</sub> value is greater than the tested threshold concentration of 100 μM.

respectively).<sup>1</sup> Compound **2** displays a notable SI > 4.2\* ( $p < 0.05$ ) against A2780 and a very moderate increase in selectivity towards MCF-7 (SI > 1.2\*,  $p < 0.05$ ) and MDA-MB-231 (SI > 1.4\*).<sup>1</sup> The amine-terminated compound **3**, is the only compound to display increased selectivity for A2780cisR when compared to PNT-2, with a SI > 1.6\* ( $p < 0.05$ ), which, albeit is very modest, is higher than the SI values observed for **CDDP** (0.6), **OXA** (0.6) and **CARB** (0.3\*). Overall, these results highlight that small structural changes to the terminal groups of these aromatic oligoamides can have a marked effect on their biological activity against the tested ovarian and breast cancer cell lines. Herein, it is shown that modification of the terminal groups from Ac to Boc leads to a notable increase in the SI against A2780 but similar SI values are observed against MDA-MD-231, whilst variation of the terminal group to NH<sub>2</sub> leads to a change in the SI of the aromatic oligoamide against A2780cisR with a slight increase in SI (>1.6\*,  $p < 0.05$ ) being observed by this amine-terminated compound.

## CONCLUSION

In conclusion, we have synthesized and characterized a series of aromatic oligoamides based on a common pyridyl carboxamide core but incorporating distinct end groups: acetyl (Ac) **1**, *tert*-butyloxycarbonyl (Boc) **2** and amine **3**. Single crystal X-ray diffraction analysis of **1–3** and 2-DMSO has identified the presence of an array of non-covalent interactions including N-H...N and N-H...O=C hydrogen-bonding interactions, a series of C-H... $\pi$  and  $\pi$ - $\pi$  stacking interactions that support the diverse crystal packing arrangements present in these aromatic oligoamides including slipped stack (**1**), herringbone (**2**) and cofacial/slipped stacked (**3**). The crystal packing of **3** also reveals the presence of hydrogen-bonded dimer formed by the presence of reciprocal intermolecular N-H...O=C hydrogen bonding interactions formed between the NH of the terminal amine groups and the O atom on the carbonyl group in the amide group of an adjacent molecule.

To understand SARs, the cytotoxicity of the compound **1–3** (and **CDDP**, **OXA** and **CARB**) were obtained via a 96 h MTT assay, and screening against human ovarian carcinomas (A2780 and A2780cisR), human breast adenocarcinomas (MCF-7 and MDA-MB-231) and non-malignant prostate cell line (PNT-2). Generally, compounds **1–3** display either moderate cytotoxicity or are non-toxic against A2780cisR, MCF-7 and MDA-MB-231 cancer cell lines. The Boc-terminated compound, **2**, is the lead candidate of the tested aromatic oligoamides displaying an IC<sub>50</sub> value of  $24 \pm 0.9 \mu\text{M}$  against A2780. Unlike the tested clinical platinum anticancer drugs, compound **2** is non-toxic towards PNT-2 (IC<sub>50</sub> > 100  $\mu\text{M}$ ), meaning it displays an SI value >4.2\*-fold towards A2780 (*cf.* PNT-2), making it more selective towards ovarian

cancer than the platinum drugs **CDDP** and **OXA** (SI values against A2780: 1.6 (**CDDP**), 6.5 (**CARB**); 2.6 (**OXA**)). The insights gained from this study, regarding the importance of small structural modifications on influencing the biological activity of aromatic oligoamides, will facilitate the future design of related compounds with improved cytotoxicity against ovarian and breast cancer cell lines.

## DATA AVAILABILITY STATEMENT

The datasets presented in this study can be found in online repositories. The names of the repository/repositories and accession number(s) can be found in the article/Supplementary Material.

## AUTHOR CONTRIBUTIONS

PD was responsible for the synthesis and characterization of compounds **1–3**. CS was responsible for the collection of crystallographic data and solving crystal structures of **2**, 2-DMSO and **3** and for the analysis of crystallographic data. LM was responsible for the collection of crystallographic data and solving crystal structure of **1**. RL was responsible for conducting the biological assays on the tested compounds, analysis of biological data and contributed to the manuscript. SP conceived the project and was responsible for analysis of crystallographic and biological data, manuscript preparation and project supervision.

## FUNDING

RL and SP thank the University of Bradford Research Development Fund for financial support. SP acknowledges the University of Birmingham for a Birmingham Fellowship. RL is a UKRI Future Leaders Fellow, and this work is supported by a UKRI Future Leaders Fellowship (MR/T041315/1). SP is a UKRI Future Leaders Fellow, and this work is supported by a UKRI Future Leaders Fellowship (MR/S035486/2).

## ACKNOWLEDGMENTS

We are grateful to the University of Bradford's Analytical Centre for support, in particular Haseeb Ul-Rehman for conducting mass spectrometry experiments. We would like to thank the Institute of Cancer Therapeutics, University of Bradford for access to Cat II laboratories and providing cell lines.

## SUPPLEMENTARY MATERIAL

The Supplementary Material for this article can be found online at: <https://www.frontiersin.org/articles/10.3389/fchem.2021.709161/full#supplementary-material>

<sup>1</sup>The IC<sub>50</sub> values of **1–3** against PNT-2 are greater than the tested threshold concentration of 100  $\mu\text{M}$  and the reported results are minimum SI values (\*) and could be greater than reported here.

## REFERENCES

- Annala, R., Suhonen, A., Laakkonen, H., Permi, P., and Nissinen, M. (2017). Structural Tuning and Conformational Stability of Aromatic Oligoamide Foldamers. *Chem. Eur. J.* 23, 16671–16680. doi:10.1002/chem.201703985
- Arifuzzaman, M., Siddiquee, T. A., Karim, M. R., Mirza, A. H., and Ali, M. A. (2013). Synthesis and Structure of Dimeric Copper (I) Complex from Bis[(2,2')-Dimethyl 2,2'-(1,10-Phenanthroline-2,9-Diyl) Bis(methan-1-Yl-1-Ylidene)-Bis(hydrazinecarbo Dithioate)]. *Csta* 02, 159–166. doi:10.4236/csta.2013.24022
- Azzarito, V., Prabhakaran, P., Bartlett, A. I., Murphy, N. S., Hardie, M. J., Kilner, C. A., et al. (2012). 2-O-Alkylated Para-Benzamide  $\alpha$ -helix Mimetics: the Role of Scaffold Curvature. *Org. Biomol. Chem.* 10, 6469. doi:10.1039/c2ob26262b
- Bao, C., Kauffmann, B., Gan, Q., Srinivas, K., Jiang, H., and Huc, I. (2008). Converting Sequences of Aromatic Amino Acid Monomers into Functional Three-Dimensional Structures: Second-Generation Helical Capsules. *Angew. Chem. Int. Ed.* 47, 4153–4156. doi:10.1002/anie.200800625
- Burslem, G. M., Kyle, H. F., Breeze, A. L., Edwards, T. A., Nelson, A., Warriner, S. L., et al. (2014). Small-Molecule Proteomimetic Inhibitors of the HIF-1 $\alpha$ -P300 Protein-Protein Interaction. *ChemBioChem* 15, 1083–1087. doi:10.1002/cbic.201400009
- Burslem, G. M., Kyle, H. F., Breeze, A. L., Edwards, T. A., Nelson, A., Warriner, S. L., et al. (2016). Towards "bionic" Proteins: Replacement of Continuous Sequences from HIF-1 $\alpha$  with Proteomimetics to Create Functional P300 Binding HIF-1 $\alpha$  Mimics. *Chem. Commun.* 52, 5421–5424. doi:10.1039/c6cc01812b
- Chang, Y.-C., Chen, Y.-D., Chen, C.-H., Wen, Y.-S., Lin, J. T., Chen, H.-Y., et al. (2008). Crystal Engineering for  $\pi$ - $\pi$  Stacking via Interaction between Electron-Rich and Electron-Deficient Heteroaromatics. *J. Org. Chem.* 73, 4608–4614. doi:10.1021/jo800546j
- Davis, J. M., Tsou, L. K., and Hamilton, A. D. (2007). Synthetic Non-peptide Mimetics of  $\alpha$ -helices. *Chem. Soc. Rev.* 36, 326–334. doi:10.1039/b608043j
- Dhar, J., Venkatramaniah, N., A., A., and Patil, S. (2014). Photophysical, Electrochemical and Solid State Properties of Diketopyrrolopyrrole Based Molecular Materials: Importance of the Donor Group. *J. Mater. Chem. C* 2, 3457–3466. doi:10.1039/c3tc32251c
- Egli, M., Tereshko, V., Mushudov, G. N., Sanishvili, R., Liu, X., and Lewis, F. D. (2003). Face-to-Face and Edge-To-Face  $\pi$ - $\pi$  Interactions in a Synthetic DNA Hairpin with a Stilbene-diether Linker. *J. Am. Chem. Soc.* 125, 10842–10849. doi:10.1021/ja0355527
- Ernst, J. T., Becerril, J., Park, H. S., Hang, Y., and Hamilton, A. D. (2003). *Angew. Chem. Int. Ed.* 42, 536. doi:10.1002/anie.200390154
- Figaro, M. K., Clayton, W., Usho, C., Brown, K., Kassim, A., Lakhani, V. T., et al. (2011). Thyroid Abnormalities in Patients Treated with Lenalidomide for Hematological Malignancies: Results of a Retrospective Case Review. *Am. J. Hematol.* 86, 467–470. doi:10.1002/ajh.22008
- Frimannsson, D. O., McCabe, T., Schmitt, W., Lawler, M., and Gunnlaugsson, T. (2010). Synthesis and Crystallographic Analysis of Short Pyridine-Based Oligoamides as DNA-Targeting Supramolecular Binders. *Supramolecular Chem.* 22, 483–490. doi:10.1080/10610278.2010.483732
- Garia, J. M., Garia, F. C., Serna, F., and de la Peña, J. L. (2010). *Prog. Polym. Sci.* 35, 623.
- Hamuro, Y., Geib, S. J., and Hamilton, A. D. (1994). Novel Molecular Scaffolds: Formation of Helical Secondary Structure in a Family of Oligoanthranilamides. *Angew. Chem. Int. Ed. Engl.* 33, 446–448. doi:10.1002/anie.199404461
- Hamuro, Y., Geib, S. J., and Hamilton, A. D. (1996). Oligoanthranilamides. Non-peptide Subunits that Show Formation of Specific Secondary Structure. *J. Am. Chem. Soc.* 118, 7529–7541. doi:10.1021/ja9539857
- Hegedus, Z., Grison, C. M., Miles, J. A., Rodriguez-Marin, S., Warriner, S. L., Webb, M. E., et al. (2019). A Catalytic Protein-Proteomimetic Complex: Using Aromatic Oligoamide Foldamers as Activators of RNase S. *Chem. Sci.* 10, 3956–3962. doi:10.1039/c9sc00374f
- Jayatunga, M. K. P., Thompson, S., and Hamilton, A. D. (2014).  $\alpha$ -Helix Mimetics: Outwards and Upwards. *Bioorg. Med. Chem. Lett.* 24, 717–724. doi:10.1016/j.bmcl.2013.12.003
- Kobayashi, K., Shimaoka, R., Kawahata, M., Yamanaka, M., and Yamaguchi, K. (2006). Synthesis and Cofacial  $\pi$ -Stacked Packing Arrangement of 6,13-Bis(alkylthio)pentacene. *Org. Lett.* 8, 2385–2388. doi:10.1021/ol060679x
- König, B., Papke, U., and Rödel, M. (2000). Synthesis of Aromatic and Heteroaromatic Oligoamides on Methoxypoly(ethylene Glycol) as Solubilizing Polymer Support. *New J. Chem.* 24, 39–45. doi:10.1039/a904289j
- Kortelainen, M., Suhonen, A., Hamza, A., Pápai, I., Nauha, E., Yliniemelä-Sipari, S., et al. (2015). Folding Patterns in a Family of Oligoamide Foldamers. *Chem. Eur. J.* 21, 9493–9504. doi:10.1002/chem.201406521
- Mader, R. M., Müller, M., and Steger, G. G. (1998). Resistance to 5-Fluorouracil. *Gen. Pharmacol. Vasc. Syst.* 31, 661–666. doi:10.1016/s0306-3623(98)00191-8
- Nishio, M. (2011). The CH/ $\pi$  Hydrogen Bond in Chemistry. Conformation, Supramolecules, Optical Resolution and Interactions Involving Carbohydrates. *Phys. Chem. Chem. Phys.* 13, 13873. doi:10.1039/c1cp20404a
- Plante, J. P., Burnley, T., Malkova, B., Webb, M. E., Warriner, S. L., Edwards, T. A., et al. (2009). Oligobenzamide Proteomimetic Inhibitors of the P53-hDM2 Protein-Protein Interaction. *Chem. Commun.*, 5091. doi:10.1039/b908207g
- Rozas, I., Alkorta, I., and Elguero, J. (1998). Bifurcated Hydrogen Bonds: Three-Centered Interactions. *J. Phys. Chem. A* 102, 9925–9932. doi:10.1021/jp9824813
- Suhonen, A., Kortelainen, M., Nauha, E., Yliniemelä-Sipari, S., Pihko, P. M., and Nissinen, M. (2016). Conformational Properties and Folding Analysis of a Series of Seven Oligoamide Foldamers. *CrystEngComm* 18, 2005–2013. doi:10.1039/c5ce02458g
- Suhonen, A., Nauha, E., Salorinne, K., Helttunen, K., and Nissinen, M. (2012). Structural Analysis of Two Foldamer-type Oligoamides - the Effect of Hydrogen Bonding on Solvate Formation, crystal Structures and Molecular Conformation. *CrystEngComm* 14, 7398. doi:10.1039/c2ce25981h
- Tageja, N., Giorgadze, T., and Zonder, J. (2011). Dermatological Complications Following Initiation of Lenalidomide in a Patient with Chronic Lymphocytic Leukaemia. *Intern. Med. J.* 41, 286–288. doi:10.1111/j.1445-5994.2011.02426.x
- Tárkányi, G., Király, P., Varga, S., Vakulya, B., and Soós, T. (2008). Edge-to-Face CH/ $\pi$  Aromatic Interaction and Molecular Self-Recognition inepi-Cinchona-Based Bifunctional Thiourea Organocatalysis. *Chem. Eur. J.* 14, 6078–6086. doi:10.1002/chem.200800197
- Tew, G. N., Liu, D., Chen, B., Doerken, R. J., Kaplan, J., Carroll, P. J., et al. (2002). De Novo design of Biomimetic Antimicrobial Polymers. *Proc. Natl. Acad. Sci.* 99, 5110–5114. doi:10.1073/pnas.082046199
- Ward, R. A., Fawell, S., Floc'h, N., Flemington, V., McKerrecher, D., and Smith, P. D. (2021). Challenges and Opportunities in Cancer Drug Resistance. *Chem. Rev.* 121, 3297–3351. doi:10.1021/acs.chemrev.0c00383
- Winocur, G., Vardy, J., Binns, M., Kerr, L., and Tannock, I. (2006). The Effects of the Anti-cancer Drugs, Methotrexate and 5-fluorouracil, on Cognitive Function in Mice. *Pharmacol. Biochem. Behav.* 85, 66–75. doi:10.1016/j.pbb.2006.07.010
- Yamato, K., Yuan, L., Feng, W., Helsel, A. J., Sanford, A. R., Zhu, J., et al. (2009). Crescent Oligoamides as Hosts: Conformation-dependent Binding Specificity. *Org. Biomol. Chem.* 7, 3643. doi:10.1039/b911653b
- Yao, Z.-F., Wang, J.-Y., and Pei, J. (2018). Control of  $\pi$ - $\pi$  Stacking via Crystal Engineering in Organic Conjugated Small Molecule Crystals. *Cryst. Growth Des.* 18, 7–15. doi:10.1021/acs.cgd.7b01385
- Yap, J. L., Cao, X., Vanommeslaeghe, K., Jung, K.-Y., Peddaboina, C., Wilder, P. T., et al. (2012). Relaxation of the Rigid Backbone of an Oligoamide-Foldamer-Based  $\alpha$ -helix Mimetic: Identification of Potent Bcl-xL Inhibitors. *Org. Biomol. Chem.* 10, 2928. doi:10.1039/c2ob07125h
- Yi, H.-P., Shao, X.-B., Hou, J.-L., Li, C., Jiang, X.-K., and Li, Z.-T. (2005). Hydrogen Bonding-Mediated Oligobenzamide Foldamer Receptors that Efficiently Bind a Triol and Saccharides in Chloroform. *New J. Chem.* 29, 1213. doi:10.1039/b508773b
- Yin, H., and Hamilton, A. D. (2005). Strategies for Targeting Protein-Protein Interactions with Synthetic Agents. *Angew. Chem. Int. Ed.* 44, 4130–4163. doi:10.1002/anie.200461786
- Yuan, L., Sanford, A. R., Feng, W., Zhang, A., Zhu, J., Zeng, H., et al. (2005). Synthesis of Crescent Aromatic Oligoamides. *J. Org. Chem.* 70, 10660–10669. doi:10.1021/jo050798a
- Yuan, L., Zeng, H., Yamato, K., Sanford, A. R., Feng, W., Atreya, H. S., et al. (2004). Helical Aromatic Oligoamides: Reliable, Readily Predictable Folding from the Combination of Rigidified Structural Motifs. *J. Am. Chem. Soc.* 126, 16528–16537. doi:10.1021/ja046857w

**Conflict of Interest:** The authors declare that the research was conducted in the absence of any commercial or financial relationships that could be construed as a potential conflict of interest.

Copyright © 2021 Delfosse, Seaton, Male, Lord and Pike. This is an open-access article distributed under the terms of the Creative Commons Attribution License (CC BY). The use, distribution or reproduction in other forums is permitted, provided the original author(s) and the copyright owner(s) are credited and that the original publication in this journal is cited, in accordance with accepted academic practice. No use, distribution or reproduction is permitted which does not comply with these terms.



# Exploiting Peptide Self-Assembly for the Development of Minimalistic Viral Mimetics

Patrizia Janković<sup>1</sup>, Iva Šantek<sup>1</sup>, Ana Sofia Pina<sup>2,3</sup> and Daniela Kalafatovic<sup>1\*</sup>

<sup>1</sup>Department of Biotechnology, University of Rijeka, Rijeka, Croatia, <sup>2</sup>Associate Laboratory i4HB - Institute for Health and Bioeconomy, NOVA School of Science and Technology, NOVA University Lisbon, Caparica, Portugal, <sup>3</sup>UCIBIO – Applied Molecular Biosciences Unit, Department of Chemistry, NOVA School of Science and Technology, NOVA University Lisbon, Caparica, Portugal

Viruses are natural supramolecular nanostructures that form spontaneously by molecular self-assembly of complex biomolecules. Peptide self-assembly is a versatile tool that allows mimicking viruses by creating their simplified versions through the design of functional, supramolecular materials with modularity, tunability, and responsiveness to chemical and physical stimuli. The main challenge in the design and fabrication of peptide materials is related to the precise control between the peptide sequence and its resulting supramolecular morphology. We provide an overview of existing sequence patterns employed for the development of spherical and fibrillar peptide assemblies that can act as viral mimetics, offering the opportunity to tackle the challenges of viral infections.

## OPEN ACCESS

### Edited by:

Jennifer Hiscock,  
University of Kent, United Kingdom

### Reviewed by:

Mustafa O Guler,  
University of Chicago, United States  
Hajime Shigemitsu,  
Osaka University, Japan

### \*Correspondence:

Daniela Kalafatovic  
daniela.kalafatovic@uniri.hr

### Specialty section:

This article was submitted to  
Supramolecular Chemistry,  
a section of the journal  
Frontiers in Chemistry

**Received:** 10 June 2021

**Accepted:** 15 July 2021

**Published:** 28 July 2021

### Citation:

Janković P, Šantek I, Pina AS and  
Kalafatovic D (2021) Exploiting Peptide  
Self-Assembly for the Development of  
Minimalistic Viral Mimetics.  
Front. Chem. 9:723473.  
doi: 10.3389/fchem.2021.723473

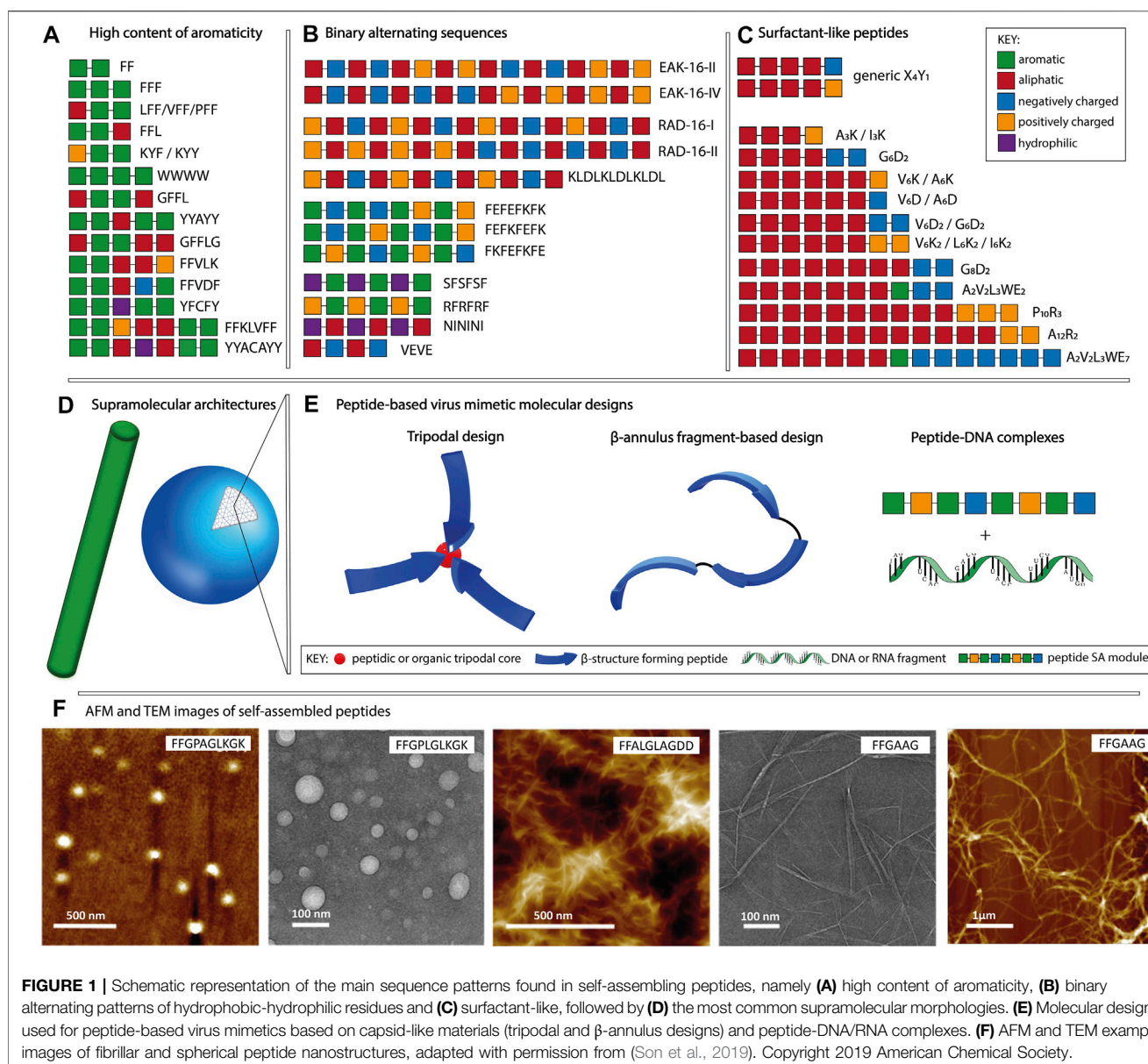
**Keywords:** self-assembly, viral mimetics, peptides, minimalistic, co-assembly

## INTRODUCTION

Designed bio-nanomaterials are often inspired by basic processes found in nature such as molecular recognition and self-assembly (Lehn, 2002; Whitesides and Grzybowski, 2002; Yang et al., 2020a). Viruses present a great source of inspiration for the design of life-like materials (Whitesides, 2015; Maslanka Figueroa et al., 2021) as they constitute simple, yet sophisticated supramolecular assemblies that contain genetic code and present well-defined rod-like or spherical morphologies. In addition, they show the ability to self-replicate, respond to physical and chemical stimuli, adapt to the environment, and evade the immune system which makes them ideal candidates to be manipulated and repurposed.

A variety of virus-mimetic materials have been developed for biological and chemical sensing (Mao et al., 2009), drug delivery (Li et al., 2016), cancer immunotherapy (Mohsen et al., 2020) and vaccine design (Abudula et al., 2020). Virus-like particles (VLPs), formed by the multimeric self-assembly of expressed viral structural proteins in absence of genetic material, are the most studied ones (Ludwig and Wagner, 2007; Ferreira and Martins, 2017; Roldão et al., 2019). The complexity of their fabrication, that requires fully folded proteins and efficient upstream and downstream strategies, impacts the production yields, and is associated to high costs. Other examples include polymer peptide nanogels (Lee et al., 2008), dendritic lipopeptides (Liang et al., 2019), iron oxide-lactoferrin magneto-responsive nanocapsules (Fang et al., 2015), peptide-DNA condensates (Cao et al., 2018), rabies-inspired gold nanorods (Lee et al., 2017) or metal-organic frameworks (Qiao et al., 2020). However, the potential of minimalistic, purely peptidic, supramolecular nanostructures to resemble the morphology and/or functionality of viruses has not been fully exploited yet.





**FIGURE 1 |** Schematic representation of the main sequence patterns found in self-assembling peptides, namely (A) high content of aromaticity, (B) binary alternating patterns of hydrophobic-hydrophilic residues and (C) surfactant-like, followed by (D) the most common supramolecular morphologies. (E) Molecular designs used for peptide-based virus mimetics based on capsid-like materials (tripodal and β-annulus designs) and peptide-DNA/RNA complexes. (F) AFM and TEM example images of fibrillar and spherical peptide nanostructures, adapted with permission from (Son et al., 2019). Copyright 2019 American Chemical Society.

Several peptide-based therapeutics have reached the market while others are in various phases of clinical development for the treatment of cancer and metabolic disorders (Vlieghe et al., 2010; Craik et al., 2013). Compared to their protein counterparts, peptides are easier to synthesize and more stable under harsh conditions (Fosgerau and Hoffmann, 2015). Furthermore, peptides can be exploited as building blocks for the fabrication of highly ordered nanostructures with varying morphologies and surface functionalities, developed for drug delivery, tissue engineering, and regenerative medicine due to their inherent biocompatibility and biodegradability (Zhang, 2003; Collier et al., 2010; Woolfson and Mahmoud, 2010; Frederix et al., 2015; Smith et al., 2015; Slocik and Naik, 2017; Lampel et al., 2018; Sharma et al., 2021).

Peptide-based nanomaterials offer simple and low costs alternatives to VLPs (Matsuura, 2012; Hendricks et al., 2017; Singh et al., 2017; Cai et al., 2020). When designing peptide-based virus mimetics, the main

strategy is capsid reconstruction through the formation of supramolecular assemblies based on peptide segments with the goal of mimicking the viral architecture and functionality of efficient cell entry, immune evasion, and targeted cargo delivery. In here, we provide an overview of sequence patterns that drive peptide self-assembly, followed by the potential to achieve dimensional control through co-assembly. Finally, examples of peptide-based building blocks used in the design of supramolecular virus mimetics are discussed.

## MORPHOLOGICAL CONTROL THROUGH SEQUENCE DESIGN

In the context of molecular self-assembly, the composition and the physico-chemical properties of amino acid side chains dictate

their behavior in different environments. In a hydrophilic environment, aromatic amino acids tend to aggregate due to hydrophobic interactions and  $\pi$ - $\pi$  stacking, whereas polar and charged amino acids promote nanostructure formation through hydrogen bonds and electrostatic interactions, respectively. In addition, the position of a particular amino acid within the sequence, as well as the type of neighboring residues, affect the formation of supramolecular assemblies and their morphologies. Although it is possible to identify distinct sequence patterns with the tendency to form a particular nanostructure, it is challenging to attribute a supramolecular morphology based solely on the amino acid composition. Peptide sequences can self-assemble into a variety of shapes, including spheres, fibers, vesicles and tubes, with diameters in the 10–100 nm range and in the case of nanofibers, reaching micrometers in length (Gazit, 2007a; Zhao et al., 2008). In this section, we will focus on three main patterns used in the design of purely peptidic materials (**Figures 1A–C**): (i) high content of aromaticity, (ii) binary alternating hydrophobic-hydrophilic and (iii) surfactant-like.

### Peptides With High Content of Aromaticity

Peptides composed of aromatic amino acids preferentially self-assemble into nanofibers with high intermolecular  $\beta$ -sheet content. Short motifs such as FF, YY, and WW constitute fundamental building blocks for self-assembly, with diphenylalanine being the most widely studied one (Gazit, 2007b; Frederix et al., 2015; Tao et al., 2017). Depending on the combination of amino acids adjacent to the FF motif and its position within the sequence, various morphologies such as fibrous and plate-like assemblies for FFF, nanospheres for CFF, helical fibrils for PFF and heterogeneous nanostructures for FFV, VFF, and LFF, are observed (Reches and Gazit, 2004; Tamamis et al., 2009; Marchesan et al., 2012; Frederix et al., 2015; Bera et al., 2019). Examples of fiber forming peptides (**Figure 1A**) having longer sequences include FFKLVFF, GFFLG, GFFL, FFAGL, FFVLK, FFVDF, and WWWW (Kalafatovic et al., 2016; Diaferia et al., 2018; Son et al., 2019; Yang et al., 2020b). Moreover, tyrosine-rich sequences including YYAYY, YYACAYY, YFCFY, KYF, and KYY were found to assemble into nanosheets, nanocapsules or nanofibers (Frederix et al., 2015; Lee et al., 2019; Sloan-Dennison et al., 2021). Amyloid-like peptides find applications in plaque-associated neurodegenerative diseases research or as biosensors and nanocarriers (Gazit, 2007b; Al-Halifa et al., 2019).

### Binary Alternating Sequences of Hydrophobic-Hydrophilic Residues

Peptides with the binary-alternating patterns rely on hydrogen bonds and/or electrostatic interactions for the formation of supramolecular assemblies. The first reported self-assembling peptide, EAK16-II (AEAEAKAKAEAEAKAK) is a repetitive segment derived from a natural yeast protein consisting of alternating hydrophobic and hydrophilic, positively, and

negatively charged amino acids (Zhang et al., 1993; Zhang, 2017). It was shown that the disposition of amino acids within the sequence and the pH of the environment influence the supramolecular morphology of EAK16 (Hong et al., 2003). At neutral pH, EAK16-II formed fibrils and its analogue EAK16-IV (AEAEAEAEAKAKAKAK) formed globular assemblies, whereas both peptides showed fibrillar assemblies at conditions above or below the neutral. Other examples (**Figure 1B**) including RAD16-I (RADARADARADADA), RAD16-II (RARADADARADADA), KLDLKLKLKL, FKFEFKFE, FEKFEFK, FEFEFKFK, VEVE, SFSFSF, RFRFRF, and NININI have been reported to self-assemble into fibers (Kisiday et al., 2002; Marini et al., 2002; Yokoi et al., 2005; Cui et al., 2009; Guilbaud et al., 2010; Mandal et al., 2014; Do et al., 2016; Gao et al., 2017; Pelin et al., 2020). In addition to linear sequences, cyclic peptides have been used as building blocks allowing for manipulation of the supramolecular morphology through monomer design (Mandal et al., 2013). Cyclic peptides having the  $[WR]_n$  structure, where  $n \in \{3,4,5\}$ , favor the formation of vesicle-type assemblies, unlike the linear designs with the binary alternating pattern, that preferentially assemble into fibrillar morphologies. The main applications of peptides classified in this category are related to their ability to form hydrogels. Such biomaterials can serve as scaffolds for tissue engineering, bioprinting, cell proliferation, regenerative medicine and drug delivery (Liu and Zhao, 2011; Levin et al., 2020; Gelain et al., 2021).

### Surfactant-Like Peptides

Surfactant-like peptides formed by combining aliphatic and charged segments have been also reported as self-assembly units. Their design is based on a hydrophobic tail composed of V, I, L, G, A or P followed by a charged head group containing K, D, R or E (**Figure 1C**). Examples include V<sub>6</sub>K, V<sub>6</sub>K<sub>2</sub>, V<sub>6</sub>D, V<sub>6</sub>D<sub>2</sub>, I<sub>3</sub>K, I<sub>6</sub>K<sub>2</sub>, A<sub>3</sub>K, A<sub>6</sub>K, A<sub>6</sub>D, G<sub>4</sub>D<sub>2</sub>, G<sub>6</sub>D<sub>2</sub>, G<sub>8</sub>D<sub>2</sub>, A<sub>12</sub>R<sub>2</sub>, A<sub>2</sub>V<sub>2</sub>L<sub>3</sub>WE<sub>2/7</sub>, P<sub>10</sub>R<sub>3</sub>, etc. (Vauthey et al., 2002; van Hell et al., 2007; Yoon et al., 2008; Wang et al., 2009; Zhao, 2009; Xu et al., 2010; Hamley et al., 2013). These sequences can assemble into various morphologies comprising micelles, fibers, vesicles and tubes. The size and shape of the formed supramolecular assemblies depend on the type of amino acids used to constitute the amphiphile as well as the number of aliphatic and charged residues. In addition, factors such as temperature, solution pH and ionic strength affect the self-assembly process. The ability to form lipid bilayer-like assemblies makes them ideal for applications in immunotherapy, gene and drug delivery. Moreover, they can be used as protective envelopes for the delivery of enzymes and other biomolecules (Dasgupta and Das, 2019).

### DIMENSIONAL CONTROL THROUGH CO-ASSEMBLY

Compared to the unimolecular assemblies described above, supramolecular co-assemblies lead to the formation of

**TABLE 1 |** Examples of peptide-based viral mimetic design strategies.

Strategy	Peptidic component / sequence	Role (structural (s) / functional (f))	Supramolecular Morphology	Development Stage	Ref.
<b>Capsid mimicking nanomaterials with C<sub>3</sub> symmetry (trigonal or based on <math>\alpha</math>-helical or <math>\beta</math>-sheet forming peptides)</b>					
Trigonal (trimesoyl) peptide conjugate	C <sup>I</sup> -FKFEFKFE <sup>II</sup> Ci-KTWTWTE <sup>III</sup> ( $\gamma$ E-C <sup>I</sup> -G) <sup>IV</sup>	i) Conjugation to core molecule (s) ii) $\beta$ -sheet self-assembly unit (s) iii) Tryptophane zipper based $\beta$ -sheet self-assembly (s) iv) self-assembly unit (s)	Nanospheres	Biophysical data	Matsuura et al. (2005) Matsuura et al. (2011) Matsuura et al. (2009)
Wheel (trimesoyl) peptide conjugate	(FKFE-C <sup>I</sup> -KFE) <sup>II</sup>	i) Conjugation to core molecule (s) ii) $\beta$ -sheet self-assembly unit (s)	Nanofibers	Biophysical data	Murasato et al. (2008)
Trigonal (tertiary amine) dipeptide conjugate	WW FF	$\beta$ -sheet self-assembly unit (s)	Nanospheres Nanotubes	Biophysical data	Ghosh et al., (2007)
Trigonal (ethyl benzene)-peptide conjugate	( $\gamma$ E-C <sup>I</sup> -G) <sup>II</sup>	i) Conjugation to core molecule (s) ii) Self-assembly unit (s)	Nanospheres	Biophysical data	Matsuura et al., (2010a)
Peptide triskelion (trilateral honeycomb symmetry)	$\beta$ AKK <sup>I</sup> -(RRWTWE) <sup>II</sup> <sup>III</sup>	i) Trigonal core (s) ii) Tryptophane zipper based $\beta$ -sheet self-assembly (s) iii) Antimicrobial activity (f)	Nanocapsules	Cell assays (RNA delivery, antimicrobial activity)	Castelletto et al. (2016)
Trigonal peptidic coiled coil heterodimers	K <sub>p</sub> AK <sub>p</sub> AK <sup>I</sup> -(KIAKLKQIKQLKAKIAKLKQ) <sub>3</sub> <sup>I</sup> C <sub>p</sub> AEISALEQEIASLEQEISALEQ <sup>III</sup>	i) Trigonal core (s) ii) Cationic, covalently bound antimicrobial component (s) iii) Anionic component for heterodimer formation (s)	Nanospheres	Cell assays (RNA delivery, antimicrobial activity)	De Santis et al., (2017)
$\beta$ -annulus fragment from TBSV capsid	INHVGTTGGAIMAPVAVTRQLVGS <sup>I</sup> INHVGTTGGAIMAPVAVTRQLVGG <sup>I</sup> CGGGKIAALKKKNAALKQKIAALKQ <sup>I</sup> EIAALEKENAALEQEIAALEQ <sup>III</sup>	i) $\beta$ -annulus segment (s) ii) Cationic component covalently bound to $\beta$ -annulus (s) iii) Anionic component for heterodimer formation (s)	Hollow nanocapsules Nanospheres	Biophysical data	Matsuura et al. (2010b); Fujita and Matsuura (2017)
$\beta$ -annulus fragment from SMV	GISMASQAQGAM <sup>I</sup> -FKFE <sup>II</sup>	i) $\beta$ -annulus segment (s) ii) $\beta$ -sheet self-assembly unit (s)	Nanospheres	Biophysical data	Matsuura et al., (2016)
Tecto-dendrimeric design	C <sup>I</sup> -GG <sup>II</sup> - EIALEQEIALEQEIALEQEIALE <sup>III</sup>	i) Disulfide crosslinking (s) ii) Glycine linker (s) iii) $\alpha$ -helical conformation promoting sequence (s)	Spherical particles	Cell assays (gene transfection)	Noble et al., (2016)
<b>Multicomponent peptide-DNA complexes</b>					
Surfactant-like sequences	I <sub>3</sub> V <sub>3</sub> A <sub>3</sub> G <sub>3</sub> <sup>I</sup> -K <sub>3</sub> <sup>II</sup>	i) $\beta$ -sheet self-assembly unit (s) ii) DNA condensing (f)	Nanosheets for peptidic component Heterogeneous morphologies via condensation with DNA	Cell assays (gene transfection)	Cao et al., (2018)
Multicomponent, glucose-peptide conjugate	GSGSGS <sup>I</sup> -K <sub>8</sub> <sup>II</sup> -GGSGGS <sup>III</sup> -(WKWE) <sub>3</sub> WG <sup>IV</sup>	i) linker (s) ii) siRNA binding site (f) iii) linker (s) iv) $\beta$ -sheet self-assembly unit (s)	$\beta$ -nanoribbons for peptidic component and for complexes with siRNA and dsDNA	Cells assays (siRNA transfection)	Lim et al., (2008)

(Continued on following page)

**TABLE 1 |** (Continued) Examples of peptide-based viral mimetic design strategies.

Strategy	Peptidic component / sequence	Role (structural (s) / functional (f))	Supramolecular Morphology	Development Stage	Ref.
Cocoon-like viral mimics based on $\beta$ -sheet forming sequences (C6 = alkyl linker)	$K_3^I-C_6-WLVFFAQQ^II-G^III-SPD^IV$ $K_3^I-C_6-X^II-G^III-SPD^IV$ where $X \in \{L_8, L_6, L_4, A_8, A_6, (L_2A_2)_2\}$	i) cationic, DNA binding region (f) ii) amyloid / $\beta$ -sheet segment (s) iii) glycine linker (s) iv) hydrophilic segment (s)	Nanoribbons for peptidic component Nanococoons <i>via</i> condensation with DNA Nanofibers for peptidic component Nanococoons <i>via</i> condensation with DNA for $L_8, L_6, L_4, (L_2A_2)_2$	Biophysical data Cell assays (gene transfection)	Ni and Chau, (2014) Ni and Chau, (2017)
Tat-LK15 conjugate	(RKRRRQRRRG <sup>I</sup> -KLLKLLKLLKLLK <sup>II</sup> ) <sup>III</sup>	i) Cell penetrating (f) ii) Membrane lytic, amphipathic (f) iii) DNA binding (f)	Peptide-DNA complex (morphology not determined)	Cells assays (gene transfection)	Saleh et al. (2010)
Multicomponent	$K_6^I-GGFLG^II-$ $FWRGNGRKRTRSA YERM CNILKGK^III$	i) DNA binding (f) ii) Enzyme cleavable (s/f) iii) Influenza-derived epitope (f)	Dimer formation through disulphide linkage for peptide component Spherical aggregates in presence of DNA	Cells assays (gene transfection)	Haines et al. (2001)
Multicomponent, bola-amphiphile	$RGD^I-GPLGLAG^II-I_3^III-G-R_8^IV$	i) Integrin binding (f) ii) enzyme cleavable (hydrophobic) (s/f) iii) structural (hydrophobic) (s) iv) Cell penetrating, DNA binding (f)	Nanospheres for peptidic component only Rod-like or spherical shapes in presence of DNA	Cells assays (gene transfection)	Wang et al. (2020)
Bi-functional bola-amphiphile with hydrocarbon (C <sub>12</sub> ) core	$RGD^I-C_{12}-R_8^II$	i) Integrin binding (f) ii) Cell penetrating, DNA binding (f)	Spherical nanoparticles <i>via</i> condensation with DNA	Cells assays (gene transfection)	Chen et al., (2013)

nanostructures with increased chemical diversity and structural complexity that can resemble natural systems. Peptides can co-assemble in cooperative, orthogonal, disruptive or random manner (Makam and Gazit, 2018). It is possible to fine-tune the morphology and dimension of nanostructures, and consequently their chemical, mechanical and physical properties, by controlling the mixing ratio of the individual building blocks. For example, the co-assembly of FF and FFF can be tuned to obtain nanorods, spherical nanovesicles, hollow nanotubes and toroid-like nanostructures (Guo et al., 2016). The disruptive co-assembly of the FF motif with its capped version Boc-FF allowed for the precise control of the nanotube length from 12 to 8  $\mu$ m by changing the mixing ratio from 20:1 to 5:1, respectively (Adler-Abramovich et al., 2016). The cooperative co-assembly of dendrimeric poly (lysine) hydrophilic heads with linear poly (leucine) hydrophobic tails allowed the morphology control of the formed peptidosomes by alternating the ratio of dendrimeric to linear component. When the ratio changed from 10:1 to 1:5, the size of the nanoparticles increased from 300 to 800 nm and their morphology changed from spherical to fusiform (Xu et al., 2012). The ability to achieve dimensional control constitutes a

promising tool for the design of peptide supramolecular materials where specific morphologies or dimensions are required. However, the co-assembly of peptide-based nanomaterials has not been researched extensively and constitutes an opportunity to improve the future design of peptide materials (Sasselli et al., 2017).

## VIRAL MIMETICS

Recently, the concept of mimicking viral capsids by creating their simplified versions through molecular self-assembly following the bottom-up strategy has emerged. Peptide self-assembly is a powerful tool to create biocompatible, tunable, low-cost supramolecular materials. It allows the conversion of chemically simple building blocks into a wide range of supramolecular architectures featuring modularity, functional diversity, adaptability and responsiveness to stimuli (Lampel, 2020). Peptides are versatile molecules for the design of virus mimetics as they can act as structural components as well as functional domains that favor selective binding, cell entry, endosomal escape or possess a specific activity (e.g., antimicrobial or catalytic). Short



peptides offer the possibility to use minimal recognition modules for the design of functional materials and offer unique platforms for mimicking complex systems (Levin et al., 2020).

In this review, we distinguish the role of peptidic components used for the fabrication of virus mimetics into structural and functional modules (**table 1**). The structural modules are based on patterns that drive the formation of ordered supramolecular nanostructures having spherical or fibrillar morphologies (**Figure 1D, F**), dictated by the sequence, as described in **section 2**. In addition, trigonal cores (peptidic or organic), linkers (glycine or alkyl), cysteine residues serving as conjugation points, coiled coil,  $\alpha$ -helical or  $\beta$ -annulus segments contribute to the design of structural modules. On the other hand, functional modules, related to the inherent biological signaling typical for peptides, are based on sequences with known activities such as cell penetration, integrin binding, DNA condensation and antimicrobial activity. Accordingly, peptide-based viral mimetic designs are divided into: i) capsid reconstruction strategies where structural modules contribute to the final supramolecular morphology and ii) simplified virus-like complexes where structural and functional peptidic modules are complexed with DNA or RNA fragments.

## Capsid-Like Nanomaterials

Viral capsids with icosahedral symmetry formed through the assembly of multiple protein subunits have inspired the design of artificial, peptide-based nanostructures for applications in gene delivery and cancer immunotherapy (Matsuura, 2018; Cai et al., 2020). In capsid reconstruction, it is important to maintain the  $n$ -fold rotational symmetry with  $n \in \{3,5\}$ . The  $C_3$  assembly can be achieved at the molecular level by designing trigonal conjugates or through folding-assembly pathways of peptides with helical conformations or  $\beta$ -annulus segments found on capsid-forming proteins (**Figure 1E**).

Trigonal designs induce the symmetry through the manipulation of the tripodal core (organic or peptidic) conjugated to peptidic structural modules that favor  $\beta$ -sheet-like self-assembly including the WTW tryptophane zipper and the FKFE-based binary alternating pattern. Examples are trymesoyl conjugates bearing three  $\beta$ -sheet-forming sequences (CFKFEFKFE or CKTWTWTE) attached through the C-terminal cysteine, that assemble into spherical morphologies (Matsuura et al., 2005, 2011). Similarly, a wheel-like trigonal design where the same core is conjugated to FKFECKFE through the central cysteine residue, self-assembled into fibers (Murasato et al., 2008). A clathrin triskelion-inspired conjugate, having a tris(2-aminoethyl) amine core linked to three aromatic di-tryptophan modules, self-assembled into nanospheres. In contrast, the conjugate containing the FF motif linked to the same core resulted in the formation of nanotubes, indicating that the morphology of the assemblies could be tuned through the dipeptide sequence (Ghosh et al., 2007). Furthermore, the choice of the core molecule can influence the properties of the obtained assemblies. For glutathione ( $\gamma$ -ECG) attached to two different cores, the 1,3,5-tris(aminomethyl)-2,4,6-triethyl benzene

showed improved conformational rigidity compared to the trimesoyl, giving rise to nanospheres with narrow size distribution (Matsuura et al., 2009; Matsuura et al., 2010a).

A purely peptidic triskelion, designed by conjugating each amino acid of the core sequence  $\beta$ AKK to the antimicrobial RRWTWE peptide containing the virus-derived tryptophane zipper, self-assembled into nanocapsules with dual function consisting of siRNA delivery and intrinsic antimicrobial activity (Castelletto et al., 2016). In this case, the RRWTWE sequence contains both the structural ( $\beta$ -sheet-forming) and functional (antimicrobial) modules. In another example, the core  $K\beta AK\beta AK$  sequence was conjugated to a positively charged antimicrobial (KIAKLKQIKQLKAKIAKLKQ) peptide to form a trigonal conjugate, that upon addition of a complementary anionic sequence ( $C\beta AEISALEQEIASLEQEISALEQ$ ), assembled in a coiled-coil hetero dimer. The resulting  $C_3$  subunit gave rise to capsid-like nanomaterials with antimicrobial activity (De Santis et al., 2017).

The reconstruction of capsid morphology based on the assembly of  $\beta$ -annulus peptide segments from Tomato bushy stunt virus (INHVGGTGGAIMAPVAVTRQLVG) and *Sesbania* mosaic virus (GISMAPSAQGAM) is able to maintain the  $C_3$  symmetry while allowing for introduction of surface modifications (Matsuura et al., 2010b; Matsuura et al., 2016). Among others, these include coating with gold nanoparticles to enhance the imaging efficiency (Matsuura et al., 2015) or with albumin to confer greater serum stability without eliciting immune response or toxicity (Matsuura and Honjo, 2019).

At the sequence level, the  $\beta$ -annulus segments can be modified with  $\beta$ -sheet promoting sequences (FKFE) to improve their assembly propensity into spherical morphologies (Matsuura et al., 2016). Moreover, with the intention of mimicking spike-bearing viruses such as Influenza and SARS-CoV-2, the  $\beta$ -annulus segment covalently linked to a cationic, coiled-coil-forming sequence at the C-terminus (CGGGKIAALKKKNAALKQKIAALKQ) gives rise to nanospheres. In the presence of a complementary anionic peptide (EIAALEKENAALEQEIAALEQ) and depending on the ratio of the cationic to anionic component, spherical (4:1) or fibrillar (1:1) assemblies with surface-exposed dimeric coiled coils are obtained (Fujita and Matsuura, 2017).

Another strategy is the use of a tecto-dendrimeric architecture as template to achieve  $C_3$  assembly into spherical particles for gene delivery. The design is based on structural coiled-coil subunits (CGG-EIARLEQEIAARLEQEIAARLEYEIAARLE) configured into helical wheels, containing a GG spacer motif adjacent to a cysteine residue allowing for disulfide crosslinking (Noble et al., 2016).

## Multicomponent Peptide-DNA Complexes

Virus-mimicking nanostructures can be formed through the complexation of peptides with DNA or RNA (**Figure 1E**), simulating the co-assembly of capsid proteins with viral genomes. Predominantly positively charged peptides have the tendency to condense negatively charged gene fragments making the resulting virus mimicking nanostructures ideal candidates for gene delivery (Miyata et al., 2012). Compared to conventional, cytotoxic DNA condensation agents such as polyelectrolytes and lipidic surfactants,

short peptides have higher biocompatibility and consequently lower toxicity. Moreover, their structure can easily be modified to obtain high affinity DNA binders (Wang et al., 2020). Furthermore, the condensation with the peptidic vector confers protection from DNases. Several peptide-DNA/RNA co-assemblies have been reported containing structural or functional modules or their combination resulting in multicomponent designs.

Peptide-DNA condensates composed of lysine modified surfactant-like, binary alternating or amyloid-like structural modules, have been reported. While the cationic region drives the binding to DNA or RNA through electrostatic attraction, peptide self-assembly and  $\beta$ -sheet formation takes place *via* hydrogen bonds and hydrophobic interactions. Surfactant-like sequences, obtained by varying the position of aliphatic amino acids (A, G, I, and L) as well as the position of the cationic ( $K_3$ ) region from N- to C-terminus, including cone-like ( $G_3A_3V_3I_3K_3$ ,  $K_3I_3V_3A_3G_3$ ), dumbbell-like ( $I_3V_3A_3G_3K_3$ ,  $K_3G_3A_3V_3I_3$ ) and irregular shaped sequences ( $V_3G_3I_3A_3K_3$ ,  $K_3A_3I_3G_3V_3$ ) gave rise to nanorods, nanosheets and nanofibrils, respectively. The  $I_3V_3A_3G_3K_3$  was the most efficient one in inducing DNA condensation showing high content of ordered domains (Cao et al., 2018). This example shows that the supramolecular morphology and content of ordered domains could be fine-tuned through sequence engineering. Furthermore, a glucose-peptide conjugate [Glucose-GSGSGS- $K_8$ -GSGSGS-(WKWE) $_3$ WG] containing a functional, cationic segment ( $K_8$ ) for siRNA binding positioned between two linkers (GSGSGS and GSGSGS) and a binary alternating structural motif (WKWE) $_3$ , assembled into bilayered  $\beta$ -nanoribbons. The carbohydrate ligand exhibited the dual function of maintaining the  $\beta$ -nanoribbons neutrally charged while enhancing the cell binding through glucose transporters (Lim et al., 2008). Therefore, this design offers the formation of a controllable filamentous morphology able to bind RNA while presenting surface functionalization that yields high transfection efficiency.

Another example is the design of the cocoon-like virus mimetics based on a sequence ( $K_3$ - $C_6$ -WLFFAQQGSPD) containing the cationic, DNA binding region ( $K_3$ ) at the N-terminus, followed by the alkyl linker ( $C_6$ ) and three structural components, namely, the amyloid-like motif (LVFFA), the glycine linker and the hydrophilic (SPD) region (Ni and Chau, 2014). The  $\beta$ -sheet forming segment can be modified from amyloid to aliphatic ( $L_8$ ,  $L_6$ ,  $L_4$ , and  $L_2A_2L_2A_2$ ) while maintaining the self-assembly propensity of the whole sequence. The peptides alone self-assemble into fibrillar aggregates, while their interaction with DNA in various ratios induces condensation into nanococoons (Ni and Chau, 2017).

Cell penetrating peptides including the arginine-rich,  $R_8$  and the HIV-1 derived, Tat (RKKRRQRRRGGG) constitute the main functional modules used for the design of DNA condensates (Kalafatovic and Giralt, 2017). The covalent conjugation of Tat to the amphipathic LK15 sequence (KLLKLLKLLKLLK) resulted in improved cellular uptake and transfection efficiency, compared to Tat or LK15 alone (Saleh et al., 2010). CL22 ( $K_6$ -GGFLG-FWRGENGRKTRSAYERMCNLIKGG) is an example of purely

peptidic design containing an enzyme cleavable segment adjacent to the DNA binding region at the N-terminus and the Influenza nucleoprotein-derived sequence at the C-terminus. It assembles into spherical aggregates in the presence of DNA and attains maximum gene transfection efficiency upon spontaneous dimerization through the disulfide bond between cysteines at the C-terminus (Haines et al., 2001). Bola amphiphiles, composed of a central hydrophobic segment flanked by two hydrophilic ones, have the ability to self-assemble into fibrillar or spherical nanostructures depending on the sequence design (Chen et al., 2013). Examples are the purely peptidic RGD-GPLGLAG- $I_3$ -G- $R_8$  (Wang et al. 2020) and the fatty acid containing RGD- $C_{12}$ - $R_8$  (Chen et al., 2013) that accommodate both functional and structural motifs, where RGD is crucial for integrin-binding and  $R_8$  for cell penetration. Additionally, the PLGLA sequence serves as an enzyme-cleavable segment, while  $I_3$  confers hydrophobicity. The main drawback of peptide-DNA/RNA co-assemblies, mainly based on functional modules, is that oppositely charged polyions often form heterogeneous aggregates. The challenges resulting from the lack of control over their morphology, degree of order and size, often hamper the efficiency of gene transfection or delivery.

The DNA fragment length and composition can affect the formation of peptide-DNA complexes but also their morphology. The mechanism of formation depends on the peptides' intrinsic ability to self-assemble. Self-assembling peptide sequences condense the DNA by reorganizing to a final morphology that is often different from the one formed by the peptide alone. On the other hand, predominantly cationic and/or cell-penetrating peptides, unable to self-assemble, tend to form irregular aggregates in the presence of DNA. Moreover, the size of the complex can be controlled by varying the length of the DNA fragment. For example, the  $I_3V_3A_3G_3K_3$ -DNA complex size decreased from 122 to 85 nm by shortening the DNA fragment from 2000 to 300 bp (base pairs). Even though most examples use  $\lambda$ -DNA (~4.8 kbp), shorter DNA fragments (2000–300 bp) were explored with the intention to improve the DNA delivery efficiency (Cao et al., 2018).

However, the key factor influencing the morphology of peptide-DNA complexes is the  $R + / -$  ratio of the positively charged peptide residues to the negatively charged DNA fragments. A stable peptide-DNA complex is formed when all the negative charges are successfully neutralized. For example, RGD-GPLGLAG- $I_3$ -G- $R_8$  that self-assembles into spheres, upon the interaction with DNA and depending on the  $R + / -$  values forms thread-like ( $R + / - = 0.5$ ) complexes or highly condensed rod-like or spherical ( $R + / - = 3$ ) nanostructures (Wang et al., 2020). In another example, the  $R + / -$  of 10 is the minimum requirement for DNA condensation with  $K_3C_6SPD$ , where the peptide alone self-assembles into nanoribbons. However, upon DNA addition, the electrostatic interactions drive the self-assembly into amorphous aggregates ( $R + / - = 5$ ), or agglomerations with small striped nanococoons ( $R + / - = 10$ ). The  $R + / - = 20$  presents the optimal ratio for nanococoon formation, while at  $R + / -$  of 25 and 50 both nanococoons and filamentous nanoribbons are formed (Ni and Chau, 2014).

## FUTURE PERSPECTIVES

The idea of exploiting known principles of peptide self-assembly to obtain spherical or fibrillar nanostructures by including important features such as cell penetration, antimicrobial activity or viral transfection is conceptually attractive. Such systems are promising as they can be easily engineered and modified to include specific sequences found on the receptor binding domains of spike proteins. In addition, they can be designed as vehicles able to deliver cargo into cells. So far, morphology rather than functionality has been mimicked and it constitutes an advantage from the point of view of easy production compared to VLPs. A step towards functionality of peptide materials is their ability to enhance viral transfection by increasing the  $\beta$ -sheet content of supramolecular nanostructures (Sieste et al., 2021). However, efforts are needed to achieve controllable and complex functions such as self-replication and catalysis in the future. Although largely unexplored for clinical use, because of the multiscale and multiparameter optimization challenges of supramolecular nanostructures (Sieste et al., 2021), we envision that peptides have great potential in becoming future nanotechnological solutions in covid-19 therapy and diagnostics.

The intention of this review is to emphasize the increasing importance of peptide self-assembly in the design and fabrication of minimalistic, synthetic models applicable to a variety of viral infections. We expect that future research in this field will deliver simple and cost-effective viral mimetics composed of peptide modules found on the surface of specific viruses, rationally designed to assemble into multivalent and multifunctional nanostructures able to selectively bind receptors of interest, penetrate cells and carry cargos. In addition to mimicking the viral morphology, such systems would partly resemble basic

functionality through the display of known functional modules and their combinations aiming for possible synergistic effects. Such an approach could lead to the development of efficient and safe platforms to study viral infections without the need of complicated genetic manipulations. Moreover, the developed models will provide screening platforms that can be rationally designed, allowing for rapid discovery of potential inhibitors or surface protein binders. Therefore, they could be used as safe alternatives for antiviral drug discovery or as vehicles for mRNA vaccines.

## AUTHOR CONTRIBUTION

PJ and DK conceived and designed the review, PJ, IŠ, AP, and DK analysed the literature and wrote the manuscript. All authors have read and approved the final version of the manuscript.

## FUNDING

This work was supported by the University of Rijeka (uniri-COV-1), the Foundation of the Croatian Academy of Sciences and Arts (HAZU) and by the Croatian Science Foundation/Hrvatska zaklada za znanost (UIP-2019-04-7999).

## ACKNOWLEDGMENTS

The authors would like to acknowledge the Centre for Artificial intelligence and cyber security (AIRI) and the Center for Advanced Computing and Modelling (CNRN) at the University of Rijeka.

## REFERENCES

- Abudula, T., Bhatt, K., Eggermont, L. J., O'Hare, N., Memic, A., and Bencherif, S. A. (2020). Supramolecular Self-Assembled Peptide-Based Vaccines: Current State and Future Perspectives. *Front. Chem.* 8, 1–11. doi:10.3389/fchem.2020.598160
- Adler-Abramovich, L., Marco, P., Arnon, Z. A., Creasey, R. C. G., Michaels, T. C. T., Levin, A., et al. (2016). Controlling the Physical Dimensions of Peptide Nanotubes by Supramolecular Polymer Coassembly. *ACS Nano*. 10, 7436–7442. doi:10.1021/acsnano.6b01587
- Al-Halifa, S., Baby, M., Zottig, X., Archambault, D., and Bourgault, S. (2019). Amyloid Self-Assembling Peptides: Potential Applications in Nanovaccine Engineering and Biosensing. *Pept. Sci.* 111, e24095–12. doi:10.1002/pep2.24095
- Bera, S., Mondal, S., Xue, B., Shimon, L. J. W., Cao, Y., and Gazit, E. (2019). Rigid Helical-like Assemblies from a Self-Aggregating Tripeptide. *Nat. Mater.* 18, 503–509. doi:10.1038/s41563-019-0343-2
- Cai, Y., Ran, W., Zhai, Y., Wang, J., Zheng, C., Li, Y., et al. (2020). Recent Progress in Supramolecular Peptide Assemblies as Virus Mimics for Cancer Immunotherapy. *Biomater. Sci.* 8, 1045–1057. doi:10.1039/c9bm01380f
- Cao, M., Wang, Y., Zhao, W., Qi, R., Han, Y., Wu, R., et al. (2018). Peptide-Induced DNA Condensation into Virus-Mimicking Nanostructures. *ACS Appl. Mater. Inter.* 10, 24349–24360. doi:10.1021/acsaami.8b00246
- Castelletto, V., De Santis, E., Alkassam, H., Lamarre, B., Noble, J. E., Ray, S., et al. (2016). Structurally Plastic Peptide Capsules for Synthetic Antimicrobial Viruses. *Chem. Sci.* 7, 1707–1711. doi:10.1039/c5sc03260a
- Chen, J.-X., Xu, X.-D., Yang, S., Yang, J., Zhuo, R.-X., and Zhang, X.-Z. (2013). Self-Assembled BolA-like Amphiphilic Peptides as Viral-Mimetic Gene Vectors for Cancer Cell Targeted Gene Delivery. *Macromol. Biosci.* 13, 84–92. doi:10.1002/mabi.201200283
- Collier, J. H., Rudra, J. S., Gasiorowski, J. Z., and Jung, J. P. (2010). Multi-component Extracellular Matrices Based on Peptide Self-Assembly. *Chem. Soc. Rev.* 39, 3413–3424. doi:10.1039/b914337h
- Craig, D. J., Fairlie, D. P., Liras, S., and Price, D. (2013). The Future of Peptide-Based Drugs. *Chem. Biol. Drug Des.* 81, 136–147. doi:10.1111/cbdd.12055
- Cui, H., Muraoka, T., Cheetham, A. G., and Stupp, S. I. (2009). Self-assembly of Giant Peptide Nanobelts. *Nano Lett.* 9, 945–951. doi:10.1021/nl802813f
- Dasgupta, A., and Das, D. (2019). Designer Peptide Amphiphiles: Self-Assembly to Applications. *Langmuir* 35, 10704–10724. doi:10.1021/acs.langmuir.9b01837
- De Santis, E., Alkassam, H., Lamarre, B., Faruqi, N., Bella, A., Noble, J. E., et al. (2017). Antimicrobial Peptide Capsids of De Novo Design. *Nat. Commun.* 8, 1–11. doi:10.1038/s41467-017-02475-3
- Diaferia, C., Balasco, N., Sibillano, T., Giannini, C., Vitagliano, L., Morelli, G., et al. (2018). Structural Characterization of Self-Assembled Tetra-Tryptophan Based Nanostructures: Variations on a Common Theme. *ChemPhysChem* 19, 1635–1642. doi:10.1002/cphc.201800026
- Do, T. D., De Almeida, N. E. C., Lapointe, N. E., Chamas, A., Feinstein, S. C., and Bowers, M. T. (2016). Amino Acid Metaclusters: Implications of Growth

- Trends on Peptide Self-Assembly and Structure. *Anal. Chem.* 88, 868–876. doi:10.1021/acs.analchem.5b03454
- Fang, J.-H., Lee, Y.-T., Chiang, W.-H., and Hu, S.-H. (2015). Magneto-responsive Virus-Mimetic Nanocapsules with Dual Heat-Triggered Sequential-Infected Multiple Drug-Delivery Approach for Combinatorial Tumor Therapy. *Small* 11, 2417–2428. doi:10.1002/smll.201402969
- Ferreira, D., and Martins, I. M. (2017). “Artificial Virus Particles,” in *Bioinspired Materials for Medical Applications* (Elsevier), 427–450. doi:10.1016/B978-0-08-100741-9.00015-2
- Fosgerau, K., and Hoffmann, T. (2015). Peptide Therapeutics: Current Status and Future Directions. *Drug Discov. Today* 20, 122–128. doi:10.1016/j.drudis.2014.10.003
- Frederix, P. W. J. M., Scott, G. G., Abul-Haija, Y. M., Kalafatovic, D., Pappas, C. G., Javid, N., et al. (2015). Exploring the Sequence Space for (Tri-)peptide Self-Assembly to Design and Discover New Hydrogels. *Nat. Chem.* 7, 30–37. doi:10.1038/nchem.2122
- Fujita, S., and Matsuura, K. (2017). Self-Assembled Artificial Viral Capsids Bearing Coiled-Coils at the Surface. *Org. Biomol. Chem.* 15, 5070–5077. doi:10.1039/c7ob00998d
- Gao, J., Tang, C., Elsayy, M. A., Smith, A. M., Miller, A. F., and Saiani, A. (2017). Controlling Self-Assembling Peptide Hydrogel Properties through Network Topology. *Biomacromolecules* 18, 826–834. doi:10.1021/acs.biomac.6b01693
- Gazit, E. (2007b). Self Assembly of Short Aromatic Peptides into Amyloid Fibrils and Related Nanostructures. *Prion* 1, 32–35. doi:10.4161/pri.1.1.4095
- Gazit, E. (2007a). Self-assembled Peptide Nanostructures: The Design of Molecular Building Blocks and Their Technological Utilization. *Chem. Soc. Rev.* 36, 1263–1269. doi:10.1039/b605536m
- Gelain, F., Luo, Z., Rioult, M., and Zhang, S. (2021). Self-assembling Peptide Scaffolds in the Clinic. *Npj Regen. Medmed.* 6, 1–8. doi:10.1038/s41536-020-00116-w
- Ghosh, S., Reches, M., Gazit, E., and Verma, S. (2007). Bioinspired Design of Nanocages by Self-Assembling Triskelion Peptide Elements. *Angew. Chem. Int. Ed.* 46, 2002–2004. doi:10.1002/anie.200604383
- Guilbaud, J.-B., Vey, E., Boothroyd, S., Smith, A. M., Ulijn, R. V., Saiani, A., et al. (2010). Enzymatic Catalyzed Synthesis and Triggered Gelation of Ionic Peptides. *Langmuir* 26, 11297–11303. doi:10.1021/la100623y
- Guo, C., Arnon, Z. A., Qi, R., Zhang, Q., Adler-Abramovich, L., Gazit, E., et al. (2016). Expanding the Nanoarchitectural Diversity through Aromatic Di- and Tri-peptide Coassembly: Nanostructures and Molecular Mechanisms. *ACS Nano* 10, 8316–8324. doi:10.1021/acsnano.6b02739
- Haines, A., Irvine, A., Mountain, A., Charlesworth, J., Farrow, N., Husain, R., et al. (2001). CL22 - A Novel Cationic Peptide for Efficient Transfection of Mammalian Cells. *Gene Ther.* 8, 99–110. doi:10.1038/sj.gt.3301314
- Hamley, I. W., Dehsorkhi, A., Castelletto, V., Seitonen, J., Ruokolainen, J., and Iatrou, H. (2013). Self-assembly of a Model Amphiphilic Oligopeptide Incorporating an Arginine Headgroup. *Soft Matter* 9, 4794–4801. doi:10.1039/c3sm50303h
- Hendricks, M. P., Sato, K., Palmer, L. C., and Stupp, S. I. (2017). Supramolecular Assembly of Peptide Amphiphiles. *Acc. Chem. Res.* 50, 2440–2448. doi:10.1021/acs.accounts.7b00297
- Hong, Y., Legge, R. L., Zhang, S., and Chen, P. (2003). Effect of Amino Acid Sequence and pH on Nanofiber Formation of Self-Assembling Peptides EAK16-II and EAK16-IV. *Biomacromolecules* 4, 1433–1442. doi:10.1021/bm0341374
- Kalafatovic, D., and Giral, E. (2017). Cell-penetrating Peptides: Design Strategies beyond Primary Structure and Amphipathicity. *Molecules* 22, 1929–1938. doi:10.3390/molecules22111929
- Kalafatovic, D., Nobis, M., Son, J., Anderson, K. I., and Ulijn, R. V. (2016). MMP-9 Triggered Self-Assembly of Doxorubicin Nanofiber Depots Halts Tumor Growth. *Biomaterials* 98, 192–202. doi:10.1016/j.biomaterials.2016.04.039
- Kisiday, J., Jin, M., Kurz, B., Hung, H., Semino, C., Zhang, S., et al. (2002). Self-assembling Peptide Hydrogel Fosters Chondrocyte Extracellular Matrix Production and Cell Division: Implications for Cartilage Tissue Repair. *Proc. Natl. Acad. Sci.* 99, 9996–10001. doi:10.1073/pnas.142309999
- Lampel, A. (2020). Biology-Inspired Supramolecular Peptide Systems. *Chem* 6, 1222–1236. doi:10.1016/j.chempr.2020.03.005
- Lampel, A., Ulijn, R. V., and Tuttle, T. (2018). Guiding Principles for Peptide Nanotechnology through Directed Discovery. *Chem. Soc. Rev.* 47, 3737–3758. doi:10.1039/c8cs00177d
- Lee, C., Hwang, H. S., Lee, S., Kim, B., Kim, J. O., Oh, K. T., et al. (2017). Rabies Virus-Inspired Silica-Coated Gold Nanorods as a Photothermal Therapeutic Platform for Treating Brain Tumors. *Adv. Mater.* 29, 1605563–1605568. doi:10.1002/adma.201605563
- Lee, E. S., Kim, D., Youn, Y. S., Oh, K. T., and Bae, Y. H. (2008). A Virus-Mimetic Nanogel Vehicle. *Angew. Chem. Int. Ed.* 47, 2418–2421. doi:10.1002/anie.200704121
- Lee, J., Ju, M., Cho, O. H., Kim, Y., and Nam, K. T. (2019). Tyrosine-Rich Peptides as a Platform for Assembly and Material Synthesis. *Adv. Sci.* 6, 1801255. doi:10.1002/advs.201801255
- Lehn, J.-M. (2002). Toward Self-Organization and Complex Matter. *Science* 295, 2400–2403. doi:10.1126/science.1071063
- Levin, A., Hakala, T. A., Schnaider, L., Bernardes, G. J. L., Gazit, E., and Knowles, T. P. J. (2020). Biomimetic Peptide Self-Assembly for Functional Materials. *Nat. Rev. Chem.* 4, 615–634. doi:10.1038/s41570-020-0215-y
- Li, Y., Lai, Y., Xu, X., Zhang, X., Wu, Y., Hu, C., et al. (2016). Capsid-like Supramolecular Dendritic Systems as pH-Responsive Nanocarriers for Drug Penetration and Site-specific Delivery. *Nanomedicine: Nanotechnology, Biol. Med.* 12, 355–364. doi:10.1016/j.nano.2015.09.015
- Liang, H., Hu, A., Chen, X., Jin, R., Wang, K., Ke, B., et al. (2019). Structure Optimization of Dendritic Lipopeptide Based Gene Vectors with the Assistance from Molecular Dynamic Simulation. *J. Mater. Chem. B* 7, 915–926. doi:10.1039/c8tb02650e
- Lim, Y.-b., Lee, E., Yoon, Y.-R., Lee, M. S., and Lee, M. (2008). Filamentous Artificial Virus from a Self-Assembled Discrete Nanoribbon. *Angew. Chem.* 120, 4601–4604. doi:10.1002/ange.200800266
- Liu, J., and Zhao, X. (2011). Design of Self-Assembling Peptides and Their Biomedical Applications. *Nanomedicine* 6, 1621–1643. doi:10.2217/nnm.11.142
- Ludwig, C., and Wagner, R. (2007). Virus-like Particles-Universal Molecular Toolboxes. *Curr. Opin. Biotechnol.* 18, 537–545. doi:10.1016/j.copbio.2007.10.013
- Makam, P., and Gazit, E. (2018). Minimalistic Peptide Supramolecular Co-assembly: Expanding the Conformational Space for Nanotechnology. *Chem. Soc. Rev.* 47, 3406–3420. doi:10.1039/c7cs00827a
- Mandal, D., Nasrolahi Shirazi, A., and Parang, K. (2014). Self-assembly of Peptides to Nanostructures. *Org. Biomol. Chem.* 12, 3544–3561. doi:10.1039/c4ob00447g
- Mandal, D., Tiwari, R. K., Nasrolahi Shirazi, A., Oh, D., Ye, G., Banerjee, A., et al. (2013). Self-assembled Surfactant Cyclic Peptide Nanostructures as Stabilizing Agents. *Soft Matter* 9, 9465–9475. doi:10.1039/c3sm50764e
- Mao, C., Liu, A., and Cao, B. (2009). Virus-based Chemical and Biological Sensing. *Angew. Chem. Int. Ed.* 48, 6790–6810. doi:10.1002/anie.200900231
- Marchesan, S., Easton, C. D., Kushkaki, F., Waddington, L., and Hartley, P. G. (2012). Tripeptide Self-Assembled Hydrogels: Unexpected Twists of Chirality. *Chem. Commun.* 48, 2195–2197. doi:10.1039/c2cc16609g
- Marini, D. M., Hwang, W., Lauffenburger, D. A., Zhang, S., and Kamm, R. D. (2002). Left-Handed Helical Ribbon Intermediates in the Self-Assembly of a  $\beta$ -Sheet Peptide. *Nano Lett.* 2, 295–299. doi:10.1021/nl015697g
- Maslanka Figueroa, S., Fleischmann, D., and Goepferich, A. (2021). Biomedical Nanoparticle Design: What We Can Learn from Viruses. *J. Controlled Release* 329, 552–569. doi:10.1016/j.jconrel.2020.09.045
- Matsuura, K. (2012). Construction of Spherical Virus-Inspired Peptide Nanoassemblies. *Polym. J.* 44, 469–474. doi:10.1038/pj.2012.16
- Matsuura, K., Fujino, K., Teramoto, T., Murasato, K., and Kimizuka, N. (2010a). Glutathione Nanosphere: Self-Assembly of Conformation-Regulated Trigonal-Glutathiones in Water. *Bcsj* 83, 880–886. doi:10.1246/bcsj.20100048
- Matsuura, K., Hayashi, H., Murasato, K., and Kimizuka, N. (2011). Trigonal Tryptophane Zipper as a Novel Building Block for pH-Responsive Peptide Nano-Assemblies. *Chem. Commun.* 47, 265–267. doi:10.1039/c0cc01324b
- Matsuura, K., and Honjo, T. (2019). Artificial Viral Capsid Dressed up with Human Serum Albumin. *Bioconjug. Chem.* 30, 1636–1641. doi:10.1021/acs.bioconjchem.9b00327
- Matsuura, K., Matsuyama, H., Fukuda, T., Teramoto, T., Watanabe, K., Murasato, K., et al. (2009). Spontaneous Self-Assembly of Nanospheres from Trigonal Conjugate of Glutathione in Water. *Soft Matter* 5, 2463–2470. doi:10.1039/b819472f



- Matsuura, K., Mizuguchi, Y., and Kimizuka, N. (2016). Peptide Nanospheres Self-Assembled from a Modified  $\beta$ -annulus Peptide of Sesbania Mosaic Virus. *Biopolymers* 106, 470–475. doi:10.1002/bip.22774
- Matsuura, K., Murasato, K., and Kimizuka, N. (2005). Artificial Peptide-Nanospheres Self-Assembled from Three-Way Junctions of  $\beta$ -Sheet-Forming Peptides. *J. Am. Chem. Soc.* 127, 10148–10149. doi:10.1021/ja052644i
- Matsuura, K. (2018). Synthetic Approaches to Construct Viral Capsid-like Spherical Nanomaterials. *Chem. Commun.* 54, 8944–8959. doi:10.1039/C8CC03844A
- Matsuura, K., Ueno, G., and Fujita, S. (2015). Self-assembled Artificial Viral Capsid Decorated with Gold Nanoparticles. *Polym. J.* 47, 146–151. doi:10.1038/pj.2014.99
- Matsuura, K., Watanabe, K., Matsuzaki, T., Sakurai, K., and Kimizuka, N. (2010b). Self-Assembled Synthetic Viral Capsids from a 24-mer Viral Peptide Fragment. *Angew. Chem. Int. Ed.* 49, 9662–9665. doi:10.1002/anie.201004606
- Miyata, K., Nishiyama, N., and Kataoka, K. (2012). Rational Design of Smart Supramolecular Assemblies for Gene Delivery: Chemical Challenges in the Creation of Artificial Viruses. *Chem. Soc. Rev.* 41, 2562–2574. doi:10.1039/c1cs15258k
- Mohsen, M. O., Speiser, D. E., Knuth, A., and Bachmann, M. F. (2020). Virus-like Particles for Vaccination against Cancer. *WIREs Nanomed Nanobiotechnol.* 12, 1–17. doi:10.1002/wnan.1579
- Murasato, K., Matsuura, K., and Kimizuka, N. (2008). Self-Assembly of Nanofiber with Uniform Width from Wheel-type Trigonal- $\beta$ -Sheet-Forming Peptide. *Biomacromolecules* 9, 913–918. doi:10.1021/bm701302p
- Ni, R., and Chau, Y. (2014). Structural Mimics of Viruses through Peptide/DNA Co-assembly. *J. Am. Chem. Soc.* 136, 17902–17905. doi:10.1021/ja507833x
- Ni, R., and Chau, Y. (2017). Tuning the Inter-nanofibril Interaction to Regulate the Morphology and Function of Peptide/DNA Co-assembled Viral Mimics. *Angew. Chem.* 129, 9484–9488. doi:10.1002/ange.201703596
- Noble, J. E., De Santis, E., Ravi, J., Lamarre, B., Castelletto, V., Mantell, J., et al. (2016). A De Novo Virus-like Topology for Synthetic Virions. *J. Am. Chem. Soc.* 138, 12202–12210. doi:10.1021/jacs.6b05751
- Pelin, J. N. B. D., Gerbelli, B. B., Edwards-Gayle, C. J. C., Aguilar, A. M., Castelletto, V., Hamley, I. W., et al. (2020). Amyloid Peptide Mixtures: Self-Assembly, Hydrogelation, Nematic Ordering, and Catalysts in Aldol Reactions. *Langmuir* 36, 2767–2774. doi:10.1021/acs.langmuir.0c00198
- Qiao, C., Zhang, R., Wang, Y., Jia, Q., Wang, X., Yang, Z., et al. (2020). Rabies Virus-Inspired Metal-Organic Frameworks (MOFs) for Targeted Imaging and Chemotherapy of Glioma. *Angew. Chem. Int. Ed.* 59, 16982–16988. doi:10.1002/anie.202007474
- Reches, M., and Gazit, E. (2004). Formation of Closed-Cage Nanostructures by Self-Assembly of Aromatic Dipeptides. *Nano Lett.* 4, 581–585. doi:10.1021/nl035159z
- Roldão, A., Silva, A. C., Mellado, M. C. M., Alves, P. M., and Carrondo, M. J. T. (2017). Viruses and Virus-like Particles in Biotechnology: Fundamentals and Applications. *Compr. Biotechnol.*, 633–656. doi:10.1016/B978-0-12-809633-8.09046-4
- Saleh, A. F., Aojula, H., Arthanari, Y., Offerman, S., Alkotaji, M., and Pluen, A. (2010). Improved Tat-Mediated Plasmid DNA Transfer by Fusion to LK15 Peptide. *J. Controlled Release*. 143, 233–242. doi:10.1016/j.jconrel.2009.12.025
- Sasselli, I. R., Moreira, I. P., Ulijn, R. V., and Tuttle, T. (2017). Molecular Dynamics Simulations Reveal Disruptive Self-Assembly in Dynamic Peptide Libraries. *Org. Biomol. Chem.* 15, 6541–6547. doi:10.1039/c7ob01268c
- Sharma, P., Pal, V. K., and Roy, S. (2021). An Overview of Latest Advances in Exploring Bioactive Peptide Hydrogels for Neural Tissue Engineering. *Biomater. Sci.* 9, 3911–3938. doi:10.1039/D0BM02049D
- Sieste, S., Mack, T., Lump, E., Hayn, M., Schütz, D., Röcker, A., et al. (2021). Supramolecular Peptide Nanofibrils with Optimized Sequences and Molecular Structures for Efficient Retroviral Transduction. *Adv. Funct. Mater.* 31, 2009382. doi:10.1002/adfm.202009382
- Singh, N., Kumar, M., Miravet, J. F., Ulijn, R. V., and Escuder, B. (2017). Peptide-Based Molecular Hydrogels as Supramolecular Protein Mimics. *Chem. Eur. J.* 23, 981–993. doi:10.1002/chem.201602624
- Sloan-Dennison, S., Lampel, A., Raßlenberg, E., Ulijn, R. V., Smith, E., Faulds, K., et al. (2021). Elucidation of the Structure of Supramolecular Polymorphs in Peptide Nanofibres Using Raman Spectroscopy. *J. Raman Spectrosc.* 1–7. doi:10.1002/jrs.6121
- Slocik, J. M., and Naik, R. R. (2017). Sequenced Defined Biomolecules for Nanomaterial Synthesis, Functionalization, and Assembly. *Curr. Opin. Biotechnol.* 46, 7–13. doi:10.1016/j.copbio.2016.11.025
- Smith, D. J., Brat, G. A., Medina, S. H., Tong, D., Huang, Y., Grahmmer, J., et al. (2015). A Multiphase Transitioning Peptide Hydrogel for Suturing Ultrasmall Vessels. *Nat. Nanotech.* 11, 95–102. doi:10.1038/nnano.2015.238
- Son, J., Kalafatovic, D., Kumar, M., Yoo, B., Cornejo, M. A., Contel, M., et al. (2019). Customizing Morphology, Size, and Response Kinetics of Matrix Metalloproteinase-Responsive Nanostructures by Systematic Peptide Design. *ACS Nano*. 13, 1555–1562. doi:10.1021/acsnano.8b07401
- Tamamis, P., Adler-Abramovich, L., Reches, M., Marshall, K., Sikorski, P., Serpell, L., et al. (2009). Self-assembly of Phenylalanine Oligopeptides: Insights from Experiments and Simulations. *Biophysical J.* 96, 5020–5029. doi:10.1016/j.bpj.2009.03.026
- Tao, K., Makam, P., Aizen, R., and Gazit, E. (2017). Self-assembling Peptide Semiconductors. *Science* 358, eaam9756. doi:10.1126/science.aam9756
- van Hell, A. J., Costa, C. I. C. A., Flesch, F. M., Sutter, M., Jiskoot, W., Crommelin, D. J. A., et al. (2007). Self-Assembly of Recombinant Amphiphilic Oligopeptides into Vesicles. *Biomacromolecules* 8, 2753–2761. doi:10.1021/bm0704267
- Vauthey, S., Santoso, S., Gong, H., Watson, N., and Zhang, S. (2002). Molecular Self-Assembly of Surfactant-like Peptides to Form Nanotubes and Nanovesicles. *Proc. Natl. Acad. Sci.* 99, 5355–5360. doi:10.1073/pnas.072089599
- Vlieghe, P., Lisowski, V., Martinez, J., and Khrestchatsky, M. (2010). Synthetic Therapeutic Peptides: Science and Market. *Drug Discov. Today*. 15, 40–56. doi:10.1016/j.drudis.2009.10.009
- Wang, J., Han, S., Meng, G., Xu, H., Xia, D., Zhao, X., et al. (2009). Dynamic Self-Assembly of Surfactant-like Peptides A6K and A9K. *Soft Matter*. 5, 3870–3878. doi:10.1039/b901653h
- Wang, Y., Nie, Y., Ding, Z., Yao, M., Du, R., Zhang, L., et al. (2020). An Amphiphilic Peptide with Cell Penetrating Sequence for Highly Efficient Gene Transfection. *Colloids Surf. A: Physicochemical Eng. Aspects*. 590, 124529. doi:10.1016/j.colsurfa.2020.124529
- Whitesides, G. M. (2015). Bioinspiration: Something for Everyone. *Interf. Focus*. 5, 20150031. doi:10.1098/rsfs.2015.0031
- Whitesides, G. M., and Grzybowski, B. (2002). Self-assembly at All Scales. *Science* 295, 2418–2421. doi:10.1126/science.1070821
- Wolfson, D. N., and Mahmoud, Z. N. (2010). More Than Just Bare Scaffolds: Towards Multi-Component and Decorated Fibrous Biomaterials. *Chem. Soc. Rev.* 39, 3464–3479. doi:10.1039/c0cs00032a
- Xu, H., Wang, Y., Ge, X., Han, S., Wang, S., Zhou, P., et al. (2010). Twisted Nanotubes Formed from Ultrashort Amphiphilic Peptide I3K and Their Templating for the Fabrication of Silica Nanotubes. *Chem. Mater.* 22, 5165–5173. doi:10.1021/cm101019p
- Xu, X., Yuan, H., Chang, J., He, B., and Gu, Z. (2012). Cooperative Hierarchical Self-Assembly of Peptide Dendrimers and Linear Polypeptides into Nanoarchitectures Mimicking Viral Capsids. *Angew. Chem. Int. Ed.* 51, 3130–3133. doi:10.1002/anie.201106080
- Yang, J., Zhang, X., Liu, C., Wang, Z., Deng, L., Feng, C., et al. (2021a). Biologically Modified Nanoparticles as Theranostic Bionanomaterials. *Prog. Mater. Sci.* 118, 100768. doi:10.1016/j.pmatsci.2020.100768
- Yang, P., Li, Y.-J., Cao, Y., Zhang, L., Wang, J.-Q., Lai, Z.-W., et al. (2020b). Rapid Discovery of Self-Assembling Peptides with One-Bead One-Compound Peptide Libraries. *Res. Sq.* 1–15. doi:10.21203/rs.3.rs-109949/v1
- Yokoi, H., Kinoshita, T., and Zhang, S. (2005). Dynamic Reassembly of Peptide RADA16 Nanofiber Scaffold. *Proc. Natl. Acad. Sci.* 102, 8414–8419. doi:10.1073/pnas.0407843102
- Yoon, Y.-R., Lim, Y.-b., Lee, E., and Lee, M. (2008). Self-assembly of a Peptide Rod-Coil: A Polyproline Rod and a Cell-Penetrating Peptide Tat Coil. *Chem. Commun.*, 1892–1894. doi:10.1039/b719868j
- Zhang, S. (2017). Discovery and Design of Self-Assembling Peptides. *Interf. Focus*. 7, 20170028. doi:10.1098/rsfs.2017.0028
- Zhang, S. (2003). Fabrication of Novel Biomaterials through Molecular Self-Assembly. *Nat. Biotechnol.* 21, 1171–1178. doi:10.1038/nbt874

- Zhang, S., Holmes, T., Lockshin, C., and Rich, A. (1993). Spontaneous Assembly of a Self-Complementary Oligopeptide to Form a Stable Macroscopic Membrane. *Proc. Natl. Acad. Sci.* 90, 3334–3338. doi:10.1073/pnas.90.8.3334
- Zhao, X. (2009). Design of Self-Assembling Surfactant-like Peptides and Their Applications. *Curr. Opin. Colloid Interf. Sci.* 14, 340–348. doi:10.1016/j.cocis.2009.07.002
- Zhao, X., Pan, F., and Lu, J. R. (2008). Recent Development of Peptide Self-Assembly. *Prog. Nat. Sci.* 18, 653–660. doi:10.1016/j.pnsc.2008.01.012

**Conflict of Interest:** The authors declare that the research was conducted in the absence of any commercial or financial relationships that could be construed as a potential conflict of interest.

**Publisher's Note:** All claims expressed in this article are solely those of the authors and do not necessarily represent those of their affiliated organizations, or those of the publisher, the editors and the reviewers. Any product that may be evaluated in this article, or claim that may be made by its manufacturer, is not guaranteed or endorsed by the publisher.

Copyright © 2021 Janković, Šantek, Pina and Kalafatovic. This is an open-access article distributed under the terms of the Creative Commons Attribution License (CC BY). The use, distribution or reproduction in other forums is permitted, provided the original author(s) and the copyright owner(s) are credited and that the original publication in this journal is cited, in accordance with accepted academic practice. No use, distribution or reproduction is permitted which does not comply with these terms.



# Spiropyran-Based Drug Delivery Systems

Andrew Fagan, Michał Bartkowski and Silvia Giordani\*

School of Chemical Sciences, Dublin City University (DCU), Dublin, Ireland

Nanocarriers are rapidly growing in popularity in the field of drug delivery. The ability of nanocarriers to encapsulate and distribute poorly soluble drugs while minimising their undesired effects is significantly advantageous over traditional drug delivery. Nanocarriers can also be decorated with imaging moieties and targeting agents, further incrementing their functionality. Of recent interest as potential nanocarriers are spiropyrans; a family of photochromic molecular switches. Due to their multi-responsiveness to endo- and exogenous stimuli, and their intrinsic biocompatibility, they have been utilised in various drug delivery systems (DDSs) to date. In this review, we provide an overview of the developments in spiropyran-based DDSs. The benefits and drawbacks of utilising spiropyrans in drug delivery are assessed and an outline of spiropyran-based drug delivery systems is presented.

**Keywords:** spiropyran, merocyanine, nanocarrier, drug delivery, smart release, nanomedicine, molecular switch

## OPEN ACCESS

### Edited by:

Jennifer Hiscock,  
University of Kent, United Kingdom

### Reviewed by:

Robert Elmes,  
Maynooth University, Ireland  
Ali Reza Mahdavian,  
Iran Polymer and Petrochemical  
Institute, Iran

### \*Correspondence:

Silvia Giordani  
silvia.giordani@dcu.ie

### Specialty section:

This article was submitted to  
Supramolecular Chemistry,  
a section of the journal  
Frontiers in Chemistry

**Received:** 03 June 2021

**Accepted:** 19 July 2021

**Published:** 29 July 2021

### Citation:

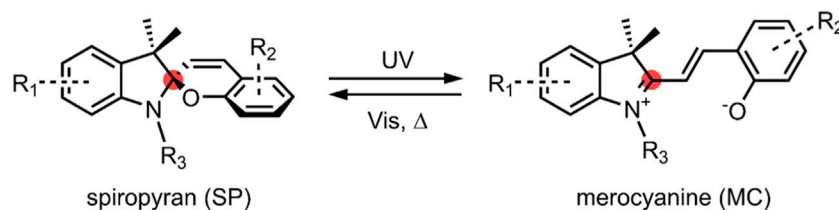
Fagan A, Bartkowski M and Giordani S  
(2021) Spiropyran-Based Drug  
Delivery Systems.  
Front. Chem. 9:720087.  
doi: 10.3389/fchem.2021.720087

## INTRODUCTION

### Nano-Based Drug Delivery Systems

At present, many significant challenges are facing the pharmaceutical industry. Most importantly, around 40% of all drugs on the market and 60% of all new chemical entities exhibit low aqueous solubility due to the increasing size, complexity, and lipophilicity of drug molecules. Associated with this is low *in vivo* stability and toxic side effects (Fahr and Liu, 2007; Wen et al., 2015). In recent years, advances in pharmaceuticals and materials science have allowed nanomaterials to be successfully studied for their use as drug delivery systems (DDS) (Mura et al., 2013). Nanomaterials exhibit unique chemical, physical and biological properties (Krishna et al., 2018). Of particular interest is their ability to encapsulate and solubilise poorly soluble therapeutics, and release them in a controlled, target-specific manner. These drug nanocarriers exhibit prolonged retention time in the blood, improved drug efficiency and reduced side effects by limiting systemic exposure (Martinho et al., 2011). There are various organic, inorganic and metallic nanostructures used in nano-based DDSs, such as polymeric micelles, liposomes, dendrimers, and mesoporous silica nanoparticles (Deng et al., 2020).

The size of nanocarriers (1–100 nm) enables them to move more freely around the body and enhance the bioavailability of drugs due to the enhanced permeation and retention (EPR) effect (Kang et al., 2019). The EPR effect allows for the passive targeting of cells with leaky surrounding vasculatures, such as tumour cells. The functionalisation of nanocarriers' surfaces with targeting agents allows for active targeting of specific receptor sites on target cells, thus improving the efficacy and reducing the toxic side effects of drugs (Patra et al., 2018). As a result, nanocarriers have been extensively studied for their ability to deliver anti-cancer therapeutics to specific tumour sites, such as DNA delivery vectors, and for their ability to cross the blood-brain barrier (Patra et al., 2018).



**FIGURE 1 |** General schematic of an SP ↔ MC reversible isomerisation. The spiro-carbon is highlighted red. In the SP form, the indoline moiety on the left of the spiro-carbon is orthogonal to the benzopyran (chromene)—the MC form is planar. A strongly electron-withdrawing nitro group is typically present at the R<sub>2</sub> position.

Active targeting, however, often falls short of the desired effect. Thus, to further improve the targeted and controlled release properties of nanocarriers, novel smart platforms have been developed to respond to a range of exogenous and endogenous stimuli, such as light, pH and temperature (Mura et al., 2013). This ability to control the release of drugs from nanocarriers in a time and site-specific manner offers the advantage of maximising drug efficacy while minimising side effects. Nanocarriers may be developed to respond to endogenous stimuli associated with a particular disorder, for example, the lower extracellular pH environment in tumour cells, or the significant increase in Zn<sup>2+</sup> ions in apoptotic cells (Vaupel et al., 1989; Franklin and Costello, 2009). An alternative method of inducing drug release is through exogenous stimuli, such as light, magnetic fields and ultrasound. Light as a stimulus offers many advantages—it can be controlled in space and time, limiting drug release to a specific target, and the intensity and wavelength of irradiation can be precisely tuned. Light is already in use clinically for photodynamic therapy, which is used to treat cancer and vascular issues associated with angiogenesis (Moore et al., 2009). However, the wavelengths required to induce drug release, typically ultraviolet (UV) and visible (Vis) light, have poor penetration in bodily tissues, and prolonged UV-irradiation has been shown to have mutagenic effects, limiting its biomedical applications (McMillan et al., 2008; Rwei et al., 2015). These problems may be overcome using lower energy near infra-red (NIR) light, which has much greater tissue penetrating ability (Lim and Park, 2017).

Smart nanocarriers that have been developed are typically hybrid materials, such as polymers or nanoparticles, which are functionalised with a responsive material that can undergo a spatial conformational change on application of a specific stimulus (Mohapatra et al., 2019). One such class of responsive materials are spiropyrans. Spiropyrans can undergo a reversible conformational change between a closed, hydrophobic spiropyran form and an open, hydrophilic merocyanine form. This can be induced by various stimuli, such as light, pH, heat and the presence of metal ions. This unique ability to switch between two distinct, stable states on the application of a stimulus has led to their incorporation into a variety of dynamic materials (Klajn, 2014).

## The Chemistry of Spiropyrans

Spiropyrans are a class of organic molecules that are structurally related by the presence of a benzopyran (chromene) moiety

linked to another heterocyclic moiety, commonly an indoline, via an sp<sup>3</sup> carbon called spiro-carbon (Figure 1). The sp<sup>3</sup> hybridisation of the spiro-carbon orientates the two heterocycles orthogonal to one another (Berkovic et al., 2000). This can be seen from the several available spiropyran crystal structures, and an excellent analysis of the crystal structures of three spiropyrans in the solid state, including a rare example of an open merocyanine form (Aakeröy et al., 2010).

Spiropyrans (SP) were first reported by Fischer and Hirschberg in the 1950's, and extensively studied in the 1960's for their photochromic behaviour (Hirschberg and Fischer, 1954a, 1954b; Heiligman-Rim et al., 1961, 1962a, 1962b). The colourless SPs become photoexcited and undergo a ring-opening upon irradiation with UV light ranging between 200–400 nm. The ring-opened intermediate that forms quickly undergoes a *cis-trans* isomerisation of the benzopyran double bond to give a stable, highly coloured open form called merocyanine (MC). The resulting MC molecule exhibits a unique absorption spectrum to the original SP molecule. This process is reversible, with the MC isomer reverting back to the more stable SP isomer under thermal conditions or by irradiation with visible light. The conversion between the SP and the MC form is not exclusively a light-responsive process. SPs exhibit acidochromism, thermochromism and solvatochromism. The MC form can also be stabilised by complexation with metal cations (Koelsch, 1951; Minkin, 2004; Kortekaas and Browne, 2019).

SP and MC are physically and chemically distinct. The SP form is neutral and non-polar. Given that the two heterocyclic moieties in the SP form are mutually perpendicular,  $\pi$ -electrons cannot move between them. As such, there is no delocalisation of  $\pi$ -electrons between the two halves of the molecule, and the molecule is not electronically conductive. As previously discussed, spiropyrans absorb in the UV region between 200–400 nm, and the absorbance spectrum is believed to be a composite of the spectra of the individual constituent moieties (Tyler and Becker, 1970). Spiropyrans are thus colourless (Eilmes, 2013; Wang and Li, 2018).

In contrast to this, upon C-O bond cleavage to the open MC form (Figure 1), a zwitterion is formed containing a phenolate anion and a positively charged indolium. The charged MCs have a much larger dipole moment (~14–18 D) than the non-polar SP form (~4–6 D) (Klajn, 2014). Also notable is that the spiro-carbon is sp<sup>2</sup> hybridised in the ring-open form, and the indoline and benzopyran moieties are co-planar. As a result of this, there is a conjugation of the  $\pi$ -electrons of the two heterocyclic moieties.



The conjugation present in the MC form leads to a significant redshift of the absorption spectrum compared to the SP spectrum, with the MC form absorbing in the visible region; MC is, therefore, intensely coloured (Pimienta et al., 1996; Kajimoto et al., 2010; Wang and Li, 2018). The MC form may be converted back to the SP form on irradiation with visible light, around 500–600 nm (Vlassioug et al., 2006).

As a result of the differences between the SP and MC forms, and the ability to switch between them repeatedly by application of an external stimulus, SP molecules have received widespread attention for their use in many various dynamic systems, including SP-functionalised polymers, biopolymers, inorganic nanoparticles, carbon nanomaterials and solid surfaces—many of which have potential biological applications (Klajn, 2014; Cardano et al., 2019); notably, in cell tracking and labelling (Keyvan Rad et al., 2015; Keyvan Rad et al., 2016; Cong et al., 2021), photothermal therapy (Keyvan Rad et al., 2018) and cell sheet engineering (Karimipour et al., 2021). These applications, however, may be restricted by the well-known tendency of the MC isomer to undergo hydrolytic decomposition in aqueous solution, resulting in the formation of salicylaldehyde and a Fischer's base derivative (Stafforst and Hilvert, 2008; Hammarson et al., 2013). This may limit the long term reversibility of SP-based molecular switches in aqueous solution. The decomposition reaction mechanism is thought to occur firstly *via* a nucleophilic attack by water on the eniminium MC form, followed by a retro-aldol reaction to give the decomposition products. Therefore, it has been proposed that the introduction of electron-donating groups, such as OMe, to the benzopyran moiety will greatly improve the hydrolytic stability of the MC form by increasing the electron density around the carbon-carbon double bond and reducing its susceptibility to nucleophilic attack (Abeyrathna and Liao, 2016; Berton et al., 2020). Additionally, the long-term reversibility of SP-based molecular switches is also limited by photofatigue (reduction in the efficiency of the switching process with repeat cycles). However, immobilisation of SPs to a support, such as a polymer, *via* covalent attachment at the nitrogen of the indoline moiety has been found to increase resistance to photofatigue by suppressing photodegradation pathways (Radu et al., 2009). Thus, careful tuning of the spiropyran structure and the overall system offers a successful route for overcoming these limitations.

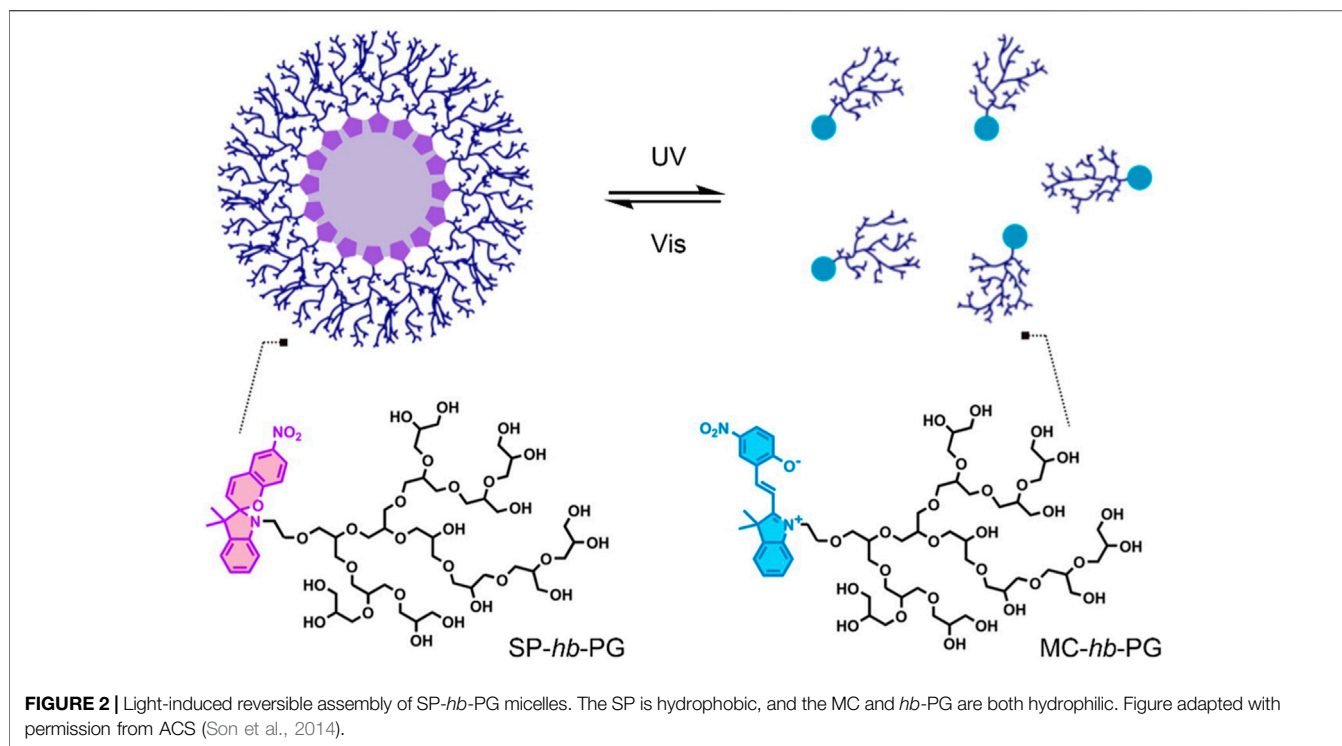
Our group has previously shown the safety of SPs for use in biological applications; in particular, bionanosensing, where the cytotoxicity of SPs in macrophage, gastric, and epithelial cells was studied. The SPs showed negligible toxic effects on the cells up to millimolar concentrations, while significant cytotoxicity was observed only at concentrations of  $10^{-3}$  M and above after exposure for 24 h, and at  $10^{-4}$  M for prolonged exposure times. The time and dose dependence of cytotoxicity was also found to be statistically significant using High Content Screening and Analysis (HCSA), validated by enzyme-linked immunosorbent assays (ELISA) (Movia et al., 2010). Of recent interest is the use of SPs in nano-based drug delivery systems—several reported spiropyran-based nanocarriers are herein reviewed.

## SPIROPYRAN-BASED NANOCARRIERS FOR DRUG DELIVERY

### Polymeric Micelles

Polymeric micelles are composed of amphiphilic block copolymers, which have distinct hydrophobic and hydrophilic domains (Zhang et al., 2014). In aqueous solutions, these amphiphilic polymers self-assemble to form micelles consisting of a hydrophobic core and a hydrophilic outer corona, with sizes ranging from 10–100 nm (Jhaveri and Torchilin, 2014). Self-assembled polymeric micelles have been studied extensively for their use in DDSs due to the enhanced solubility and circulation lifetime of the encapsulated drug, the tunability of their physicochemical properties by changing the functionalities present along the polymer backbone, and, most importantly, the EPR effect in tumours as a result of their size (Ahmad et al., 2014). The latter advantage makes them very appealing for anti-cancer drug delivery. Polymeric micelles also show promise for their use in light-controlled DDSs. Spiropyran-based micelles in which the non-polar SP form is present in the hydrophobic core surrounded by a hydrophilic shell have been recently developed. The SP form undergoes a ring-opening to form the polar MC isomer on irradiation with a specific wavelength of light. This leads to a disassembly/change in morphology of the micelle with a subsequent release of the encapsulated drug (Lee et al., 2007). This process is entirely reversible. The polymers used must be biodegradable and biocompatible. Poly (ethylene glycol) (PEG) is a commonly used hydrophilic polymer, whereas polyesters, such as poly (lactic acid), are typically used as hydrophobic polymers to make up the block copolymer backbone (Zhang et al., 2014). The light-induced isomerisation of spiropyran makes these polymeric micelles ideal for controlled release formulations, where light offers spatiotemporal control of drug release by irradiating specific sites in the body, such as tumour cells. These systems may also be used to enhance the aqueous solubility of poorly soluble drugs, which are becoming increasingly problematic in the pharmaceutical industry (Khan et al., 2010).

In 2014, Son et al. investigated the potential of amphiphilic spiropyran-initiated hyperbranched polyglycerols (SP-*hb*-PG) for light-controlled release of therapeutic agents (Figure 2) (Son et al., 2014). In solution, the amphiphilic SP-*hb*-PG chains self-assembled into micelles with an average diameter of approximately 33 nm. However, upon irradiation with UV light at 365 nm for 30 min, it was found that the diameter decreased significantly (to about 0.1 nm), suggesting the complete disassembly of the micelle into individual polymer chains. A new absorption band in the UV-Vis spectra at 550 nm, and the solutions' colour change (from colourless to light pink), suggested that the micellar disassembly was caused by the photo-induced conversion of the amphiphilic SP-*hb*-PG to the hydrophilic MC-*hb*-PG. Upon irradiation with visible light at 620 nm for 30 min, the measured diameter returned to an average of 30 nm. This indicated the MC-*hb*-PG → SP-*hb*-PG reversion with subsequent micellar reformation, as confirmed by the

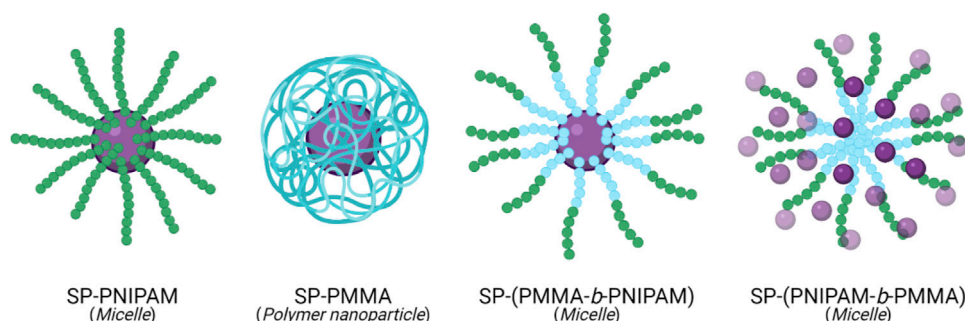


disappearance of the absorption band at 550 nm in the UV-Vis spectra. The potential of this system as a nanocarrier was evaluated, using pyrene as a model hydrophobic molecule. Successful loading of pyrene into the micelle nanocarriers was achieved. The fluorescent spectrum of pyrene was observed upon irradiation with UV light at 254 nm. A decrease in fluorescence intensity with irradiation time suggested the release of pyrene from the micelles. The intensity increased again upon irradiation with visible light to about 40% of the initial intensity, suggesting partial reloading of the pyrene into the reformed micelles. *In vitro* cytotoxicity was investigated using HeLa and WI-38 cells. SP-*hb*-PG was found to be non-toxic and showed excellent biocompatibility with both cell lines (Son et al., 2014).

A similar investigation was performed using a smart DDS composed of a light-responsive amphiphilic block copolymer spiropyran-poly (2-methacryloyloxyethyl phosphorylcholine) (SP-PMPC) (Shen et al., 2015). This amphiphilic SP-PMPC system, similarly to the aforementioned SP-*hb*-PG DDS (Son et al., 2014), took advantage of the hydrophobic-hydrophilic balance in micelles. Micellar disassembly occurred upon UV-irradiation (365 nm) due to SP-PMPC  $\rightarrow$  MC-PMPC isomerisation. Reassembly was observed upon visible light irradiation (620 nm), as the MC form was converted back to the SP form. Drug loading and release were also studied, using doxorubicin (DOX) as a model therapeutic. The release of DOX from the SP-PMPC micellar nanocarrier was found to increase significantly on UV-irradiation—approx. 50% of DOX was released after 24 h, whilst less than 20% was found to release in the absence of UV-irradiation after 24 h. The photo-induced on/off switching of drug release from this DDS was confirmed using the fluorescent molecule coumarin-102. Furthermore,

SP-PMPC micelles were found to have no *in vitro* cytotoxic effects on huvec and HeLa cell lines, with and without UV-irradiation. Whereas the DOX loaded SP-PMPC micelles showed cytotoxicity with and without UV-irradiation. The DOX loaded micelles were also observed to have better cytotoxicity when irradiated with UV light compared to those not exposed to UV light—thus showing that the anti-cancer activity was predominantly a result of DOX release from the SP-PMPC micellar nanocarriers (Shen et al., 2015).

In 2017, Aibani et al. investigated a novel light-responsive DDS, which showed both controlled release of the loaded therapeutic agent and simultaneous real-time analysis of the quantity of therapeutic remaining in the micellar nanocarrier (Aibani et al., 2017). The micellar drug carrier was composed of an amphiphilic copolymer, which consisted of a hydrophilic PEG monomer and a hydrophobic C10 decyl chain monomer, both containing a methacrylate functional group; this amphiphilic copolymer was previously shown to be biocompatible (Yildiz et al., 2011). An SP-ibuprofen (SP-IBU) analogue was prepared and incorporated into the micelles' hydrophobic core, along with a BODIPY dye. Upon irradiation with UV light, SP-IBU  $\rightarrow$  MC-IBU isomerisation occurred, leading to the MC-IBU prodrug release from the micelle. It is believed that upon prodrug release *in situ*, the MC-IBU would undergo hydrolysis by an esterase enzyme, thus releasing the active IBU drug. The absorbance spectrum of the MC-IBU form overlaps with the emission spectrum of the BODIPY dye in the hydrophobic core, which enabled Förster Resonance Energy Transfer (FRET) to occur. FRET is a mechanism by which one donor chromophore transfers energy to another acceptor chromophore *via* dipole-dipole coupling (Helms, 2019). FRET is a distance-dependent



**FIGURE 3** | Self-assembly of SP (purple) chain end-group polymers, PNIPAM (green) and PMMA (blue), and their respective copolymers, into polymeric particles and micelles (Razavi et al., 2020).

phenomenon; the further the two chromophores are from one another, the weaker the energy transfer. In this investigation, the SP-IBU (acceptor) and BODIPY dye (donor) act as a FRET pair. When the micelles were irradiated with UV light, an SP-IBU  $\rightarrow$  MC-IBU isomerisation occurred, and MC-IBU quenched the BODIPY dye's fluorescence in the hydrophobic core due to its overlapping emission signature to that of the BODIPY. The quenching of the BODIPY dye's emission decreased when MC-IBU was released from the core, or converted back to SP-IBU in heat and visible light conditions. This FRET communication allowed for temporal analysis of the quantity of prodrug remaining in the micelles' core after irradiation with UV light. The system was also investigated in HeLa cells for its *in vitro* triggered encapsulated cargo release. It was shown that after 12 min, a 24 and 5% release was achieved, with and without UV-irradiation, respectively. Overall, this system shows promise for its ability to incorporate various hydrophobic APIs, thus offering a route for solubilising them. Also, drug release can be monitored by taking advantage of FRET communication between two different chromophores in the micelles' hydrophobic core (Aibani et al., 2017).

An amphiphilic block copolymer composed of a temperature-responsive poly (*N*-isopropylacrylamide) (PNIPAM) block, and a hydrophobic poly (methyl methacrylate) (PMMA) block, with light-responsive SP chain end-groups, was investigated by Razavi et al. for its use as a dual stimuli-responsive DOX DDS (Razavi et al., 2020). Self-assembly of the block copolymer was investigated, varying the arrangement of the PNIPAM and PMMA. The particle size was found to be affected by the proximity of the SP molecule to the PNIPAM block. The composition of the micelles also varied depending on the block neighbouring the SP molecule. Micelles formed from the SP-(PMMA-*b*-PNIPAM) copolymer had a hydrophobic core containing the PMMA block and the SP molecules, and a hydrophilic corona composed of the PNIPAM block. In contrast, in micelles formed from the SP-(PNIPAM-*b*-PMMA) copolymer, the SP molecules were distributed throughout the hydrophilic corona (**Figure 3**). Drug release in this system resulted from the light and temperature-induced shrinkage of the micellar nanocarriers. In all self-assemblies, the SP chain end-groups underwent SP  $\rightarrow$  MC isomerisation upon UV-irradiation

(365 nm), resulting in a migration of the polar MC molecules to the micelles' surface—subsequently resulting in a large decrease in particle size, inducing DOX release. This process was entirely reversible on irradiation with visible light. The SP  $\leftrightarrow$  MC isomerisation was significantly affected by the neighbouring block's polarity, with the polar PNIPAM block stabilising the polar MC form. PNIPAM has a low critical solution temperature (LCST) range of 31–33°C. Heating the PNIPAM-based self-assemblies above the LCST (to 45°C) resulted in a significant decrease in particle size. The LCST showed light-dependence; upon UV-irradiation, the LCST increased to 37°C (close to body temperature) due to the polar MC form's presence. This increase in the PNIPAM's LCST is significant from a controlled-release perspective as the micelles' temperature responsivity can be light-controlled. Moreover, the multi-responsive nature of DOX-loaded SP-PNIPAM, SP-(PMMA-*b*-PNIPAM) and SP-(PNIPAM-*b*-PMMA) micelles was investigated *in vitro*, where the release profiles were examined at pH 5.3 (25°C) and 7.4 (25°C and 40°C), and under UV irradiation at 365 nm (pH 7.4). Minimal drug release (<30%) was observed at pH 7.4 for all micellar assemblies after 48 h, whereas a significant increase in drug release was recorded in acidic media, at temperatures above the PNIPAM's LCST (40°C), and also when irradiated with UV light. These results indicate the potential use of the micellar nanocarriers as smart DDSs, with highly efficient pH, temperature and UV light-controlled drug release. However, further investigations must be carried out to determine the ideal backbone composition for controlled release (Razavi et al., 2020).

## Polymeric Nanoparticles

In a similar fashion to micelles, amphiphilic block copolymers may self-assemble in aqueous solutions to form solid nanoparticles. The structure formed on self-assembly is dependent on the fraction of the copolymer that is hydrophilic. Polymeric nanoparticles can be classified based on their structure into nanospheres and nanocapsules. Nanospheres consist of a continuous polymeric matrix, in which a drug can be encapsulated by surface adsorption or dispersion throughout the inner matrix. Nanocapsules have a vesicular structure, composed of a hydrophobic oily core, into which hydrophobic drugs are

typically dissolved, surrounded by a polymeric outer shell. As with micelles, polymeric nanoparticles have received attention as drug delivery vectors due to their favourable properties. Their small size allows for improved intracellular uptake, particularly in tumour cells due to the EPR effect. Additionally, the ability of polymeric nanoparticles to solubilise hydrophobic drugs enhances the stability, bioavailability and circulation time of the therapeutics (Begines et al., 2020; Zielińska et al., 2020). Notwithstanding the benefits of polymeric nanoparticles, one challenge associated with this nanomaterial is controlled drug release. To overcome this challenge, polymeric nanoparticles have been functionalised with SPs to develop a DDS that can deliver therapeutic agents in a controlled and site-specific manner.

In 2019, Wang et al. reported a novel pH and light-responsive polymeric nanoparticle exhibiting both dual-colour fluorescence and excellent controlled release properties (Wang et al., 2019). The nanoparticle was composed of a methyl ether poly (ethylene glycol)-poly ( $\beta$ -amino esters) (MPEG-PAE) copolymer, with fluorescent naphthalimide (NAPH) and photochromic SP moieties introduced along the polymer backbone *via* quaternisation. In an aqueous solution, the functionalised copolymer self-assembled to form nanoparticles with an average diameter of 40–80 nm, with the PAE, SP and NAPH composing the hydrophobic core and the MPEG forming the hydrophilic shell. On irradiation with UV light at 365 nm, there was an observable swelling and aggregation of the nanoparticles, attributed to the photo-induced conversion of the hydrophobic SP form to the hydrophilic MC form causing a disruption of the hydrophobic-hydrophilic balance in the nanoparticles. Partial reformation of nanoparticles with diameters of 10–30 nm was observed on irradiation with visible light at 520 nm, indicating reversion of the MC form back to the SP form. The SP  $\leftrightarrow$  MC isomerisation was confirmed by the appearance of an absorbance band at 560 nm, after irradiation with UV light, coupled with a yellow  $\rightarrow$  purple change in colour, which is indicative of the presence of the MC form. The intensity of the absorbance band decreased again on visible light irradiation, accompanied by the reappearance of the yellow colour. The photoisomerisation also resulted in a change in the fluorescence of the nanoparticles from green to orange/red, with NAPH (donor), excited at 440 nm, and the MC isomer (acceptor) acting as a FRET pair. Acidic conditions were also found to cause changes in the nanoparticle morphology. At pH 5.5, swelling of the nanoparticles was observed, attributed to the protonation of amino groups in the PAE block, which increased its hydrophilicity. As a result of these dual stimuli responsive properties, the controlled release behaviour of the polymeric nanoparticles was investigated. The fluorescent dye coumarin-102 was used as a model hydrophobic molecule. Successful loading of coumarin-102 into the nanoparticles was confirmed by observing the fluorescence at 490 nm. A gradual decrease in the fluorescent intensity of coumarin-102 was observed on irradiation with UV light at 365 nm and pH 7, indicating the release of coumarin-102 from the nanoparticles. 83% of the loaded coumarin-102 was found to release after 35 min irradiation with UV light, while minimal release was observed in the absence of UV light. Gradual decrease in fluorescent

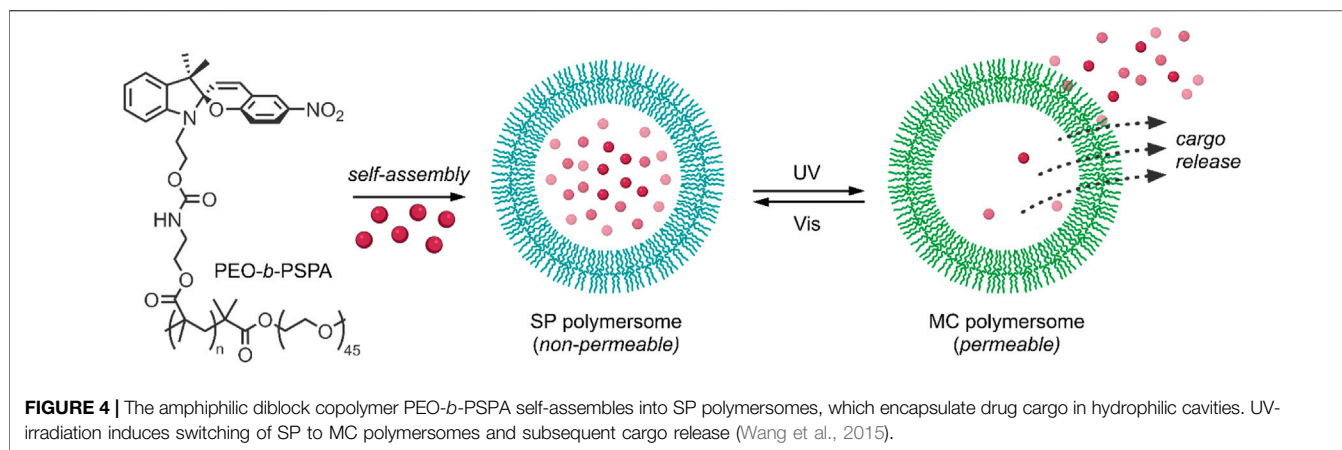
intensity was also observed at pH 5.5, with and without UV irradiation. In the absence of UV irradiation, a release of approx. 90% was observed after 6 h, while the same release was observed after 25 min in the presence of UV light. This indicated that a combination of UV irradiation and acidic conditions could be used to achieve a rapid release of cargo from the polymeric nanoparticles, while acidic conditions alone allow for sustained release of the cargo over a longer period of time. In summary, the polymeric nanocarrier developed by Wang et al. exhibited reversible dual-colour fluorescence and dual-stimuli responsive release of a model cargo (Wang et al., 2019). However, there remains significant issues that must be addressed before the potential of this system can be fully appreciated. The loading efficiencies and biocompatibility of the nanoparticles must be examined. Additionally, the use of UV irradiation and, indeed, the irradiation times required (35 min at pH 7; 25 min at pH 5.5) challenge the clinical viability of this system given the shortcomings of using UV irradiation in a clinical setting.

## Polymersomes

As described above, the self-assembly of amphiphilic copolymers can result in the formation of micelles and nanoparticles. Polymersomes are another type of polymeric vesicles, with structures similar to liposomes; they are composed of hydrophobic bilayer membranes enclosing hollow hydrophilic cavities. This vesicular bilayer structure makes polymersomes highly attractive for their potential in encapsulation and controlled release of therapeutic agents, where hydrophobic drugs may be loaded into the hydrophobic membrane, and hydrophilic drugs may be encapsulated in the hydrophilic core (Alibolandi et al., 2015). Additionally, the ability to carefully select the constituent polymers and introduce functionalities at the supramolecular level enables a high degree of control over polymersomes' properties; including their size, biocompatibility, and stimuli-responsiveness. Therefore, polymersomes have received widespread attention not only for their use as nanocarriers but also for their ability to mimic cellular organelles due to their bilayer membrane structure (Sun et al., 2009). The applicability of polymersomes in drug delivery is vitally dependent on membrane permeability, as the hydrophobic nature of the bilayer membrane may prevent the loading of hydrophilic drugs into the central cavity. This has led to the construction of polymersomes from stimuli-responsive polymers, enabling the modulation of properties, such as membrane permeability, so that a high degree of control over drug release can be achieved (Che and van Hest, 2016).

Most methods of enhancing the membrane permeability of polymersomes, such as the introduction of stimuli-responsive bilayers, are irreversible, and the change in the hydrophobic-hydrophilic balance may lead to the undesirable disintegration of the polymersomes. To overcome this issue, Wang et al. investigated photochromic poly (ethylene oxide)-*b*-PSPA (PEO-*b*-PSPA) based polymersomes (Figure 4), composed of hydrophilic cavities encapsulated by hydrophobic PSPA (SP-based monomer with a carbamate linker) bilayers with PEO inner and outer coronas (Wang et al., 2015). The polymersomes were developed on the principle that membrane





permeability could be reversibly switched between non-permeable and selectively permeable by photoinduced isomerisation between SP and MC moieties present in the membrane bilayer, respectively. On irradiation with UV light at 365 nm, the neutral SP moieties were converted into zwitterionic MC moieties, as indicated by the appearance of an absorbance band at 574 nm associated with the MC isomer. This transition was accompanied by a corresponding change in the hydrophilicity and permeability of the membrane bilayer, as indicated by a decrease in the fluorescent intensity of coumarin-102 loaded into the hydrophobic membrane of the polymersomes. The absorbance band was attenuated on irradiation with visible light at 530 nm, indicating the reversion of the MC form back to the SP form. However, this transition was much slower than the SP  $\rightarrow$  MC transition due to the increased stability of the MC polymersomes relative to the SP polymersomes. To ensure that the physical integrity of the polymersomes was maintained during the SP  $\leftrightarrow$  MC switching process, the authors took advantage of cooperative non-covalent interactions such as H-bonding and hydrophobic interactions to stabilise the membranes of the SP polymersomes. In contrast, the emergence of additional zwitterionic and  $\pi$ - $\pi$  stacking interactions between MC isomers within the bilayer membrane provided extreme stability to the MC polymersomes. These properties were further exploited to investigate the drug release behaviour of the SP and MC polymersomes, using 2'-deoxy-5-fluorouridine (5-dFu) as a model, small, hydrophilic anti-cancer drug. 5-dFu was encapsulated into the hydrophilic cavities of the polymersomes during self-assembly, and the release behaviour of both SP and MC polymersomes was studied. It was found that <10% of 5-dFu was released from the SP polymersomes after 8 h, while ~90% of the drug was released after 8 h when the polymersomes were first irradiated with UV light for 2 min. The release rate of the drug from the MC polymersomes decreased over time, given the reversion of the MC isomer back to the SP isomer and corresponding reduction of membrane permeability, and the release rate was easily halted by irradiation with visible light. This reversible bilayer permeability was further investigated *in vitro*. The release of the fluorescent DNA intercalating agent 4',6-diamidino-2-phenylindole (DAPI)

from the cavities of the polymersomes in HeLa cells was examined using confocal laser scanning microscopy. As expected, in the absence of UV irradiation, minimal release of the model drug was observed from the SP polymersomes, while on UV irradiation at 405 nm for 2 min, an increase in membrane permeability and efficient release of DAPI was observed. It is clear from these results that the incorporation of SP-based monomers into the bilayers of polymersomes provides a promising route to overcome the issue of poor membrane permeability associated with traditional polymersomes. Their ability to reversibly switch membrane permeability on and off through UV/Vis light triggers also makes them highly attractive for use as controlled and sustained release nanocarriers (Wang et al., 2015).

## Interpenetrating Polymer Networks

Although the self-assembled polymeric systems described above exhibit great promise for site-specific, on-demand drug delivery, particularly with the introduction of the stimuli-responsive SP moieties, there remain several intrinsic limitations that may hinder their successful application *in vivo*. In general, self-assembled nanocarriers, particularly micelles, are unstable and may dissociate in solution, potentially giving rise to unwanted premature release or leaching of the drug from the nanocarrier. The use of biodegradable polymers also means that a burst release is common to these nanocarriers instead of sustained drug release. Additionally, drug release mechanisms typically associated with stimuli-responsive self-assembled polymeric systems, such as stimuli-triggered nanocarrier disassembly, may restrict the ability to halt drug release after the initial application of a release stimulus. Toxic side reactions may also occur due to the release of residual polymeric materials into the cell on nanocarrier disassembly (Soleymani Abyaneh et al., 2015; Venditti, 2019; Yadav et al., 2020).

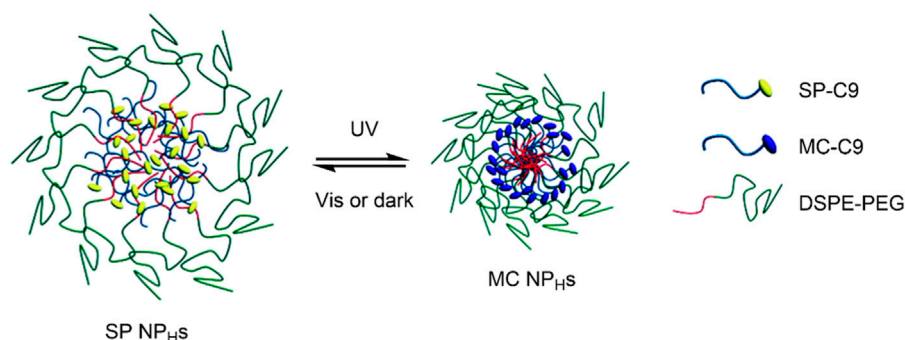
An alternative to self-assembled polymeric systems are interpenetrating polymer networks (IPNs). IPNs are combinations of two or more polymers in the form of a network, with at least one being synthesised in the presence of another polymer, such that a novel multi-component polymeric system is produced. The properties of the individual polymer network constituents are maintained, allowing for a synergistic

and incremental augmentation of the overall properties of the IPN itself. These properties include high stability, biocompatibility and capacity for swelling without loss of structural integrity. Together, they position IPNs as an attractive alternative to self-assembled polymeric nanocarriers (Raina et al., 2019). The beneficial properties of IPNs have been exploited to develop stimuli-responsive DDSs. These DDSs leverage the change in interactions between the polymers, loaded drug molecules and solvent on stimuli application, thus enabling highly controlled drug delivery without disruption to the structure of the IPNs (Ghani et al., 2021a; 2021b).

In a recent paper, Ghani et al. utilised supercritical CO<sub>2</sub> technology to develop an efficient photo-responsive IPN for reversible and on-demand drug release (Ghani et al., 2021a). The IPN was constructed by impregnating a silicone elastomer with different SP-functionalised guest polymers. A Hansen solubility parameter-based thermodynamic model was used to optimise the polymer composition to enable a high degree of control over drug release. The thermodynamic model worked on the principle that a high work of adhesion between the loaded drug and the guest polymer would reduce premature drug release, as the adsorption of a drug to the guest polymer would be energetically favourable. In contrast, low work of adhesion would result in increased premature release. To test the feasibility of the model, the light-triggered release of a model drug doxycycline from multiple IPNs with different guest polymer compositions was investigated. Firstly, the photochromic properties of the IPNs were examined on exposure to UV and visible radiation, and reversible SP  $\leftrightarrow$  MC isomerisation was confirmed to be retained in the IPN. Next, the loading of doxycycline into the IPNs was achieved through passive diffusion—the presence of a protic solvent caused the swelling of IPNs by inducing spontaneous and irreversible SP  $\rightarrow$  MC isomerisation, allowing the doxycycline molecules to diffuse into the IPN. Finally, the release properties of several IPNs varying in hydrophilicity were analysed, and the poly (BMA-co-HEMA-co-SPMA) IPN with 8.5% HEMA was determined to be the optimal IPN for drug delivery. This IPN showed considerable controlled release behaviour, where drug release was increased on irradiation with UV light and decreased or even halted on irradiation with visible light. The hydrophobic BMA and SPMA blocks were found to minimise premature drug release by maintaining a high work of adhesion, as predicted by the model. At the same time, the addition of small amounts of the hydrophilic HEMA allowed for maximal cumulative release in the presence of UV light and inhibition of premature release in its absence. The effect of drug hydrophobicity on the triggered release properties of the IPN was further investigated using five model drugs with increasing hydrophobicity, namely: doxycycline, dopamine, L-dopa, prednisone and curcumin. On irradiation with UV light, 80–90% triggered release was observed for dopamine, L-dopa and prednisone, while triggered releases of ~60 and 26% were observed for doxycycline and curcumin, respectively. The hydrophilicity of doxycycline accounts for its preference to stay in the loading media rather than adsorb to the IPN. At the same time, the hydrophobicity of curcumin likely caused a reduction in its release from the IPN, in addition to

potentially causing its binding to the silicone matrix. Finally, the biocompatibility of the IPN was investigated in human neural stem cells (hNSCs). The IPN was found to have minimal adverse effects on cell viability in the presence or absence of UV light. The IPN was also found to allow successful differentiation of hNSCs into neurons with no morphological damage. Overall, this photo-responsive IPN displayed good light-controlled drug release, with minimal premature release. However, the maximum cumulative release of the model drug doxycycline achievable was still less than those achieved using more hydrophilic IPNs, which were plagued by high premature release (Ghani et al., 2021a).

In an alternative approach, Ghani et al. investigated a SP-photogated IPN-based DDS for on-demand delivery (Ghani et al., 2021b). The IPN was synthesised as follows: firstly, a silicone elastomer prepared using supercritical CO<sub>2</sub> technology was impregnated with a hydrophilic poly (HEMA-co-PEGMEA) hydrogel. Subsequently, carboxyl-containing SP molecules (SPCOOH) were grafted onto the IPN surface. By introducing the photochromic SP onto the IPN surface, rather than as part of the polymer network itself, it was proposed that the SP would instead act as a molecular gate, allowing for high drug loading efficiency while minimising unwanted premature release. In the hydrophobic SP form, the molecular gate would be closed, generating a hydrophobic layer surrounding the IPN and preventing premature drug release. Irradiation with UV light would stimulate the conversion of the SP isomer into the hydrophilic MC isomer, causing the gate to open. This change in hydrophilicity would allow increased diffusion of water molecules into the IPN, causing it to swell and release the loaded drug molecules. Post-synthesis analysis confirmed the successful functionalisation of the hydrogel surface with SPs. The photo-responsive properties of the SP moieties were also successfully retained on surface binding. An investigation of the IPN's water uptake in the presence and absence of UV light was carried out. It was found that water uptake was higher in the presence of UV light, confirming that when the gate is closed, the hydrophobic SP layer prevents surface wetting. In contrast, on conversion to the hydrophilic MC isomer, water molecules were found to diffuse much more readily into the IPN's interior. This increase in water uptake in the presence of UV light was, however, dependent on the amount of hydrogel present on the silicone elastomer—the greater the amount of hydrogel present, the lower the increase in water uptake. As with the previous IPN-based DDS (Ghani et al., 2021a), the triggered release of the model drug doxycycline from the SP-photogated IPN was investigated. The IPN was indeed found to effectively inhibit premature doxycycline release in the absence of UV light. This ability to inhibit premature release was, however, found to be dependent on the hydrogel content. IPNs with hydrogel contents of 40 and 50% exhibited very high premature release of doxycycline. In contrast, IPNs with hydrogel contents of 20 and 30% showed much lower premature release. Regardless, all IPNs showed an increase in the cumulative release of doxycycline on UV-irradiation, indicating that the SP molecular gate did indeed work effectively. Although, the cumulative release was significantly less for those IPNs with lower hydrogel contents (20 and 30%) than those with higher hydrogel contents (40 and 50%). These results indicate that the



**FIGURE 5** | Schematic of the UV-induced shrinkage of the SP NP<sub>Hs</sub> system due to SP → MC conversion. Figure adapted with permission from ACS (Tong et al., 2012).

proposed SP-photogated IPN does indeed show promise for on-demand delivery of hydrophilic drugs. However, careful tuning of hydrogel composition is required in order to ensure a compromise is reached between high cumulative drug release and minimal premature release (Ghani et al., 2021b).

## Lipid-Based Nanoparticles

Lipid-based nanocarriers have attracted much attention due to their ability to enhance the solubility and bioavailability of drugs. There are various lipid-based nanocarriers, which are broken down into two categories: vesicular and non-vesicular, such as liposomes and solid lipid nanocarriers, respectively. Lipids enable transport across the mucosal walls of the gastrointestinal tract and protect the encapsulated API from oxidation. The major advantage of incorporating lipids into a DDS is that they are biocompatible and easily broken down by the body (Mihai Grumezescu, 2018). As with other drug carriers, drug release may be unpredictable and systemic rather than local. Thus, there has been an increased interest in developing stimuli-responsive drug release, along with increasing the number of possible doses from a single administration (Timko et al., 2010).

Tong, Kohane et al. described a hybrid SP/lipid-PEG nanoparticle (SP NP<sub>Hs</sub>), which was composed of a C9 alkyl chain SP derivative (SP-C9), 1,2-distearoyl-*sn*-glycero-3-phosphoethanolamine-*N*-carboxy (polyethylene glycol)-5,000 (DPSE-PEG), and lecithin (Tong et al., 2012). In solution, the amphiphilic PEGylated lipid underwent self-assembly to form a monodisperse nanoparticle, with the SP-C9 chains composing the hydrophobic core and the PEG chains forming the hydrophilic outer layer. This nanoparticle exhibited light-induced size reduction on irradiation with UV light due to the increase in polarity of the PEGylated lipids on the conversion of the SP NP<sub>Hs</sub> to MC NP<sub>Hs</sub> (Figure 5). This was reversible in dark conditions or on visible light irradiation. Seven compounds, namely rhodamine B, coumarin 6, cyanine 5, paclitaxel, docetaxel (DTXL), proparacaine, and DOX, were encapsulated in the core of the lipid nanoparticle to show its broad applicability in drug delivery. The toxicity of the unloaded SP NP<sub>Hs</sub> was assessed in HeLa, PC-3 and huvec cells, showing minimal cytotoxicity in all cell types at standard concentrations.

However, the SP NP<sub>Hs</sub> showed photofatigue, with the absorption intensity decreasing after repeated irradiation. This highlighted the potential use of these nanocarriers for delivering multiple dosages from the same administration. The UV-induced shrinkage of the SP NP<sub>Hs</sub>, as it was converted into MC NP<sub>Hs</sub>, was shown to result in drug release. When the fluorescent molecule calcein was incorporated into the SP NP<sub>Hs</sub> system, no fluorescence was observed due to self-quenching as calcein was stored within the nanoparticle. However, upon UV-irradiation (365 nm), strong fluorescence was observed ( $\lambda_{\text{max}}$  510 nm), indicating rapid calcein release from the nanocarrier. This was observed on calcein loaded SP NP<sub>Hs</sub> in HeLa cells, strongly suggesting the release of calcein through UV-induced particle size reduction. In the second part of this study, the functionalisation of the SP NP<sub>Hs</sub> surface was examined. It was found that when the surface was functionalised with a cell-penetrating protein, the cytotoxicity of DOX loaded SP NP<sub>Hs</sub> was significantly increased compared to that of the non-functionalised nanocarrier. This highlights the possibility of using biomolecules to enhance targeted drug delivery in these systems. The group also found that the SP NP<sub>Hs</sub> → MC NP<sub>Hs</sub> particle size reduction improved drug diffusion through collagen matrices and cornea cadavers, indicating the potential for improved drug penetration and controlled release to tumour cells on target site photo-irradiation (Tong et al., 2012).

In a follow-up paper, the group improved the SP NP<sub>Hs</sub> nanocarrier by introducing cholesterol (SP NP<sub>HC</sub>) (Tong et al., 2013). It was shown that the introduction of cholesterol to DTXL loaded SP NP<sub>Hs</sub> significantly reduced the release of DTXL in the absence of UV-irradiation. However, drug release remained rapid on irradiation with UV light. The drug release followed the same mechanism described in the previous paper; UV-induced SP NP<sub>Hs</sub> → MC NP<sub>HC</sub> conversion led to particle size reduction and subsequent drug release. It was found that the diffusion of DTXL and its distribution in mice tumour cells was increased upon UV-irradiation of the DTXL loaded SP NP<sub>HC</sub> nanocarriers. An increased intra-tumoural penetration accompanied this. This is a significant advance, given that the dense matrix present in tumour cells limits the penetration of traditional therapies (Netti et al., 2000). Overall, the nanocarrier showed both spatiotemporal control over drug release and an enhanced tumour penetration on

irradiation with UV light, and reduced systemic exposure in the absence of UV-irradiation (Tong et al., 2013).

## Upconversion Nanoparticles

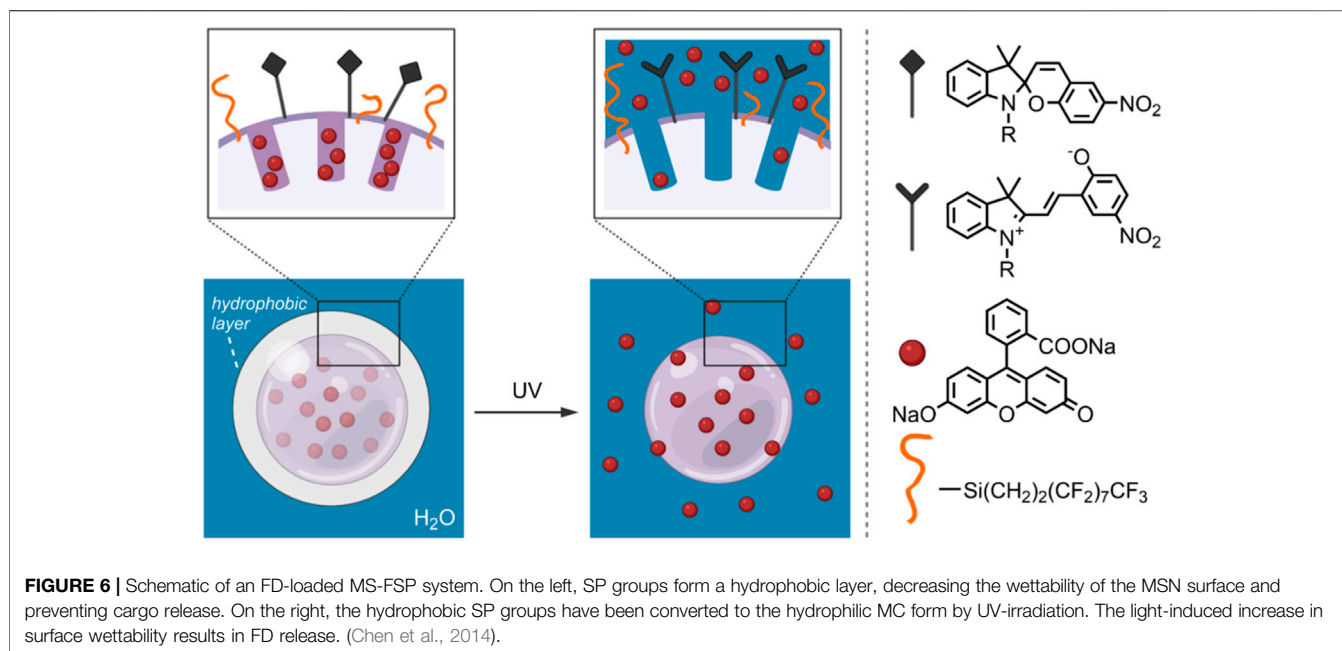
Although light as a stimulus is very convenient, tunable, and offers spatiotemporal control of drug release, the wavelengths required for light-induced drug release from SP-based DDSs limit their applicability. Prolonged exposure to UV light is known to have cytotoxic and mutagenic effects on healthy cells (McMillan et al., 2008). Furthermore, chromophores within bodily tissues, such as haemoglobin and water, have wavelength-dependent extinction coefficients and are strongly absorbing in the UV-Vis region, thus decreasing tissue penetration (Rwei et al., 2015). However, the extinction coefficients of these chromophores are lowest in the NIR region between 650–900 nm; as such, NIR light has a much greater tissue penetrating ability. In addition, NIR light is non-invasive and causes minimal cellular damage (Weissleder, 2001; Ash et al., 2017). Therefore, NIR light is a promising practical alternative to UV-Vis light, having applications in photothermal therapy, stimulus-responsive drug release and *in vivo* deep-tissue imaging (Lim and Park, 2017). However, NIR light does not have enough energy to induce a ring-opening in an SP molecule. One solution to this is two-photon excitation. SP molecules have been shown to isomerise using NIR light due to this effect (Klajn, 2014). However, this may reduce the absorption cross-section for the NIR photons and extend the irradiation time required (Schumers et al., 2010). Alternatively, lanthanide-doped upconversion nanoparticles (UCNPs) have been introduced into DDSs to convert low-energy NIR radiation into higher energy radiation, driving  $SP \leftrightarrow MC$  isomerisation. The lanthanide group of elements are commonly used in UCNPs as they have partially filled inner 4f orbitals. An electron in inner 4f orbitals may be excited by a low energy photon (NIR) and, given that f-f transitions are formally forbidden, its excited state has a long lifetime; up to several milliseconds (Tu et al., 2015). As a result, a second low-energy photon may be absorbed, and a higher excited state may be reached. Upon relaxation to the ground state, a photon of higher energy than those absorbed is emitted (Bettinelli et al., 2015). This is known as the anti-Stokes (upconversion) process, by which two or more long-wavelength photons are converted into a single photon of a shorter wavelength (Li et al., 2015). Lanthanide dopants commonly used include  $Yb^{3+}$ ,  $Er^{3+}$ ,  $Tm^{3+}$ , and  $Ho^{3+}$  (Lee and Park, 2018). UCNPs are typically hydrophobic, limiting their biomedical application. However, this can be overcome by introducing hydrophilic polymers onto their surface, allowing for a photoresponsive moiety and a drug molecule to be attached to the surface of the UCNP. Alternatively, this can be achieved by forming a nanocomposite, where the UCNPs, drug molecules and SP groups are incorporated into a polymer matrix (Bagheri et al., 2016).

In 2013, Zhou, Qu et al. reported a facile route for the synthesis of hollow  $NaYF_4$ : 18% $Yb^{3+}$ /2% $Er^{3+}$  UCNP using DNA without needing a sacrificial template nanoparticle that is commonly required to synthesise UCNPs. It was found that increasing the DNA concentration led to a decrease in particle size, but when less DNA was used, the particles obtained were spherical

and hollow, allowing for control of both shape and size (Zhou et al., 2013). To test the loading capacity and photoresponsivity of the UCNPs, MC was immobilised onto their surface (UCNP-MC). The absorption spectra of the UCNP-MC were recorded on irradiation with NIR light at 980 nm, and visible-light-induced  $MC \rightarrow SP$  isomerisation was observed, as facilitated by the upconversion luminescence ( $\lambda_{em}$  520, 538 and 652 nm) of the UCNPs. Given its charged characteristic, the UCNP-MC form was investigated for both its ability to bind proteins, and its NIR light-triggered release properties, for which  $\beta$ -galactosidase ( $\beta$ -gal) was used as a model enzyme. It was found that the enzyme adsorption to the UCNP-MC surface (UCNP-MC- $\beta$ -gal) was greatly influenced by the positive charge on the MC groups, with enzyme release only observed as UCNP-MC was converted into UCNP-SP upon NIR irradiation. The system's *in vitro* behaviour was studied in HeLa cells—the UCNP-MC- $\beta$ -gal nanocarrier was found to endocytose and accumulate in the cytoplasm. The system showed no cytotoxicity on NIR irradiation, and the NIR-triggered protein release into cells was confirmed. Furthermore, the released enzyme retained its biological activity, thus indicating this nanoparticles' ability to act as a protein delivery system. This MC-UCNP nanocarrier displayed good spatiotemporal control over protein release, highlighting its potential application beyond protein-delivery for possible light-controlled drug delivery. (Zhou et al., 2013).

In an alternative approach, Chen et al. reported a successful DDS composed of a photo- and pH-responsive SP-functionalised amphiphilic polymer and UCNP based nanocomposite (Chen et al., 2016). In their investigation, a poly (*N*-isopropylacrylamide-*co*-SP methacrylate) amphiphilic block copolymer and a  $NaYF_4$ : 25% $Yb^{3+}$ /0.5% $Tm^{3+}$  UCNP were synthesised. In an aqueous solution, the amphiphilic polymers self-assembled into micellar nanoparticles with the *N*-isopropylacrylamide block forming the hydrophilic shell, and the SP-containing methacrylate block forming the hydrophobic core. The hydrophobicity of the micelle core was exploited to encapsulate the UCNPs. The emission spectra of UCNPs on NIR-irradiation (980 nm) were shown to have a  $\lambda_{max}$  at 360 nm, which overlapped with the absorption spectra of the SP groups. Moreover, it was shown that on NIR-irradiation, the absorption band at 525 nm in the nanocomposites' UV-Vis spectra increased, indicating  $SP \rightarrow MC$  conversion. On irradiation with visible light at 520 nm, the absorption spectra reverted to the original, indicating reversible  $SP \leftrightarrow MC$  isomerisation in the nanocomposites. Fluorescent coumarin-102 guest molecules were then loaded into the nanocomposites hydrophobic core to investigate their dual photo/pH-controlled encapsulation and release properties. Coumarin-102 release was observed on NIR-irradiation due to the conversion of the hydrophobic SP groups to hydrophilic MC groups, which disrupted the hydrophobic-hydrophilic balance and subsequently caused the micelles to dissociate. Interestingly, low pH conditions led to the swelling of the self-assemblies and subsequent drug release. Reduction in the pH from seven to five and NIR-irradiation led to an increase in coumarin-102 release due to the protonation of the SP to the MC form, indicated by the nanocomposites' emission spectra. Critically, the





nanocomposites were shown to have minimal cytotoxicity *in vitro* on U-87 MG cancer cells, while when loaded with DOX, the nanocomposites caused significant cell death on NIR-irradiation. Overall, these UCNP SP-copolymer nanocomposites show a potential application in anti-cancer treatment—the low-pH tumour environment combined with NIR-irradiation can improve site-specific drug release properties while minimising phototoxic effects (Chen et al., 2016).

## Mesoporous Silica Nanoparticles

Mesoporous silica nanoparticles (MSNs) are solid silica ( $\text{SiO}_2$ ) frameworks with honeycomb-like porous structures (Pednekar et al., 2017). Mesoporous materials are characterised by pore diameters ranging from 2–50 nm (Rouquerol et al., 1994)—this porous nature of MSNs allows loading and release of therapeutics, with pore size and volume being highly tunable to accommodate a variety of guest molecules. The vast quantity of Si-OH groups present on the MSN surface allows for surface modification with responsive materials, commonly polymers, for controlled-release of therapeutics (Yang et al., 2012; Manzano and Vallet-Regi, 2019). By coating the MSN surface with a hydrophobic polymer, the pores are effectively covered by a hydrophobic layer, thus decreasing the nanoparticle's wettability and consequently minimising drug release. In contrast, in the presence of a hydrophilic polymer, the surface wettability is increased, which allows for loaded therapeutics to diffuse out of the MSNs (Yang et al., 2012). This process has been exploited by modifying the Si-OH groups with SP-containing polymers. An endo- or exogenous stimuli may induce these to switch from the hydrophobic SP form to the hydrophilic MC form. Thus, allowing for targeted and controlled release of the loaded therapeutic. In addition, MSNs show very good biocompatibility and their size enables efficient cellular uptake by endocytosis, highlighting their

potential as nanocarriers for anti-cancer therapeutics (Li et al., 2012; Argyo et al., 2013).

The ability to control drug release by influencing MSN surface wettability through photo-induced SP isomerisation was investigated by Chen et al., in 2014 (Chen et al., 2014). In their study, 300 nm diameter MSNs were treated with 3-aminopropyltriethoxysilane (APTES) and perfluorodecyltriethoxysilane (PFDTES). The resulting amine- and fluorinated-silane modified MSNs (MS-FNH<sub>2</sub>) were subsequently functionalised with carboxylic acid-terminated SP, yielding the final hydrophobic DDS (MS-FSP). Using fluorescein disodium (FD) as model cargo, the light-responsive release properties of the MS-FSP were investigated. It was found that rapid release occurred when the surface was functionalised with SP only (MS-SP). However, by increasing the surface hydrophobicity through a high PFDTES: SP ratio, minimal FD release from MS-FSP pores was observed without UV-irradiation—thus, creating a hydrophobic surface layer that effectively prevented undesired FD release. On UV-irradiation, the SP form was converted to the MC form, increasing the MSNs surface hydrophilicity—in this case, FD release was observed (Figure 6). To further investigate the system's drug-delivery potential, camptothecin (CPT) was loaded into the MS-FSP (MS-FSP-CPT) as a model anticancer drug. The *in vitro* release properties were investigated in EA.hy926 and HeLa cells. After 24 h, minimal cytotoxicity was observed for MS and MS-FSP, with and without a 5 min exposure to UV-irradiation, up to concentrations of 100  $\mu\text{g}/\text{ml}$ . Decreased cell viability was observed for both cell types loaded with MS-FSP-CPT, with increased cell death observed when irradiated with UV light, indicating successful light-induced CPT release. Overall, this system has good potential for the controlled release of anti-cancer drugs, having good biocompatibility and photoresponsive characteristics (Chen et al., 2014).

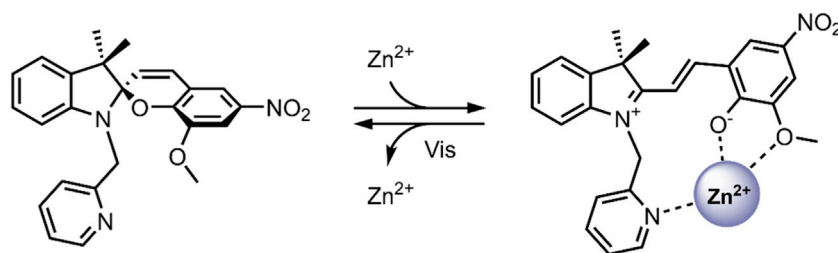
In an alternative approach, Xing et al. examined the drug-delivery feasibility of a hollow MSN (HMSN) coated with an amphiphilic SP-containing copolymer *via* self-assembly (Xing et al., 2014). HMSNs have been increasingly studied for their drug loading ability due to their increased volume for storing therapeutics (Liu et al., 2016). In this investigation, the amphiphilic copolymer was composed of a rhodamine B (2-hydroxyethyl acrylate) ester (RBM) block, a hydrophilic MAPEG block, and a spiropyran methacrylate (SPMA) block. The amphiphilic copolymer, labelled PRMS, was then conjugated with folic acid (FA), which is known to target folate receptors (FR) in tumour cells (Fernández et al., 2018). The absorption bands of the SPMA at 365 nm were found to overlap well with the emission bands of the RBM. Thus, a FRET process could be utilised, with RBM acting as the donor and SPMA acting as the acceptor. This was indeed observed as the fluorescent intensity of the rhodamine B moiety, excited at 510 nm, significantly decreased on irradiation with UV light at 365 nm. This was a result of the conversion of the closed SP form to the open, visible light absorbing MC form, leading to the quenching of the rhodamine B fluorescence. The polymer was then coated onto the surface of an HMSN modified with C-18 alkyl chains by self-assembly through hydrophobic interactions between the C-18 chains and the polymer's hydrophobic blocks. The coating process was shown to block the pores of the HMSN by forming a hydrophobic layer at the HMSN surface. The HMSN/C-18/PRMS-FA nanocarrier's controlled-release properties were investigated, using DOX as a model therapeutic. The amphiphilic polymer on the HMSN surface effectively blocked the pores, preventing the release of DOX in the absence of UV and visible light, and minimising the quantity released after 8 h. Rapid release was observed with UV-irradiation, with 70 wt% of DOX released in 100 h, and the initial rapid release was found to halt immediately upon switching to a visible irradiation source. Moreover, the drug release was found to co-occur with the FRET process, allowing for real-time monitoring of the DOX levels in the HMSNs. The HMSN/C-18/PRMS-FA nanocarriers showed good biocompatibility and good targeting in FR containing tumour cells compared to non-FR containing tumour cells due to the FA moiety in the polymer. Based on these results, this system shows promise for its biomedical applications; particularly, the targeted and controlled release of anti-cancer drugs to FR containing tumour cells (Xing et al., 2014).

Although MSNs have many benefits, they have been shown to have low renal clearance and poor biodegradability (Croissant et al., 2017). In addition, the limitations associated with using UV light, as previously discussed (*Polymersomes* Section), are pertinent. In light of this, He et al. recently proposed a system that addresses both of these issues (He et al., 2020). The system was composed of an SP and fluorinated silane (FS) modified ultrasmall mesoporous silica nanoparticle (SP-FS-USMSN; approx. 12 nm diameter)—the FS was used to increase surface hydrophobicity. In a pH 7.4 PBS solution, the SP-FS-USMSN self-assembled through hydrophobic interactions into nanoclusters (approx. 110 nm diameter). The clusters were shown to dissociate at pH 4.5 and 5.5—the low pH caused the

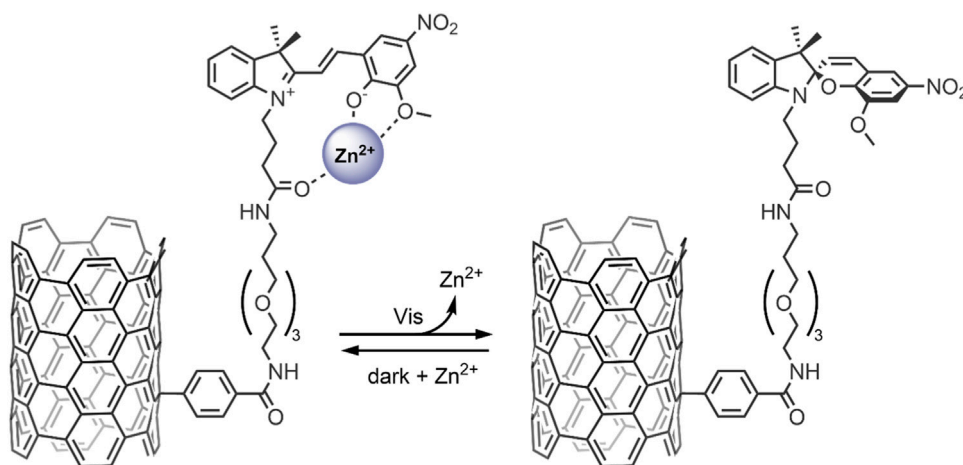
hydrophobic SP form to convert to the hydrophilic MC form, thus resulting in cluster dissociation. These nanoclusters were used for co-delivery of DOX and curcumin (CUR). DOX was loaded into the pores of SP-FS-USMSNs by electrostatic interactions with the surface silanol groups. The DOX-loaded SP-FS-USMSN were then allowed to assemble *via* hydrophobic interactions with CUR, to form DOX and CUR-loaded SP-FS-USMSN nanoclusters. The systems release properties were then studied, and a significant increase in drug release was observed at pH 5.5 and 4.5 for both DOX and CUR. This low-pH-induced release is a contrast to the decreased release observed at pH 7.4 and 6.5. Through *in vitro* studies, the nanoclusters were shown to exhibit significant cellular uptake in HepG2 cells due to the EPR effect. Through DOX and CUR fluorescence monitoring, the drugs were shown to be widely distributed in HepG2 cells after 8 h. This desirable biodistribution is believed to result from the low-pH environment of endosomes, causing the SP → MC conversion-induced disassociation of the nanoclusters and subsequent release of the loaded therapeutics. The *in vitro* cytotoxicity of DOX- and CUR and DOX-loaded SP-FS-USMSN nanoclusters was also investigated. The dual loaded CUR-DOX-SP-FS-USMSN displayed a higher cytotoxicity than that of the DOX-loaded SP-FS-USMSN, indicating the combinatorial anti-tumour effects of CUR and DOX. The SP-FS-USMSN cluster, on the other hand, showed no inhibitory effect on cell viability, indicating its biocompatibility. HepG2-xenografted nude mice were used to determine the *in vivo* properties of the system. DOX and CUR loaded SP-FS-USMSN showed a 74% tumour growth inhibition rate and were found to cause dramatic cell shrinkage and necrosis. Further *in vivo* studies in mice showed large amounts of silica present in both urine and faeces, indicating that the USMSN could be rapidly cleared from the body upon disassociation of the clusters at low pH. This DDS shows promise for their use in anti-cancer therapy for its considerable accumulation in tumour cells, the potential for effective co-delivery of complementary therapeutics, its rapid clearance from the body, and the fact that harmful UV-irradiation is not required to induce drug-release in this system (He et al., 2020).

## SP-Metal Ion Complexes and Carbon Nanomaterials

The attention given to the complexation of SPs with metal cations has been increasing in the scientific community over recent years (Natali et al., 2010a; Del Canto et al., 2012; Heng et al., 2018; Cardano et al., 2019). The planar, open MC form contains an anionic phenolate shown to reversibly chelate to electron-poor metal ions differing in softness/hardness, such as  $\text{Zn}^{2+}$  and  $\text{Cu}^{2+}$ , with optical control (**Figure 7**) (Phillips et al., 1965; Natali and Giordani, 2012a). Also, functionalisation of the benzopyran and indoline moieties with additional chelating groups can influence the metal ion-spiropyran complex stoichiometry and geometry without significantly affecting the SP ↔ MC isomerisation (Görner and Chibisov, 1998; Natali and Giordani, 2012b; Klajn, 2014; Baldrighi et al., 2016). The on/off switching ability of SP-metal ion complexation has found many



**FIGURE 7** | Schematic of the photo-reversible SP  $\rightarrow$  MC- $\text{Zn}^{2+}$  complex formation (Natali et al., 2010b).

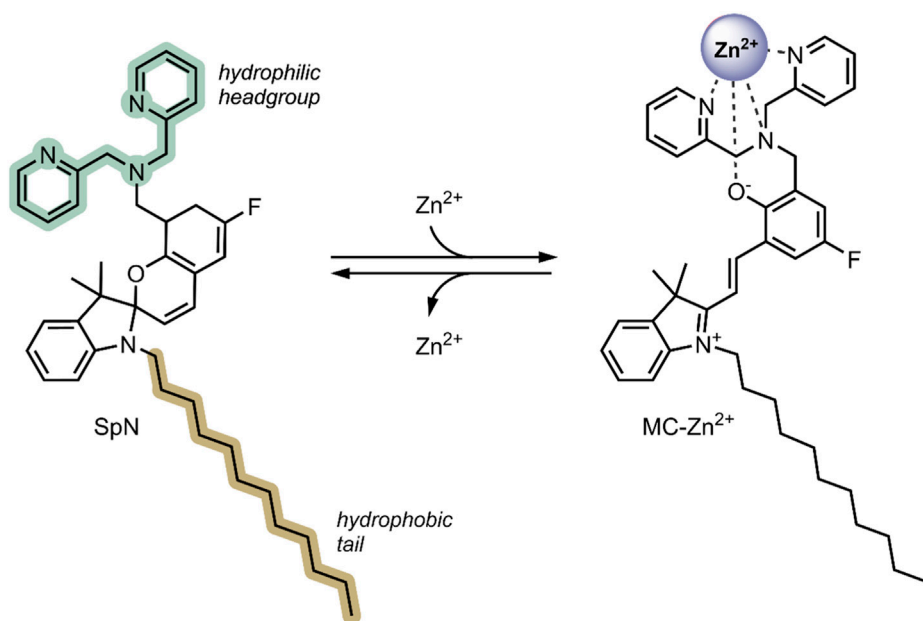


**FIGURE 8** | Light-induced MC  $\rightarrow$  SP conversion in the functionalised SWNT nanocarrier, resulting in the release of  $\text{Zn}^{2+}$  ions from the MC molecules anchored to the SWNT surface (Del Canto et al., 2012).

biomedical applications, particularly in biosensors (Radu et al., 2009; Ali et al., 2020). More recently, the potential of SPs has been exploited for the stimuli-controlled ion and drug release from nanocarriers (Del Canto et al., 2012; Heng et al., 2018; Cardano et al., 2019).

Carbon nanomaterials (CNMs) are chemically stable, and their surfaces can be easily modified, allowing for robust control of their physicochemical properties and functions within the body—as such, they lend to many biological applications, especially in the case of photoresponsive CNMs (Cardano et al., 2018). In particular, single-walled carbon nanotubes (SWNTs) and graphene show potential for their use in light-controlled DDSs, when modifying their surface with photochromic SP molecules (Del Canto et al., 2012; Nahain et al., 2013). It has been shown that when bound to the surface of these nanomaterials, SPs retain their ability to bind to metal ions and have shown SP  $\rightarrow$  MC isomerisation when exposed to  $\text{Zn}^{2+}$  (Del Canto et al., 2010; Perry et al., 2015). These findings have been exploited to design smart SP-functionalised SWNTs for the light-controlled release of  $\text{Zn}^{2+}$  (Del Canto et al., 2012). In our 2012 study, we investigated the ability of an SP bound to the surface of a SWNT as a receptor to reversibly uptake  $\text{Zn}^{2+}$  in response to light (**Figure 8**) (Del

Canto et al., 2012). The SP molecules were bound to the SWNT surface *via* a PEG linker, which was used to enhance biocompatibility and promote the nanocarrier's renal clearance. The SWNTs were first purified to remove the toxic metal catalysts and then covalently modified using a Tour reaction to introduce benzoic acid moieties, which further improved the nanocarrier's dispersibility. The benzoic acid moieties were then coupled with a PEG linker and the SP derivative *via* an amidation reaction. The absorbance maximum of SP-SWNT ( $\lambda_{\text{max}}$  416 nm) was redshifted relative to that of free SP in solution, confirming the successful functionalization of the surface of the SWNT. An absorption maximum at 585 nm was obtained after UV-irradiation (365 nm for 2 min), which disappeared after 3 min in the dark, indicating reversible SP  $\leftrightarrow$  MC isomerisation. Emission spectroscopy was used to confirm the formation of the MC- $\text{Zn}^{2+}$  complex, and light/darkness cycles showed the sequential uptake and release of  $\text{Zn}^{2+}$  by the SWNT-anchored SP molecules. These findings highlight the potential of SP/SWNT-based systems to be used for drug delivery, where the photo-controlled switching of SWNT-anchored SP molecules may modulate the release of bound therapeutic agents at target locations (Del Canto et al., 2012).

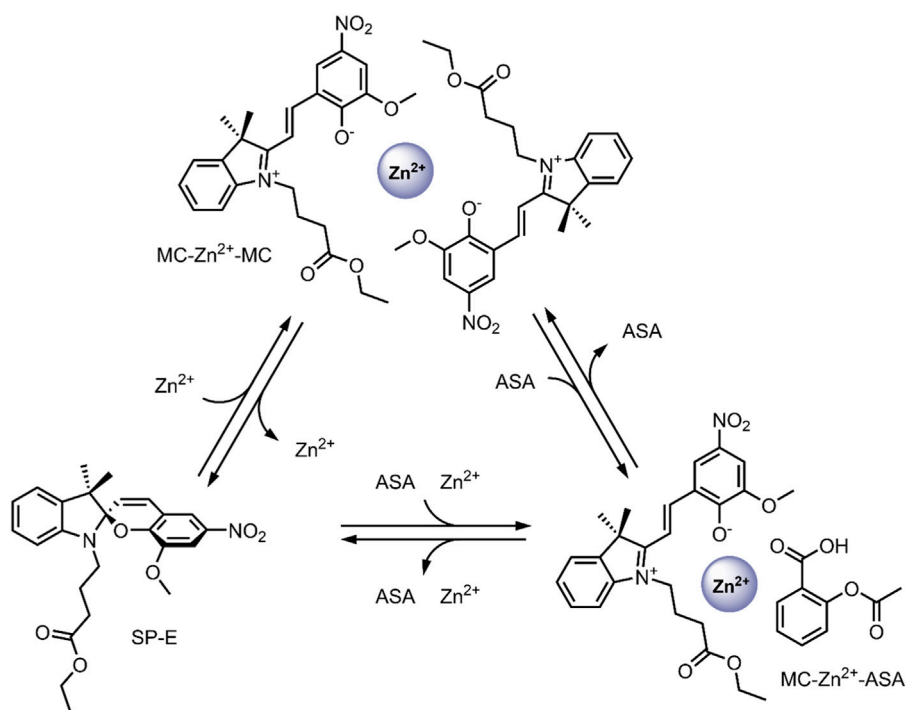


**FIGURE 9** | The structure of the SpN is shown on the left. The presence of high levels of  $\text{Zn}^{2+}$  in tumour cells induces a ring-opening and formation of a fluorescent MC- $\text{Zn}^{2+}$  complex, shown on the right. The three nitrogen atoms in the bis(2-pyridyl)methyl)amine group and the phenolate oxygen were involved in chelating to the  $\text{Zn}^{2+}$  ion (Heng et al., 2018).

In 2018, Heng et al. reported a  $\text{Zn}^{2+}$  responsive SP-based nanocarrier (Heng et al., 2018). Some tumour cells have elevated  $\text{Zn}^{2+}$  levels compared to healthy cells—these  $\text{Zn}^{2+}$  levels tightly regulate the activity of specific caspases, which are known to induce apoptosis (Brown and Attardi, 2005). Thus, the reported system took advantage of the favourable conversion of the SP form to the MC form in the presence of high levels of  $\text{Zn}^{2+}$ , resulting in the swelling of the nanocarriers and the release of encapsulated therapeutic. The system (SpN) was composed of an SP molecule containing a hydrophobic C-12 substituent on the nitrogen of the indolenine moiety and a hydrophilic bis(2-pyridyl)methyl)amine group on the benzopyran moiety (Figure 9). The SpN self-assembled in an aqueous solution to form a micelle-like nanocarrier of an average diameter of 575 nm. The particle diameter was found to increase linearly with increasing  $\text{Zn}^{2+}$  concentration, owing to the SP form switching to the fluorescent MC- $\text{Zn}^{2+}$  complex. Using the fluorophores 7-hydroxycoumarin and 1-hydroxypyrene, the nanocarriers' encapsulation and release properties were investigated in apoptotic and healthy HEK293 cells. In apoptotic HEK293 cells, elevated levels of  $\text{Zn}^{2+}$ , intense fluorescence, and distribution in the cells were observed for both fluorophores. This was not the case in healthy cells. This indicated that in the absence of  $\text{Zn}^{2+}$ , the molecules remained trapped in the nanocarriers, but are released in the presence of  $\text{Zn}^{2+}$  due to complex formation and swelling of the nanocarrier. The fluorescent intensity increased linearly with increasing  $\text{Zn}^{2+}$  concentration, highlighting potential use in real-time  $\text{Zn}^{2+}$  sensing. The nanocarriers were further used to encapsulate and deliver Azure B, a caspase inhibitor, into apoptotic HEK293 cells and a potent proteasome inhibitor to breast

cancer cell lines, T46D and MDA-MB-468. Caspase inhibition by Azure B released from the SpN was observed, validated by time-lapsed cell microscopy. Significant cytotoxicity was observed in the breast cancer cell lines due to the release of the proteasome inhibitor in the presence of  $\text{Zn}^{2+}$ . No cytotoxicity was observed in the absence of  $\text{Zn}^{2+}$ . Both the Azure B and proteasome inhibitor's therapeutic activity depended on  $\text{Zn}^{2+}$  concentration, where increased inhibition was observed with increasing  $\text{Zn}^{2+}$  concentration. The  $\text{Zn}^{2+}$  responsive nature of this system enabled targeted release of anti-cancer therapeutics in tumour cells, limiting systemic exposure, and the fluorescent nature of the complex formed enabled real-time analysis of the  $\text{Zn}^{2+}$  concentration, indicating early or late-stage apoptosis (Heng et al., 2018).

In 2019, our group probed the use of modified SPs for dual co-delivery applications (Cardano et al., 2019). For this study, a  $\text{Zn}^{2+}$  and acetylsalicylic acid (ASA) pair was chosen as model cargo, given their excellent anti-inflammatory activity (Prasad, 2014; Jarosz et al., 2017). A spiropyran ester (SP-E) derivative was synthesised in our previous work, and its interactions with divalent metal cations ( $\text{Zn}^{2+}$ ,  $\text{Cu}^{2+}$ , and  $\text{Mg}^{2+}$ ) were extensively studied—XRD analysis indicated that the metal cations chelate the SP-E molecule's through their phenolate and methoxy moieties (Baldrighi et al., 2016). Our study found that the SP-E forms a stable ternary complex in the MC form with  $\text{Zn}^{2+}$  and ASA (Figure 10). The ternary complex formation was found to occur only when the components were added without any pre-complexation, and the ternary complex was stable for 1 month. The system's photo-responsiveness was then investigated—the conversion of the SP-E moiety from ring-opened MC form to the ring closed SP form was observed on



**FIGURE 10 |** Schematic representation of the formation and dissociation of the MC-Zn<sup>2+</sup>-ASA and MC-Zn<sup>2+</sup>-MC ternary complexes (Cardano et al., 2019).

visible light irradiation, leading to the release of Zn<sup>2+</sup> and ASA. The ternary complex was found to reform within 2 h in the dark. The ability to switch the SP-E moiety between open/closed forms on Vis-irradiation highlights its potential as a smart DDS for light-controlled co-delivery of anti-inflammatory agents to areas of the body with direct exposure to visible light; such as the skin (Cardano et al., 2019). Prospectively, the development of optical fibres may allow for this ternary DDS to co-deliver therapeutics to targets within the body which are not penetrable by visible light (Keiser, 2019).

## CONCLUSION

The photochromic behaviour of spiropyrans (SP) has been extensively studied since it was first observed in the 1950s by Fischer and Hirshberg. On the application of a stimulus, most commonly light, the SP form undergoes a ring-opening to a physically and chemically distinct merocyanine (MC) form, with a corresponding redshift in the UV-Vis spectrum. With the extraordinary advances in pharmaceutical and materials science, there has been a resurgent interest in the ability of SPs to switch between two distinct, stable isomers, lending to their biomedical applications, particularly in biosensing and nano-based drug delivery. The present review highlights several promising SP-based nanocarriers that leverage stimulus-induced SP → MC conversion for site-specific and dose-controlled release of drugs. In particular, SPs have found successful incorporation into polymeric micelles, lipid

nanoparticles, upconversion nanoparticles (UCNPs), and mesoporous silica nanoparticles (MSNs), as a result of their broad-range compatibility with nanomaterials. These systems show good biocompatibility, bioavailability, and the versatility of the nanomaterials used allows for their release properties to be tuned such that minimal drug release is observed in the absence of a stimulus, but is rapid on stimulus application. Also, by incorporating a second chromophore into the systems, the Förster Resonance Energy Transfer (FRET) mechanism may be exploited for real-time quantification of drug release. SP-based nanocarriers also show responsivity to a variety of endogenous and exogenous stimuli, such as pH, heat and light. Due to its spatiotemporal control over drug release, light is the most commonly used stimulus in SP-based drug-delivery systems (DDSs). However, due to the well-known mutagenic effects of UV light and its insufficient penetration power through bodily tissues, its biomedical applications are limited. This is overcome by using longer wavelength NIR light, which may be 'upconverted' into higher-energy light capable of driving the SP → MC conversion, thus releasing the loaded therapeutic. This process can be achieved through the use of lanthanide-doped UCNPs. In an alternative approach, divalent metal ions, particularly Zn<sup>2+</sup>, can be used to induce SP ↔ MC isomerisation, with the MC form favourably forming MC-Zn<sup>2+</sup> complexes. Overall, spiropyran prove to be a versatile material that shows promise in light-controlled drug delivery.

The need to move beyond traditional therapies to achieve greater control over drug delivery drives the continued development of responsive materials and smart DDSs. A



large focus of SP-based DDS research has been placed on optimising the fabrication of nanocarriers to ensure biocompatibility, high drug loading efficiency, and effective release in the presence of a stimulus, while minimising premature release. However, very little *in vivo* preclinical data has been reported thus far. While biocompatibility will remain of utmost importance, several challenges must be overcome to advance the field toward successful clinical outcomes. Firstly, many of the DDSs developed, particularly self-assembled systems, typically undergo irreversible disassembly/disintegration on the application of a release stimulus. This limits the number of doses that can be delivered with a single administration to one and prevents the halting of drug release after the initial stimulus. Drug delivery vectors such as IPNs and MSNs do not suffer from this issue and may offer a promising alternative to self-assembled systems. Additionally, the excellent physicochemical properties of CNMs have led to their potential use as efficient DDSs, as successfully explored in recent years (Pattnaik et al., 2020). Nevertheless, the research on the introduction of SPs into these IPN, MSN and CNM-based DDSs for triggered, on-demand drug delivery is still in its infancy, with further work required to determine their clinical viability. A second factor to consider is the choice of drug-release stimuli. Although UV-light is the most effective stimulus, the drawbacks in a clinical setting are well-known. The use of NIR light instead offers the obvious benefits of enhanced penetration and reduced cellular damage. However, to achieve the desired effect (SP  $\leftrightarrow$  MC

isomerisation) through two photon NIR excitation, much longer irradiation times are required. For this reason, UCNPs are commonly utilised for NIR to UV light upconversion. However, the health effects of UCNPs are still not well understood (Gnach et al., 2015). The use of different endogenous stimuli, such as temperature, pH and metal ions, has also been investigated to some success. However, their inherent variability *in vivo* makes it difficult to achieve precise control over drug delivery.

## AUTHOR CONTRIBUTIONS

AF wrote the initial draft of the manuscript. MB prepared the Figures and edited the manuscript. SG conceived the original idea, supervised and edited the manuscript.

## FUNDING

Financial assistance in the form of a Government of Ireland Postgraduate Scholarship (GOIPG) to MB (GOIPG/2019/1820) from the Irish Research Council (IRC) is gratefully acknowledged.

## ACKNOWLEDGMENTS

Figures 3, 4, 6 were partially created with BioRender.

## REFERENCES

- Aakeröy, C. B., Hurley, E. P., Desper, J., Natali, M., Douglass, A., and Giordani, S. (2010). The Balance between Closed and Open Forms of Spiropyran in the Solid State. *CrytEngComm* 12, 1027–1033. doi:10.1039/b914566d
- Abeyrathna, N., and Liao, Y. (2016). Stability of Merocyanine-type Photoacids in Aqueous Solutions. *J. Phys. Org. Chem.* 30, e3664. doi:10.1002/poc.3664
- Ahmad, Z., Shah, A., Siddiq, M., and Kraatz, H.-B. (2014). Polymeric Micelles as Drug Delivery Vehicles. *RSC Adv.* 4, 17028–17038. doi:10.1039/c3ra47370h
- Aibani, N., da Costa, P. F., Masterson, J., Marino, N., Raymo, F. M., Callan, J., et al. (2017). The Integration of Triggered Drug Delivery with Real Time Quantification Using FRET; Creating a Super 'smart' Drug Delivery System. *J. Controlled Release* 264, 136–144. doi:10.1016/j.jconrel.2017.08.013
- Ali, A. A., Kharbush, R., and Kim, Y. (2020). Chemo- and Biosensing Applications of Spiropyran and its Derivatives - A Review. *Analytica Chim. Acta* 1110, 199–223. doi:10.1016/j.aca.2020.01.057
- Alibolandi, M., Ramezani, M., Abnous, K., Sadeghi, F., and Hadizadeh, F. (2015). Comparative Evaluation of Polymersome versus Micelle Structures as Vehicles for the Controlled Release of Drugs. *J. Nanopart. Res.* 17, 1–16. doi:10.1007/s11051-015-2878-8
- Argy, C., Weiss, V., Bräuchle, C., and Bein, T. (2013). Multifunctional Mesoporous Silica Nanoparticles as a Universal Platform for Drug Delivery. *Chem. Mater.* 26, 435–451. doi:10.1021/cm402592t
- Ash, C., Dubec, M., Donne, K., and Bashford, T. (2017). Effect of Wavelength and Beam Width on Penetration in Light-Tissue Interaction Using Computational Methods. *Lasers Med. Sci.* 32, 1909–1918. doi:10.1007/s10103-017-2317-4
- Bagheri, A., Arandian, H., Boyer, C., and Lim, M. (2016). Lanthanide-Doped Upconversion Nanoparticles: Emerging Intelligent Light-Activated Drug Delivery Systems. *Adv. Sci.* 3, 1500437. doi:10.1002/adv.201500437
- Baldrighi, M., Locatelli, G., Desper, J., Aakeröy, C. B., and Giordani, S. (2016). Probing Metal Ion Complexation of Ligands with Multiple Metal Binding Sites: The Case of Spiropyran. *Chem. Eur. J.* 22, 13976–13984. doi:10.1002/chem.201602608
- Begines, B., Ortiz, T., Pérez-Aranda, M., Martínez, G., Merinero, M., Argüelles-Arias, F., et al. (2020). Polymeric Nanoparticles for Drug Delivery: Recent Developments and Future Prospects. *Nanomaterials* 10, 1403. doi:10.3390/nano10071403
- Berkovic, G., Krongauz, V., and Weiss, V. (2000). Spiropyran and Spirooxazines for Memories and Switches. *Chem. Rev.* 100, 1741–1754. doi:10.1021/cr9800715
- Berton, C., Busiello, D. M., Zamuner, S., Solari, E., Scopelliti, R., Fadaei-Tirani, F., et al. (2020). Thermodynamics and Kinetics of Protonated Merocyanine Photoacids in Water. *Chem. Sci.* 11, 8457–8468. doi:10.1039/d0sc03152f
- Bettinelli, M., Carlos, L., and Liu, X. (2015). Lanthanide-doped Upconversion Nanoparticles. *Phys. Today* 68, 38–44. doi:10.1063/pt.3.2913
- Brown, J. M., and Attardi, L. D. (2005). The Role of Apoptosis in Cancer Development and Treatment Response. *Nat. Rev. Cancer* 5, 231–237. doi:10.1038/nrc1560
- Canto, E. D., Natali, M., Movia, D., and Giordani, S. (2012). Photo-controlled Release of Zinc Metal Ions by Spiropyran Receptors Anchored to Single-Walled Carbon Nanotubes. *Phys. Chem. Chem. Phys.* 14, 6034. doi:10.1039/c2cp40275k
- Cardano, F., Del Canto, E., and Giordani, S. (2019). Spiropyran for Light-Controlled Drug Delivery. *Dalton Trans.* 48, 15537–15544. doi:10.1039/c9dt02092f
- Cardano, F., Frascioni, M., and Giordani, S. (2018). Photo-Responsive Graphene and Carbon Nanotubes to Control and Tackle Biological Systems. *Front. Chem.* 6, 102. doi:10.3389/fchem.2018.00102
- Che, H., and van Hest, J. C. M. (2016). Stimuli-responsive Polymersomes and Nanoreactors. *J. Mater. Chem. B* 4, 4632–4647. doi:10.1039/c6tb01163b

- Chen, L., Wang, W., Su, B., Wen, Y., Li, C., Zhou, Y., et al. (2014). A Light-Responsive Release Platform by Controlling the Wetting Behavior of Hydrophobic Surface. *ACS Nano* 8, 744–751. doi:10.1021/nn405398d
- Chen, S., Gao, Y., Cao, Z., Wu, B., Wang, L., Wang, H., et al. (2016). Nanocomposites of Spiropyran-Functionalized Polymers and Upconversion Nanoparticles for Controlled Release Stimulated by Near-Infrared Light and pH. *Macromolecules* 49, 7490–7496. doi:10.1021/acs.macromol.6b01760
- Cong, Y., Wang, X., Zhu, S., Liu, L., and Li, L. (2021). Spiropyran-Functionalized Gold Nanoclusters with Photochromic Ability for Light-Controlled Fluorescence Bioimaging. *ACS Appl. Bio Mater.* 4, 2790–2797. doi:10.1021/acsabm.1c00011
- Croissant, J. G., Fatiev, Y., Almalik, A., and Khashab, N. M. (2017). Mesoporous Silica and Organosilica Nanoparticles: Physical Chemistry, Biosafety, Delivery Strategies, and Biomedical Applications. *Adv. Healthc. Mater.* 7, 1700831. doi:10.1002/adhm.201700831
- Del Canto, E., Flavin, K., Natali, M., Perova, T., and Giordani, S. (2010). Functionalization of Single-Walled Carbon Nanotubes with Optically Switchable Spiropyrans. *Carbon* 48, 2815–2824. doi:10.1016/j.carbon.2010.04.012
- Deng, Y., Zhang, X., Shen, H., He, Q., Wu, Z., Liao, W., et al. (2020). Application of the Nano-Drug Delivery System in Treatment of Cardiovascular Diseases. *Front. Bioeng. Biotechnol.* 7, 489. doi:10.3389/fbioe.2019.00489
- Eilmes, A. (2013). Spiropyran to Merocyanine Conversion: Explicit versus Implicit Solvent Modeling. *J. Phys. Chem. A* 117, 2629–2635. doi:10.1021/jp3117209
- Fahr, A., and Liu, X. (2007). Drug Delivery Strategies for Poorly Water-Soluble Drugs. *Expert Opin. Drug Delivery Drug Deliv.* 4, 403–416. doi:10.1517/17425247.4.4.403
- Fernández, M., Javadi, F., and Chudasama, V. (2018). Advances in Targeting the Folate Receptor in the Treatment/imaging of Cancers. *Chem. Sci.* 9, 790–810. doi:10.1039/C7SC04004K
- Franklin, R. B., and Costello, L. C. (2009). The Important Role of the Apoptotic Effects of Zinc in the Development of Cancers. *J. Cel. Biochem.* 106, 750–757. doi:10.1002/jcb.22049
- Ghani, M., Heiskanen, A., Kajtez, J., Rezaei, B., Larsen, N. B., Thomsen, P., et al. (2021a). On-Demand Reversible UV-Triggered Interpenetrating Polymer Network-Based Drug Delivery System Using the Spiropyran-Merocyanine Hydrophobicity Switch. *ACS Appl. Mater. Inter.* 13, 3591–3604. doi:10.1021/acsami.0c19081
- Ghani, M., Heiskanen, A., Thomsen, P., Alm, M., and Emnéus, J. (2021b). Molecular-Gated Drug Delivery Systems Using Light-Triggered Hydrophobic-To-Hydrophilic Switches. *ACS Appl. Bio Mater.* 4, 1624–1631. doi:10.1021/acsabm.0c01458
- Gnach, A., Lipinski, T., Bednarkiewicz, A., Rybka, J., and Capobianco, J. A. (2015). Upconverting Nanoparticles: Assessing the Toxicity. *Chem. Soc. Rev.* 44, 1561–1584. doi:10.1039/c4cs00177j
- Görner, H., and Chibisov, A. K. (1998). Complexes of Spiropyran-Derived Merocyanines with Metal Ions Thermally Activated and Light-Induced Processes. *Faraday Trans.* 94, 2557–2564. doi:10.1039/A803330G
- Hammarson, M., Nilsson, J. R., Li, S., Beke-Somfai, T., and Andréasson, J. (2013). Characterization of the Thermal and Photoinduced Reactions of Photochromic Spiropyran in Aqueous Solution. *J. Phys. Chem. B* 117, 13561–13571. doi:10.1021/jp408781p
- He, Y., Shao, L., Usman, I., Hu, Y., Pan, A., Liang, S., et al. (2020). A pH-Responsive Dissociable Mesoporous Silica-Based Nanoparticle Enabling Efficient Dual-Drug Co-delivery and Rapid Clearance for Cancer Therapy. *Biomater. Sci.* 8, 3418–3429. doi:10.1039/d0bm00204f
- Heiligman-Rim, R., Hirshberg, Y., and Fischer, E. (1961). 29. Photochromism in Some Spiropyranes. Part III. The Extent of Phototransformation. *J. Chem. Soc.* 156. doi:10.1039/jr9610000156
- Heiligman-Rim, R., Hirshberg, Y., and Fischer, E. (1962a). Photochromism in Spiropyranes. Part IV.1 Evidence for the Existence of Several Forms of the Colored Modification. *J. Phys. Chem.* 66, 2465–2470. doi:10.1021/j100818a035
- Heiligman-Rim, R., Hirshberg, Y., and Fischer, E. (1962b). Photochromism in Spiropyranes. Part V.1 on the Mechanism of Phototransformation. *J. Phys. Chem.* 66, 2470–2477. doi:10.1021/j100818a036
- Helms, V. (2019). *Principles of Computational Cell Biology: From Protein Complexes to Cellular Networks*. 2nd ed. Wiley VCH. doi:10.1628/978-3-16-157957-8
- Heng, S., Zhang, X., Pei, J., Adwal, A., Reineck, P., Gibson, B. C., et al. (2018). Spiropyran-Based Nanocarrier: A New Zn<sup>2+</sup>-Responsive Delivery System with Real-Time Intracellular Sensing Capabilities. *Chem. Eur. J.* 25, 854–862. doi:10.1002/chem.201804816
- Hirshberg, Y., and Fischer, E. (1954a). Photochromism and Reversible Multiple Internal Transitions in Some Spiropyranes at Low Temperatures. Part I. *J. Chem. Soc.* 297. doi:10.1039/jr9540000297
- Hirshberg, Y., and Fischer, E. (1954b). Photochromism and Reversible Multiple Internal Transitions in Some Spiropyranes at Low Temperatures. Part II. *J. Chem. Soc.* 3129. doi:10.1039/jr9540003129
- Jarosz, M., Olbert, M., Wyszogrodzka, G., Mlyniec, K., and Librowski, T. (2017). Antioxidant and Anti-inflammatory Effects of Zinc. Zinc-dependent NF- $\kappa$ B Signaling. *Inflammopharmacol.* 25, 11–24. doi:10.1007/s10787-017-0309-4
- Jhaveri, A. M., and Torchilin, V. P. (2014). Multifunctional Polymeric Micelles for Delivery of Drugs and siRNA. *Front. Pharmacol.* 5, 77. doi:10.3389/fphar.2014.00077
- Kajimoto, S., Mori, A., and Fukumura, H. (2010). Photo-controlled Phase Separation and Mixing of a Mixture of Water and 2-butoxyethanol Caused by Photochromic Isomerisation of Spiropyran. *Photochem. Photobiol. Sci.* 9, 208. doi:10.1039/b9pp00137a
- Kang, H., Rho, S., Stiles, W. R., Hu, S., Baek, Y., Hwang, D. W., et al. (2019). Size-Dependent EPR Effect of Polymeric Nanoparticles on Tumor Targeting. *Adv. Healthc. Mater.* 9, 1901223. doi:10.1002/adhm.201901223
- Karimipour, K., Keyvan Rad, J., Shirvalilou, S., Khoei, S., and Mahdavian, A. R. (2021). Spiropyran-based Photoswitchable Acrylic Nanofibers: A Stimuli-Responsive Substrate for Light Controlled C6 Glioma Cells Attachment/detachment. *Colloids Surf. B: Biointerfaces* 203, 111731. doi:10.1016/j.colsurfb.2021.111731
- Keiser, G. (2019). “Optical Fibers for Biomedical Applications,” in Handbook Of Optical Fibers. Editor G.-D. Peng (Springer).
- Keyvan Rad, J., Mahdavian, A. R., Khoei, S., and Janati Esfahani, A. (2016). FRET-based Acrylic Nanoparticles with Dual-Color Photoswitchable Properties in DU145 Human Prostate Cancer Cell Line Labeling. *Polymer* 98, 263–269. doi:10.1016/j.polymer.2016.06.042
- Keyvan Rad, J., Mahdavian, A. R., Khoei, S., and Shirvalilou, S. (2018). Enhanced Photogeneration of Reactive Oxygen Species and Targeted Photothermal Therapy of C6 Glioma Brain Cancer Cells by Folate-Conjugated Gold-Photoactive Polymer Nanoparticles. *ACS Appl. Mater. Inter.* 10, 19483–19493. doi:10.1021/acsami.8b05252
- Keyvan Rad, J., Mahdavian, A. R., Salehi-Mobarakeh, H., and Abdollahi, A. (2015). FRET Phenomenon in Photoreversible Dual-Color Fluorescent Polymeric Nanoparticles Based on Azocarbazole/Spiropyran Derivatives. *Macromolecules* 49, 141–152. doi:10.1021/acs.macromol.5b02401
- Khan, F., Katara, R., and Ramteke, S. (2010). Enhancement of Bioavailability of Cefpodoxime Proxetil Using Different Polymeric Microparticles. *AAPS PharmSciTech* 11, 1368–1375. doi:10.1208/s12249-010-9505-x
- Klajn, R. (2014). Spiropyran-based Dynamic Materials. *Chem. Soc. Rev.* 43, 148–184. doi:10.1039/C3CS60181A
- Koelsch, C. F. (1951). Steric Factors in Thermochromism of Spiropyranes and in Reactivities of Certain Methylene Groups. *J. Org. Chem.* 16, 1362–1370. doi:10.1021/jo50003a005
- Kortekaas, L., and Browne, W. R. (2019). The Evolution of Spiropyran: Fundamentals and Progress of an Extraordinarily Versatile Photochrome. *Chem. Soc. Rev.* 48, 3406–3424. doi:10.1039/c9cs00203k
- Krishna, V. D., Wu, K., Su, D., Cheeran, M. C. J., Wang, J.-P., and Perez, A. (2018). Nanotechnology: Review of Concepts and Potential Application of Sensing Platforms in Food Safety. *Food Microbiol.* 75, 47–54. doi:10.1016/j.fm.2018.01.025
- Lee, G., and Park, Y. (2018). Lanthanide-Doped Upconversion Nanocarriers for Drug and Gene Delivery. *Nanomaterials* 8, 511. doi:10.3390/nano8070511
- Lee, H.-i., Wu, W., Oh, J. K., Mueller, L., Sherwood, G., Peteanu, L., et al. (2007). Light-Induced Reversible Formation of Polymeric Micelles. *Angew. Chem. Int. Ed.* 46, 2453–2457. doi:10.1002/anie.200604278
- Li, X., Zhang, F., and Zhao, D. (2015). Lab on Upconversion Nanoparticles: Optical Properties and Applications Engineering via Designed Nanostructure. *Chem. Soc. Rev.* 44, 1346–1378. doi:10.1039/c4cs00163j
- Li, Z., Barnes, J. C., Bosoy, A., Stoddart, J. F., and Zink, J. I. (2012). Mesoporous Silica Nanoparticles in Biomedical Applications. *Chem. Soc. Rev.* 41, 2590. doi:10.1039/c1cs15246g

- Lim, D.-J., and Park, H. (2017). Near-infrared Light for On-Demand Drug Delivery. *J. Biomater. Sci. Polym. Edition* 29, 750–761. doi:10.1080/09205063.2017.1398994
- Liu, J., Luo, Z., Zhang, J., Luo, T., Zhou, J., Zhao, X., et al. (2016). Hollow Mesoporous Silica Nanoparticles Facilitated Drug Delivery via cascade pH Stimuli in Tumor Microenvironment for Tumor Therapy. *Biomaterials* 83, 51–65. doi:10.1016/j.biomaterials.2016.01.008
- Manzano, M., and Vallet-Regí, M. (2019). Mesoporous Silica Nanoparticles for Drug Delivery. *Adv. Funct. Mater.* 30, 1902634. doi:10.1002/adfm.201902634
- Martinho, N., Damgé, C., and Reis, C. P. (2011). Recent Advances in Drug Delivery Systems. *Jbnb* 02, 510–526. doi:10.4236/jbnb.2011.225062
- McMillan, T. J., Leatherman, E., Ridley, A., Shorrocks, J., Tobi, S. E., and Whiteside, J. R. (2010). Cellular Effects of Long Wavelength UV Light (UVA) in Mammalian Cells. *J. Pharm. Pharmacol.* 60, 969–976. doi:10.1211/jpp.60.8.0004
- Mihai Grumezescu, A. (2018). *Lipid Nanocarriers for Drug Targeting*. Oxford William Andrew Applied Science Publishers, An Imprint Of Elsevier.
- Minkin, V. I. (2004). Photo-, Thermo-, Solvato-, and Electrochromic Spiroheterocyclic Compounds. *Chem. Rev.* 104, 2751–2776. doi:10.1021/cr020088u
- Mohapatra, S. S., Ranjan, S., Dasgupta, N., Mishra, R. K., and Thomas, S. (2019). *Nanocarriers for Drug Delivery: Nanoscience and Nanotechnology in Drug Delivery*. Ma: Elsevier PP - Cambridge.
- Moore, C. M., Pendsé, D., and Emberton, M. (2009). Photodynamic Therapy for Prostate Cancer-A Review of Current Status and Future Promise. *Nat. Rev. Urol.* 6, 18–30. doi:10.1038/ncpuro1274
- Movia, D., Prina-Mello, A., Volkov, Y., and Giordani, S. (2010). Determination of Spiropyran Cytotoxicity by High Content Screening and Analysis for Safe Application in Bionanosensing. *Chem. Res. Toxicol.* 23, 1459–1466. doi:10.1021/tx100123g
- Mura, S., Nicolas, J., and Couvreur, P. (2013). Stimuli-responsive Nanocarriers for Drug Delivery. *Nat. Mater.* 12, 991–1003. doi:10.1038/nmat3776
- Nahain, A.-A., Lee, J.-E., Jeong, J. H., and Park, S. Y. (2013). Photoresponsive Fluorescent Reduced Graphene Oxide by Spiropyran Conjugated Hyaluronic Acid for *In Vivo* Imaging and Target Delivery. *Biomacromolecules* 14, 4082–4090. doi:10.1021/bm4012166
- Natali, M., Aakeröy, C., Desper, J., and Giordani, S. (2010a). The Role of Metal Ions and Counterions in the Switching Behavior of a Carboxylic Acid Functionalized Spiropyran. *Dalton Trans.* 39, 8269. doi:10.1039/c0dt00242a
- Natali, M., and Giordani, S. (2012a). Interaction Studies between Photochromic Spiropyran and Transition Metal Cations: the Curious Case of Copper. *Org. Biomol. Chem.* 10, 1162–1171. doi:10.1039/c1ob06375h
- Natali, M., and Giordani, S. (2012b). Molecular Switches as Photocontrollable “Smart” Receptors. *Chem. Soc. Rev.* 41, 4010. doi:10.1039/c2cs35015g
- Natali, M., Soldi, L., and Giordani, S. (2010b). A Photoswitchable Zn (II) Selective Spiropyran-Based Sensor. *Tetrahedron* 66, 7612–7617. doi:10.1016/j.tet.2010.07.035
- Netti, P. A., Berk, D. A., Swartz, M. A., Grodzinsky, A. J., and Jain, R. K. (2000). Role of Extracellular Matrix Assembly in Interstitial Transport in Solid Tumors. *Cancer Res.* 60, 2497–2503.
- Patra, J. K., Das, G., Fraceto, L. F., Campos, E. V. R., Rodriguez-Torres, M. d. P., Acosta-Torres, L. S., et al. (2018). Nano Based Drug Delivery Systems: Recent Developments and Future Prospects. *J. Nanobiotechnol.* 16, 71. doi:10.1186/s12951-018-0392-8
- Pattnaik, S., Surendra, Y., Rao, J. V., and Swain, K. (2020). Carbon Family Nanomaterials for Drug Delivery Applications. *Nanoeng. Biomater. Adv. Drug Deliv.*, 421–445. doi:10.1016/b978-0-08-102985-5.00018-8
- Pednekar, P. P., Godiyal, S. C., Jadhav, K. R., and Kadam, V. J. (2017). “Chapter 23 - Mesoporous Silica Nanoparticles: a Promising Multifunctional Drug Delivery System,” in *ScienceDirect*. Editors A. Ficaí and A. M. Grumezescu (Elsevier).
- Perry, A., Green, S. J., Horsell, D. W., Horne, S. M., and Wood, M. E. (2015). A Pyrene-Appended Spiropyran for Selective Photo-Switchable Binding of Zn(II): UV-Visible and Fluorescence Spectroscopy Studies of Binding and Non-covalent Attachment to Graphene, Graphene Oxide and Carbon Nanotubes. *Tetrahedron* 71, 6776–6783. doi:10.1016/j.tet.2015.07.035
- Phillips, J. P., Mueller, A., and Przystal, F. (1965). Photochromic Chelating Agents. *J. Am. Chem. Soc.* 87, 4020. doi:10.1021/ja01095a067
- Pimienta, V., Lavabre, D., Levy, G., Samat, A., Guglielmetti, R., and Micheau, J. C. (1996). Kinetic Analysis of Photochromic Systems under Continuous Irradiation. Application to Spiropyran. *J. Phys. Chem.* 100, 4485–4490. doi:10.1021/jp9531117
- Prasad, A. S. (2014). Zinc Is an Antioxidant and Anti-inflammatory Agent: Its Role in Human Health. *Front. Nutr.* 1, 14. doi:10.3389/fnut.2014.00014
- Radu, A., Byrne, R., Alhashimi, N., Fusaro, M., Scarmagnani, S., and Diamond, D. (2009). Spiropyran-based Reversible, Light-Modulated Sensing with Reduced Photofatigue. *J. Photochem. Photobiol. A: Chem.* 206, 109–115. doi:10.1016/j.jphotochem.2009.05.022
- Raina, N., Rani, R., Khan, A., Nagpal, K., and Gupta, M. (2019). Interpenetrating Polymer Network as a pioneer Drug Delivery System: a Review. *Polym. Bull.* 77, 5027–5050. doi:10.1007/s00289-019-02996-5
- Razavi, B., Abdollahi, A., Roghani-Mamaqani, H., and Salami-Kalajahi, M. (2020). Light- and Temperature-Responsive Micellar Carriers Prepared by Spiropyran-Initiated Atom Transfer Polymerization: Investigation of Photochromism Kinetics, Responsivities, and Controlled Release of Doxorubicin. *Polymer* 187, 122046. doi:10.1016/j.polymer.2019.122046
- Rouquerol, J., Avnir, D., Fairbridge, C. W., Everett, D. H., Haynes, J. M., Pernicone, N., et al. (1994). Recommendations for the Characterization of Porous Solids (Technical Report). *Pure Appl. Chem.* 66, 1739–1758. doi:10.1351/pac199466081739
- Rwei, A. Y., Wang, W., and Kohane, D. S. (2015). Photoresponsive Nanoparticles for Drug Delivery. *Nano Today* 10, 451–467. doi:10.1016/j.nantod.2015.06.004
- Schumers, J.-M., Fustin, C.-A., and Gohy, J.-F. (2010). Light-Responsive Block Copolymers. *Macromol. Rapid Commun.* 31, 1588–1607. doi:10.1002/marc.201000108
- Shen, H., Zhou, M., Zhang, Q., Keller, A., and Shen, Y. (2015). Zwitterionic Light-Responsive Polymeric Micelles for Controlled Drug Delivery. *Colloid Polym. Sci.* 293, 1685–1694. doi:10.1007/s00396-015-3550-7
- Soleymani Abyaneh, H., Vakili, M. R., Zhang, F., Choi, P., and Lavasanifar, A. (2015). Rational Design of Block Copolymer Micelles to Control Burst Release at a Nanoscale Dimension. *Acta Biomater.* 24, 127–139. doi:10.1016/j.actbio.2015.06.017
- Son, S., Shin, E., and Kim, B.-S. (2014). Light-Responsive Micelles of Spiropyran Initiated Hyperbranched Polyglycerol for Smart Drug Delivery. *Biomacromolecules* 15, 628–634. doi:10.1021/bm401670t
- Stafforst, T., and Hilvert, D. (2008). Kinetic Characterization of Spiropyran in Aqueous media. *Chem. Commun.*, 287–288. doi:10.1039/b818050d
- Sun, G., Fang, H., Cheng, C., Lu, P., Zhang, K., Walker, A. V., et al. (2009). Benzaldehyde-Functionalized Polymer Vesicles. *ACS Nano* 3, 673–681. doi:10.1021/nn8007977
- Timko, B. P., Dvir, T., and Kohane, D. S. (2010). Remotely Triggerable Drug Delivery Systems. *Adv. Mater.* 22, 4925–4943. doi:10.1002/adma.201002072
- Tong, R., Chiang, H. H., and Kohane, D. S. (2013). Photoswitchable Nanoparticles for *In Vivo* Cancer Chemotherapy. *Proc. Natl. Acad. Sci.* 110, 19048–19053. doi:10.1073/pnas.1315336110
- Tong, R., Hemmati, H. D., Langer, R., and Kohane, D. S. (2012). Photoswitchable Nanoparticles for Triggered Tissue Penetration and Drug Delivery. *J. Am. Chem. Soc.* 134, 8848–8855. doi:10.1021/ja211888a
- Tu, L., Liu, X., Wu, F., and Zhang, H. (2015). Excitation Energy Migration Dynamics in Upconversion Nanomaterials. *Chem. Soc. Rev.* 44, 1331–1345. doi:10.1039/c4cs00168k
- Tyer, N. W., and Becker, R. S. (1970). Photochromic Spiropyran. I. Absorption Spectra and Evaluation of the  $\pi$ -electron Orthogonality of the Constituent Halves. *J. Am. Chem. Soc.* 92, 1289–1294. doi:10.1021/ja00708a031
- Vaupel, P., Kallinowski, F., and Okunieff, P. (1989). Blood Flow, Oxygen and Nutrient Supply, and Metabolic Microenvironment of Human Tumors: A Review. *Cancer Res.* 49, 6449–6465.
- Venditti, I. (2019). Morphologies and Functionalities of Polymeric Nanocarriers as Chemical Tools for Drug Delivery: A Review. *J. King Saud Univ. - Sci.* 31, 398–411. doi:10.1016/j.jksus.2017.10.004
- Vlassioudis, I., Park, C.-D., Vail, S. A., Gust, D., and Smirnov, S. (2006). Control of Nanopore Wetting by a Photochromic Spiropyran: A Light-Controlled Valve and Electrical Switch. *Nano Lett.* 6, 1013–1017. doi:10.1021/nl060313d
- Wang, D., Zhang, T., Wu, B., Ye, C., Wei, Z., Cao, Z., et al. (2019). Reversibly Photoswitchable Dual-Color Fluorescence and Controlled Release Properties of

- Polymeric Nanoparticles. *Macromolecules* 52, 7130–7136. doi:10.1021/acs.macromol.9b01735
- Wang, L., and Li, Q. (2018). Photochromism into Nanosystems: towards Lighting up the Future Nanoworld. *Chem. Soc. Rev.* 47, 1044–1097. doi:10.1039/c7cs00630f
- Wang, X., Hu, J., Liu, G., Tian, J., Wang, H., Gong, M., et al. (2015). Reversibly Switching Bilayer Permeability and Release Modules of Photochromic Polymersomes Stabilized by Cooperative Noncovalent Interactions. *J. Am. Chem. Soc.* 137, 15262–15275. doi:10.1021/jacs.5b10127
- Weissleder, R. (2001). A Clearer Vision for *In Vivo* Imaging. *Nat. Biotechnol.* 19, 316–317. doi:10.1038/86684
- Wen, H., Jung, H., and Li, X. (2015). Drug Delivery Approaches in Addressing Clinical Pharmacology-Related Issues: Opportunities and Challenges. *AAPS J.* 17, 1327–1340. doi:10.1208/s12248-015-9814-9
- Xing, Q., Li, N., Chen, D., Sha, W., Jiao, Y., Qi, X., et al. (2014). Light-responsive Amphiphilic Copolymer Coated Nanoparticles as Nanocarriers and Real-Time Monitors for Controlled Drug Release. *J. Mater. Chem. B* 2, 1182. doi:10.1039/C3TB21269F
- Yadav, S., Sharma, A. K., and Kumar, P. (2020). Nanoscale Self-Assembly for Therapeutic Delivery. *Front. Bioeng. Biotechnol.* 8, 127. doi:10.3389/fbioe.2020.00127
- Yang, P., Gai, S., and Lin, J. (2012). Functionalized Mesoporous Silica Materials for Controlled Drug Delivery. *Chem. Soc. Rev.* 41, 3679. doi:10.1039/c2cs15308d
- Yildiz, I., Impellizzeri, S., Deniz, E., McCaughan, B., Callan, J. F., and Raymo, F. M. (2011). Supramolecular Strategies to Construct Biocompatible and Photoswitchable Fluorescent Assemblies. *J. Am. Chem. Soc.* 133, 871–879. doi:10.1021/ja107341f
- Zhang, Y., Huang, Y., and Li, S. (2014). Polymeric Micelles: Nanocarriers for Cancer-Targeted Drug Delivery. *AAPS PharmSciTech* 15, 862–871. doi:10.1208/s12249-014-0113-z
- Zhou, L., Chen, Z., Dong, K., Yin, M., Ren, J., and Qu, X. (2013). DNA-mediated Construction of Hollow Upconversion Nanoparticles for Protein Harvesting and Near-Infrared Light Triggered Release. *Adv. Mater.* 26, 2424–2430. doi:10.1002/adma.201304437
- Zielińska, A., Carreiró, F., Oliveira, A. M., Neves, A., Pires, B., Venkatesh, D. N., et al. (2020). Polymeric Nanoparticles: Production, Characterization, Toxicology and Ecotoxicology. *Molecules* 25, 3731. doi:10.3390/molecules25163731

**Conflict of Interest:** The authors declare that the research was conducted in the absence of any commercial or financial relationships that could be construed as a potential conflict of interest.

**Publisher's Note:** All claims expressed in this article are solely those of the authors and do not necessarily represent those of their affiliated organizations, or those of the publisher, the editors and the reviewers. Any product that may be evaluated in this article, or claim that may be made by its manufacturer, is not guaranteed or endorsed by the publisher.

Copyright © 2021 Fagan, Bartkowski and Giordani. This is an open-access article distributed under the terms of the Creative Commons Attribution License (CC BY). The use, distribution or reproduction in other forums is permitted, provided the original author(s) and the copyright owner(s) are credited and that the original publication in this journal is cited, in accordance with accepted academic practice. No use, distribution or reproduction is permitted which does not comply with these terms.





# Chaotropic and Kosmotropic Anions Regulate the Outcome of Enzyme-Mediated Dynamic Combinatorial Libraries of Cyclodextrins in Two Different Ways

Andreas Erichsen, Dennis Larsen and Sophie R. Beeren\*

Department of Chemistry, Technical University of Denmark, Kongens Lyngby, Denmark

## OPEN ACCESS

### Edited by:

Anna McConnell,  
University of Kiel, Germany

### Reviewed by:

Werner M. Nau,  
Jacobs University Bremen, Germany  
Nicholas White,  
Australian National University,  
Australia

### \*Correspondence:

Sophie R. Beeren  
sopbee@kemi.dtu.dk

### Specialty section:

This article was submitted to  
Supramolecular Chemistry,  
a section of the journal  
Frontiers in Chemistry

Received: 07 June 2021

Accepted: 12 July 2021

Published: 03 August 2021

### Citation:

Erichsen A, Larsen D and Beeren SR  
(2021) Chaotropic and Kosmotropic  
Anions Regulate the Outcome of  
Enzyme-Mediated Dynamic  
Combinatorial Libraries of  
Cyclodextrins in Two Different Ways.  
Front. Chem. 9:721942.  
doi: 10.3389/fchem.2021.721942

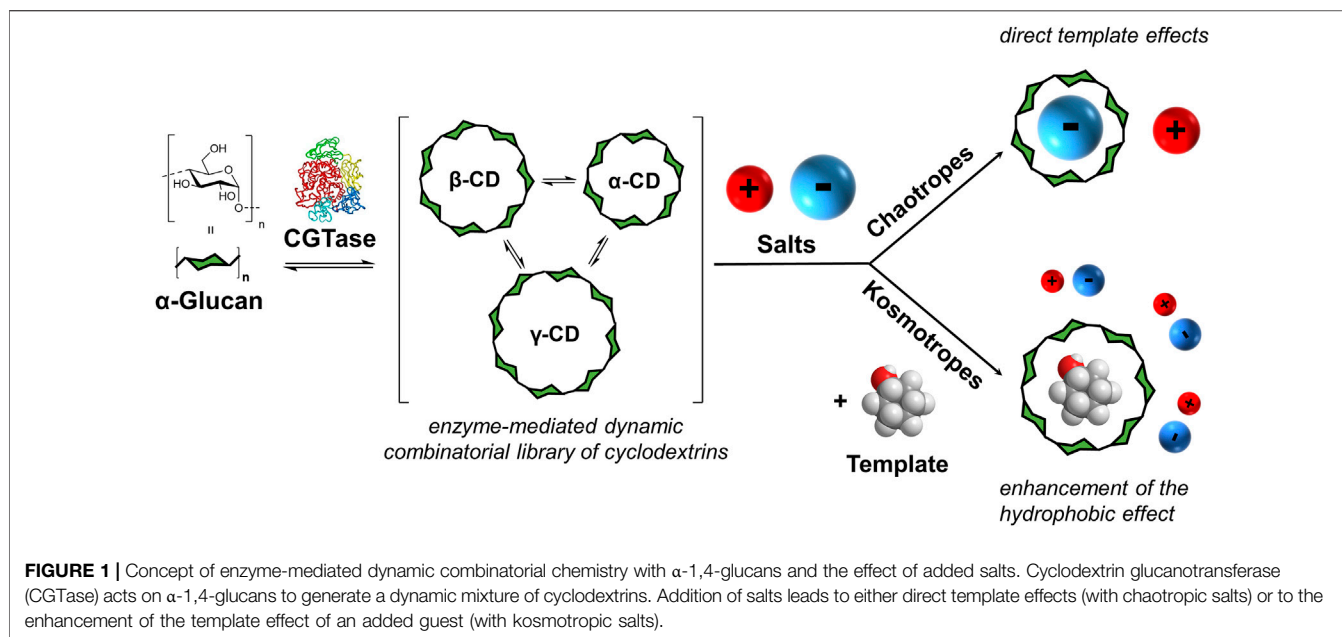
We demonstrate how different anions from across the Hofmeister series can influence the behavior of enzyme-mediated dynamic combinatorial libraries of cyclodextrins (CDs). Using cyclodextrin glucanotransferase to catalyze reversible transglycosylation, dynamic mixtures of interconverting cyclodextrins can be formed wherein the relative concentrations of  $\alpha$ -CD,  $\beta$ -CD and  $\gamma$ -CD is determined by their intrinsic stabilities and any stabilizing influences of added template (guest) molecules. Here, we find that addition of high concentrations of kosmotropic anions can be used to enhance the effects of added hydrophobic templates, while chaotropic anions can themselves act as templates, causing predictable and significant changes in the cyclodextrin composition due to weak, but specific, binding interactions with  $\alpha$ -CD.

**Keywords:** dynamic combinatorial chemistry, supramolecular chemistry, anions, cyclodextrins, cyclodextrin glucanotransferase, templated synthesis, systems chemistry

## INTRODUCTION

Since the groundbreaking work of Franz Hofmeister more than a century ago into how salts affect the solubility of proteins (Hofmeister, 1888), countless studies have repeatedly revealed the Hofmeister series of anions:  $F^-$ ,  $SO_4^{2-}$ ,  $AcO^-$ ,  $Cl^-$ ,  $Br^-$ ,  $NO_3^-$ ,  $ClO_3^-$ ,  $I^-$ ,  $ClO_4^-$  and  $SCN^-$ . Kosmotropes, such as  $F^-$  and  $SO_4^{2-}$ , generally decrease the solubility of proteins and other solutes (salting out), and while the rules governing these phenomena are not fully understood, these ions are said to enhance the hydrophobic effect (Gibb, 2011). Chaotropes, such as  $ClO_4^-$  and  $SCN^-$ , generally increase the solubility of proteins and other solutes (salting in), cause the denaturation of proteins at high concentrations and diminish the hydrophobic effect. The affinity of chaotropic anions towards hydrophobic surfaces allow them to compete with the interactions between hydrophobic solutes (Gibb and Gibb, 2011). Chaotropic anions form complexes with hosts that have hydrophobic cavities, such as cavitands and cyclodextrins (CDs) (Sullivan et al., 2018). The binding of chaotropic anions to hydrophobic solutes is associated with a certain thermodynamic fingerprint—a favorable enthalpy and an entropic penalty—which has recently been characterized as a generic driving force under the term “the chaotropic effect” by Nau and coworkers (Assaf et al., 2015; Assaf and Nau, 2018). These authors stressed that the chaotropic effect should be distinguished from the classical hydrophobic effect, where the thermodynamic signature is a favorable entropic term. Understanding the different influences of kosmotropes, chaotropes and hydrophobes on self-assembly processes in aqueous solution, both as modulators of solvent effects (Kunz et al., 2004;





Gibb, 2011, Gibb, 2019; van der Vegt and Nayar, 2017) and as recognition motifs (Busschaert et al., 2015; Hillyer and Gibb, 2016; Assaf and Nau, 2018), is key to the successful design of supramolecular systems. In this work, we examine how the interplay between kosmotropic, chaotropic and hydrophobic effects modulates the behavior of an enzyme-mediated dynamic system of cyclodextrins.

Dynamic combinatorial chemistry (DCC) is a powerful method to explore molecular self-assembly and the templated synthesis of complex molecular architectures using reversible bond formation under thermodynamic control (Otto et al., 2002; Corbett et al., 2006; Lehn, 2007; Ponnuswamy et al., 2012; Li et al., 2013). We have previously described how dynamic combinatorial libraries (DCLs) of interconverting cyclodextrins can be generated by employing an enzyme that enables reversible transglycosylation (Larsen and Beeren, 2019, Larsen and Beeren, 2020, Larsen and Beeren, 2021). Cyclodextrins are macrocycles formed from α-1,4-linked glucopyranose units. The native cyclodextrins, α-CD, β-CD and γ-CD, with six, seven, and eight glucopyranose units, respectively, exhibit truncated cone-like structures and are widely utilized hosts for the encapsulation of hydrophobic molecules in the foods, pharmaceutical and cosmetics industries (Hedges, 1998; Del Valle, 2004; Sharma and Baldi, 2016). Cyclodextrin glucanotransferase (CGTase) catalyzes both fast, reversible inter- and intramolecular transglycosylation and slow hydrolysis of α (1–4)-glycosidic bonds (Terada et al., 1997; Tewari et al., 1997; Uitdehaag et al., 2002). Exposure of an α-1,4-glucan source to CGTase, therefore, generates a dynamic mixture of linear α-1,4-glucans (maltooligosaccharides) and cyclic α-1,4-glucans (cyclodextrins) (Larsen and Beeren, 2019). As α-CD, β-CD and γ-CD are intrinsically more stable than their linear counterparts, a complex dynamic system is formed in which α-CD, β-CD and γ-CD are kinetically trapped and transiently

form as the primary products before being eventually converted to glucose.

We previously showed that even though α-CD, β-CD and γ-CD form out-of-equilibrium in this enzyme-mediated dynamic system, they exist in a subsystem that operates under *pseudo*-thermodynamic control (Larsen and Beeren, 2019). The distribution of products formed can be controlled by addition of a template that binds selectively to specific cyclodextrins. We were able to produce α-CD, β-CD or γ-CD with 99% selectivity using sodium dodecyl sulfate, 1-adamantanecarboxylic acid and sodium tetraphenylborate as templates (Larsen and Beeren, 2019, Larsen and Beeren, 2020). While investigating different reaction conditions, it was also found that CGTase could not only tolerate very high concentrations of NaNO<sub>3</sub> (up to 7.5 M) but that the presence of NaNO<sub>3</sub> altered the distribution of cyclodextrins in the DCL that was formed. These results encouraged us to explore how the addition of a range of sodium salts in high concentrations would influence the cyclodextrin distribution in our dynamic system. Here, we present how the addition of salts to CGTase-mediated DCLs of cyclodextrins can either enhance the template effects of added guests, in the case of kosmotropes, or lead to direct template effects, in the case of chaotropes (Figure 1).

## MATERIALS, INSTRUMENTATION AND METHODS

### Materials

All chemicals and solvents of HPLC (high performance liquid chromatography) grade were obtained from commercial suppliers and used as received. High purity water used both in reactions and chromatographic analysis was obtained using a Merck Millipore Synergy UV water purification system. Colorless Corning CoStar 0.65 ml centrifuge tubes were used for enzymatic

reactions and sample preparation (dilution and centrifugation), while colorless 2 ml glass vials with PTFE-lined screw-cap septa and 0.2 ml glass inserts were used for short-term sample storage and injection on HPLC equipment. A stock solution of the enzyme CGTase derived from *Bacillus macerans* was received as a kind gift from Amano Enzyme, Inc., Nagoya, Japan. The stock solution was stored at 5°C and used as received.

## Instrumentation

Chromatographic analysis was performed on a Thermo Scientific Dionex Ultimate 3000 HPLC (ultra-high pressure) system equipped with a Waters Acquity UPLC BEH Amide 1.7  $\mu\text{m}$  2.1  $\times$  150 mm column maintained at 30°C, and an autosampler module maintained at 20°C. Detection was carried out using an Agilent Technologies 1,260 Infinity ELSD (evaporative light scattering detector), operating with the evaporator at 90°C, nebulizer at 70°C, and a  $\text{N}_2$  gas flow of 1.0 L/min. The ELSD enables the detection of the chromophore-lacking oligosaccharides. Calibration curves from 0.01 mg/ml to 10 mg/ml for  $\alpha$ -,  $\beta$ - and  $\gamma$ -CD and linear  $\alpha$ -1,4-glucans up to maltooctaose were used to correct for differences in the ELS detector response for different oligosaccharides. The calibrations were based on masses injected (0.018–3.66  $\mu\text{g}$ ) and the resulting response curves were fitted to a simple power equation  $M = kA^p$  (where  $M$  is the injected mass of compound,  $A$  is the area under the peak in the chromatogram and  $k$  and  $p$  are fitted parameters) using non-linear curve fitting (in OriginPro 2018b from OriginLab Corp.) See recent paper for details (Larsen and Beeren, 2021). The gradient profile for HPLC runs was a linear gradient from 75% acetonitrile in water to 55% acetonitrile in water over 8 min with a flow rate of 0.6 ml/min. Both eluents contained 0.1% formic acid by volume.

## Enzymatic Reactions and Analysis

Reaction mixtures with the desired concentrations of salts were prepared by mixing appropriate amounts of two types of stock solutions in buffered water (50 mM sodium phosphate at pH 7.5): 1) a solution containing  $\alpha$ -CD (10 mg/ml) and various salts (4.0 M); and 2) a solution containing  $\alpha$ -CD (10 mg/ml). In templated experiments, cyclohexanol or cyclohexanecarboxylic acid was dissolved in these resulting mixtures at a concentration of 10 mM. For the experiments with a higher concentration of sodium phosphate buffer, a stock solution of  $\alpha$ -CD (10 mg/ml) in 0.45 M sodium phosphate buffer at pH 7.5 was prepared. The starting mixtures containing salt,  $\alpha$ -CD and template (if any) in buffer were then aliquoted (165–365  $\mu\text{l}$ ) into reaction vessels and kept at ambient temperature. All reactions were then initiated by adding CGTase stock solution (50  $\mu\text{l}$  per ml of starting mixture) to the starting mixtures followed by thorough mixing. The reactions were then monitored at various time points: Aliquots for analysis (4–5  $\mu\text{l}$ ) were taken out and rapidly diluted (31 fold) in a 1% trifluoroacetic acid (TFA) solution in 3:1 acetonitrile/water with 10 mM ammonium chloride to stop the enzymatic reaction. For experiments with NaCl, aliquots for analysis (20  $\mu\text{l}$ ) were taken out and rapidly diluted (six fold) in a 1% TFA solution in water. Samples were then centrifuged (10,000 RPM for 4 min) to prevent column blockage by insoluble species such as enzyme

and salts, and the top fractions (leaving behind 20  $\mu\text{l}$ ) were then transferred to 2 ml glass vials with 0.2 ml glass inserts, kept at 20°C and then injected on the HPLC instrument within 48 h. Injection volumes were 10  $\mu\text{l}$  or 2  $\mu\text{l}$  (for 31-fold and 6-fold diluted samples, respectively). Peaks in the chromatograms corresponding to  $\alpha$ -CD,  $\beta$ -CD and  $\gamma$ -CD and linear  $\alpha$ -1,4-glucans up to maltooctaose were identified by comparison with authentic samples obtained from commercial suppliers.

## Simulations of Dynamic Combinatorial Libraries

Simulations of dynamic combinatorial libraries (DCLs) with and without the anion  $\text{SCN}^-$  were carried out using the *DCLSim* software developed in the Otto group (Corbett et al., 2004) and kindly made available to us. The program requires input of the concentration of the building block (glucopyranose units in this case), the composition of the oligomers (library members) formed in the DCL ( $\alpha$ -CD,  $\beta$ -CD and  $\gamma$ -CD, with six, seven or eight glucose units in this case), the relative formation constants  $K_f$  of the library members (determined from the *pseudo*-equilibrium composition of  $\alpha$ -,  $\beta$ -, and  $\gamma$ -CD in an untemplated library), the binding constants ( $K_a$ ) of each library member to the template ( $\text{SCN}^-$ ) and the concentration of the template. Details about how the relative formation constants  $K_f$  of  $\alpha$ -,  $\beta$ -, and  $\gamma$ -CD were calculated can be found in the **Supplementary Material**. The binding constants used were obtained from a study carried out by Tokunaga and coworkers, where the authors used  $^1\text{H}$ -NMR spectroscopy to determine binding constants between inorganic anions and cyclodextrins (Matsui et al., 1997).

## RESULTS AND DISCUSSION

### The Influence of a Series of Anions on Cyclodextrin DCLs

To explore the influence of anions on CGTase-mediated DCLs of cyclodextrins, we examined a series of DCLs prepared in the presence of different sodium salts at concentrations up to 4 M. The following series of anions was investigated, ranked according to the Hofmeister series:  $\text{HPO}_4^{2-}/\text{H}_2\text{PO}_4^- > \text{Cl}^- > \text{NO}_3^- > \text{Br}^- > \text{ClO}_4^- > \text{SCN}^-$ . The libraries were prepared by addition of CGTase (50  $\mu\text{l}$  stock solution per ml reaction mixture) to solutions of  $\alpha$ -CD (10 mg/ml) with the desired sodium salts at various concentrations up to 4 M concentration in phosphate buffer (50 mM, pH 7.5). Despite the lower solubility of sodium phosphates, we chose also to include phosphate buffer in this study albeit at a maximum of 0.45 M. The library compositions were monitored as the dynamic system evolved over time using hydrophilic interaction liquid chromatography (HILIC) with an evaporative light scattering detector (ELSD), which enabled the separation and quantification of the chromophore-lacking glucan mixtures. The influence of varying concentrations of different salts on the equilibrium cyclodextrin distribution and the time taken to reach this steady distribution is summarized for all anions tested in **Table 1**.

**TABLE 1** | Summary of results (relative CD yield at *pseudo*-equilibrium and time to *pseudo*-equilibrium) for CGTase-mediated Dynamic Combinatorial Libraries (DCLs) of cyclodextrins in the presence of different sodium salts.

Entry #	Salt <sup>a</sup>	Salt concentration (M)	Time to <i>pseudo</i> -equilibrium (h) <sup>b</sup>	Relative CD yield at <i>pseudo</i> -equilibrium (% by weight) <sup>c</sup>		
				$\alpha$ -CD	$\beta$ -CD	$\gamma$ -CD
1	No salt	—	1	32	57	11
2	HPO <sub>4</sub> <sup>2-</sup> /H <sub>2</sub> PO <sub>4</sub> <sup>-</sup>	0.45	1	36	54	10
3	NaCl	1	1	37	54	10
4	NaCl	2	2	37	54	9
5	NaCl	3	2	37	53	9
6	NaCl	4	4	40	52	8
7	NaNO <sub>3</sub>	1	1	48	45	7
8	NaNO <sub>3</sub>	2	1.5	49	45	6
9	NaNO <sub>3</sub>	3	2	51	43	6
10	NaNO <sub>3</sub>	4	2	55	40	5
11	NaBr	1	1	41	50	8
12	NaBr	2	1.5	44	49	7
13	NaBr	3	2.5	48	46	6
14	NaBr	4	4	54	40	5
15	NaClO <sub>4</sub>	1	3	62	36	2
16	NaClO <sub>4</sub>	2	6	65	34	1
17	NaClO <sub>4</sub>	3	<sup>d</sup>	—	—	—
18	NaSCN	1	2	72	26	2
19	NaSCN	2	8	75	23	2
20	NaSCN	3	<sup>d</sup>	—	—	—

<sup>a</sup>Conditions:  $\alpha$ -CD (10 mg/ml) in sodium phosphate buffer (50 mM, pH 7.5) treated with CGTase at room temperature.

<sup>b</sup>Estimated time (to the nearest half hour) until a steady distribution of CDs was obtained.

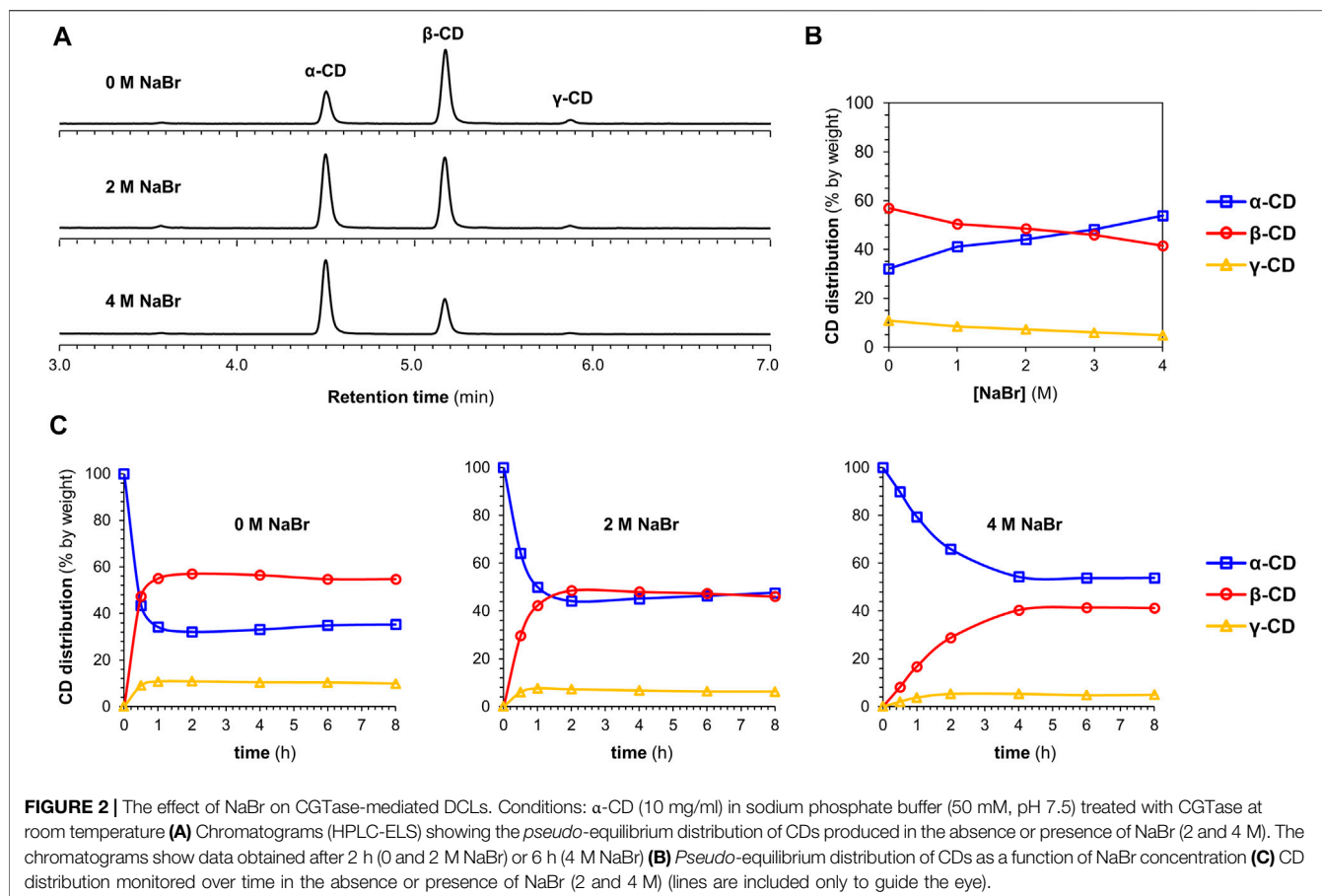
<sup>c</sup>Values taken from a single data point after a steady distribution of CDs was obtained. (Instrumental uncertainty of about  $\pm 2\%$  points in the relative CD yields).

<sup>d</sup>Zero or close to zero enzyme activity, presumably due to enzyme denaturation.

**Figure 2** shows representative data obtained for DCLs of cyclodextrins prepared in the presence of increasing amounts of NaBr. **Figure 2A** depicts chromatograms showing the distributions of  $\alpha$ -1,4-glucan products formed after *pseudo*-equilibrium is obtained (2–6 h) in the absence and presence of different concentrations of NaBr. It is immediately evident that the relative concentration of  $\alpha$ -CD increased at the expense of  $\beta$ -CD and  $\gamma$ -CD in the presence of increasing concentrations of NaBr. Amplifications of  $\alpha$ -CD were seen for all the anions tested, but the magnitude of the effect was anion-dependent (**Table 1**). The evolution of each DCL was monitored over time (**Supplementary Figures 1–6**). For all DCLs, the CD yield decreased gradually overtime, due to background hydrolysis and the consequent build-up of short linear  $\alpha$ -1,4-glucan and glucose. For the DCL without salt, a steady distribution of  $\alpha$ -CD,  $\beta$ -CD and  $\gamma$ -CD was obtained after approximately one hour, when a *pseudo*-thermodynamic equilibrium of cyclodextrins was reached. At this point >90% of the glucan material was still present as cyclodextrins. With increasing concentrations of NaBr, the evolution of the DCL became slower, and it took up to approximately four hours (with 4 M NaBr) to reach a steady distribution of cyclodextrins (**Figure 2C**). In all cases, addition of anions led to a slower evolution of the dynamic enzymatic system (**Supplementary Figures 1–6**). With the chaotropic anions ClO<sub>4</sub><sup>-</sup> and SCN<sup>-</sup> (**Table 1**, entries 15–20) this retardation was quite significant at 1–2 M concentrations, and at concentrations of 3 M and higher, the activity of the enzyme was zero or close to zero within just 30 min of

being exposed to the salt solutions (**Supplementary Figure 8**), presumably due to denaturation of the enzyme under these conditions.

The equilibrium cyclodextrin distributions obtained in the presence of different anions at 2 M concentration are summarized in **Figure 3**. Following a largely systematic trend, the relative yield of  $\alpha$ -CD increases upon moving from the most kosmotropic anions (HPO<sub>4</sub><sup>2-</sup>/H<sub>2</sub>PO<sub>4</sub><sup>-</sup>, Cl<sup>-</sup>, minor changes) to the most chaotropic anions (ClO<sub>4</sub><sup>-</sup>, SCN<sup>-</sup>, large changes). These results suggest that all the tested anions have a specific, albeit weak affinity for  $\alpha$ -CD and function as templates in the enzyme-mediated DCL of cyclodextrins. Selected binding constants for Cl<sup>-</sup>, NO<sub>3</sub><sup>-</sup>, Br<sup>-</sup>, SCN<sup>-</sup> and ClO<sub>4</sub><sup>-</sup> interacting with  $\alpha$ -CD,  $\beta$ -CD and  $\gamma$ -CD have previously been reported (**Table 2**). These binding constants were determined using a variety of techniques: <sup>1</sup>H-NMR spectroscopy (Matsui et al., 1997), conductance (Wojcik and Rohrbach, 1975), potentiometry (Gelb et al., 1983), spectrophotometry (Buvári and Barcza, 1979), volatilization (Sanemasa et al., 1988) and isothermal titration calorimetry (Sullivan et al., 2018). While the numeric values of the binding constants vary somewhat depending on the method, the trends are certainly clear. In the kosmotropic end of the Hofmeister series, the binding of Cl<sup>-</sup> to  $\alpha$ -CD was found to be negligible in most cases, which corresponds well with our data, where only minor changes in the cyclodextrin distribution occur upon addition of Cl<sup>-</sup> (**Table 1**, entries 3–6). The minor increase in the relative yield of  $\alpha$ -CD, from 32 to 37%, does, however, indicate that there could

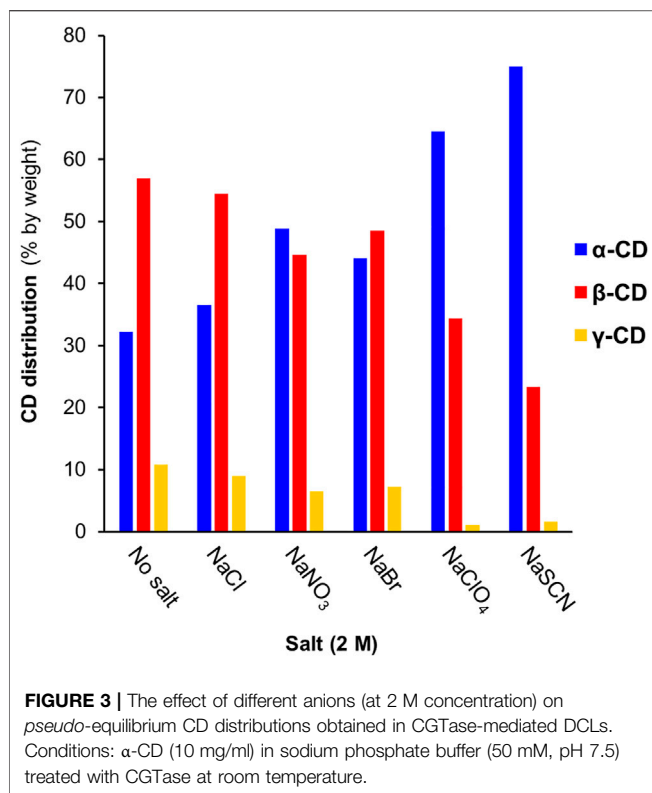


be a very weak binding between  $\alpha$ -CD and  $\text{Cl}^-$ , as found in some cases in the literature (Wojcik and Rohrbach, 1975). Next in the series, both  $\text{NO}_3^-$  and  $\text{Br}^-$  bind to  $\alpha$ -CD with small and similar binding constants ( $1\text{--}4\text{ M}^{-1}$ ), which matches the small but significant amplification of  $\alpha$ -CD observed with these anions (Table 1, entries 7–14). The chaotropic anions  $\text{SCN}^-$  and  $\text{ClO}_4^-$  have significantly higher affinities for  $\alpha$ -CD ( $16\text{--}46\text{ M}^{-1}$ ) and led to much larger changes in the cyclodextrin distribution (Table 1, entries 15–20). The fact that the amplification of  $\alpha$ -CD is larger with  $\text{SCN}^-$  than  $\text{ClO}_4^-$  can be explained by the relatively higher competing affinity of  $\text{ClO}_4^-$  for  $\beta$ -CD, as the distribution obtained in a DCL is influenced by the binding interaction of the template with all members of a library. It is noteworthy that each of the small anions tested amplified and bound most strongly to  $\alpha$ -CD, whereas we have previously observed the amplification of larger CDs with 8, 9, and 10 glucopyranose units in the presence of the large superchaotropic anion  $\text{B}_{12}\text{I}_{12}^{2-}$  (diameter 11.7 Å) (Larsen and Beeren, 2019). There is clearly, thus, a relationship between the size of the anion (Table 2 column 3) and the preferential formation of the CD(s) with a suitable size cavity. Overall, we found that the addition of anions in high concentrations to the CGTase-mediated DCLs of cyclodextrins leads to changes characteristic of template effects, and remarkably, the

system remains dynamic even at 2 M concentrations of the denaturing salts NaSCN and  $\text{NaClO}_4$ .

## DCL Simulation to Support Templating Effects of Chaotropes

To gain further support for our conclusion that chaotropic anions influence the production of specific cyclodextrins in CGTase-mediated dynamic systems through direct template effects, we sought to simulate the DCL generated in the presence of increasing concentrations of NaSCN. *DCLSim* is a software developed in the Otto group (Corbett et al., 2004) that enables the prediction of product distributions in templated DCLs operating under thermodynamic control. To simulate the DCLs, binding constants for the interaction of the template with each library member ( $\alpha$ -CD,  $\beta$ -CD and  $\gamma$ -CD) is required, and this was available for  $\text{SCN}^-$  (Table 2, column 1, Matsui et al., 1997). The relative formation constants  $K_f$  for  $\alpha$ -CD,  $\beta$ -CD and  $\gamma$ -CD are also needed for the simulation and these could be calculated from the relative concentrations of  $\alpha$ -CD,  $\beta$ -CD and  $\gamma$ -CD generated at equilibrium in the DCL without salt. We simulated DCLs of cyclodextrins with  $\text{SCN}^-$  at 0, 1 and 2 M concentrations. The results, summarized in Figure 4, show that the simulations correlate well with the experimental results, supporting the conclusion that chaotropic anions function as



**TABLE 2 |** Binding constants ( $K_a$ ) for anions with α-CD, β-CD and γ-CD reported by various authors and the size (diameter,  $d$ ) of the anions.

Host	Guest	$d$ (Å) <sup>c</sup>	$K_a$ (M <sup>-1</sup> ) <sup>a</sup>					
			I	II	III	IV	V	VI
α-CD	Cl <sup>-</sup>	3.6	—	<1	—	~0	3	No binding
	NO <sub>3</sub> <sup>-</sup>	4.0	1.4	1.4	2.31	—	4	— <sup>b</sup>
	Br <sup>-</sup>	3.9	1.6	3.5	0.96	—	—	—
	SCN <sup>-</sup>	4.3	28.4	18.7	33.5	—	—	16
	ClO <sub>4</sub> <sup>-</sup>	4.8	33.0	28.9	45.8	—	35	23
β-CD	NO <sub>3</sub> <sup>-</sup>	—	—	—	—	0.2	—	—
	Br <sup>-</sup>	—	—	—	0.45	1.1	—	—
	SCN <sup>-</sup>	—	9.2	9.9	9.2	5.7	—	—
	ClO <sub>4</sub> <sup>-</sup>	—	13.6	—	—	9.0	—	—
γ-CD	SCN <sup>-</sup>	—	4.1	—	—	—	—	—

<sup>a</sup>Binding constants for anions (as Na<sup>+</sup> or K<sup>+</sup> salts) to α, β and γ-CD measured in H<sub>2</sub>O or D<sub>2</sub>O at 20°C or 25°C with various techniques: I) <sup>1</sup>H-NMR spectroscopy (Matsui et al., 1997); II) Conductance (Wojcik and Rohrbach, 1975); III) Potentiometry (Gelb et al., 1983); IV) Spectrophotometry (Buvári and Barcza, 1979); V) Volatilization (Sanemasa et al., 1988); VI) Isothermal titration calorimetry (Sullivan et al., 2018).

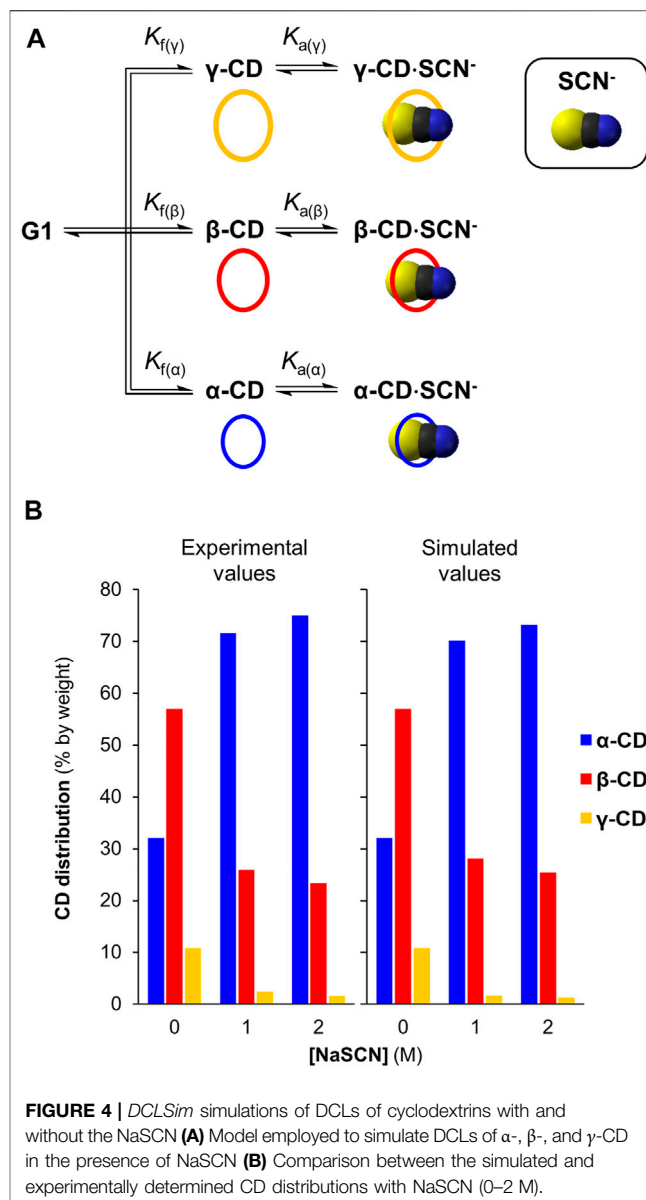
<sup>b</sup>Binding too weak to determine a binding constant.

<sup>c</sup>From reference (Marcus, 1994, 1997).

templates in this system, and at high concentrations can strongly influence the product selectivity in CGTase-mediated cyclodextrin synthesis.

## Increasing the Template Effect of Hydrophobic Guests by Addition of a Kosmotropic Salt

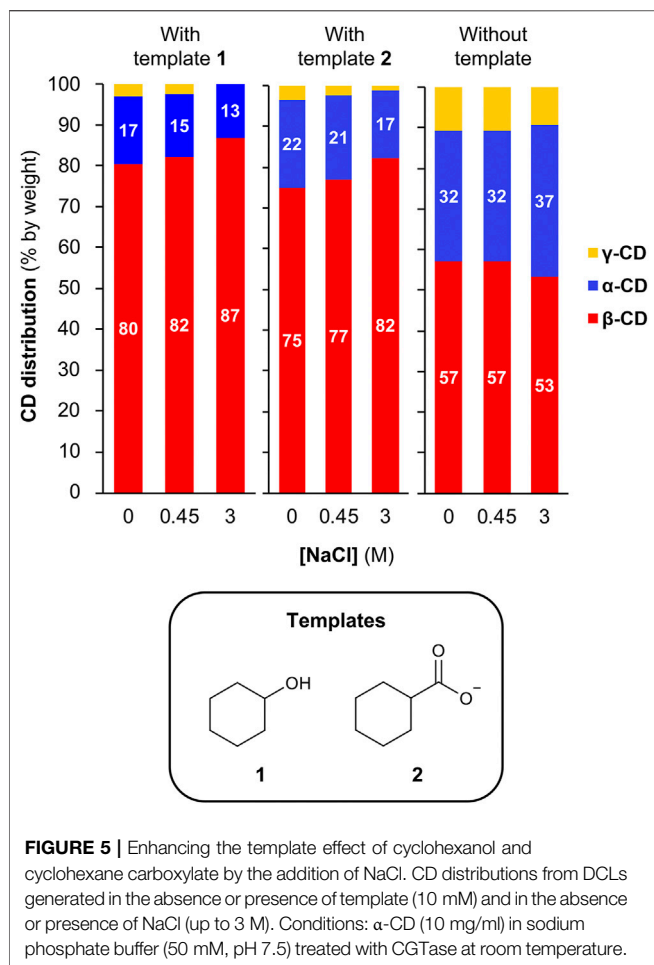
As kosmotropic salts can lead to stronger binding between cyclodextrins and hydrophobic guests (Buvári and Barcza,



**FIGURE 4 |** DCLSim simulations of DCLs of cyclodextrins with and without the NaSCN (A) Model employed to simulate DCLs of α-, β-, and γ-CD in the presence of NaSCN (B) Comparison between the simulated and experimentally determined CD distributions with NaSCN (0–2 M).

1979; Holm et al., 2014), we sought to investigate whether we could enhance the template effect of hydrophobic templates in this dynamic cyclodextrin system by using high concentrations of NaCl. For these experiments, we chose to employ cyclohexanol (**template 1**) and cyclohexanecarboxylate (**template 2**) as templates, as both guests have a relatively low affinity for β-CD in the absence of salts (ca. 700 and ca. 300 M<sup>-1</sup>, respectively) (Gelb and Schwartz, 1989; Rekharsky et al., 1994), thus giving room for a possible improvement in templating effect upon addition of NaCl. A series of CGTase-mediated DCLs were set-up starting from α-CD (10 mg/ml) with template (10 mM) in phosphate buffer (50 mM, pH 7.5) with 0–3 M NaCl (Supplementary Figure 7). It was found that the addition of NaCl in increasing concentrations up to 3 M did in fact lead to a moderate increase in the selectivity for β-CD obtained in





the presence of each template (from 80 to 87% for template 1 and from 75 to 82% for template 2) (Figure 5). It is worth noting that increasing the concentration of NaCl from 0 to 3 M in the absence of template also changes the cyclodextrin distribution, but in the opposite direction, with a decrease in the relative yield of β-CD from 57 to 53%, thus counteracting the observed increase in the template effect with 1 and 2. Accordingly, the actual kosmotrope-induced increase in the template effect is potentially larger than the effect observed here.

## CONCLUSION

In this work, we have systematically explored the influence of different anions on the behavior of CGTase-mediated dynamic combinatorial libraries of cyclodextrins and distinguished two key effects. On the one hand, we observed that NaCl (which lies towards the kosmotropic end of the Hofmeister series) could subtly enhance the templating effects of hydrophobic guest added to the DCLs. On the other hand, we observed direct templating effects due to specific interactions between chaotropes and cyclodextrins. These interactions are very

weak ( $K_a < 50 \text{ M}^{-1}$ ), but, when present in high concentrations (2–4 M), chaotropes can, nevertheless, cause significant changes in the distribution of α-CD, β-CD and γ-CD generated. For example, addition of 2 M NaSCN led to a shift in selectivity from 32% α-CD to 75% α-CD. The observed amplifications of α-CD correlated well with reported binding constants, and simulation of DCLs templated with NaSCN matched well to the experimental results, which is further evidence that the observed effects are due to specific anion-cyclodextrin binding interactions rather than the global influence of the high salt concentration on the bulk solvent. In fact, this dynamic system potentially provides a new method to identify very weak binding of guests to CDs, which would be very difficult to detect otherwise. Finally, we note that the CGTase used in these experiments was remarkably stable at high salt concentrations. Our study showcases how the interplay between kosmotropes, chaotropes and hydrophobes in dynamic supramolecular systems can be utilized to alter the outcome of these systems in predictable and systematic ways.

## DATA AVAILABILITY STATEMENT

The original contributions presented in the study are included in the article/Supplementary Material, further inquiries can be directed to the corresponding author.

## AUTHOR CONTRIBUTIONS

AE performed the experiments. All authors contributed to the experiment design. DL and SB conceived the concept and supervised the research. AE prepared figures and the original draft of the article. All authors contributed to the preparation and editing of the article.

## FUNDING

The authors are grateful to the Villum Foundation (Grant No. 15482), the Carlsberg Foundation (Grant No. CF19-0510) and the Novo Nordisk Foundation (Grant No. NNF19OC0057672) for financial support for salaries, equipment and running costs.

## ACKNOWLEDGMENTS

The authors are grateful to Amano Enzyme, Inc., Nagoya, Japan, for the kind gift of a stock solution of the enzyme CGTase.

## SUPPLEMENTARY MATERIAL

The Supplementary Material for this article can be found online at: <https://www.frontiersin.org/articles/10.3389/fchem.2021.721942/full#supplementary-material>

## REFERENCES

- Assaf, K. I., and Nau, W. M. (2018). The Chaotropic Effect as an Assembly Motif in Chemistry. *Angew. Chem. Int. Ed.* 57, 13968–13981. doi:10.1002/anie.201804597
- Assaf, K. I., Ural, M. S., Pan, F., Georgiev, T., Simova, S., Rissanen, K., et al. (2015). Water Structure Recovery in Chaotropic Anion Recognition: High-Affinity Binding of Dodecaborate Clusters to  $\gamma$ -Cyclodextrin. *Angew. Chem. Int. Ed.* 54, 6852–6856. doi:10.1002/anie.201412485
- Busschaert, N., Caltagirone, C., Van Rossom, W., and Gale, P. A. (2015). Applications of Supramolecular Anion Recognition. *Chem. Rev.* 115, 8038–8155. doi:10.1021/acs.chemrev.5b00099
- Buvári, Á., and Barcza, L. (1979).  $\beta$ -Cyclodextrin Complexes of Different Type with Inorganic Compounds. *Inorg. Chim. Acta* 33, 179–180. doi:10.1016/S0020-1693(00)89441-4
- Corbett, P. T., Leclaire, J., Vial, L., West, K. R., Wietor, J.-L., Sanders, J. K. M., et al. (2006). Dynamic Combinatorial Chemistry. *Chem. Rev.* 106, 3652–3711. doi:10.1021/cr020452p
- Corbett, P. T., Otto, S., and Sanders, J. K. M. (2004). Correlation between Host-Guest Binding and Host Amplification in Simulated Dynamic Combinatorial Libraries. *Chem. Eur. J.* 10, 3139–3143. doi:10.1002/chem.200400300
- Del Valle, E. M. M. (2004). Cyclodextrins and Their Uses: A Review. *Process Biochem.* 39, 1033–1046. doi:10.1016/S0032-9592(03)00258-9
- Gelb, R. I., and Schwartz, L. M. (1989). Complexation of Carboxylic Acids and Anions by Alpha and Beta Cyclodextrins. *J. Incl. Phenom. Macrocycl. Chem.* 7, 465–476. doi:10.1007/BF01079783
- Gelb, R. I., Schwartz, L. M., Radeos, M., and Laufer, D. A. (1983). Cycloamylose Complexation of Inorganic Anions. *J. Phys. Chem.* 87, 3349–3354. doi:10.1021/j100240a033
- Gibb, B. C. (2019). Hofmeister's Curse. *Nat. Chem.* 11, 963–965. doi:10.1038/s41557-019-0355-1
- Gibb, B. C. (2011). Supramolecular Assembly and Binding in Aqueous Solution: Useful Tips Regarding the Hofmeister and Hydrophobic Effects. *Isr. J. Chem.* 51, 798–806. doi:10.1002/ijch.201100058
- Gibb, C. L. D., and Gibb, B. C. (2011). Anion Binding to Hydrophobic Concavity Is central to the Salting-In Effects of Hofmeister Chaotropes. *J. Am. Chem. Soc.* 133, 7344–7347. doi:10.1021/ja202308n
- Hedges, A. R. (1998). Industrial Applications of Cyclodextrins. *Chem. Rev.* 98, 2035–2044. doi:10.1021/cr970014w
- Hillyer, M. B., and Gibb, B. C. (2016). Molecular Shape and the Hydrophobic Effect. *Annu. Rev. Phys. Chem.* 67, 307–329. doi:10.1146/annurev-physchem-040215-112316
- Hofmeister, F. (1888). Zur Lehre von der Wirkung der Salze. *Archiv F. Experiment. Pathol. U. Pharmacol.* 25, 1–30. doi:10.1007/BF01838161
- Holm, R., Schönbeck, C., Somprasit, P., Westh, P., and Mu, H. (2014). A Study of Salt Effects on the Complexation between  $\beta$ -cyclodextrins and Bile Salts Based on the Hofmeister Series. *J. Incl. Phenom. Macrocycl. Chem.* 80, 243–251. doi:10.1007/s10847-014-0383-9
- Kunz, W., Lo Nostro, P., and Ninham, B. W. (2004). The Present State of Affairs with Hofmeister Effects. *Curr. Opin. Colloid Interf. Sci.* 9, 1–18. doi:10.1016/j.cocis.2004.05.004
- Larsen, D., and Beeren, S. R. (2021). Building up Cyclodextrins from Scratch - Templated Enzymatic Synthesis of Cyclodextrins Directly from Maltose. *Chem. Commun.* 57, 2503–2506. doi:10.1039/d1cc00137j
- Larsen, D., and Beeren, S. R. (2019). Enzyme-mediated Dynamic Combinatorial Chemistry Allows Out-Of-Equilibrium Template-Directed Synthesis of Macrocyclic Oligosaccharides. *Chem. Sci.* 10, 9981–9987. doi:10.1039/c9sc03983j
- Larsen, D., and Beeren, S. R. (2020). Tuning the Outcome of Enzyme-Mediated Dynamic Cyclodextrin Libraries to Enhance Template Effects. *Chem. Eur. J.* 26, 11032–11038. doi:10.1002/chem.202001076
- Lehn, J.-M. (2007). From Supramolecular Chemistry towards Constitutional Dynamic Chemistry and Adaptive Chemistry. *Chem. Soc. Rev.* 36, 151–160. doi:10.1039/b616752g
- Li, J., Nowak, P., and Otto, S. (2013). Dynamic Combinatorial Libraries: From Exploring Molecular Recognition to Systems Chemistry. *J. Am. Chem. Soc.* 135, 9222–9239. doi:10.1021/ja402586c
- Marcus, Y. (1997). *Ion Properties*. New York: Marcel Dekker.
- Marcus, Y. (1994). ViscosityB-coefficients, Structural Entropies and Heat Capacities, and the Effects of Ions on the Structure of Water. *J. Solution Chem.* 23, 831–848. doi:10.1007/BF00972677
- Matsui, Y., Ono, M., and Tokunaga, S. (1997). NMR Spectroscopy of Cyclodextrin-Inorganic Anion Systems. *Bcsj* 70, 535–541. doi:10.1246/bcsj.70.535
- Otto, S., Furlan, R. L. E., and Sanders, J. K. M. (2002). Selection and Amplification of Hosts from Dynamic Combinatorial Libraries of Macrocyclic Disulfides. *Science* 297, 590–593. doi:10.1126/science.1072361
- Ponnuswamy, N., Cougnon, F. B. L., Clough, J. M., Pantos, G. D., and Sanders, J. K. M. (2012). Discovery of an Organic Trefoil Knot. *Science* 338, 783–785. doi:10.1126/science.1227032
- Rekharsky, M. V., Schwarz, F. P., Tewari, Y. B., Goldberg, R. N., Tanaka, M., and Yamashoji, Y. (1994). Thermodynamic and NMR Study of the Interactions of Cyclodextrins with Cyclohexane Derivatives. *J. Phys. Chem.* 98, 4098–4103. doi:10.1021/j100066a032
- Sanemasa, I., Fujiki, M., and Deguchi, T. (1988). A New Method for Determining Cyclodextrin Complex Formation Constants with Electrolytes in Aqueous Medium. *Bcsj* 61, 2663–2665. doi:10.1246/bcsj.61.2663
- Sharma, N., and Baldi, A. (2016). Exploring Versatile Applications of Cyclodextrins: An Overview. *Drug Deliv.* 23, 729–747. doi:10.3109/10717544.2014.938839
- Sullivan, M. R., Yao, W., Tang, D., Ashbaugh, H. S., and Gibb, B. C. (2018). The Thermodynamics of Anion Complexation to Nonpolar Pockets. *J. Phys. Chem. B* 122, 1702–1713. doi:10.1021/acs.jpcc.7b12259
- Terada, Y., Yanase, M., Takata, H., Takaha, T., and Okada, S. (1997). Cyclodextrins Are Not the Major Cyclic  $\alpha$ -1,4-Glucans Produced by the Initial Action of Cyclodextrin Glucanotransferase on Amylose. *J. Biol. Chem.* 272, 15729–15733. doi:10.1074/jbc.272.25.15729
- Tewari, Y. B., Goldberg, R. N., and Sato, M. (1997). Thermodynamics of the Hydrolysis and Cyclization Reactions of  $\alpha$ -,  $\beta$ -, and  $\gamma$ -cyclodextrin. *Carbohydr. Res.* 301, 11–22. doi:10.1016/s0008-6215(97)00073-6
- Uitdehaag, J. C. M., van der Veen, B. A., Dijkhuizen, L., and Dijkstra, B. W. (2002). Catalytic Mechanism and Product Specificity of Cyclodextrin Glycosyltransferase, a Prototypical Transglycosylase from the  $\alpha$ -amylase Family. *Enzyme Microb. Tech.* 30, 295–304. doi:10.1016/S0141-0229(01)00498-7
- van der Vegt, N. F. A., and Nayar, D. (2017). The Hydrophobic Effect and the Role of Cosolvents. *J. Phys. Chem. B* 121, 9986–9998. doi:10.1021/acs.jpcc.7b06453
- Wojcik, J. F., and Rohrbach, R. P. (1975). Small Anion Binding to Cycloamylose. Equilibrium Constants. *J. Phys. Chem.* 79, 2251–2253. doi:10.1021/j100588a010

**Conflict of Interest:** The authors declare that the research was conducted in the absence of any commercial or financial relationships that could be construed as a potential conflict of interest.

**Publisher's Note:** All claims expressed in this article are solely those of the authors and do not necessarily represent those of their affiliated organizations, or those of the publisher, the editors and the reviewers. Any product that may be evaluated in this article, or claim that may be made by its manufacturer, is not guaranteed or endorsed by the publisher.

Copyright © 2021 Erichsen, Larsen and Beeren. This is an open-access article distributed under the terms of the Creative Commons Attribution License (CC BY). The use, distribution or reproduction in other forums is permitted, provided the original author(s) and the copyright owner(s) are credited and that the original publication in this journal is cited, in accordance with accepted academic practice. No use, distribution or reproduction is permitted which does not comply with these terms.



# The Importance of Spin State in Chiral Supramolecular Electronics

Ana M. Garcia, Gabriel Martínez and Amparo Ruiz-Carretero \*

Institute Charles Sadron, University of Strasbourg, CNRS, Strasbourg, France

## OPEN ACCESS

### Edited by:

Anna McConnell,  
University of Kiel, Germany

### Reviewed by:

Ron Naaman,  
Weizmann Institute of Science, Israel  
Carmen Herrmann,  
University of Hamburg, Germany

### \*Correspondence:

Amparo Ruiz-Carretero  
amparo.ruiz@ics-cnrs.unistra.fr

### Specialty section:

This article was submitted to  
Supramolecular Chemistry,  
a section of the journal  
Frontiers in Chemistry

**Received:** 09 June 2021

**Accepted:** 21 July 2021

**Published:** 04 August 2021

### Citation:

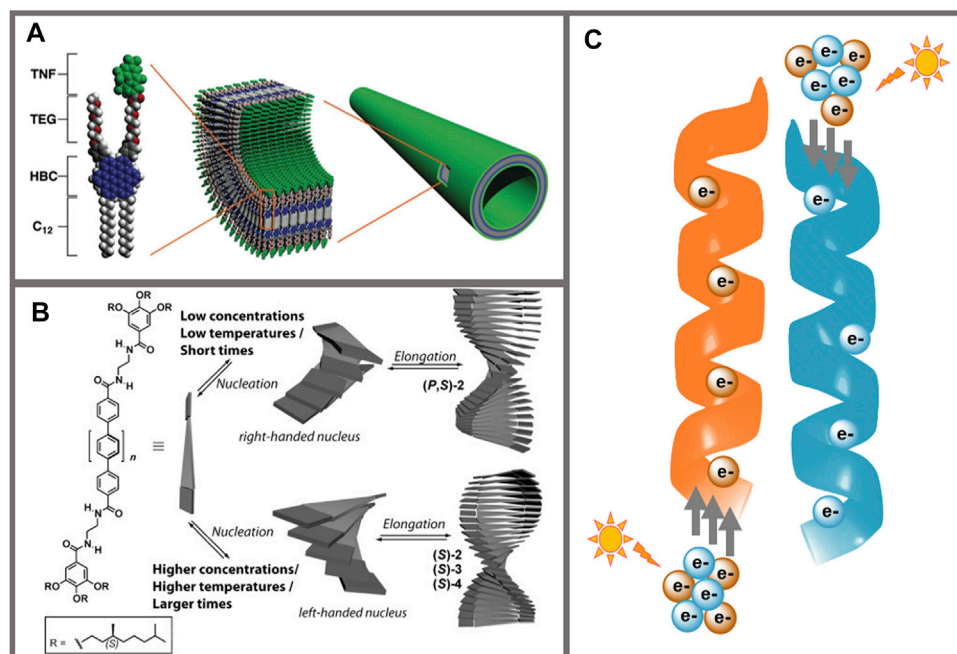
Garcia AM, Martínez G and  
Ruiz-Carretero A (2021) The  
Importance of Spin State in Chiral  
Supramolecular Electronics.  
Front. Chem. 9:722727.  
doi: 10.3389/fchem.2021.722727

The field of spintronics explores how magnetic fields can influence the properties of organic and inorganic materials by controlling their electron's spins. In this sense, organic materials are very attractive since they have small spin-orbit coupling, allowing long-range spin-coherence over times and distances longer than in conventional metals or semiconductors. Usually, the small spin-orbit coupling means that organic materials cannot be used for spin injection, requiring ferromagnetic electrodes. However, chiral molecules have been demonstrated to behave as spin filters upon light illumination in the phenomenon described as chirality-induced spin selectivity (CISS) effect. This means that electrons of certain spin can go through chiral assemblies of molecules preferentially in one direction depending on their handedness. This is possible because the lack of inversion symmetry in chiral molecules couples with the electron's spin and its linear momentum so the molecules transmit the one preferred spin. In this respect, chiral semiconductors have great potential in the field of organic electronics since when charge carriers are created, a preferred spin could be transmitted through a determined handedness structure. The exploration of the CISS effect in chiral supramolecular semiconductors could add greatly to the efforts made by the organic electronics community since charge recombination could be diminished and charge transport improved when the spins are preferentially guided in one specific direction. This review outlines the advances in supramolecular chiral semiconductors regarding their spin state and its influence on the final electronic properties.

**Keywords:** supramolecular chirality, self-assembly, CISS effect, spin state, supramolecular electronics

## INTRODUCTION

The field of supramolecular electronics bridges the gap between molecular and plastic electronics (Meijer and Schenning, 2002; Schenning and Meijer, 2005; Moulin et al., 2013). In this sense, supramolecular chemistry represents the bridge, providing the tools to achieve highly organized structures with superior properties than those of the individual components. The presence of noncovalent interactions in organic semiconductors has been demonstrated to enhance the charge transport properties and device efficiency (Ghosh et al., 2017), finding exciting results in literature where  $\pi$ - $\pi$  stacking interactions (Lee et al., 2011), hydrogen bonds (Huang et al., 2005; Ruiz-Carretero et al., 2013; Aytun et al., 2015; Carretero et al., 2020) metallophilic interactions (Che et al., 2011; Ruiz-Carretero et al., 2019) or a combination of several noncovalent interactions (Yamamoto et al., 2006; Schulze et al., 2014; Stupp and Palmer, 2014; Weldeab et al., 2018) were used to boost the properties of supramolecular electronic systems (Figure 1A). The dynamic nature of noncovalent interactions allows to tune the optoelectronic properties by controlling the self-assembly processes. In this regard, parameters such as temperature, concentration or solvent polarity can impact the self-



**FIGURE 1 | (A)** Representation of the monomer (left) and the resulting supramolecular nanotube containing a coaxial p/n-heterojunction (right). The donor moiety in the monomer is HBC (blue), and the acceptor is trinitrofluorenone (green); TEG (red) and C12 chains (white) in the monomer provide solubility. From Yamamoto et al. 2006. Reprinted with permission from AAAS. **(B)** Schematic representation of the kinetically controlled modulation of the supramolecular helical organization of chiral oligo-p-phenylene-based organogelators. Structures of opposite handedness are obtained depending on the concentration, temperature, and times of formation. Reprinted with permission from Aparicio et al. (2014). Copyright 2014 Wiley-VCH. **(C)** Schematic representation of the CISS effect. The panel shows helical supramolecular structures where, after illumination with circular polarized light, electrons with opposite spins (orange and blue spheres) can be selectively transported through right-handed (orange) or left-handed (blue) helices, respectively.

assembly and hence, the properties (Aida et al., 2012). The incorporation of chiral centers into  $\pi$ -conjugated materials also affects the self-assembly properties. In this case, the chiral information of the monomer is transferred along the assembly yielding the final chiral configuration to the structure (Liu et al., 2015) (Figure 1B). Recently, chiral supramolecular structures have raised as very interesting systems in the field of spintronics (Wolf et al., 2001) since chiral and helical structures have been demonstrated to behave as spin filters upon light illumination in the phenomenon described as Chirality-Induced Spin Selectivity (CISS) effect (Naaman and Waldeck, 2012) (Figure 1C). Organic materials are very attractive for spintronic devices due to their small spin-orbit coupling (SOC), which increases the spin relaxation time as compared to inorganic materials usually containing heavy atoms, resulting in long-range spin transport in organic materials (Rocha et al., 2005). However, this affirmation should be taken carefully since the mobility of organic materials is rather inferior to those of inorganic materials, meaning that even if spin relaxation times are high, the spin polarized charges do not travel long distances (Szulcowski et al., 2009).

The small SOC implies that organic materials cannot be used for spin injection, requiring ferromagnetic electrodes (Awschalom and Flatté, 2007). However, the CISS effect

indicates that organic molecules are not considered as passive elements but as spin filters because the lack of inversion symmetry in chiral molecules couples with the electron's spin and its linear momentum, so the molecules transmit one preferred spin.

The scope of this review is to introduce the reader to chiral supramolecular electronic materials and the importance of the electron's spin in the final properties of such materials. The CISS effect will be presented, as well as examples of supramolecular semiconductors where the roles of chirality and the spin have been highlighted but not related to the CISS effect. Finally, we focus on the latest insights into supramolecular systems based on chiral  $\pi$ -conjugated materials and the impact of controlling the spin state on the final electronic processes.

## THE CISS EFFECT

### Discovery and Definition

The CISS effect was firstly identified by Naaman and coworkers in 1999, who determined the scattering asymmetry in electrons transmission in Langmuir-Blodgett films made of L- and D-stearoyl lysine (Ray et al., 1999). Their results showed that the quantum yield of photoelectrons depended both on the



relative polarization of the light, and the chirality of the molecules. They started the study of the main factors that influence the CISS effect using self-assembled monolayers (SAMs) of double-stranded (ds) DNA and oligopeptides, demonstrating that spin selectivity is correlated to the supramolecular organization of single molecules, and its magnitude increases with the length of the DNA strands or peptide sequence, respectively (Carmeli et al., 2002; Ray et al., 2006; Göhler et al., 2011; Xie et al., 2011; Kettner et al., 2015; Aragonès et al., 2017; Kiran et al., 2017; Tassinari et al., 2018; Torres-Cavanillas et al., 2020). These studies pointed out the previously ignored role of the spin in electron-biomolecule interactions, as well as the potential of SAMs of chiral molecules that work as spin filters at room temperature (Michaeli et al., 2016; Naaman et al., 2019).

## Theoretical Models

Several theoretical models have been described to explain the spin-selective transport through chiral molecules, using helical-shaped molecules and dsDNA (Guo and Sun, 2012; Gutierrez et al., 2012; Medina et al., 2012). The first models found in literature share two important features: chirality is essential to reach spin polarization, and a helical potential based on the Rashba-like SOC term needs to be considered to calculate the SO interaction (Naaman and Waldeck, 2012). Later on, Dalum and Hedegard suggested a novel mechanism for CISS based on perturbative approach calculations, that need to be concretized to specific systems (Dalum and Hedegård, 2019). First-principle calculations were used by Gutierrez and coworkers to study the geometry-dependent spin polarization using an atomistic model of oligoglycine. The helical symmetry displayed a much higher spin polarization than the  $\beta$ -strand conformation, highlighting the role of helical geometry in the CISS effect (Maslyuk et al., 2018). In this sense, Herrmann et al. analyzed the crucial role of the imaginary terms in the Hamiltonian matrix for nonvanishing spin polarization in helical structures (Zöllner et al., 2020).

Furthermore, recent studies remark the important role of phonons and polarons to reach high spin polarization. Fransson showed the importance of cooperation of electron-phonon and spin-dependent couplings to get an exchange splitting between the spin channels that is reasonable for CISS (Fransson, 2020). In particular, he investigated systems of chiral molecules coupled to metals, where molecular vibrations (phonons) represent a mechanism able to break the spin symmetry of the molecule (Fransson, 2021). On their side, Zhang et al. assessed spin polaron transport in chiral molecules and, unlike previous theoretical explanations, their results showed that both type of polarons (spin-up and spin-down) can traverse the chiral molecule, although with different spin dynamics, i.e., the ones with antiparallel orientation experiment spin switching (Zhang et al., 2020).

Overall, there is not a general consensus as of now that theoretically rationalizes the astounding value experimentally observed for the CISS effect. Nevertheless, the investigations mentioned above suggest several reasons to explain this effect that range from the buildup of spin polarization at the interface to the electron-phonon interactions and polaron transport, and very

recently, to the topological orbital texture combined with SOC in the substrate (Liu et al., 2021). Further theoretical investigations are currently ongoing that are expected to give more insights into these theoretical points.

## Experimental Measurements

There are multiple experimental methods to investigate the CISS effect (Naaman and Waldeck, 2015). Photoelectron spectroscopy has been used to characterize spin orientation through a SAM of chiral molecules adsorbed in a gold substrate when irradiating with circularly polarized light. The spin of the transmitted electrons is detected using a Mott polarimeter (Göhler et al., 2011). Conductive-probe atomic force microscopy (cp-AFM) is another technique that measures the spin-dependent conduction through single molecules (Xie et al., 2011; Kettner et al., 2015; Bullard et al., 2019). With this technique, the current-voltage (J-V) curves are registered on a SAM of chiral molecules adsorbed on a ferromagnetic substrate (normally nickel), while gold nanoparticles are attached to the tail of some of these molecules. It can be considered one of the best techniques to evaluate the real spin selectivity as it does not detect electrons from non-covered areas of the surface.

Spin polarization Hall devices measure Hall voltage and cyclic voltammetry response on chiral SAMs (Kumar et al., 2017; Bullard et al., 2019). The sign of the observed Hall voltage depends on the chirality of the molecule.

Recently, a technique that combines time-resolved microwave conductivity (TRMC), electron paramagnetic resonance (EPR) and optical spectroscopy has been used to study charge carrier mobility and spin state in p-type semiconductors (Tsutsui et al., 2018). Chemical doping using iodine vapors generates radicals that allow to determine the species with different spin state present in the sample.

## CHIRAL SUPRAMOLECULAR $\pi$ -CONJUGATED MATERIALS. SPIN AND OPTOELECTRONIC PROPERTIES

The importance of chirality and the spin state in organic electronics has been reported in many literature examples even if they were not connected to the CISS effect. Yet, the number of works linking conductivity to chirality is still scarce despite the emergent properties observed in organic semiconductors as a consequence of chirality (Yang et al., 2017). For instance, Zhu et al. reported optically active chiral electronic wires based on oligo-arylene-ethynylene and 1,1'-bi-2-naphthol (BINOL) (Zhu et al., 2006). The (R)- and (S)-derivatives were prepared and self-assembled onto gold surfaces. The electrical transport properties were studied measuring the J-V curves for the pure enantiomers and different enantiomeric mixtures, finding that the optically pure compounds exhibited greater conductivity than the mixtures. The authors hypothesized that the result could be due to very different packing structures between homochiral and heterochiral molecules. Later on, several works were reported on the influence of stereoisomerism on the crystallization, optoelectronic properties and device efficiency



of  $\pi$ -conjugated materials functionalized with asymmetric branched alkyl chains. Liu et al. reported (Liu et al., 2013) the differences among the mesomer, the RR-isomer and the SS-isomer of diketopyrrolopyrrole (DPP) molecules functionalized with asymmetrical branched alkyl chains. The stereoisomers, isolated by a HPLC equipped with a chiral column, were also compared to the as-synthesized compound. The enantiomers showed very similar crystal structures, thin film morphology and field effect transistor (FET) properties, and they were the best structures to grow single crystals, while the mesomer had the greatest crystallization tendency in spin-cast films. The latter resulted in the highest charge carrier mobilities due to a coplanar conjugated backbone that favors intermolecular  $\pi$ - $\pi$  stacking compared to the twisted backbone of the RR- and SS-isomers. Similarly, Zerdan et al. reported the influence of the solubilizing chain stereochemistry on photovoltaic devices made with small molecules and fullerene derivatives (Zerdan et al., 2014). In this case, the authors reported DPP derivatives with RR-, SS- and RS-ethylhexyl alkyl tails. Bulk heterojunction solar cells were fabricated with the pure isomers and compared to isomer mixtures from the purchased derivative. The authors found that when crystallization was induced by thermal annealing, important differences were found in the molecular packing between the different stereoisomers. Later on, Stolte et al. showed the impact of ethylhexyl stereoisomers on organic thin film transistors of  $\pi$ -conjugated materials (Stolte et al., 2016). In this case, the highest mobility is found for dyes bearing 2-ethylhexyl substituents that include a mixture of (R,R) (S,S) and (R,S) stereoisomers. The authors argue that this was possible due to the superior  $\pi$ - $\pi$  contacts between DPP dyes. The result agreed with the previous studies pioneered by Liu and collaborators (Liu et al., 2013). The same group reported the impact of 2-ethylhexyl stereoisomers on single crystal field-effect transistors (FET) (He et al., 2018). In this case, the (R,S) mesomer was the most promising stereoisomer, being the mobility values superior to those of the pure enantiomers.

Other systems showing the influence of chirality in  $\pi$ -conjugated materials are optically active polymers (Grenier et al., 2007; Vanormelingen et al., 2008; Kane-Maguire and Wallace, 2010, 2010), thiophene-based block copolymers (Van den Bergh et al., 2010; Verswyvel et al., 2011), copolymers of chiral poly(ethylenedioxythiophene) (PEDOT) (Jeong and Akagi, 2011), supramolecular helical nanostructures (Hafner et al., 2018) and tetrathiafulvalene systems (Pop et al., 2013, 2014).

Likewise, the role of the spin state was highlighted in other series of works. The spin state is a very important parameter in the kinetic control of recombination in organic photovoltaics (Rao et al., 2013) and in charge transfer (CT) states (Chang et al., 2015). While cascade structures allow the spatial separation of photogenerated electrons and holes in biological systems, the photogenerated excitons in organic photovoltaic devices are dissociated exclusively at the donor-acceptor heterojunction. However, the nanoscale morphology of photovoltaic devices promotes the encounters of charges and hence, recombination. Yet, there are examples of organic photovoltaic devices with quantum efficiency close to unity (Park et al., 2009), meaning that recombination can be avoided. Rao et al. (2013)

demonstrated using time-resolved spectroscopy that the recombination of bound states is mediated not only by energetics, but also by the spin delocalization, allowing free carriers to be formed again and suppressing recombination. Along the same lines, Janssen et al. demonstrated that the spin-based particle reactions happening in polymer-fullerene blends can be tuned using magnetoresistance lineshapes and voltage dependencies (Janssen et al., 2013). The authors showed non-spin-polarized organic semiconductor devices, which in the absence of magnetic elements presented large room temperature magnetoresistance effect at small magnetic fields. This effect is known as organic magnetoresistance (OMAR) and it is very appealing because it can unravel unknown phenomena happening due to the intrinsically magnetic field-dependent charge transport properties of organic semiconductors. The authors explored the possible mechanisms to explain OMAR, categorized as reactions of polarons with the same charge into bipolarons, reactions of polarons with opposite charge into excitons, and reactions of triple excitons with polarons or with other triplet excitons. As a result of their study, the authors conclude that by choosing the right materials to alter the alignment of triplet excitons and CT states, important effects on the reaction pathways and the resulting OMAR can be achieved, influencing the device physics and efficiency.

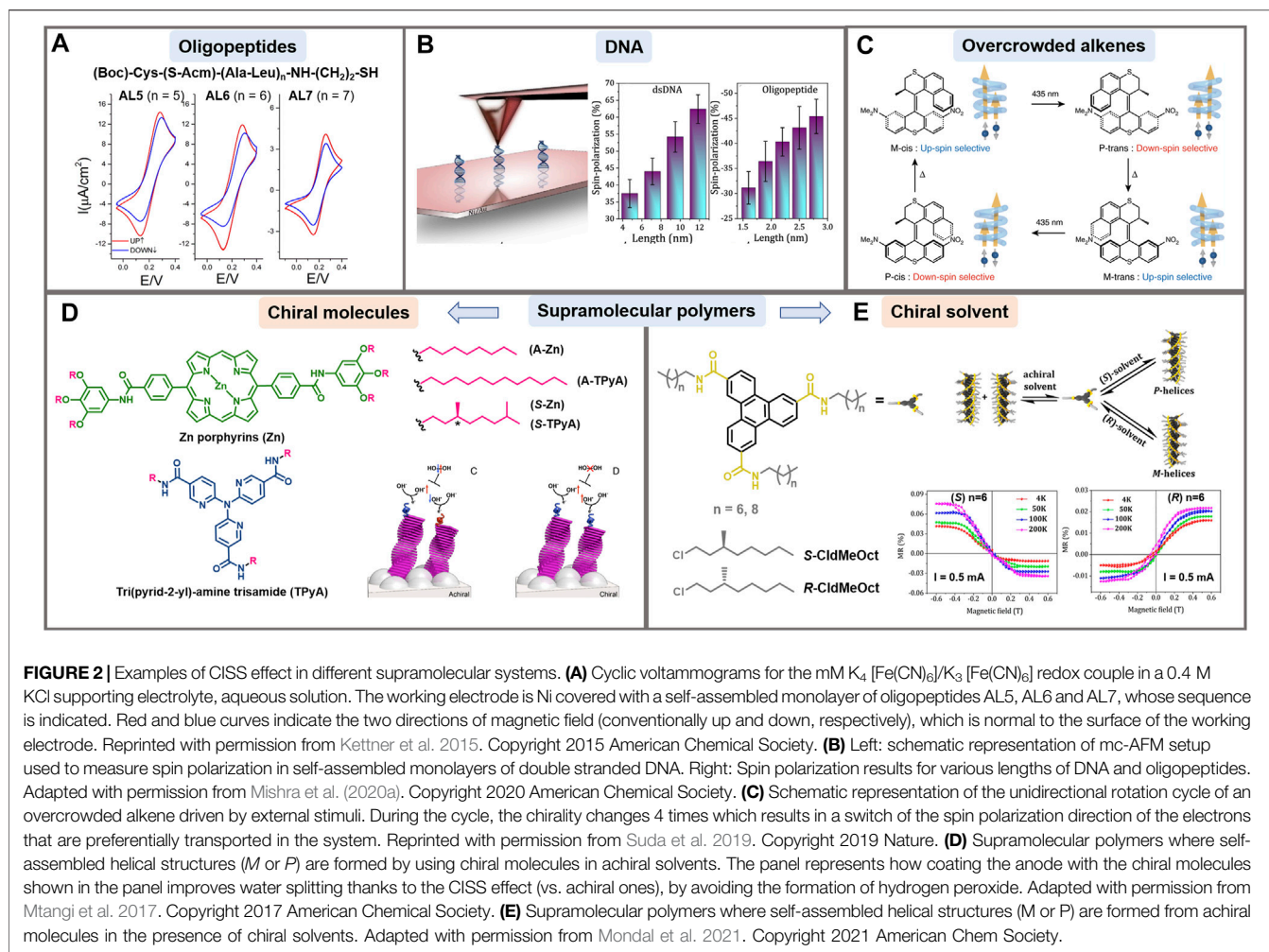
## MAIN SUPRAMOLECULAR STRUCTURES WHERE CISS EFFECT HAS BEEN STUDIED

One of the main research areas of the CISS effect has been understanding its role in electron transfer in biology-related systems. It explains not only why it is so efficient in biological processes such as photosynthesis or respiration, but also the reasons for preferred enantioselective recognition in living organisms (Michaeli et al., 2016). In addition, other processes in which electrons are transferred in a way that only one spin state prevails are interesting for many applications in chemistry and electronics, since it enables the fabrication of electronic devices using chiral organic molecules instead of ferromagnets (Dor et al., 2013; Mathew et al., 2014; Koplovitz et al., 2017; Mtangi et al., 2017; Mondal et al., 2021).

In the next paragraphs we will describe the main supramolecular  $\pi$ -conjugated systems where the CISS effect has been studied.

### Peptides

Since the identification of the CISS effect, big efforts have been made to understand it in a wide variety of molecular systems, including biologically relevant molecules as DNA and peptides (Naaman and Waldeck, 2015). Only recently, several key parameters in spin polarization and its magnitude have been disclosed. The dependence of spin selectivity on the molecular length was demonstrated by varying the number of amino acid residues in oligopeptide sequences using cyclic voltammetry (Figure 2A) and cp-AFM (Kettner et al., 2015; Kiran et al., 2017), finding that spin selectivity decreases when increasing



**FIGURE 2 |** Examples of CISS effect in different supramolecular systems. **(A)** Cyclic voltammograms for the mK<sub>4</sub> [Fe(CN)<sub>6</sub>]/K<sub>3</sub> [Fe(CN)<sub>6</sub>] redox couple in a 0.4 M KCl supporting electrolyte, aqueous solution. The working electrode is Ni covered with a self-assembled monolayer of oligopeptides AL5, AL6 and AL7, whose sequence is indicated. Red and blue curves indicate the two directions of magnetic field (conventionally up and down, respectively), which is normal to the surface of the working electrode. Reprinted with permission from Kettner et al. 2015. Copyright 2015 American Chemical Society. **(B)** Left: schematic representation of mc-AFM setup used to measure spin polarization in self-assembled monolayers of double stranded DNA. Right: Spin polarization results for various lengths of DNA and oligopeptides. Adapted with permission from Mishra et al. (2020a). Copyright 2020 American Chemical Society. **(C)** Schematic representation of the unidirectional rotation cycle of an overcrowded alkene driven by external stimuli. During the cycle, the chirality changes 4 times which results in a switch of the spin polarization direction of the electrons that are preferentially transported in the system. Reprinted with permission from Suda et al. 2019. Copyright 2019 Nature. **(D)** Supramolecular polymers where self-assembled helical structures (M or P) are formed by using chiral molecules in achiral solvents. The panel represents how coating the anode with the chiral molecules shown in the panel improves water splitting thanks to the CISS effect (vs. achiral ones), by avoiding the formation of hydrogen peroxide. Adapted with permission from Mtangi et al. 2017. Copyright 2017 American Chemical Society. **(E)** Supramolecular polymers where self-assembled helical structures (M or P) are formed from achiral molecules in the presence of chiral solvents. Adapted with permission from Mondal et al. 2021. Copyright 2021 American Chem Society.

the tip-loading force. Following these studies, Aragonès and coworkers proved current asymmetry in chiral single molecular junctions by scanning tunneling microscopy break-junction (STM-BJ). They used 22-mer L- and D-oligopeptide systems, a magnetized nickel tip and a gold electrode (Aragonès et al., 2017). The spin selectivity in electron transfer was also noted when 12-mer oligopeptides were attached to ferrocene, where oxidation or reduction were favored depending on the L- or D-enantiomer and the direction of the magnetic field (Tassinari et al., 2018). Importantly, a polyproline chiral system (Pro<sub>8</sub>) conjugated to zinc porphyrins showed that the spin-polarized generated currents were further transmitted over distances surpassing the length of chiral molecules (Bullard et al., 2019). Very recently, ds peptide nucleic acids (PNAs) have been proposed to study the CISS effect. Their spin-filtering capabilities were directly correlated to the molecular helicity, highlighting the worth of the dsPNAs for systematic studies of the CISS effect (Möllers et al., 2021).

## DNA

The helical structure of dsDNA is very attractive in spintronics because it has played a critical role in charge transport processes

through long molecular distances (Kiran et al., 2017). In 2011, Göhler and collaborators presented the first example of spin filters based on DNA. They obtained spin polarization exceeding 60% at room temperature measured by Mott polarimetry with dsDNA monolayers adsorbed on gold (Göhler et al., 2011). Densely packed single stranded (ss) and dsDNA films with a redox-active probe adsorbed on a gold-capped nickel surface were analyzed by cyclic voltammetry. Only the dsDNA films displayed variations of up to 16% in the electrochemical reduction depending on the orientation of the magnetic field. This states that the chiral supramolecular organization prevails over the chirality of the individual components (Zwang et al., 2016). The linear dependence of the spin polarization on the length of dsDNA oligonucleotides has also been demonstrated by cp-AFM using lengths of 20 up to 50 base pairs (Mishra et al., 2020a) (Figure 2B). Later, Banerjee-Ghosh et al. proved experimentally that there is an enantiospecific interaction between chiral molecules and perpendicularly polarized substrates. They followed the kinetics of the enantioselective adsorption of dsDNA on a magnetized Ni/Au surface, finding that the rate of absorption was considerably different for up and down magnetization of the substrate (Banerjee-Ghosh et al., 2018).

Additionally, researchers have investigated the effect of oxidative damage on the spin transport through monolayers of dsDNA using a Hall device (Bullard et al., 2019). Unexpectedly, dsDNA having one and two oxidative damages in the base pairs had higher spin polarization than undamaged dsDNA films. It seems that due to the damage of the bases most of the conduction goes through the backbone of the DNA structure, which is chiral and hence, more spin selective.

## Helicenes and Overcrowded Alkenes

Helicenes are fully conjugated molecules without stereogenic carbons. The repulsion between the termini of these molecules makes the helicenes adopt permanent helical conformations with *M* (left-handed enantiomer) and *P* (right-handed enantiomer) configurations (OuYang and Crassous, 2018). Kiran et al. have shown that cationic [4] helicenes behaved as spin filters when they were uniformly absorbed and oriented on a pyrolytic graphite surface (Kiran et al., 2016). Spin polarizations of more than 40% were obtained with preferred opposite spin orientation for *P* and *M* configurations. In another report, monolayers made of enantiopure [7] helicenes were deposited on Cu (332), Ag (110), and Au (111) surfaces, which have a wide range of SOC values (Kettner et al., 2018). Very similar results of spin selectivity were obtained, proving the dominant role of chirality in the spin filtering ability of helicenes over the SOC of the surfaces. Interestingly, some authors have pointed out improved charge transport properties on racemic mixtures of helicenes compared to enantiopure composition in organic electronic devices (Yang et al., 2017). Important morphological differences between the racemic and enantiopure systems were found, as well as an 80-fold increase in hole mobility in FETs. On the other hand, Josse et al. compared device efficiency fabricated with enantiopure and racemic naphthalimide end-capped [6] helicenes as electron acceptors (Josse et al., 2017), observing a two-fold increase in electron mobility, and a five-fold increase of the power conversion efficiency in devices fabricated with the enantiopure material compared to the racemic. These contradictory results emphasize the need to further investigate the impact of solid-state organization in chiral supramolecular systems in organic electronic devices. In 2019, it was presented for the first time the change of spin selectivity by modifying the handedness of chiral molecules by external stimuli (Suda et al., 2019) (Figure 2C). An artificial molecular motor based on an overcrowded alkene was synthesized. It was able to switch its chirality generating a unidirectional rotation cycle driven by temperature or light, with spin selectivity values of up to 44%.

## Conjugated Polymers/ $\pi$ -Conjugated Molecules Incorporating Amino Acids (Chirality)

Chirality has been demonstrated crucial for spin filtering also in different polymers and  $\pi$ -conjugated molecules, as for example in organic light emitting diodes (OLEDs). Thanks to the CISS effect, chiral polymers represent a great alternative for spin polarization and injection with high spin selectivity. For instance, thin films of thiophene-based polymers incorporating cysteine exhibited high

spin filter ability at room temperature, as shown using a solid-state device to determine magnetoresistance and electrochemical measurements (Mondal et al., 2015). Another intriguing example illustrating the importance of selective spin transport in supramolecular structures is the improvement in water splitting by avoiding the formation of hydrogen peroxide (Figure 2D). In this case, the anode was coated with a helix-forming chiral organic semiconductor that enhanced the desired process thanks to the CISS effect (Mtangi et al., 2017). Later on, the importance of supramolecular chirality rather than the number of chiral centers present in the molecule was demonstrated using coronene bisimide and porphyrin-like polymers with chiral (or achiral) alkoxyphenyl chains (Kulkarni et al., 2020). In principle, supramolecular helicity is expected to be inverted depending on the stereoconfiguration of the chiral centers in the  $\pi$ -conjugated molecule or polymer. However, it was shown that both, *M* and *P* chiral helicity can also emerge from a monomer with the same chirality (e.g., *L*-derivative). In this sense, the secondary arrangement can be inverted by changing the temperature (+20°C or -10°C) (Kulkarni et al., 2020), or by using a different solvent (Mishra et al., 2020b). More recently, spin polarization was identified in achiral polymers with a preferred helical arrangement induced by the use of chiral solvents. The authors used triphenylene-2,4,10-tricarboxamide derivatives, whose supramolecular chirality is biased to get either *P*- or *M*-helices when using chiral solvents (Mondal et al., 2021) (Figure 2E). The inversion of supramolecular chirality by means of temperature and solvent when using the same enantiomer affects spin selectivity, and confirms the importance of supramolecular orientation in selective spin transport. In fact, very recently, Meijer and coworkers claimed the pivotal role of chiral supramolecular order rather than the number of chiral centers in discrete molecules in the CISS effect using squaraine dyes (Rösch et al., 2021).

## Inorganic and Hybrid Inorganic-Organic Materials

Inorganic and hybrid inorganic-organic materials have shown as well properties as spin filters. Hybrid materials of perovskites frameworks integrating a chiral organic sublattice have presented spin selectivity much larger than previously reported in SAM systems (Waldeck et al., 2021). Recently, Lu et al. achieved spin polarizations of up to 86% in oriented R- and S-chiral 2D-layered Pb-iodide hybrid organic-inorganic perovskite (HOIP) films. Weak thickness dependence was displayed in films from 20–100 nm (Lu et al., 2019). In another report, Huang et al. demonstrated that chiral-HOIPs are capable of changing the magnetization of an adjacent NiFe ferromagnetic substrate. The sign of the magnetization studied by Magneto-optic Kerr rotation effect depended on the chirality of the HOIP (Huang et al., 2020). Recently, a spin-polarized LED at room temperature without magnetic or ferromagnetic contacts, which are normally required has been reported (Kim et al., 2021). Furthermore, bioinspired chiral metal-organic Cu(II) phenylalanine (D- or L-) crystals have shown to present CISS electron conduction

over long ranges (300 nm) at room temperature measured by magnetic cp-AFM. Interestingly, the authors also reported a thermally activated ferromagnetic behavior, which had only been identified in inorganic materials (Huang et al., 2020).

In 2019 Ghosh et al. prepared copper oxide films capable of spin polarize photoelectrons and act as electrocatalyst for the conversion of water to oxygen. The spin filtering ability of chiral CuO avoids the generation of side products such as  $H_2O_2$  (Ghosh et al., 2019). In another example by the same group, chiral cobalt oxide films used as electrocatalysts in the oxygen evolution reaction achieved a 1.4-fold increase in the production of oxygen (Ghosh et al., 2020).

## FUTURE DIRECTIONS IN THE FIELD

The CISS effect has been identified and studied in many different systems, especially over the last 20 years. Although it is still at its infancy, experimental studies of this phenomenon and the attempts to give an accurate theoretical explanation have paved the way for a better understanding of the effect itself. Over the next years, its application in the fabrication and the development of novel devices is expected, where miniaturization and reduction of energy consumption can be envisaged, as the use of ferromagnets, and more complicated interfaces can be avoided. The goal is to achieve the proper supramolecular organization to ensure spin polarization and filtering, either using pure chiral entities or in combination with achiral molecules where

supramolecular chirality can be achieved as described by the “sergeants-and-soldiers” effect. Overall, the study and application of the CISS effect can revolutionize spin-based devices in the organic electronics field.

## AUTHOR CONTRIBUTIONS

AG, GM, and AR-C carried out literature searching and wrote the manuscript. AR-C supervised and revised the writing of the manuscript. All authors approved it for publication.

## FUNDING

Graduate School of Complex Systems Chemistry (CSC) of Strasbourg (doctoral fellowship of GM) funded by the French National Research Agency (CSC-IGS ANR-17-EURE-0016) and University of Strasbourg Institute for Advance Science (USIAS) fellowship 2020. LabEx Emerging Investigator 2018 (awarded to ARC).

## ACKNOWLEDGMENTS

All the authors thank the CNRS for providing the tools to start working on this project and to the rest of the team for fruitful discussions.

## REFERENCES

- Aida, T., Meijer, E. W., and Stupp, S. I. (2012). Functional Supramolecular Polymers. *Science* 335, 813–817. doi:10.1126/science.1205962
- Aparicio, F., Nieto-Ortega, B., Nájera, F., Ramírez, F., Navarrete, J., Casado, J., et al. (2014). *Inversion of Supramolecular Helicity in Oligo-p-phenylene-Based Supramolecular Polymers: Influence of Molecular Atropisomerism*. *Angewandte Chemie International Edition*, 1397–1401.
- Aragónes, A. C., Medina, E., Ferrer-Huerta, M., Gimeno, N., Teixidó, M., Palma, J. L., et al. (2017). Measuring the Spin-Polarization Power of a Single Chiral Molecule. *Small* 13, 1602519. doi:10.1002/sml.201602519
- Awschalom, D. D., and Flatté, M. E. (2007). Challenges for Semiconductor Spintronics. *Nat. Phys* 3, 153–159. doi:10.1038/nphys551
- Aytun, T., Barreda, L., Ruiz-Carretero, A., Lehrman, J. A., and Stupp, S. I. (2015). Improving Solar Cell Efficiency through Hydrogen Bonding: A Method for Tuning Active Layer Morphology. *Chem. Mater.* 27, 1201–1209. doi:10.1021/cm503915t
- Banerjee-Ghosh, K., Ben Dor, O., Tassinari, F., Capua, E., Yochelis, S., Capua, A., et al. (2018). Separation of Enantiomers by Their Enantiospecific Interaction with Achiral Magnetic Substrates. *Science* 360, 1331–1334. doi:10.1126/science.aar4265
- Bullard, G., Tassinari, F., Ko, C.-H., Mondal, A. K., Wang, R., Mishra, S., et al. (2019). Low-Resistance Molecular Wires Propagate Spin-Polarized Currents. *J. Am. Chem. Soc.* 141, 14707–14711. doi:10.1021/jacs.9b06142
- Carmeli, I., Skakalova, V., Naaman, R., and Vager, Z. (2002). Magnetization of Chiral Monolayers of Polypeptide: A Possible Source of Magnetism in Some Biological Membranes. *Angew. Chem.*, 114, 2-K: CO, 787–790. doi:10.1002/1521-3757(20020301)114:5<787::AID-ANGE787>3.0.CO;2-K
- Carretero, A. R., Miltzer, S., Nishimura, N., Ávila-Rovelo, N. R., Matsuda, W., Schwaller, D., et al. (2020). Impact of Chirality on Hydrogen-bonded
- Supramolecular Assemblies and Photoconductivity of Diketopyrrolopyrrole Derivatives. *Chem. – A Eur. J.* doi:10.1002/chem.202001540
- Chang, W., Congreve, D. N., Hontz, E., Bahlke, M. E., McMahon, D. P., Reineke, S., et al. (2015). Spin-dependent Charge Transfer State Design Rules in Organic Photovoltaics. *Nat. Commun.* 6, 6415. doi:10.1038/ncomms7415
- Che, C.-M., Chow, C.-F., Yuen, M.-Y., Roy, V. A. L., Lu, W., Chen, Y., et al. (2011). Single Microcrystals of Organoplatinum(II) Complexes with High Charge-Carrier Mobility. *Chem. Sci.* 2, 216–220. doi:10.1039/C0SC00479K
- Dalum, S., and Hedegård, P. (2019). Theory of Chiral Induced Spin Selectivity. *Nano Lett.* 19, 5253–5259. doi:10.1021/acs.nanolett.9b01707
- Dor, O. B., Yochelis, S., Mathew, S. P., Naaman, R., and Paltiel, Y. (2013). A Chiral-Based Magnetic Memory Device without a Permanent Magnet. *Nat. Commun.* 4, 2256. doi:10.1038/ncomms3256
- Fransson, J. (2021). Charge Redistribution and Spin Polarization Driven by Correlation Induced Electron Exchange in Chiral Molecules. *Nano Lett.* 21, 3026–3032. doi:10.1021/acs.nanolett.1c00183
- Fransson, J. (2020). Vibrational Origin of Exchange Splitting and “Chiral-Induced Spin Selectivity”. *Phys. Rev. B* 102, 235416. doi:10.1103/PhysRevB.102.235416
- Ghosh, K. B., Zhang, W., Tassinari, F., Mastai, Y., Lidor-Shalev, O., Naaman, R., et al. (2019). Controlling Chemical Selectivity in Electrocatalysis with Chiral CuO-Coated Electrodes. *J. Phys. Chem. C* 123, 3024–3031. doi:10.1021/acs.jpcc.8b12027
- Ghosh, S., Bloom, B. P., Lu, Y., Lamont, D., and Waldeck, D. H. (2020). Increasing the Efficiency of Water Splitting through Spin Polarization Using Cobalt Oxide Thin Film Catalysts. *J. Phys. Chem. C* 124, 22610–22618. doi:10.1021/acs.jpcc.0c07372
- Ghosh, T., Panicker, J., and Nair, V. (2017). Self-Assembled Organic Materials for Photovoltaic Application. *Polymers* 9, 112. doi:10.3390/polym9030112
- Göhler, B., Hamelbeck, V., Markus, T. Z., Kettner, M., Hanne, G. F., Vager, Z., et al. (2011). Spin Selectivity in Electron Transmission through Self-Assembled



- Monolayers of Double-Stranded DNA. *Science* 331, 894–897. doi:10.1126/science.1199339
- Grenier, C. R. G., George, S. J., Joncheray, T. J., Meijer, E. W., and Reynolds, J. R. (2007). Chiral Ethylhexyl Substituents for Optically Active Aggregates of  $\pi$ -Conjugated Polymers. *J. Am. Chem. Soc.* 129, 10694–10699. doi:10.1021/ja068461t
- Guo, A.-M., and Sun, Q.-f. (2012). Spin-Selective Transport of Electrons in DNA Double Helix. *Phys. Rev. Lett.* 108, 218102. doi:10.1103/PhysRevLett.108.218102
- Gutierrez, R., Diaz, E., Naaman, R., and Cuniberti, G. (2012). Publisher's Note: Spin-Selective Transport through Helical Molecular Systems [Phys. Rev. B85, 081404(R) (2012)]. *Phys. Rev. B* 85, 199902. doi:10.1103/PhysRevB.85.199902
- Hafner, R. J., Tian, L., Brauer, J. C., Schmaltz, T., Sienkiewicz, A., Balog, S., et al. (2018). Unusually Long-Lived Photocharges in Helical Organic Semiconductor Nanostructures. *ACS Nano* 12, 9116–9125. doi:10.1021/acsnano.8b03165
- He, T., Leowanawat, P., Burschka, C., Stepanenko, V., Stolte, M., and Würthner, F. (2018). Impact of 2-Ethylhexyl Stereoisomers on the Electrical Performance of Single-Crystal Field-Effect Transistors. *Adv. Mater.* 30, 1804032. doi:10.1002/adma.201804032
- Huang, C.-H., McClenaghan, N. D., Kuhn, A., Hofstra, J. W., and Bassani, D. M. (2005). Enhanced Photovoltaic Response in Hydrogen-Bonded All-Organic Devices. *Org. Lett.* 7, 3409–3412. doi:10.1021/ol050966l
- Huang, Z., Bloom, B. P., Ni, X., Georgieva, Z. N., Marciesky, M., Vetter, E., et al. (2020). Magneto-Optical Detection of Photoinduced Magnetism via Chirality-Induced Spin Selectivity in 2D Chiral Hybrid Organic-Inorganic Perovskites. *ACS Nano* 14, 10370–10375. doi:10.1021/acsnano.0c04017
- Janssen, P., Cox, M., Wouters, S. H. W., Kemerink, M., Wienk, M. M., and Koopmans, B. (2013). Tuning Organic Magnetoresistance in Polymer-Fullerene Blends by Controlling Spin Reaction Pathways. *Nat. Commun.* 4, 2286. doi:10.1038/ncomms3286
- Jeong, Y. S., and Akagi, K. (2011). Control of Chirality and Electrochromism in Copolymer-type Chiral PEDOT Derivatives by Means of Electrochemical Oxidation and Reduction. *Macromolecules* 44, 2418–2426. doi:10.1021/ma102861t
- Josse, P., Favereau, L., Shen, C., Dabos-Seignon, S., Blanchard, P., Cabanetos, C., et al. (2017). Enantiopure versus Racemic Naphthalimide End-Capped Helicene Non-fullerene Electron Acceptors: Impact on Organic Photovoltaics Performance. *Chem. Eur. J.* 23, 6277–6281. doi:10.1002/chem.201701066
- Kane-Maguire, L. A. P., and Wallace, G. G. (2010). Chiral Conducting Polymers. *Chem. Soc. Rev.* 39, 2545. doi:10.1039/b908001p
- Kettner, M., Göhler, B., Zacharias, H., Mishra, D., Kiran, V., Naaman, R., et al. (2015). Spin Filtering in Electron Transport through Chiral Oligopeptides. *J. Phys. Chem. C* 119, 14542–14547. doi:10.1021/jp509974z
- Kettner, M., Maslyuk, V. V., Nürenberg, D., Seibel, J., Gutierrez, R., Cuniberti, G., et al. (2018). Chirality-Dependent Electron Spin Filtering by Molecular Monolayers of Helicenes. *J. Phys. Chem. Lett.* 9, 2025–2030. doi:10.1021/acs.jpclett.8b00208
- Kim, Y.-H., Zhai, Y., Lu, H., Pan, X., Xiao, C., Gaubling, E. A., et al. (2021). Chiral-induced Spin Selectivity Enables a Room-Temperature Spin Light-Emitting Diode. *Science* 371, 1129–1133. doi:10.1126/science.abf5291
- Kiran, V., Cohen, S. R., and Naaman, R. (2017). Structure Dependent Spin Selectivity in Electron Transport through Oligopeptides. *J. Chem. Phys.* 146, 092302. doi:10.1063/1.4966237
- Kiran, V., Mathew, S. P., Cohen, S. R., Hernández Delgado, I., Lacour, J., and Naaman, R. (2016). Helicenes-A New Class of Organic Spin Filter. *Adv. Mater.* 28, 1957–1962. doi:10.1002/adma.201504725
- Koplovitz, G., Primc, D., Ben Dor, O., Yochelis, S., Rotem, D., Porath, D., et al. (2017). Magnetic Nanoplatelet-Based Spin Memory Device Operating at Ambient Temperatures. *Adv. Mater.* 29, 1606748. doi:10.1002/adma.201606748
- Kulkarni, C., Mondal, A. K., Das, T. K., Grinbom, G., Tassinari, F., Mabesoone, M. F. J., et al. (2020). Highly Efficient and Tunable Filtering of Electrons' Spin by Supramolecular Chirality of Nanofiber-Based Materials. *Adv. Mater.* 32, 1904965. doi:10.1002/adma.201904965
- Kumar, A., Capua, E., Kesharwani, M. K., Martin, J. M. L., Sitbon, E., Waldeck, D. H., et al. (2017). Chirality-induced Spin Polarization Places Symmetry Constraints on Biomolecular Interactions. *Proc. Natl. Acad. Sci. USA* 114, 2474–2478. doi:10.1073/pnas.1611467114
- Lee, O. P., Yiu, A. T., Beaujuge, P. M., Woo, C. H., Holcombe, T. W., Millstone, J. E., et al. (2011). Efficient Small Molecule Bulk Heterojunction Solar Cells with High Fill Factors via Pyrene-Directed Molecular Self-Assembly. *Adv. Mater.* 23, 5359–5363. doi:10.1002/adma.201103177
- Liu, J., Zhang, Y., Phan, H., Sharenko, A., Moonsin, P., Walker, B., et al. (2013). Effects of Stereoisomerism on the Crystallization Behavior and Optoelectrical Properties of Conjugated Molecules. *Adv. Mater.* 25, 3645–3650. doi:10.1002/adma.201300255
- Liu, M., Zhang, L., and Wang, T. (2015). Supramolecular Chirality in Self-Assembled Systems. *Chem. Rev.* 115, 7304–7397. doi:10.1021/cr500671p
- Liu, Y., Xiao, J., Koo, J., and Yan, B. (2021). Chirality-driven Topological Electronic Structure of DNA-like Materials. *Nat. Mater.* 20, 638–644. doi:10.1038/s41563-021-00924-5
- Lu, H., Wang, J., Xiao, C., Pan, X., Chen, X., Brunecky, R., et al. (2019). Spin-dependent Charge Transport through 2D Chiral Hybrid lead-iodide Perovskites. *Sci. Adv.* 5, eaay0571. doi:10.1126/sciadv.aay0571
- Maslyuk, V. V., Gutierrez, R., Dianat, A., Mujica, V., and Cuniberti, G. (2018). Enhanced Magnetoresistance in Chiral Molecular Junctions. *J. Phys. Chem. Lett.* 9, 5453–5459. doi:10.1021/acs.jpclett.8b02360
- Mathew, S. P., Mondal, P. C., Moshe, H., Mastai, Y., and Naaman, R. (2014). Non-magnetic Organic/inorganic Spin Injector at Room Temperature. *Appl. Phys. Lett.* 105, 242408. doi:10.1063/1.4904941
- Medina, E., López, F., Ratner, M. A., and Mujica, V. (2012). Chiral Molecular Films as Electron Polarizers and Polarization Modulators. *EPL* 99, 17006. doi:10.1209/0295-5075/99/17006
- Meijer, E. W., and Schenning, A. P. H. J. (2002). Material Marriage in Electronics. *Nature* 419, 353–354. doi:10.1038/419353a
- Michaeli, K., Kantor-Uriel, N., Naaman, R., and Waldeck, D. H. (2016). The Electron's Spin and Molecular Chirality - How Are They Related and How Do They Affect Life Processes?. *Chem. Soc. Rev.* 45, 6478–6487. doi:10.1039/C6CS00369A
- Mishra, S., Mondal, A. K., Pal, S., Das, T. K., Smolinsky, E. Z. B., Siligardi, G., et al. (2020a). Length-Dependent Electron Spin Polarization in Oligopeptides and DNA. *J. Phys. Chem. C* 124, 10776–10782. doi:10.1021/acs.jpcc.0c02291
- Mishra, S., Mondal, A. K., Smolinsky, E. Z. B., Naaman, R., Maeda, K., Nishimura, T., et al. (2020b). Spin Filtering along Chiral Polymers. *Angew. Chem. Int. Ed.* 59, 14671–14676. doi:10.1002/anie.202006570
- Möllers, P. V., Ulku, S., Jayarathna, D., Tassinari, F., Nürenberg, D., Naaman, R., et al. (2021). Spin-selective Electron Transmission through Self-assembled Monolayers of Double-stranded Peptide Nucleic Acid. *Chirality* 33, 93–102. doi:10.1002/chir.23290
- Mondal, A. K., Preuss, M. D., Ślęczkowski, M. L., Das, T. K., Vantomme, G., Meijer, E. W., et al. (2021). Spin Filtering in Supramolecular Polymers Assembled from Achiral Monomers Mediated by Chiral Solvents. *J. Am. Chem. Soc.* 143, 7189–7195. doi:10.1021/jacs.1c02983
- Mondal, P. C., Kantor-Uriel, N., Mathew, S. P., Tassinari, F., Fontanesi, C., and Naaman, R. (2015). Chiral Conductive Polymers as Spin Filters. *Adv. Mater.* 27, 1924–1927. doi:10.1002/adma.201405249
- Moulin, E., Cid, J.-J., and Giuseppone, N. (2013). Advances in Supramolecular Electronics - from Randomly Self-Assembled Nanostructures to Addressable Self-Organized Interconnects. *Adv. Mater.* 25, 477–487. doi:10.1002/adma.201201949
- Mtangi, W., Tassinari, F., Vankayala, K., Vargas Jentzsch, A., Adelizzi, B., Palmans, A. R. A., et al. (2017). Control of Electrons' Spin Eliminates Hydrogen Peroxide Formation during Water Splitting. *J. Am. Chem. Soc.* 139, 2794–2798. doi:10.1021/jacs.6b12971
- Naaman, R., Paltiel, Y., and Waldeck, D. H. (2019). Chiral Molecules and the Electron Spin. *Nat. Rev. Chem.* 3, 250–260. doi:10.1038/s41570-019-0087-1
- Naaman, R., and Waldeck, D. H. (2012). Chiral-Induced Spin Selectivity Effect. *J. Phys. Chem. Lett.* 3, 2178–2187. doi:10.1021/jz300793y
- Naaman, R., and Waldeck, D. H. (2015). Spintronics and Chirality: Spin Selectivity in Electron Transport through Chiral Molecules. *Annu. Rev. Phys. Chem.* 66, 263–281. doi:10.1146/annurev-physchem-040214-121554
- OuYang, J., and Crassous, J. (2018). Chiral Multifunctional Molecules Based on Organometallic Helicenes: Recent Advances. *Coord. Chem. Rev.* 376, 533–547. doi:10.1016/j.ccr.2018.08.015

- Park, S. H., Roy, A., Beaupré, S., Cho, S., Coates, N., Moon, J. S., et al. (2009). Bulk Heterojunction Solar Cells with Internal Quantum Efficiency Approaching 100%. *Nat. Photon* 3, 297–302. doi:10.1038/nphoton.2009.69
- Pop, F., Auban-Senzier, P., Canadell, E., Rikken, G. L. J. A., and Avarvari, N. (2014). Electrical Magnetochiral Anisotropy in a Bulk Chiral Molecular Conductor. *Nat. Commun.* 5, 3757. doi:10.1038/ncomms4757
- Pop, F., Auban-Senzier, P., Frackowiak, A., Ptaszyński, K., Olejniczak, I., Wallis, J. D., et al. (2013). Chirality Driven Metallic versus Semiconducting Behavior in a Complete Series of Radical Cation Salts Based on Dimethyl-Ethylenedithio-Tetrathiafulvalene (DM-EDT-TTF). *J. Am. Chem. Soc.* 135, 17176–17186. doi:10.1021/ja408350r
- Rao, A., Chow, P. C. Y., Gélinas, S., Schlenker, C. W., Li, C.-Z., Yip, H.-L., et al. (2013). The Role of Spin in the Kinetic Control of Recombination in Organic Photovoltaics. *Nature* 500, 435–439. doi:10.1038/nature12339
- Ray, K., Ananthavel, S. P., Waldeck, D. H., and Naaman, R. (1999). Asymmetric Scattering of Polarized Electrons by Organized Organic Films of Chiral Molecules. *Science* 283, 814–816. doi:10.1126/science.283.5403.814
- Ray, S. G., Daube, S. S., Leitius, G., Vager, Z., and Naaman, R. (2006). Chirality-Induced Spin-Selective Properties of Self-Assembled Monolayers of DNA on Gold. *Phys. Rev. Lett.* 96, 036101. doi:10.1103/PhysRevLett.96.036101
- Rocha, A. R., García-suárez, V. M., Bailey, S. W., Lambert, C. J., Ferrer, J., and Sanvito, S. (2005). Towards Molecular Spintronics. *Nat. Mater* 4, 335–339. doi:10.1038/nmat1349
- Rösch, A. T., Zhu, Q., Robben, J., Tassinari, F., Meskers, S. C. J., Naaman, R., et al. (2021). Helicity Control in the Aggregation of Achiral Squaraine Dyes in Solution and Thin Films. *Chem. Eur. J.* 27, 298–306. doi:10.1002/chem.202002695
- Ruiz-Carretero, A., Atoini, Y., Han, T., Operamolla, A., Ippolito, S., Valentini, C., et al. (2019). Charge Transport Enhancement in Supramolecular Oligothiophene Assemblies Using Pt(II) Centers as a Guide. *J. Mater. Chem. A* 7, 16777–16784. doi:10.1039/C9TA04364K
- Ruiz-Carretero, A., Aytun, T., Bruns, C. J., Newcomb, C. J., Tsai, W.-W., and Stupp, S. I. (2013). Stepwise Self-Assembly to Improve Solar Cell Morphology. *J. Mater. Chem. A* 1, 11674. doi:10.1039/c3ta12411h
- Schenning, A. P. H. J., and Meijer, E. W. (2005). Supramolecular Electronics; Nanowires from Self-Assembled  $\pi$ -conjugated Systems. *Chem. Commun.* 0, 3245–3258. doi:10.1039/B501804H
- Schulze, B. M., Shewmon, N. T., Zhang, J., Watkins, D. L., Mudrick, J. P., Cao, W., et al. (2014). Consequences of Hydrogen Bonding on Molecular Organization and Charge Transport in Molecular Organic Photovoltaic Materials. *J. Mater. Chem. A* 2, 1541–1549. doi:10.1039/C3TA13529B
- Stolte, M., Suraru, S.-L., Diemer, P., He, T., Burschka, C., Zschieschang, U., et al. (2016). Diketopyrrolopyrrole Organic Thin-Film Transistors: Impact of Alkyl Substituents and Tolerance of Ethylhexyl Stereoisomers. *Adv. Funct. Mater.* 26, 7415–7422. doi:10.1002/adfm.201602994
- Stupp, S. I., and Palmer, L. C. (2014). Supramolecular Chemistry and Self-Assembly in Organic Materials Design. *Chem. Mater.* 26, 507–518. doi:10.1021/cm403028b
- Suda, M., Thathong, Y., Promarak, V., Kojima, H., Nakamura, M., Shiraogawa, T., et al. (2019). Light-driven Molecular Switch for Reconfigurable Spin Filters. *Nat. Commun.* 10, 2455. doi:10.1038/s41467-019-10423-6
- Szulcowski, G., Sanvito, S., and Coey, M. (2009). A Spin of Their Own. *Nat. Mater* 8, 693–695. doi:10.1038/nmat2518
- Tassinari, F., Jayarathna, D. R., Kantor-Uriel, N., Davis, K. L., Varade, V., Achim, C., et al. (2018). Chirality Dependent Charge Transfer Rate in Oligopeptides. *Adv. Mater.* 30, 1706423. doi:10.1002/adma.201706423
- Torres-Cavanillas, R., Escorcia-Ariza, G., Brotons-Alcázar, I., Sanchis-Gual, R., Mondal, P. C., Rosaleny, L. E., et al. (2020). Reinforced Room-Temperature Spin Filtering in Chiral Paramagnetic Metallopeptides. *J. Am. Chem. Soc.* 142, 17572–17580. doi:10.1021/jacs.0c07531
- Tsutsui, Y., Okamoto, H., Sakamaki, D., Sugiyasu, K., Takeuchi, M., and Seki, S. (2018). Landscape of Charge Carrier Transport in Doped Poly(3-Hexylthiophene): Noncontact Approach Using Ternary Combined Dielectric, Paramagnetic, and Optical Spectroscopies. *J. Phys. Chem. Lett.* 9, 3639–3645. doi:10.1021/acs.jpclett.8b01465
- Van den Bergh, K., Cosemans, I., Verbiest, T., and Koeckelberghs, G. (2010). Expression of Supramolecular Chirality in Block Copoly(thiophene)s. *Macromolecules* 43, 3794–3800. doi:10.1021/ma100266b
- Vanormelingen, W., Van den Bergh, K., Verbiest, T., and Koeckelberghs, G. (2008). Conformational Transitions in Chiral, Gallic Acid-Functionalized Poly(dithienopyrrole): A Comparative UV-vis and CD Study. *Macromolecules* 41, 5582–5589. doi:10.1021/ma8012114
- Verswyvel, M., Monnaie, F., and Koeckelberghs, G. (2011). AB Block Copoly(3-Alkylthiophenes): Synthesis and Chiroptical Behavior. *Macromolecules* 44, 9489–9498. doi:10.1021/ma2021503
- Waldeck, D. H., Naaman, R., and Paltiel, Y. (2021). The Spin Selectivity Effect in Chiral Materials. *APL Mater.* 9, 040902. doi:10.1063/5.0049150
- Weldeab, A. O., Steen, A., Starkenburg, D. J., Williams, J. S. D., Abboud, K. A., Xue, J., et al. (2018). Tuning the Structural and Spectroscopic Properties of Donor-Acceptor-Donor Oligomers via Mutual X-Bonding, H-Bonding, and  $\pi$ - $\pi$  Interactions. *J. Mater. Chem. C* 6, 11992–12000. doi:10.1039/C8TC00074C
- Wolf, S. A., Awschalom, D. D., Buhrman, R. A., Daughton, J. M., Molnár, S. von., Roukes, M. L., et al. (2001). Spintronics: A Spin-Based Electronics Vision for the Future. *Science* 294, 1488–1495. doi:10.1126/science.1065389
- Xie, Z., Markus, T. Z., Cohen, S. R., Vager, Z., Gutierrez, R., and Naaman, R. (2011). Spin Specific Electron Conduction through DNA Oligomers. *Nano Lett.* 11, 4652–4655. doi:10.1021/nl2021637
- Yamamoto, Y., Fukushima, T., Suna, Y., Ishii, N., Saeki, A., Seki, S., et al. (2006). Photoconductive Coaxial Nanotubes of Molecularly Connected Electron Donor and Acceptor Layers. *Science* 314, 1761–1764. doi:10.1126/science.1134441
- Yang, Y., Rice, B., Shi, X., Brandt, J. R., Correa da Costa, R., Hedley, G. J., et al. (2017). Emergent Properties of an Organic Semiconductor Driven by its Molecular Chirality. *ACS Nano* 11, 8329–8338. doi:10.1021/acsnano.7b03540
- Zerdan, R. B., Shewmon, N. T., Zhu, Y., Mudrick, J. P., Chesney, K. J., Xue, J., et al. (2014). The Influence of Solubilizing Chain Stereochemistry on Small Molecule Photovoltaics. *Adv. Funct. Mater.* 24, 5993–6004. doi:10.1002/adfm.201401030
- Zhang, L., Hao, Y., Qin, W., Xie, S., and Qu, F. (2020). Chiral-induced Spin Selectivity: A Polarized Transport Model. *Phys. Rev. B* 102, 214303. doi:10.1103/PhysRevB.102.214303
- Zhu, Y., Gergel, N., Majumdar, N., Harriott, L. R., Bean, J. C., and Pu, L. (2006). First Optically Active Molecular Electronic Wires. *Org. Lett.* 8, 355–358. doi:10.1021/ol0517168
- Zöllner, M. S., Varela, S., Medina, E., Mujica, V., and Herrmann, C. (2020). Insight into the Origin of Chiral-Induced Spin Selectivity from a Symmetry Analysis of Electronic Transmission. *J. Chem. Theor. Comput.* 16, 2914–2929. doi:10.1021/acs.jctc.9b01078
- Zwang, T. J., Hürlimann, S., Hill, M. G., and Barton, J. K. (2016). Helix-dependent Spin Filtering through the DNA Duplex. *J. Am. Chem. Soc.* 138, 15551–15554. doi:10.1021/jacs.6b10538

**Conflict of Interest:** The authors declare that the research was conducted in the absence of any commercial or financial relationships that could be construed as a potential conflict of interest.

**Publisher's Note:** All claims expressed in this article are solely those of the authors and do not necessarily represent those of their affiliated organizations, or those of the publisher, the editors and the reviewers. Any product that may be evaluated in this article, or claim that may be made by its manufacturer, is not guaranteed or endorsed by the publisher.

Copyright © 2021 Garcia, Martínez and Ruiz-Carretero. This is an open-access article distributed under the terms of the Creative Commons Attribution License (CC BY). The use, distribution or reproduction in other forums is permitted, provided the original author(s) and the copyright owner(s) are credited and that the original publication in this journal is cited, in accordance with accepted academic practice. No use, distribution or reproduction is permitted which does not comply with these terms.



# Evolution of Supramolecular Systems Towards Next-Generation Biosensors

Sujeung Lim<sup>1</sup>, Yuyao Kuang<sup>1</sup> and Herdeline Ann M. Ardoña<sup>1,2,3,4\*</sup>

<sup>1</sup>Department of Chemical and Biomolecular Engineering, Samueli School of Engineering, University of California, Irvine, Irvine, CA, United States, <sup>2</sup>Department of Biomedical Engineering, Samueli School of Engineering, University of California, Irvine, Irvine, CA, United States, <sup>3</sup>Department of Chemistry, School of Physical Sciences, University of California, Irvine, Irvine, CA, United States, <sup>4</sup>Sue & Bill Gross Stem Cell Research Center, University of California, Irvine, Irvine, CA, United States

## OPEN ACCESS

### Edited by:

Jennifer Hiscock,  
University of Kent, United Kingdom

### Reviewed by:

Tony D. James,  
University of Bath, United Kingdom  
Yong Yao,  
Nantong University, China

### \*Correspondence:

Herdeline Ann M. Ardoña  
hardona@uci.edu

### Specialty section:

This article was submitted to  
Supramolecular Chemistry,  
a section of the journal  
Frontiers in Chemistry

**Received:** 10 June 2021

**Accepted:** 09 August 2021

**Published:** 19 August 2021

### Citation:

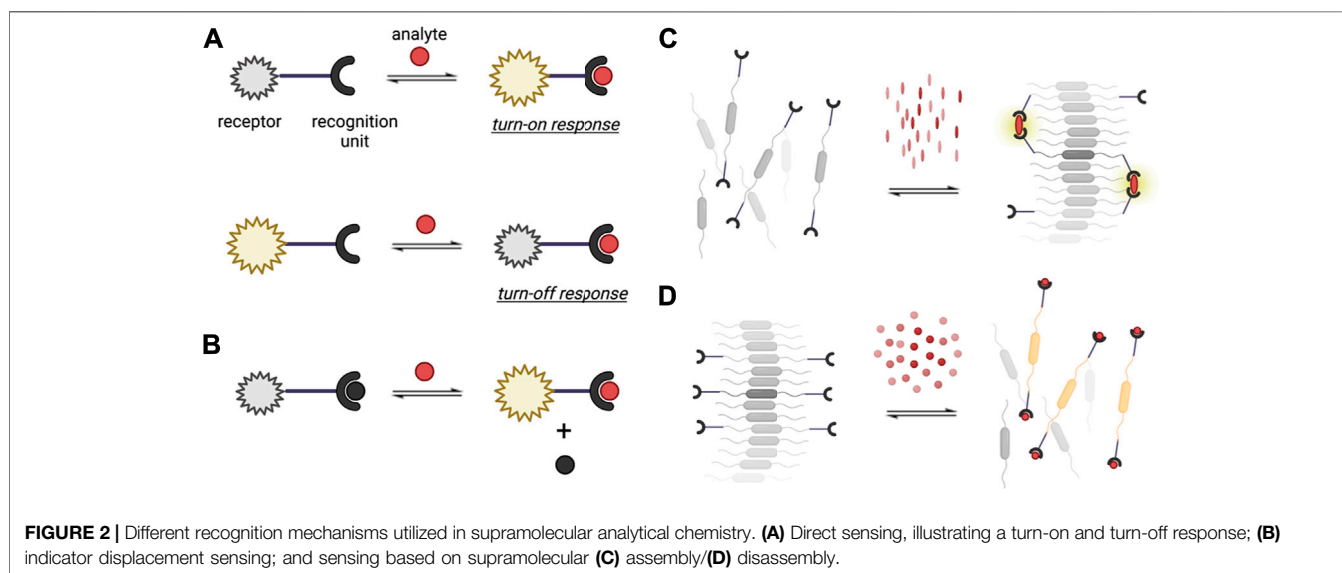
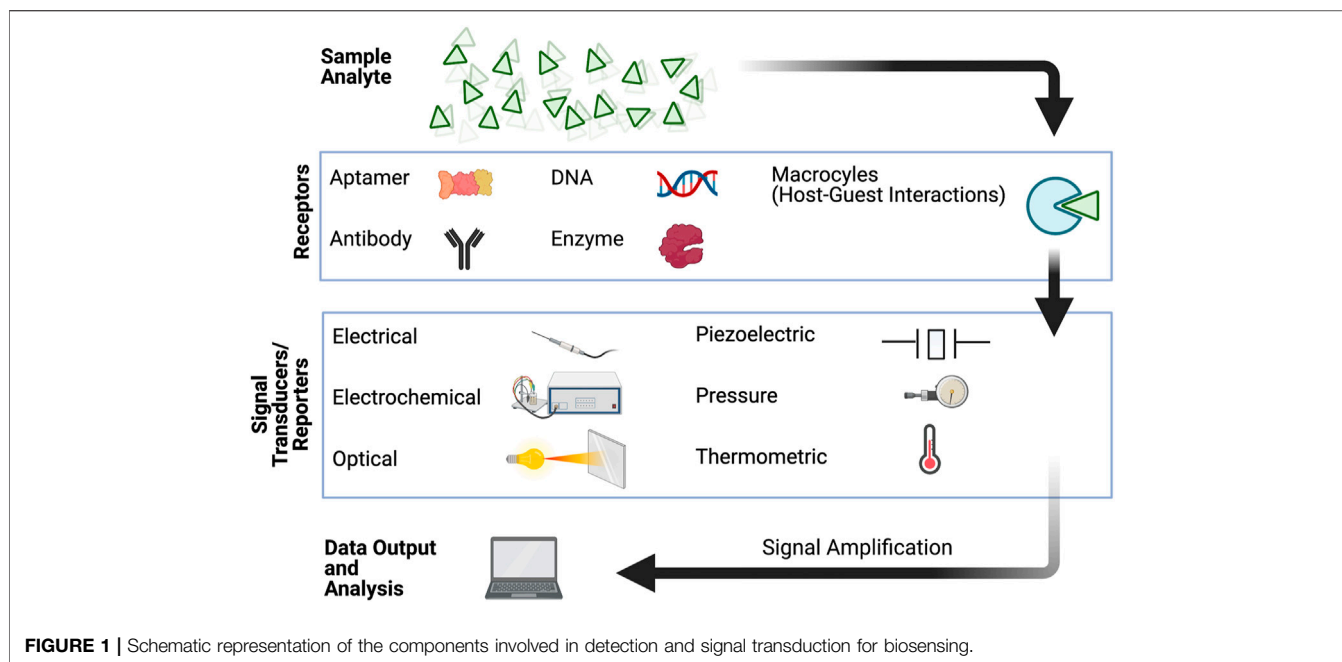
Lim S, Kuang Y and Ardoña HAM  
(2021) Evolution of Supramolecular  
Systems Towards Next-  
Generation Biosensors.  
Front. Chem. 9:723111.  
doi: 10.3389/fchem.2021.723111

Supramolecular materials, which rely on dynamic non-covalent interactions, present a promising approach to advance the capabilities of currently available biosensors. The weak interactions between supramolecular monomers allow for adaptivity and responsiveness of supramolecular or self-assembling systems to external stimuli. In many cases, these characteristics improve the performance of recognition units, reporters, or signal transducers of biosensors. The facile methods for preparing supramolecular materials also allow for straightforward ways to combine them with other functional materials and create multicomponent sensors. To date, biosensors with supramolecular components are capable of not only detecting target analytes based on known ligand affinity or specific host-guest interactions, but can also be used for more complex structural detection such as chiral sensing. In this Review, we discuss the advancements in the area of biosensors, with a particular highlight on the designs of supramolecular materials employed in analytical applications over the years. We will first describe how different types of supramolecular components are currently used as recognition or reporter units for biosensors. The working mechanisms of detection and signal transduction by supramolecular systems will be presented, as well as the important hierarchical characteristics from the monomers to assemblies that contribute to selectivity and sensitivity. We will then examine how supramolecular materials are currently integrated in different types of biosensing platforms. Emerging trends and perspectives will be outlined, specifically for exploring new design and platforms that may bring supramolecular sensors a step closer towards practical use for multiplexed or differential sensing, higher throughput operations, real-time monitoring, reporting of biological function, as well as for environmental studies.

**Keywords:** supramolecular, biosensors, self-assembly, host-guest interactions, supramolecular analytical chemistry

## INTRODUCTION

The development of sensing platforms that can detect target analytes in biological milieu has since transformed the workflow in fields such as disease diagnostics, drug discovery, and food industry (Bhalla et al., 2016; Vigneshvar et al., 2016). These biosensors commonly rely on chemical, immunological, or enzymatic sensing elements whereby the kinetics and affinity of receptor-target binding at the molecular level are critical to their efficiency (Bhalla et al., 2016; Lim and



Ahmed, 2017). There are currently several forms of biosensors that can successfully monitor biological analytes by reporting chemical, optical, electrical, or a combination of these signals (Figure 1). For example, biosensors are used not only to screen pathogens and prevent food contamination, but also, they are used to identify and detect the level of glucose, heart failure, and other diseases (Mehrotra, 2016). Since the development of the first biosensor in 1962 (Clark and Lyons, 1962), which was used for oxygen detection, the range of analytes that can be detected by these biosensors have now expanded from ionic species or small, neutral organic molecules, to cellular phenotypes (Mehrotra, 2016; Mako et al., 2019). Despite several advancements in the

area of biosensing, currently available biosensors are reported to still have challenges associated with them, such as long-term stability, low sensitivity, selectivity at low target concentrations, and most importantly—the ability to perform under real-world environments.

More recently, supramolecular materials brought together by dynamic non-covalent interactions, such as host-guest interactions mediated by H-bonding, have been utilized as biosensing elements. The reversible nature of bonds that hold supramolecular monomers together provide several advantages for biosensing and for monitoring biologically-relevant analytes or signals in a continuous manner (Webber et al., 2016; Pinalli



et al., 2018). Supramolecular analytical chemistry explores new design and properties of synthetic structures that can afford signal modulating molecular recognition and self-assembly processes *via* dynamic interactions (You et al., 2015). The non-covalent and adaptive nature of synthetic supramolecular units allow for multiple mechanisms of detection (Figure 2) that lead to increased signal-to-noise ratio and broadened range of analytes. Three general detection schemes, particularly for sensing systems that generate optical read-outs are the following: 1) direct sensing, whereby a signal output is generated upon the direct binding of an analyte to the receptor (Figure 2A); 2) indicator displacement, which involves the signal change upon the displacement of an indicator by an analyte from the sensory unit (Figure 2B); and 3) aggregation/disaggregation of sensory units in the presence of absence of the analyte (Figure 2C,D). The low energy barrier for disassembly and reassembly of supramolecular structure (Li J. et al., 2020), specifically those that are based on aggregates held by  $\pi$ - $\pi$  interactions, also support good signal amplification. Currently available supramolecular materials have been made from inorganic systems, organic structures, polymers, hybrid materials, charged molecules, crystals, gels, metallic nanoparticles, and others by combining various types of non-covalent interactions (Martins et al., 2015; Wang et al., 2016). Many of these materials and their composites can be functionalized in a facile manner to achieve water solubility, making such supramolecular building blocks more relevant for sensing biological analytes under aqueous environments (Wang et al., 2016). Compared to top-down fabrication approaches such as etching and photolithography, the bottom-up fabrication of supramolecular materials allows the formation of biosensor elements with nanoscale dimensions (Nguyen et al., 2001; Aida et al., 2012; Kumar et al., 2018). Beyond harnessing unique signal transduction mechanisms from nanomaterials, the utility of supramolecular ensembles with nanoscale dimensions enables the miniaturization of biosensors which positively benefits the performance and applicability of biosensors. The higher surface area-to volume ratio increases the active sensing area, both enhancing the signal-to-noise-ratio and reducing the non-specific binding in biosensors (Adams et al., 2008; Soleymani and Li, 2017). Biosensors based on supramolecular ensembles also present higher local concentration of binding sites and lower interference from water molecules solvating the assemblies, resulting in highly sensitive recognition processes (Wang et al., 2016). Considering all of these properties, supramolecular materials are promising candidates for analytical applications and have the potential to address some existing challenges in the field of biosensors.

Herein, we will highlight key advancements in developing supramolecular systems for biosensing and use this as a roadmap to describe the next-generation of supramolecular biosensors. First, we will provide examples of supramolecular structure designs that serve as building blocks for biosensors operating *via* different signal transduction mechanisms. We will then feature representative examples of how certain supramolecular materials are used and implemented for various biosensing

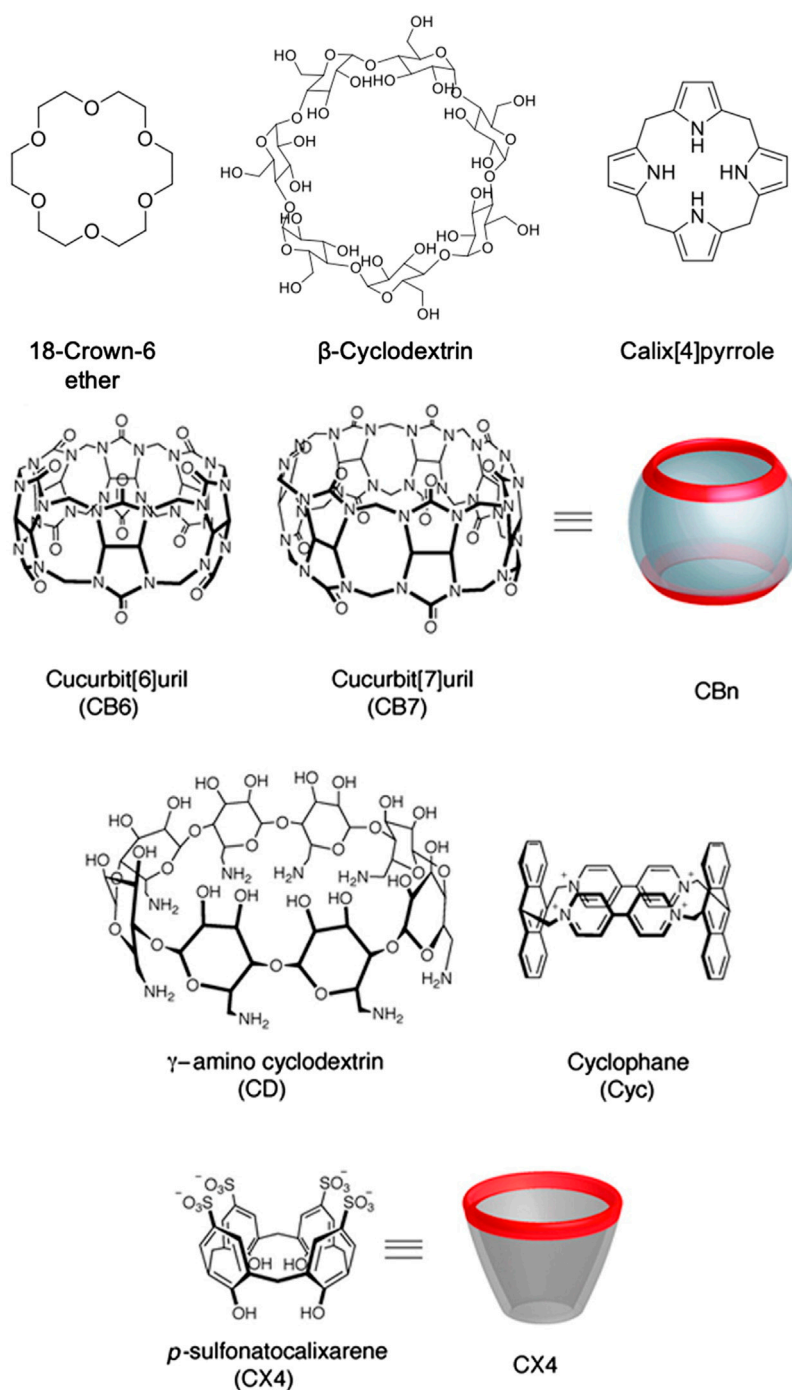
devices. To conclude, we will draw attention to emerging approaches for utilizing supramolecular systems, particularly how these may be adapted in the future towards better addressing the existing challenges in biosensing. The unique characteristics of supramolecular materials and the evolution in the design of their structures or device implementation will enable next-generation biosensors to measure a broader range of analytes, biological functionalities or responses with improved performance—towards positively contributing in environmental, pharmaceutical, and biomedical applications.

## SUPRAMOLECULAR SYSTEMS AS RECOGNITION AND REPORTER UNITS FOR BIOSENSING

### Macrocycles as Recognition Units

Natural receptors, such as enzyme-substrate, protein-ligand, and antibody-antigen rely on non-covalent interactions, shape recognition, and binding site complementarities with high specificity. Several biosensors have employed these interactions to enhance selectivity (Kalantar-zadeh, 2013). In a similar fashion, synthetic supramolecular host-guest interactions, which typically involve macrocyclic systems, have been established as recognition elements in biosensors (Figure 3). For most macrocyclic hosts, the molecular recognition mechanism is based on the non-covalent entrapment of analytes as guest molecules in the host cavity. Macrocycles are considered to be chemically stable, easy to functionalize, and are suitable receptors for a wide range of analytes as guest molecules (Ghale and Nau, 2014; Pinalli et al., 2018). A variety of macrocycle functionalities can be achieved by the cyclization of different motifs based on aryl groups connected *via* short linkers—often resulting in macrocycles with a hydrophobic inner part and hydrophilic outer part (Braegelman and Webber, 2019).

Among the most commonly used macrocyclic host is cyclodextrin (CD), which is synthesized through cyclization of glucose polysaccharides with  $\alpha$ -1,4-linkage and can have tunable cavity sizes (Diehl et al., 2015; Wajs et al., 2016; Braegelman and Webber, 2019). The inner part of CDs is hydrophobic, whereas the outer part consists of hydroxyl moieties that facilitate water solubility. While adamantane-cyclodextrin is a widely used host-guest interaction for detection, CDs can also bind to a variety of nonpolar small molecule guests with binding affinities usually ranging from 100–1000 M<sup>-1</sup> (Mako et al., 2019). Cucurbiturils (CB[n]s) is another class of water-soluble supramolecular host with a rigid cavity that can bind strongly with larger organic or metal cations (Diehl et al., 2015; Mako et al., 2019). CB[n]s are synthesized by the condensation of glycoluril and formaldehyde under acidic conditions, whereby the number of glycoluril groups defines the size of the CB[n] cavity (Pinalli et al., 2018). The macrocycle rim of cucurbiturils are lined with carbonyls that result in a negative charge density at the cavity, which drives the binding of positively-charged guests along with solvation effects (Ling et al., 2016; Kaifer, 2018). Beyond sensing, cucurbiturils can



**FIGURE 3 |** Examples of macrocycles used as supramolecular recognition units for biosensing. Adapted from Ghale et al., 2014. Copyright 2014 American Chemical Society.

also act as delivery vehicles for many hydrophobic drugs due to the hydrophobic nature of the host cavity (Diehl et al., 2015).

Another established class of macrocyclic supramolecular host is calix[n]arenes, which have been used as a receptor for both small cations and anions (Mako et al., 2019). Calixarenes can be formed by the condensation of a *p*-substituted phenol, resorcinol,

or pyrogallol with an aldehyde. Calixarenes conjugated with naphthylidene have been reported to be capable of detecting amino acids such as cysteine, histidine, aspartic acid, and glutamic acid (Chinta et al., 2009). Hamuro and coworkers showed that calix[4]arenes could target a protein (cytochrome C) and inhibit the protein-protein interactions (Hamuro et al.,

1997). Calixpyrroles, which are calixarene derivatives with conical conformation, have been demonstrated to bind to cations or anions depending on structural modification (Gale et al., 1996). Crown ether adds to this list of common macrocycles that can serve as a receptor for many metal ions chemical species, which is often incorporated in fluorescence-based sensor systems (Li et al., 2017). Unlike the other macrocycles discussed above, the binding affinities of neutral crown ethers for metal cations in organic solvents are generally stronger than in aqueous solution (Diehl et al., 2015). For example, 18-crown-6 binding of  $K^+$  has an association constant of  $10^6 M^{-1}$  methanol, whereas in water, it is only  $10^2 M^{-1}$  (Lamb et al., 1980). Preferential binding among different cations, such as between lithium vs. manganese cations, has also been demonstrated for crown ethers (Pauric et al., 2016).

Among the most recently explored class of macrocyclic host is pillar[n]arenes, composed of *p*-dialkoxybenzene-based repeating units connected by methylene bridges (Li Q. et al., 2020). Pillar[n]arenes can be synthesized *via* one-pot Friedel-Crafts alkylation of 1,4-dialkoxybenzenes, to form rigid macrocycles (Cai et al., 2021). They utilize ion-dipole interactions, solvophobic effects, and C-H- $\pi$  interactions to interact with the guest compounds. These driving forces provide host-guest selectivity for different types of target analytes (Cai et al., 2021). Their electron-rich cavities can bind with cationic (e.g., toxic heavy metal ions) and neutral guests, but these cavities can also be functionalized to bind with anionic guests (Li Q. et al., 2020). For instance, Yin and co-workers have developed a sensor based on a water-soluble pillar[5]arene host and a planar chromophoric guest to detect  $Fe^{3+}$  ions with a  $2.13 \times 10^{-7}$  mol/L limit of detection (Yao et al., 2017). Apart from sensing and detection, pillar[n]arenes can also be used for targeted live cell imaging. Yao and co-workers have reported a supramolecular system with a two-step, sequential red fluorescence enhancement using pillar[5]arene-based host-guest recognition for mitochondria-targeted cell imaging (Guo et al., 2020). With this imaging construct, pillar[5]arene formed a complex with bicanostilbene derivative (BSC8) due to the presence of two *N*-methylpyridin-1-ium groups. When pillar[5]arene/BSC8 complex was co-assembled with sodium dodecyl benzene sulfonate (SDBS), the red fluorescence was enhanced. In addition to pillar[n]arenes, prismarenes are also emerging macrocycles for supramolecular sensing. Gaeta and co-workers recently reported a templation-based thermodynamically controlled synthesis of primarenes, which have been demonstrated to have a good affinity for quaternary ammonium guests (Della Sala et al., 2020).

## $\pi$ -Conjugated Assemblies as Reporter Systems

Supramolecular sensory ensembles with large  $\pi$ -systems or chromophores have emerged in recent years as effective reporter units for biosensing. These are often comprised of self-assembling  $\pi$ -systems with aggregation-induced changes in physical properties, such as absorption, fluorescence, or impedance, upon exposure to an analyte or other external triggers. For example, perylene-3,4,9,10-bis(dicarboximide) or perylene bisimide (PBI) is considered as an ideal fluorophore

for sensors because it is an electron acceptor and exhibits strong fluorescence in its monomeric and small oligomeric states (Jones et al., 2004; Zhao et al., 2007). PBI and its analogues have been extensively studied as sensory units not only due to their excellent optoelectronic properties, but also for their stability under thermal and oxidative stress. The planar  $\pi$ -electron conjugation of PBIs allow for  $\pi$ - $\pi$  stacking interactions amongst repeating units to form aggregates, resulting in fluorescence quenching and a hypsochromic shift of the absorption upon assembly (Zheng et al., 2005; Tang et al., 2007). PBI derivatives can be easily functionalized, which makes it more attractive for sensing with high specificity. In a recent example, the assembly system of a PBI derivative, *N,N'*-bis(2-(trimethylammonium)ethylene)perylene bisimide dichloride, was used as a reporter element for detecting biogenic amines based on electronic communication and effect of these amines on the aggregation (and therefore, photophysical properties) of dicationic PBI units (Bettini et al., 2019). Pyrene is another widely used chromophore for biosensors that has a large extinction coefficient, strong tendency towards  $\pi$ - $\pi$  interactions, and good stability in aqueous solution when functionalized appropriately. The emission of pyrene is excimeric in nature, as characterized by a structureless fluorescence profile that is red-shifted by *ca.* 100 nm from the monomer emission (Wang et al., 2016). Charged pyrene derivatives are often designed to probe analytes that can electrostatically influence the aggregation of pyrene, which can be monitored by the increase or quenching of excimer emission. More examples of self-assembling  $\pi$ -systems for biosensing with optical readouts will be discussed in the subsequent sections.

Graphene is another interesting supramolecule that has caught attention for sensing applications in the recent years (Cho et al., 2020). While it is well known for its high mechanical strength, thermal conductivity, and elasticity (Pumera et al., 2010), the high surface-to-volume ratio of graphene enables the absorption of a large amount of aromatic biomolecules through  $\pi$ - $\pi$  interactions (Geim and Novoselov, 2007), making it a favorable candidate for biosensing applications. Similarly, the high specific surface area of graphene allows for direct contact with analytes resulting in high specificity and allows receptors to be efficiently immobilized on the graphene surface (Justino et al., 2017; Szunerits and Boukherroub, 2018). One limitation of graphene is that its native, unfunctionalized form has poor dispersion ability in aqueous medium. On the other hand, graphene oxide (GO) is easier to disperse and its nanoscale analogues have size-enabled properties that have already been leveraged for differential sensing of proteins, cells, and bacteria together with different fluorophores (Chou et al., 2012; Pei et al., 2012).

## Coordination Complexes as Reporter Units

Supramolecular coordination complexes (SCCs) with  $\pi$ -conjugated ligands, controllable coordination geometries, and tunable cavity architecture present several advantages for sensing applications (Cook et al., 2013; Liu et al., 2015; Dey and Haynes, 2021). Contrary to conventional fluorophores in small molecule probes, which experience signal quenching due to analyte-induced aggregation, many SCCs display a higher signal-to-noise

ratio due to aggregation-induced emission behavior in the presence of an analyte or trigger. The first wave of designs for these complexes were primarily designed for ion sensing. To date, 2D-metallacycles and 3D-metallacages have been used to probe larger ionic analytes, biomolecules, gases, and antibiotics based on changes in fluorescence emission intensities or quantum yields. Pt(II) complexes have been among the most widely used SCC for sensing applications. Recent examples include a Pt-based SCC capable of serving as a dual selective probe to detect both cations and anions, such as  $\text{Zn}^{2+}$  and pyrophosphate (Wong et al., 2021). Yam and co-workers demonstrated another recent example of an SCC involving Pt(II) complex used to detect RNA, RNA synthesis inhibitor, and nucleolus (Law et al., 2021). This guanidinium-functionalized alkynylplatinum(II) complex exhibited low cytotoxicity against HeLa and Chinese hamster ovary (CHO) cells, along with a low detection limit of 73.5 ng/ml for its luminescence-based sensing mechanism. Other examples of metal complexes have also now been used for chirality recognition of biomolecules (Folmer-Andersen et al., 2005; Folmer-Andersen et al., 2006; Dong et al., 2017; Mendez-Arroyo et al., 2017). Several efforts have also been dedicated to explore the influence of microenvironments on the sensing efficiency of SCCs as optical biosensors, which is important due to the heterogeneity of analyte environments for real-world applications. For example, Stang and co-workers demonstrated the effect of the number of metallacycle appendages and solvent polarity for SCC sensing (Tang et al., 2018). Their group reported other factors, such as the shape of coordination complexes, counter-anion, or substituent effects, that may influence the photophysical properties and sensing performance of SCCs (Yan et al., 2016; Zhou et al., 2016; Zhang M. et al., 2017). To explore the practical applicability of SCCs, Duan and co-workers reported SCCs with optical responses that can be utilized to detect amino acids even in human blood serum sample. They were able to show that their synthesized material (cerium-based tetrahedron with twelve hydrogen-bonding amide linkages and four triphenylamines) can selectively detect tryptophan/tryptophan-containing peptides in DMF-water mixtures (He et al., 2012).

## Advancing Detection Schemes Using Nanoparticle Constructs

The sections above described general classes of compounds used for recognition and/or signal transduction. Under this section, presented are sensing elements that are specifically packaged to have structures within the nanoscale. This strategy often allows for enhanced signaling, multifunctionality, or better compatibility with bioimaging techniques due to improved systemic circulation dynamics. Nanoparticles for sensing that have been previously reported span the range of organic-inorganic composites, polymeric materials, and bioconjugated structures. Carbon-based nanoparticles, nanofibers, or nanotubes are widely used as nano-biosensors because they can be modified easily with functional groups and have high chemical stability. Carbon nanotubes (CNTs) are mainly used as electrochemical

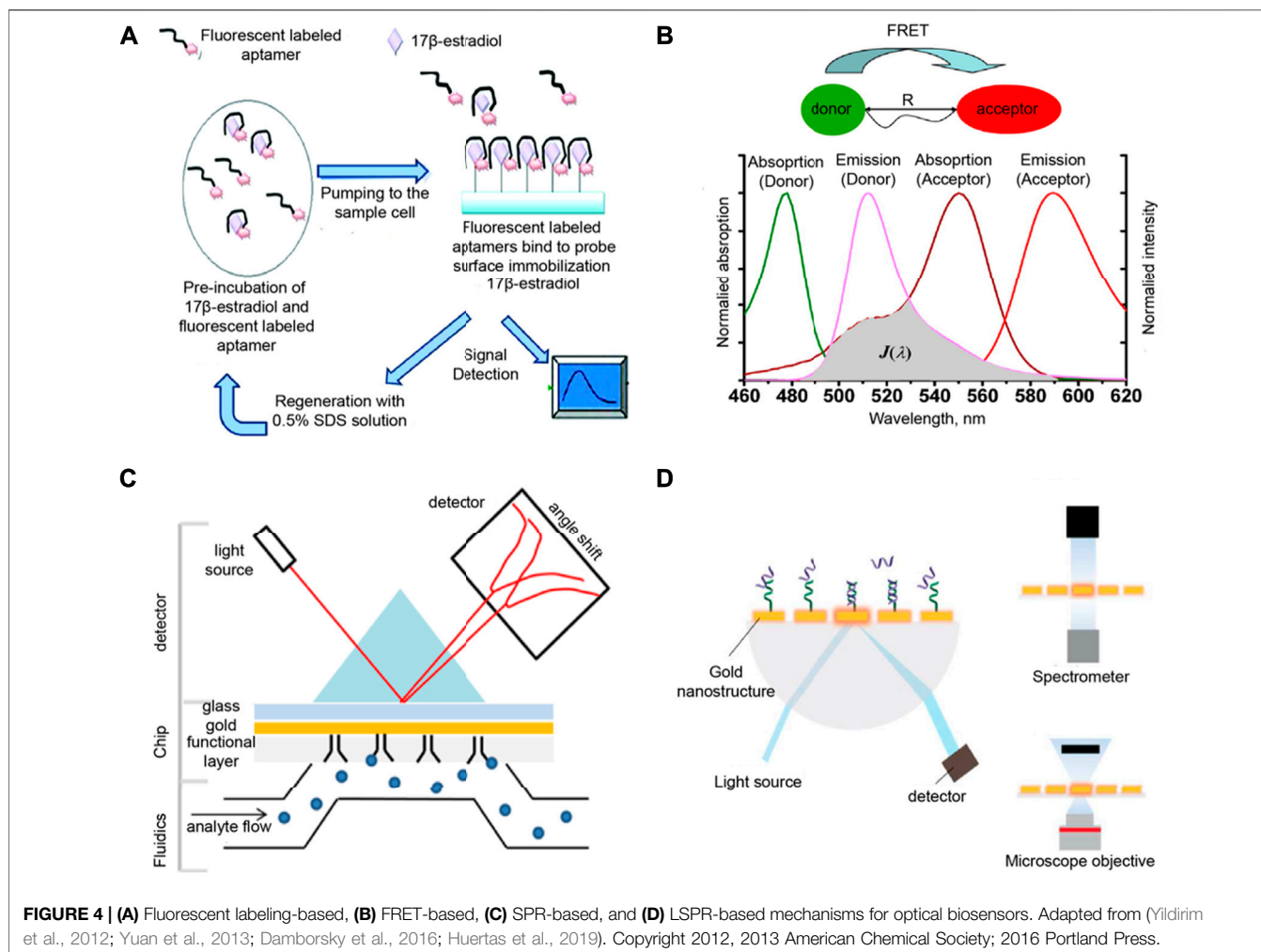
transducers in biosensors because of their large surface area, allowing an increase of immobilization of enzymes to the reaction area with high sensitivity and high electrical conductivity (Zhang et al., 2016; Cho et al., 2018). Similarly, the innate surface properties of CNTs allow biomolecules such as DNA and proteins to adsorb easily. CNTs can also be functionalized with hydrophilic units resulting in higher carrier capacity (Rao et al., 2011). Considering the relevance of these carbon-based nanomaterials for biological sensing, there have been several efforts focused on surface-functionalizing CNTs (e.g., with amino acids) or investigating the biodegradation of CNTs due to oxidative enzymes (Bianco et al., 2011; Tilmaciu and Morris, 2015). A previous report showed CNT biodegradation due to human myeloperoxidase, demonstrating the potential of CNT-based DNA sensors for long-term biological use (Kagan et al., 2010). Fullerenes, which are considered as 0-D nanomaterials with low toxicity and good stability, have also been reported to be useful in electrochemical biosensors with low detection limits (Yuan et al., 2018; Wang et al., 2020).

Development of stimuli-responsive, amphiphilic nanomaterials or amphiphile-induced aggregation of nanoparticles have also emerged as a strategy to reduce concerns with instability under biological environments and toxicity. An early report from Heinze and co-workers demonstrated an optical chemical/biochemical biosensor that is nanophase-separated due to amphiphilic polymeric networks (Hanko et al., 2006). This design allows for one phase to interact with the sensing elements, and another for the target analytes. Moreover, using amphiphilic sensors have high applicability for analytes that are also amphiphilic in character such as glycolipids (Xu et al., 2018). Specific applications that have used amphiphilic structures for sensing include bacterial detection (Nandi et al., 2015) or assessment of pH-fluctuations in cancer cells or tumor tissues (Kim et al., 2020).

As a step towards developing sensing platforms for high throughput screening, nanoparticle array have also been developed for detecting biomacromolecule libraries. Rotello and co-workers have made huge strides on this front, particularly on using metal nanoparticle bioconjugates that utilize characteristic fingerprints for pattern recognition (Miranda et al., 2010b; Bunz and Rotello, 2010; Mout et al., 2012). For example, their group developed arrays of gold nanoparticle-fluorescent polymer complexes that were able to provide quantitative differentiation of multiple proteins with varying structural characteristics (Moyano et al., 2011). In another approach, enzyme-amplified array sensing (EAAS) was developed with gold nanoparticles,  $\beta$ -galactosidase as the enzyme, and an enzyme-activatable fluorescent probe (Miranda et al., 2010a). More recent versions of nanoparticle sensor arrays from Rotello and co-workers have been used to identify different mammalian cell types/states or to detect bacteria (Bajaj et al., 2010; Chen et al., 2015).

In the subsequent sections, we will be highlighting more examples of biosensors based on supramolecular systems, but with more emphasis on the mechanisms involved for signal transduction.





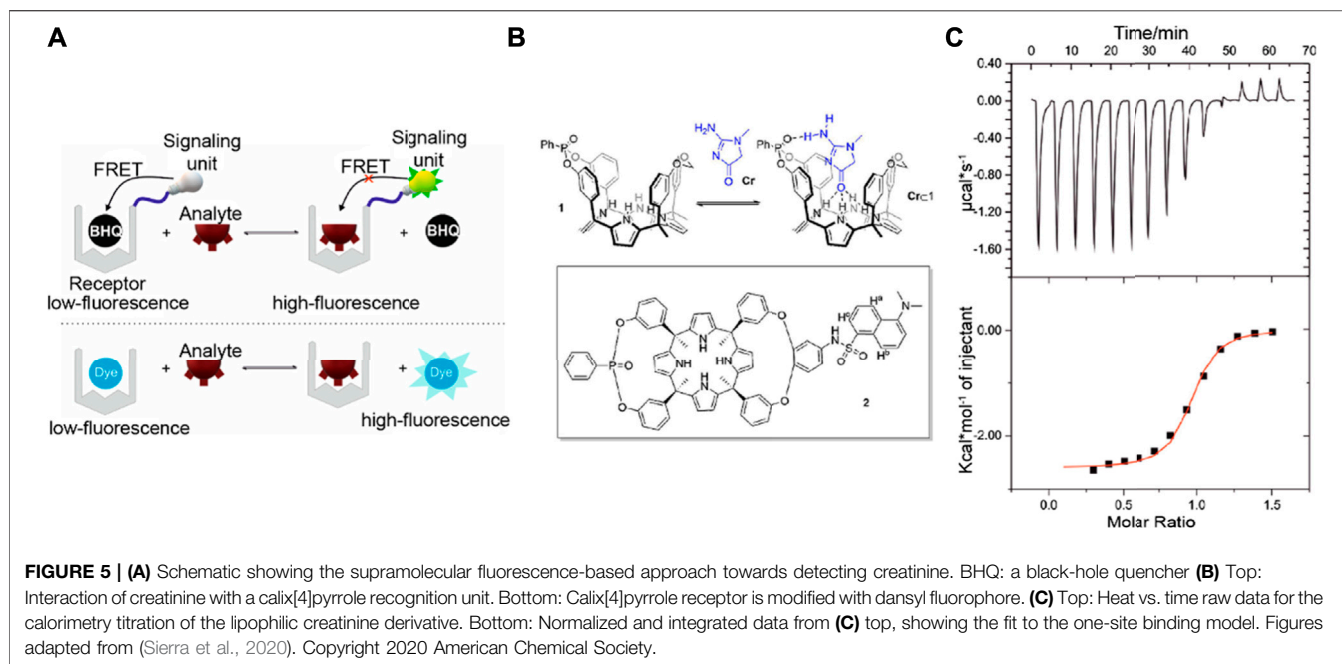
## OPTICAL SUPRAMOLECULAR BIOSENSORS

Supramolecular biosensors with readouts based on changes in absorption, reflectance, emission, or interferometric pattern can operate under label-free or label-based sensing (Peltomaa et al., 2018). Regardless of the photonic process involved, optical biosensors are often considered to be highly sensitive, reproducible, and simple to use. The discussion below highlights a couple of optical processes utilized for biosensing (Figure 4).

Several optical sensors used for biologically relevant analytes utilize fluorescent probes, which either provide a “turn-on” or “turn-off” response. Sensors that use a “turn-on” response are deemed to be more generally favorable due to less background noise than a “turn-off” response. Early reports on supramolecular fluorescence sensors are largely based on chromophores that are able to change their emission upon binding of metal ions (Fabrizzi and Poggi, 1995). For example, an anthracene-based supramolecular sensor with 3,8-bis-pyridin-4-ylethynyl [1,10]-phenanthroline (BPP) ligand was reported to be sensitive to micromolar concentrations of  $\text{Ni}^{2+}$ ,  $\text{Cd}^{2+}$ , or  $\text{Cr}^{3+}$  (Resendiz

et al., 2004). When BPP is self-assembled with 1,8-platinum-functionalized anthracene, the complex formed acts as a unit molecular clip which enables the optical sensing of transition metals. In a recent report by Gu and co-workers, a platform for highly selective detection of an endocrine disrupting compound (17 $\beta$ -estradiol) utilized a fluorescence-labeled DNA aptamer targeted for this analyte (Yildirim et al., 2012). Their portable, inexpensive, and reusable biosensor allows for real-time monitoring of 17 $\beta$ -estradiol through covalently immobilized recognition units onto the optical fiber sensor surface (Figure 4A).

Another widely used fluorescence-based phenomenon in biosensing is fluorescence resonance energy transfer (FRET), which occurs when energy transfer between donor and acceptor units occur as two interacting dipoles (Yuan et al., 2013; Mako et al., 2019; Wu et al., 2020a). FRET probes require the modulation of donor-acceptor distance or spectral overlap integral based on the analyte to be detected (Figure 4B). As an example, Wei et al. reported a metal ion FRET sensor that is highly selective towards potassium ion constructed using crown ether, carbon dots, and graphene (Wei et al., 2012). The dynamic carbon dots and 18-crown-6-ether-reduced



graphene oxide hybrids (18C6E-rGO-Am-CD) complex were assembled. This platform can detect  $K^+$  concentrations relevant to the  $K^+$  content in the blood (3.5–5.3 mM). Moreover, this supramolecular sensor showed higher selectivity towards  $K^+$  as compared to other cations, which implies that the variation in the physiological concentrations of other ions have negligible effects on the read-outs. Sensitivity for other cations or even other biomolecules can be tuned for this sensor by combining different derivatives of crown ethers with carbon dots-reduced-graphene oxide. Additionally, the excitation (>450 nm) and emission (>500 nm) wavelengths of the sensing unit can minimize the background fluorescence from biological fluids. A more recent study by Nau and co-workers used a supramolecular FRET-based system for salmon sperm DNA sensing (Zhang et al., 2019). CB[7] was used as the recognition unit that was attached to a carboxyfluorescein (CF) dye as the FRET acceptor. The FRET donor is 4',6-diamidino-2-phenylindole (DAPI), which can then intercalate with DNA. Upon increasing the DNA concentrations, DAPI moves farther from CB[7]-CF and does not serve as FRET donor. This relocation causes the fluorescence intensity ratio to linearly increase in picomolar range (up to 20  $\mu\text{g/ml}$ ), with a limit of detection of *ca.* 60 ng/ml. This ratiometric, FRET-based sensing platform can be used as another method for DNA quantification with high sensitivity and reliability. Supramolecular biosensors with FRET probes have also been used for sensing metabolites such as creatinine. In the work by Sierra et al., calix[4]pyrrole phosphate-cavitands were used to sense creatinine and its lipophilic derivative hexylcreatinine (Figure 5; Sierra et al., 2020). They reported the use of calix[4]pyrrole modified with dansyl fluorophore to examine hexylcreatinine binding. The molecular recognition

mechanism of the developed supramolecular biosensor for creatinine utilizes a combination of H-bonding,  $\pi$ - $\pi$ , C-H- $\pi$  interactions of polar groups of the receptor unit. Data from calorimetric titration revealed a one-site binding model for this system, as suggested by the sigmoidal binding isotherm with an inflection point around a host:guest ratio of 1:1. This sensor for creatinine is advantageous over other creatinine sensors because of the excellent binding ability to neutral polar species, mono- and polyatomic anions from cone conformation of the reporter unit. However, this reported supramolecular biosensor needs improvement in its selectivity to distinguish creatinine from other biologically relevant analytes such as proline and urea.

As mentioned in an earlier section, optical biosensors that depend on supramolecular assembly or aggregation of chromophores as triggered by the presence of analytes are also widely used. A fast, responsive humidity sensor reported by Mogera et al. used nanofibers built from self-assembled coronene tetracarboxylate (donor) and dodecyl methyl viologen (acceptor), which are photoactive components that can generate electrical readouts (Mogera et al., 2014). The response time of this sensor to relative humidity was reported to be only 10 milliseconds. This supramolecular sensing system is stable under ambient conditions and can even be stored up to 8 months. Other biosensors depend on conjugated aromatic compounds known as aggregation-induced emission luminogens (AIEgens), which often consist of flexible molecular moieties that can consume the energy of the excited state upon photoexcitation through intramolecular motion in the dispersed state. The fluorescence of AIEgens can be attributed to the restriction of intermolecular motion (Li J. et al., 2020). Supramolecular materials based on AIEgens could result in high luminescence efficiency and can be constructed easily to

give controlled and tunable architectures (Li J. et al., 2020). Tang and co-workers reported the first AIEgen using tetraphenylethylene (TPE) as the supramolecular reporter unit (Hong et al., 2008). A more recent example from Lee and co-workers utilized a fluorescent “turn-on” peptide-modified TPE probe to detect heparin. This probe used electrostatic interactions and self-assembly to form supramolecular nanoparticles. The limit of detection of this sensor was 138.0 pM in water and 2.6 nM in serum sample (Lee et al., 2018). This sensor is the first example that shows the dual role of a fluorescent probe to detect and inhibit *via* the recognition process. Compared to the previously reported fluorescence methods for detecting oversulfated chondroitin sulfate, known as the heparin contaminant that can cause hypotension and angioedema, this fluorescence probe does not require a large amount of the enzyme and can be easily utilized for fast high-throughput screening.

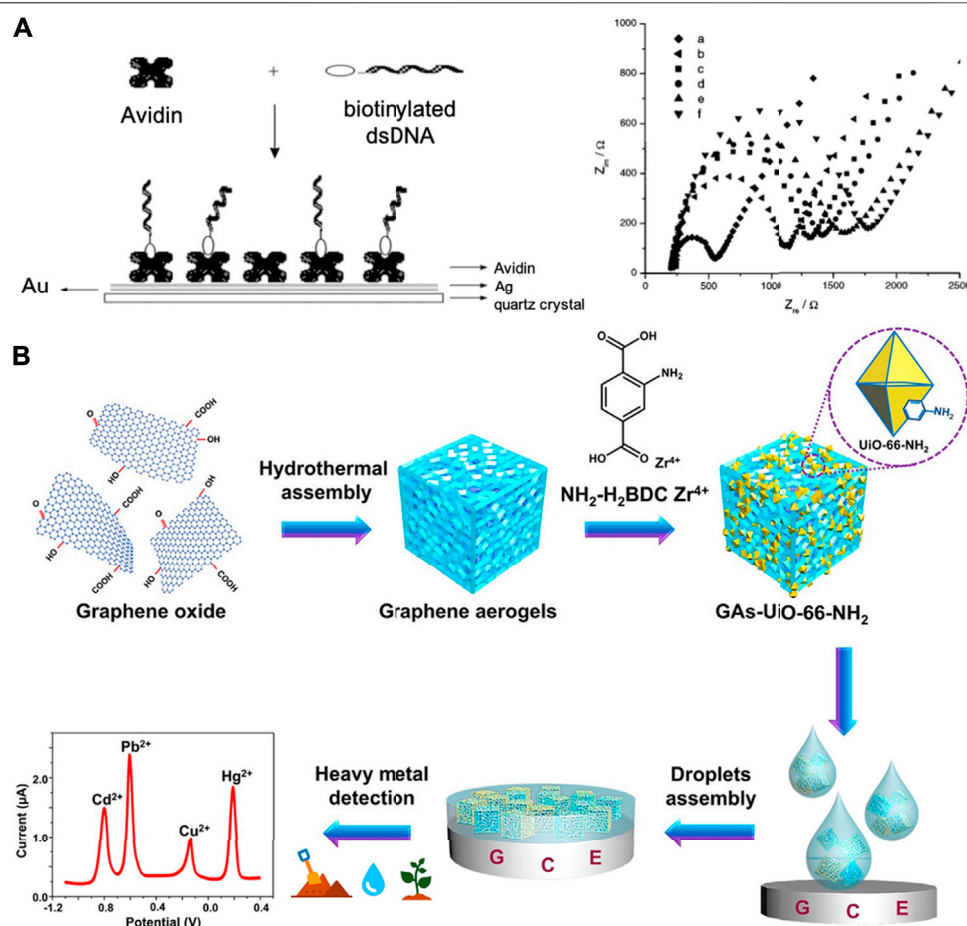
Finally, under this section, we highlight surface plasmon resonance (SPR) as a widely utilized optical phenomenon for biosensors (Ogoshi and Harada, 2008; Dey and Goswami, 2011; Huertas et al., 2019; Chen and Wang, 2020). SPR allows for changes in refractive index to be measured in response to binding of analytes on the surface. This phenomenon occurs when the polarized light is reflected on the surface of metal at the interface of two media at a certain angle (Figure 4C). For example, Chen et al. used a hydrogel-gold nanoparticle supramolecular sphere to develop a label-free and real-time SPR imaging biosensor and specifically detect prostate cancer cell-derived exosomes (Chen et al., 2020). DNA probes on the gold chip surface modified with antibodies can capture the targets by forming polymers. Although the reported limit of detection for this biosensor is  $1 \times 10^5$  particles/mL, which is relatively inferior than the reported values of other nanomaterial-based methods for detecting exosomes, this sensor platform provided high response signals and also shows specificity against exosomes derived from different cells lines. This SPR imaging biosensor has the potential to be utilized in the clinical applications for early diagnosis and real time treatment monitoring of prostate cancer. On the other hand, localized SPR (LSPR) presents a modified SPR configuration that relies on distinct optical processes that occur due to the interaction of light with metallic nanostructures (Figure 4D). LSPR involves photoexcitation of metallic nanostructures that induces a collective electron charge oscillation and impacts the UV-visible absorbance (Damborsky et al., 2016). Sensing platforms based on LSPR offer a similar performance SPR systems without requiring high surface densities of recognition molecules.

## SUPRAMOLECULAR SENSING WITH ELECTROCHEMICAL AND ELECTRICAL READ-OUTS

Since the conception of the first electrochemical biosensor based on glucose oxidase, electrochemical read-outs have been predominantly used for biosensors, primarily due to their efficiency in metabolite monitoring (Chaubey and Malhotra, 2002; Turner, 2013; Hammond et al., 2016). Application of

supramolecular materials in electrochemical biosensors not only improves the selectivity detection of biochemical reactions, but also increases the signal-to-noise ratio by minimizing the electrochemical sensor elements to nano-scale or micro-scale (Schoning and Poghosian, 2002). Electrochemical sensing in the presence of chemical and biological analytes typically involves electron transfer due to non-covalent interactions, which consequentially, alters the electrical properties of supramolecular systems in response to analyte exposure. This alteration can be converted to electrical signals and analyzed by various electrical read-out techniques such as potentiometry and amperometry (Grieshaber et al., 2008). Supramolecular systems that utilize electrochemical processes or electrical read-outs (Figure 6; Yan and Sadik, 2001; Lu et al., 2019) for analyte recognition has been widely used for ion quantification, protein sensing, nucleic acid analysis, and small molecule detection. To date, pushing the limit of detection to sub-nanomolar range has been a major driving factor for the development of potentiometric and amperometric biosensors (Bakker and Pretsch, 2005; Paul and Srivastava, 2018). One of the advantages of potentiometric biosensors is their independence from sample volume and biosensor size. This provides the potential to minimize the biosensor size and achieve high sensitivity at the same time (Ding and Qin, 2020). On the other hand, signal generation for supramolecular amperometric biosensors is based on charge-transfer processes that can produce measurable currents for the analysis. An amperometric biosensor offers advantages such as short response and analysis time, ease of use without sample pretreatment, broad detection range, and the possibility of miniaturization (Luo et al., 2018; Kawai et al., 2019; Takeda et al., 2021).

Healthcare diagnostics, such as the quantitative detection of disease-related proteins, is a major application of supramolecular electrochemical biosensors (Hewitt and Wilson, 2017; Merks et al., 2019). As an alternative to PCR-based nucleic acid analysis techniques, an increasing number of studies apply electrochemical detection due to its rapid detection speed with high accuracy (Espy et al., 2006; Song et al., 2016; Fu et al., 2018; Drame et al., 2020). Zhao and co-workers developed a self-assembled supramolecular nanocomposite for the sensitive and selective electrochemical detection of CD44, an important surface biomarker of breast cancer stem cell (Zhao et al., 2018). Nanospheres self-assembled by diphenylalanine (FF) provide surfaces for gold and silver nanoparticle deposition to amplify the electrochemical signal. CB[8] links nanoparticles through host-guest interactions to aggregate at the electrode surface (Figure 7A). The recognition stability of this sensor is increased by using binding peptides as recognition units. Furthermore, the utility of gold and silver nanoparticles not only facilitates interactions between sensing elements, but also enable an ultra-high sensitivity for CD44 detection (Figure 7B,C). Aptamer-based electrochemical supramolecular biosensor is another promising platform due to its advantages, such as high sensitivity and fast response (Rivas et al., 2015; Yu et al., 2016a; Pereira et al., 2020). Yu et al. proposed a new strategy for using smart protein biogates in electrochemical detection of



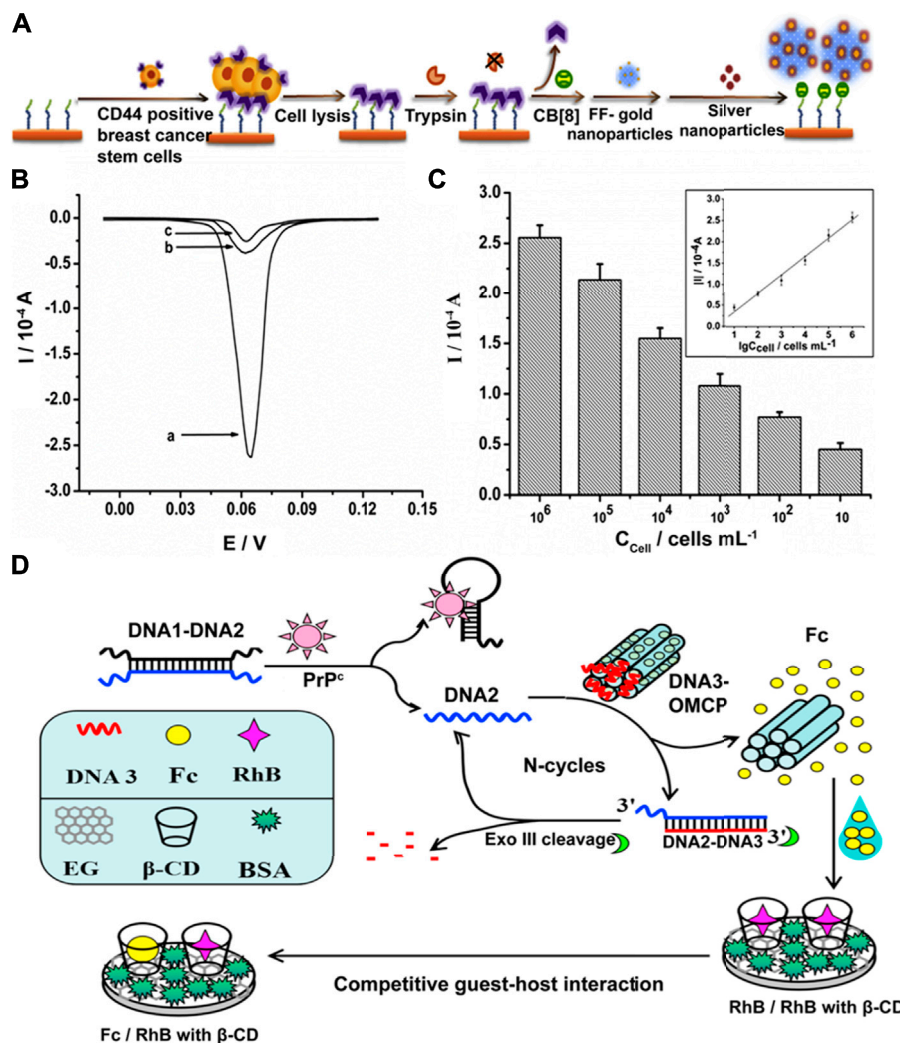
**FIGURE 6 |** Examples of supramolecular biosensors with electrical readouts. **(A)** Sensor interface immobilized with double-stranded DNA onto electrodeposited avidin monolayer (left) and impedance measurements in the presence of  $\text{Fe}(\text{CN})_6^{3-/4-}$  using Au-based electrode with different surface modification (right). **(B)** Electrochemical sensor based on a composite of graphene aerogel and metal-organic framework for simultaneous detection of multiple heavy-metal ions in aqueous solutions. Adapted from (Yan and Sadik, 2001; Lu et al., 2019). Copyright 2001, 2019 American Chemical Society.

prion protein ( $\text{PrP}^{\text{C}}$ ) (Yu et al., 2015). The quantitative analysis of prion can be achieved on the basis of ratiometric electrochemical sensing using methylene blue (MB) and ferrocenecarboxylic acid (Fc). Protein biogates formed by the prion aptamer with MB strongly bind with  $\beta$ -CD on the electrode surface and prevent competitive binding by Fc. Taking advantage of only one single-labeled target aptamer enables a low detection limit (16 fM) and offers the potential for a facile, large-scale production of this biosensor. Later, the same research group proposed the first cascaded, dual-signaling, amplified electrochemical strategy for aptamer-based prion detection as shown in **Figure 7D** (Yu et al., 2016b). The free DNA2 released by specific and selective binding between  $\text{PrP}^{\text{C}}$  and DNA1 with  $\text{PrP}^{\text{C}}$ -binding aptamer can hybridize with DNA3 to release the electroactive Fc from ordered mesoporous carbon probe (OMCP). This dual-signaling amplification can be achieved *via* the competitive guest-host interaction between Fc molecule/Rhodamine B (RhB) and  $\beta$ -CD for the high selectivity of detection. Recycling of DNA2 can be realized by dissociation through Exo III cleavage, which presents the advantage of being able to

perform specific, repeatable, and robust assays using this sensor. Moreover, the application of enzymes for DNA recycling has the potential to be used in other DNA-based biosensors.

Reusability of sensors is another important design factor that has been realized with a couple of electrochemical biosensors. Yang and coworkers developed a pioneering example of a recyclable and immobilization-free electrochemical supramolecular biosensor for breast cancer early diagnostics (Yang et al., 2016). They reported a stable DNA sandwich structure formed by hybridization of MB-labeled signal DNA and alkylamino-modified capture DNA for a highly selective and ultra-sensitive detection of breast cancer susceptibility gene (BRCA). At the same time, host-guest interactions between this DNA sandwich structure with trithiocarbonate modified pillar[5]arene (P5A-CTA) allows for sensor regeneration by simple washing. This immobilization-free technology based on the host-guest interaction and homogeneous DNA hybridization has a high potential for practical applications due to its high reproducibility, ease of use, and reusability. Macrocycles such as  $\beta$ -CD and calixarenes have also been widely studied as a



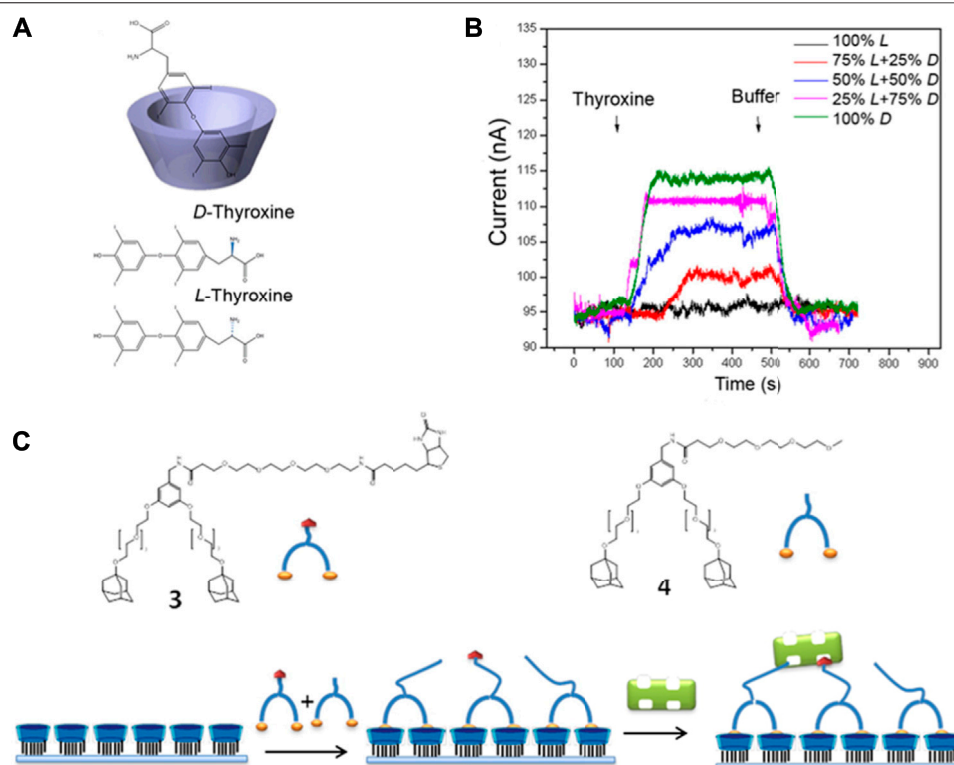


**FIGURE 7 | (A)** Schematic illustration of detection of CD44 in cell samples. **(B)** Linear sweep voltammetry scans obtained in the presence of CD44-positive breast cancer stem cells (BCSCs) (curve a), CD44-negative cell BT474 (curve b) or in the absence of cell samples (curve c). **(C)** Peak currents obtained in different concentrations of BCSCs. Inset shows a linear relationship between the absolute value of the peak current and the logarithm of cell concentration from  $10^1$  cells/mL to  $10^6$  cells/mL. Figures are adapted from (Zhao et al., 2018). **(D)** Schematic illustration of the label-free and cascaded dual-signaling amplified electrochemical strategy for cellular prion protein detection. Figure is adapted from (Yu et al., 2016b). Copyright 2016, 2018 Elsevier.

recognition element for nucleic acid electroanalysis due to good selectivity and fast readouts (Wang et al., 2005; Jiang et al., 2017; Barakat et al., 2020). For instance, supramolecular complex formed by ferrocenyl- $\beta$ -CD and adamantyl-naphthalene diimide not only yields strong electrochemical signals, but also stabilizes the whole target system due to threading intercalation with DNA strands (Sato et al., 2004). Furthermore, electrochemically active ferrocene is first masked by  $\beta$ -CD, and then released in the presence of target DNA. This allows for the analysis to be primarily based on the rise of an electrochemical signal instead of a drop, thereby operating under a “turn-on” detection scheme. In another example, Gorbachuk et al. studied DNA damage using a copolymer of tetrasubstituted thiacalix[4] arene and oligolactic acid, then measuring changes on the polymer film properties such as permeability, charge

distribution, and the charge transfer resistance (Gorbachuk et al., 2017).

For the detection of biologically-relevant small molecules using supramolecular electrochemical sensors, signal specificity and binding selectivity are currently the most critical challenges for performance optimization. To determine two low-molecular weight tumor markers with similar structures, Shishkanova et al. reported a supramolecular receptor by functionalizing Troger's base with amino- and coumarin-units to selectively bind with vanillylmandelic acid (VMA) in the presence of homovanillic acid (HVA) (Shishkanova et al., 2016). The spatial arrangement and accessibility of binding sites played a critical role in the selectivity of this biosensor. Control over receptor geometry provides a mechanism that utilizes spatial factor to enable high sensor specificity. In another example,

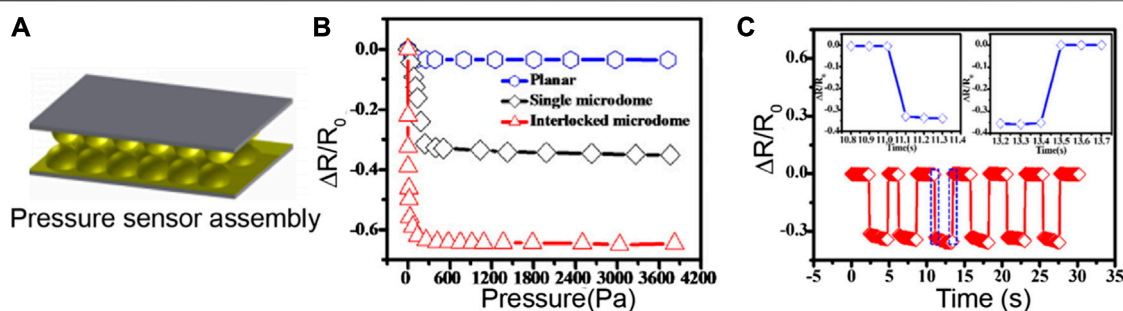


**FIGURE 8 | (A, B)** Detection of 1 nM *L*- and *D*-thyroxine enantiomers using Si NWFETs functionalized with  $\beta$ -CD. **(C)** Adsorption scheme for the sensing of streptavidin through a mixture of adamantyl-biotin (3) and adamantyl-oligo(ethylene glycol) (4) at the surface. Modified from (Duan et al., 2013). Copyright 2013 American Chemical Society.

Uppachai et al. applied supramolecular chemistry with surfactant assemblies to improve electrochemical sensor sensitivity for dopamine detection. The supramolecular assemblies formed by tetra-butylammonium bromide and sodium dodecyl sulphate enhance the electron transfer of dopamine due to hydrophobic interaction and electrostatic attraction between dopamine and gold nanoparticles on the modified glassy carbon electrode (Uppachai et al., 2020). Shen et al. reported a supramolecular aptamer self-assembled by the thiolated aptamer probe and a biotin-labeled analog in the presence of cocaine. This dual amplification resulting from the binding of linear DNA molecule and catalysis of the  $\alpha$ -naphthylphosphate ( $\alpha$ -NP) hydrolysis improves the limit of detection for cocaine to 1.3 nM (Shen et al., 2015). The mechanism of this rolling circle amplification is possible to be applied to the other detection of drug abuse in a fast and sensitive manner with suitable supramolecular aptamers.

Lastly, it is important to highlight supramolecular sensing methods that rely on changes in electrical properties such as *via* impedance measurements and field effect transistors (FETs). Supramolecular sensing of enantiomeric composition using field-effect transistors (FET) has been reported with cyclodextrin-functionalized silicon nanowire FET (Si NWFET) (Duan et al.,

2013). The supramolecular interface of this device was able to distinguish *L*- and *D*-enantiomers of thyroxine molecules (Figure 8). The reported affinity constants for *L*- and *D*-thyroxine are  $1.02 \pm 10^5 \text{ M}^{-1}$  and  $7.11 \pm 10^8 \text{ M}^{-1}$ , respectively. The involved mechanism shed the light on supramolecular interface built by functionalization of Si NWFET with cyclodextrin to benefit both practical device design and fundamental research study. Another example of supramolecular FET-based sensing was demonstrated with CB [7] derivatives to detect amphetamine-type stimulants (ATS) (Jang et al., 2017). This OFET-based wireless sensing platform offered a sensitive, flexible, and rapid approach for real-time liquid phase ATS detection. The limit of detection generated by this supramolecular biosensor was on the picomolar range, showing the highest sensitivity towards ATS to date. Moreover, the OFET based mechanism enables the feasibility to fabricate this portable and miniaturized sensor to drive the development of on-site real-time detection. Currently, there are several other macrocyclic receptors used in electrical sensors not only for solution-based analytes, but also for vapors. Calixarenes, porphyrins, and cyclodextrins are among those that have demonstrated good selectivity and fast readouts when coupled with electrical transducers for biosensing (Phillips et al., 2020).



**FIGURE 9 |** (A) Pressure sensor based on a flexible PDMS film, micropatterned using a colloid self-assembly technology. (B) The pressure sensitivities of sensor films with planar, and single microdome, and interlocked microdome surfaces. (C) Time-dependent response of the microdome-patterned PDMS sensor at a constant pressure of 100 Pa. Adapted from (Zhang Y. et al., 2017). Copyright 2017 American Chemical Society.

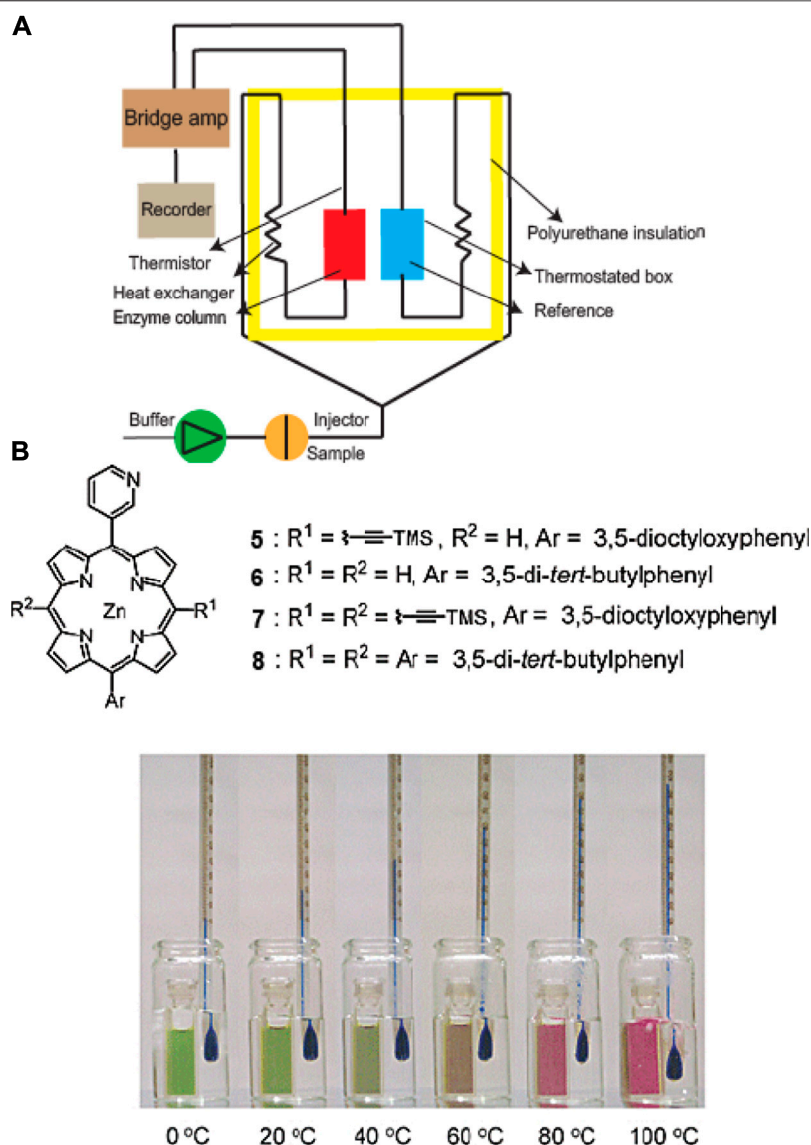
## OTHER TRANSDUCTION MECHANISMS FOR SUPRAMOLECULAR BIOSENSORS

While conventional biosensors that solely rely on photonic or electronic processes are widely used, there are other transduction mechanisms used for sensing which may offer unique advantages in terms of selectivity and sensitivity. These include, but are not limited to, piezoelectric, thermometric, magnetic, and micromechanical transducers. Discussed below are some examples of sensor systems based on supramolecular materials that utilize less common signal transduction mechanisms.

Biosensors that rely on pressure or force sensing do not require an analyte to bind to the sensors to initiate a readout. With this, pressure-based and piezoelectric biosensors have the potential to be used in portable devices for healthcare applications at home and point-of-care settings (Yu et al., 2021; Pohanka, 2018). In the report by Zhang et al., elastic microstructured polydimethylsiloxane (PDMS) film was constructed by using self-assembly method with monodispersed polystyrene (PS) microsphere as a monolayer (**Figure 9A**) (Zhang Y. et al., 2017). The surface microstructure, along with material durability and stability, were critical factors in determining the sensitivity of this supramolecular-based pressure sensor. This sensor exhibited a detection capacity at low pressures, affording a real-time change in resistance measurement by simply putting a dry rose flower on the top of the sensor. As the process of removing and placing the dry rose was repeated, the resistance values also increased and decreased, confirming the good limit of detection for this sensor. Moreover, by enhancing the size of the microdomes, the pressure sensors showed highly sensitive detection capability ( $\sim 15 \text{ kPa}^{-1}$ ), fast response time of 100 ms, and a low limit of detection of 4 Pa (**Figures 9B,C**). In addition, its tunability and facile fabrication process with low cost make this supramolecular pressure sensor potentially useful for real-time human health monitoring using wearable electronics. There have also been reports on supramolecular, stretchable pressure sensors such as the conductive self-healable gels (CSGs) by Khan and co-workers (Khan et al., 2020). This study reported a supramolecular gel, containing polythiolic

acid (PTA), pyromellitic acid (PA),  $\text{Fe}^{3+}$  and a polyaniline (PANI) network, that is highly sensitive ( $2.8 \text{ kPa}^{-1}$ ), stretchable ( $>5,000\%$ ), and has good strain sensitivity (gauge factor of 11). This supramolecular, self-healable gel sensor is injectable, making it an excellent candidate to be used in future biomedical applications. Quartz crystal resonators are also commonly used as piezoelectric biosensors because of the linear relationship that can be established between deposited mass and frequency response of the crystal standing wave (Pohanka, 2018; Chalklen et al., 2020). In a report by Liu et al., a piezoelectric supramolecular sensor was coated with  $\beta$ -cyclodextrin and calixarene derivatives to show high sensitivity and selectivity toward aliphatic amines. The frequency data demonstrates the sensitivity of this piezoelectric quartz crystal sensor to the size and the shape of the aliphatic amine analytes (Liu et al., 2002). In this case, the microstructural change of the host molecule dictates how sensitively the piezoelectric quartz crystal sensor coated with cyclodextrin derivatives detects the amine guests. For the piezoelectric quartz crystal sensors coated with calixarene derivatives, there are two main sensing mechanisms—formation of complex inside (*endo*) and outside (*exo*) the macrocycle—depending on the interaction with the amine guests. Further illustrating the advantages of a piezoelectric transducer, CB[6] was used for a sensor that can rapidly detect cocaine with high sensitivity (Menezes et al., 2017). This piezoelectric sensing platform also offers reusability for detecting drugs. These representative examples suggest that macrocyclic receptors can be systematically tuned to impart selectivity on piezoelectric systems for rapid sensing.

On the other hand, thermal biosensors offer the advantage of long-term stability since there is often no chemical contact needed between transducer and sample. A general workflow for a thermometric biosensor is shown in **Figure 10A**, which specifically illustrates an enzyme thermistor (Zhou et al., 2012). The thermostated box can regulate the physiological temperature, whereby the heat generated reduces thermistor resistance and the bridge amplifier reads the signal (Zheng et al., 2006; Zhou et al., 2012). A pioneering study on a supramolecular thermochromic system utilized a zinc-porphyrin complex with a metal-ligating 3-pyridyl group (Tsuda et al., 2003). This sensor



**FIGURE 10 | (A)** Schematic diagram of a thermal biosensor. **(B)** Thermochromism exhibited by a zinc complex of alkynyl-functionalized (3-pyridyl)porphyrin in toluene. Adapted from (Tsuda et al., 2003; Zhou et al., 2012). Copyright 2003 American Chemical Society.

takes advantage of the ability of the complex to have a thermally-induced change in axial coordination dynamics, ultimately leading to an altered absorption profile (**Figure 10B**). The temperature-dependent molecular transformation leads to a change in effective  $\pi$ -electronic conjugation length, resulting in absorption spectral shifts that are highly dependent on alkynyl group. In particular, one of the conditions led the zinc complex in toluene to change its color from green to yellow to red as the temperature increased. Without any alkynyl group, the color only slightly changed from orange to pink and having two alkynyl groups did not result in a dramatic color change as the temperature increased from 0 to  $100^\circ\text{C}$ . This reported sensor presents an example of wide-range thermochromism, thus, has the potential to be used as a multicolor thermometer with easy

visualization of the colors representing corresponding temperatures. Another example of a supramolecular temperature sensor is reported by Sambe et al., whereby the sensor was constructed based on the host-guest interactions with hydrophilic tetracationic macrocyclic host cyclobis(paraquat-*p*-phenylene) tetrachloride ( $\text{CBPQT}^{4+}$ ) with a programmable functionality (Sambe et al., 2014). Finally, as an example of a sensor array system that utilizes a hybrid approach for signal read-outs, Zhang and co-workers developed a thermochemiluminescence (TCL)-based platform for protein and cell discrimination. The fingerprint TCL signals are uniquely generated as a function of thermal catalytic oxidation (Kong et al., 2011). The reported cross-reactive sensing array system, which can be categorized under a class of vapor-



based sensors known as “chemical noses,” is composed of nanomaterials that are solid catalysts with good stability. This TCL-based sensing system is advantageous over other types due to enhanced sensitivity, reversibility, and fast generation of read-outs.

## EMERGING TRENDS AND CURRENT CHALLENGES

Our discussion up to this point has demonstrated the rich variety of exemplar molecular designs and signal transduction mechanisms used for supramolecular biosensors to date. These previously reported supramolecular sensors have afforded the detection of charged species, not limited to metal cations and anions, but also organics species such as amino acids. Beyond broadening the scope of target analytes, it is logical that the next steps in the field would be to explore ways that could increase the sensitivity, selectivity, and stability of supramolecular materials for biosensing. Optimization of these characteristics have been among the longstanding challenges that are relevant towards the practical applications of supramolecular sensors for biological imaging (Reineck and Gibson, 2017), technologies for national security (Sun et al., 2015), or food industry (Zhou et al., 2018)—to name a few. On a similar note, the rise of newer device platforms that enable real-time sensing and high throughput screening (e.g., microfluidics or flexible sensors) requires compatibility and stability of supramolecular structures present in real biological environments. Among the pioneering examples of microfluidic integration is the supramolecular optical chemosensor by Nocera and co-workers, which uses cyclodextrin modified with a  $\text{Tb}^{3+}$  macrocycle to detect polyaromatic hydrocarbons in aqueous solutions at sub-micromolar concentrations even without signal amplification (Rudzinski et al., 2002). Recently, gel-based supramolecular sensors have been emerging as a platform that provides a unique kinetics and dynamics for the sensing process (Cao et al., 2019; Ma et al., 2019; Sebastian and Prasad, 2020). For example, supramolecular copper metallogel has been used for sensing toxic cyanide ions (Sebastian and Prasad, 2020). This work presented cyanide sensing based on deprotonation in aqueous medium caused by very high solvation energy of cyanide ion in water. Beyond these aforementioned themes, discussed below are other promising trajectories that have been emerging in the field of supramolecular biosensors.

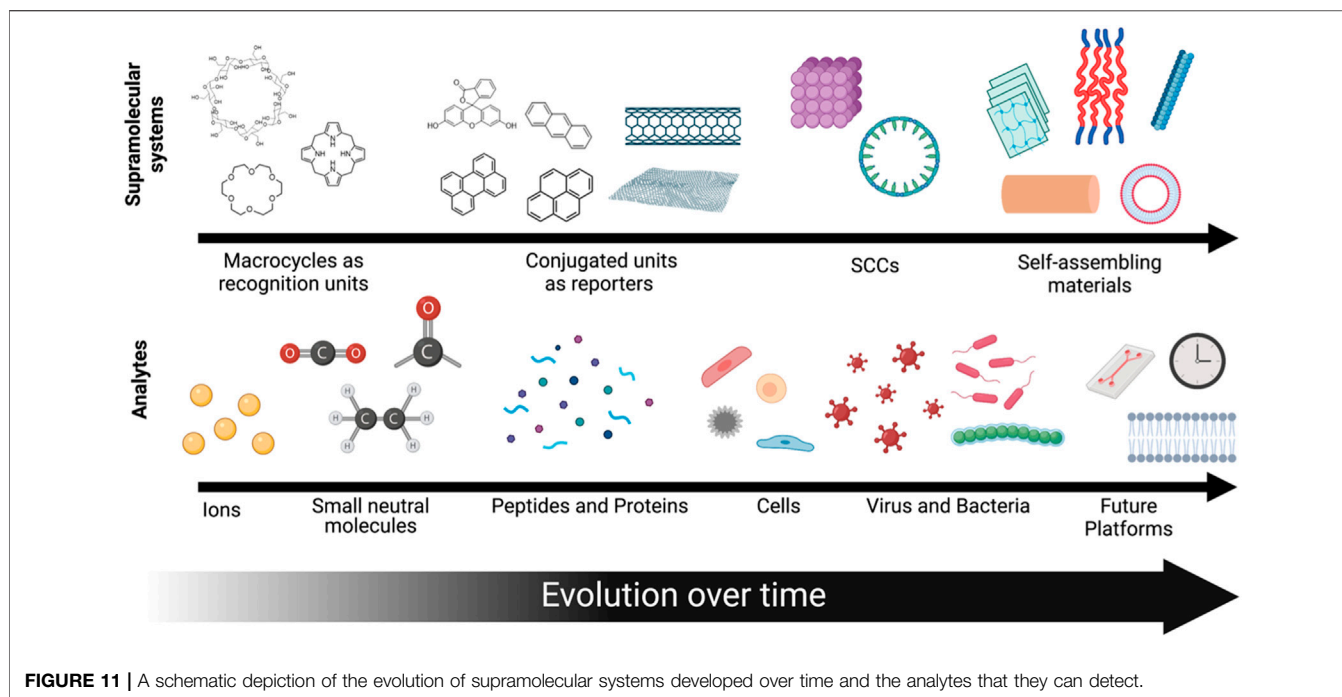
First, we are currently in an era where molecular machines (rotaxanes, catenanes, or molecular rotors) exist and continue to be explored for analytical applications. These complex structures offer the advantage of having fast-motion response that is fatigue-resistant, which may be used to detect submolecular movement (Erbaş-Cakmak et al., 2015). Interlocked structures of molecular machines are advantageous for optically sensing small guest molecules. In a study by Cornell and co-workers, a biosensor with a self-assembled lipid bilayer embedded with gramicidin A ion

channels has been developed to act as a biological switch (Moradi-Monfared et al., 2012). This rapid and sensitive diagnostic device, which preserves its accuracy even in the presence of human serum, plasma and whole blood, can be used as an alternative for enzyme-linked immunosorbent assay (ELISA) that does not require pre- or post-processing steps. A recent work from Stoddart and co-workers demonstrates the use of electrochemically switchable bistable [2]rotaxane with a fluorescent molecular rotor, which may be used in the future for electro-optical sensing applications (Wu Y. et al., 2020). Cyclodextrin-based catenanes and rotaxanes have also been reported for use in sensing many cations and anions (Bak et al., 2020). For example, it was reported that rotaxane was used to sense  $\text{Au}^{3+}$  using fluorophores like anthracene (Chan et al., 2019).

New approaches towards differential sensing or multiplexing using supramolecular materials have also gained attention over the past decade. Sensor arrays that mimic the human sensory system (i.e., artificial nose or tongue) have been used to discriminate between multiple analytes. For example, Eker et al., reported a supramolecular luminescent sensor platform with five parallel sensing self-assembled monolayers incorporated in a microfluidic device that can detect multiple analytes (phosphate anions and aromatic carboxylic acids) (Eker et al., 2011). Other examples that involve supramolecular arrays for differentially sensing biomolecular analytes used antibody-free systems for the detection of the histone code (Minaker et al., 2012) and gold nanoclusters for nucleotide sensing (Rana et al., 2012; Pezzato et al., 2013), and even mammalian cell types or cancer states (Bajaj et al., 2010).

Since many biologically relevant molecules are chiral, and different enantiomers have varying biological activity or functionality, methods for chirality analysis are of high significance for biological analyte sensing. Supramolecular materials used for chiral sensing commonly utilize optical sensing mechanisms. Wolf and co-workers made several advances in this area, primarily by using achiral chromophores that exhibit induced circular dichroism and only show strong Cotton effects in the UV-Vis region upon addition of the chiral analyte. Several metal complexes have also been used for circular dichroism-based sensing. Additionally, combining circular dichroism readouts with SPR and FET sensors have been previously reported (Ariga et al., 2010). A recent report on chiral supramolecular biocoordination polymers with photochromic, photoluminescent, photoconductive, and chemiresistive characteristics present a future for chiral sensing whereby one system may afford multiple signal transduction mechanisms (Shang et al., 2018).

Next, advancements in platform engineering is required to achieve sensors that are portable, inexpensive, and can be used multiple times over. Reusability or recyclability of sensors is a well-sought property since many available sensors are based upon irreversible interactions. The supramolecular-based sensors achieve high stability during the recycling due to the unique interactions between sensor elements and analytes. For instance, Qu et al., developed a reusable



**FIGURE 11** | A schematic depiction of the evolution of supramolecular systems developed over time and the analytes that they can detect.

supramolecular sensing platform using  $\beta$ -CD as a host to detect bacteria and proteins. They showed that it could be used to detect bacteria (*E. coli*) and protein (Concanavalin A) several times without losing bioactivity (Qu et al., 2017a). Another example is from Lu et al., which involves a silver nanocluster-based pH sensor together with a copolymer ligand that has *N*-heterocyclic groups of 8-hydroxyquinoline and *N*-isopropylacrylamide (Lu et al., 2018). This reversible sensing system was able to be reused to sense a pH range of 3.04–5.25 up to six times. Sonication or rinsing the sensor surface with a solution at a specific pH (Duan et al., 2015), surfactant addition (Tang et al., 2016; Qu et al., 2017b), or utilization of competitive binding (Jia et al., 2016; Lei et al., 2016) are other strategies that have been reported to effectively regenerate supramolecular sensing units.

Lastly, interfacing supramolecular sensors directly with living system—whether for mammalian cell screening or detection of bacteria or virus—is an area that continuously receives high interest in biosensing. This has been proven to be challenging due to the complex and dynamic microenvironments within or surrounding these target living systems. Nonetheless, the examples of supramolecular materials used for differentially screening or identifying cells (e.g., tumorigenic vs. healthy) and bacteria highlighted in earlier sections suggest that the field is now significantly past establishing the proof-of-principle for detecting these analytes. Recent studies that explore the supramolecular assembly dynamics within cellular environments or sub-cellular localization present the future potential of having more controlled detection schemes within the biological milieu (Krivitsky et al., 2019; Bai et al., 2020; He et al., 2020; Pieszka et al., 2020).

## OUTLOOK

In this Review, we summarized the key technological advancements in the area of supramolecular biosensors (Figure 11). We have highlighted the evolution of utility of supramolecular components in biosensing platforms, from recognition units, to now being able to be both detectors and transducers. Advancements in supramolecular analytical chemistry have led to innovative designs for high performing biosensors that have transformed the types of analytes and biological niches where these sensors can be applied—from small ionic species, to now being able differentially detect proteins, cell phenotypes, and bacteria. The analytical supramolecular systems developed to date are getting closer to truly mimicking the natural sensory systems of higher order species, relying on selective interactions with a broad range of analytes instead of a specific interaction with just one type of analyte. As such, beyond the single analyte sensing paradigm, supramolecular sensors can now report environmental parameters (such as temperature and pressure), differentiate between stereoisomers, and perform multiplexed sensing. While this review is not meant to provide a comprehensive history of every iteration of supramolecular sensor design reported to date, we hope to have highlighted the key advancements that has led to the state-of-the-art supramolecular biosensors nowadays.

Due to the innumerable variations of supramolecular structures that may be designed and synthesized, one can expect that the next-generation of supramolecular structures can open doors for more complex recognition and transduction functionalities that are yet to be realized. Such advancements can bring supramolecular-based biosensors a

step closer towards its practical use for real-time drug delivery monitoring, reporting of tissue function of 3D organ models, or as commercial components of wearable health monitors. Overall, supramolecular biosensing has evolved over the years into a rich, transdisciplinary field with high promise towards more practical applications in future technologies.

## AUTHOR CONTRIBUTIONS

SL, YK, and HAMA performed the literature review and wrote the manuscript. All authors listed have made a substantial, direct,

and intellectual contribution to the work and approved it for publication.

## ACKNOWLEDGMENTS

We acknowledge partial support from the National Science Foundation Materials Research Science and Engineering Center program through the UC Irvine Center for Complex and Active Materials (DMR-2011967). **Figures 1, 2, and 11** were created with BioRender.com.

## REFERENCES

- Adams, K. L., Puchades, M., and Ewing, A. G. (2008). *In Vitro* Electrochemistry of Biological Systems. *Annu. Rev. Anal. Chem.* 1, 329–355. doi:10.1146/annurev.anchem.1.031207.113038
- Aida, T., Meijer, E. W., and Stupp, S. I. (2012). Functional Supramolecular Polymers. *Science* 335, 813–817. doi:10.1126/science.1205962
- Ariga, K., Richards, G. J., Ishihara, S., Izawa, H., and Hill, J. P. (2010). Intelligent Chiral Sensing Based on Supramolecular and Interfacial Concepts. *Sensors* 10, 6796–6820. doi:10.3390/s100706796
- Bai, H., Liu, Z., Zhang, T., Du, J., Zhou, C., He, W., et al. (2020). Multifunctional Supramolecular Assemblies with Aggregation-Induced Emission (AIE) for Cell Line Identification, Cell Contamination Evaluation, and Cancer Cell Discrimination. *ACS Nano* 14, 7552–7563. doi:10.1021/acsnano.0c03404
- Bajaj, A., Rana, S., Miranda, O. R., Yawe, J. C., Jerry, D. J., Bunz, U. H. F., et al. (2010). Cell Surface-Based Differentiation of Cell Types and Cancer States Using a Gold Nanoparticle-GFP Based Sensing Array. *Chem. Sci.* 1, 134–138. doi:10.1039/c0sc00165a
- Bakker, E., and Pretsch, E. (2005). Potentiometric Sensors for Trace-Level Analysis. *Trac Trends Anal. Chem.* 24, 199–207. doi:10.1016/j.trac.2005.01.003
- Barakat, F., Gaudin, K., Vialet, B., Bathany, K., Benizri, S., Barthélémy, P., et al. (2020). Analysis of Lipid-Oligonucleotide Conjugates by Cyclodextrin-Modified Capillary Zone Electrophoresis. *Talanta* 219, 121204. doi:10.1016/j.talanta.2020.121204
- Bettini, S., Syrgiannis, Z., Pagano, R., Đorđević, L., Salvatore, L., Prato, M., et al. (2019). Perylene Bisimide Aggregates as Probes for Subnanomolar Discrimination of Aromatic Biogenic Amines. *ACS Appl. Mater. Inter.* 11, 17079–17089. doi:10.1021/acami.9b04101
- Bhalla, N., Jolly, P., Formisano, N., and Estrela, P. (2016). Introduction to Biosensors. *Essays Biochem.* 60, 1–8. doi:10.1042/ebc20150001
- Bianco, A., Kostarelos, K., and Prato, M. (2011). Making Carbon Nanotubes Biocompatible and Biodegradable. *Chem. Commun.* 47, 10182–10188. doi:10.1039/c1cc13011k
- Braegelman, A. S., and Webber, M. J. (2019). Integrating Stimuli-Responsive Properties in Host-Guest Supramolecular Drug Delivery Systems. *Theranostics* 9, 3017–3040. doi:10.7150/thno.31913
- Bunz, U. H. F., and Rotello, V. M. (2010). Gold Nanoparticle-Fluorophore Complexes: Sensitive and Discerning “noses” for Biosystems Sensing. *Angew. Chem. Int. Edition* 49, 3268–3279. doi:10.1002/anie.200906928
- Bak, K. M., Porfyrakis, K., Davis, J. J., and Beer, P. D. (2020). Exploiting the Mechanical Bond for Molecular Recognition and Sensing of Charged Species. *Mater. Chem. Front.* 4, 1052–1073.
- Cai, Y., Zhang, Z., Ding, Y., Hu, L., Wang, J., Chen, T., et al. (2021). Recent Development of Pillar[n]arene-Based Amphiphiles. *Chin. Chem. Lett.* 32, 1267–1279. doi:10.1016/j.ccl.2020.10.036
- Cao, X., Li, Y., Yu, Y., Fu, S., Gao, A., and Chang, X. (2019). Multifunctional Supramolecular Self-Assembly System for Colorimetric Detection of Hg<sup>2+</sup>, Fe<sup>3+</sup>, Cu<sup>2+</sup> and Continuous Sensing of Volatile Acids and Organic Amine Gases. *Nanoscale* 11, 10911–10920. doi:10.1039/c9nr01433k
- Chalklen, T., Jing, Q., and Kar-Narayan, S. (2020). Biosensors Based on Mechanical and Electrical Detection Techniques. *Sensors (Basel)* 20, 5605. doi:10.3390/s20195605
- Chan, S.-M., Tang, F.-K., Kwan, C.-S., Lam, C.-Y., Hau, S. C. K., and Leung, K. C.-F. (2019). Water-compatible Fluorescent [2]rotaxanes for Au<sup>3+</sup> Detection and Bioimaging. *Mater. Chem. Front.* 3, 2388–2396. doi:10.1039/c9qm00476a
- Chaubey, A., and Malhotra, B. D. (2002). Mediated Biosensors. *Biosens. Bioelectron.* 17, 441–456. doi:10.1016/s0956-5663(01)00313-x
- Chen, C., and Wang, J. (2020). Optical Biosensors: an Exhaustive and Comprehensive Review. *Analyst* 145, 1605–1628. doi:10.1039/c9an01998g
- Chen, J., Jiang, Z., Ackerman, J. D., Yazdani, M., Hou, S., Nugen, S. R., et al. (2015). Electrochemical Nanoparticle-Enzyme Sensors for Screening Bacterial Contamination in Drinking Water. *Analyst* 140, 4991–4996. doi:10.1039/c5an00637f
- Chen, W., Li, J., Wei, X., Fan, Y., Qian, H., Li, S., et al. (2020). Surface Plasmon Resonance Biosensor Using Hydrogel-AuNP Supramolecular Spheres for Determination of Prostate Cancer-Derived Exosomes. *Microchim. Acta* 187, 590. doi:10.1007/s00604-020-04573-4
- Chinta, J. P., Acharya, A., Kumar, A., and Rao, C. P. (2009). Spectroscopy and Microscopy Studies of the Recognition of Amino Acids and Aggregation of Proteins by Zn(II) Complex of Lower Rim Naphthylidene Conjugate of Calix[4]arene. *J. Phys. Chem. B* 113, 12075–12083. doi:10.1021/jp903099b
- Cho, I.-H., Kim, D. H., and Park, S. (2020). Electrochemical Biosensors: Perspective on Functional Nanomaterials for On-Site Analysis. *Biomater. Res.* 24, 6. doi:10.1186/s40824-019-0181-y
- Cho, I. H., Lee, J., Kim, J., Kang, M. S., Paik, J. K., Ku, S., et al. (2018). Current Technologies of Electrochemical Immunosensors: Perspective on Signal Amplification. *Sensors (Basel)* 18, 207. doi:10.3390/s18010207
- Chou, S. S., De, M., Luo, J., Rotello, V. M., Huang, J., and Dravid, V. P. (2012). Nanoscale Graphene Oxide (nGO) as Artificial Receptors: Implications for Biomolecular Interactions and Sensing. *J. Am. Chem. Soc.* 134, 16725–16733. doi:10.1021/ja306767y
- Clark, L. C., Jr., and Lyons, C. (1962). Electrode Systems for Continuous Monitoring in Cardiovascular Surgery. *Ann. N. Y. Acad. Sci.* 102, 29–45. doi:10.1111/j.1749-6632.1962.tb13623.x
- Cook, T. R., Vajpayee, V., Lee, M. H., Stang, P. J., and Chi, K.-W. (2013). Biomedical and Biochemical Applications of Self-Assembled Metallacycles and Metallacages. *Acc. Chem. Res.* 46, 2464–2474. doi:10.1021/ar400010v
- Damborský, P., Švitel, J., and Katrlík, J. (2016). Optical Biosensors. *Essays Biochem.* 60, 91–100. doi:10.1042/ebc20150010
- Della Sala, P., Del Regno, R., Talotta, C., Capobianco, A., Hickey, N., Geremia, S., et al. (2020). Prismarenes: A New Class of Macrocyclic Hosts Obtained by Templation in a Thermodynamically Controlled Synthesis. *J. Am. Chem. Soc.* 142, 1752–1756. doi:10.1021/jacs.9b12216
- Dey, D., and Goswami, T. (2011). Optical Biosensors: a Revolution towards Quantum Nanoscale Electronics Device Fabrication. *J. Biomed. Biotechnol.* 2011, 348218. doi:10.1155/2011/348218
- Dey, N., and Haynes, C. J. E. (2021). Supramolecular Coordination Complexes as Optical Biosensors. *ChemPlusChem* 86, 418–433. doi:10.1002/cplu.202100004
- Diehl, K. L., Bachman, J. L., Chapin, B. M., Edupuganti, R., Rogelio Escamilla, P., Gade, A. M., et al. (2015). “Chapter 2. Design and Synthesis of Synthetic Receptors for Biomolecule Recognition,” in *Synthetic Receptors for Biomolecules: Design Principles and Applications* (London: The Royal Society of Chemistry), 39–85. doi:10.1039/9781782622062-00039
- Ding, J. W., and Qin, W. (2020). Recent Advances in Potentiometric Biosensors. *Trac-Trends Anal. Chem.* 124, 115803. doi:10.1016/j.trac.2019.115803

- Dong, J., Tan, C., Zhang, K., Liu, Y., Low, P. J., Jiang, J., et al. (2017). Chiral NH-Controlled Supramolecular Metallacycles. *J. Am. Chem. Soc.* 139, 1554–1564. doi:10.1021/jacs.6b11422
- Dramé, M., Tabue Teguo, M., Proye, E., Hequet, F., Hentzien, M., Kanagaratnam, L., et al. (2020). Should RT-PCR Be Considered a Gold Standard in the Diagnosis of COVID-19? *J. Med. Virol.* 92, 2312–2313. doi:10.1002/jmv.25996
- Duan, X., Mu, L., Sawtelle, S. D., Rajan, N. K., Han, Z., Wang, Y., et al. (2015). Functionalized Polyelectrolytes Assembling on Nano-BioFETs for Biosensing Applications. *Adv. Funct. Mater.* 25, 2279–2286. doi:10.1002/adfm.201500002
- Duan, X., Rajan, N. K., Routenberg, D. A., Huskens, J., and Reed, M. A. (2013). Regenerative Electronic Biosensors Using Supramolecular Approaches. *ACS Nano* 7, 4014–4021. doi:10.1021/nn306034f
- Eker, B., Yilmaz, M. D., Schlautmann, S., Gardeniers, J. G., and Huskens, J. (2011). A Supramolecular Sensing Platform for Phosphate Anions and an Anthrax Biomarker in a Microfluidic Device. *Int. J. Mol. Sci.* 12, 7335–7351. doi:10.3390/ijms12117335
- Erbas-Cakmak, S., Leigh, D. A., McInnes, C. T., and Nussbaumer, A. L. (2015). Artificial Molecular Machines. *Chem. Rev.* 115, 10081–10206. doi:10.1021/acs.chemrev.5b00146
- Espy, M. J., Uhl, J. R., Sloan, L. M., Buckwalter, S. P., Jones, M. F., Vetter, E. A., et al. (2006). Real-time PCR in Clinical Microbiology: Applications for Routine Laboratory Testing. *Clin. Microbiol. Rev.* 19, 165–256. doi:10.1128/cmr.19.1.165-256.2006
- Fabrizzi, L., and Poggi, A. (1995). Sensors and Switches from Supramolecular Chemistry. *Chem. Soc. Rev.* 24, 197–202. doi:10.1039/cs9952400197
- Folmer-Andersen, J. F., Kitamura, M., and Anslyn, E. V. (2006). Pattern-Based Discrimination of Enantiomeric and Structurally Similar Amino Acids: An Optical Mimic of the Mammalian Taste Response. *J. Am. Chem. Soc.* 128, 5652–5653. doi:10.1021/ja061313i
- Folmer-Andersen, J. F., Lynch, V. M., and Anslyn, E. V. (2005). Colorimetric Enantiodiscrimination of  $\alpha$ -Amino Acids in Protic Media. *J. Am. Chem. Soc.* 127, 7986–7987. doi:10.1021/ja052029e
- Fu, Y., Zhou, X., and Xing, D. (2018). Integrated Paper-Based Detection Chip with Nucleic Acid Extraction and Amplification for Automatic and Sensitive Pathogen Detection. *Sensors Actuators B: Chem.* 261, 288–296. doi:10.1016/j.snb.2018.01.165
- Gale, P. A., Sessler, J. L., Král, V., and Lynch, V. (1996). Calix[4]pyrroles: Old yet New Anion-Binding Agents. *J. Am. Chem. Soc.* 118, 5140–5141. doi:10.1021/ja960307r
- Geim, A. K., and Novoselov, K. S. (2007). The Rise of Graphene. *Nat. Mater.* 6, 183–191. doi:10.1038/nmat1849
- Ghale, G., and Nau, W. M. (2014). Dynamically Analyte-Responsive Macrocyclic Host-Fluorophore Systems. *Acc. Chem. Res.* 47, 2150–2159. doi:10.1021/ar500116d
- Gorbachuk, V. V., Porfireva, A. V., Stepanova, V. B., Kuzin, Y. I., Evtugyn, V. G., Shamagumova, R. V., et al. (2017). Co-polymers of Oligo(lactic Acid and Tetrasubstituted Thiocalix[4]arenes as a New Material for Electrochemical Sensor Development. *Sensors Actuators B: Chem.* 246, 136–145. doi:10.1016/j.snb.2017.02.061
- Grieshaber, D., Mackenzie, R., Vörös, J., and Reimhult, E. (2008). Electrochemical Biosensors - Sensor Principles and Architectures. *Sensors* 8, 1400–1458. doi:10.3390/s80314000
- Guo, H., Yan, X., Lu, B., Wang, J., Yuan, X., Han, Y., et al. (2020). Pillar[5]arene-based Supramolecular Assemblies with Two-step Sequential Fluorescence Enhancement for Mitochondria-Targeted Cell Imaging. *J. Mater. Chem. C* 8, 15622–15625. doi:10.1039/d0tc04343e
- Hammond, J. L., Formisano, N., Estrela, P., Carrara, S., and Tkac, J. (2016). Electrochemical Biosensors and Nanobiosensors. *Essays Biochem.* 60, 69–80. doi:10.1042/ebc20150008
- Hamuro, Y., Calama, M. C., Park, H. S., and Hamilton, A. D. (1997). A Calixarene with Four Peptide Loops: An Antibody Mimic for Recognition of Protein Surfaces. *Angew. Chem. Int. Ed. Engl.* 36, 2680–2683. doi:10.1002/anie.199726801
- Hanko, M., Bruns, N., Rentmeister, S., Tiller, J. C., and Heinze, J. (2006). Nanophase-Separated Amphiphilic Conetworks as Versatile Matrixes for Optical Chemical and Biochemical Sensors. *Anal. Chem.* 78, 6376–6383. doi:10.1021/ac060634+
- He, C., Wang, J., Wu, P., Jia, L., Bai, Y., Zhang, Z., et al. (2012). Fluorescent Differentiation and Quantificational Detection of Free Tryptophan in Serum within a Confined Metal-Organic Tetrahedron. *Chem. Commun.* 48, 11880–11882. doi:10.1039/c2cc36932j
- He, H., Guo, J., Lin, X., and Xu, B. (2020). Enzyme-Instructed Assemblies Enable Mitochondria Localization of Histone H2B in Cancer Cells. *Angew. Chem. Int. Ed.* 59, 9330–9334. doi:10.1002/anie.202000983
- Hewitt, S. H., and Wilson, A. J. (2017). Protein Sensing and Discrimination Using Highly Functionalised Ruthenium(ii) Tris(bipyridyl) Protein Surface Mimetics in an Array Format. *Chem. Commun.* 53, 12278–12281. doi:10.1039/c7cc06175g
- Hong, Y., Häußler, M., Lam, J. W. Y., Li, Z., Sin, K. K., Dong, Y., et al. (2008). Label-Free Fluorescent Probing of G-Quadruplex Formation and Real-Time Monitoring of DNA Folding by a Quaternized Tetraphenylethene Salt with Aggregation-Induced Emission Characteristics. *Chem. Eur. J.* 14, 6428–6437. doi:10.1002/chem.200701723
- Huertas, C. S., Calvo-Lozano, O., Mitchell, A., and Lechuga, L. M. (2019). Advanced Evanescent-Wave Optical Biosensors for the Detection of Nucleic Acids: An Analytic Perspective. *Front. Chem.* 7, 724. doi:10.3389/fchem.2019.00724
- Jang, Y., Jang, M., Kim, H., Lee, S. J., Jin, E., Koo, J. Y., et al. (2017). Point-of-Use Detection of Amphetamine-type Stimulants with Host-Molecule-Functionalized Organic Transistors. *Chem.* 3, 641–651. doi:10.1016/j.chempr.2017.08.015
- Jia, J., Chen, H. G., Feng, J., Lei, J. L., Luo, H. Q., and Li, N. B. (2016). A Regenerative Ratiometric Electrochemical Biosensor for Selective Detecting Hg<sup>2+</sup> Based on Y-Shaped/hairpin DNA Transformation. *Analytica Chim. Acta* 908, 95–101. doi:10.1016/j.aca.2015.12.028
- Jiang, J., Lin, X., and Diao, G. (2017). Smart Combination of Cyclodextrin Polymer Host-Guest Recognition and Mg<sup>2+</sup>-Assistant Cyclic Cleavage Reaction for Sensitive Electrochemical Assay of Nucleic Acids. *ACS Appl. Mater. Inter.* 9, 36688–36694. doi:10.1021/acsami.7b13132
- Jones, B. A., Ahrens, M. J., Yoon, M.-H., Facchetti, A., Marks, T. J., and Wasielewski, M. R. (2004). High-mobility Air-Stable N-type Semiconductors with Processing Versatility: Dicyanoperylene-3,4,9,10-Bis(dicarboximides). *Angew. Chem. Int. Ed.* 43, 6363–6366. doi:10.1002/anie.200461324
- Justino, C. I. L., Duarte, A. C., and Rocha-Santos, T. A. P. (2017). Recent Progress in Biosensors for Environmental Monitoring: A Review. *Sensors (Basel)* 17, 2918. doi:10.3390/s17122918
- Kagan, V. E., Konduru, N. V., Feng, W., Allen, B. L., Conroy, J., Volkov, Y., et al. (2010). Carbon Nanotubes Degraded by Neutrophil Myeloperoxidase Induce Less Pulmonary Inflammation. *Nat. Nanotech.* 5, 354–359. doi:10.1038/nnano.2010.44
- Kaifer, A. E. (2018). Portal Effects on the Stability of Cucurbituril Complexes. *Isr. J. Chem.* 58, 244–249. doi:10.1002/ijch.201700097
- Kalantar-Zadeh, K. (2013). *Sensors: An Introductory Course*. NY: Springer Science+Business Media.
- Kawai, H., Kitazumi, Y., Shirai, O., and Kano, K. (2019). Performance Analysis of an Oxidase/peroxidase-Based Mediatorless Amperometric Biosensor. *J. Electroanalytical Chem.* 841, 73–78. doi:10.1016/j.jelechem.2019.04.012
- Khan, A., Kisannagar, R. R., Gouda, C., Gupta, D., and Lin, H.-C. (2020). Highly Stretchable Supramolecular Conductive Self-Healable Gels for Injectable Adhesive and Flexible Sensor Applications. *J. Mater. Chem. A* 8, 19954–19964. doi:10.1039/d0ta07543d
- Kim, S. Y., Podder, A., Lee, H., Cho, Y.-J., Han, E. H., Khatun, S., et al. (2020). Self-assembled Amphiphilic Fluorescent Probe: Detecting pH-Fluctuations within Cancer Cells and Tumour Tissues. *Chem. Sci.* 11, 9875–9883. doi:10.1039/d0sc03795h
- Kong, H., Liu, D., Zhang, S., and Zhang, X. (2011). Protein Sensing and Cell Discrimination Using a Sensor Array Based on Nanomaterial-Assisted Chemiluminescence. *Anal. Chem.* 83, 1867–1870. doi:10.1021/ac200076c
- Krivitsky, V., Zverzhinetsky, M., Krivitsky, A., Hsiung, L.-C., Naddaka, V., Gabriel, I., et al. (2019). Cellular Metabolomics by a Universal Redox-Reactive Nanosensors Array: From the Cell Level to Tumor-On-A-Chip Analysis. *Nano Lett.* 19, 2478–2488. doi:10.1021/acs.nanolett.9b00052
- Kumar, M., Ing, N. L., Narang, V., Wijerathne, N. K., Hochbaum, A. I., and Ulijn, R. V. (2018). Amino-acid-encoded Biocatalytic Self-Assembly Enables the



- Formation of Transient Conducting Nanostructures. *Nat. Chem.* 10, 696–703. doi:10.1038/s41557-018-0047-2
- Lamb, J. D., Izatt, R. M., Swain, C. S., and Christensen, J. J. (1980). A Systematic Study of the Effect of Macrocyclic Ring Size and Donor Atom Type on the Log K<sub>D</sub>.DELTA.H, and T.DELTA.S of Reactions at 25.degree.C in Methanol of Mono- and Divalent Cations with crown Ethers. *J. Am. Chem. Soc.* 102, 475–479. doi:10.1021/ja00522a005
- Law, A. S.-Y., Lee, L. C.-C., Lo, K. K.-W., and Yam, V. W.-W. (2021). Aggregation and Supramolecular Self-Assembly of Low-Energy Red Luminescent Alkynylplatinum(II) Complexes for RNA Detection, Nucleolus Imaging, and RNA Synthesis Inhibitor Screening. *J. Am. Chem. Soc.* 143, 5396–5405. doi:10.1021/jacs.0c13327
- Lee, H., In, B., In, P. K., Kishore, M. Y. L. N., and Lee, K.-H. (2018). Dual Role of a Fluorescent Peptidyl Probe Based on Self-Assembly for the Detection of Heparin and for the Inhibition of the Heparin-Digestive Enzyme Reaction. *ACS Appl. Mater. Inter.* 10, 2282–2290. doi:10.1021/acsami.7b15411, In,
- Lei, Y.-M., Zhao, M., Wang, A., Yu, Y.-Q., Chai, Y.-Q., Yuan, R., et al. (2016). Electrochemiluminescence of Supramolecular Nanorods and Their Application in the "On-Off-On" Detection of Copper Ions. *Chem. Eur. J.* 22, 8207–8214. doi:10.1002/chem.201504995
- Li, J., Wang, J., Li, H., Song, N., Wang, D., and Tang, B. Z. (2020a). Supramolecular Materials Based on AIE Luminogens (AIEgens): Construction and Applications. *Chem. Soc. Rev.* 49, 1144–1172. doi:10.1039/c9cs00495e
- Li, J., Yim, D., Jang, W.-D., and Yoon, J. (2017). Recent Progress in the Design and Applications of Fluorescence Probes Containing crown Ethers. *Chem. Soc. Rev.* 46, 2437–2458. doi:10.1039/c6cs00619a
- Li, Q., Zhu, H., and Huang, F. (2020b). Pillararene-Based Supramolecular Functional Materials. *Trends Chem.* 2, 850–864. doi:10.1016/j.trechm.2020.07.004
- Lim, S. A., and Ahmed, M. U. (2017). "CHAPTER 1 Introduction to Food Biosensors," in *Food Biosensors* (London: The Royal Society of Chemistry), 1–21.
- Ling, X., Saretz, S., Xiao, L., Francescon, J., and Masson, E. (2016). Water vs. Cucurbituril Rim: a Fierce Competition for Guest Solvation. *Chem. Sci.* 7, 3569–3573. doi:10.1039/c5sc04475h
- Liu, M., Zhang, L., and Wang, T. (2015). Supramolecular Chirality in Self-Assembled Systems. *Chem. Rev.* 115, 7304–7397. doi:10.1021/cr500671p
- Liu, Y., You, C.-C., Kang, S.-Z., Wang, C., Chen, F., and He, X.-W. (2002). Synthesis of Novel  $\beta$ -Cyclodextrin and Calixarene Derivatives and Their Use in Gas Sensing on the Basis of Molecular Recognition. *Eur. J. Org. Chem.* 2002, 607–613. doi:10.1002/1099-0690(200202)2002:4<607::aid-efoc607>3.0.co;2-i
- Lu, J., Fu, Y., Wang, D. L., and Lu, C. (2018). Thermo-Responsive Copolymer Stabilized Fluorescent Silver Nanoclusters and Their Application in pH Sensing. *Sens. Actuators, B* 254, 996. doi:10.1016/j.snb.2017.07.180
- Lu, M., Deng, Y., Luo, Y., Lv, J., Li, T., Xu, J., et al. (2019). Graphene Aerogel-Metal-Organic Framework-Based Electrochemical Method for Simultaneous Detection of Multiple Heavy-Metal Ions. *Anal. Chem.* 91, 888–895. doi:10.1021/acs.analchem.8b03764
- Luo, X., Yu, H., and Cui, Y. (2018). A Wearable Amperometric Biosensor on a Cotton Fabric for Lactate. *IEEE Electron. Device Lett.* 39, 123–126. doi:10.1109/led.2017.2777474
- Ma, Y., Cametti, M., Džolić, Z., and Jiang, S. (2019). Selective Cu(II) Sensing by a Versatile AIE Cyanostilbene-Based Gel System. *Soft Matter* 15, 6145–6150. doi:10.1039/c9sm00955h
- Mako, T. L., Racicot, J. M., and Levine, M. (2019). Supramolecular Luminescent Sensors. *Chem. Rev.* 119, 322–477. doi:10.1021/acs.chemrev.8b00260
- Martins, T. D., Ribeiro, A. C. C., Colmati, F., De Souza, G. A., De Camargo, H. S., Dias, D. L., et al. (2015). "Supramolecular Materials for Optical and Electrochemical Biosensors," in *Biosensors-Micro and Nanoscale Applications* (London: INTECH).
- Mehrotra, P. (2016). Biosensors and Their Applications - A Review. *J. Oral Biol. Craniofac. Res.* 6, 153–159. doi:10.1016/j.jobcr.2015.12.002
- Mendez-Arroyo, J., d'Aquino, A. I., Chinen, A. B., Manraj, Y. D., and Mirkin, C. A. (2017). Reversible and Selective Encapsulation of Dextromethorphan and  $\beta$ -Estradiol Using an Asymmetric Molecular Capsule Assembled via the Weak-Link Approach. *J. Am. Chem. Soc.* 139, 1368–1371. doi:10.1021/jacs.6b10027
- Menezes, M., Balbino, M., Castro, A., Eleotério, I., Demets, G., Oliveira, O., et al. (2017). Chemically Modified Piezoelectric Devices to Detect Seized Marijuana and Cocaine Samples: A New Tool for Forensic Chemistry. *SM J. Forensic Res. Criminology* 1, 1003.
- Merkx, M., Smith, B., and Jewett, M. (2019). Engineering Sensor Proteins. *ACS Sens.* 4, 3089–3091. doi:10.1021/acssensors.9b02459
- Minaker, S. A., Daze, K. D., Ma, M. C. F., and Hof, F. (2012). Antibody-Free Reading of the Histone Code Using a Simple Chemical Sensor Array. *J. Am. Chem. Soc.* 134, 11674–11680. doi:10.1021/ja303465x
- Miranda, O. R., Chen, H.-T., You, C.-C., Mortenson, D. E., Yang, X.-C., Bunz, U. H. F., et al. (2010a). Enzyme-Amplified Array Sensing of Proteins in Solution and in Biofluids. *J. Am. Chem. Soc.* 132, 5285–5289. doi:10.1021/ja1006756
- Miranda, O. R., Czeran, B., and Rotello, V. M. (2010b). Array-based Sensing with Nanoparticles: 'chemical Noses' for Sensing Biomolecules and Cell Surfaces. *Curr. Opin. Chem. Biol.* 14, 728–736. doi:10.1016/j.cbpa.2010.07.021
- Mogera, U., Sagade, A. A., George, S. J., and Kulkarni, G. U. (2014). Ultrafast Response Humidity Sensor Using Supramolecular Nanofibre and its Application in Monitoring Breath Humidity and Flow. *Sci. Rep.* 4, 4103. doi:10.1038/srep04103
- Moradi-Monfared, S., Krishnamurthy, V., and Cornell, B. (2012). A Molecular Machine Biosensor: Construction, Predictive Models and Experimental Studies. *Biosens. Bioelectron.* 34, 261–266. doi:10.1016/j.bios.2012.02.018
- Mout, R., Moyano, D. F., Rana, S., and Rotello, V. M. (2012). Surface Functionalization of Nanoparticles for Nanomedicine. *Chem. Soc. Rev.* 41, 2539–2544. doi:10.1039/c2cs15294k
- Moyano, D. F., Rana, S., Bunz, U. H. F., and Rotello, V. M. (2011). Gold Nanoparticle-Polymer/biopolymer Complexes for Protein Sensing. *Faraday Discuss.* 152, 33–42. doi:10.1039/c1fd00024a
- Nandi, S., Ritenberg, M., and Jelinek, R. (2015). Bacterial Detection with Amphiphilic Carbon Dots. *Analyst* 140, 4232–4237. doi:10.1039/c5an00471c
- Nguyen, S. T., Gin, D. L., Hupp, J. T., and Zhang, X. (2001). Supramolecular Chemistry: Functional Structures on the Mesoscale. *Proc. Natl. Acad. Sci.* 98, 11849–11850. doi:10.1073/pnas.201373898
- Ogoshi, T., and Harada, A. (2008). Chemical Sensors Based on Cyclodextrin Derivatives. *Sensors* 8, 4961–4982. doi:10.3390/s8084961
- Paul, A., and Srivastava, D. N. (2018). Amperometric Glucose Sensing at Nanomolar Level Using MOF-Encapsulated TiO<sub>2</sub> Platform. *Acs Omega* 3, 14634–14640. doi:10.1021/acsomega.8b01968
- Pauric, A. D., Jin, S., Fuller, T. J., Balogh, M. P., Halalay, I. C., and Goward, G. R. (2016). NMR Determination of the Relative Binding Affinity of Crown Ethers for Manganese Cations in Aprotic Nonaqueous Lithium Electrolyte Solutions. *J. Phys. Chem. C* 120, 3677–3683. doi:10.1021/acs.jpcc.5b12142
- Pei, H., Li, J., Lv, M., Wang, J., Gao, J., Lu, J., et al. (2012). A Graphene-Based Sensor Array for High-Precision and Adaptive Target Identification with Ensemble Aptamers. *J. Am. Chem. Soc.* 134, 13843–13849. doi:10.1021/ja305814u
- Peltomaa, R., Glahn-Martínez, B., Benito-Peña, E., and Moreno-Bondí, M. C. (2018). Optical Biosensors for Label-free Detection of Small Molecules. *Sensors (Basel)* 18, 4126. doi:10.3390/s18124126
- Pereira, A. R., Araújo, A. N., Montenegro, M. C. B. S. M., and Amorim, C. M. P. G. (2020). A Simpler Potentiometric Method for Histamine Assessment in Blood Sera. *Anal. Bioanal. Chem.* 412, 3629–3637. doi:10.1007/s00216-020-02597-6
- Pezzato, C., Lee, B., Severin, K., and Prins, L. J. (2013). Pattern-based Sensing of Nucleotides with Functionalized Gold Nanoparticles. *Chem. Commun.* 49, 469–471. doi:10.1039/c2cc38058g
- Phillips, B., Banerjee, S., Tu, X., and Fang, L. (2020). Electrical Vapour Sensing with Macrocyclic Molecular Receptors. *Supramolecular Chem.* 32, 165. doi:10.1080/10610278.2020.1726916
- Pieszka, M., Han, S., Volkmann, C., Graf, R., Lieberwirth, I., Landfester, K., et al. (2020). Controlled Supramolecular Assembly inside Living Cells by Sequential Multistaged Chemical Reactions. *J. Am. Chem. Soc.* 142, 15780–15789. doi:10.1021/jacs.0c05261
- Pinalli, R., Pedrini, A., and Dalcanale, E. (2018). Biochemical Sensing with Macrocyclic Receptors. *Chem. Soc. Rev.* 47, 7006–7026. doi:10.1039/c8cs00271a
- Pohanka, M. (2018). Overview of Piezoelectric Biosensors, Immunosensors and DNA Sensors and Their Applications. *Materials (Basel)* 11, 448. doi:10.3390/ma11030448

- Pumera, M., Ambrosi, A., Bonanni, A., Chng, E., and Poh, H. (2010). Graphene for Electrochemical Sensing and Biosensing. *Trac-Trends Anal. Chem.* 29, 954. doi:10.1016/j.trac.2010.05.011
- Qu, Y., Wei, T., Zhan, W., Hu, C., Cao, L., Yu, Q., et al. (2017a). A Reusable Supramolecular Platform for the Specific Capture and Release of Proteins and Bacteria. *J. Mater. Chem. B* 5, 444–453. doi:10.1039/c6tb02821g
- Qu, Y., Wei, T., Zhan, W., Hu, C., Cao, L., Yu, Q., et al. (2017b). A Reusable Supramolecular Platform for the Specific Capture and Release of Proteins and Bacteria. *J. Mater. Chem. B* 5, 444–453. doi:10.1039/c6tb02821g
- Rana, S., Singla, A. K., Bajaj, A., Elci, S. G., Miranda, O. R., Mout, R., et al. (2012). Array-Based Sensing of Metastatic Cells and Tissues Using Nanoparticle-Fluorescent Protein Conjugates. *ACS Nano* 6, 8233–8240. doi:10.1021/nn302917e
- Rao, V. K., Suresh, S., Sharma, M., Gupta, A., and R. V. (2011). “Carbon Nanotubes - A Potential Material for Affinity Biosensors,” in *Carbon Nanotubes - Growth and Applications*. doi:10.5772/16836
- Reineck, P., and Gibson, B. (2017). Near-Infrared Fluorescent Nanomaterials for Bioimaging and Sensing. *Adv. Opt. Mater.* 5, 1600446. doi:10.1002/adom.201600446
- Resendiz, M. J. E., Noveron, J. C., Disteldorf, H., Fischer, S., and Stang, P. J. (2004). A Self-Assembled Supramolecular Optical Sensor for Ni(II), Cd(II), and Cr(III). *Org. Lett.* 6, 651–653. doi:10.1021/ol035587b
- Rivas, L., Mayorga-Martinez, C. C., Quesada-González, D., Zamora-Gálvez, A., de la Escosura-Muñiz, A., and Merkoçi, A. (2015). Label-Free Impedimetric Aptasensor for Ochratoxin-A Detection Using Iridium Oxide Nanoparticles. *Anal. Chem.* 87, 5167–5172. doi:10.1021/acs.analchem.5b00890
- Rudzinski, C. M., Young, A. M., and Nocera, D. G. (2002). A Supramolecular Microfluidic Optical Chemosensor. *J. Am. Chem. Soc.* 124, 1723–1727. doi:10.1021/ja010176g
- Sambe, L., de La Rosa, V. R., Belal, K., Stoffelbach, F., Lyskawa, J., Delattre, F., et al. (2014). Programmable Polymer-Based Supramolecular Temperature Sensor with a Memory Function. *Angew. Chem. Int. Ed. Engl.* 53, 5044–5048. doi:10.1002/anie.201402108
- Sato, S., Nojima, T., and Takenaka, S. (2004). Electrochemical Gene Detection Based on Supramolecular Complex Formation by Ferrocenyl- $\beta$ -Cyclodextrin and Adamantyl-naphthalene Diimide Bound to Double Stranded DNA. *J. Organomet. Chem.* 689, 4722–4728. doi:10.1016/j.jorganchem.2004.08.039
- Schöningh, M. J., and Poghossian, A. (2002). Recent Advances in Biologically Sensitive Field-Effect Transistors (BioFETs). *Analyst* 127, 1137–1151. doi:10.1039/b204444g
- Sebastian, A., and Prasad, E. (2020). Cyanide Sensing in Water Using a Copper Metallogel through “Turn-On” Fluorescence. *Langmuir* 36, 10537–10547. doi:10.1021/acs.langmuir.0c01803
- Shang, X., Song, I., Jung, G. Y., Choi, W., Ohtsu, H., Lee, J. H., et al. (2018). Chiral Self-Sorted Multifunctional Supramolecular Biocoordination Polymers and Their Applications in Sensors. *Nat. Commun.* 9, 3933. doi:10.1038/s41467-018-06147-8
- Shen, B., Li, J., Cheng, W., Yan, Y., Tang, R., Li, Y., et al. (2015). Electrochemical Aptasensor for Highly Sensitive Determination of Cocaine Using a Supramolecular Aptamer and Rolling circle Amplification. *Microchim. Acta* 182, 361–367. doi:10.1007/s00604-014-1333-3
- Shishkanova, T. V., Havlík, M., Dendisová, M., Matějka, P., and Král, V. (2016). Synthesis and Deposition of a Tröger’s Base Polymer on the Electrode Surface for Potentiometric Detection of a Neuroblastoma Tumor Marker Metabolite. *Chem. Commun.* 52, 11991–11994. doi:10.1039/c6cc06203b
- Sierra, A. F., Hernández-Alonso, D., Romero, M. A., González-Delgado, J. A., Pischel, U., and Ballester, P. (2020). Optical Supramolecular Sensing of Creatinine. *J. Am. Chem. Soc.* 142, 4276–4284. doi:10.1021/jacs.9b12071
- Soleymani, L., and Li, F. (2017). Mechanistic Challenges and Advantages of Biosensor Miniaturization into the Nanoscale. *ACS Sens.* 2, 458–467. doi:10.1021/acssensors.7b00069
- Song, C., Li, B., Yang, X., Wang, K., Wang, Q., Liu, J., et al. (2016). Use of  $\beta$ -cyclodextrin-tethered Cationic Polymer Based Fluorescence Enhancement of Pyrene and Hybridization Chain Reaction for the Enzyme-free Amplified Detection of DNA. *Analyst* 142, 224–228. doi:10.1039/c6an02269c
- Sun, X., Wang, Y., and Lei, Y. (2015). Fluorescence Based Explosive Detection: From Mechanisms to Sensory Materials. *Chem. Soc. Rev.* 44, 8019–8061. doi:10.1039/c5cs00496a
- Szunerits, S., and Boukherroub, R. (2018). Graphene-based Biosensors. *Interf. Focus* 8, 20160132. doi:10.1098/rsfs.2016.0132
- Takeda, K., Kusuoka, R., Inukai, M., Igarashi, K., Ohno, H., and Nakamura, N. (2021). An Amperometric Biosensor of L-Fucose in Urine for the First Screening Test of Cancer. *Biosens. Bioelectron.* 174, 112831. doi:10.1016/j.bios.2020.112831
- Tang, J.-H., Sun, Y., Gong, Z.-L., Li, Z.-Y., Zhou, Z., Wang, H., et al. (2018). Temperature-Responsive Fluorescent Organoplatinum(II) Metallacycles. *J. Am. Chem. Soc.* 140, 7723–7729. doi:10.1021/jacs.8b04452
- Tang, T., Peneva, K., Müllen, K., and Webber, S. E. (2007). Photophysics of Water Soluble Perylene Diimides in Surfactant Solutions. *J. Phys. Chem. A* 111, 10609–10614. doi:10.1021/jp073782s
- Tang, Y., Long, F., Gu, C., Wang, C., Han, S., and He, M. (2016). Reusable Split-Aptamer-Based Biosensor for Rapid Detection of Cocaine in Serum by Using an All-Fiber Evanescent Wave Optical Biosensing Platform. *Analytica Chim. Acta* 933, 182–188. doi:10.1016/j.aca.2016.05.021
- Tilmaç, C.-M., and Morris, M. C. (2015). Carbon Nanotube Biosensors. *Front. Chem.* 3, 59. doi:10.3389/fchem.2015.00059
- Tsuda, A., Sakamoto, S., Yamaguchi, K., and Aida, T. (2003). A Novel Supramolecular Multicolor Thermometer by Self-Assembly of  $\Delta\pi$ -Extended Zinc Porphyrin Complex. *J. Am. Chem. Soc.* 125, 15722–15723. doi:10.1021/ja038349k
- Turner, A. P. F. (2013). Biosensors: Sense and Sensibility. *Chem. Soc. Rev.* 42, 3184–3196. doi:10.1039/c3cs35528d
- Uppachai, P., Srijaranai, S., Poosittisak, S., Md Isa, I., and Mukdasai, S. (2020). Supramolecular Electrochemical Sensor for Dopamine Detection Based on Self-Assembled Mixed Surfactants on Gold Nanoparticles Deposited Graphene Oxide. *Molecules* 25, 2528. doi:10.3390/molecules25112528
- Vigneshvar, S., Sudhakumari, C. C., Senthilkumaran, B., and Prakash, H. (2016). Recent Advances in Biosensor Technology for Potential Applications - an Overview. *Front. Bioeng. Biotechnol.* 4, 11. doi:10.3389/fbioe.2016.00011
- Wajs, E., Fernández, N., and Frago, A. (2016). Supramolecular Biosensors Based on Electropolymerised Pyrrole-Cyclodextrin Modified Surfaces for Antibody Detection. *Analyst* 141, 3274–3279. doi:10.1039/c6an00532b
- Wang, Q., Li, Z., Tao, D.-D., Zhang, Q., Zhang, P., Guo, D.-P., et al. (2016). Supramolecular Aggregates as Sensory Ensembles. *Chem. Commun.* 52, 12929–12939. doi:10.1039/c6cc06075g
- Wang, Z., Hu, T., Liang, R., and Wei, M. (2020). Application of Zero-Dimensional Nanomaterials in Biosensing. *Front. Chem.* 8, 320. doi:10.3389/fchem.2020.00320
- Wang, Z., Xiao, S., and Chen, Y. (2005). Electrocatalytic and Analytical Response of  $\beta$ -Cyclodextrin Incorporated Carbon Nanotubes-Modified Electrodes toward Guanine. *Electroanalysis* 17, 2057–2061. doi:10.1002/elan.200503333
- Webber, M. J., Appel, E. A., Meijer, E. W., and Langer, R. (2016). Supramolecular Biomaterials. *Nat. Mater.* 15, 13–26. doi:10.1038/nmat4474
- Wei, W., Xu, C., Ren, J., Xu, B., and Qu, X. (2012). Sensing Metal Ions with Ion Selectivity of a crown Ether and Fluorescence Resonance Energy Transfer between Carbon Dots and Graphene. *Chem. Commun.* 48, 1284–1286. doi:10.1039/c2cc16481g
- Wong, Y.-S., Ng, M., Yeung, M. C.-L., and Yam, V. W.-W. (2021). Platinum(II)-Based Host-Guest Coordination-Driven Supramolecular Co-assembly Assisted by Pt–Pt and  $\pi$ - $\pi$  Stacking Interactions: A Dual-Selective Luminescence Sensor for Cations and Anions. *J. Am. Chem. Soc.* 143, 973–982. doi:10.1021/jacs.0c11162
- Wu, L., Huang, C., Emery, B. P., Sedgwick, A. C., Bull, S. D., He, X.-P., et al. (2020a). Förster Resonance Energy Transfer (FRET)-based Small-Molecule Sensors and Imaging Agents. *Chem. Soc. Rev.* 49, 5110–5139. doi:10.1039/c9cs00318e
- Wu, Y., Frascioni, M., Liu, W.-G., Young, R. M., Goddard, W. A., Wasielewski, M. R., et al. (2020b). Electrochemical Switching of a Fluorescent Molecular Rotor Embedded within a Bistable Rotaxane. *J. Am. Chem. Soc.* 142, 11835–11846. doi:10.1021/jacs.0c03701
- Xu, M., Kelley, S. P., and Glass, T. E. (2018). A Multi-Component Sensor System for Detection of Amphiphilic Compounds. *Angew. Chem. Int. Ed.* 57, 12741–12744. doi:10.1002/anie.201807221
- Yan, F., and Sadik, O. A. (2001). Enzyme-Modulated Cleavage of dsDNA for Supramolecular Design of Biosensors. *Anal. Chem.* 73, 5272–5280. doi:10.1021/ac015516v

- Yan, X., Wang, M., Cook, T. R., Zhang, M., Saha, M. L., Zhou, Z., et al. (2016). Light-Emitting Superstructures with Anion Effect: Coordination-Driven Self-Assembly of Pure Tetraphenylethylene Metallacycles and Metallacages. *J. Am. Chem. Soc.* 138, 4580–4588. doi:10.1021/jacs.6b00846
- Yang, S., Liu, L., You, M., Zhang, F., Liao, X., and He, P. (2016). The Novel Pillar[5]arene Derivative for Recyclable Electrochemical Sensing Platform of Homogeneous DNA Hybridization. *Sensors Actuators B: Chem.* 227, 497–503. doi:10.1016/j.snb.2015.12.090
- Yao, Q., Lü, B., Ji, C., Cai, Y., and Yin, M. (2017). Supramolecular Host-Guest System as Ratiometric Fe<sup>3+</sup> Ion Sensor Based on Water-Soluble Pillar[5]arene. *ACS Appl. Mater. Inter.* 9, 36320–36326. doi:10.1021/acsami.7b12063
- Yildirim, N., Long, F., Gao, C., He, M., Shi, H.-C., and Gu, A. Z. (2012). Aptamer-Based Optical Biosensor for Rapid and Sensitive Detection of 17 $\beta$ -Estradiol in Water Samples. *Environ. Sci. Technol.* 46, 3288–3294. doi:10.1021/es203624w
- You, L., Zha, D., and Anslyn, E. V. (2015). Recent Advances in Supramolecular Analytical Chemistry Using Optical Sensing. *Chem. Rev.* 115, 7840–7892. doi:10.1021/cr5005524
- Yu, P., Zhang, X., Zhou, J., Xiong, E., Li, X., and Chen, J. (2015). Smart Protein Biogate as a Mediator to Regulate Competitive Host-Guest Interaction for Sensitive Ratiometric Electrochemical Assay of Prion. *Sci. Rep.* 5, 16015. doi:10.1038/srep16015
- Yu, P., Liu, Y., Zhang, X., Zhou, J., Xiong, E., Li, X., et al. (2016a). A Novel Electrochemical Aptasensor for Bisphenol A Assay Based on Triple-Signaling Strategy. *Biosens. Bioelectron.* 79, 22–28. doi:10.1016/j.bios.2015.12.007
- Yu, P., Zhang, X., Xiong, E., Zhou, J., Li, X., and Chen, J. (2016b). A Label-free and Cascaded Dual-Signaling Amplified Electrochemical Aptasensing Platform for Sensitive Prion Assay. *Biosens. Bioelectron.* 85, 471–478. doi:10.1016/j.bios.2016.05.047
- Yu, Z., Cai, G., Liu, X., and Tang, D. (2021). Pressure-Based Biosensor Integrated with a Flexible Pressure Sensor and an Electrochromic Device for Visual Detection. *Anal. Chem.* 93, 2916–2925. doi:10.1021/acs.analchem.0c04501
- Yuan, L., Lin, W., Zheng, K., and Zhu, S. (2013). FRET-based Small-Molecule Fluorescent Probes: Rational Design and Bioimaging Applications. *Acc. Chem. Res.* 46, 1462–1473. doi:10.1021/ar300273v
- Yuan, Q., He, J., Niu, Y., Chen, J., Zhao, Y., Zhang, Y., et al. (2018). Sandwich-type Biosensor for the Detection of  $\alpha$ 2,3-sialylated Glycans Based on Fullerene-Palladium-Platinum alloy and 4-mercaptophenylboronic Acid Nanoparticle Hybrids Coupled with Au-Methylene Blue-MAL Signal Amplification. *Biosens. Bioelectron.* 102, 321–327. doi:10.1016/j.bios.2017.11.043
- Zhang, M., Yin, S., Zhang, J., Zhou, Z., Saha, M. L., Lu, C., et al. (2017a). Metallacycle-cored Supramolecular Assemblies with Tunable Fluorescence Including white-light Emission. *Proc. Natl. Acad. Sci. USA* 114, 3044–3049. doi:10.1073/pnas.1702510114
- Zhang, S., Assaf, K. I., Huang, C., Hennig, A., and Nau, W. M. (2019). Ratiometric DNA Sensing with a Host-Guest FRET Pair. *Chem. Commun.* 55, 671–674. doi:10.1039/c8cc09126a
- Zhang, X., Li, C.-R., Wang, W.-C., Xue, J., Huang, Y.-L., Yang, X.-X., et al. (2016). A Novel Electrochemical Immunosensor for Highly Sensitive Detection of Aflatoxin B1 in Corn Using Single-Walled Carbon Nanotubes/chitosan. *Food Chem.* 192, 197–202. doi:10.1016/j.foodchem.2015.06.044
- Zhang, Y., Hu, Y., Zhu, P., Han, F., Zhu, Y., Sun, R., et al. (2017b). Flexible and Highly Sensitive Pressure Sensor Based on Microdome-Patterned PDMS Forming with Assistance of Colloid Self-Assembly and Replica Technique for Wearable Electronics. *ACS Appl. Mater. Inter.* 9, 35968–35976. doi:10.1021/acsami.7b09617
- Zhao, C., Zhang, Y., Li, R., Li, X., and Jiang, J. (2007). Di(alkoxy)- and Di(alkylthio)-Substituted Perylene-3,4,9,10-Tetracarboxy Diimides with Tunable Electrochemical and Photophysical Properties. *J. Org. Chem.* 72, 2402–2410. doi:10.1021/jo062150j
- Zhao, J., Tang, Y., Cao, Y., Chen, T., Chen, X., Mao, X., et al. (2018). Amplified Electrochemical Detection of Surface Biomarker in Breast Cancer Stem Cell Using Self-Assembled Supramolecular Nanocomposites. *Electrochimica Acta* 283, 1072–1078. doi:10.1016/j.electacta.2018.07.002
- Zheng, Y., Long, H., Schatz, G. C., and Lewis, F. D. (2005). Duplex and Hairpin Dimer Structures for Perylene Diimide-Oligonucleotide Conjugates. *Chem. Commun.*, 4795–4797. doi:10.1039/b509754a
- Zheng, Y.-H., Hua, T.-C., Sun, D.-W., Xiao, J.-J., Xu, F., and Wang, F.-F. (2006). Detection of Dichlorvos Residue by Flow Injection Calorimetric Biosensor Based on Immobilized Chicken Liver Esterase. *J. Food Eng.* 74, 24–29. doi:10.1016/j.jfoodeng.2005.02.009
- Zhou, J.-W., Zou, X.-M., Song, S.-H., and Chen, G.-H. (2018). Quantum Dots Applied to Methodology on Detection of Pesticide and Veterinary Drug Residues. *J. Agric. Food Chem.* 66, 1307–1319. doi:10.1021/acs.jafc.7b05119
- Zhou, Y., Chiu, C.-W., and Liang, H. (2012). Interfacial Structures and Properties of Organic Materials for Biosensors: an Overview. *Sensors* 12, 15036–15062. doi:10.3390/s121115036
- Zhou, Z., Yan, X., Saha, M. L., Zhang, M., Wang, M., Li, X., et al. (2016). Immobilizing Tetraphenylethylene into Fused Metallacycles: Shape Effects on Fluorescence Emission. *J. Am. Chem. Soc.* 138, 13131–13134. doi:10.1021/jacs.6b07173

**Conflict of Interest:** The authors declare that the research was conducted in the absence of any commercial or financial relationships that could be construed as a potential conflict of interest.

**Publisher's Note:** All claims expressed in this article are solely those of the authors and do not necessarily represent those of their affiliated organizations, or those of the publisher, the editors and the reviewers. Any product that may be evaluated in this article, or claim that may be made by its manufacturer, is not guaranteed or endorsed by the publisher.

Copyright © 2021 Lim, Kuang and Ardoña. This is an open-access article distributed under the terms of the Creative Commons Attribution License (CC BY). The use, distribution or reproduction in other forums is permitted, provided the original author(s) and the copyright owner(s) are credited and that the original publication in this journal is cited, in accordance with accepted academic practice. No use, distribution or reproduction is permitted which does not comply with these terms.



# Elucidation of Charge Contribution in Iridium-Chelated Hydrogen-Bonding Systems

Barbora Balónová<sup>†</sup> and Barry A. Blight<sup>\*†</sup>

Department of Chemistry, University of New Brunswick, Fredericton, NB, Canada

## OPEN ACCESS

### Edited by:

Cally Jo Elizabeth Haynes,  
University College London,  
United Kingdom

### Reviewed by:

Tangxin Xiao,  
Changzhou University, China  
Xin Wu,  
The University of Sydney, Australia

### \*Correspondence:

Barry A. Blight  
b.blight@unb.ca

### <sup>†</sup>ORCID:

Barbora Balónová  
orcid.org/0000-0001-9029-5460  
Barry A. Blight  
orcid.org/0000-0003-1166-6206

### Specialty section:

This article was submitted to  
Supramolecular Chemistry,  
a section of the journal  
Frontiers in Chemistry

Received: 21 May 2021

Accepted: 20 July 2021

Published: 24 August 2021

### Citation:

Balónová B and Blight BA (2021)  
Elucidation of Charge Contribution in  
Iridium-Chelated Hydrogen-  
Bonding Systems.  
Front. Chem. 9:712698.  
doi: 10.3389/fchem.2021.712698

We present two iridium complexes **1H<sup>+</sup>** and **2H<sup>+</sup>** that contain cationic ligands to extend the knowledge of charge-assisted hydrogen bonding (CAHB), which counts among the strongest non-covalent bonding interactions. Upon protonation, both complexes were converted into new hydrogen-bonding arrays with various selectivity for respective H-bonding partners. This study compares the association strengths of four hydrogen-bonding co-systems, emphasizing the roles of CAHB in supramolecular systems. We determined that the cationic charge in these systems contributed up to 2.7 kJ mol<sup>-1</sup> in the H-bonding complexation processes.

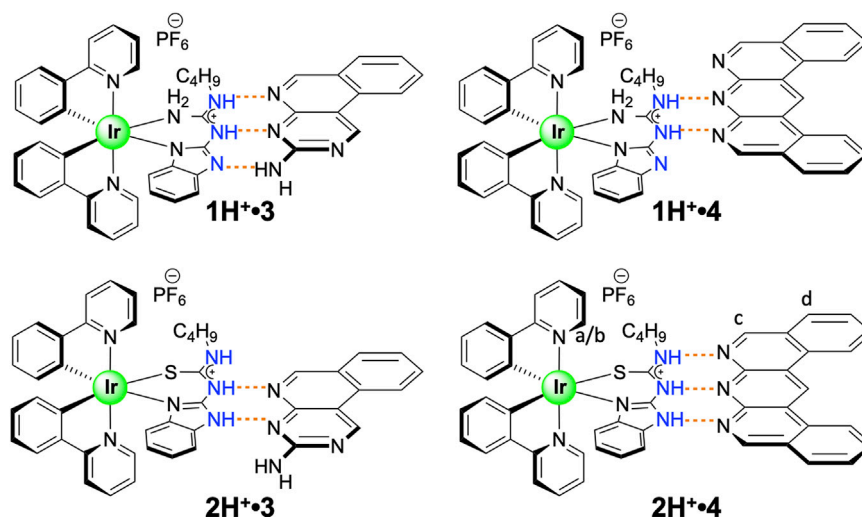
**Keywords:** H-bonding array, charge-assisted, ligand non-innocence, non-covalent interactions, self-assembly

## INTRODUCTION

Hydrogen-bonding is a type of interaction that plays a crucial role in most branches of science (Marechal, 2007). Not surprisingly, this interaction is often used in biochemical processes (Moran et al., 2012), materials science (Chowdhury and Gillespie, 2018), and many applicative areas of supramolecular chemistry (Kuhn et al., 2010; Persch et al., 2015). The electrostatic interaction occurs between the partial positively charged hydrogen atom X-H (donor) and a partial negatively charged hydrogen acceptor atom Y, where X and Y are electronegative atoms (such as N, O, or S). In addition to hydrogen bonds (H-bonds), supramolecular systems can be reinforced by the cooperative interactions between binding partners in the assembly (Prins et al., 2001). An important example of this statement is charge-assisted H-bonding (CAHB), which can be described as an interaction of the X-H<sup>+</sup>...Y<sup>-</sup> type, where the X-H donor belongs to the cation, and the Y acceptor belongs to the anion. Here, the charge assisted bonds X-H<sup>+</sup>...Y<sup>-</sup>, also known as a salt bridge, combine the inherent strength and directionality of the hydrogen bond with favorable localization of the ionic charges while being easily obtained via an acid-base reaction (Braga et al., 2000). Previously reported strategies for the preparation of CAHB systems often involve strategies incorporating nitrogen-based compounds (amines, amides, amidines), which can accept a proton from a carboxylic acid, for example, leading to the formation of N-H<sup>+</sup>...O<sup>-</sup> interactions (Papoutsakis et al., 1999; Félix et al., 2000; Schmuck and Wienand, 2003) with free energies ranging from 4.0–5.2 kJ mol<sup>-1</sup> (Horovitz et al., 1990).

Leigh and coworkers presented quadruple hydrogen-bonding complexes, including protonated salts with four N-H...N interactions that include an ion-dipole N-H<sup>+</sup>...N array (Leigh et al., 2013). These interactions can be switched on/off by the controlled addition of acid and base (Blight et al., 2011). Such configurations may be useful for designing responsive materials, such as nanofibers, gels, and supramolecular polymers. CAHBs tend to possess stronger interactions than a simple hydrogen bond due to the additional electrostatic interaction involved, resulting from one or more of the components bearing a charge (Papmeyer et al., 2016; Pop et al., 2016). Experimental deconvolution





**FIGURE 1** | Four complementary charge-assisted H-bonding systems featured in this study.

of sole-charge contribution in CAHB systems has yet to be quantified in assemblies where multiple hydrogen bonding arrays are employed. Several reports have shown that CAHB systems have found application in crystal engineering (Liu et al., 2019), synthesis of pharmaceutical salts/co-crystals (Wang et al., 2014), and in organometallic systems (Braga et al., 2004), making the elucidation of this energetic contribution critical in predicting materials properties.

In this study, we explore the effect of CAHB through the protonation of guanidine and thiourea-based ligands. According to the study conducted by Taylor and Kennard, N-H donors with a formal positive charge tend to form shorter bonds than uncharged N-H groups (Taylor and Kennard, 1984), which indicates a stronger association strength. Guanidinium derivatives represent a versatile functional group with unique properties (Blondeau et al., 2007; Han et al., 2008; Gale et al., 2013), and together with thiourea derivatives (Lee et al., 2002), have been widely investigated as part of the supramolecular systems. As such, we present here a comprehensive study of non-covalent self-assembly of the ionic iridium (III) complexes  $1H^+$  and  $2H^+$  (illustrated in Figure 1) with two different guest molecules **3** (Balónová et al., 2018) and **4** (Blight et al., 2009). These cationic complexes were found to exhibit stronger association constants than with the neutral species **1** (Balónová et al., 2018) and **2** (Balónová et al., 2020) when combined with complementary binding partners **3** and **4**. Chelation of the iridium (III) center by the guanidine and thiourea ligands eliminates any destructive rotational energy allowing us to accurately determine the contribution of the cationic charge to the association strength *via* experimentation.

## RESULTS AND DISCUSSION

We have previously reported the synthesis and characterization data of thiourea and guanidine-based ligands used for the

**TABLE 1** | Experimentally determined association constants for  $1H^+$  and  $2H^+$  with two different guest molecules, **3** and **4**, and their neutral parent complexes.

Co-system	Association	$-\Delta G$ (kJ mol <sup>-1</sup> )	Sartorius (kJ mol <sup>-1</sup> )
	Constant <sup>a</sup> ( $K_a$ )		
<b>1•3</b> <sup>b</sup>	$K_{11} = 9.1 \times 10^5 \text{ M}^{-1}$ $K_{12} = 3.2 \times 10^4 \text{ M}^{-1}$	34.0 25.7	23.7 —
<b>1•4</b> <sup>c</sup>	$K_{11} = 9.9 \times 10^4 \text{ M}^{-1}$ $K_{12} = 4.2 \times 10^3 \text{ M}^{-1}$	28.5 20.7	21.6 —
<b>1H<sup>+</sup>•3</b> <sup>b</sup>	$K_{11} = 1.9 \times 10^6 \text{ M}^{-1}$ $K_{12} = 3.4 \times 10^4 \text{ M}^{-1}$	35.9 25.9	23.7 —
<b>1H<sup>+</sup>•4</b> <sup>c</sup>	$K_a = 1.5 \times 10^3 \text{ M}^{-1}$	18.1	21.6
<b>2•3</b> <sup>d</sup>	$K_a = 2.1 \times 10^3 \text{ M}^{-1}$	19.0	23.7
<b>2•4</b> <sup>d</sup>	$K_a = 1.6 \times 10^3 \text{ M}^{-1}$	18.3	21.6
<b>2H<sup>+</sup>•3</b> <sup>c</sup>	$K_a = 4.8 \times 10^3 \text{ M}^{-1}$	21.0	21.6
<b>2H<sup>+</sup>•4</b> <sup>c</sup>	$K_{11} = 2.0 \times 10^4 \text{ M}^{-1}$ $K_{12} = 8.6 \times 10^3 \text{ M}^{-1}$	24.5 22.4	35.3 —

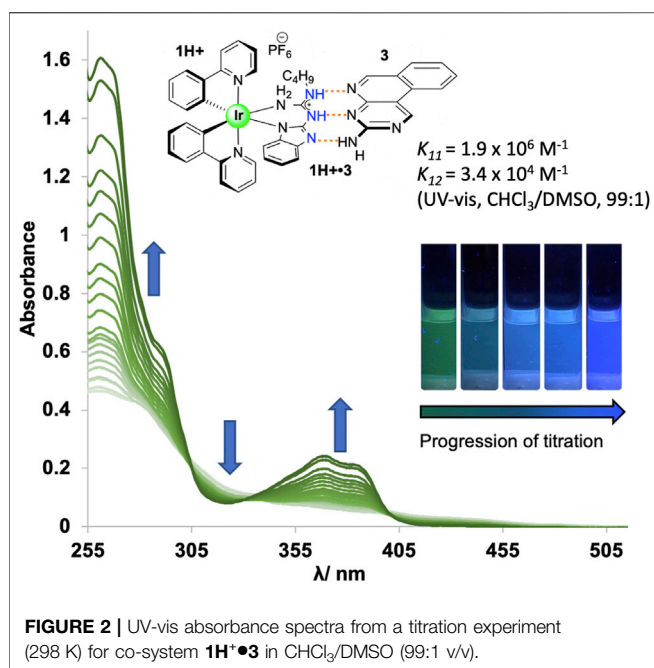
<sup>a</sup>Measured by UV-vis absorption spectroscopy in CHCl<sub>3</sub>/DMSO (99:1 v/v), 298 K.

<sup>b</sup>Data modelled using *sivvu.org*.

<sup>c</sup>Data modelled using *Bindfit* from *supramolecular.org*.

<sup>d</sup>Data from previously reported work (Balónová et al., 2020).

synthesis of iridium complexes  $1H^+$  and  $2H^+$  (Balónová et al., 2018; Balónová et al., 2020). Synthetic details for cationic complexes  $1H^+$  and  $2H^+$  are presented in the supplementary material for this article (**Supplementary Section S1**). Iridium  $\mu$ -chloro-bridged dimer [Ir(ppy)<sub>2</sub>Cl]<sub>2</sub> (ppyH = phenylpyridine) dimer was prepared by the procedure reported by Nonoyama (Nonoyama, 1974). Complex  $1H^+$  was synthesized using 1-(1H-benzo [d]imidazole-2-yl)-3-butylguanidine as a ligand followed by the ligand exchange using potassium hexafluorophosphate (KPF<sub>6</sub>) as the source of PF<sub>6</sub><sup>-</sup> counterion. Iridium complex  $2H^+$

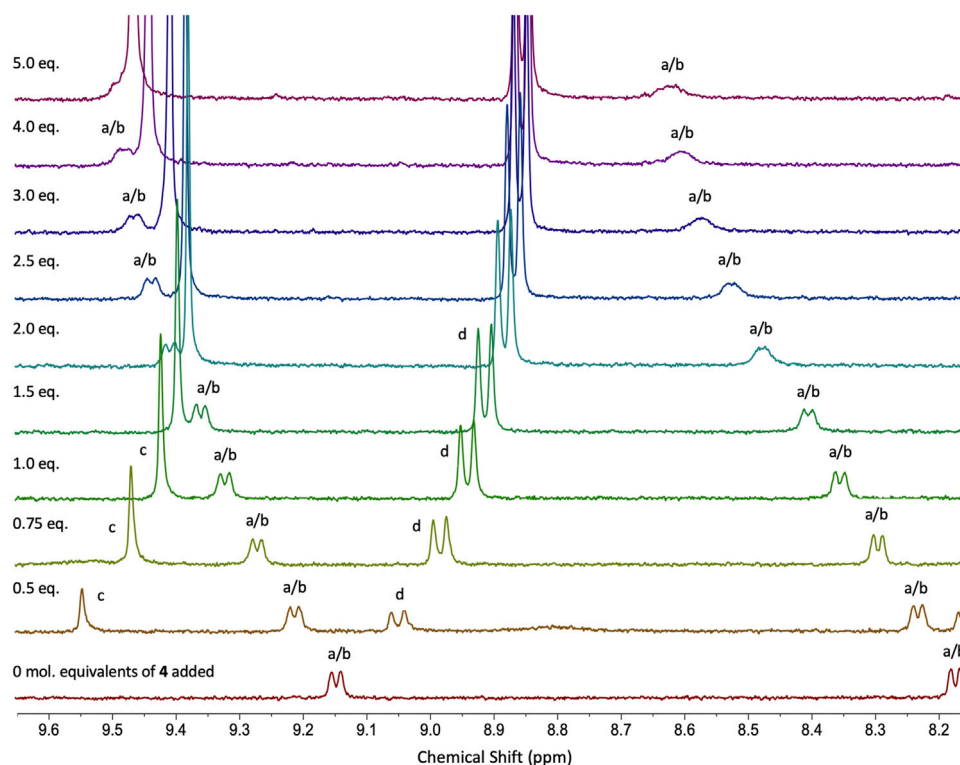


was synthesized by refluxing 1-(1H-benzo [d]imidazole-2-yl)-3-butylthiourea ligand with the iridium  $\mu$ -chloro-bridged dimer  $[Ir(ppy)_2Cl]_2$  in toluene, and similarly followed by the ion exchange with  $KPF_6^-$  counterion for the cationic complex  $2H^+$ . Complexes  $1H^+$  and  $2H^+$  were paired with binding partners **3** and **4** (Figure 1), and association constants were determined. UV-vis absorption spectroscopy titration methods were used to measure the association constants for complexes  $1H^+\bullet 3/4$  and  $2H^+\bullet 3/4$ , and all data were analyzed with the program BindFit (Thordarson, 2011; Supplementary Section S5) or sivvu.org as noted. The titrations were carried out in HPLC grade  $CHCl_3$  with 1% of DMSO to support the solubility of binding partners **3** and **4**. The self-association ( $K_{dim}$ ) of compounds **3** and **4** was determined to be  $K_{dim} < 50 M^{-1}$  and considered negligible for this study.

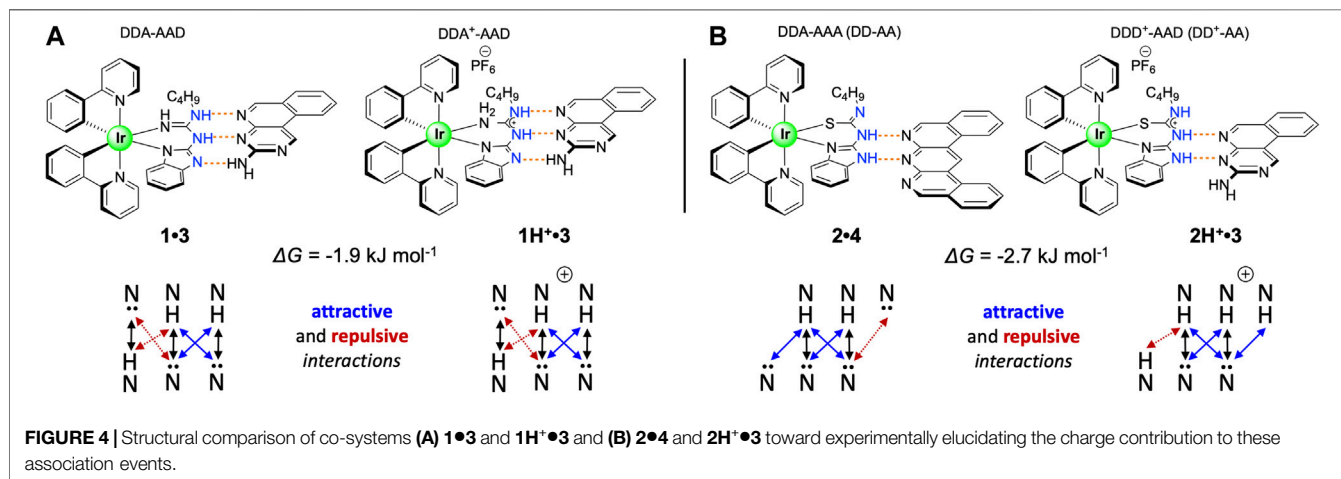
Cationic guanidine-based complex  $1H^+$  was paired with binding partners **3** and **4**, and association constants were determined through UV-vis absorption titration studies, with results summarized in Table 1. Due to the increased acidity of NH protons in the guanidinium moiety in complex  $1H^+$ , higher association constants were expected for systems  $1H^+\bullet 3/4$  in comparison to the association constants for thiourea based systems  $2H^+\bullet 3/4$ . Gibbs free energies for all co-systems, together with the predicted energy values from the empirical model, are also presented in Table 1. Titration study for co-system  $1H^+\bullet 3$  (Figure 2; Supplementary Section S5) revealed an increased association constants  $K_{11} = 1.9 \times 10^6 M^{-1}$  and  $K_{12} = 3.4 \times 10^4 M^{-1}$  (UV-vis,  $CHCl_3/DMSO$ , (99:1 v/v)) in comparison to neutral system **1** $\bullet 3$  (Table 1). To our surprise, experimental results obtained from UV-vis absorption titration studies with binding partner **4** did not align with our hypothesis. Admittedly, the association strength for protonated co-system  $1H^+\bullet 4$  (DDD<sup>+</sup>-AAA array) – where protonation of the benzimidazole would lead

to a DDD<sup>+</sup> system, a perfect complement to **4**—did not increase compared to neutral co-system **1** $\bullet 4$  (DDA-AAA array). As reported by Wisner and coworkers, the association strength can be decreased or increased by changing the structure of the interacting site to the other isomeric form (Linares Mendez et al., 2019). We posit that prototropy of the guanidinium ligand, made possible by the multiple basic sites that guanidine offers, gives rise to a protonated state that does not give rise to the desired DDD<sup>+</sup> arrangement, but an ADD<sup>+</sup> array (Supplementary Section S1), as evidenced by the lower-than-expected association constant for  $1H^+\bullet 4$ , with a modest increase of binding strength observed for  $1H^+\bullet 3$ .

Compound  $2H^+$  was separately paired with guests **3** and **4**, and their interactions were examined through UV-vis spectroscopic analysis (Supplementary Section S5) to quantify their respective association constants and compared with neutral systems **2** $\bullet 3$  and **2** $\bullet 4$  (Table 1). The co-system  $2H^+\bullet 3$  can be described as a double bonding DD<sup>+</sup>-AA motif with three attractive and one repulsive secondary interaction within the structure. The strength of this association was assessed via UV-vis absorption titration of  $2H^+$  with **3** in  $CHCl_3/DMSO$  (99:1 v/v), revealing an association constant  $K_a = 4.8 \times 10^3 M^{-1} \pm 0.4\%$  and the binding energy of  $-21.6 kJ mol^{-1}$ , which is almost identical to the value obtained from the Sartorius empirical model that assigns weighted interaction values as the number of interactions increase (Sartorius and Schneider, 1996). This value is almost doubled compared to the neutral co-system **2** $\bullet 3$ , which can be explained by the increased number of attractive secondary interactions and electrostatic-charge assistance contributing to the stability and binding energy of the  $2H^+\bullet 3$  system (Table 1). The association constant for co-system  $2H^+\bullet 4$  was also investigated, and according to the strong influence of secondary interactions, the complementary DDD<sup>+</sup>-AAA system was predicted to be among the most stable arrays presented in this study. As has been previously investigated (and noted above), the binding strength is maximized if all the donor atoms are located on one component and all acceptor atoms are on the binding partner (Jorgensen and Pranata, 1990; Pranata et al., 1991). The planar compound **4** has been previously reported to improve stability and give rise to high association constants in triple DDD-AAA systems (Blight et al., 2009). The neutral complex **2** formed a double H-bonding DD-AA array with **4** ( $K_a = 1.6 \times 10^3 M^{-1} \pm 0.1\%$ ; Figure 2), and through simple protonation, the multiplicity was increased to triple H-bonding DDD<sup>+</sup>-AAA system  $2H^+\bullet 4$ . Multiple examples of DDD-AAA complexes have been reported to date (only two DDD<sup>+</sup>), but none of them considered thiourea ligands as binding partners in the assemblies (Balónová et al., 2020; Djurdjevic et al., 2007). Addition of **4** to  $2H^+$  in  $CHCl_3/DMSO$  (99:1 v/v) was monitored by UV-vis absorption titration analysis and association constants  $K_{11} = 2.0 \times 10^4 M^{-1} \pm 0.1\%$ ,  $K_{12} = 8.6 \times 10^3 M^{-1} \pm 0.2\%$  for co-system  $2H^+\bullet 4$  were determined (confirmed by <sup>1</sup>H NMR; Figure 3; Supplementary Sections S4, S5). Compared to the neutral co-system **2** $\bullet 4$ , protonation of complex **2** resulted in  $\sim 12$ -fold increase in the association constant when combined with compound **4** in  $CHCl_3/DMSO$  (99:1 v/v). <sup>1</sup>H NMR titrations illustrate the putative interactions between  $2H^+$  and **4** with protons *a/b* of  $2H^+$  (*o*-protons of both



**FIGURE 3** | Stacked  $^1\text{H}$  NMR (400 MHz, 298 K) spectra from titration experiment for co-system  $2\text{H}^+\bullet 4$  in  $\text{CDCl}_3/\text{DMSO}-d_6$  (99:1 v/v). **4** ( $c = 1 \times 10^{-3}$  M) was titrated into a solution of  $2\text{H}^+$  ( $c = 1 \times 10^{-4}$  M) in  $\text{CDCl}_3/\text{DMSO}-d_6$  (99:1 v/v).cs.



**FIGURE 4** | Structural comparison of co-systems (A)  $1\bullet 3$  and  $1\text{H}^+\bullet 3$  and (B)  $2\bullet 4$  and  $2\text{H}^+\bullet 3$  toward experimentally elucidating the charge contribution to these association events.

pyridine moieties) being shifted down-field by approx. 0.5 ppm and protons *c* and *d* of **4** showing a reciprocal shift up-field as its concentration is increased in the presence of host  $2\text{H}^+$ .

Based on these results, we were able to use an empirical approach to calculate the contribution of charge to the association strength for two of our systems. Protonation of **1** gives rise to the  $1\text{H}^+$ , where complex prototropy (Supplementary Section S1) inhibits identification of the extra proton location.

Given that there is a large increase in  $K_a$  for  $1\text{H}^+\bullet 3$  and not for  $1\text{H}^+\bullet 4$ , which would represent a  $\text{DDD}^+$ -AAA array, we propose that  $1\text{H}^+\bullet 3$  exists as an  $\text{ADD}^+$  array (vs  $\text{DDD}^+$ ) complemented by **3** (DAA; Figure 4A), which allows us to directly compare its  $K_a$  with that of  $1\bullet 3$  (ADD-DAA) given that they have the same number of primary H-bonds and secondary electrostatic interactions. Comparing the neutral guanidine-based co-system  $1\bullet 3$  ( $\Delta G_{1:1} = -34.0 \text{ kJ mol}^{-1}$ ) with the cationic  $1\text{H}^+\bullet 3$

( $\Delta G_{1:1} = -35.9 \text{ kJ mol}^{-1}$ ), we calculated the overall charge contribution to the association, as the difference in Gibbs free energy, to be  $-1.9 \text{ kJ mol}^{-1}$  ( $-0.45 \text{ kcal mol}^{-1}$ ). As presented in **Figure 4B**, thiourea-based systems **2•4** and **2H<sup>+</sup>•3** empirically have the same number of primary hydrogen bonds and attractive/repulsive secondary interactions within the structures, assuming that the different secondary electrostatic interactions contribute equally. Based on this structural arrangement, the charge contribution was calculated. From the comparison of neutral thiourea-based co-system **2•4** ( $\Delta G = -18.3 \text{ kJ mol}^{-1}$ ) with the cationic **2H<sup>+</sup>•3** ( $\Delta G = -21.0 \text{ kJ mol}^{-1}$ ) we calculated the charge contribution in this instance to be  $-2.7 \text{ kJ mol}^{-1}$  ( $-0.65 \text{ kcal mol}^{-1}$ ). We note the difference in values in the two different systems and acknowledge that these are using the  $K_{1:1}$  values from these equilibria to do this comparison. We posit that the competitive 1:2 equilibria will interfere with determining a wholly discrete cation contribution. However, to the best of our knowledge, the discrete charge contribution to association strength in H-bonding arrays has never been determined before. If comparing the Gibbs free energy of charge contribution to salt bridges as determined by Horowitz and coworkers ( $4.0\text{--}5.2 \text{ kJ mol}^{-1}$ ; Horowitz et al., 1990) the charge contributions elucidated in this study are in agreement, given that the present study includes only one of the charged partners.

In summary, we prepared two new cationic iridium (III) complexes **1H<sup>+</sup>** and **2H<sup>+</sup>**. Both complexes **1H<sup>+</sup>** and **2H<sup>+</sup>** represent rare examples of charged complexes where the ancillary ligand carries the formal charge (ligand non-innocence). This work further examined the self-assembly of complexes **1H<sup>+</sup>** and **2H<sup>+</sup>** with guest molecules **3** and **4**, respectively, to determine the charge contribution to the association strength. Guanidine based complex **1H<sup>+</sup>** with component **3** in DDA-AAD alignment represents the strongest H-bonding system ( $K_{11} = 1.9 \times 10^6 \text{ M}^{-1}$  and  $K_{12} = 3.4 \times 10^4 \text{ M}^{-1}$ , UV-vis,  $\text{CHCl}_3/\text{DMSO}$ , (99:1 v/v)) in this study due to increased acidity of NH protons in the cationic **1H<sup>+</sup>** system, a 2-fold increase over its neutral system. In addition, simple protonation of thiourea-based complex **2** results in a ~12-fold increase in the association strength of co-system **2H<sup>+</sup>•4** in comparison to its neutral version **2•4**. Furthermore, from UV-vis absorption titration studies, we were able to determine the

contribution of the charge to the association strength by comparing neutral systems **1•3** and **2•4** with their respective complements **1H<sup>+</sup>•3** and **2H<sup>+</sup>•3** to be  $-1.9 \text{ kJ mol}^{-1}$  ( $-0.45 \text{ kcal mol}^{-1}$ ) and  $-2.7 \text{ kJ mol}^{-1}$  ( $-0.65 \text{ kcal mol}^{-1}$ ), respectively). Elucidating the energetics of CAHB interactions will contribute to developing empirical models that allow for more accurate prediction of system dynamics. Based on these results, incorporating CAHB interactions into H-bonding arrays can increase association strengths, leading to higher-order materials and a significant role in more competitive and complex systems.

## DATA AVAILABILITY STATEMENT

The datasets presented in this study can be found in online repositories. The names of the repository/repositories and accession number(s) can be found below: <https://doi.org/10.25545/6TZWCG>.

## AUTHOR CONTRIBUTIONS

BB helped design and completed all experiments, and wrote the first draft of the manuscript. BAB directly supervised BB, helped design experiments and completed the manuscript.

## FUNDING

BAB is grateful for financial support from University of New Brunswick, New Brunswick Foundation for Innovation (NBIF), and Natural Science and Engineering Council of Canada (NSERC; RGPIN-2018-04021).

## SUPPLEMENTARY MATERIAL

The Supplementary Material for this article can be found online at: <https://www.frontiersin.org/articles/10.3389/fchem.2021.712698/full#supplementary-material>

## REFERENCES

- Balónová, B., Martir, D. R., Clark, E. R., Shepherd, H. J., Zysman-Colman, E., and Blight, B. A. (2018). Influencing the Optoelectronic Properties of a Heteroleptic Iridium Complex by Second-Sphere H-Bonding Interactions. *Inorg. Chem.* 57, 8581–8587. doi:10.1021/acs.inorgchem.8b01326
- Balónová, B., Shepherd, H. J., Serpell, C. J., and Blight, B. A. (2020). IrIII as a Strategy for Preorganisation in H-Bonded Motifs. *Supramolecular Chem.* 32, 1–12. doi:10.1080/10610278.2019.1649674
- Blight, B. A., Camara-Campos, A., Djurdjevic, S., Kaller, M., Leigh, D. A., McMillan, F. M., et al. (2009). AAA-DDD Triple Hydrogen Bond Complexes. *J. Am. Chem. Soc.* 131, 14116–14122. doi:10.1021/ja906061v
- Blight, B. A., Hunter, C. A., Leigh, D. A., McNab, H., and Thomson, P. I. T. (2011). An AAAA-DDDD Quadruple Hydrogen-Bond Array. *Nat. Chem.* 3, 244–248. doi:10.1038/nchem.987
- Blondeau, P., Segura, M., Pérez-Fernández, R., and de Mendoza, J. (2007). Molecular Recognition of Oxoanions Based on Guanidinium Receptors. *Chem. Soc. Rev.* 36, 198–210. doi:10.1039/B603089K
- Braga, D., Maini, L., Grepioni, F., De Cian, A., Fe'lix, O., Fischer, J., et al. (2000). Charge-assisted N-H(+)...O(-) and O-H...O(-) Hydrogen Bonds Control the Supramolecular Aggregation of Ferrocenedicarboxylic Acid and Bis-Amidines. *New J. Chem.* 24, 547–553. doi:10.1039/B002061N
- Braga, D., Polito, M., and Grepioni, F. (2004). Novel Organometallic Building Blocks for Molecular Crystal Engineering. 3. Synthesis, Characterization, and Hydrogen Bonding of the Crystalline Mono- and Bis-Amide Derivatives of [CoIII(η5-C5H4-COOH)2]+ and of the Cationic Zwitterion [CoIII(η5-C5H4CONHC5H4NH)(η5-C5H4COO)]+. *Cryst. Growth Des.* 4, 769–774. doi:10.1021/cg049942w
- Chowdhury, S. C., and Gillespie, J. W. (2018). A Molecular Dynamics Study of the Effects of Hydrogen Bonds on Mechanical Properties of Kevlar crystal. *Comput. Mater. Sci.* 148, 286–300. doi:10.1016/j.commatsci.2018.02.055



- Djordjevic, S., Leigh, D. A., McNab, H., Parsons, S., Teobaldi, G., and Zerbetto, F. (2007). Extremely Strong and Readily Accessible AAA-DDD Triple Hydrogen Bond Complexes. *J. Am. Chem. Soc.* 129, 476–477. doi:10.1021/ja067410t
- Félix, O., Hosseini, M. W., De Cian, A., and Fischer, J. (2000). Crystal Engineering of 2-D Hydrogen Bonded Molecular Networks Based on the Self-Assembly of Anionic and Cationic Modules. *Chem. Commun.* 4, 281–282. doi:10.1039/A909093B
- Gale, P. A., Pérez-Tomás, R., and Quesada, R. (2013). Anion Transporters and Biological Systems. *Acc. Chem. Res.* 46, 2801–2813. doi:10.1021/ar400019p
- Han, J., Yau, C.-W., Lam, C.-K., and Mak, T. C. W. (2008). Designed Supramolecular Assembly of Hydrogen-Bonded Anionic Rosette Layers. *J. Am. Chem. Soc.* 130, 10315–10326. doi:10.1021/ja802425q
- Horovitz, A., Serrano, L., Avron, B., Bycroft, M., and Fersht, A. R. (1990). Strength and Co-operativity of Contributions of Surface Salt Bridges to Protein Stability. *J. Mol. Biol.* 216, 1031–1044. doi:10.1016/S0022-2836(99)80018-7
- Jorgensen, W. L., and Pranata, J. (1990). Importance of Secondary Interactions in Triply Hydrogen Bonded Complexes: Guanine-Cytosine vs Uracil-2,6-Diaminopyridine. *J. Am. Chem. Soc.* 112, 2008–2010. doi:10.1021/ja00161a061
- Kuhn, B., Mohr, P., and Stahl, M. (2010). Intramolecular Hydrogen Bonding in Medicinal Chemistry. *J. Med. Chem.* 53, 2601–2611. doi:10.1021/jm100087s
- Lee, D. H., Lee, H. Y., and Hong, J.-I. (2002). Anion Sensor Based on the Indoaniline-Thiourea System. *Tetrahedron Lett.* 43, 7273–7276. doi:10.1016/S0040-4039(02)01455-7
- Leigh, D. A., Robertson, C. C., Slawin, A. M. Z., and Thomson, P. I. T. (2013). AAAA-DDDD Quadruple Hydrogen-Bond Arrays Featuring NH...N and CH...N Hydrogen Bonds. *J. Am. Chem. Soc.* 135, 9939–9943. doi:10.1021/ja404504m
- Linares Mendez, I. J., Pleizier, J. S., Wang, H.-B., and Wisner, J. A. (2018). 1 H NMR-Based Method for the Determination of Complexation Equilibrium Parameters and Chemical Shifts in a Hydrogen-Bonded System with Dynamic Composition. *J. Phys. Org. Chem.* 31, e3805. doi:10.1002/poc.3805
- Liu, L., Zou, D., Zhang, Y., Zhang, D., Zhang, Y., Zhang, Q., et al. (2019). Assembly of Three Pharmaceutical Salts/Cocrystals of Tetrahydroberberine with Sulfophenyl Acids: Improving the Properties by Formation of Charge-Assisted Hydrogen Bonds. *New J. Chem.* 43, 4886–4894. doi:10.1039/C9NJ00131J
- Marechal, Y. (2007). *The Hydrogen Bond and the Water Molecule: The Physics and Chemistry of Water, Aqueous and Bio media*. Amsterdam, Netherlands: Elsevier Science & Technology.
- Moran, L. A., Horton, H. R., Scrimgeour, K. G., and Perry, M. D. (2012). *Principles of Biochemistry*. 5th ed. New York: Pearson Education.
- Nonoyama, M. (1974). Benzo[h]quinolin-10-yl-Niridium(III) Complexes. *Bcsj* 47, 767–768. doi:10.1246/bcsj.47.767
- Papmeyer, M., Vuilleumier, C. A., Pavan, G. M., Zhurov, K. O., and Severin, K. (2016). Molecularly Defined Nanostructures Based on a Novel AAA-DDD Triple Hydrogen-Bonding Motif. *Angew. Chem.* 128, 1717–1721. doi:10.1002/anie.20151042310.1002/ange.201510423
- Papoutsakis, D., Kirby, J. P., Jackson, J. E., and Nocera, D. G. (1999). From Molecules to the Crystalline Solid: Secondary Hydrogen-Bonding Interactions of Salt Bridges and Their Role in Magnetic Exchange. *Chem. Eur. J.* 5, 1474–1480. doi:10.1002/(SICI)1521-3765(19990503)5:5<1474::AID-CHEM1474>3.0.CO;2-T
- Persch, E., Dumele, O., and Diederich, F. (2015). Molecular Recognition in Chemical and Biological Systems. *Angew. Chem. Int. Ed.* 54, 3290–3327. doi:10.1002/anie.201408487
- Pop, L., Hadade, N. D., van der Lee, A., Barboiu, M., Grosu, I., and Legrand, Y.-M. (2016). Occurrence of Charge-Assisted Hydrogen Bonding in Bis-Amidine Complexes Generating Macrocycles. *Cryst. Growth Des.* 16, 3271–3278. doi:10.1021/acs.cgd.6b00246
- Pranata, J., Wierschke, S. G., and Jorgensen, W. L. (1991). OPLS Potential Functions for Nucleotide Bases. Relative Association Constants of Hydrogen-Bonded Base Pairs in Chloroform. *J. Am. Chem. Soc.* 113, 2810–2819. doi:10.1021/ja00008a002
- Prins, L. J., Reinhoudt, D. N., and Timmerman, P. (2001). Non-covalent Synthesis Using Hydrogen Bonding. *Angew. Chem. Int. Ed.* 40, 2382–2426. doi:10.1002/1521-3773(20010702)40:13<2382::AID-ANIE2382>3.0.CO;2-G
- Sartorius, J., and Schneider, H.-J. (1996). A General Scheme Based on Empirical Increments for the Prediction of Hydrogen-Bond Associations of Nucleobases and of Synthetic Host-Guest Complexes. *Chem. Eur. J.* 2, 1446–1452. doi:10.1002/chem.19960021118
- Schmuck, C., and Wienand, W. (2003). Highly Stable Self-Assembly in Water: Ion Pair Driven Dimerization of a Guanidiniocarbonyl Pyrrole Carboxylate Zwitterion. *J. Am. Chem. Soc.* 125, 452–459. doi:10.1021/ja028485+
- Taylor, R., and Kennard, O. (1984). Hydrogen-Bond Geometry in Organic Crystals. *Acc. Chem. Res.* 17, 320–326. doi:10.1021/ar00105a004
- Thordarson, P. (2011). Determining Association Constants from Titration Experiments in Supramolecular Chemistry. *Chem. Soc. Rev.* 40, 1305–1323. doi:10.1039/c0cs00062k
- Wang, H., Gurau, G., Shamshina, J., Cojocaru, O. A., Janikowski, J., MacFarlane, D. R., et al. (2014). Simultaneous Membrane Transport of Two Active Pharmaceutical Ingredients by Charge Assisted Hydrogen Bond Complex Formation. *Chem. Sci.* 5, 3449–3456. doi:10.1039/C4SC01036A

**Conflict of Interest:** The authors declare that the research was conducted in the absence of any commercial or financial relationships that could be construed as a potential conflict of interest.

**Publisher's Note:** All claims expressed in this article are solely those of the authors and do not necessarily represent those of their affiliated organizations, or those of the publisher, the editors and the reviewers. Any product that may be evaluated in this article, or claim that may be made by its manufacturer, is not guaranteed or endorsed by the publisher.

Copyright © 2021 Balónová and Blight. This is an open-access article distributed under the terms of the Creative Commons Attribution License (CC BY). The use, distribution or reproduction in other forums is permitted, provided the original author(s) and the copyright owner(s) are credited and that the original publication in this journal is cited, in accordance with accepted academic practice. No use, distribution or reproduction is permitted which does not comply with these terms.



# Advances in the Supramolecular Chemistry of Tetracoordinate Boron-Containing Organic Molecules into Organogels and Mesogens

Sanchita Shah, Parvati Marandi and P. P. Neelakandan\*

Energy and Environment Unit, Institute of Nano Science and Technology, Mohali, India

## OPEN ACCESS

### Edited by:

Claudia Caltagirone,  
University of Cagliari, Italy

### Reviewed by:

Alessandra Garau,  
University of Cagliari, Italy  
Xiao-Yu Hu,  
Nanjing University of Aeronautics and  
Astronautics, China

### \*Correspondence:

P. P. Neelakandan  
ppn@inst.ac.in

### Specialty section:

This article was submitted to  
Supramolecular Chemistry,  
a section of the journal  
Frontiers in Chemistry

**Received:** 12 May 2021

**Accepted:** 23 August 2021

**Published:** 07 September 2021

### Citation:

Shah S, Marandi P and  
Neelakandan PP (2021) Advances in  
the Supramolecular Chemistry of  
Tetracoordinate Boron-Containing  
Organic Molecules into Organogels  
and Mesogens.  
Front. Chem. 9:708854.  
doi: 10.3389/fchem.2021.708854

Boron-containing organic compounds are well accepted as a class of compounds having excellent photophysical properties. In addition to the unique photophysical properties, the ease of synthesis and structural robustness make tetracoordinate boron complexes ideal for a variety of applications. While significant light has been thrown on their luminescence properties, there is no collective attention to their supramolecular chemistry. In this mini review, we discuss the progress made in the supramolecular chemistry of these compounds which includes their utility as building blocks for liquid crystalline materials and gels largely driven by various non-covalent interactions like H-bonding, CH- $\pi$  interactions, BF- $\pi$  interactions and Van der Waals forces. The organoboron compounds presented here are prepared from easy-to-synthesize chelating units such as imines, diiminates, ketoiminates and diketonates. Moreover, the presence of heteroatoms such as nitrogen, oxygen and sulfur, and the presence of aromatic rings facilitate non-covalent interactions which not only favor their formation but also helps to stabilize the self-assembled structures.

**Keywords:** luminescence, self-assembly, boron, gels, liquid crystals

## INTRODUCTION

Organoboron compounds are typically employed in organic chemistry as reagents and catalysts. However, boron has emerged as a key element for organic luminescent materials in the recent past. Several tri- and tetra-coordinated boron containing organic compounds have been synthesized and were demonstrated to have excellent photophysical properties (Loudet and Burgess, 2007; Li et al., 2013; Frath et al., 2014; Mukherjee and Thilagar, 2016). Properties such as environment sensitive luminescence, long lifetimes and high carrier mobility has allowed the usage of boron-containing organic compounds as organic light-emitting diodes, organic field-effect transistors, photoresponsive materials, photosensitizers, sensors and imaging materials (K. Tanaka and Chujo, 2012; Anthony, 2012; Awuah and You, 2012; Rao and Wang, 2011; Jäkle, 2010; Entwistle and Marder, 2002).

The delocalization of the  $\pi$ -electrons of organic chelates to the vacant  $p$ -orbitals of boron rigidifies the boron-containing organic compounds and thus stabilizes the  $\pi$ -conjugated skeletons (Shah et al., 2018). Such ring-fused structures not only constrain the  $\pi$ -conjugated framework to intensify the emission but also lower the energy levels of the lowest unoccupied molecular orbital. The type of the ligands and the nature of the substituted groups on either the ligands or boron have a great influence on the photophysical properties of these compounds. A variety of ligands have been investigated as

boron coordination motifs and the fluorescence of the resulting organoboron compounds cover a wide spectral range in the UV and visible region. Several reviews have been published that compile the optical properties and applications of different classes of boron-containing organic molecules (Boens et al., 2012; Kamkaew et al., 2013; Li et al., 2013; Maeda and Bando, 2013; Frath et al., 2014; Mukherjee and Thilagar, 2016; Chen et al., 2017b; Matsuoka and Nabeshima, 2018).

Supramolecular chemistry of the organoboron compounds pertains to their usage as chemosensors, inclusion compounds, liquid crystalline materials, gels and luminescent materials. Among the various classes of self-assembled structures, gels and liquid crystals are interesting because their nanostructure and properties can be tuned by subtle modifications in the chemical composition. The formation of both gels and mesogens is driven by the balance between various non-covalent interactions such as hydrogen bonding, electrostatic interactions, hydrophobic forces, CH- $\pi$  interactions, BF- $\pi$  interactions and Van der Waals forces. The presence of hetero atoms in boron-containing organic compounds along with the  $\pi$ -conjugated core offers a stable platform for the formation of gels and mesogens. Although their supramolecular chemistry is as intriguing as their luminescence properties, their self-assembly properties have not been reviewed extensively. This mini-review focusses on the supramolecular assemblies such as gels and liquid crystals formed by tetra-coordinate boron-containing organic molecules containing chelates such as imines, diiminates, ketoiminates and diketonates. Boron-dipyrrromethenes (BODIPYs) are the most famous members of the organoboron family. But, as there are several reviews that summarize the developments in the chemistry of BODIPYs (Loudet and Burgess, 2007; Galbraith and James, 2010; Boens et al., 2012; Kamkaew et al., 2013; Lu et al., 2014; Cherumukil et al., 2018), we do not intent to discuss any BODIPY compounds. We have subdivided the mini-review into two sections namely gels and mesogens with one figure representing each section.

## SELF-ASSEMBLY INTO GELS

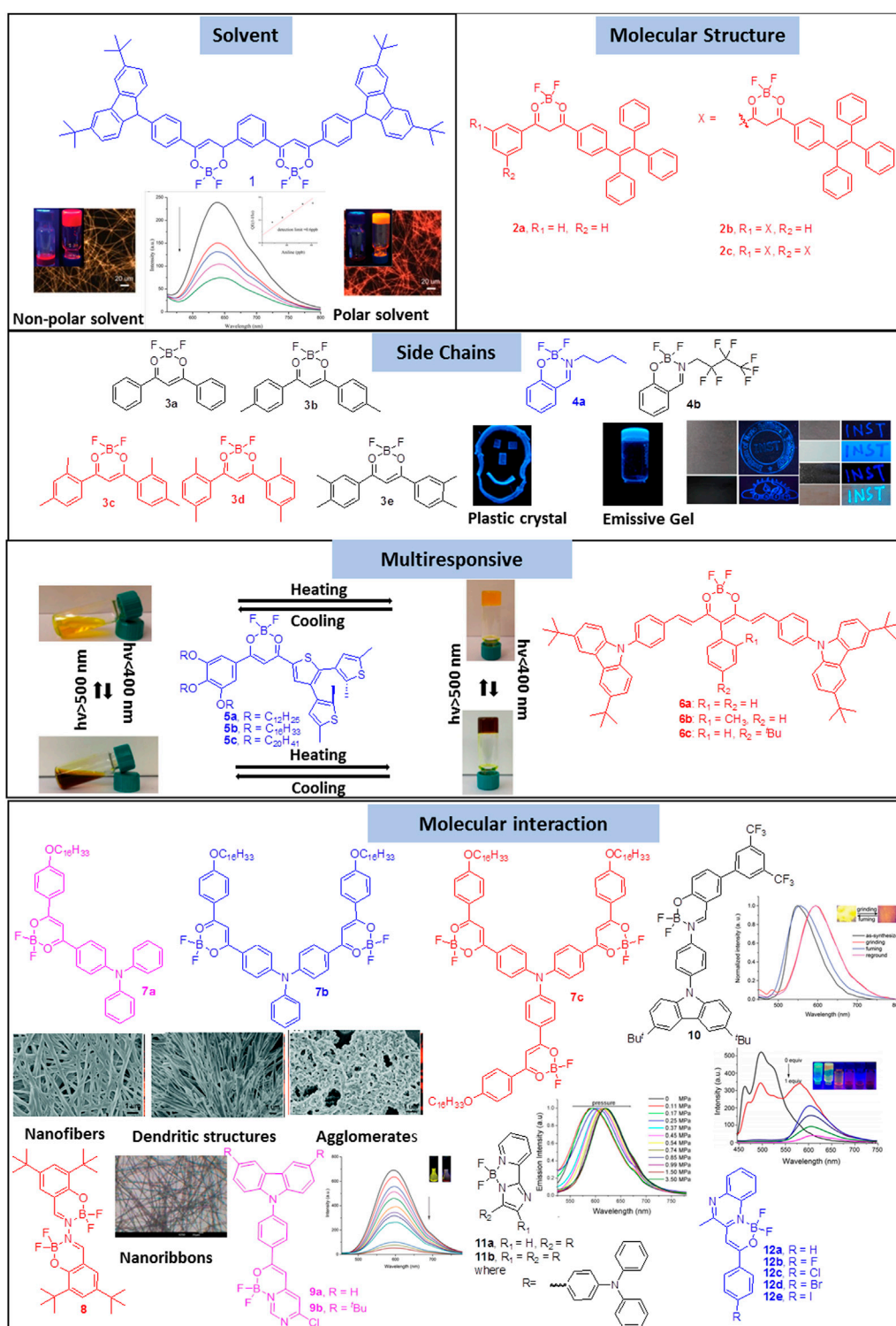
Organogels are semisolids composed of a gelling molecule organized into a continuous network *via* physical or chemical crosslinking that exhibits no flow in the steady state. The formation of organogels depends on various factors such as the nature of the gelator, solvent, temperature and the time for gelation. Organogels are widely employed as matrices for inks, paints and cosmetics, and their stimuli-responsive properties allow them to be used for applications wherein sustained and controlled release is necessary (Abdallah and Weiss, 2000; Varaprasad et al., 2017; Crump et al., 2021; Das et al., 2021; Esposito and Kirilov, 2021). Boron-difluoride complexes are emerging as an important class of organogelators because they can promote non-covalent interactions through the hetero atoms that are present inherently in their structure. Moreover, these compounds are easy to synthesize and functionalization with traditional gelation-inducing moieties could be circumvented. Further, their excellent

stability and photophysical properties such as high fluorescence in solution and solid state, high electron affinity and large molar extinction coefficients make them excellent building blocks for gelation. In this mini review, we have classified the gelation of boron-difluoride compounds on the basis of the effect of solvent, molecular structure, effect of substituents and intermolecular interactions (Figure 1).

One of the crucial factors for gelation is the ability of the gelator to trap solvent molecules. The balance between the interaction of the gelator with itself and with the solvent is determined by the solvent as solvent plays a critical role in the nucleation and growth processes of self-assembly. Sun et al. showed that the polarity of the solvent affects the gelation properties of  $\beta$ -diketonate difluoroboron complex **1** functionalized with *tert*-butyl carbazole moiety (Sun et al., 2018). Complex **1** formed two different colored organogels: a red gel was formed in low polar solvent mixtures such as *o*-dichlorobenzene/cyclohexane (*v/v* = 1/5) whereas an orange gel was formed in high polar solvent mixtures like *o*-dichlorobenzene/cyclohexane (*v/v* = 1/2). The difference in the color of the gels were attributed to the formation of *J*- and *H*-aggregates in these solvent mixtures which resulted in the formation of twisted and straight nanofibers, respectively. Further, xerogel based films of complex **1** were found to be sensitive towards *n*-propylamine and aniline with a detection limit of 1 ppb and 0.6 ppb respectively.

In addition to solvent, chemical composition of the molecule also plays a vital role in the self-assembly pattern of tetra coordinated difluoroboron complexes. Zhai et al. illustrated that a boomerang shaped  $\beta$ -diketone difluoroboron complex without traditional gelation groups forms organogels with the introduction of tetraphenylethylene unit **2a-c** (Zhai et al., 2017). The xerogel of **2b** obtained from *p*-xylene formed nanorods with strong orange red emission having diameters in the range of 0.67–1.78  $\mu\text{m}$  due to the favorable boomerang shaped  $\pi$ -conjugated skeleton that facilitated self-assembly whereas **2a** and **2c** did not form gel. Furthermore, XRD measurements indicated that molecules of **2b** were packed in an anti-parallel bimolecular layered structure in the gel state. It was interesting to observe that the emission of **2** in xerogel-based film was quenched significantly in the presence of triethylamine vapors.

Similar to the molecular structure, appropriately placed substituents also exert a significant influence on the self-assembly and the gelation properties of the tetra coordinated boron difluoride complexes. Zhu et al. demonstrated the importance of methyl group in the gelation of  $\beta$ -diketone difluoroboron complexes **3a-e** (Zhu et al., 2020). The self-assembly of these complexes were studied in various solvents like hexane, cyclohexane, petroleum ether and toluene. Xerogels **3c** and **3d** were observed to form flake-like lamellar structures with porous networks which implied that a large volume of solvent was entrapped in the gel state. The gels were also found to be super-hydrophobic with water contact angles ranging from 145–153°. Detailed investigation into the self-assembly pattern revealed that the number and position of methyl groups played a vital role in the self-assembly. Intermolecular  $\pi$ - $\pi$  stacking and non-covalent bonding



**FIGURE 1** | Gelation of boron-difluoride compounds on the basis of the effect of solvent, molecular structure, effect of substituents and intermolecular interactions.

Reproduced with permission from Sun et al., 2018, copyright 2018 Royal Society of Chemistry. Reproduced from Naim et al., 2021, copyright 2021 American Chemical Society. Reproduced from Wong et al., 2017, copyright 2017 American Chemical Society. Reproduced with permission from Qian et al., 2015, copyright 2015 Royal Society of Chemistry. Reproduced with permission from Gong et al., 2015, copyright 2015 Royal Society of Chemistry. Reproduced with permission from Mi et al., 2018, copyright 2018 Royal Society of Chemistry. Reproduced with permission from Sun et al., 2017, copyright 2017 Royal Society of Chemistry. Reproduced with permission from Wang et al., 2017, copyright 2017 WILEY-VCH. Reproduced with permission from Wu et al., 2017, copyright 2017 WILEY-VCH.



between methyl groups and the neighboring molecules were ascertained to be the driving forces for gelation. Our group recently showed that the chemical composition of the sidechain has a significant influence on the self-assembly as well as the mechanical and luminescent properties of boron difluoride complexes (Naim et al., 2021). While complex 4a with an alkyl chain formed plastic crystals whereas the complex 4b with a fluoroalkyl chain favored the formation of organogels. Based on crystallography and NMR data, it was established that the ability of 4a and 4b to form strong and weak C–H...F and B–F... $\pi$  interactions, respectively, was the key in defining the different self-assembly behavior. It was also demonstrated that 4b could be used as a fluorescent security marker on a variety of surfaces such as paper, granite and wood.

A combination of the above mentioned effects, *viz.* the effect of the solvent, molecular structure and substituents, can lead to organogels with multi-responsive properties. Wong et al. reported a few  $\beta$ -diketonate boron complexes (5) that functioned as photo-responsive organogelators with photo-switchable behavior (Wong et al., 2017). Among the different compounds, only 5c with a long alkoxy chain formed gels with fibrous structure in toluene and benzene. The gel of 5c in benzene exhibited green luminescence while in 1,4-dioxane, a bluish-green luminescence was observed. Moreover on heating the benzene/toluene gels of 5c, a color change was observed from orange to yellow because of the photocyclization of the dithienylethylene moiety. Zhai et al. reported a few  $\beta$ -diketone difluoroboron complexes that formed luminescent gels *via* self-assembly into one-dimensional nanorods (Zhai et al., 2019). Detailed investigations revealed that  $\pi$ - $\pi$  interactions were the main driving force for the molecules to pack into parallel layered structures in the gel state. Organogels of the compound 6c were emissive in the red region and their xerogels were observed to be sensitive towards aniline with a detection limit of 2 ppb.

The presence of aromatic core that favors  $\pi$ - $\pi$  interactions is another factor that contributes to gelation. The directionality and rigidity of these interactions are vital in deciding the spatial arrangements of the molecules during gelation. Several strategies have been developed to tune the strength of  $\pi$ - $\pi$  interactions by elongating the conjugation or by appropriately introducing functional groups. Qian et al. showed that molecular structure as well as balanced  $\pi$ - $\pi$  interactions play a vital role in the gelation property exhibited by  $\beta$ -diketones difluoroboron complexes. In a series of triphenylamine functionalized  $\beta$ -diketones difluoroboron complexes 7, it was reported that the asymmetric complex 7a exhibited a better gelation property in comparison to the symmetric complexes 7b and 7c (Qian et al., 2015). The difference in the self-assembly behavior was explained on the basis of the formation of different types of nanostructures. While 7a self-assembled into a three-dimensional network of straight nanofibers, 7b self-assembled into numerous nanofibers forming dendritic structures. On the other hand, 7c self-assembled into three-dimensional network of ill-defined agglomerates. Similarly, Gong et al. showed that salicylaldehyde-hydrazone based  $\beta$ -ketoiminatodifluoroboron complexes 8 self-assembled into nanoribbon-like features resulting in the formation of gels

with intense blue emission (Gong et al., 2015). In the complex 8 the non-planar aromatic unit experienced large steric hindrance from the *tert*-butyl group thereby decreasing the strength of  $\pi$ - $\pi$  interactions thereby inducing gelation. On the other hand, on further extending the conjugation no gel formation was observed due to an imbalance in  $\pi$ - $\pi$  interactions. Another similar report by Mi et al. showed that the pyrimidine containing  $\beta$ -iminoenolate-difluoroboron complexes 9a–b self-assembled into organogels upon the introduction of *tert*-butyl group which provided an optimum strength to  $\pi$ - $\pi$  interactions (Mi et al., 2018). The xerogel-based film of 9b was observed to emit yellow light and was used as a fluorescent sensor to detect vapors of trifluoroacetic acid with a decay time and detection limit of 0.8 s and 260 ppb, respectively.

Sun et al. showed that both *tert*-butyl and trifluoromethyl groups are important in the formation of organogels in the case of carbazole based salicylideneimine-boron complexes 10 (Sun et al., 2017). Only 10 containing both the *tert*-butyl and trifluoromethyl group formed gels with a three dimensional network of intertwined nanofibers. These nanofibers were also observed to be emissive due to the formation of *J*-aggregates in the gel state and exhibited reversible piezofluorochromic behavior. Another gelator based on balanced  $\pi$ - $\pi$  interactions was reported by Wang et al. which consisted of triphenylamine-functionalized boron complexes 11a and 11b containing 2-(2'-pyridyl)imidazole moieties that self-assembled into gels and showed piezochromic property wherein dried gel exhibited better sensitivity to pressure as compared to the regular crystalline powder (Wang et al., 2017). Using a series of halogenated  $\beta$ -iminoenolate difluoroboron complexes 12a–h, Wu et al. showed that not only the conjugation but the electronic effect also plays a vital role in the gelation abilities (Wu et al., 2017). It was observed that for excellent gelation, strong  $\pi$ - $\pi$ , CH...F, and CH...Br interactions played a key role. Interestingly, 12c–e were found to be emissive not only in solution but also in organogels and xerogel based films. The nanofiber films of 12d were sensitive towards trifluoroacetic acid with a decay time and detection limit of 0.5 s and 0.17 ppm, respectively.

## SELF-ASSEMBLY INTO MESOGENS

Liquid crystals (LCs) have been long known from 1888 which grew into a multibillion dollar industry over the time (Mitov, 2014). LCs can be defined as a state of matter characterized by the regularity in the periodic arrangement of atoms/molecules as in solids as well as the anisotropy as in liquids. They display a unique blend of the long range order and mobility. Materials that display liquid crystal phases are called mesogens. LCs are typically formed by calamitic (rod-like), discotic (disc-shaped) or bent core (banana-shaped) molecules. One major class of LCs is the thermotropic LCs which have the ability to display mesomorphic behavior as a function of temperature and as a result the molecules/atoms self-assemble into three different kinds of arrangements: namely nematic, smectic and cholesteric. In nematic phase, molecules are aligned with the director axis parallel to each other, but there is no positional order. When

these molecules further organize into layered arrangements stacking into two dimensional manner, smectic phase is formed which display a degree of translational order not present in nematic phases. Cholesteric LCs have the director axis spiraling around with a pitch, these are mainly the nematic mesogens that consist of a chiral center. Columnar mesophase fall into another category which are represented by stacked columns of molecules packed together to form an array. They are shaped liked disks instead of long rods. As LCs are responsive to various stimuli, their molecular order rapidly responds to environmental factors like temperature, electric fields, magnetic fields or chemical adsorption. While LCs are immensely popular for their application in flat panel displays, their special properties have been used in a number of other applications as well such as organic electronics, nanoparticle organization, LC colloids, LC elastomer actuators, and chemical and biological sensors. Apart from these, liquid crystals have also found utility in thin-film thermometers and switchable display windows (Lagerwall and Scalia, 2012; Iino et al., 2015; Urbanski et al., 2017; Chen et al., 2021).

Boron-containing organic molecules have been studied for their mesogenic properties along with luminescence properties (Camerel et al., 2007; Maeda et al., 2010; Olivier et al., 2010; Sánchez et al., 2010; Turanova et al., 2010; Benstead et al., 2011a, 2011b; Maeda et al., 2011; Olivier et al., 2012; Bando et al., 2013; Giziroglu et al., 2014; Sánchez et al., 2014; Fang et al., 2017; Feng et al., 2018; Xiong et al., 2018; Cheng et al., 2019; Liu et al., 2019). The very first reports were put forward by Turanova et al. wherein the boron difluoride-diketonate complex obtained from a non-mesogenic diketonate exhibited liquid crystalline properties along with photoluminescent properties (Turanova et al., 2006). In concurrence with the previous section, this mini-review will focus on the advances made using diketonates and ketoiminates in the past few years (Figure 2).

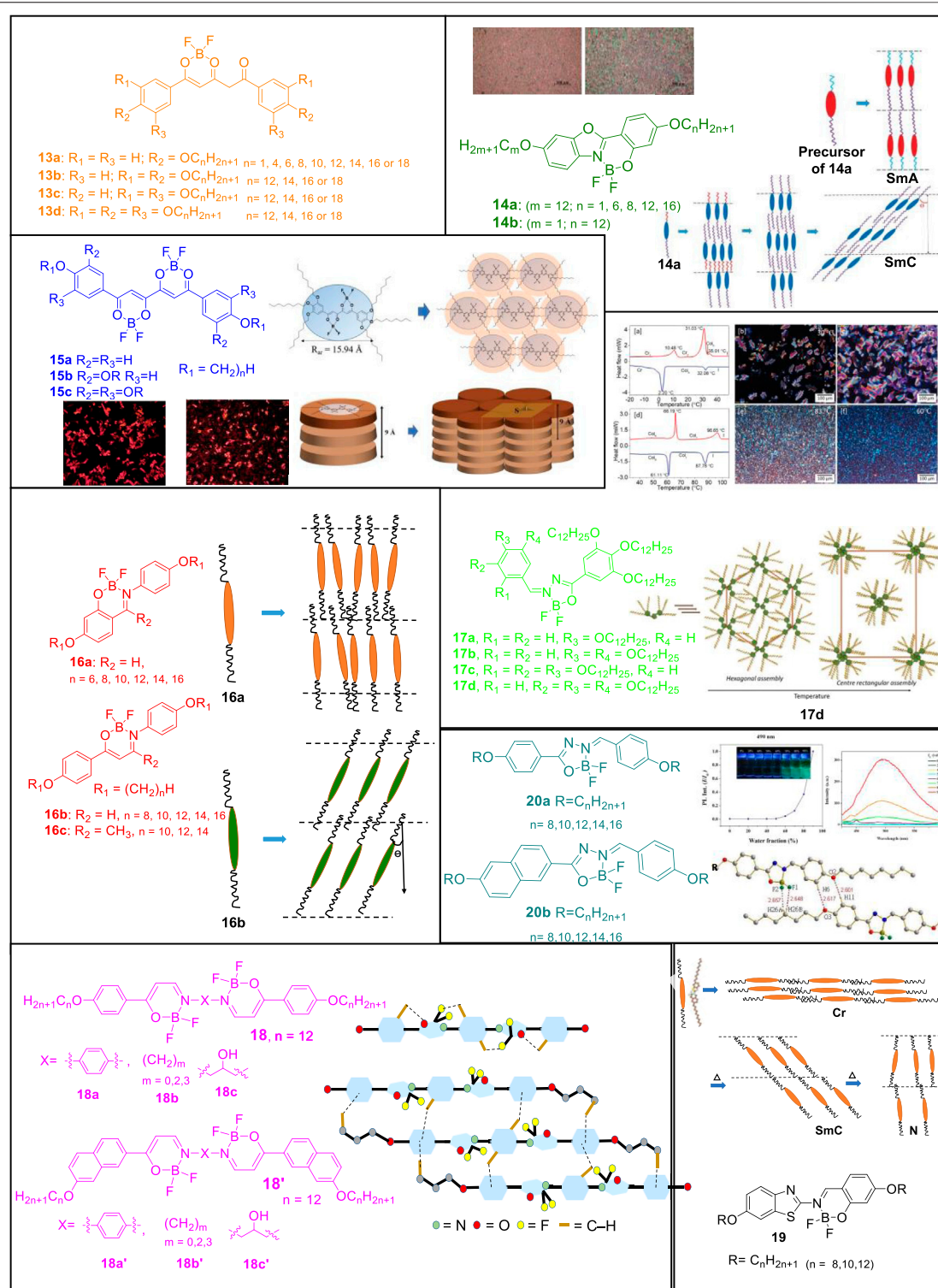
Sánchez et al. reported alkyloxyphenyl-substituted  $\beta,\delta$ -triketonatedifluoroboron complexes 13 wherein the presence of varying alkyl chains in each aromatic group of the triketonate ligand dictated the mesomorphic behavior of the compound (Sánchez et al., 2016). Smectic C mesophases were found for compounds carrying two lateral chains whereas those consisting of four or six chains led to discotic lamellar and hexagonal columnar mesophases, respectively. Compounds 13a with long-tailed substituents ( $n = 16, 18$ ) showed liquid crystal behavior, while derivatives with shorter alkyl chains ( $n < 14$ ) showed crystalline polymorphism and a direct melt to isotropic liquid. Contrary to previous reports on non-mesogenic monocatenar symmetrically alkoxyphenyl substituted  $\beta$ -diketonate containing difluoroboron complexes, the reported long chain monocatenar aryl-substituted triketonate derivatives showed liquid crystal properties. This was presumably due to an appropriate length-to-width molecular ratio, which is favored with long chains and extensive conjugation in triketones. Presence of the large and rigid molecular core with extended  $\pi$  conjugation and molecular polarization effectively induced mesomorphism in the difluoroboron complexes. While molecular asymmetry with respect to the length of chains and the presence of varying number of alkyl chains at both phenyl

rings was a prerequisite to achieve mesomorphism in  $\beta$ -diketonates, this requirement was not mandatory when using  $\beta,\delta$ -triketonate ligands for  $\text{BF}_2$  coordination in which liquid crystal behavior was achieved even at room temperature. Compounds containing one chain or two adjacent chains in each phenyl group exhibited smectogenic behavior stemming clearly from the rod-like molecular shape. In contrast, disk-shaped complexes were obtained when two alternate or three alkyl chains were attached to the aromatic system. Consequently the complexes form lamellar discotic or hexagonal columnar mesophases, respectively.

Chen et al. further reported the liquid crystalline properties of the benzoxazoles derived boron complexes 14 (Chen et al., 2017a). The mesomorphic behavior of complexes 14 was altered upon complexation to boron difluoride and the clearing temperatures increased than the uncoordinated benzoxazoles. While the precursor benzoxazoles formed monotropic Smectic A phases, the corresponding boron difluoride complexes 14a ( $n = 6, 8, 12, 16$ ) exhibited monotropic Smectic C mesophases. Molecules in the 14b category was not found to be mesogenic owing to the presence of the methoxy group which was assumed as not being polar enough to induce a stable mesophase. Intermolecular F...H bonds as observed in the crystal lattices of 14a ( $m = 12, n = 8$ ) facilitated the molecules to align in head-to-head arrangements which is one of the requirements for the induction of mesophases.

Coordination to boron difluoride plays an interesting role towards appearance of liquid crystal properties as tetrahedral geometry allows a dipole strong enough to induce the mesophase. But at the same time the small size of  $\text{BF}_2$  does not interrupt the molecular arrangement of the mesophases. Otherwise generally, a tetrahedral or bulky core does not favor the formation of mesophases. Along with weak H bonding interactions, the lone-pair of electrons located on the two fluorine atoms also repelled other atoms intra- and intermolecularly, facilitating the weaker interactions required for the formation of kinetically stable mesophases. Chen et al. also reported a series of bis(boron difluoride) complexes derived from the corresponding substituted tetraketones (Chen et al., 2017b). While compounds 15a and 15b carrying varying alkyl lengths were not mesogenic, compounds 15c ( $n = 8, 10, 12$ ) exhibited enantiotropic columnar mesophases where a single disc-shaped molecule was stacked within columns in hexagonal columnar phases. While the precursors of 15a were mesogenic forming enantiotropic nematic or nematic/smectic C phases, the precursors of 15b-c formed crystalline phases because the overall molecular shapes of these two compounds were more likely catenar shaped, instead of linear or disc-shaped. It is noteworthy that most of the known  $\alpha,\beta$ -diketonates were not mesogenic due to their bent structures which do not favor mesophases formation. A more linear core in the tetraketone structure and a small dihedral angle of  $\sim 1.564^\circ$  resulted in the induction of mesophases compared to other non-mesogenic  $\alpha,\beta$ -diketonates.

Lei et al. further reported  $\text{BF}_2$  complexes 16 obtained from substituted salicylideneamine and  $\beta$ -enaminoketonates (Lei et al., 2018). Four complexes 16a ( $n = 8, 10, 12, 14$ ) showed monotropic



**FIGURE 2** | Chemical structures and schematic representation of boron-difluoride compounds self-assembling into mesogens. Reproduced with permission from Chen et al., 2017a, copyright 2017 Royal Society of Chemistry. Reproduced with permission from Chen et al., 2017b, copyright 2017 Royal Society of Chemistry. Reproduced with permission from R. Vinayakumara et al., 2019, copyright 2019 Royal Society of Chemistry. Reproduced with permission from Cai et al., 2021, copyright 2021 Royal Society of Chemistry.

mesogenic behavior, whereas the other two derivatives ( $n = 6, 16$ ) were not mesogenic. 16b ( $n = 8, 10, 12, 14, 16$ ) exhibited enantiotropic Smectic C phases and the better mesomorphic behavior of 16b was attributed to being a better rod/linear shaped molecule owing to the presence of  $\beta$ -enaminoketonate moiety in 16b than that of salicylideneamine in 16a. Also  $\beta$ -enaminoketonate 16b has more extended conjugation length than the salicylideneamine moiety in 16a. The imine moiety here not only played the role of linking group but also carried a dipole moment that enhanced the thermal stability of mesophases. An improved core planarity resulting from various weak intra- and intermolecular H-bonds facilitated a more ordered arrangement in mesogenic states. In the crystal structure, along with the H-bonding interactions, the intermolecular F...H interactions were found to be crucial, which facilitated molecules to align in a head-to-head manner. While only one complex 16c ( $n = 12$ ) showed monotropic mesomorphic behavior, the other two complexes in 16c were not mesogenic as both  $-\text{BF}_2$  and  $-\text{CH}_3$  could have slightly twisted the layer packing in the crystal and liquid crystalline states. Large dihedral angle of  $81.3^\circ$  between the two phenyl rings of 16c was supposed to be the main reason behind the lack of liquid crystallinity.

Vinayakumara et al. reported benzylidenehydrazones substituted  $\text{BF}_2$  complexes 17 wherein the precursor compounds benzylidenehydrazones exhibited a columnar mesophase with a hexagonal structure which could be attributed to co-operative intermolecular hydrogen bonding (R. Vinayakumara et al., 2019). Their corresponding  $\text{BF}_2$  complexes showed thermotropic phase behavior. The number and position of chains around the aromatic core greatly affected the mesomorphic properties of these hemi-discoidal boron complexes. As a result, isomeric complexes showed different thermotropic phase behavior and exhibited distinct columnar mesophase at different temperature ranges. While the alkyl chains around the planar core moiety helped to acquire disc-shaped molecules, the central core-system consisting of three rings adopted an entirely planar geometry which supported the stabilization of the columnar arrangement.

Lei et al. derived liquid crystals of bis( $\text{BF}_2$ ) complexes 18 from Schiff base  $\beta$ -enaminoketones (Lei et al., 2020). Mesomorphic properties were observed to be dependent on the structure of the central spacer and terminal groups and most of the synthesized molecules formed SmC or SmA phase except complexes 18b ( $m = 2, 3; n = 12$ ) and 18c ( $n = 12$ ). The structure of 18a was linear enough to be considered as rod-shaped which favored the layered smectic arrangement. While compound 18b wherein  $m = 0$  was purely mesogenic, the other two compounds 18b ( $m = 2, 3$ ) showed crystalline phases and the absence of mesogenic behavior for derivatives with  $m = 2$  and 3 was attributed to the more flexible ethylene and propylene spacer units. Upon incorporation of ethylene or propylene group in compounds 18b ( $n = 12$ ), all clearing temperatures were significantly lowered. Also, the mesogenic behavior did not improve upon introduction of a hydroxyl group in the C2-atom of compound 18c as a bulky-OH group incorporated closer to core center could not favor the molecules to pack in the solid or liquid crystal state. Introduction of a terminal naphthalenyl moiety significantly improved the

mesomorphic properties and thermal stabilities of all four compounds 18' as compared to their homologues 18. Compound 18c' ( $n = 12$ ) was truly mesogenic and its improved mesomorphic behavior from 18c was attributed to more balanced intermolecular  $\pi$ - $\pi$  interactions by terminal naphthalenyl ring and hydrogen bonding by central hydroxy-OH group. "Shape-effect" of the compound 18c' also had a role to play along with an appropriate aspect ratio necessary for the induction of the mesophases. Elongation of the rigid molecular core also resulted in broadening of the mesophases. Boron complexes 18' with terminal naphthalenyl ring were found to be more stable in higher temperatures than 18.

Hsu et al. reported boron difluoride complexes 19 from benzothiazoles that formed nematic and smectic phases as is common for rod shaped molecules (Hsu et al., 2020). In the crystal lattice, all alkoxy chains were slightly interdigitated, giving a smaller layer distance both in N and SmC phases upon heating. The intramolecular H-bonds in the benzothiazole moiety kept the phenolic ring nearly coplanar to the benzo ring which favored a better packing. Upon complexation to  $\text{BF}_2$  moiety, three complexes 19 ( $n = 8, 10, 12$ ) formed enantiotropic N or/and SmC phases. All clearing temperatures were higher than those of the precursor compounds. The presence of sulfur atom led to better polarization thereby resulting in better mesomorphic behavior and luminescence properties over the benzoxazole analogues too.

Recently, Cai et al. reported boron difluoride complexes 20 derived from aroylhydrazines that showed mesomorphic behavior and AIE properties (Cai et al., 2021). All precursor ligands of 20a–b were crystalline and non-mesogenic but all complexes 20 formed SmC or/and N phases. These  $\text{BF}_2$  complexes were fluorescent and the compound 20a was AIE active. As observed in single crystal of 20a ( $n = 8$ ) the overall molecule was quite flat and a dihedral angle of  $\sim 3.298^\circ$  and  $\sim 5.750^\circ$  between the central core and the surrounding phenyl rings was observed. Weak intramolecular hydrogen bonds kept the central molecule as planar as possible making it easy for the molecules to pack in the crystal and liquid crystal states. Along with other intermolecular F...H interactions, formation of dimeric structures through hydrogen bonds along with other weak interactions further favored mesophase formation. Two derivatives 20a ( $n = 10$ ) and 20b ( $n = 8$ ) formed monotropic SmC phases and complexes 20b have a wider temperature range of SmC phase than that of complexes 20a that were attributed to more efficient  $\pi$ - $\pi$  interactions between the cores upon naphthalene substitution. Compound 20a ( $n = 12$ ) was found to be AIE active.

## CONCLUSION AND FUTURE OUTLOOK

In this mini-review, we have summarized the recent developments in the supramolecular chemistry of tetra-coordinate boron-containing organic molecules. Organoboron compounds prepared from chelating units such as imines, diiminates, ketoiminates, diketones, etc. are easy to synthesize and often afford good to excellent synthetic yields.



As the chelating units are synthesized from simple starting materials like amines and aldehydes/ketones, this strategy allows for the synthesis of a variety of compounds whose properties may be tuned by an appropriate selection of the reactants. Further, the presence of heteroatoms and aromatic rings in these systems helps in stabilizing the self-assembled structures through various non-covalent interactions like H-bonding, CH- $\pi$  and F- $\pi$  interactions without the need for specific functionalization. As exemplified by various reports, a majority of these compounds exhibit excellent luminescence properties, and most of them have been used for sensing applications. However, a majority of these systems absorb UV or visible light and only limited success has been achieved in the synthesis of near-infrared absorbing dyes using this chemistry. NIR absorbing dyes are superior for biological applications and thus extension of this methodology for the synthesis of long-wavelength absorbing dyes would be beneficial for applications in biology. As these supramolecular assemblies are inherently dynamic and reversible, and have the ability to respond to external stimuli, a synergy between adaptive properties and NIR optical properties could lead to next-generation soft materials for biomedical applications. Another area with scope for improvement is the appropriate functionalization of

organoboron compounds so as to obtain supramolecular hydrogels which will enable and extend the utility of these systems for wound healing, cell therapies, artificial tissue development and anticancer treatments. In order to be commercially successful, these compounds must be explored from the application perspective which in our opinion lacks to date. We hope that this mini-review gives a comprehensive understanding of the capabilities of the highly stable tetra-coordinate boron containing molecules to the readers and opens up new avenues towards real life applications.

## AUTHOR CONTRIBUTIONS

SS and PM conducted the literature review, and have contributed equally to the manuscript. All authors contributed to the writing and editing of the manuscript.

## FUNDING

We thank financial support from Institute of Nano Science and Technology, Mohali.

## REFERENCES

- Abdallah, D. J., and Weiss, R. G. (2000). Organogels and Low Molecular Mass Organic Gelators. *Adv. Mater.* 12, 1237–1247. doi:10.1002/1521-4095(200009)12:17<1237::aid-adma1237>3.0.co;2-b
- Anthony, S. P. (2012). Organic Solid-State Fluorescence: Strategies for Generating Switchable and Tunable Fluorescent Materials. *ChemPlusChem* 77, 518–531. doi:10.1002/cplu.201200073
- Auwah, S. G., and You, Y. (2012). Boron Dipyrromethene (BODIPY)-based Photosensitizers for Photodynamic Therapy. *RSC Adv.* 2, 11169–11183. doi:10.1039/c2ra21404k
- Bando, Y., Sakurai, T., Seki, S., and Maeda, H. (2013). Corannulene-Fused Anion-Responsive  $\pi$ -Conjugated Molecules that Form Self-Assemblies with Unique Electronic Properties. *Chem. Asian J.* 8, 2088–2095. doi:10.1002/asia.201300635
- Benstead, M., Rosser, G. A., Beeby, A., Mehl, G. H., and Boyle, R. W. (2011a). Addressing Fluorescence and Liquid crystal Behaviour in Multi-Mesogenic BODIPY Materials. *New J. Chem.* 35, 1410–1417. doi:10.1039/c0nj00990c
- Benstead, M., Rosser, G. A., Beeby, A., Mehl, G. H., and Boyle, R. W. (2011b). Mesogenic BODIPYs: an Investigation of the Correlation between Liquid Crystalline Behaviour and Fluorescence Intensity. *Photochem. Photobiol. Sci.* 10, 992–999. doi:10.1039/c0pp00388c
- Boens, N., Leen, V., and Dehaen, W. (2012). Fluorescent Indicators Based on BODIPY. *Chem. Soc. Rev.* 41, 1130–1172. doi:10.1039/c1cs15132k
- Cai, Y.-H., Chih, H.-Y., Lee, G.-H., and Lai, C. K. (2021). Aggregation-induced Emissions in the Mesogenic BF<sub>2</sub> Complexes of Aroylhydrazines. *New J. Chem.* 45, 12557–12568. doi:10.1039/d1nj02001c
- Camerel, F., Ulrich, G., Barberá, J., and Ziessel, R. (2007). Ionic Self-Assembly of Ammonium-Based Amphiphiles and Negatively Charged Bodipy and Porphyrin Luminesophores. *Chem. Eur. J.* 13, 2189–2200. doi:10.1002/chem.200601475
- Chen, H.-Q., Wang, X.-Y., Bisoyi, H. K., Chen, L.-J., and Li, Q. (2021). Liquid Crystals in Curved Confined Geometries: Microfluidics Bring New Capabilities for Photonic Applications and beyond. *Langmuir* 37, 3789–3807. doi:10.1021/acs.langmuir.1c00256
- Chen, Y.-W., Lee, G.-H., and Lai, C. K. (2017a). Fluorescent Mesogenic boron Difluoride Complexes Derived from Heterocyclic Benzoxazoles. *Dalton Trans.* 46, 12274–12283. doi:10.1039/c7dt02937c
- Chen, Y.-W., Lin, Y.-C., Kuo, H.-M., and Lai, C. K. (2017b). Fluorescent Columnar Bis(boron Difluoride) Complexes Derived from Tetraketonates. *J. Mater. Chem. C* 5, 5465–5477. doi:10.1039/c7tc01425b
- Cheng, J., Zheng, S., Lin, L., Guo, H., and Yang, F. (2019). Novel Near-Infrared Fluorescent Liquid crystal: Bodipy Bearing Multiple Alkyl Chains with Columnar Mesophase. *Liquid Crystals* 46, 1127–1135. doi:10.1080/02678292.2018.1558464
- Cherumukil, S., Vedhanarayanan, B., Das, G., Praveen, V. K., and Ajayaghosh, A. (2018). Self-Assembly of Bodipy-Derived Extended  $\pi$ -Systems. *Bcsj* 91, 100–120. doi:10.1246/bcsj.20170334
- Crump, M. R., Biding, S. L., Pavinatto, F. J., Gong, A. T., Sweet, R. M., and MacKenzie, J. D. (2021). Sensorized Tissue Analogues Enabled by a 3D-Printed Conductive Organogel. *NPJ Flex. Electron.* 5, 1–8. doi:10.1038/s41528-021-00104-0
- Das, J., Bhattacharjee, B., Dutta, J. J., and Paul, T. (2021). Organogel: An Ideal Drug Delivery Carrier. *World J. Pharm. Res.* 10, 446–465. doi:10.20959/wjpr20218-20878
- Entwistle, C. D., and Marder, T. B. (2002). Boron Chemistry Lights the Way: Optical Properties of Molecular and Polymeric Systems C.D.E. Thanks EPSRC for a Postgraduate Studentship and Syngenta for a Postgraduate Scholarship, and T.B.M. Thanks the University of Durham for Support and Prof. Dr. K. Tamao for a Preprint of Ref. 32. *Angew. Chem. Int. Ed.* 41, 2927–2931. doi:10.1002/1521-3773(20020816)41:16<2927::aid-anie2927>3.0.co;2-I
- Esposito, C. L., and Kirilov, P. (2021). Preparation, Characterization and Evaluation of Organogel-Based Lipstick Formulations: Application in Cosmetics. *Gels* 7, 97. doi:10.3390/gels7030097
- Fang, X., Guo, H., Yang, F., and Lin, J. (2017). Near-infrared Fluorescent and Columnar Liquid crystal: Synthesis, and Photophysical and Mesomorphic Properties of Triphenylene-BODIPY-Triphenylene Triad. *RSC Adv.* 7, 23657–23662. doi:10.1039/c7ra00982h
- Feng, H., Geng, X., Lin, J., Guo, H., and Yang, F. (2018). Novel Fluorescent Liquid Crystals: Synthesis, Mesomorphism and Fluorescence of Triphenylene-BODIPY Derivatives Based on 1,3,5-triazine Core. *Liq. Cryst.* 45, 1470–1476. doi:10.1080/02678292.2018.1446554
- Fraht, D., Massue, J., Ulrich, G., and Ziessel, R. (2014). Luminescent Materials: Locking  $\pi$ -Conjugated and Heterocyclic Ligands with Boron(III). *Angew. Chem. Int. Ed.* 53, 2290–2310. doi:10.1002/anie.201305554

- Galbraith, E., and James, T. D. (2010). Boron Based Anion Receptors as Sensors. *Chem. Soc. Rev.* 39, 3831–3842. doi:10.1039/b926165f
- Giziroglu, E., Nesrullajev, A., and Orhan, N. (2014). 1,3-Dimethyl-5-(3,4,5-tris(alkoxy)benzoyl) Barbituric Acid Derivatives and Their Liquid Crystalline Difluoroboron Complexes: Synthesis, Characterization and Comparative Investigations of Mesomorphic, Thermotropic and Thermomorphologic Properties. *J. Mol. Struct.* 1056–1057, 246–253. doi:10.1016/j.molstruc.2013.10.038
- Gong, P., Yang, H., Sun, J., Zhang, Z., Sun, J., Xue, P., et al. (2015). Salicylaldimine Difluoroboron Complexes Containing Tert-Butyl Groups: Nontraditional  $\pi$ -gelator and Piezofluorochromic Compounds. *J. Mater. Chem. C* 3, 10302–10308. doi:10.1039/c5tc02484f
- Hsu, Y. C., Wang, C. Y., Hsiao, P. C., Cai, Y.-H., Lee, G. H., and Lai, C. K. (2020). Polarization Effect in Luminescent Mesogenic BF<sub>2</sub> Complexes Derived from Heterocyclic Benzothiazoles. *J. Mol. Liquids* 297, 111660. doi:10.1016/j.molliq.2019.111660
- Iino, H., Usui, T., and Hanna, J.-i. (2015). Liquid Crystals for Organic Thin-Film Transistors. *Nat. Commun.* 6, 6828. doi:10.1038/ncomms7828
- Jäkle, F. (2010). Advances in the Synthesis of Organoborane Polymers for Optical, Electronic, and Sensory Applications. *Chem. Rev.* 110, 3985–4022. doi:10.1021/cr100026f
- Kamkaew, A., Lim, S. H., Lee, H. B., Kiew, L. V., Chung, L. Y., and Burgess, K. (2013). BODIPY Dyes in Photodynamic Therapy. *Chem. Soc. Rev.* 42, 77–88. doi:10.1039/c2cs35216h
- Lagerwall, J. P. F., and Scalia, G. (2012). A new era for Liquid crystal Research: Applications of Liquid Crystals in Soft Matter Nano-, Bio- and Microtechnology. *Curr. Appl. Phys.* 12, 1387–1412. doi:10.1016/j.cap.2012.03.019
- Lei, Z.-Y., Cai, Y.-H., Lee, G.-H., and Lai, C. K. (2020). Luminescent Mesogenic Dimeric Boron difluoride Complexes. *Liq. Cryst.* 48, 1–19. doi:10.1080/02678292.2020.1836277
- Lei, Z.-Y., Lee, G.-H., and Lai, C. K. (2018). Luminescent Mesogenic Boron difluoride Complexes with the Schiff Bases Containing Salicylideneamines and  $\beta$ -aminoketones Core Systems. *J. Mol. Liq.* 260, 44–56. doi:10.1016/j.molliq.2018.03.047
- Li, D., Zhang, H., and Wang, Y. (2013). Four-coordinate Organoboron Compounds for Organic Light-Emitting Diodes (OLEDs). *Chem. Soc. Rev.* 42, 8416–8433. doi:10.1039/c3cs60170f
- Liu, C., Ding, W., Liu, Y., Zhao, H., and Cheng, X. (2019). Self-assembled star-shaped Aza-BODIPY Mesogen Affords white-light Emission. *New J. Chem.* 44, 102–109.
- Loudet, A., and Burgess, K. (2007). BODIPY Dyes and Their Derivatives: Syntheses and Spectroscopic Properties. *Chem. Rev.* 107, 4891–4932. doi:10.1021/cr078381n
- Lu, H., Mack, J., Yang, Y., and Shen, Z. (2014). Structural Modification Strategies for the Rational Design of Red/NIR Region BODIPYs. *Chem. Soc. Rev.* 43, 4778–4823. doi:10.1039/c4cs00030g
- Maeda, H., and Bando, Y. (2013). Recent Progress in Research on Anion-Responsive Pyrrole-Based  $\pi$ -conjugated Acyclic Molecules. *Chem. Commun.* 49, 4100–4113. doi:10.1039/c2cc35759c
- Maeda, H., Naritani, K., Honsho, Y., and Seki, S. (2011). Anion Modules: Building Blocks of Supramolecular Assemblies by Combination with  $\pi$ -Conjugated Anion Receptors. *J. Am. Chem. Soc.* 133, 8896–8899. doi:10.1021/ja203880d
- Maeda, H., Terashima, Y., Haketa, Y., Asano, A., Honsho, Y., Seki, S., et al. (2010). Discotic Columnar Mesophases Derived from 'rod-Like'  $\pi$ -Conjugated Anion-Responsive Acyclic Oligopyrroles. *Chem. Commun.* 46, 4559–4561. doi:10.1039/c0cc00551g
- Matsuoka, R., and Nabeshima, T. (2018). Functional Supramolecular Architectures of Dipyrrin Complexes. *Front. Chem.* 6, 349. doi:10.3389/fchem.2018.00349
- Mi, W., Qu, Z., Sun, J., Zhang, F., Zhai, L., and Ye, K. (2018). Pyrimidine Containing  $\beta$ -Iminoenolate Difluoroboron Complexes Acting as Non-Traditional  $\pi$ -Gelators and Mechanofluorochromic Dyes. *New J. Chem.* 42, 12882–12890. doi:10.1039/c8nj01508b
- Mitov, M. (2014). Liquid-Crystal Science from 1888 to 1922: Building a Revolution. *ChemPhysChem* 15, 1245–1250. doi:10.1002/cphc.201301064
- Mukherjee, S., and Thilagar, P. (2016). Stimuli and Shape Responsive 'boron-containing' Luminescent Organic Materials. *J. Mater. Chem. C* 4, 2647–2662. doi:10.1039/c5tc02406d
- Naim, K., Sahoo, S. C., Venugopalan, P., and Neelakandan, P. P. (2021). Remarkable Self-Assembly of Salicylideneimine-Boron Complexes into Plastic Crystals and Organogels. *Cryst. Growth Des.* 21, 3798–3806. doi:10.1021/acs.cgd.1c00132
- Olivier, J.-H., Barberá, J., Bahaidarah, E., Harriman, A., and Ziesel, R. (2012). Self-Assembly of Charged BODIPY Dyes to Form Cassettes that Display Intracomplex Electronic Energy Transfer and Accrete into Liquid Crystals. *J. Am. Chem. Soc.* 134, 6100–6103. doi:10.1021/ja3007935
- Olivier, J.-H., Camerel, F., Ulrich, G., Barberá, J., and Ziesel, R. (2010). Luminescent Ionic Liquid Crystals from Self-Assembled BODIPY Disulfonate and Imidazolium Frameworks. *Chem. - A Eur. J.* 16, 7134–7142. doi:10.1002/chem.201000339
- Qian, C., Liu, M., Hong, G., Xue, P., Gong, P., and Lu, R. (2015). Luminescent Organogels Based on Triphenylamine Functionalized  $\beta$ -diketones and Their Difluoroboron Complexes. *Org. Biomol. Chem.* 13, 2986–2998. doi:10.1039/c4ob02612h
- Rao, Y.-L., and Wang, S. (2011). Four-Coordinate Organoboron Compounds with a  $\pi$ -Conjugated Chelate Ligand for Optoelectronic Applications. *Inorg. Chem.* 50, 12263–12274. doi:10.1021/ic200658v
- Sánchez, I., Fernández-Lodeiro, A., Oliveira, E., Campo, J. A., Torres, M. R., Cano, M., et al. (2016). Triketonate Difluoroboron Complexes. Substitution-dependent Liquid crystal and Photophysical Properties. *Dyes Pigm.* 135, 184–200. doi:10.1016/j.dyepig.2015.10.029
- Sánchez, I., Mayoral, M. J., Ovejero, P., Campo, J. A., Heras, J. V., Cano, M., et al. (2010). Luminescent Liquid crystal Materials Based on Unsymmetrical boron Difluoride  $\beta$ -diketonate Adducts. *New J. Chem.* 34, 2937–2942. doi:10.1039/c0nj00503g
- Sánchez, I., Núñez, C., Campo, J. A., Torres, M. R., Cano, M., and Lodeiro, C. (2014). Polycatenar Unsymmetrical  $\beta$ -diketonate Ligands as a Useful Tool to Induce Columnar Mesomorphism on Highly Luminescent boron Difluoride Complexes. *J. Mater. Chem. C* 2, 9653–9665. doi:10.1039/c4tc01373e
- Shah, S., Bajaj, A., Shibu, A., Ali, M. E., and Neelakandan, P. P. (2018). Iodo-Functionalized Salicylideneimine-Boron Complexes: Synthesis and Photosensitized Degradation of Organic Water Pollutants. *Chem. Eur. J.* 24, 18788–18794. doi:10.1002/chem.201804376
- Sun, J., Qian, C., Xu, S., Jia, X., Zhai, L., Zhao, J., et al. (2018). H- and J-Aggregates Formed from a Nontraditional  $\pi$ -gelator Depending on the Solvent Polarity for the Detection of Amine Vapors. *Org. Biomol. Chem.* 16, 7438–7445. doi:10.1039/c8ob01596a
- Sun, J., Sun, J., Mi, W., Xue, P., Zhao, J., Zhai, L., et al. (2017). Carbazole Modified Salicylaldimines and Their Difluoroboron Complexes: Effect of the Tert-Butyl and Trifluoromethyl Terminal Groups on Organogelation and Piezofluorochromism. *New J. Chem.* 41, 763–772. doi:10.1039/c6nj03063g
- Tanaka, K., and Chujo, Y. (2012). Advanced Luminescent Materials Based on Organoboron Polymers. *Macromol. Rapid Commun.* 33, 1235–1255. doi:10.1002/marc.201200239
- Turanova, O. A., Garifzyanova, G. G., and Turanov, A. N. (2010). Liquid crystal Polymorphism of boron Difluoride  $\beta$ -diketonates. *Russ. J. Gen. Chem.* 80, 2317–2322. doi:10.1134/s1070363210110150
- Turanova, O. A., Turanov, A. N., Lapaev, D. V., Gnezdilov, O. I., Lobkov, S. V., and Galyametdinov, Y. G. (2006). The First Mesogenic Derivative of boron Difluoride  $\beta$ -diketonate. *Russ. J. Gen. Chem.* 76, 730–732. doi:10.1134/s1070363206050124
- Urbanski, M., Reyes, C. G., Noh, J., Sharma, A., Geng, Y., Subba Rao Jampani, V., et al. (2017). Liquid Crystals in Micron-Scale Droplets, Shells and Fibers. *J. Phys. Condens. Matter* 29, 133003. doi:10.1088/1361-648x/aa5706
- Varaprasad, K., Raghavendra, G. M., Jayaramudu, T., Yallapu, M. M., and Sadiku, R. (2017). A Mini Review on Hydrogels Classification and Recent Developments in Miscellaneous Applications. *Mater. Sci. Eng. C* 79, 958–971. doi:10.1016/j.msec.2017.05.096
- Vinayakumara, D. R. D., Swamyathan, K., Kumar, S., and Adhikari, A. V. (2019). Columnar Self-Assembly of Novel Benzylidenehydrazones and Their Difluoroboron Complexes: Structure-Property Correlations. *New J. Chem.* 43, 7099–7108. doi:10.1039/c9nj01192g
- Wang, S., Lan, H., Xiao, S., Tan, R., and Lu, Y. (2017). Highly Fluorescent Non-conventional Boron-Difluoride-Based  $\pi$  Organogel with Gelation-Assisted Piezochromism. *Chem. Asian J.* 12, 198–202. doi:10.1002/asia.201601492

- Wong, C.-L., Poon, C.-T., and Yam, V. W.-W. (2017). Photoresponsive Organogelator: Utilization of Boron(III) Diketonate as a Building Block to Construct Multiresponsive Materials. *Organometallics* 36, 2661–2669. doi:10.1021/acs.organomet.7b00274
- Wu, Z., Sun, J., Zhang, Z., Yang, H., Xue, P., and Lu, R. (2017). Nontraditional  $\pi$  Gelators Based on  $\beta$ -Iminoenolate and Their Difluoroboron Complexes: Effect of Halogens on Gelation and Their Fluorescent Sensory Properties towards Acids. *Chem. Eur. J.* 23, 1901–1909. doi:10.1002/chem.201604573
- Xiong, Y., Zheng, S., Zhu, L., Guo, H., and Yang, F. (2018). Novel Liquid Crystals with High Fluorescence: Synthesis, Mesomorphic and Photophysical Properties of Cholesterol-Triazine-BODIPY Trimers. *J. Mol. Struct.* 1164, 311–316. doi:10.1016/j.molstruc.2018.03.093
- Zhai, L., Sun, M., Liu, M., Shu, Y., Sun, J., Zhang, F., et al. (2019).  $\beta$ -Diketone Difluoroboron Complexes-Based Luminescent  $\pi$ -gelators and Mechanofluorochromic Dyes with Low-Lying Excited States. *Dyes Pigm.* 160, 467–475. doi:10.1016/j.dyepig.2018.08.025
- Zhai, L., Zhang, F., Sun, J., Liu, M., Sun, M., and Lu, R. (2017). New Non-traditional Organogelator of  $\beta$ -diketone-boron Difluoride Complexes with Terminal Tetraphenylethene: Self-Assembling and Fluorescent Sensory Properties towards Amines. *Dyes Pigm.* 145, 54–62. doi:10.1016/j.dyepig.2017.05.047
- Zhu, P., Yan, X., Li, Y., Lan, H., and Xiao, S. (2020). Non-conventional Low-Molecular-Weight Organogelators with Superhydrophobicity Based on Fluorescent  $\beta$ -diketone-boron Difluorides. *Dyes Pigm.* 175, 108176. doi:10.1016/j.dyepig.2019.108176
- Conflict of Interest:** The authors declare that the research was conducted in the absence of any commercial or financial relationships that could be construed as a potential conflict of interest.
- Publisher's Note:** All claims expressed in this article are solely those of the authors and do not necessarily represent those of their affiliated organizations, or those of the publisher, the editors and the reviewers. Any product that may be evaluated in this article, or claim that may be made by its manufacturer, is not guaranteed or endorsed by the publisher.

Copyright © 2021 Shah, Marandi and Neelakandan. This is an open-access article distributed under the terms of the Creative Commons Attribution License (CC BY). The use, distribution or reproduction in other forums is permitted, provided the original author(s) and the copyright owner(s) are credited and that the original publication in this journal is cited, in accordance with accepted academic practice. No use, distribution or reproduction is permitted which does not comply with these terms.



# Looking for Options to Sustainably Fixate Nitrogen. Are Molecular Metal Oxides Catalysts a Viable Avenue?

Rebeca González-Cabaleiro<sup>1\*</sup>, Jake A. Thompson<sup>2</sup> and Laia Vilà-Nadal<sup>2\*</sup>

<sup>1</sup>Department of Biotechnology, Delft University of Technology, Delft, Netherlands, <sup>2</sup>School of Chemistry, University of Glasgow, Glasgow, United Kingdom

## OPEN ACCESS

### Edited by:

Jennifer Hiscock,  
University of Kent, United Kingdom

### Reviewed by:

Subhamay Pramanik,  
University of Kansas, United States  
Matthew A. Addicoat,  
Nottingham Trent University,  
United Kingdom

### \*Correspondence:

Rebeca González-Cabaleiro  
r.gonzalezcabaleiro@tudelft.nl  
Laia Vilà-Nadal  
laia.vila-nadal@chem.gla.ac.uk

### Specialty section:

This article was submitted to  
Supramolecular Chemistry,  
a section of the journal  
Frontiers in Chemistry

Received: 16 July 2021

Accepted: 17 August 2021

Published: 14 September 2021

### Citation:

González-Cabaleiro R, Thompson JA  
and Vilà-Nadal L (2021) Looking for  
Options to Sustainably Fixate Nitrogen.  
Are Molecular Metal Oxides Catalysts a  
Viable Avenue?  
Front. Chem. 9:742565.  
doi: 10.3389/fchem.2021.742565

Fast and reliable industrial production of ammonia (NH<sub>3</sub>) is fundamentally sustaining modern society. Since the early 20<sup>th</sup> Century, NH<sub>3</sub> has been synthesized *via* the Haber–Bosch process, running at conditions of around 350–500°C and 100–200 times atmospheric pressure (15–20 MPa). Industrial ammonia production is currently the most energy-demanding chemical process worldwide and contributes up to 3% to the global carbon dioxide emissions. Therefore, the development of more energy-efficient pathways for ammonia production is an attractive proposition. Over the past 20 years, scientists have imagined the possibility of developing a milder synthesis of ammonia by mimicking the nitrogenase enzyme, which fixes nitrogen from the air at ambient temperatures and pressures to feed leguminous plants. To do this, we propose the use of highly reconfigurable molecular metal oxides or polyoxometalates (POMs). Our proposal is an informed design of the polyoxometalate after exploring the catabolic pathways that cyanobacteria use to fix N<sub>2</sub> in nature, which are a different route than the one followed by the Haber–Bosch process. Meanwhile, the industrial process is a “brute force” system towards breaking the triple bond N–N, needing high pressure and high temperature to increase the rate of reaction, nature first links the protons to the N<sub>2</sub> to later easier breaking of the triple bond at environmental temperature and pressure. Computational chemistry data on the stability of different polyoxometalates will guide us to decide the best design for a catalyst. Testing different functionalized molecular metal oxides as ammonia catalysts laboratory conditions will allow for a sustainable reactor design of small-scale production.

**Keywords:** nitrogen fixation, polyoxometalate, nitrogenase, computational chemistry, metabolic modelling, Haber Bosch, catalyst—N

## INTRODUCTION

Multicellular organisms are unable to metabolize atmospheric N<sub>2</sub> because of its high bond enthalpy and zero dipole moment. Instead, they source nitrogen from fixed resources such as nitrate and ammonia (Sadeghi et al., 2015). The process known as biological nitrogen fixation in which N<sub>2</sub> is converted into assimilable forms is carried out by a specialized group of microorganisms that possess nitrogenases which are enzymes able to reduce atmospheric nitrogen into ammonia (NH<sub>3</sub>). At the start of the last century the only solid natural forms of nitrogen to enrich the soil were Peruvian guano and Chilean nitrate but in 1913, the Haber–Bosch process changed the course of the 20<sup>th</sup> Century allowing mass production of ammonia. In fact, ammonia production is the base of



agriculture supporting between a third and a half of human food intake. Despite technical improvements for industrial NH<sub>3</sub> production, it still requires both high temperature (350–500°C) and high pressure (15–20 MPa) consuming more than 1% of world-wide energy production and being one of the main world-wide producers of carbon dioxide and nitrous oxide emissions, both tagged as green-house gases (Foster et al., 2018). We can reduce travelling to mitigate climate change, but definitely, we cannot stop eating (Erisman et al., 2008), and massive industrial ammonia production of NH<sub>3</sub> is fundamental in sustaining the human population (50% of the nitrogen found in human tissues originates from the Haber–Bosch process). However, the abuse of ammonia fertilizers, of which only about 50% are efficiently absorbed in soils, has led to an accumulation of nitrogen in natural waterbodies with negative consequences (such as limitation of natural diversity and proliferation of toxic algae) (Fields, 2004). Therefore, sustainable nitrogen fixation has remained as a critical area of research at the frontiers of inorganic, organometallic, coordination chemistry, and biochemistry for decades. Finding efficient alternatives to the Haber–Bosch process is a challenge because of the extraordinarily complicated characteristics of the reaction. In fact, ammonia synthesis is currently the most well-characterized heterogeneous catalytic reaction.

The overall reaction of ammonia synthesis from N<sub>2</sub> is accessible thermodynamically at standard conditions ( $\Delta G^\circ = -16.4 \text{ kJ mol}^{-1}$ ) (Lide, 2005), which indicates that this reaction could occur without external energy input at low temperatures. However, it does not take place spontaneously (Jia and Quadrelli, 2014). Kinetics, and endergonic production of intermediates, dictate operation at ca 350–500°C and elevated pressures are needed to achieve acceptable process yields at an industrial level (Hargreaves et al., 2020). The detailed thermodynamic analysis presented in (Jia and Quadrelli, 2014) also shows that although the overall reaction of fixing N<sub>2</sub> is exergonic, the kinetic routes that lead to them demand high amounts of energy. Indeed, diazene and hydrazine are intermediates of the overall reaction with very high enthalpies of formation (Van Der Ham et al., 2014).

Given its global impact, the fundamentals of the Haber–Bosch process have hardly changed at all over the past 100 years. It still relies on an iron catalyst with potassium oxide and alumina acting as electronic and structural promoters, respectively (Galloway et al., 2013). In the early 1900s, Alwin Mittasch conducted a large-scale screening experiment to find a substitute for Haber's osmium- and uranium-based catalysts (Hargreaves, 2014). Approximately 3,000 catalyst compositions were evaluated in over 20,000 small-scale tests. He developed a Fe-based catalyst, which is still used today, but in the 1970s ruthenium (Ru) was acknowledged as the best elemental metal catalyst for industrial ammonia production.

In recent years, there has been a large amount of research on reducing the temperature and pressure of the Haber–Bosch process using a variety of advanced catalysts such as promoted-iron, supported-ruthenium, and metal nitrides (Humphreys et al., 2021). Today we know that Ru has much higher activity than Fe, at least near thermodynamic equilibrium.

However, due to the higher cost of Ru and its shorter catalytic lifetime, promoted Ru catalysts have only recently begun to challenge iron-based catalysts (Ross, 2019). Also, it has been long accepted that d-block metals can bind the abundant dinitrogen molecule, however, only a few are able to catalyze the conversion of dinitrogen to ammonia. Indeed, the main impediment to N<sub>2</sub> fixation is primarily of kinetic nature (Jia and Quadrelli, 2014). After carefully analyzing existing thermodynamic experimental data, Borden provided an insightful explanation to the energetics of bonding H<sub>2</sub> to N<sub>2</sub> (Borden, 2017). The study showed how the difficulty associated to N<sub>2</sub> fixation, is only partly due to the strength of one of the three N–N  $\pi$  bond that is broken in this reaction. In fact, the relative weakness of the intermediate sp<sup>2</sup> N–H  $\sigma$  bonds in E–HN = NH obtained in this reaction plays a slightly larger role which allows us to conclude that reactivity of the intermediates rely on a delicate balance between the bonds that are formed and broken towards the yielding of the final product (Nicolaidis and Borden, 1991).

Under the current global scenario of environmental emergency, it is urgent to find sustainable solutions to fulfil the ammonia demands of the human population. Novel design of catalysts is required to efficiently produce NH<sub>3</sub> at low temperatures and with less energy requirements. Ideally, these catalyzers could drive N<sub>2</sub> fixation at small scale, tailoring the operation for specific demands and contributing to the reduction of synthetic NH<sub>3</sub> accumulation in the environment. But in developing these alternative solutions, it is necessary to design new catalysts which can follow alternative pathways that substitute the endergonic dissociative mechanism used in the Haber–Bosch process, and reduce the industrial energy spilt accounted for NH<sub>3</sub> synthetic production.

## NITROGENASES

Nature, contrary to chemists, has found a way to use the abundant N<sub>2</sub> gas effectively at room temperature and neutral pH by using natural catalysts, enzymes, called nitrogenases. The nitrogenase can channel electrons and energy from different sources in anaerobic and aerobic conditions to form bioavailable NH<sub>3</sub> breaking the triple bond of the (almost inert) molecules of N<sub>2</sub> gas. Three homologous nitrogenases have been reported, distinguished by their metal-centred catalytic cofactors: molybdenum (MoFe), iron (FeFe) and vanadium (VFe) (Hu and Ribbe, 2015). Although the three homologous enzymes have been associated with specific activities, our understanding of the nitrogenase metal cofactors and their role is still incomplete (Rutledge and Tezcan, 2020).

The more ancient, abundant, efficient, and studied nitrogenase is the molybdenum containing system (Curatti et al., 2006). This nitrogenase is composed of two proteins, an homodimeric iron (FeP) protein (~66 kDa) and the  $\alpha_2\beta_2$  heterotetrameric molybdenum-iron (MoFe) protein (~240 kDa, with two complex metalloclusters). The FeP protein contains an ATP-binding site within each subunit interface of the protein, and it oversees the shuttle of eight electrons towards the reduction of

**TABLE 1** | Efficiencies of selected novel catalysts for N<sub>2</sub> fixation under ambient temperatures and pressures. RHE = Reversible Hydrogen Electrode / SCE = Standard Calomel Electrode.

Catalyst	Efficiency (mol NH <sub>3</sub> e <sup>-1</sup> )	Ammonia rate (μgNH <sub>3</sub> mg <sub>cat.</sub> <sup>-1</sup> h <sup>-1</sup> )	Electronic promotor	Ref
<b>Electrocatalysts</b>				
Ru SAs/N-C	0.0493	120.90	-0.20 V vs RHE	Geng et al. (2018)
Pd/C	0.0137	4.50	0.10 V vs RHE	Wang et al. (2018)
MoO <sub>3</sub> nanosheets	0.0032	29.43	-0.50 V vs RHE	Han et al. (2018)
Bi <sub>4</sub> V <sub>2</sub> O <sub>11</sub> /CeO <sub>2</sub>	0.0169	23.21	-0.20 V vs RHE	Lv et al. (2018)
Mo <sub>2</sub> N nanorod	0.0075	78.40	-0.30 V vs RHE	Ren et al. (2018)
Au/TiO <sub>2</sub>	0.0135	21.40	-0.20 V vs RHE	Shi et al. (2017)
CN-C <sub>500</sub>	0.0280	2.90	-0.30 V vs RHE	Peng et al. (2020)
<b>Photocatalysts</b>				
Bi <sub>2</sub> MoO <sub>6</sub>	0.0012	22.14	Xe lamp (λ = 500 nm)	Hao et al. (2016)
<b>Synthetic electron donor</b>				
[Co(N <sub>2</sub> )( <sup>t</sup> BuPNP)]	0.0442	47.22	KC <sub>8</sub>	Kuriyama et al. (2016)
<b>MOF-Polyoxometalate Catalysts PMo<sub>12</sub>@MIL-100 (Fe) precursor</b>				
FeMo-based material	0.0912	105.30	-0.40 V vs RHE	Wang et al. (2020)
<b>Enzymatic Fuel Cells</b>				
MoFe / Cobaltocene	0.0583	12.72	-1.25 V vs SCE	Milton et al. (2016)
MoFe / Methyl viologen	0.0440	2.44	-0.85 V vs SCE	Milton et al. (2017)

1 mole of N<sub>2</sub>. Concomitantly, 1 mole of H<sub>2</sub> is produced per mole of N<sub>2</sub> fixed. The explanation for this H<sub>2</sub> reduction and apparent waste of equivalent power remains elusive but considering that H<sub>2</sub> reduction by nitrogenase occurs only in the presence of N<sub>2</sub>, it has been proposed that production of H<sub>2</sub> activates the FeMo-protein. Together, the oxidation of the low-potential [4Fe-4S]<sup>1+</sup> cluster requires activation, and this happens when the hydrolysis of ATP takes place (Barsukova-Stuckart et al., 2012). Commonly, the ATP requirement of nitrogenase is evaluated as 2 moles of ATP are hydrolyzed into ADP and inorganic phosphate (P<sub>i</sub>) per mole of electrons transferred, although more efficient ratios (down to 1 mole of ATP consumed per mole of electron) have been reported (Tan et al., 2016; Poudel et al., 2018). With this, the overall stoichiometry of natural N<sub>2</sub> fixation remains as presented in Eq. 1.



The detailed explanation for the necessary loss of a cell's energy currency (ATP) associated with nitrogenase activity remains elusive (Rabo and Schoonover, 2001; Milton et al., 2017) but it is assumed to be essential to reduce the activation barriers associated to the catalysis of the intermediates that lead to the overall reaction (Van Der Ham et al., 2014) and to activate the transfer of electrons (Rutledge and Tezcan, 2020). Also, the electron transfer to the substrate in nitrogenase seems to follow the description drawn in 1978 by Thorneley and colleagues (Thorneley et al., 1978), but the delicate and precise donation of electrons, protons and energy is not fully deciphered yet. Meanwhile, this optimized coordinated mechanism plays a fundamental role in maintaining the high efficiency of the non-selective nitrogenase enzyme (Kang et al., 2021).

After the donation of electrons, the [4Fe-4S]<sup>1+</sup> cluster must be reduced again. This can happen by subsequent reduction by flavodoxin in aerobic or facultative anaerobic organisms, or by ferredoxin (more sensitive to O<sub>2</sub> presence) in anaerobic ones. Phylogenetic analyses suggested the use of flavodoxin as strategy for diversification of nitrogenases in aerobic environments (Boyd et al., 2015). The electrons that feed flavodoxin and/or ferredoxin come directly from pyruvate or H<sub>2</sub> oxidation (mostly in anaerobic organisms) or NAD(P)H electron carriers (aerobic, facultative anaerobes, and anoxygenic phototrophs) (Poudel et al., 2018). Indeed, the reduction of flavodoxin or ferredoxin starts the cycle towards N<sub>2</sub> fixation again.

Although some research efforts have been trying to take advantage of the high efficiency of nitrogenase using the two-protein mechanism to directly catalyze N<sub>2</sub> fixation (Harris et al., 2018), the high efficiency of electrons donated per mole of N<sub>2</sub> fixed by nitrogen-fixing bacteria (8 electrons per mole of NH<sub>3</sub> produced), has not been achieved by any *in vitro* system using the MoFe protein, the nitrogenase enzyme or any inorganic catalysts (Table 1). Engineering of nitrogenase in eukaryotic cells is another promising avenue but still requires overcoming fundamental challenges (Yang et al., 2014; Vicente and Dean, 2017). Therefore, other efforts have been directed towards the generation of enzymatic fuel cells, which has been approached using methyl viologen as solely electron mediator between a cathodic surface and a nitrogenase (Milton et al., 2017). This is a rather difficult catalysis as it requires an ATP regenerating system to activate the FeP protein, and anaerobic conditions, with remarkably low efficiencies reported. To remove the necessity of an ATP regeneration, bioelectrocatalysis of N<sub>2</sub> fixation has been explored using only the MoFe protein of the nitrogenase and

cobaltocene as electron mediator (Milton et al., 2016). However, production of NH<sub>3</sub> was only reported with the reduction of N<sub>3</sub><sup>−</sup> or NO<sub>2</sub><sup>−</sup>.

Few electrochemical systems that produce convincing amounts of NH<sub>3</sub> have been reported with the most successful so far being the molybdenum based ones (see, Table 1). However, the poor Faradaic efficiency of these systems due to their low selectivity competing with H<sub>2</sub> production, makes them, in many cases more energy demanding than Haber–Bosch process (Van Der Ham et al., 2014). These inefficiencies can only be surpassed by the design of other catalysts able to follow a more feasible reaction pathway at room temperature. The reliability of experimental electrochemical nitrogen reduction reaction (ENRR) experiments was questioned in a recent publication by Choi et al. detailing the complexity that arises from the potential intrusion of airborne contaminants. The reduction of nitrogen oxides (NO, NO<sub>2</sub>, etc.) are more thermodynamically favorable than direct ENRR (Choi et al., 2020). Failure to control this has led to contentious Faradaic efficiencies and ammonia yields.

The design of novel bio-inspired catalysts, containing multiple active sites, has the potential to bypass the obvious limitations associated with exploitation of the complex nitrogenase enzyme, although competitive CO<sub>2</sub> and H<sub>2</sub> selectivity must be overcome with concomitant effectiveness in N<sub>2</sub> adsorption and mechanistic delivery of electrons and protons (Bagger et al., 2021). Other authors, have reported that the use of a bio-inspired catalysts operating via an associative mechanism, like the one described for nitrogenases, are able to fix N<sub>2</sub>, CO<sub>2</sub> and CH<sub>4</sub> simultaneously at room temperature (Revilla-López et al., 2020). This can open the avenue for the development of new industrial processes able to combine N<sub>2</sub> fixation with carbon homologation.

## MOLECULAR METAL OXIDES OR POLYOXOMETALATES

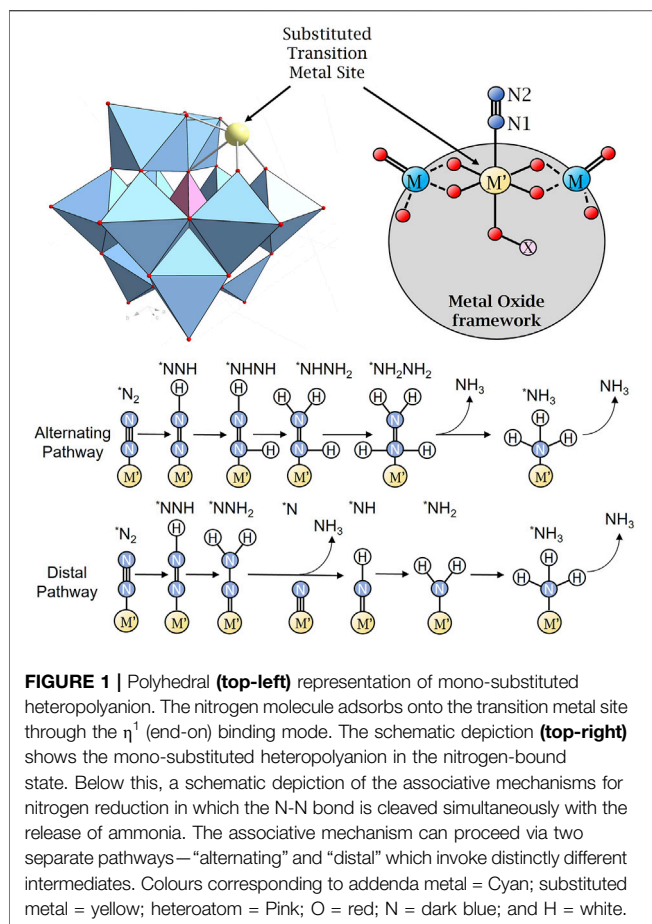
Molecular metal oxides, or polyoxometalates (POMs) offer a route to design efficient ENRR using Earth abundant transition metals. POMs are primarily comprised of early-transition-metal (*d-block*) elements in their highest oxidation states. A great majority of these structures are anionic and consequently salts with charge balancing cations. In fact, POMs are an archetypal family of self-assembled molecular clusters that display a vast range of physical properties, structural features and sizes (Vilà-Nadal and Cronin, 2017). POMs are mainly formed by Mo<sup>6+</sup> and W<sup>6+</sup> combined with a main group oxyanion (phosphate, silicate, etc.). Simply speaking, the synthesis of POM clusters in a “one-pot” solution involves dissolving the [MO<sub>4</sub>]<sup>n−</sup> (M = W, Mo) salt in aqueous solution followed by acidification, addition of electrophiles, buffer, additional cations and in some cases a reducing agent (Proust et al., 2012). The solution can then be processed by normal, microwave or hydrothermal heating followed by controlled precipitation to yield the cluster in crystalline form so that the structure of the cluster can be elucidated by single crystal X-ray

diffraction (Long et al., 2004). This route has been used in 99% of all cases in POM chemistry and is very convenient to yield complex structures from “one-pot” but suffers a great deal from dependence on initial reaction conditions, reproducibility, and the ability to systematically investigate parameter space to design new cluster architectures. In this respect, during the last decade the field of POMs has been transformed by trapping reactive building blocks and generating an accessible building block library as a function of pH, template, linker heteroatoms, and cation type (Miras et al., 2020). The key aspect here is that the heteroatom mediated assembly of the anionic metal-oxo units to building blocks which then link to clusters, can be used to form new types of materials with novel and unprecedented architectures (Zheng et al., 2018). In fact, POM structures and functionalities make them ideal candidates as model systems for metal-oxide-anchored single atom catalysts (POM-SAC) (Liu and Streb, 2021). POMs are polynuclear metal oxide anions that are molecular analogues of solid-state metal oxides. Diverse fields such as, water oxidation catalysts (Blasco-Ahicart et al., 2018), photocatalysis (Costa-Coquelard et al., 2010), molecular electronics (Busche et al., 2014), quantum computation (Gaita-Ariño et al., 2019), biology (Gumerova and Rompel, 2021) and medicinal science (Lu et al., 2021) have all been impacted by POM chemistry. Current findings demonstrate the feasibility of hydrogen-production using silicotungstic acid, H<sub>6</sub>[SiW<sub>12</sub>O<sub>4</sub>], by coupling low-pressure oxygen production via water oxidation linked to non-electrolyzer catalytic hydrogen production (Rausch et al., 2014). Given their structural diversity and versatility of POM cluster applications, they are ideal candidates to provide further insight into the heterogeneous Haber–Bosch catalyst or the low-energy nitrogenase enzymes that directly make ammonia.

## DISCUSSION

Ammonia is a viable hydrogen energy vector, and its pre-existing industry, which produces, stores, and trades millions of tons of ammonia annually, means that the infrastructure necessary to jump-start the hydrogen economy already exists. The United Kingdom has developed detailed plans for the next decade to use “green” ammonia as an energy storage material for renewable electricity (The Royal Society, 2020).

The global cycling of nitrogen through the biosphere depends upon a heavy element: molybdenum and requires bacteria in the fixation of nitrogen (Hille, 2002). However, when extensively starved nitrogen-fixing bacteria *A. vinelandii* were grown in a medium that lacked molybdate but that contained tungstate, *A. vinelandii* synthesized the regular storage protein but with tungstate. This is perhaps not surprising since tungsten, lies below molybdenum in the d-block, and is consequently expected to feature chemical properties related to those of molybdenum. Recent work indicated that molybdenum and tungsten-based enzymes are incredibly ancient and their enzymatic role and functionality has been preserved (Vitousek et al., 2002). It is thought that in the reducing environment of the



primordial world tungsten-enzymes were favoured. In those days, oxygen atom transfer reactions were more challenging than in our oxidic modern world, with its preference for molybdenum-enzymes (Schemberg et al., 2007). By deepening our understanding of the microbial populations that cycle nitrogen, we can find opportunities to deliver more efficient bioengineering solutions. To date, no one has systematically explored the new biotechnologies for nitrogen removal that can emerge from this new knowledge because a purely empirical exploration would require significant investigation. To achieve low-temperature, cost-effective and efficient electrochemical ammonia synthesis requires a multidisciplinary approach able to characterise natural biocatalysts (nitrogenases) that efficiently catalyse N<sub>2</sub> reduction, as well as develop heterogeneous (molecular) catalytic systems informed by current computational theory developments in the area that can direct efficiently experimental investigation (Foster et al., 2018).

We will start by looking into transition metal substituted lacunary Keggin anions, as shown in **Figure 1**. Such structures are derivatives from the parent anion  $[XM_{12}O_{40}]^{n-}$ , where X is the heteroatom (most commonly are P<sup>5+</sup>, Si<sup>4+</sup>, or B<sup>3+</sup>), and M = W, Mo, inspired by recent work in the area, (Lin et al., 2020)

which investigated the Gibbs free energy change for the reductive adsorption of \*N<sub>2</sub> and \*H on four Keggin-POM-supported Ru single atom electrocatalysts. The phosphorus-templated tungstate- and molybdate-Keggin clusters presented high nitrogen-binding selectivity, whereas the silicon-templated analogues prefer hydrogen binding. Our aim is to explore the functionalization of molecular dinitrogen and its catalytic conversion in POMs by combining our expertise in inorganic chemistry with exploring the catalytic conversion *d*-block metals. This will be our theoretical model structure, bearing in mind that the pH increases the Mo- and W-based Keggin ions gradually disintegrate (Kondinski and Parac-Vogt, 2018). Computational chemistry will help us to describe the intermediates of bioinspired reaction pathways. These results will complement in-depth metabolic analyses of highly efficient nitrogenases at ambient temperature and pressure. We will work closely with experimentalists in the area that will help us to translate our theoretical results into effective experimental N<sub>2</sub> reduction catalysis.

## DATA AVAILABILITY STATEMENT

The original contributions presented in the study are included in the article/supplementary material, further inquiries can be directed to the corresponding authors.

## AUTHOR CONTRIBUTIONS

LV-N conceived the idea, designed the project and together with RG-C coordinated the efforts of the research team. LV-N and RG-C co-wrote the paper with input from JAT.

## FUNDING

Financial support for this work was provided by University of Glasgow and the Engineering and Physical Sciences Research Council Grants (EP/S030603/1; EP/R513222/1; EP/T517896/1), Royal Society of Chemistry RSC Hardship Grant (Covid-19). We also thank the University of Glasgow Early Career Development Programme (ECDP) for support.

## ACKNOWLEDGMENTS

The authors acknowledge Justin Hargreaves from the School of Chemistry at the University of Glasgow for useful ongoing discussions in this project and proof reading the manuscript. We acknowledge Cindy Smith from the School of Engineering at the University of Glasgow for ongoing discussions on environmental controls of the microorganisms driving the nitrogen cycle.



## REFERENCES

- Bagger, A., Wan, H., Stephens, I. E. L., and Rossmeisl, J. (2021). Role of Catalyst in Controlling N<sub>2</sub> Reduction Selectivity: A Unified View of Nitrogenase and Solid Electrodes. *ACS Catal.* 11, 6596–6601. doi:10.1021/acscatal.1c01128
- Barsukova-Stuckart, M., Izarova, N. V., Barrett, R. A., Wang, Z., van Tol, J., Kroto, H. W., et al. (2012). Polyoxopalladates Encapsulating 8-Coordinated Metal Ions, [MO<sub>8</sub>PdII<sub>12</sub>L<sub>8</sub>]n<sup>−</sup> (M = Sc<sup>3+</sup>, Mn<sup>2+</sup>, Fe<sup>3+</sup>, Co<sup>2+</sup>, Ni<sup>2+</sup>, Cu<sup>2+</sup>, Zn<sup>2+</sup>, Lu<sup>3+</sup>; L = PhAsO<sub>3</sub><sup>2−</sup>, PhPO<sub>3</sub><sup>2−</sup>, SeO<sub>3</sub><sup>2−</sup>). *Inorg. Chem.* 51, 13214–13228. doi:10.1021/ic301537n
- Blasco-Ahicart, M., Soriano-López, J., Carbó, J. J., Poblet, J. M., and Galan-Mascaros, J. R. (2018). Polyoxometalate Electrocatalysts Based on Earth-Abundant Metals for Efficient Water Oxidation in Acidic media. *Nat. Chem.* 10, 24–30. doi:10.1038/NCHEM.2874
- Borden, W. T. (2017). Why Are Addition Reactions to N<sub>2</sub> Thermodynamically Unfavorable? *J. Phys. Chem. A* 121, 1140–1144. doi:10.1021/acs.jpca.6b11728
- Boyd, E. S., Costas, A. M. G., Hamilton, T. L., Mus, F., and Peters, J. W. (2015). Evolution of Molybdenum Nitrogenase during the Transition from Anaerobic to Aerobic Metabolism. *J. Bacteriol.* 197, 1690–1699. doi:10.1128/JB.02611-14
- Busche, C., Vilà-Nadal, L., Yan, J., Miras, H. N., Long, D.-L., Georgiev, V. P., et al. (2014). Design and Fabrication of Memory Devices Based on Nanoscale Polyoxometalate Clusters. *Nature* 515, 545–549. doi:10.1038/nature13951
- Choi, J., Suryanto, B. H. R., Wang, D., Du, H.-L., Hodgetts, R. Y., Ferrero Vallana, F. M., et al. (2020). Identification and Elimination of False Positives in Electrochemical Nitrogen Reduction Studies. *Nat. Commun.* 11, 1–10. doi:10.1038/s41467-020-19130-z
- Costa-Coquelard, C., Sorgues, S., and Ruhlmann, L. (2010). Photocatalysis with Polyoxometalates Associated to Porphyrins under Visible Light: An Application of Charge Transfer in Electrostatic Complexes. *J. Phys. Chem. A* 114, 6394–6400. doi:10.1021/jp101261n
- Curatti, L., Ludden, P. W., and Rubio, L. M. (2006). NifB-dependent *In Vitro* Synthesis of the Iron-Molybdenum Cofactor of Nitrogenase. *Proc. Natl. Acad. Sci.* 103, 5297–5301. doi:10.1073/pnas.0601115103
- Erisman, J. W., Sutton, M. A., Galloway, J., Klimont, Z., and Winiwarter, W. (2008). How a century of Ammonia Synthesis Changed the World. *Nat. Geosci.* 1, 636–639. doi:10.1038/ngeo325
- Fields, S. (2004). Global Nitrogen: Cycling Out of Control. *Environ. Health Perspect.* 112, 556–563. doi:10.1289/ehp.112-a556
- Foster, S. L., Bakovic, S. I. P., Duda, R. D., Maheshwari, S., Milton, R. D., Minter, S. D., et al. (2018). Catalysts for Nitrogen Reduction to Ammonia. *Nat. Catal.* 1, 490–500. doi:10.1038/s41929-018-0092-7
- Gaita-Ariño, A., Luis, F., Hill, S., and Coronado, E. (2019). Molecular Spins for Quantum Computation. *Nat. Chem.* 11, 301–309. doi:10.1038/s41557-019-0232-y
- Galloway, J. N., Leach, A. M., Bleeker, A., and Erisman, J. W. (2013). A Chronology of Human Understanding of the Nitrogen Cycle. *Phil. Trans. R. Soc. B* 368, 20130120. doi:10.1098/rstb.2013.0120
- Geng, Z., Liu, Y., Kong, X., Li, P., Li, K., Liu, Z., et al. (2018). Achieving a Record-High Yield Rate of 120.9 μgNH<sub>3</sub> mgcat<sup>−1</sup> H<sup>−1</sup> for N<sub>2</sub> Electrochemical Reduction over Ru Single-Atom Catalysts. *Adv. Mater.* 30, 1803498–1803507. doi:10.1002/adma.201803498
- Gumerova, N. I., and Rompel, A. (2021). Interweaving Disciplines to Advance Chemistry: Applying Polyoxometalates in Biology. *Inorg. Chem.* 60, 6109–6114. doi:10.1021/acs.inorgchem.1c00125
- Han, J., Ji, X., Ren, X., Cui, G., Li, L., Xie, F., et al. (2018). MoO<sub>3</sub> Nanosheets for Efficient Electrocatalytic N<sub>2</sub> Fixation to NH<sub>3</sub>. *J. Mater. Chem. A* 6, 12974–12977. doi:10.1039/c8ta03974g
- Hao, Y., Dong, X., Zhai, S., Ma, H., Wang, X., and Zhang, X. (2016). Hydrogenated Bismuth Nanoframe for Efficient Sunlight-Driven Nitrogen Fixation from Air. *Chem. Eur. J.* 22, 18722–18728. doi:10.1002/chem.201604510
- Hargreaves, J. S. J., Chung, Y.-M., Ahn, W.-S., Hisatomi, T., Domen, K., Kung, M. C., et al. (2020). Minimizing Energy Demand and Environmental Impact for Sustainable NH<sub>3</sub> and H<sub>2</sub>O<sub>2</sub> Production: A Perspective on Contributions from Thermal, Electro-, and Photo-Catalysis. *Appl. Catal. A: Gen.* 594, 117419. doi:10.1016/j.apcata.2020.117419
- Hargreaves, J. S. J. (2014). Nitrides as Ammonia Synthesis Catalysts and as Potential Nitrogen Transfer Reagents. *Appl. Petrochem. Res.* 4, 3–10. doi:10.1007/s13203-014-0049-y
- Harris, D. F., Lukoyanov, D. A., Shaw, S., Compton, P., Tokmina-Lukaszewska, M., Bothner, B., et al. (2018). Mechanism of N<sub>2</sub> Reduction Catalyzed by Fe-Nitrogenase Involves Reductive Elimination of H<sub>2</sub>. *Biochemistry* 57, 701–710. doi:10.1021/acs.biochem.7b01142
- Hille, R. (2002). Molybdenum and Tungsten in Biology. *Trends Biochem. Sci.* 27, 360–367. doi:10.1016/S0968-0004(02)02107-2
- Hu, Y., and Ribbe, M. W. (2015). Nitrogenase and Homologs. *J. Biol. Inorg. Chem.* 20, 435–445. doi:10.1007/s00775-014-1225-3
- Humphreys, J., Lan, R., and Tao, S. (2021). Development and Recent Progress on Ammonia Synthesis Catalysts for Haber-Bosch Process. *Adv. Energ. Sustain. Res.* 2, 2000043. doi:10.1002/aesr.202000043
- Jia, H.-P., and Quadrelli, E. A. (2014). Mechanistic Aspects of Dinitrogen Cleavage and Hydrogenation to Produce Ammonia in Catalysis and Organometallic Chemistry: Relevance of Metal Hydride Bonds and Dihydrogen. *Chem. Soc. Rev.* 43, 547–564. doi:10.1039/c3cs60206k
- Kang, W., Lee, C. C., Jasiewski, A. J., Ribbe, M. W., and Hu, Y. (2021). Response to Comment on "Structural Evidence for a Dynamic Metallocofactor during N<sub>2</sub> Reduction by Mo-Nitrogenase". *Science* 371, eabe5856–1385. doi:10.1126/science.abe5856
- Kondinski, A., and Parac-Vogt, T. N. (2018). Keggin Structure, Quó Vádis? *Front. Chem.* 6, 1–7. doi:10.3389/fchem.2018.00346
- Kuriyama, S., Arashiba, K., Tanaka, H., Matsuo, Y., Nakajima, K., Yoshizawa, K., et al. (2016). Direct Transformation of Molecular Dinitrogen into Ammonia Catalyzed by Cobalt Dinitrogen Complexes Bearing Anionic PNP Pincer Ligands. *Angew. Chem.* 128, 14503–14507. doi:10.1002/ange.201606090
- Lide, D. R. (2005). *CRC Handbook of Chemistry and Physics: A Ready-Reference of Chemical and Physical Data, 85th ed Edited by David R. Lide*. Boca Raton, FL: CRC Press LLC, 2313–2314.
- Lin, L., Gao, L., Xie, K., Jiang, R., and Lin, S. (2020). Ru-polyoxometalate as a Single-Atom Electrocatalyst for N<sub>2</sub> Reduction to NH<sub>3</sub> with High Selectivity at Applied Voltage: A Perspective from DFT Studies. *Phys. Chem. Chem. Phys.* 22, 7234–7240. doi:10.1039/d0cp00698j
- Liu, R., and Streib, C. (2021). Polyoxometalate-Single Atom Catalysts (POM-SACs) in Energy Research and Catalysis. *Adv. Energ. Mater.* 11, 2101120. doi:10.1002/aenm.202101120
- Long, D.-L., Kögerler, P., and Cronin, L. (2004). Old Clusters with New Tricks: Engineering S...S Interactions and Novel Physical Properties in Sulfite-Based Dawson Clusters. *Angew. Chem. Int. Ed.* 43, 1817–1820. doi:10.1002/anie.200352896
- Lu, F., Wang, M., Li, N., and Tang, B. (2021). Polyoxometalate-Based Nanomaterials toward Efficient Cancer Diagnosis and Therapy. *Chem. Eur. J.* 27, 6422–6434. doi:10.1002/chem.202004500
- Lv, C., Yan, C., Chen, G., Ding, Y., Sun, J., Zhou, Y., et al. (2018). An Amorphous Noble-Metal-Free Electrocatalyst that Enables Nitrogen Fixation under Ambient Conditions. *Angew. Chem. Int. Ed. Engl.* 57, 6073–6076. doi:10.1002/adma.20180349810.1002/anie.201801538
- Milton, R. D., Abdellaoui, S., Khadka, N., Dean, D. R., Leech, D., Seefeldt, L. C., et al. (2016). Nitrogenase Bioelectrocatalysis: Heterogeneous Ammonia and Hydrogen Production by MoFe Protein. *Energy Environ. Sci.* 9, 2550–2554. doi:10.1039/c6ee01432a
- Milton, R. D., Cai, R., Abdellaoui, S., Leech, D., De Lacey, A. L., Pita, M., et al. (2017). Bioelectrochemical Haber-Bosch Process: An Ammonia-Producing H<sub>2</sub> /N<sub>2</sub> Fuel Cell. *Angew. Chem. Int. Ed.* 56, 2680–2683. doi:10.1002/anie.201612500
- Miras, H. N., Mathis, C., Xuan, W., Long, D.-L., Pow, R., and Cronin, L. (2020). Spontaneous Formation of Autocatalytic Sets with Self-Replicating Inorganic Metal Oxide Clusters. *Proc. Natl. Acad. Sci. USA* 117, 10699–10705. doi:10.1073/pnas.1921536117
- Nicolaides, A., and Borden, W. T. (1991). Ab Initio calculations of the Relative Strengths of the .Pi. Bonds in Acetylene and Ethylene and of Their Effect on the Relative Energies of .pi.-bond Addition Reactions. *J. Am. Chem. Soc.* 113, 6750–6755. doi:10.1021/ja00018a005
- Peng, G., Wu, J., Wang, M., Niklas, J., Zhou, H., and Liu, C. (2020). Nitrogen-Defective Polymeric Carbon Nitride Nanolayer Enabled Efficient

- Electrocatalytic Nitrogen Reduction with High Faradaic Efficiency. *Nano Lett.* 20, 2879–2885. doi:10.1021/acs.nanolett.0c00698
- Poudel, S., Colman, D. R., Fixen, K. R., Ledbetter, R. N., Zheng, Y., Pence, N., et al. (2018). Electron Transfer to Nitrogenase in Different Genomic and Metabolic Backgrounds. *J. Bacteriol.* 200, 1–19. doi:10.1128/JB.00757-17
- Proust, A., Matt, B., Villanneau, R., Guillemot, G., Gouzerh, P., and Izzet, G. (2012). Functionalization and post-functionalization: a Step towards Polyoxometalate-Based Materials. *Chem. Soc. Rev.* 41, 7605–7622. doi:10.1039/c2cs35119f
- Rabo, J. a., and Schoonover, M. W. (2001). Early Discoveries in Zeolite Chemistry and Catalysis at Union Carbide, and Follow-Up in Industrial Catalysis. *Appl. Catal. A: Gen.* 222, 261–275. doi:10.1016/S0926-860X(01)00840-7
- Rausch, B., Symes, M. D., Chisholm, G., and Cronin, L. (2014). Decoupled Catalytic Hydrogen Evolution from a Molecular Metal Oxide Redox Mediator in Water Splitting. *Science* 345, 1326–1330. doi:10.1126/science.1257443345
- Ren, X., Cui, G., Chen, L., Xie, F., Wei, Q., Tian, Z., et al. (2018). Electrochemical N<sub>2</sub>fixation to NH<sub>3</sub>under Ambient Conditions: Mo<sub>2</sub>N Nanorod as a Highly Efficient and Selective Catalyst. *Chem. Commun.* 54, 8474–8477. doi:10.1039/c8cc03627f
- Revilla-López, G., Sans, J., Casanovas, J., Bertran, O., Puiggali, J., Turon, P., et al. (2020). Analysis of Nitrogen Fixation by a Catalyst Capable of Transforming N<sub>2</sub>, CO<sub>2</sub> and CH<sub>4</sub> into Amino Acids under Mild Reactions Conditions. *Appl. Catal. A: Gen.* 596, 117526. doi:10.1016/j.apcata.2020.117526
- Ross, J. R. H. (2019). An Introduction to Heterogeneous Catalysis and its Development through the Centuries-Chemistry in Two Dimensions, 3, 38). doi:10.1016/b978-0-444-63474-0.00001-1
- Rutledge, H. L., and Tezcan, F. A. (2020). Electron Transfer in Nitrogenase. *Chem. Rev.* 120, 5158–5193. doi:10.1021/acs.chemrev.9b00663
- Sadeghi, O., Zakharov, L. N., and Nyman, M. (2015). Aqueous Formation and Manipulation of the Iron-Oxo Keggin Ion. *Science* 347, 1359–1362. doi:10.1126/science.aaa4620
- Schemberg, J., Schneider, K., Demmer, U., Warkentin, E., Müller, A., and Ermler, U. (2007). Towards Biological Supramolecular Chemistry: A Variety of Pocket-Templated, Individual Metal Oxide Cluster Nucleations in the Cavity of a Mo/W-Storage Protein. *Angew. Chem. Int. Ed.* 46, 2408–2413. doi:10.1002/anie.200604858
- Shi, M.-M., Bao, D., Wulan, B.-R., Li, Y.-H., Zhang, Y.-F., Yan, J.-M., et al. (2017). Au Sub-nanoclusters on TiO<sub>2</sub>toward Highly Efficient and Selective Electrocatalyst for N<sub>2</sub>Conversion to NH<sub>3</sub>at Ambient Conditions. *Adv. Mater.* 29, 1606550–1606557. doi:10.1002/adma.201606550
- Tan, M. L., Perrin, B. S., Niu, S., Huang, Q., and Ichiye, T. (2016). Protein dynamics and the all-ferrous [Fe<sub>4</sub>S<sub>4</sub>] cluster in the nitrogenase iron protein. *Protein Sci.* 25, 12–18. doi:10.1002/pro.2772
- The Royal Society (2020). *Ammonia: Zero-Carbon Fertiliser, Fuel and Energy Store*. London: Policy Briefing.
- Thorneley, R. N. F., Eady, R. R., and Lowe, D. J. (1978). Biological Nitrogen Fixation by Way of an Enzyme-Bound Dinitrogen-Hydride Intermediate. *Nature* 272, 557–558. doi:10.1038/272557a0
- Van Der Ham, C. J. M., Koper, M. T. M., and Hetterscheid, D. G. H. (2014). Challenges in Reduction of Dinitrogen by Proton and Electron Transfer. *Chem. Soc. Rev.* 43, 5183–5191. doi:10.1039/c4cs00085d
- Vicente, E. J., and Dean, D. R. (2017). Keeping the Nitrogen-Fixation Dream Alive. *Proc. Natl. Acad. Sci. USA* 114, 3009–3011. doi:10.1073/pnas.1701560114
- Vilà-Nadal, L., and Cronin, L. (2017). Design and Synthesis of Polyoxometalate-Framework Materials from Cluster Precursors. *Nat. Rev. Mater.* 2. doi:10.1038/natrevmats.2017.54
- Vitousek, P. M., Cassman, K., Cleveland, C., Crews, T., Christopher, B., Grimm, N. B., et al. (2002). Towards an Ecological Understanding of Biological Nitrogen Fixation Rastetter and Janet I . Sprent Published By : Springer Stable URL . *Biogeochemistry* 57, 1–45. doi:10.1007/978-94-017-3405-9\_1
- Wang, J., Yu, L., Hu, L., Chen, G., Xin, H., and Feng, X. (2018). Ambient Ammonia Synthesis via Palladium-Catalyzed Electrohydrogenation of Dinitrogen at Low Overpotential. *Nat. Commun.* 9. doi:10.1038/s41467-018-04213-9
- Wang, X., Feng, Z., Xiao, B., Zhao, J., Ma, H., Tian, Y., et al. (2020). Polyoxometalate-based Metal-Organic Framework-Derived Bimetallic Hybrid Materials for Upgraded Electrochemical Reduction of Nitrogen. *Green. Chem.* 22, 6157–6169. doi:10.1039/d0gc01149e
- Yang, J., Xie, X., Wang, X., Dixon, R., and Wang, Y.-P. (2014). Reconstruction and Minimal Gene Requirements for the Alternative Iron-Only Nitrogenase in *Escherichia coli*. *Proc. Natl. Acad. Sci.* 111, E3718–E3725. doi:10.1073/pnas.1411185111
- Zheng, Q., Vilà-Nadal, L., Lang, Z., Chen, J.-J., Long, D.-L., Mathieson, J. S., et al. (2018). Self-Sorting of Heteroanions in the Assembly of Cross-Shaped Polyoxometalate Clusters. *J. Am. Chem. Soc.* 140, 2595–2601. doi:10.1021/jacs.7b11982

**Conflict of Interest:** The authors declare that the research was conducted in the absence of any commercial or financial relationships that could be construed as a potential conflict of interest.

**Publisher's Note:** All claims expressed in this article are solely those of the authors and do not necessarily represent those of their affiliated organizations, or those of the publisher, the editors and the reviewers. Any product that may be evaluated in this article, or claim that may be made by its manufacturer, is not guaranteed or endorsed by the publisher.

Copyright © 2021 González-Cabaleiro, Thompson and Vilà-Nadal. This is an open-access article distributed under the terms of the Creative Commons Attribution License (CC BY). The use, distribution or reproduction in other forums is permitted, provided the original author(s) and the copyright owner(s) are credited and that the original publication in this journal is cited, in accordance with accepted academic practice. No use, distribution or reproduction is permitted which does not comply with these terms.



# Self-Assembled Materials Incorporating Functional Porphyrins and Carbon Nanoplatforms as Building Blocks for Photovoltaic Energy Applications

Boyang Mao<sup>1,2\*</sup>, Benjamin Hodges<sup>1,3</sup>, Craig Franklin<sup>1</sup>, David G. Calatayud<sup>1,4\*</sup> and Sofia I. Pascu<sup>1,3\*</sup>

<sup>1</sup>Department of Chemistry, University of Bath, Bath, United Kingdom, <sup>2</sup>Cambridge Graphene Centre, Engineering Department, University of Cambridge, Cambridge, United Kingdom, <sup>3</sup>Centre for Sustainable and Circular Technologies (CSCT), University of Bath, Bath, United Kingdom, <sup>4</sup>Department of Electroceramics, Instituto de Ceramica y Vidrio (CSIC), Madrid, Spain

## OPEN ACCESS

### Edited by:

Jennifer Hiscock,  
University of Kent, United Kingdom

### Reviewed by:

Tsukuru Minamiki,  
National Institute of Advanced  
Industrial Science and Technology  
(AIST), Japan  
Dönüs Tuncel,  
Bilkent University, Turkey

### \*Correspondence:

Sofia I. Pascu  
s.pascu@bath.ac.uk  
Boyang Mao,  
bym573@cam.ac.uk  
David G. Calatayud  
dgcalatayud@icv.csic.es

### Specialty section:

This article was submitted to  
Supramolecular Chemistry,  
a section of the journal  
Frontiers in Chemistry

**Received:** 18 June 2021

**Accepted:** 13 August 2021

**Published:** 01 October 2021

### Citation:

Mao B, Hodges B, Franklin C,  
Calatayud DG and Pascu SI (2021)  
Self-Assembled Materials  
Incorporating Functional Porphyrins  
and Carbon Nanoplatforms as Building  
Blocks for Photovoltaic  
Energy Applications.  
Front. Chem. 9:727574.  
doi: 10.3389/fchem.2021.727574

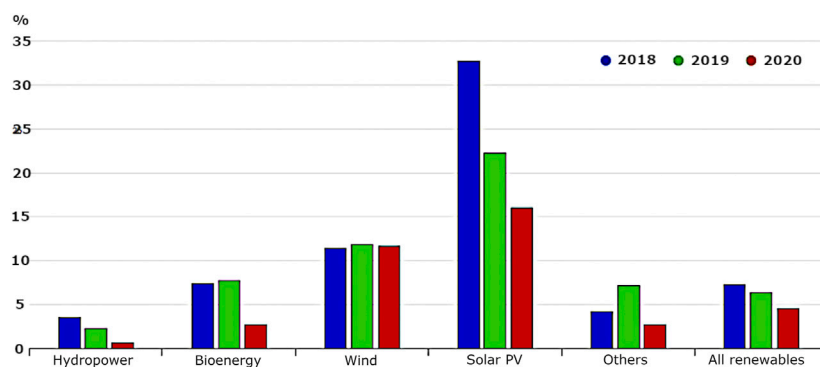
As a primary goal, this review highlights the role of supramolecular interactions in the assembly of new sustainable materials incorporating functional porphyrins and carbon nanoplatforms as building blocks for photovoltaics advancements.

**Keywords:** supramolecular chemistry, functional graphene materials, porphyrins, donor/acceptor interactions, net zero, sustainable processes

## SUSTAINABLE ENERGY PRODUCTION IN CURRENT SOCIOECONOMIC CONTEXT

Production and consumption of energy is a basic element in daily life and crucial to societal development. The demand for energy is increased continuously with the evolution of civilisations. The increase of the human population, urbanisation, modernisation, and technology development all go along with the increased demand for energy supply. It is predicted that the growth in global energy demand will rise harshly over the coming year rendering the current reliance on fossil fuels, which is a bottleneck for continuous economic growth worldwide. Currently, the world heavily relies on fossil fuels to meet the vast majority of its energy needs. Fossil fuels, for instance, oil, gas, and coal, which were generated by natural processes such as anaerobic decomposition of buried, dead organisms over million years, are providing almost 80% of the global energy demands (Asif and Muneer, 2007; World Energy Outlook, 2020 – Analysis – IEA). The fact that humanity faces is that a significant amount of energy currently being consumed across the world has adverse implications on the environment of the Planet, and this triggered the current race to “net zero.” The dominant purveyors of global energy, fossil fuels, are seen as placing merciless effects on ecosystems. The significant consumption of fossil fuels leads to the dramatic emission of greenhouse gas (CO<sub>2</sub>, CH<sub>4</sub>, etc.), which impact directly the environment and contribute to climate change. It has been reported that 160,000 people die each year due to the side effects of climate change, which includes malnutrition, malaria, and spread of epidemic diseases, which follow in the wake of floods, droughts, and warmer Earth temperatures, and the numbers of victims may double by the end of 2020, according to the World Health Organization (2018) (Climate change and health; Asif and Muneer, 2007).

It has been well known that the amount of fossil fuel generated by the current sources decrease and, by facing the difficult climate challenges, the current energy system is unable to cope with future energy demands. The production and consumption of nuclear energy, which is mainly employed in developed counties, together with fossil fuels are strictly linked to increased threats to biological



**FIGURE 1 |** Annual growth for renewable electricity generation by source.

diversity, environmental degradation that affects human health and quality of life and affects ecological balance. Therefore, if the rapidly increasing global energy needs are to be met without irrevocable environmental damage, there should have to be a worldwide drive to create and exploit energy systems that are not detrimental to the life of current and future generations and do not exceed the current carrying capacity of ecosystems. This situation has become even more crucial in recent years, the variability in the price of crude oil (World Energy Outlook, 2020 – Analysis – IEA), considerations about natural gas fracking and the economic crisis, make people less concerned about achieving sustainable energy development that does not compromise the future.

Sustainable energy sources, which are naturally replenished, inexhaustible, and widely available on a human timescale such as sunlight, wind, rain, tides, and geothermal heat, have the potential to provide energy services with almost nil emissions of both air pollutants and greenhouse gases. Sustainable energy can replace fossil fuels in four distinct areas: electricity generation, hot water/space heating, motor fuels, and rural energy services. Currently, sustainable energy is only contributing to 13.5% (Asif and Muneer, 2007; Department for Business, 2020; Renewables – Global Energy Review, 2020 – Analysis – IEA; Report extract Renewables, 2020; World Energy Outlook, 2020 – Analysis – IEA) of the total energy needs. Sustainable energy resources have the capacity to meet the current and future energy requirements of the world and minimise the reliance on fossil or nuclear fuels.

The development and use of sustainable energy sources have significant benefits including the enhancement of diversity in energy supply markets, help reduce local and global environmental impacts, provide commercially alternative options to meet specific energy service demands, and contribute to securing long-term sustainable energy supplies and also creating new employment opportunities practically in developing country and rural area. It is also noticed that the cost of energy generated from these renewable resources is significantly reduced with the development of high technology.

Over the last two decades, solar and wind energy systems have experienced rapid growth and dominated the sustainable energy market (Chu and Majumdar, 2012; Department for Business, 2020; Renewables – Global Energy Review, 2020 – Analysis – IEA;

Report extract Renewables, 2020; World Energy Outlook, 2020 – Analysis – IEA). This rapid growth was contributed by several reasons, like the decreasing capital cost and continued improvement in performance characterisation. Compared with wind energy, solar energy is still being investigated and has huge potential in the technology revolution. The economic and policy mechanisms for developing solar energy support the widespread dissemination and rapid evolution. Chemists, material scientists, and other physical scientists have started the race for high-performance materials of relevance to sustainable energy applications.

Therefore, the topic of sustainable energy production raised to prominence in both academic research and governmental policy over the past 20 years. The diminishing supplies of oil, increased population, and the increase in the demand for energy mean that alternative methods for the production of energy are greatly desired. This is in line with global developments whereby renewable electricity generation rose by nearly 5% in 2020 (notwithstanding the current COVID-related challenges that caused supply chain disruptions that have paused or delayed economic activities in several key regions) and is expected to continue to rise at this rate globally throughout to the end of 2021 (Renewables – Global Energy Review, 2020 – Analysis – IEA). Within the United Kingdom, the total energy consumption in 2019 (pre-COVID crisis) raised to 3,600 kWh per annum for electricity and 13,600 kWh per annum for gas (Department for Business, 2020).

Although overall the demand for electricity has generally been declining since 2010 due to the introduction of energy-saving systems throughout the country, the domestic production of energy is rapidly falling as production and consumption of primary energy sources such as coal and gas are reduced for both financial reasons and the meeting of carbon emission targets. This means that energy produced from sustainable sources such as wind, hydro, and solar energy is being employed to make up the difference, increasing at a steady rate since 1990. Overall, in the United Kingdom, the renewable energy sources have grown at an average annual rate of 2.0%, which is slightly higher than the growth rate of world TES, 1.8%. Growth has been especially high for solar PV and wind power, which grew at average annual rates of 36.5 and

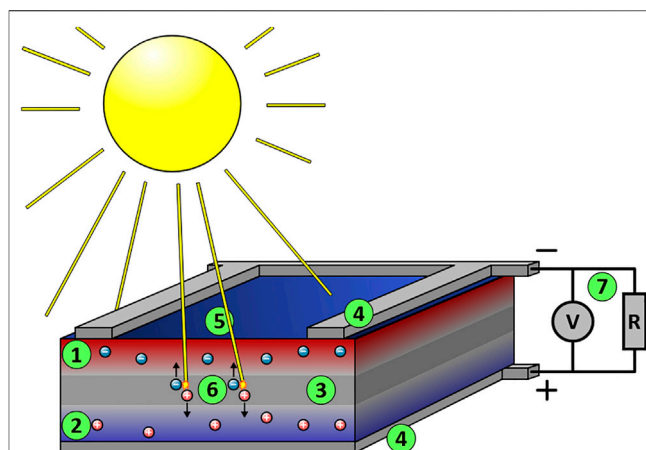


23.0%, respectively **Figure 1**). Interestingly, a marked increase was seen from 2012 to 2013 when the energy produced from sustainable sources in the United Kingdom grew by 30% to contribute to a total of 14.9% overall of the electricity produced in the United Kingdom at that date and continue to make a significant contribution to the energy consumption.

Current solar cell technologies rely on materials and processes that require a large input of energy and thus increase their overall CO<sub>2</sub> equivalence. Studies have shown that PV systems based on silicon produce 50–250 g-CO<sub>2</sub>/kWh over their lifetime which is higher than most other renewable sources of electricity (although still lower than conventional coal, oil, or gas systems) (Renewables – Global Energy Review, 2020 – Analysis – IEA; Report extract Renewables, 2020; World Energy Outlook, 2020 – Analysis – IEA). Producing low-cost and low-impact solar cells is the key to the continuation of this rising technology.

Industrially, several different classes of devices and underlining materials are being produced for applications in sustainable technologies. These include (but are not limited to) the organic electronic areas of relevance to organic photovoltaics, organic photodiodes, OLEDs, and thin-film transistors development. Using organic semiconductors as the basis of device manufacturing in sustainable technologies is widely acknowledged due to the low-cost manufacturing methods, based on evaporating or printing on a variety of substrates.

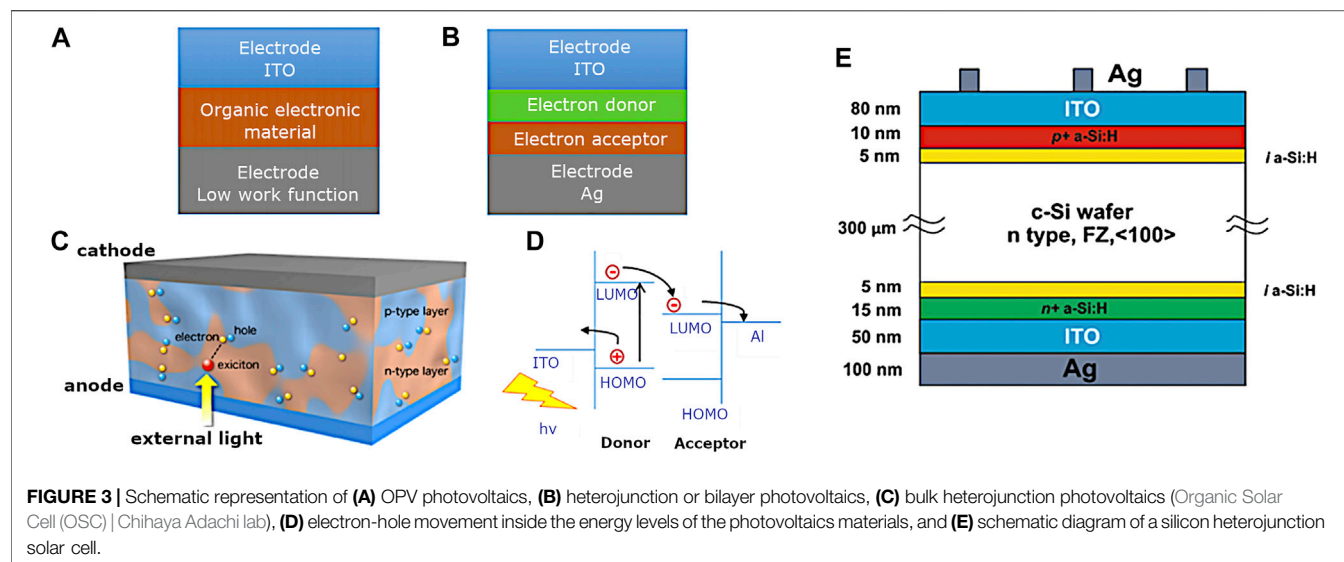
On the other hand, direct storage of solar energy is very difficult and even unworkable outside research environments; in this sense, solar energy is usually first converted into other forms of energy and then stored (Badenhorst, 2019; Brunetti et al., 2019). The most commonly used methods currently are the conversion of energy into thermal energy (Dahash et al., 2019), conversion into biomass energy (Bentsen and Møller, 2017), conversion into chemical energy (Wang et al., 2020), and conversion and storage of solar energy electrochemically (Meng et al., 2019; Wang et al., 2021a), being the last one which offers the best practical prospects. To realise the potential of solar-to-electrochemical energy conversion and storage, the integration of solar cells with electrochemical energy storage (EES) devices is necessary (Gurung and Qiao, 2018). Specifically, this involves a solar cell as the energy harvesting unit and an EES device [e.g., a rechargeable battery or supercapacitor (SC)] as the energy storage unit, resulting in what is known as a “photo-charging” process. Thus, the involvement of innovative EES units is as important as solar cells. Like in the case of solar cells, carbon-based functional materials can also improve the performance of rechargeable batteries and SCs (Ren et al., 2020). As is well known, carbon black can greatly increase the conductivity of electrode materials, thus bringing better charge/discharge characteristics to batteries. Carbon coatings on the surface of electrode materials can also improve the cyclic stability of EES units in integrated devices. For example, the involvement of novel materials such as carbon nanotubes (CNTs) and graphene in the design elements can be considered, by directly using these as active electrode



**FIGURE 2 |** Schematic representation of a silicon monocrystalline solar cell. The circles present the excited electrons and holes. They are then extracted to the conductance band of an n-type conductor and from there passed around a circuit and eventually returned to the valence band of the p-type conductor. (1) The upper silicon layer is interspersed with electron donors (e.g., phosphorus atoms), negatively doped. There are too many electrons here (n-layer). (2) The lower silicon layer is interspersed with electron acceptors (e.g., boron atoms), positively doped. Here, there are too few electrons, i.e., too many defects or holes (p-layer). (3) In the border region of the two layers, the excess electrons of the electron donors bind loosely to the vacancies of the electron acceptors (they occupy the vacancies in the valence band) and form a neutral zone (p-n junction). (4) Since there is now a lack of electrons at the top and a lack of vacancies at the bottom, a constantly present electric field forms between the upper and lower contact surfaces. (5) Photons (light quanta, “sun rays”) enter the transition layer. (6) Photons with sufficient energy transfer their energy to the loosely bound electrons in the valence band of the electron acceptors in the neutral zone. This releases these electrons from their bond and lifts them into the conduction band as free charge carriers. Many of these free charge carriers (electron-hole pairs) disappear again after a short time through recombination. Some charge carriers drift—moved by the electric field—to the contacts in the similarly doped zones (see above); i.e., the electrons are separated from the holes, the electrons drift upwards, and the holes downwards. A voltage and a usable current are created as long as further photons continuously generate free charge carriers. (7) The “electron” current flows through the “outer circuit” to the lower contact surface of the cell and recombines there with the holes left behind (Paetzold, 2018).

materials for batteries and SCs, due to their high electronic conduction, large surface area, and tuneable electrochemical activity (Li et al., 2019; Wang et al., 2021b). Apart from the aforementioned functions, nanocarbon arrays (e.g., CNT- and graphene-based fibres and membranes) can act as ideal flexible substrate materials for integrated devices to achieve flexibility, portability, and wearability (Lu et al., 2019; Guo et al., 2021).

Overall, it is clear that carbon materials and their analogues play very critical roles in the configuration design and performance enhancement of integrated devices of high relevance to sustainable technology applications (Shi et al., 2019). However, due to the breadth of the topic, the authors will focus in this review on the energy harvesting component and particularly on aspects of molecular designs involved in innovative solar cells technologies and related applications.



## OVERVIEW ON SOLAR CELL TECHNOLOGIES

The sun provides  $3 \times 10^{15}$  GJ a year or about 10,000 times more than the global population currently consumes. This would easily satisfy our needs, provided a large enough proportion of the Earth was covered with solar cells (0.1% of the Earth's surface with solar cells with an efficiency of 10%) (Grätzel, 2005). The discovery of the ability to convert solar energy into electricity was originally published by Becquerel who noted a photocurrent when platinum electrodes, covered with silver bromide or silver chloride, were illuminated in an aqueous solution (strictly speaking, this demonstrates a photoelectrochemical effect). A while later, Smith and Adams were the first to publish reports on photoconductivity, in 1873 and 1876, respectively, working with selenium. The use of this technology was not taken up until after further work, such as the development of the p-n junction in silicon electronics, leading to the discovery of the silicon-based solar cell.

The modern solar cells were developed by D. M. Chapin and C. S. Fuller in 1954 at Bell Labs using a solid-state semiconductor junction (Chapin et al., 1954). Since the good quality silicon wafers can be produced in the 1950s, the silicon electronics became the main source materials for the PV industry. Its potential application in space exploration led to the first use of a solar cell being on the satellite Vanguard 1 in 1958.

Dr. Ching W. Tang reported the first organic cell and published his research results in 1986 (Tang, 1986). In 1991, Grätzel and O'Regan found the first dye-sensitized photovoltaic device which has efficiency in the full sunlight of 7.1% (O'Regan and Grätzel, 1991). Since then, Perovskite materials have been first incorporated into a solar cell as reported by Miyasaka et al. in 2009; this cell was based on a dye-sensitized solar cell and generated only 3.8% power conversion efficiency (Kojima et al., 2009). A power conversion efficiency of 16% at AM 1.5G one sun illumination was reported (Lee et al., 2014), and the efficiency increased rapidly beyond 20% with the

developments of new functional materials and blends (Thomas and Thankappan, 2018). Solar cells technologies rely on the occurrence of the photovoltaic effect, which is the generation of a direct current electrical power from semiconductors when they are illuminated by photons. All solar cells require a light-absorbing material in the cell structure to absorb photons and generate free electrons by the photovoltaic effect. In a standard p-n junction solar cell, the light hitting the junction between a hole conducting and electron-conducting semiconductor can create electron-hole pairs which in turn leads to a potential difference across the interface (see Figure 2) (Luque and Hegedus, 2011).

It remains the case that the first generation solar cells remain largely still in production industrially during the first decades of the 21st century. These are based on single-junction silicon wafers, including common amorphous silicon systems, such as silicon carbide, silicon germanium, and silicon nitride. Crystalline silicon allows for an increase in the efficiency of the cell but at a cost (Parida et al., 2011); however, cost, in terms of £/W, remains the greatest barrier to further expansion of PV-generated power and cost reduction is the prime goal of the PV sector (Bagnall and Boreland, 2008).

Second generation solar cell technologies are based on thin-film technology that reduces the cost of the cell by reducing the amount of material required. These thin films are chemically or physically deposited on low-cost substrates such as glass creating a cheaper cell with similar efficiencies to the first generation cells (Soteris, 2018). The third generation is a step beyond the single-junction cells that include not only multijunction cells but also polymer and organic and dye-sensitized solar cells (DSSCs) (Dragonetti and Colombo, 2021).

Fundamentally, the basis of PV device construction relies on sensing technologies reliant on photodiodes. A diode is an electrical component that allows current to flow only in one direction. A photodiode is a type of photodetector which converts light into current or voltage, whereby an organic photodiode is made of highly conjugated organic material. If the electrodes of a

photodiode are connected by a wire, in the dark, no current will flow however in light current flows from cathode to anode. When the material absorbs a photon, an exciton is formed. This is known as the inner photovoltaic effect. The exciton is then separated, holes move to the anode, and the electrons move to the cathode. Once they are separated, a photocurrent is produced.

Commonly encountered device structures include single layer OPV whereby the organic electronic material is sandwiched between a high work function electrode and a low work function metal, whereby the difference in work function establishes an electric field within the organic layer. The potential created by the two electrodes separates the exciton (**Figure 3A**).

Additionally, heterojunction or bilayer photovoltaics incorporate the two materials that have different electron affinities and ionisation energies. The differences need to be large so the electric field is strong enough to separate the exciton (**Figure 3B**). Bulk heterojunction PV incorporate devices whereby the acceptor and donor materials are mixed together to form a polymer blend. The working principle relies on light excitation generating an exciton, which is then broken at the interface between donor and acceptor material and the charges transfer to the electrodes. The open-circuit voltage is in turn dependent on the band gap between the highest occupied molecular orbit (HOMO) and the lowest unoccupied molecular orbit (LUMO), whilst the photocurrent is determined by the voltage. Excitons must diffuse to a p-n interface to separate. Small exciton diffusion length may be overcome by mixing donor and acceptor to shorten the distance to the interface. Morphology and phase separation of the blend are crucial to solar cell performance.

For another classification often used in the solar cells industry, the traditional silicon solar cells technique belongs to the first generation technologies. The first generation silicon solar cells use mono- or multicrystalline silicon as the main materials for the production of solar cells. **Figure 3E** shows a typical monocrystalline silicon solar cell. This kind of silicon solar cells is a single-junction solar cell in different regions; n-type or p-type semiconducting materials are doped (Bagnall and Boreland, 2008). The efficiency of these single-junction solar cells can rise up 20%. The improvements of silicon single-junction solar cells were addressed by silicon heterojunction solar cells (De Wolf et al., 2012; Qu et al., 2021). **Figure 3E** shows a typical structure of silicon heterojunction solar cell. Although the efficiency of this kind of solar cell is relatively very high in comparison with that of organic solar cells, the high cost and the pollution causing in the production process set back the development of the PV industry (Nelson, 2003).

The second generation solar cells incorporate the thin-film solar cells produce thinner layer crystals than the first generation materials film, made by depositing one or more thin layers or thin film of photovoltaic material on a substrate, such as glass, plastic, or metal. It was reported that using CdTe and CIGS (Copper Indium Gallium Selenide) thin film to generate single-junction solar cells, the efficiency of these thin-film solar cells can raise up to 21% (Pearce et al., 2007). However, they involve a technically demanding of high requirement for producing process and it was

found that it is very difficult to transfer this technology from laboratory scale to commercial-scale products.

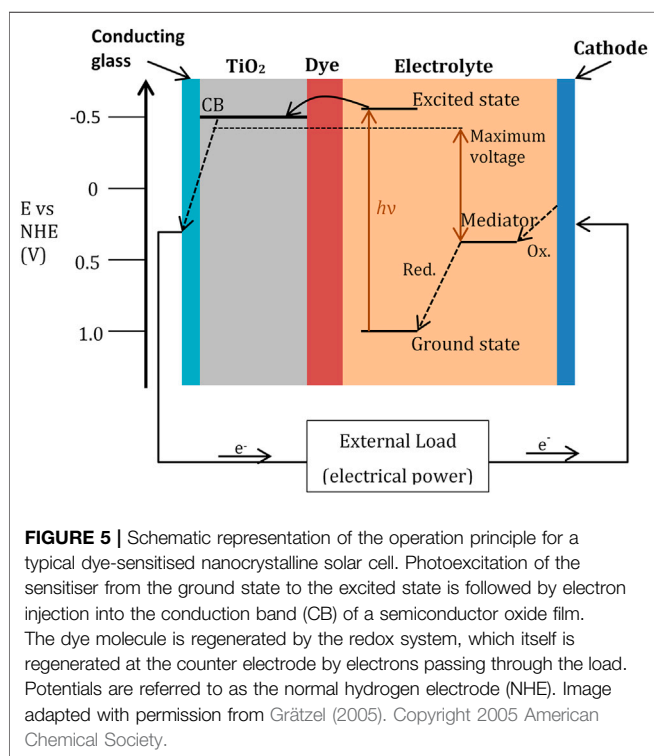
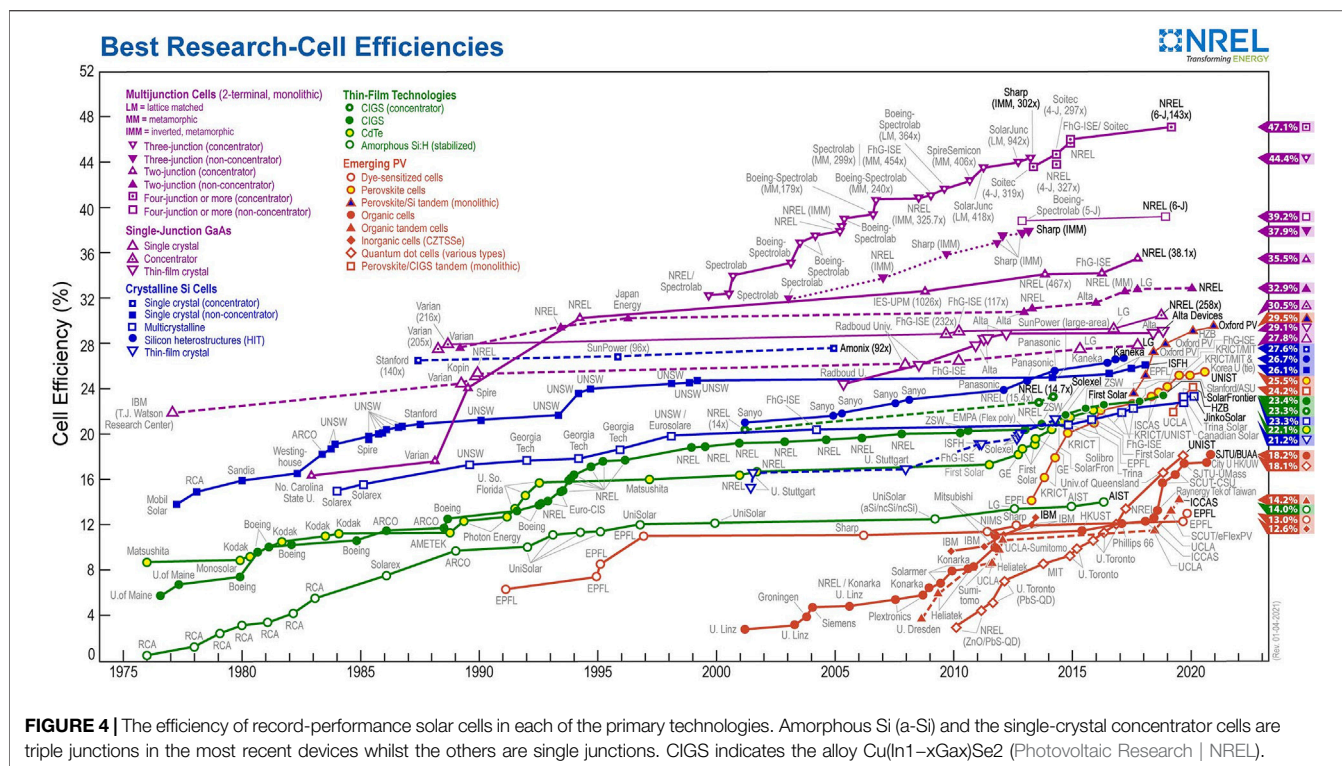
The third generation solar cells incorporate organic solar cells and several different types of DSSCs, and so on. The organic solar cells include Schottky-type solar cell, bilayer heterojunction solar cell, and bulk heterojunction solar cell (BHJ) (Hoppe and Sariciftci, 2004). The Schottky-type solar cells have a typical metal-organic-metal sandwich structure. From R. O. Loutfy and J. H. Sharp's research, macrocyclic molecules such as porphyrins and phthalocyanines were considerable material choices for the organic layer present in the sandwich structure (Loutfy and Sharp, 1979). In 1985, Tang et al. first reported the bilayer heterojunction solar cells. The efficiency of the organic solar cell was then improved significantly. In his work, small molecules of copper phthalocyanine and a perylene tetracarboxylic derivative were used as the active layer of the solar cell (Tang, 1986). However, the diffusion of excitons only occurs in several nanometres near the interface of two organic materials in the bilayer heterojunction solar cell, which constituted one of the main limitations for the bilayer heterojunction solar cell. In order to solve this problem, bulk heterojunction solar cell, which relies on the mixing of the electron donor and acceptor materials together, was introduced (Hiramoto et al., 1992; Yu et al., 1995). The bulk heterojunction is an interpenetrating network of acceptor and donor where the phase separation is commonly between 10 and 20 nm, which is within the effective diffusion length of an exciton. The emergence of bulk heterojunction is a breakthrough in organic solar cell.

Alternative third generation solar cell is the dye-sensitised photovoltaic device, which was firstly founded in 1991 by O'Regan and Grätzel (1991). Dye-sensitised solar cell combines organic and inorganic components together and assembly nanomaterial together to build up a multilayer structure. The dye molecules are working as a light-harvesting material in the cell structure to absorb photos and generate free electrons by the photovoltaic effect. Modern DSSCs are composed of a porous layer of titanium dioxide nanoparticles, covered with a molecular dye that absorbs sunlight. The titanium dioxide is immersed under an electrolyte solution, above which is a platinum-based catalyst. As in a conventional alkaline battery, titanium dioxide regarded as an anode and platinum regarded as a cathode are placed on either side of a liquid/solid electrolyte conductor.

Devices assembly involve layering methods include spin coating, blade coating, drop casting, and evaporation either by thermal or electron beam. Developments showed a departure from the classical solid-state junction device, by replacing the phase in contact with the semiconductor by an electrolyte (liquid, gel, or organic solid), thereby forming a photoelectrochemical device. **Figure 4** shows a comparison of the efficiencies of the different types of solar cells; this presents the efficiency of recorded best research solar cells performance, generated by the National Centre for Photovoltaics in the United States.

Perovskite solar cells are a relatively recent discovery, where a solid-state material such as a perovskite was first used as a light absorber (Kojima et al., 2009). These are adaptations of dye-sensitized solar cells, the fact of continuing to use organic dyes, in





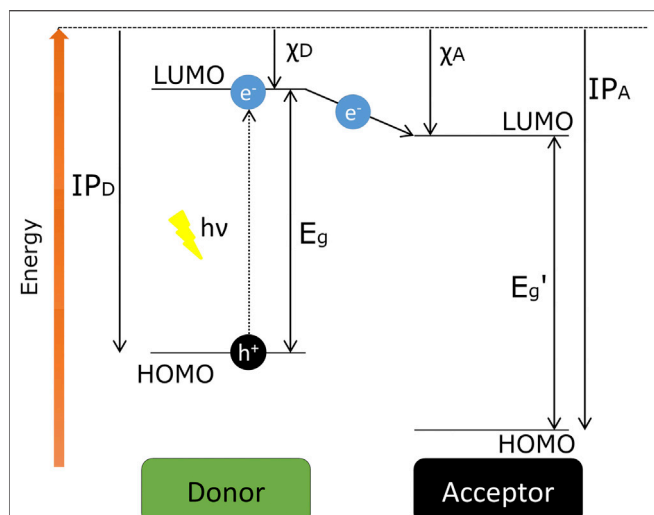
technical terms, limits the use of this range of solar cells based on cheap and readily available materials. The most commonly studied perovskite absorber is methylammonium lead trihalide ( $\text{CH}_3\text{NH}_3\text{PbX}_3$ , where X is a halogen ion such as  $\text{I}^-$ ,  $\text{Br}^-$ , and  $\text{Cl}^-$ ),

with a bandgap between 2.30 and 1.57 eV depending on halide content. It was first used as a replacement of the dye in DSSCs in order to solve the problem of limited light harvesting of organic dye (Kojima et al., 2009). However, the perovskite was found to easily dissolve or decompose in the liquid electrolyte, and it even degraded in a few minutes when it was first designed. A solid-state hole-transporting conductor was then applied to solve the instability of perovskite. In 2021, researchers at South Korea's Ulsan National Institute of Science and Technology (UNIST) and the Swiss Federal Institute of Technology Lausanne (EPFL) have achieved a new record conversion efficiency of 25.6% in a single-junction perovskite solar cell (Jeong et al., 2021).

## A Deeper Incursion Into DSSCs

The prototype for this family of devices was discovered by Grätzel at the Ecole Polytechnique Fédérale de Lausanne which involved using ruthenium-based dyes adsorbed onto nanocrystalline films of titanium dioxide. The ruthenium dye serves as a p-type conductor and absorbs the photon producing an excited electron which is then injected into the conduction band of the n-type conductor ( $\text{TiO}_2$ ). To complete the circuit, the dye must be regenerated by electron transfer from a redox species at the counter electrode, usually an iodide/triiodide electrochemical couple (Figure 5). The initial experiments were very successful, with up to 80% of the incident photons being converted into electrical current and an overall light-to-electricity yield of 7.1–7.9% (O'Regan and Grätzel, 1991). The electrons injected into the solid permeate very rapidly across the  $\text{TiO}_2$  layer and during this diffusion of electrons maintain their high electrochemical potential equal to the quasi-Fermi level of the





**FIGURE 6 |** Representation of the energy levels diagram of a donor-acceptor system, where IP is the ionisation potentials,  $\chi$  is the electron affinity, and  $E_g$  is the bandgap energy. The arrow between the LUMO levels indicates the photoinduced ET, which is the first step for generating free charge carriers. Adapted from Reference Scharber and Sariciftci (2013).

semiconductor under illumination. Thus, the principal function of the oxide, apart from supporting the sensitizer, is that of charge collection and conduction. Although  $\text{TiO}_2$  has been the material of choice, alternative wide-bandgap oxides such as  $\text{ZnO}$  and  $\text{Nb}_2\text{O}_5$  have also been investigated (Grätzel, 2005). The dye used in these cells has to withstand the conditions encountered in the practical application of the solar cell and remain serviceable for 20 years, corresponding to 50–100 million turnovers for the dye (Grätzel, 2005).

Enhancing the efficiency of a DSSC is critically dependent upon the charge separation processes, whilst at the same time reducing the energetic losses required to drive these reactions. Addressing this challenge is fundamental to the challenges of enhancing the voltage output of devices and of utilising sensitizer dyes with lower optical bandgaps and therefore enhanced spectral overlap with the solar spectrum.

A further challenge is to move towards materials which can achieve similar device performance but with enhanced stability and/or processability, they must also have high light-to-electricity conversion efficiencies, ease of fabrication, and low production costs (Bessho et al., 2010). There is an increasing appreciation that meeting these challenges is a multidimensional problem, where any one materials change impacts upon several processes within the device (Listorti et al., 2011).

## Organic Bulk Heterojunction Solar Cells

Organic materials have the advantage of being cheap and easy to process, as well as being flexible compared to most inorganic sensitizers. The choice of materials is also practically unlimited, and specific parts of the solar spectrum can be selectively absorbed. Mimicking the natural light harvesting in photosynthesis, in which a number of chlorophylls and carotenoids are involved in light collection, suggests that it is

likely that optimal photosensitization in DSSCs will only occur using a mixture of dyes (Campbell et al., 2004; Radivojevic et al., 2012).

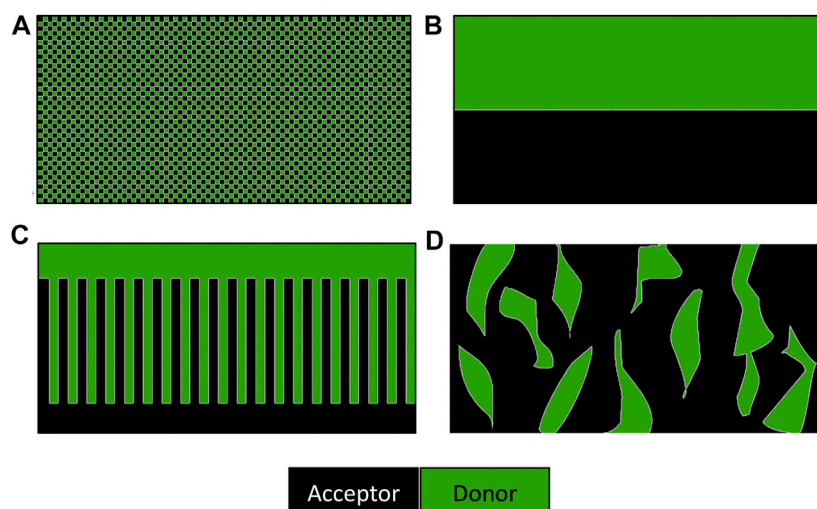
The removal of a metal-based system to a more flexible organic-based system leads to several advantages including the following:

- Low weight and flexibility of the PV modules.
- Semitransparency.
- Easy integration into other products.
- New market opportunities, e.g., wearable PV.
- Significantly lower manufacturing costs compared to conventional inorganic technologies.
- Manufacturing in a continuous process using printing tools.
- Short energy recovery times and low environmental impact during manufacturing and operations (Scharber and Sariciftci, 2013).

This type of solar cells has the potential not only to overcome the inherent cost problem of current cells but also to move the technology into new markets. Despite these advantages, organic cells are still considerably less efficient than single-crystal gallium, arsenide, or silicon, although one way these efficiencies can increase is through the increase in the number of p-n junctions, like in most third generation cells (Green, 2006). The difference here however is that bulk donor-acceptor heterojunctions can be formed simply by blending two organic materials, one serving as an electron donor (p-type conductor) and the other an electron acceptor (n-type conductor). This means that the distance between the two materials is reduced into the nanometre range, overcoming the unfavourable ratio of exciton (a bound electron-hole pair) diffusion length to optical absorption length (Sauvé and Fernando, 2015).

To be effective, when an exciton is produced by absorption of light, the pair must reach the junction and there dissociate into two free charge carriers (Figure 6). However, excitons typically diffuse only a few nanometres before recombining. Light is absorbed (and generates excitons) throughout the composite material, so the smaller the distance between each junction is, the more chance the exciton has of reaching the junction before recombination. Hence, photoinduced charge separation can occur very efficiently (Grätzel, 2001), and crucial to this is the understanding of the donor-acceptor interactions that are taking place between these junctions.

Due to the low dielectric constant of most organic materials, there is a strong Coulomb attraction between the electron-hole pair and so dissociation of the exciton at ambient conditions is very unlikely. A simple model on an electron-hole pair separated by 1 nm with a dielectric number of 3–4 would have a binding energy of 0.35–0.50 eV. This binding energy exceeds the thermal energy at room temperature by an order of magnitude and electron acceptor molecules need to be added to an organic semiconductor donor to facilitate the generation of free charge carriers (Scharber and Sariciftci, 2013). It is for this reason that an acceptor molecule is required to be the driving force behind the production of free charge carriers with the



**FIGURE 7 |** Schematic representation of the cross-section of the nanomorphologies of bulk heterojunction solar cells. **(A)** Fine mixture of donor and acceptor molecules, **(B)** bilayer arrangement, **(C)** ideal morphology of a bulk heterojunction solar cells, and **(D)** typical morphology of a solution processes device (Scharber and Sariciftci, 2013).

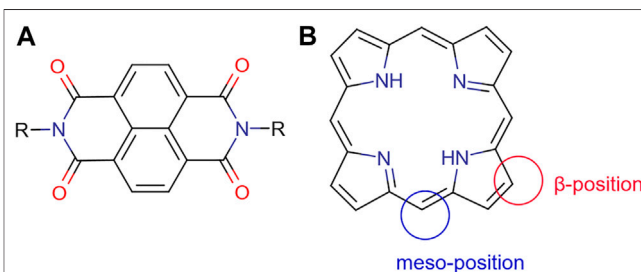
**TABLE 1 |** Comparison of recently reported cell efficiencies for traditional solar cell types.

Classification	Efficiency (%)	References
Si (crystalline)	25.6 ± 0.5	Green et al. (2014)
Si (multicrystalline)	20.4 ± 0.5	Schultz et al. (2004)
Si (microcrystalline)	11.0 ± 0.3	Petermann et al. (2012)
Si (amorphous)	10.1 ± 0.3	Green et al. (2014)
GaAs (thin film)	28.3 ± 0.9	Green et al. (2014)
Dye sensitised	11.9 ± 0.4	Komiya et al. (2011)
Bulk heterojunction	10.7 ± 0.3	Scharber and Sariciftci (2013)

energy difference between the LOMOs of the two molecules being the predominant factor (Sariciftci et al., 1992).

The construction of supramolecular structures of  $\pi$ -conjugated molecules via self-assembly has been recognised as an important approach to manipulate their optical and electronic properties to generate “supramolecular electronics.” Due to the relatively short (<1 ns) exciton lifetime in organic semiconductors, quantitative charge generation requires very fast charge separation. To achieve efficient charge generation, excitons must be generated within their diffusion length to the nearest donor-acceptor interface relative to their lifetime. Recent measurements indicate that this diffusion length is in the range of 10 nm for several prototype conjugated polymers used in bulk heterojunction solar cells, which means that an intermixing of the donor and the acceptor moieties on the nanometre scale is required (Mikhnenko et al., 2012).

There is still no full consensus on how the ideal nanomorphology of a bulk heterojunction cell should be arranged. A very fine dispersion of the acceptor in the donor material, shown in (a) in **Figure 7**, would lead to efficient charge generation but poor charge transport. Ideal charge transport



**FIGURE 8 | (A)** General molecular structure of naphthyl diimides (NDIs); **(B)** framework structure of a free-base porphyrin presenting *meso*-position and  $\beta$ -position, which may be functionalised. Additionally, the  $\text{NH}$ 's are available for deprotonation and subsequent metallations.

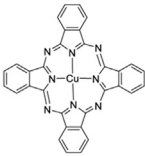

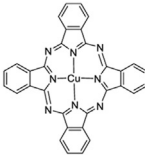

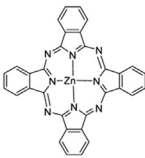

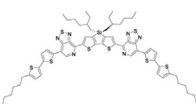
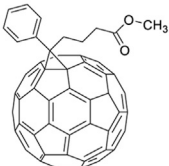
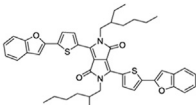
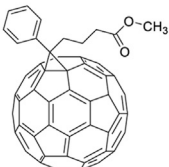
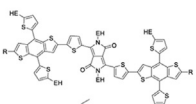
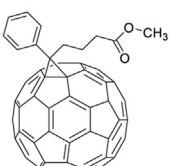
could be achieved by arranging the donor and acceptor in by bilayer stack (b). However, charge generation overall will be poor as it only happens at the interface between the two. Calculations and morphology simulation work have suggested that the arrangement shown in (c) should lead to ideal performance (Watkins et al., 2005). In addition to this loss of efficiency due to the recombination of the excitons or charge-transfer states prior to separation (called geminate recombination), further losses in efficiency have been shown to be caused by the recombination between pairs of dissociated electrons and holes, where each is generated by a different absorption event (called nongeminate recombination) (Dibb et al., 2011).

Bulk heterojunction (BHJ) solar cells offer a promising, low-cost, large-area, flexible, light weight, clean, and quiet alternative energy source for both indoor and outdoor applications. **Table 1** shows the comparison of the efficiencies of different types of solar cells, showing that BHJs are not far off the efficiency of more common inorganic based cells. What is more, due to the wide range of organic dyes that are available for these cells, the

**TABLE 2** | Small molecules used in organic solar cells.

Small molecule organic solar cells	Acceptor	<p>Fullerene and its derivatives</p>	
		Non- fullerene	<p>Perylene Diimide and its derivatives</p>
			<p>Pentacene and its derivatives</p>
			<p>Vinazene and its derivatives</p>
	Donor	<p>Diketopyrrolopyrrole(DPP) and its derivatives</p>	
	Acceptor/ donor dyad	<p>Oligothiophenes(OT) and its derivatives</p>	
		<p>Triphenylamine (TPA) and its derivatives</p>	
	Acceptor/ donor dyad	<p>Anthradithiophene and its derivatives</p>	
		<p>Oligo(p-phenylenevinylene)-fullerene</p> <p>Zn-phthalocyanine-fullerene</p>	

**TABLE 3 |** Small molecule based on fullerene and its derivatives used in organic solar cells and their structure.

Types	OSCs structure	Donor	Acceptor	Efficiency
Bi-layer	ITO/CuPc/PV/Ag	 CuPc	 PV	1%
BHJ	ITO/CuPc,C <sub>60</sub> /C <sub>60</sub> /BCP/Ag	 CuPc	 C <sub>60</sub>	3.5%
BHJ	ITO/PEDOT:PSS/m-MTDATA/ZnPc,C <sub>60</sub> /n-MPP/Al	 ZnPc	 C <sub>60</sub>	3.37%
BHJ	ITO/MoOx/DTS(P TTh <sub>2</sub> ) <sub>2</sub> ,PC <sub>70</sub> BM/Al	 DTS(PTTh <sub>2</sub> ) <sub>2</sub>	 PC <sub>71</sub> BM	6.67%
BHJ	ITO/DPP(TPFu) <sub>2</sub> ,P CBM /PEDOT:PSS/Al	 DPP(TBFu) <sub>2</sub>	 PC <sub>71</sub> BM	4.4%
BHJ	ITO/PEDOT/BDB, PCBM/Al	 BDB	 PC <sub>71</sub> BM	0.91%



application can be thought of as more than just a functional energy device, especially when considering the colour and relatively thin width of the final cell.

This tuneable colour leads to photonic nanostructures incorporated with photovoltaics capable of producing desirable colours in the visible band and utilise the absorbed light to simultaneously generate electrical powers. In contrast to the traditional colourant-based filters, these devices offer great advantages for electrooptic applications (Park et al., 2011).

Improvements in efficiency and stability, namely, minimising loss mechanisms and improving light harvesting, are required to commercialise this technology (Werner et al., 2010). These organic dyes are also less stable in common working conditions, in high-temperature and high light environments. Although it has been found that some changes to the donor molecule can increase the stability (García-Iglesias et al., 2011), there is still more to be done to create an efficient and stable organic molecule for light-harvesting applications.

Organic solar cells, as one of the most studied types of PVs to date, are based on donor-acceptor heterojunctions and attract increasing interest due to the advantages of light weight, low cost, and flexible as well as due to the fact that a vast range of materials with tuneable band gaps are available (Brabec et al., 2001; Chen et al., 2013). Organic solar cells were first discovered due to the study of the perylene-iodine complex in 1954 (Akamatu et al., 1954). As described in the previous section, the organic solar cell is limited by the low dielectric constant of organic semiconductor, which leads to the slow mobility of electrons and holes and the exciton diffusion length of the charge carrier is significantly limited. It is reported that the diffusion length of organic semiconductor is believed to be 5–20 nm (Lunt et al., 2009). As a result, the thickness of phase separation and the active layer should be extremely carefully controlled. When this is reduced into nanometre ranges, the interface between donor and acceptor materials is enhanced. Thus, new forms of donor-acceptor blended structures can improve the efficiency of PV.

In bulk heterojunction solar cells, the donors are typically organic systems having an electron-rich structure, whilst the acceptor normally shows conjugated  $\pi$  bonds, which due to the electron affinity can be the active part with the role to transport electrons (Figure 8). Another important factor for donor-acceptor is the energy level of the donor and acceptor, which should be well matched. As a result, ideally, in organic bulk heterojunction solar cells, the LUMO of the donor systems should be at least 0.3–0.4 eV higher than the acceptor's LUMO energy level, which is needed to address the efficient exciton dissociation (Mishra and Bäuerle, 2012). At the same time, the bandgap between the donor's HOMO energy level and the acceptor's LUMO energy level should not be too large to become positive to electron exchange. The bandgaps between donor HOMO energy level and the acceptor LUMO energy level determine the open-circuit voltage and a big energy gap can lead to an energy loss, causing a lower open-circuit voltage for the resulting solar cell.

To optimise the performance of a selection of PVs, donor and acceptor material combinations have been studied and tested so

far (Sariciftci et al., 1992). Compared with the use of polymers, small molecules were studied for bulk heterojunction solar cells assembly over a longer period of time, due to the following advantages: relatively easy to prepare and purify and offer a significantly improved reproducibility.

More importantly, with the advancement of supramolecular chemistry, the modification of small molecule of the classes listed in Table 1.1 becomes accomplishable (Mikhnenko et al., 2012). For instance, changing the variety or adding functional side groups became possible, which means that the HOMO and LUMO energy level of the small molecule can be easily tuned. This modification is very important for bulk heterojunction solar cells production and design of other solar cells incorporates small molecule in their systems. It means that solar cells can be designed and optimised not only at the assembly stage but also from the start, despite the careful choice of the material. The small molecule can be classified by their working role in bulk heterojunction solar cells: donor, acceptor, and acceptor/donor dyad, which can simultaneously function as either donor or acceptor depending on the environment (Zhang et al., 2018). Table 2 shows the common small molecule used in organic solar cells.

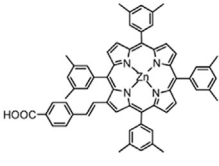
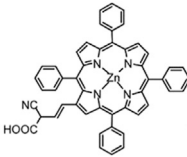
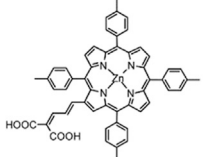
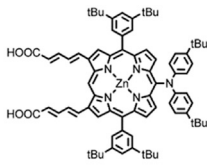
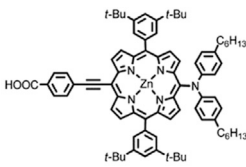
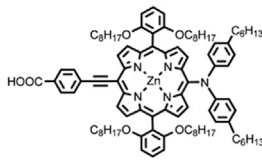
As shown in Table 2, acceptor materials used in organic solar cells can be classified into two groups: one is fullerene and its derivatives, and the other one includes nonfullerene and functional derivatives. From the class of fullerene and its derivatives, PC<sub>71</sub>BM (molecule structure shown in Table 3) shows an impressive performance for its good electron mobility and solubility (Ganesamoorthy et al., 2017).

Recently, the research of acceptor dyad and triad systems based on perylene tetracarboxylic diimide and fullerenes also show promising properties (Chamberlain et al., 2011b). For donor materials, phthalocyanine (Pc) and its metallations present good property in light absorption and had been applied in the first bilayer structure. Also reported by Uchida, a homogeneous layer of CuPc and C<sub>60</sub> homogeneous layer, the active layer corresponds with a C<sub>60</sub> and 2,9-dimethyl-4,7-diphenyl-1,10-phenanthroline cathode. This system exhibits a 3.5% efficiency (Uchida et al., 2004). Diketopyrrolopyrrole (DPP) and its derivatives donor materials also display good properties. A 4.4% efficiency and 0.9 eV open-circuit voltage were reported as using DPP (TBFu)<sub>2</sub> as donor and PCBM as acceptor (Walker et al., 2009). Recently, Zhang reported using modified DPP in organic bulk heterojunction solar cells to enhance the hole mobility from  $4.14 \times 10^{-4}$  to  $7.75 \times 10^{-3} \text{ cm}^2 \text{ V}^{-1} \text{ s}^{-1}$  and raise the fill factor from 27 to 57% when blended with PC71BM (Zhang et al., 2014). Table 3 exhibits some of the small molecules in organic bulk heterojunction solar cells.

## Dye-Sensitised Solar Cells (DSSCs)

Dye-sensitised solar cells-based technologies (DSSCs) are widely studied and longstanding candidates for the current and next generation of solar cells (NREL; Rockett, 2010; Sharma et al., 2018). As mentioned devices above, although it was Edmond Becquerel who discovered the photovoltaic effect (which describes the conversion of sun light into electricity), it was not until 1991 when Grätzel and O'Regan reported the first

**TABLE 4 |** Porphyrin molecules used in some DSSCs which obtain high efficiency.

Types	Dye molecules	Photoelectrode	Efficiency
DSSCs	 Zn-1a	TiO <sub>2</sub>	4.8%
DSSCs	 Zn-3	TiO <sub>2</sub>	5.6%
DSSCs	 GD2	TiO <sub>2</sub>	7.1%
DSSCs	 tda-2b-bd-Zn	TiO <sub>2</sub>	7.5%
DSSCs	 YD2	TiO <sub>2</sub>	11%
DSSCs	 YD2-oC8 co-sensitization of another organic dye	TiO <sub>2</sub>	12.3%

modern dye-sensitised photovoltaic device, thus introducing a mesoporous semiconductor electrode with a high internal surface area which should be an efficiency in the full sunlight of 7.1% (O'Regan and Grätzel, 1991). This discovery led to a paradigm shift in the fields of photoelectrochemistry and photovoltaics in general (Grätzel, 2005). Before the report on Grätzel and O'Regan work, previous efforts to develop DSSCs all failed due to the fact that there was no smooth semiconductor surface introduced, specifically that of the  $\text{TiO}_2$  thin film, in the system. In 2006, Y. Chiba et al. reported a DSSC with an efficiency of 11.1% (Chiba et al., 2006). A typical DSSC includes four major components: photoelectrode, dye molecule, electrolyte, and counter electrode.

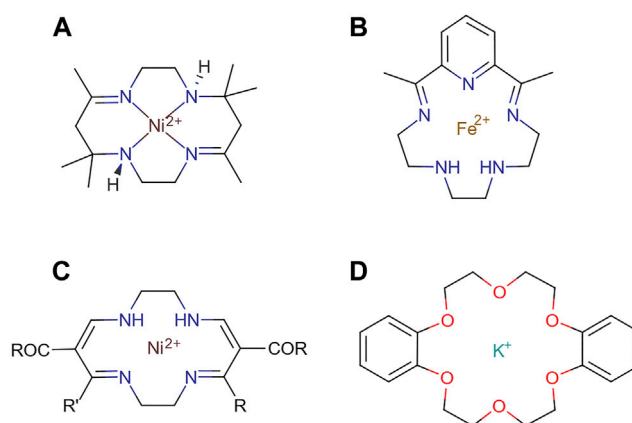
Compared with other types of solar cells, the DSSCs have several different advantages. First of all, the cost of manufacturing a DSSC is relatively low since these combine simple synthetically available organic and inorganic components, which are assembled on the nanoscale leading to the build-up of complicated hybrid structures. Additionally, the fabrication process of DSSCs is relatively simple compared with conventional p-n semiconductor solar cells, where electron-hole pairs are generated in the bulk material and then there is a need for these to diffuse to the p-n interface in order to be extracted. The charge generation in DSSCs only takes place at the material surface; as a result, the requirement for material purity is dramatically reduced. Furthermore, the fabrication process is relatively simple despite the need for specialised equipment; it does not require a high vacuum, ultrahigh temperatures, and processing in a cleanroom (Ito et al., 2008). Due to their layered structure, the DSSCs can be generated by using a printing technique, which makes them accessible to an industrial-scale generation of such device (Ito et al., 2007). The operating principles of DSSCs rely on the following processes: 1) dye molecule photoexcitation, 2) electron ejection, 3) regeneration of dye molecule with electrolyte, 4) recombination of  $\text{TiO}_2$ , and 5) regeneration of electrolyte.

One of the most commonly used wide-gap semiconductors for DSSCs photoelectrodes is  $\text{TiO}_2$  due to the fact that this is a material which is stable and nontoxic and has an energy gap of  $\sim 3.0$  eV. An important requirement for the photoelectrode semiconductor is the high transport mobility of the charge carrier, which is needed to reduce the electron transport resistance (Petermann et al., 2012). As an alternative, ZnO having different nanostructures has been actively been studied in this context due to its similar bandgap and conduction band edge (Matsumura et al., 1977; Matsumura et al., 1981; Jose et al., 2009). Yang et al. also reported a dense array of oriented crystalline ZnO nanowires with a surface area up to one-fifth of that of  $\text{TiO}_2$ , which had a sun conversion efficiency of 1.5% (Zhang and Cao, 2011). Compared to similar ZnO-based devices with power efficiency of up to 1.6%, ZnO nanotube-based cells showed exceptional photovoltage, but the higher surface area may absorb excess dye molecules (Martinson et al., 2007). Besides ZnO, some other binary metal oxides, such as  $\text{Fe}_2\text{O}_3$ ,  $\text{ZrO}_2$ ,  $\text{Nb}_2\text{O}_5$ ,  $\text{Al}_2\text{O}_3$ , and  $\text{CeO}_2$ , and ternary compounds, such as  $\text{SrTiO}_3$  and  $\text{Zn}_2\text{SnO}_4$ , have been also studied and tested as photoelectrodes in DSSC, but their efficiency is significantly lower with respect to that of  $\text{TiO}_2$  (Moharam et al., 2021).

Along with the photoelectrode, a key component of the DSSC is the photosensitiser, a dye molecule, which functions as a light absorber and injects electrons into the conduction band of the photoelectrodes. To be regarded as a competitive dye sensitiser, a molecule should have good solubility in a range of organic solvents, strong light absorption in the visible and near-IR region. The photosensitiser should have anchoring groups, such as  $-\text{COOH}$ ,  $-\text{H}_2\text{PO}_3$ , and  $-\text{SO}_3\text{H}$ ; their role is to bind the dye strongly onto the semiconductor surface. The dye of choice must have good thermal stability and good chemical stability and more importantly, it should also have suitable HOMO and LUMO energy levels to match with other molecular components used in the same DSSCs (Carella et al., 2018). The dye molecule design is made that it does not favour its self-stacking/self-aggregation. It was also reported that, through optimisation of the molecular structure of the dye or by addition of coabsorbers that prevent aggregation, the unfavourable dye aggregation on the semiconductor surface could be avoided and the cell performance can be improved (Mann et al., 2008).

According to reports, coordination complexes of Ru and Os supported by squaraines, porphyrins, phthalocyanines, perylenes, pentacene, cyanines, and coumarins can be used as competitive dye molecules (Hagfeldt et al., 2010). It was reported that the most efficient ( $>10\%$ ) DSSCs incorporate the ruthenium polypyridyl complex N3 and a similar structure slat  $(\text{Bu}_4\text{N})_2 [\text{Ru} (4\text{-carboxy}, 4\text{-carboxylato-2,2-bipyridine})_2(\text{NCS})_2]$  (N719) (Nazeeruddin et al., 2005; Chiba et al., 2006). However, ruthenium is toxic and in low abundance on Earth. Furthermore, ruthenium-based dye molecules are not sustainable options likely to afford the large scale solar cells development in the long term. As stated above, some other types of small organic dyes molecules have also been tested in DSSCs: 9% efficient with indoline (Ito et al., 2006); 6.5% efficient with coumarin (Wang et al., 2007); 5.2% efficient with hemicyanine (Chen et al., 2005); 4.5% efficient with squarine (Yum et al., 2007); 7.1% efficient with porphyrin (Campbell et al., 2007); 3.5% efficient with phthalocyanine (Cid et al., 2007). Rather than changing the type of the supporting ligand and molecule, the substitution of the coordinating metal centre has also been used in dye molecule optimisation (Armél et al., 2011).

As another electron transfer part, the electrolyte plays a very important role in the DSSCs by facilitating the transport of charge between the dye molecule and the counter electrodes. The ideal liquid phase electrolyte and its solution should have low viscosity, negligible vapour pressure, high boiling point, and high dielectric properties. Additionally, factors like robustness, environmental sustainability, and ease of processing also need to be considered prior to DSSCs industrial fabrication. As initially observed by Grätzel for his systems, all reports of efficient DSSCs to date ( $>4\%$  at 1 sun illumination) have utilised the  $\text{I}_3^-/\text{I}^-$  couple as the redox shuttle of choice. The good performance of  $\text{I}_3^-/\text{I}^-$  in these cells was due to the attribution of efficient dye regeneration combined with exceedingly slow electron transfer from  $\text{TiO}_2$  to  $\text{I}_3^-$ . For example, when  $\text{I}_3^-/\text{I}^-$  was employed with compound N3, the regeneration yield was found to be quantitative. In addition, loss



**FIGURE 9 |** Schematic representations of the pioneering examples of molecules forming the building blocks of systems with supramolecular interactions reported by (A) Curtis, (B) Busch, (C) Jäger, and (D) Pederson.

of electrons *via* interception by  $\text{I}_3^-$  is at short-circuit and can be negligible, which allowed photoinjected electrons to be collected with near-unity efficiency (Clifford et al., 2007). Other attempts were also made to find an alternative redox system in DSSCs, for instance,  $\text{Br}_3^-/\text{Br}^-$  (Wang et al., 2005b),  $\text{Co}^{2+}/\text{Co}^{3+}$  (Nusbaumer et al., 2001),  $\text{Fe}^{2+}/\text{Fe}^{3+}$  (Tian and Tatsuma, 2005), triethanolamine (Nakanishi et al., 1998), two pseudohalogen couples  $(\text{SeCN})_2/\text{SeCN}^-$  and  $(\text{SCN})_2/\text{SCN}^-$  (Oskam et al., 2001), and other mixed systems of redox couples. Water-based electrolytes for DSSCs have also been investigated (Murakami et al., 2003b; Law et al., 2010).

Additionally, naphthyl diimides (**Figure 8**) have been explored in the context of organic substrates for PV assembly on basis of their tendency to form n-type over p-type semiconductor materials (Katz et al., 2000). They are versatile materials capable of self-assembly with other aromatic species such as graphene which make them ideal for donor-acceptor systems and are photoactive; also recent microwave technologies gave rise to functional NDIs available in high yield and high purity and easy to isolate. Research led to halogen-modified structures, to study the effect on binding substrates and predict possible device assembly capabilities and performance (Hu et al., 2012; Tyson et al., 2016b). Studies on the incorporation of NDIs in a BHJ OPV in conjunction with a standard p-type material are underway (Rundel et al., 2017; Valero et al., 2020).

As the generation of solar cells developed from both the perspectives of theory and fabrication techniques, the structural improvement of DSSCs benefited from some emerging new ideas of cell design. The evolution of the solar cell technology forms the original idea of the electrolyte-based mesoscopic DSSC (introduced by Grätzel and O'Regan), and after the attempts of replacing the electrolyte with an organic p-type hole conductor, solid-state DSSCs (ssDSSC) were emerged (Murakoshi et al., 1997; Bach et al., 1998). The extremely thin absorbers (ETA) cell as introduced as the dye molecule is replaced with a semiconductor layer (Lévy-Clément et al., 2005; Kamat, 2013). For the *meso*-superstructured solar cell (MSSC), the ETA layer was replaced by a perovskite absorber and the n-type  $\text{TiO}_2$

layer was replaced with a porous insulating scaffold (Lee et al., 2012).

As stated above, the perovskite solar cells and DSSCs are following the similar operating principles but they differ in terms of choice of materials and structure. From a recent review by Henry J. Snaith (2013), three future directions for the DSSCs and perovskite solar cells technology were proposed: firstly, the  $\text{Al}_2\text{O}_3$  could be removed but the perovskite is directly structured to give a porous film which can be subsequently filled with a charge conductor, giving a porous perovskite distributed p–n heterojunction solar cells. Secondly, thin-film p–i–n perovskite solar cells could be addressed, where no porosity is required and the device takes on an intrinsic or ambipolar structure where a thin perovskite film is sandwiched between p- and n-type charge-extracting contacts (Babu et al., 2020). The third possibility includes semiconductor MSSCs, where any solution-processed semiconductor, such as SbS (Itzhak et al., 2009), can be structured by the porous scaffold to deliver the *meso*-superstructured materials. These systems are all currently processed in parallel with current developments in DSSCs.

## PORPHYRINS AS SOLAR ENERGY ABSORBERS

One of the most attractive strategies is the development of organic solar cells that mimic natural photosynthesis in the conversion and storage of solar energy (Hasobe et al., 2005). For this application, porphyrins, with their extensive adsorption throughout the visible spectrum, show great promise as light-harvesting sensitizers for solar cells. Their high electronic excitation energy, typically exceeding 2.0 eV, powers a strong electron transfer, allowing a good conversion between light and chemical/electrical energy (Werner et al., 2010). One of the most attractive strategies is the development of dye molecules in organic solar cells, given that these mimic natural photosynthesis processes in the conversion and storage of



solar energy. As chosen by nature, chlorophylls in plants function as antennae specifically designed to harvest light for the conversion of solar energy in complicated photosynthetic processes. Inspired by natural photosynthesis, scientists already utilised artificial chlorophylls model components, the porphyrins, as efficient light-harvesting centres due to their capability to absorb light and convert to electric energy in solar cells (Eichhorn et al., 1995).

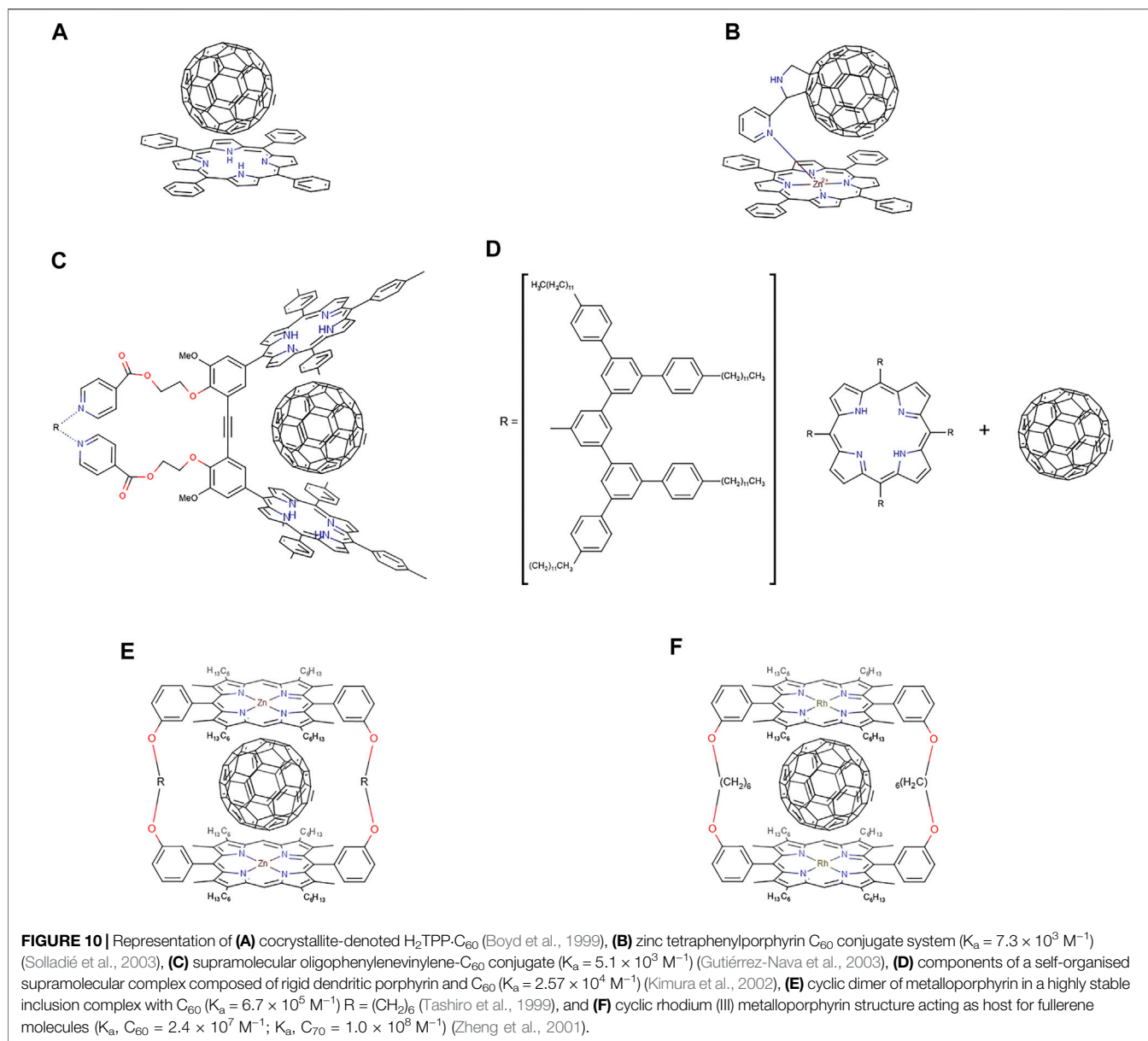
Porphyrins are a group of heterocyclic macrocycle organic compounds, composed of four modified pyrrole subunits interconnected at their  $\alpha$  carbon atoms via methine bridges ( $=CH-$ ) (Figure 8). The porphyrin macrocycle rings have rich redox chemistry and a highly delocalised  $\pi$ -electron system; this structure makes porphyrin useful in both photosynthesis and respiration (Kadish et al., 1999). Porphyrins have also attracted a great deal of attention because of their strong Soret (400–450 nm) and moderate Q-bands (550–600 nm) absorption properties as well as their photochemical and electrochemical stabilities, known synthetic process, and handy control of redox potential by metallation (Xiang et al., 2011). For photochemistry applications, the porphyrin framework provides high electronic excitation energy, normally exceeding 2.0 eV, and this can power a strong electron transfer process, which is essentially the main reason behind the fact that porphyrins have good conversion between light and chemical/electrical energy (Werner et al., 2010). The porphyrins units can incorporate a metal atom through a chemical reaction usually termed as metallation, and the coordination chemistry of the metal centre can be used to introduce additional components and features to the overall assembly of porphyrin motifs as the organic dyes of choice for PV applications. The most common porphyrin systems studied for DSSCs are free-base and zinc derivatives of the *meso*-benzoic acid substituted porphyrin TCP [tetrakis(4-carboxyphenyl)porphyrin]. These have an appropriate LUMO level that resides above the conduction band of  $TiO_2$  and a HOMO level that lies below the redox couple in the electrolyte solution, required for charge separation at the surface of the solar cell (Campbell et al., 2004). All above properties render porphyrin ligands as promising candidates in organic solar cells which allow them to act as “donor” molecule in DSSCs.

There are three main kinds of light-harvesting dye molecules and their recorded DSSC efficiency. The ruthenium-based sensitizers, which were first developed as dye molecules, show high power conversion efficiency, reported at around 10–11%. However, due to the toxicity and availability in low abundance on Earth, the ruthenium-based sensitizers are not suited for large scale fabrication and are not deemed environmentally friendly. The efficiencies of metal-free organic dyes were reported to be 9–10% during the recent 5 years, whereby the best-performed organic dye is C219, reaching  $\eta = 10.3\%$  (Zeng et al., 2010). But, the trend in the performance progress of metal-free organic sensitizers seems to reach a bottleneck for their further development and there was no breakthrough discovery following on once direction has been proposed.

Table 4 shows some of the porphyrin molecules that have been applied and the cell power conversion efficiency. It can be seen that recent porphyrin-based DSSC development shows a promising advance with the progress curve. Porphyrin molecule applied as dye molecule in DSSCs was pioneering as reported by Kay and Grätzel; a mesoporphyrin IX dye was used and achieved a 2.6% (Kay and Graetzel, 1993). From then, there was no breaking research released, until 2004 when Md. K. Nazeeruddin reported that, by using a zinc centre porphyrin, corresponding to Zn-1a in Table 4, the DSSC efficiency can rise up to 4.6% (Nazeeruddin et al., 2004). Followed by their work, by applying Zn-3, Q. Wang and coworkers reported DSSCs with a 5.6% efficiency (Wang et al., 2005a). In 2007, the same group reported porphyrin sensitizers in another series, in which porphyrin GD2 in Table 4 exhibits a 7.1% efficiency (Campbell et al., 2007). As reaching 7.1% efficiency, porphyrins work as dye molecules in DSSCs could compete with organic small molecule even ruthenium sensitizers and open a great opportunity to enhance the efficiency by modifying their structure. In 2009, Kim and coworkers reported a zinc porphyrin (td-2b-bd-Zn) with a diarylamino group and reached an efficiency of 7.5% (Park et al., 2008). More excitingly, Yeh and Diau reported YD2 porphyrin with two long alkyl chains to improve the thermal and photochemical stability and obtain 11% efficiency (Bessho et al., 2010). Grätzel and coworkers reported an optimised performance DSSCs by using YD2-o-C8 and a cosensitized organic dye Y123 (Dualet et al., 2011; Tsao et al., 2011); this cell efficiency can be up to 12.3%; the reason for this promising improvement is due to the upward shift of the  $TiO_2$  conduction band and the enhanced electron lifetime (Yella et al., 2011). The long alkyl chains play an essential role in diminishing the degree of porphyrin dye molecule aggregation.

As described above, the development of cells efficiency goes along with the porphyrin molecule modification. A very obvious modification method for the porphyrin molecule is to convert the free-base porphyrin into metalloporphyrin. Both experimental results and computer simulations have demonstrated that, by adding a metal centre, the absorption behaviours of porphyrin can be varied (Flamigni et al., 2000; Shubina et al., 2007). Zinc porphyrin molecules were the most common and widely used dye molecule in DSSCs due to the low cost and being nontoxic (D'Souza et al., 2001). Alongside metallation of the porphyrin core, the substitution of groups on the porphyrin can also allow tuning of the absorption the wavelengths, tailing of molar absorption coefficient, as a result of the HOMO/LUMO energy level modifications (Baerends et al., 2002; Zhang et al., 2005). As a result, grafting different groups around porphyrin ring have become one of the main pathways to improve electrochemical properties of porphyrins and thus improve the efficiency of DSSCs.

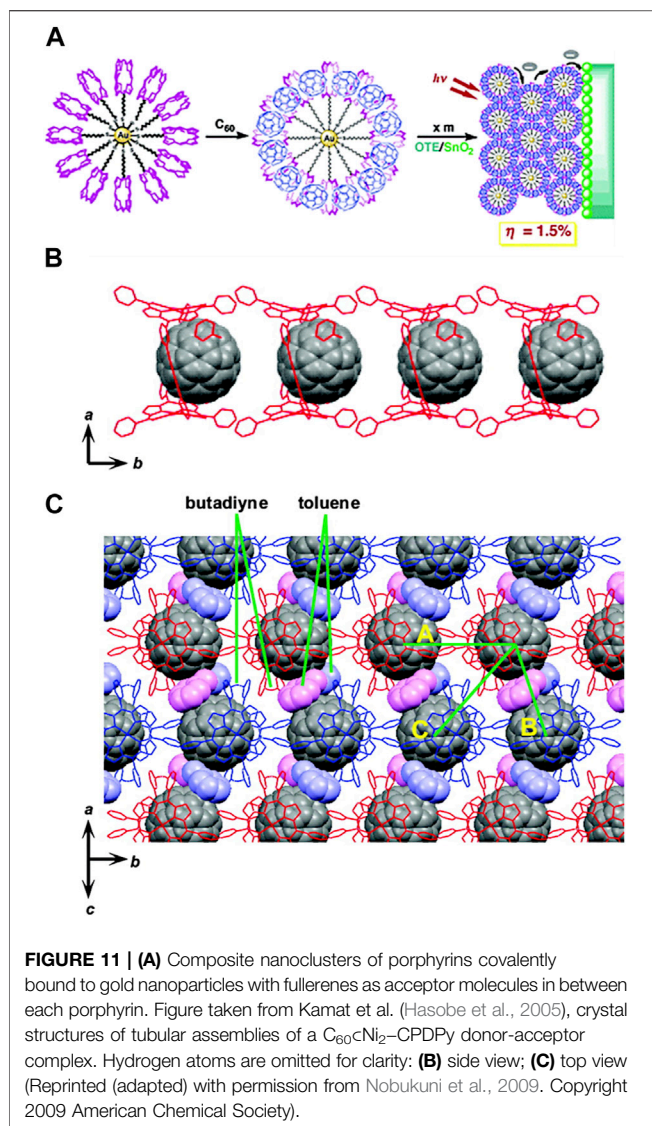
Functionalization and modification of porphyrin ligands have been carried out to overcome the problems presented by unfunctionalized porphyrins, which have previously been used as dye molecules in DSSCs. Porphyrins are highly conjugated and planar systems, which means that porphyrin has an inherent



tendency to self-aggregate in solution at high concentrations. As stated above, the dipole/dipole interactions allow a rapid migration of the excited state between neighbouring dye molecules and this could lead to the annihilation of excitons, which in turn dramatically decrease the dye efficiency. Thus, the modification of the porphyrin ligand should not allow a high level of aggregation to occur. To date, it is generally accepted that the laboratory scale synthesis of the porphyrins is more challenging than that of most other dye molecules under investigation for DSSCs. The main reason is still due to the high aggregation trends but also due to purification issues, as the solubility in the most organic solvent is similar for the starting materials, intermediates, and final product. The flexibility in the synthesis of metalloporphyrins is introduced as much cheaper metals such as iron and zinc can be incorporated, which then contributes to

the tuneable absorption wavelengths due to the nature of the  $\pi$ -electron network (Campbell et al., 2004). By altering the functional groups around the porphyrin, it is possible to alter the  $\pi$ -electron density on the ligand plane, which is then beneficial to the interactions of porphyrins and its versatility in engaging in donor-acceptor interactions is supramolecular system formation. Therefore, the strategy of modifying porphyrin molecules by introducing new functional groups around porphyrin was of interest recently (Wang et al., 2011). Porphyrin-based hybrid systems are able to avoid self-aggregation and capable of altering electron density and the injection pathway is of interest in DSSCs design.

As shown in **Figure 8**, there are two types of positions in the porphyrin molecule that can be used for molecule modification: the four *meso*-positions and eight  $\beta$ -positions. By introducing the



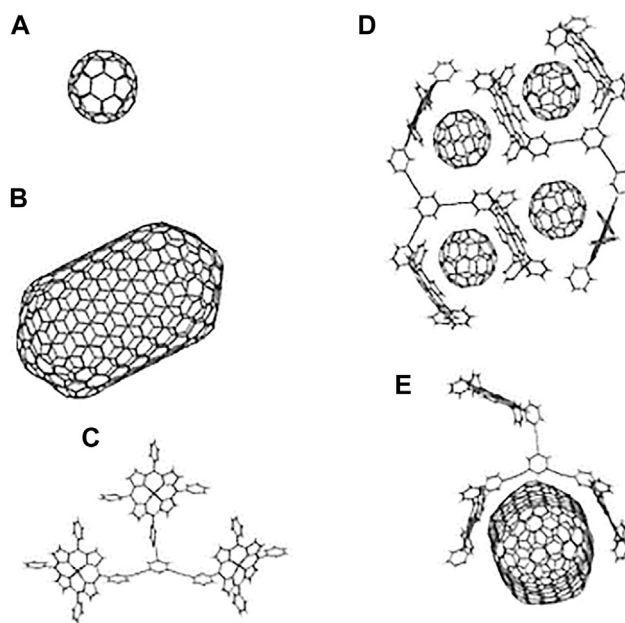
functional group at the  $\beta$ -position, the resulting system can have an enhanced capability of electronic coupling of the dye with the surface of  $TiO_2$ . This concept, to design  $\beta$ -functionalised porphyrin sensitisers, was initially explored by Kim and coworkers (Park et al., 2008). They demonstrated that zinc (II) porphyrin (tda-2b-bd-Zn, shown in Table 4) with two equivalent  $\pi$ -conjugated malonic-acid linkers effectively enhanced the efficiency of electron injection and retarded the charge recombination. Whilst the substituted linkers at the four *meso*-positions of the porphyrin have been used to suppress dye aggregation, the porphyrin YD2 (presented as Table 4) represented an attractive example of a *meso*-position modification. The functional groups introduced can be either highly conjugated groups or long alkyl chains. The long alkyl chains in porphyrins play an important role in diminishing effectively the degree of dye aggregation, which is crucial for an improved device performance since they generate interspace in the extended networks (Ripolles-Sanchis et al., 2012).

Modifications of the porphyrin core through either the *meso*-position or the  $\beta$ -position linkage can lead to efficiency improvements of dye molecule towards DSSCs applications. Regardless of precise positions and choice of functional groups, the role of those modifications needs to overcome the problem of self-aggregation and enhance the electron injection properties when employing porphyrins as dye molecules in DSSCs.

We, and others, focussed on developing new and modified, functionalised porphyrins including of the groups at both the *meso*-position and  $\beta$ -positions (e.g., conjugated groups, and long alkyl chains) on a laboratory scale aiming to improve understand the challenges in the use of these dye molecules in PVs assembly (Mao et al., 2016; Mao et al., 2017; Mao et al., 2019). Substitution of the groups on the porphyrin molecule allows tuning of the adsorption wavelength, molar absorption coefficient, and the HOMO/LUMO levels (Seo et al., 2012). Various studies have shown that chemical substitution of porphyrin derivatives alters the donating efficiency in the DSSCs on the photovoltaic properties, due in part to either metallation modifying the transfer pathway from the porphyrin (Suzuki et al., 2011; Cooling et al., 2012) or the ability of electron-donating or withdrawing groups to increase or lower respectively the level of the (HOMO) of the porphyrin molecule (Archer and Nozik, 2008). Porphyrins with aromatic rings fused to the  $\beta$ -positions of the pyrrole residues are referred to as  $\pi$ -extended porphyrins, with the increased conjugation afforded by the fused rings to the porphyrin macrocycle leading to enhanced light absorption and efficient emission in the near-infrared (near-IR) region of the spectrum (Sommer et al., 2011).

Despite the advantages of using porphyrins as dyes in solar cells, there are still two main problems associated with porphyrin as components of a DSSC. The first is that, due to the highly conjugated and planar systems, porphyrins have an inherent tendency to self-aggregate at high concentrations unless bulky substituents are incorporated to separate the planes. Secondly, dipole/dipole interactions in aggregations allow rapid migration of the excited state between neighbouring dyes, increasing the probability of exciton annihilation (Campbell et al., 2004). It is therefore important to design systems that do not allow a high amount of aggregation to occur as this will reduce the cell efficiency. There are methods to overcome this problem such as protecting the porphyrin with an alkane thiolate. Here, the molecules still exhibit high light-harvesting capabilities whilst suppressing undesirable energy transfer quenching of the porphyrin singlet excited state (Hasobe et al., 2005).

The synthesis of porphyrins is considered more challenging than that of other dyes such as the original ruthenium-based dyes, the main reason being due to the same aggregation which prevents efficient separation during synthesis. However, it is the flexibility in the synthesis of porphyrins, as well as the ability to use much cheaper metals such as iron and zinc rather than ruthenium, which leads to the important properties of the dye (such as the mentioned tuneable absorption wavelengths and varied  $\pi$ -electron systems). Firstly, by altering the



**FIGURE 12** | DFT-level optimised structures for the hosts and guests studied: **(A)**  $C_{60}$  molecule; **(B)** [10,10] capped SWNT; **(C)** simplified tripodal porphyrin host 1 (ZnP); **(D)** a 4 : 2  $C_{60}$ : porphyrin (ZnP) host complex; **(E)** porphyrin host (ZnP) [10,10] capped SWNT composite. Reproduced with permission from Pascu et al. (2008).

functional groups around the porphyrin, it is possible to alter the  $\pi$ -electronic density. This can be beneficial to the rational design of porphyrin-based supramolecular systems, for example, the separation of aromatic compounds via aromatic interactions (such as selective extraction of higher fullerenes) and in the design and synthesis of new materials with optoelectronic properties (Tong et al., 2011). It has also been demonstrated that there may be an optimum sensitizer orientation (or distance from surface) and linker length (or conjugation) dependence, wherein interfacial charge separation is still efficient but the charge recombination is inhibited (Campbell et al., 2004). Altering the structure of the porphyrin allows the tuning of the way it interacts with the surface of the cell, in both distance and orientation. Energy conversion efficiencies as high as 11% have recently been achieved, with a donor-acceptor substituted porphyrin sensitizer and an organic solvent-based electrolyte, thus making this family of dyes attractive for commercial application in DSSCs. The advantages of porphyrin sensitizers include reduced fabrication cost, a simple synthetic pathway, and a larger molar extinction coefficient compared to ruthenium-based sensitizers (Armél et al., 2011).

## Supramolecular Self-Assembly Processes of Relevance to DSSCs

Self-assembly in supramolecular chemistry is concerned with the spontaneous association of molecular components resulting in the generation of either discrete oligomolecular supermolecules or extended polymolecular assemblies (Beer et al., 1999). These multicomponent entities owe

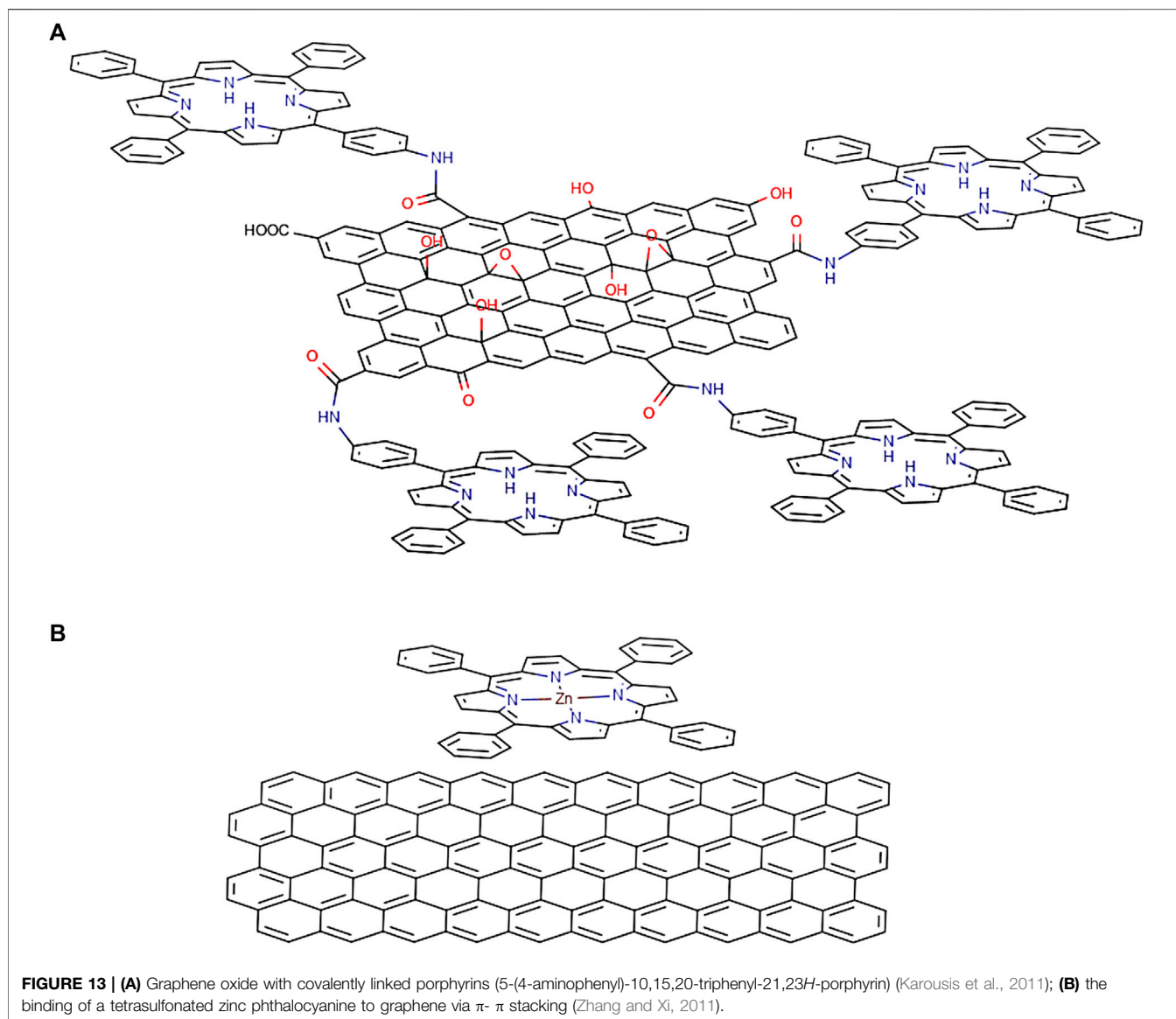
their existence to reversible interactions and so may dissociate and reform in response to particular chemical or environmental changes. The aggregation of these components gives rise to new entities with different properties that often behave in entirely novel and unexpected ways. The entropic loss in the generation of highly organized arrays in supramolecules is outweighed by the overall enthalpic gain (Beer et al., 1999).

Self-assembly may also be defined as the process by which a supramolecular species forms spontaneously from its components (Darcy et al., 2001). Namely, the total intermolecular interaction will rarely be greater than around  $100 \text{ kJ mol}^{-1}$  (whilst the weakest covalent bonds are on the order of  $150 \text{ kJ mol}^{-1}$ ) (Darcy et al., 2001).

The most famous example of supramolecular self-assembly is the double-helical form of DNA found in nature. Acidic hydrogen atoms donate to both oxygen and nitrogen accepting atoms. In synthetic chemistry, however, a range of intramolecular forces are employed including ion-ion interactions, ion-dipole interactions, dipole-dipole interactions, hydrogen bonding, interactions involving  $\pi$ -systems, van der Waals forces, close packing forces, and hydrophobic effects.

The first reported example of a supramolecular molecule, one where two or more molecules are interacting via intramolecular forces, was given by Neil F. Curtis and coworkers in 1961 (Curtis and House, 1961), comprising a Schiff's base macrocycle from acetone and ethylene diamine. Further examples of supramolecular interaction based on this metal-ligand coordination were given by Busch and Jäger in 1964 and Pederson in 1967 with the structures shown in **Figure 9** (Steed and Atwood, 2009).

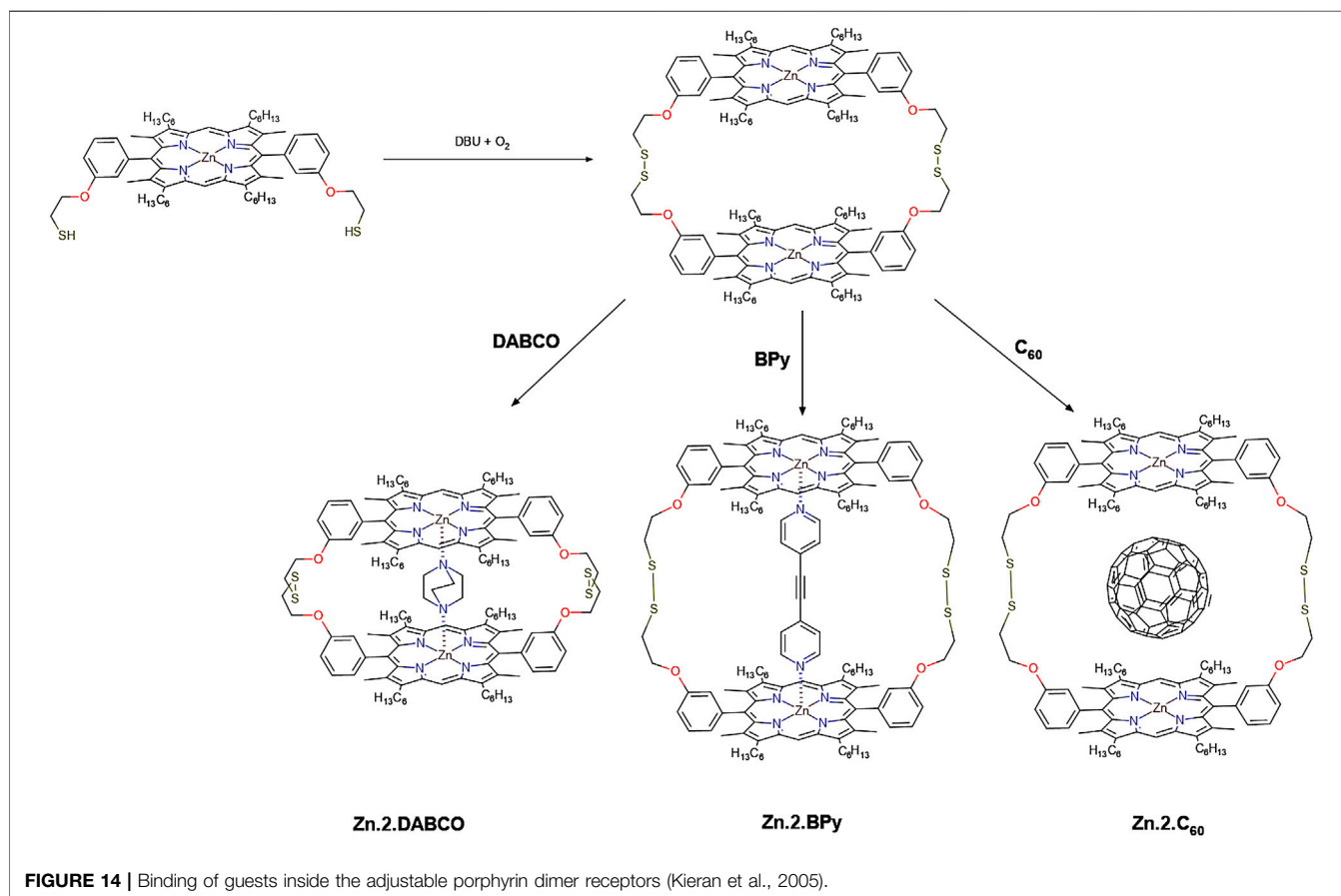




Host systems can be divided into several categories. Those with predominantly electrostatic forces are considered complexes. Those with nondirectional, less specific forces are split into two further categories: *cavitands* which contain intramolecular cavities, i.e., a “hole” in the molecule, and *clathrands* which feature extramolecular cavities (Vögtle et al., 1985). The driving force for the formation of these cavitand and clathrand supramolecular systems is the gain in entropy from the thermodynamically more favourable dense packing within the crystal structures (Cramer, 1956). Perhaps the best way to appreciate the applicability of this noncovalent approach in directing the synthesis of supramolecules is the one-step construction of nanometre-sized molecules using dynamic metal-ligand interactions. In most cases, gentle heating is required to reach thermodynamic equilibrium and the final products (from simple cages, bowls, boxes, capsules, and spheres to

other high-symmetry three-dimensional architectures resembling Platonic and Archimedean solids) with extremely high kinetic stability can be obtained in high yields (Stang and Olenyuk, 1997).

Fullerenes, a class of  $\pi$ -carbon molecules such as  $C_{60}$  and  $C_{70}$  forming ball structures, are spontaneously attracted to porphyrins and metalloporphyrins. This particular type of supramolecular recognition was first discovered with cocrystallates of  $C_{60}$  and  $C_{70}$  with tetraarylporphyrins (Sun et al., 1997) and octaethylmetalloporphyrins (Hoebe et al., 2005). The unexpectedly strong interaction between a curved  $\pi$  surface and a flat  $\pi$  surface ( $C_{fullerene}$ -to-porphyrin plane distance  $\sim 2.7$  Å) is largely van der Waals in origin (Boyd et al., 1999). It is still not possible to reliably predict the type of supramolecular structure that may form in the crystal in a given case, due to the competitive nature of the weak, noncovalent interactions involved and because the



crystal formation is severely affected by subtle differences in the crystallisation environment (reflected often in pseudopolymorphism) (Diskin-Posner et al., 2002).

The combination of porphyrin as an electron donor and fullerene as an electron acceptor seems to be a promising candidate because of the following considerations:

- 1) The high light-harvesting efficiency of porphyrin throughout the solar spectrum.
- 2) Supramolecular complexation between porphyrin and fullerene due to  $\pi$ - $\pi$  interactions (Imahori et al., 1996).
- 3) The efficient production of a long-lived, highly energetic charge-separated state by photoinduced electron transfer (ET) due to the small reorganisation energy involved in the ET (Imahori et al., 1996).

To further give light to these interactions, a macrocyclic extended tetrathiafulvalene (exTTF) host efficiently incorporates  $C_{60}$  or  $C_{70}$  with binding constants that range from  $4.2 \times 10^4$  to  $3.8 \times 10^6 \text{ M}^{-1}$ . The binding is driven in large by charge-transfer interactions (Grimm et al., 2011). To date, three main subcategories of interactions of  $\pi$ -systems, D-H... $\pi$ ,  $\pi$ ... $\pi$ , and cation... $\pi$ , were receiving significant attention in the literature. The  $\pi$ - $\pi$  interaction (stacking  $\sim 0$ – $50 \text{ kJ mol}^{-1}$ ) is a nondirectional, electrostatic attractive force, which occurs when the attraction between  $\pi$ -electrons

and  $\pi$ -framework overcome the unfavourable  $\pi$ - $\pi$  repulsions. This interaction gives rise mostly to typical geometries such as edge to face (herringbone pattern) and offset face to face. Interestingly, it has been reported that a direct face-to-face geometry leads to a repulsive interaction.

Other features such as the polarisation of  $\pi$ -systems by heteroatoms may lead to direct face-to-face geometry. Such interactions are of significance both in nature (e.g., DNA structure) and in artificial systems, but are difficult to predict and control (due to their weak directionality and strength). The cation... $\pi$  interactions ( $5$ – $80 \text{ kJ mol}^{-1}$ ) occur between metallic or organic cations and aromatic or double/triple bonded regions of the molecule. These are based on electrostatic forces but relate also to the polarizability of the aromatics and have been associated with ion-induced dipole, donor-acceptor, charge-transfer, or dispersion forces interactions.

## Porphyrin Host-Guest Chemistry

Key components of the porphyrin (acting as a “host”) contribute to the supramolecular interaction through  $\pi$ - $\pi$  interactions (from the extended aromatic  $\pi$  ring). Free-base porphyrins are capable of D-H- $\pi$  interactions and metal porphyrins can form cation- $\pi$  interactions to the neighbouring aromatic systems. Extensively conjugated  $\pi$ -frameworks such as these give rise to rich electrochemical and photophysical properties. The valuable

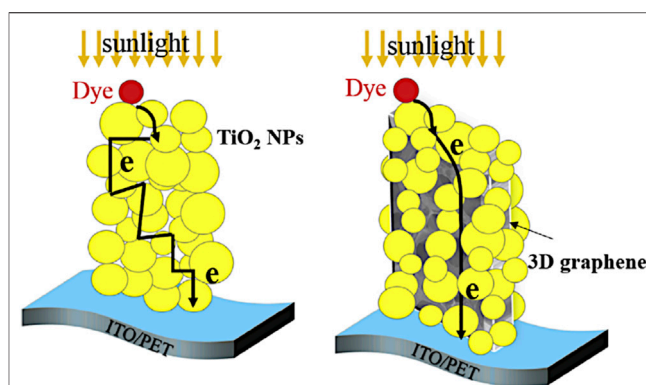
spectroscopic properties of porphyrins (UV; NMR) help monitor reaction progress and also facilitate the characterisation of the final product. Moreover, the insertion of various metal ions into the porphyrin centre offers almost infinite possibilities for coordination and photophysical chemistry (Smith et al., 2002).

Broadly divided into two main categories, the assembling process can be achieved through axial coordination or bridging through external metal centres. Because of their photochemical and biomimetic properties and also the relatively large association constant ( $\sim 10^3 \text{ M}^{-1}$  in chlorinated solvents), porphyrin assemblies relying on the Zn-N (pyridine or imidazole) interactions are well-documented (Sessler et al., 1995).

## Porphyrin-Fullerene Blends

Porphyrin-fullerene supramolecular or covalently linked systems are considered to be very interesting classes of compounds due to their rich photo- and redox chemistry, remarkable photoactive, structural, and magnetic properties (Vijayaraghavan et al., 2012). Fullerenes present extraordinary electron-accepting characteristics, promoting ultrafast charge separation and exhibiting very slow charge recombination characteristics due to the low reorganisation energies involved. This in turn leads to the generation of a long-lived charge-separated state and a high quantum yield (D'Souza and Ito, 2009). The curved  $\pi$  surface of  $\text{C}_{60}$  shows a tendency to interact with other molecules, making it an interesting target for engineering supramolecular arrays (Boyd et al., 1999). Hoffman in 1995 (Eichhorn et al., 1995), looking for charge-transfer molecular crystals, obtained the crystal structure of octakis(dimethylamino)porphyrine with  $\text{C}_{60}$  in a three-dimensional network where each  $\text{C}_{60}$  is sandwiched between two porphyrines. With these crystals grown from toluene solution, they determined a distance from the centre of the porphyrine to the centroid of the fullerene of  $6.3 \text{ \AA}$  and they established the existence of van der Waals contact between them. As such there are numerous examples of combinations of porphyrins and fullerenes in the literature, both covalently (D'Souza et al., 2001; Imahori and Fukuzumi, 2004; Cho et al., 2005; Lehtivuori et al., 2006; Schuster et al., 2006; Uneyama and Imahori, 2006; Mathew et al., 2008; Iehl et al., 2011; Charvet et al., 2012; Tolkki et al., 2012) and noncovalently bound (Boyd et al., 1999; Konarev et al., 2002; Hasobe et al., 2005; D'Souza and Ito, 2009; Fathalla et al., 2009; Konarev et al., 2009; Nobukuni et al., 2009; Bhyrappa and Karunanithi, 2010; Hasobe, 2010; Oku et al., 2010; Wessendorf et al., 2010; Iehl et al., 2011; Kahnt et al., 2011; Sprafke et al., 2011; Wang et al., 2011; Konarev et al., 2012).

In 1997, Boyd & Reed (Sun et al., 1997) investigated if monosubstituted fullerides ( $\text{C}_{60}^{1-}$ ) retained much of its parent  $\text{C}_{60}$  character. They prepared a pyrrolidine-linked tetraphenylporphyrin/ $\text{C}_{60}$  dyad and found that, in the solid state, it packs forming self-assembled dimers. In two distinct crystallographic contacts, intradimer and interdimer, the distance between the closest  $\text{C}_{60}$  carbon atoms to the mean plane of the 16-atom inner core of the porphyrin ring is very short:  $2.78 \text{ \AA}$  (interdimer) and  $2.79 \text{ \AA}$  (intradimer). Graphite and other typical arene-arene separations are in the range of  $3.3\text{--}3.5 \text{ \AA}$ , porphyrin-porphyrin separations are  $>3.2 \text{ \AA}$



**FIGURE 15 |** Schematic illustration of the devices and electron transport path without and with graphene (ITO-indium tin oxide; PET-polyethylene terephthalate) (Zhi et al., 2015).

(Hunter, 1994), fullerene-arene separations lie in the range  $3.0\text{--}3.5 \text{ \AA}$  (Balch and Olmstead, 1999), and fullerene-fullerene separations are typically ca.  $3.2 \text{ \AA}$ . This observation suggested that the  $\pi$ - $\pi$  interaction between  $\text{C}_{60}$  and the porphyrin unit is substantially augmented probably due to strong donor-acceptor interactions. In contrast to the usual view of  $\text{C}_{60}$  as an acceptor, the sense of this donor-acceptor relationship might be with  $\text{C}_{60}$  acting as a donor and the porphyrin unit being the acceptor. If this was the case, one could expect that the more electron-rich bonds of the fullerene (6:6 junctures) should preferentially interact with the porphyrin unit.

In 1999, Boyd & Reed (Boyd et al., 1999) showed that the association of  $\text{C}_{60}/\text{C}_{70}$  and tetraphenylporphyrins (TPPs) is also found in untethered cocrystallates and that this type of interaction also exists in solution. The TPPs used in the study possess aliphatic substituents and favourable "solvation"  $\text{CH}-\pi$  interactions of these residues with  $\text{C}_{60}$  and  $\text{C}_{70}$  were observed in the solid structures. This seems to be the next most important type of interaction in these systems after  $\pi$ - $\pi$  interactions and is consistent with the relative solubility of  $\text{C}_{60}$  in arenes versus alkenes (Ruoff et al., 1993).

Ito et al. (Nojiri et al., 1998) in 1998 described an ET process that occurs when one of the two partners, the fullerene or the Zn porphyrin, is photoexcited and encounters the other in solution. It is a bimolecular process controlled by diffusion and it is possible if the concentration of the two species is high (they work around  $10^{-4} \text{ M}$ ). The transient absorption bands for highly conjugated molecules such as  $\text{C}_{60}/\text{C}_{70}$  are supposed to appear in the near-IR region of the spectrum. When the  $\text{C}_{60}/\text{C}_{70}$  chromophore was predominantly photoexcited, ET took place from the ZnTPP ground state to the lower energy triplet excited state of the fullerene,  $3\text{C}_{60}^*/3\text{C}_{70}^*$ , yielding the corresponding fulleride ( $\text{C}_{60}^{\cdot-}/\text{C}_{70}^{\cdot-}$ ). On the contrary, when the species predominantly excited was the ZnTPP unit, it is the triplet state  $3\text{ZnTPP}^*$  that donates the electron to the ground state of the fullerene producing the corresponding anion radical  $\text{C}_{60}^{\cdot-}/\text{C}_{70}^{\cdot-}$ . The efficiency of the ET via photoexcitation to the triplet state of the fullerene is higher than the route involving the ZnTPP triplet state. This work highlights the potential of these systems as electronic materials.

In 1999, Diederich et al. (Armaroli et al., 1999) reported the binding of ZnTPP with a methanofullerene derivative bearing a pyridyl moiety. The photophysical properties of the assembly were studied and compared to the analogous fullerene monomalonate without the pyridyl group, which did not show any sign of complexation with the ZnTPP at  $\mu\text{M}$  concentration. The association constant value determined for the 1:1 complex,  $3\bullet\text{ZnTPP}$ , using  $^1\text{H}$  NMR titrations in  $\text{C}_6\text{D}_6$  solution was  $K_a = 3.6 \times 10^3 \text{ M}^{-1}$ . This value is in good agreement with the one derived from the luminescence experiment in toluene,  $K_a = 3.0 \times 10^3 \text{ M}^{-1}$ .

The addition of large amounts of fullerene to the solution of ZnTPP produced a 50% diminution of the porphyrin fluorescence. Moreover, the absorption spectrum of the mixture showed a 10 nm redshift in the Soret band with respect to the free ZnTPP. A similar redshift is characteristic for axial binding of pyridine ligands to zinc porphyrins. This was the first noncovalent assembly, using coordination chemistry, reported in solution between fullerene and a porphyrin.

The fluorescence quenching of porphyrin in the presence of fullerene was attributed to a fast photoinduced energy transfer to the fullerene unit. Nevertheless, this statement is simply based on the reported preference of ET to occur in toluene when the porphyrin and the fullerene moieties are facing each other, whilst energy transfer happens when the components are located at longer distances (Kuciauskas et al., 1996). Additional proof favouring this hypothesis was derived from the known fast energy transfer mechanism reported through noncovalent bonds (Armaroli et al., 1997).

The reasons for this porphyrin-fullerene compatibility have been attributed to many factors. Among these are compatible shapes leading to numerous van der Waals contacts (Armaroli et al., 1997),  $\pi$ - $\pi$  interactions between the fullerene surface and the porphyrin plane (Sun et al., 2000), charge-transfer interactions between the metal ions, such as Fe(II) or Co(II), and the fullerene acting as an electron acceptor (Sutton et al., 2004) or between the metal ion, e.g., Fe(III) and a fullerene acting as an electron donor (Evans et al., 1999), whilst dispersive (Liu and Schneider, 2002) and electrostatic interactions (Wang and Reed, 2003) were also considered. A recent review by Boyd and Reed (2005) summarises the complexity of the porphyrin-fullerene interactions and concludes that is “essentially van der Waals in nature but is perturbed by weak electrostatic and possible charge-transfer effects.”

**Figure 10** shows a selected range of supramolecular complexes of porphyrin-fullerene complexes which demonstrate the variety of interactions between the two molecules. Where known, the association constant ( $K_a$ ) has been included to highlight the strength of these interactions.

In addition to supramolecular architects, covalent interactions allow the orientation and distances between the donors and acceptors to be designed prior to synthesis. Usually, highly conjugated connectors are used to allow for an efficient ET; however, this disrupts the  $\pi$ -electron system of the fullerene. Noncovalent binding and hydrogen bonding allow for the charge transfer without disruption of the  $\pi$ -system, as well as requiring no energy input to form the complex. This also means that the nanomaterials have scope

for recycling as the two can be separated simply in solution by competitive solvation. However, the binding is understandably a lot weaker with noncovalent systems as it is limited to  $\pi$ - $\pi$  interactions. Noncovalent binding however allows for some more creative systems, examples of which are shown in **Figure 11**.

A study by Kamat et al. demonstrated the importance of the metal centre within the porphyrin. They proved that the driving force of charge separation between excited zinc porphyrin and  $\text{C}_{60}$  is larger than a free-base porphyrin because the one-electron reduction potential of the singlet excited state of ZnP ( $-1.0 \text{ V}$  vs. normal hydrogen electrode (NHE)) is more negative than that of  $\text{H}_2\text{P}$ . Similarly, the shape of the acceptor fullerene molecule was also important, where replacing  $\text{C}_{60}$  with  $\text{C}_{70}$  as an electron acceptor in the composite electrode system may have different steric effects on the accommodation of  $\text{C}_{70}$  between two porphyrin rings as compared to  $\text{C}_{60}$  (Hasobe et al., 2005).

As mentioned before, one of the major reductions in efficiency arises from the recombination of charge carriers subsequent to absorption of a photon. Interface properties determine the electronic energy alignment in donor/acceptor interfaces and play an important role in controlling how the charge is separated and therefore preventing recombination (Kahnt et al., 2011). For example, a key issue in the electronic structure of organic interfaces is the donor-acceptor energy level alignment (Sai et al., 2012).

It is clear that this optimised orientation and energy level alignment are the most crucial elements to highly efficient light-harvesting properties. In some cases the stacking of porphyrin and fullerene molecules lead to interactions between the continuous domains of each, allowing for charge transfer in an oligomer-like manner (Wang et al., 2011). It is also possible for the porphyrins to form a single plane upon which the fullerene can then be deposited which can facilitate the efficient charge transport in heterojunction based solar cell devices (Zhong et al., 2012). A DFT study by S. Vijayaraghavan et al. showed that not only can the porphyrin molecule change its shape to a bowl-like structure to accommodate the fullerene molecule, but also the fullerene existed in three separate orientations, each with a unique level of conductance (Vijayaraghavan et al., 2012).

The interactions of porphyrins and fullerenes are still proving to be a widely researched topic, with applications in bulk heterojunction solar cells being the predominant application. There is still a wide range of porphyrins to synthesise, as well as many aspects of the interactions to solve meaning that this field has a lot of scope for further study.

## Carbon Nanotubes and Porphyrin Composites

Single-walled carbon nanotubes (SWCNTs) have recently become the focus of intense multidisciplinary study due to their unique structure, high mechanical strength and good chemical stability. They have been explored for several applications, ranging from solar cells to drug delivery, with each application requiring some modification of the nanotube. For their application in solar cells, SWCNTs can be seen as an



expansion of a fullerene and thus fullerenes can be used to predict the interactions of porphyrins and nanotubes.

The advantage of using nanotubes is that not only is there the potential for several donor molecules per acceptor, but also due to the ballistic movement of electrons through the nanotube, the charge carriers can move through the nanotube from one donor to another almost at the speed of light (Mathew et al., 2008). Much like the noncovalent fullerene composites, supramolecular functionalisation of single-walled carbon nanotubes (SWNTs) has become a field of growing interest as this does not alter the  $sp^2$ -bonded nanotube walls, thus maintaining the physical properties of the carbon nanotubes (Pascu et al., 2008). Noncovalent complexation is also an important method for improving the solubility of nanotubes and for introducing functionality, whilst not damaging the electronic structure. Composites based on this concept are being developed for sensors, field-effect transistors, hydrogen generation, and biomedical applications (D'Souza and Ito, 2009; Sprafke et al., 2011) (Figure 12).

## Graphene and Related 2D Carbon Nanomaterials in Porphyrin-Based Composites

A graphene sheet is essentially a dissected SWCNT and preserves the merit as a good electron acceptor due to its low reduction potential but does not suffer from the drawback of carbon nanotubes that could be either metallic or semiconducting (Zhang and Xi, 2011). Additionally, transparent, conductive, graphene electrodes for DSSCs have been reported, thus highlighting another potential utility of graphene in future nanotechnological applications (Karousis et al., 2011).

Ongoing research work to investigate porphyrin-carbon nanomaterial interactions is aimed at advancing the understanding towards improved porphyrin-based nanohybrids (Figure 13). The development of donor-acceptor based materials for solar cell applications is hampered by the limited availability of functional porphyrins accessible mainly on an analytical scale (Tong et al., 2011). Their laboratory scale synthesis and purification still represented significant challenges and the full understanding of their interactions with fullerenes and carbon nanomaterials represented uncharted territory.

Porphyrin cores used as either zinc(II) substituted or free-base centres as well as the incorporating peripheral substituents are meant to allow the fine-tuning of the electron density in the  $\pi$ -system. The inclusion of lengthy organic groups as the design elements was used as they were deemed necessary not only to help to “wrap” around carbon support (fullerene or carbon nanotube) to increase the binding strength but also to help to prevent self-aggregation due to aromatic stacking.

Approaches for functional porphyrins evolved from that initially designed for analytical work to a scalable process and is now amenable to laboratory scale synthetic routes (milligrams scale and beyond). Synthesis of functional porphyrins incorporating metal ions and/or lengthy organic chains as peripheral substituents was found to offer the additional

practical benefit in that the separation of the final product is much simpler than that of standard porphyrin compounds reported to date, which do not incorporate long hexyl chains.

## Interactions Between Within Porphyrin Molecules and Carbon Nanomaterials

As stated above, fullerenes are suitable systems acting as electron acceptor materials of relevance to organic solar cells, due to their capability of acting as highly efficient ET reduction media (Hunter, 1994). In some types of organic solar cells, the efficient induced ET occurs at the interface between the donor molecule and the fullerene layer interface. Whilst porphyrins can be regarded as one of the most efficient dye molecules in DSSCs due to present remarkable light-harvesting ability, as discussed above, their application in the presence of fullerenes, giving rise to donor and acceptor complex systems, seems to be ideal as an approach in solar cells applications. Figure 14 shows an example of the fullerene-porphyrin complex and its supramolecular assembly.

Porphyrins and fullerenes are known to form supramolecular complexes, which contain close contacts between one of the electron-rich module led ring bonds of the guest fullerene acting as a “donor” and the molecule of the host porphyrin acting as a “host” (Sun et al., 1997; Boyd et al., 1999; Sun et al., 2000; Sun et al., 2002a; Sun et al., 2002b). The contact distances in porphyrins and  $C_{60}$  are of the order of 2.7–3.0 Å, which is much longer than normal metal-olefin bonding distances commonly found in organometallic complexes (Balch and Olmstead, 1999). The porphyrin-fullerene interaction energies are reported to be in the range from –16 to –18 kcal mol<sup>–1</sup> (Wang and Lin, 2003), which is a very strong force capable of driving the formation of porphyrin and  $C_{60}$  supramolecular complexes. The interactions between porphyrin and fullerene can be explained by  $\pi$ - $\pi$  interaction involving van der Waals forces. But, it is worth noticing that, in a study by Reed, a free-base porphyrin was found to bind to a fullerene exhibiting a more strong link than metalloporphyrins and a suggested explanation was due to the importance of electrostatic interactions involved. The noncovalently binding and hydrogen bonding allow the charge transfer without disruption of the  $\pi$ -system. Also, no additional input energy is required at the formation of such hybrids. In some cases, the metal centre in the metalloporphyrin can be linked with  $C_{60}$  in a combination with metal-ligand coordination interaction. An example is shown in Figure 14 and this linking strategy also provides a novel noncovalently bonding type in fullerene-porphyrin complex design.

The functionalised Zn(II)-porphyrins of interest for this project have been isolated on an analytical scale for dynamic combinatorial chemistry studies. Dynamic combinatorial chemistry methods were also applied to generate new compounds held together by fullerene and porphyrin donor-acceptor interactions. Dynamic combinatorial chemistry relies on molecular recognition and is a new approach to synthesise molecules and their complexes on an analytical scale (Corbett et al., 2006). Dynamic combinatorial libraries were carried out by

linking simple building blocks together with a reversible reaction under thermodynamic control. The libraries are allowing a constant interchange of building blocks resulting in a mixture of library members in equilibrium (Corbett et al., 2006). In the fullerene and porphyrin system, the dynamic combinational concept was applied by regarding a porphyrin dimer as a receptor and fullerene as a guest. Amy L. Kieran reported several approaches in porphyrin and fullerene dynamic combinatorial chemistry, but the limitation of that work was the tiny scale on which the new compounds were isolated (Kieran et al., 2005; Kieran et al., 2005).

The combination of fullerene and porphyrins can also be addressed by covalently linking such molecules (Drovetzkaya et al., 1995; D'Souza et al., 2002; de la Torre et al., 2005). The covalent binding or the donor and the acceptor allow the orientation and distances between porphyrin and fullerene to be designed in advance. In the covalently linked complexes, highly conjugated linking groups are employed to allow for an efficient ET, but this change can alter the  $\pi$ -electron system in both the porphyrin and the fullerene systems.

It has been shown that complexes incorporating a fullerene and a porphyrin show great promise as synthetic scaffolds for new functional materials for photovoltaic applications but due to the synthetic challenges so far, only a few investigations into the device fabrication based on porphyrin oligomers and carbon nanotubes or graphene/graphene oxide could be carried out (Murakami et al., 2003a). It is known that, from the class of carbon-based nanomaterials, carbon nanotubes and graphene/graphene oxides also have promising electronic and mechanical properties in their own right, which makes them even more interesting when combined with porphyrin molecules as the resulting nanohybrids can act as a donor and acceptor system. Nakashima first reported that a complex formed by porphyrin and single-walled carbon nanotubes via noncovalent interactions (Murakami et al., 2003a). After this study, some research has been carried out in this area: Raghu Chitta reported zinc (II)-porphyrin noncovalently linked to single-walled carbon nanotubes and showed that these syntheses are held together by  $\pi$ - $\pi$  interactions (Chitta et al., 2007). The covalent linking strategies were investigated to an even more limited extent: Zhen Guo reported a method to covalently link porphyrin with SWNTs by a diazonium group (Guo et al., 2006). Similar reactions were carried out between graphene/graphene oxides with a porphyrin substrate. Nikolaos Karousis reported a covalently linked porphyrin with graphene by diazonium group, as a direct adaptable converting from Zhen Guo's research (Karousis et al., 2012). In 2012, Murali Krishna reported a covalently linked porphyrin and graphene oxide with metal or metal-free porphyrin by using the defects group on the edge of graphene oxide (Krishna et al., 2012).

New modes of assembling between carbon nanomaterials and porphyrins are being investigated. These showed great promise as new synthetic scaffolds for functional materials for photovoltaic applications (Tong et al., 2008). Our new nanohybrids have been designed to incorporate with SWNTs and graphene/graphene oxide and explore by both supramolecular self-assembly method (which typically leads to the  $\pi$ -system of the carbon

nanomaterials to remain unaltered) and a more synthetically demanding route, living a covalent approach to link the donor and acceptor (but disruptive for the experimental aromatic synthesis) (Tong et al., 2008).

## CARBON NANOMATERIALS

As one of the most abundant elements on the planet, carbon is the *materia prima* for life and the basis of all organic chemistry. Other than the naturally formed carbon allotropes, human-made carbon allotropes also presented promising properties. Fullerenes, regarded as zero-dimensional materials are the molecules where carbon atoms are arranged spherically and carbon atoms in this molecule fill the  $sp^2$  orbital (Andreoni, 2000). Recently, Andrey Chuvilin et al. directly visualised a process of fullerene formation from a graphene sheet using aberration-corrected transmission electron microscopy (Chuvilin et al., 2010a). Carbon nanotubes can be regarded by rolling graphene sheet along a certain direction and then relinking the carbon bonds. Thus, carbon nanotubes can vary in length and be thought of as one-dimensional material. The discovery of carbon nanotubes was converted from  $C_{60}$ . The synthesis of multiwalled carbon nanotubes (MWNTs) was firstly reported by Iijima in 1991 (Iijima, 1991), as a result of an experiment where he pursued the synthesis of fullerenes via the arc discharge method. After further study, single-walled carbon nanotubes (SWNTs) were then reported in 1993 (Iijima and Ichihashi, 1993), and a method was specifically designed to produce such higher fullerenes by adding transition-metal catalysts (for example, Ni and Y) to the graphite in an arc discharge method. Since then carbon nanotubes have been extensively considered for applications in many different research fields, due to their structural, physical, and electronic properties such as high chemical and thermal stability, high elasticity, tensile strength, metallic conductivity, and large surface area (Terrones, 2003). SWNTs have diameters 0.5–5.0 nm (commonly around 1–2 nm), whereas the diameter of MWNTs is 2–100 nm (commonly around 10 nm). The lengths of carbon nanotubes are typically in the micrometres range, but in some reports, it has been shown that these can be up to millimetres or even centimetres (Zhu et al., 2002). The inner space of carbon nanotubes, which are encapsulated, is employed as a nanoreactor, to monitor or control the reactivity of fullerene and other small molecules to form some unusual supramolecular and covalent structures (Khlobystov, 2011).

## Functionalisation of Carbon Nanotubes

The functionalisation of carbon nanotubes has already become a very important research field. As some functional groups are grafted on the surface or trapped within the inner space of carbon nanotubes, those functional groups can alter the properties of carbon nanotubes, such as increasing the SWNTs solubility, exfoliate and monodisperse bundles of the tube, include higher-order structures using self-assembly, and so on. Although the functionalisation of SWNTs has attracted some significant attention, the chemistry of functionalised carbon

nanotubes is very challenging due to the poor solubility and low reactivity of the SWNTs. The functionalised results could be very hard to characterise due to batch-to-batch recording in SWNTs starting materials available.

The strategies of functionalisation of carbon nanotubes could be divided into five types: 1) surface defect-group functionalisation, 2) covalent sidewall functionalisation, 3) noncovalent stacking functionalisation with surfactants, 4) noncovalent stacking functionalisation with polymers, and 5) endohedral functionalisation with nanoparticles. The covalent functionalised strategies include surface defect-group functionalisation and covalent sidewall functionalisation. The oxygen-containing surface defects can be introduced onto the surface of SWNTs by oxidation reactions (Zhang et al., 2003). It has been reported that the use of highly reactive reagents to directly attack the side wall is another way to functionalise carbon nanotubes (Strano et al., 2003). The use of reactive agents and methods, borrowed and adapted from  $C_{60}$  chemistry, such as the Bingel (Coleman et al., 2003) reaction and radical trapping reaction (Liu et al., 2006) have been particularly successful.

It has been found that the noncovalent functionalisation strategies for carbon nanotubes can avoid the introduction of defects into the carbon nanotubes structure. The noncovalently functionalisation methods are based on surface association and van der Waals Interactions (Rance et al., 2010). For example, a lot of effort has been devoted to study the interaction between long chains of DNA and nanotubes (Meng et al., 2007; Tu et al., 2009). It is believed that the nanotubes are in the hydrophobic interiors of the corresponding micelles, which results in stable dispersions. When the hydrophobic part of the amphiphile contains an aromatic group, an especially strong interaction results, because of an effective and cooperative, extended  $\pi$ - $\pi$  stacking interactions which can then be formed with the graphitic sidewalls of the SWNTs. This effect was demonstrated in the aggregation of CNTs with N-succinimidyl-1-pyrenebutanoate (Chen et al., 2001).

For the endohedral functionalisation strategy,  $C_{60}$  molecules have also been found to be encapsulated into the inner space of nanotube to form a hybrid  $C_{60}$ @SWNTs structure (Okada et al., 2001; del Carmen Giménez-López, 2011). Filling nanotubes with metal nanoparticles have been also successful in both original growth methods (Demony et al., 1998) and liquid phase filling methods (Hsin et al., 2001; del Carmen Giménez-López et al., 2011). Research reporting the encapsulation of metallofullerene has also been published (Chuvilin et al., 2010b; Zhang et al., 2011; Chamberlain et al., 2011a; Maggini et al., 2014). It is also reported that graphene nanoribbons are easier self-assembly together inside the inner space of carbon nanotubes (Chuvilin et al., 2011). Since carbon nanotubes are highly heterogeneous, many functionalisation techniques have been used in an attempt to separate single-wall nanotubes samples, which include dielectrophoresis, selective functionalisation, wrapping with DNA and density gradient centrifugation (Hersam, 2008). All those methods are limited to small volume and low yield, but once the single-walled carbon nanotubes are separated, the unique diameter and chirality of SWNTs could be studied, and it was

shown that, depending on diameters and lengths, such SWNTs can be highly coloured (Tu et al., 2009).

## Carbon Nanotubes as Synthetic Scaffolds for Photovoltaics

Carbon nanotubes have a variety of attractive features which make them a suitable material for electrochemistry: high electrical conductivity; natural hydrophobic and adjustable porosity. One application for which these have been widely studied results in the use of carbon nanotubes in electrochemistry, and the application of carbon nanotubes as substrates is considered for the improvement of traditional solar cell electrode designs. In addition, the carbon nanotube can absorb light in both UV and near-IR range. It has been investigated that the use of SWNTs can add benefits both in terms of performance and durability of PVs (Du Pasquier et al., 2005; Rowell et al., 2006).

For organic bulk heterojunction solar cells, the diffusion ranges of excitons remained a problem since the diffusion can only occur in a couple of nanometres near the interface between donors and acceptors. In this case, one of the improvements of OSCs is the introduction of mixed donor and acceptor species and provides the device with a much larger contact interface between donors and acceptors. The diffusion range of excitons in an organic photovoltaic device is approximately in the order of 10 nm. When mixing the donors materials and carbon-based nanomaterials acceptor materials together, the actual size of the donor layer and that of the acceptor are smaller than the diffusion range and the domain can be reduced to several nanometres. Thus, the excitons can diffuse to the interface much easier and quicker. SWNTs can potentially be applied as the acceptor material in this improvement, due to their unique properties, like low electrical resistance and large surface area. Until recently, followed by this principle, some studies reported that SWNTs have been introduced in OSCs as the acceptor materials (Cataldo et al., 2012). Luyao Lu and coworkers have demonstrated a method to use N-doped multiwall carbon nanotubes as acceptor materials which led to the achievement of highly efficient polymer bulk heterojunction solar cells (Lu et al., 2013). It has also been found that, in DSSCs, the electron injection from the excited state of the dye molecule occurs on timescales much faster than the excited state decay and recombination of the injected electron with the dye cation (Haque et al., 1998; Tachibana et al., 2002). Thus, similar to BHJ, it has been found that when single-walled nanotubes were used as the material of choice for providing solar cells with necessary electrochemical properties, the resulting solar cells have been significantly improved in terms of efficiency (Kongkanand et al., 2007; Brown et al., 2008; Yan et al., 2013). Therefore, it is always demonstrated that SWNTs can play an important role in improving the charge separation, and it was shown that the injected electrons for conduction become faster in the presence of the SWNT scaffold (Demele et al., 2013). Some recent researches also showed that when a quantum dot-single-wall carbon nanotube complex is used as an additive, the resulting solar cell shows a good performance of light covert efficacy (Landi et al., 2005).

## Introduction of Graphene Oxide and Graphene as Materials of Choice for PV Applications

Graphene rapidly became one of the most popular research areas since it was discovered by A. K. Geim and K. S. Novoselov at the University of Manchester, by using a deceptively simple Scotch tape method (Geim and Novoselov, 2007). The reason behind this rapid development of this material is due to its promising properties: graphene has a significant large surface area,  $2,630\text{ m}^2\text{ g}^{-1}$ , which is nearly hundreds times larger than normal carbon material; it has high intrinsic mobility,  $200,000\text{ cm}^2\text{ V}^{-1}\text{ s}^{-1}$ ; graphene also obtains high Young's modulus, around 1.0 TPa; the thermal conductivity of graphene is  $5,000\text{ W m}^{-1}\text{ K}^{-1}$  and its optical transmittance is up to 97.7%. Besides these physical characteristics, graphene sheets have a special electronic structure, giving this material remarkable electronic properties, for instance, the anomalous quantum Hall effect (Novoselov et al., 2007) and its amazingly high carrier mobility at a relatively high charge carrier concentration and at room temperature (Bolotin et al., 2008). All these properties rendered graphene as a new material considered to be in next-generation applications of several different types of nanoelectronic devices of relevance to sensing and biosensing, transparent conductive films construction, fuel cells, electrical energy storage, and also structural materials design. The lattice of a monolayer of graphene sheet lattice consists of two equivalent sublattices of carbon atoms bonded together with  $\sigma$  bonds. The delocalised network of electrons within a graphene sheet is due to each carbon atom in the graphene lattice obtaining a  $\pi$  orbital.

There are normally three strategies to produce graphene: 1) exfoliation of graphite in solvents, 2) micromechanical exfoliation, and 3) epitaxial graphene. The production of graphene by micromechanical exfoliation was introduced by Ruoff and coworkers (Lu et al., 1999). Although the micromechanical exfoliated graphene has high quality and leads to the rapid development of graphene characterisation, this method is not suitable for larger material production scales and thus cannot meet the requirements for most commercial applications. The direct production of graphene by exfoliating graphite in common organic solvents, such as DMF and NMP, was introduced, and this included a prolonged time under the ultrasound treatment (Hernandez et al., 2008). This direct conversion can produce graphene with low a defect ratio, but besides the fact that it is time- and energy-consuming, it is still limited by the large size and thickness of the sheets produced (Lotya et al., 2009). It is also reported that a high-quality thin graphene film could be produced from fast electrochemical exfoliation (Su et al., 2011). The epitaxial graphene is introduced by chemical vapour deposition (CVD) on metallic catalysts. This method has been shown to be used in the generation of a high-quality monolayer or several layers of graphene with very thin dimensions and which is highly conductive (Reina et al., 2008; Li et al., 2009; Losurdo et al., 2011). The epitaxial graphene production is currently the most widely studied method. The large scale production of graphene of

high carbon purity by CVD approaches could provide the desired material in sufficient quantity for a host of likely applications, as well as for fundamental science. But, the challenge for epitaxial graphene production is the efficient transfer of the generated graphene sheets from the metal substrate to other substrates. Until recently, a new method for graphene generation is emerging, which is described as a substrate-free gas-phase synthesis of graphene (Dato et al., 2008). This method provides a new approach to the synthesis of graphene.

As discussed above, although graphene has several different promising properties, the large generation is still very challenging. In order to find a cost-effective method for the production of graphene, graphene oxide reemerged as an intense research area (Dreyer et al., 2010). The graphene oxide has similar structural properties compared with graphene. Graphene oxide can be regarded as a defective graphene sheet, which functionalised by introducing oxygen-containing groups (including carboxyl groups, hydroxyl groups, and carbonyl groups) onto its surface. The properties of graphene oxide change with the changing of the percentage of oxygen groups.

The generation of graphene oxide is via the direct exfoliation of graphite oxide. Graphite oxide has a similar structure to graphite, but the plane of carbon atoms in graphite oxide is heavily decorated with oxygen-containing groups, which not only enlarge the distance between each layer but also make the thin layer hydrophilic and thus they are increasing soluble in the aqueous phase. Thus, graphene oxide can be exfoliated from graphite oxide by moderate sonication. Generally, graphite oxide is synthesised by either Brodie (1860), Staudenmaier (1898) or Hummers method (Hummers and Offeman, 1958). Brodie and Staudenmaier used a combination of potassium chlorate ( $\text{KClO}_3$ ) with nitric acid ( $\text{HNO}_3$ ) to oxidise graphite, whilst the Hummers method involves the treatment of graphite with potassium permanganate ( $\text{KMnO}_4$ ) and sulfuric acid ( $\text{H}_2\text{SO}_4$ ). The level of the oxidation can be varied on the basis of the method, the reaction conditions and the precursor graphite used.

After the introduction of oxygen-containing groups onto the surface of a graphene sheet, graphene oxide sheets are significantly hydrophilic and the water molecules can intercalate into the inner layer space (Buchsteiner et al., 2006). Thus, the graphene oxide can form a stable aqueous colloidal suspension. The inner distance between each graphene oxide sheet in a water colloidal suspension could vary from 6 to  $12\text{ Å}$ , depending on the increasing humidity and oxidation, and this can make its characterisation particularly challenging (Buchsteiner et al., 2006). Recent studies showed that the water dispersed graphene oxide exhibits a negative surface charge (Li et al., 2008). The negative charge on the graphene oxide surface leads to electrostatic repulsion between negatively charged graphene oxide sheets and contribute to making the aqueous suspensions very stable. The negatively charged surface of graphene oxide in water dispersions is a very important property when applied to the role of graphene oxide in substrate deposition processes from dispersed phases as the surface charge of the substrate material should be matched (Li et al., 2008).



## Reduced Graphene Oxide

The reduction of graphene oxide was applied as one of the alternative ways to produce graphene in bulk generation. The reduction of graphene oxide can be carried out by several methods. Graphene oxide can be reduced by a high-temperature annealing process. The thermal reduced process can decompose the oxygen-containing groups and exfoliate graphene oxide sheet at the same time. According to Gao's research, the critical dissociation temperature ( $T_c$ ) of hydroxyl groups attached to the edges of GO is 650°C and only above this temperature hydroxyl groups can be fully removed. After the thermal annealing at temperatures of 700–1,200°C in a vacuum, the hydroxyl groups can be fully eliminated (Gao et al., 2009). The good reduction effect by thermal annealing at around 1,000°C was also proved by the high conductivity reported by Becerril et al. (2008) and Wang et al. (2008). As theory predicted, the common annealing reduction has to be carried out at 900–1,100°C, such that the oxygen groups on the surface of graphene oxide can be efficiently removed and the ratio of C/O may be significantly increased (Eda et al., 2008). As an alternative process, microwave irradiation reduction of graphene oxide has been carried out (Hassan et al., 2009; Zhu et al., 2010). The main advantage of microwave irradiation over other heating sources is that the heating of substances can be uniform and rapid. By treating graphite oxide powders in a commercial microwave oven, graphene oxide can be readily reduced to the product within 1 min.

Another type of graphene reduction is carried out by introducing chemical reducing agents. The chemical reduced graphene oxide can be obtained by processes carried out at room temperature or moderate heating atmosphere. The most common and widely used reducing reagent is hydrazine or hydrogen hydrate (Gómez-Navarro et al., 2007; Stankovich et al., 2007; Mattevi et al., 2009). The reduction by hydrazine and its derivatives, such as dimethylhydrazine (Stankovich et al., 2006), can be addressed by adding the liquid reagents to a GO aqueous dispersion. This results in the formation of agglomerated graphene-based nanosheets due to the increase of synthetic's hydrophobicity. The use of  $\text{NaBH}_4$  for this process was also reported recently. This can be used as the reducing reagent to produce rGO (Shin et al., 2009). As discussed above, the use of thermally reducing and chemically reducing reagents are the most common methods applied in the reducing progress of graphene oxide. A novel method that combines thermal and chemical reducing methods together emerged recently: a hydrothermal process where overheated supercritical water can play the role of a reducing agent (Zhou et al., 2009b; Dubin et al., 2010).

Other methods, like photoreduction (Zhang et al., 2010), photocatalyst reduction (Williams et al., 2008), and electrochemical reduction (Zhou et al., 2009a), have all been reported for rGO production, used to reduce graphene oxide, compared with the thermal reduction and chemical reagent reduction methods; these methods are not suitable in bulk reduction of graphene, as the reducing rates are not very applicable for large scale applications.

## Graphene and Graphene Oxide as Material Scaffolds in Photovoltaic

Since the graphene sheets hold promising thermally conductive, electronic, and mechanical properties, graphene and its divertive/graphene oxide are considered as scaffolds towards the construction of next-generation flexible photovoltaic devices. It was reported by Xuan Wang and coworkers by employing graphene as a material for the electrode of DSSCs. As made, obtained graphene films exhibit a high conductivity of 550 S/cm and transparency of more than 70% over 1,000–3,000 nm (Wang et al., 2008). Gurpreet Singh Selopal reported that, by employing graphene as a transparent front contact layer material, a value of photoconversion efficiency as high as 2% has been recorded for the best cell, under one sun irradiation (Selopal et al., 2014).

Similarly, with the care of SWNTs, the graphene and graphene oxide can also be used as electron acceptors due to their low reduction potential. For graphene sheets, the electrons can freely move at room temperature. This significant electron transport ability renders graphene an ideal material to assist the charge separation and conduction in solar cells systems. Considering its size, a graphene sheet can measure up to the micrometre range, which is a thousand times larger than the common donor molecules used in DSSCs. As a result, graphene can provide abundant space for donor molecule to attach either covalently or noncovalently.

Additionally, to the considerations discussed above, Jacob Tse-Wei Wang also reported an electron collection layer consisting of graphene- $\text{TiO}_2$  nanocomposites as components of thin-film perovskite solar cells. This showed a remarkable photovoltaic performance with a power conversion efficiency of up to 15.6% (Wang et al., 2013). Recently, Jian Zhi demonstrated that graphene,  $\text{TiO}_2$ , and a dye molecule complex anode structure (as showing in **Figure 15**) can achieve a power conversion efficiency of 6.41%. This is 56% higher than the care when the pristine  $\text{TiO}_2$  material was used for the anode (Zhi et al., 2015). This design confirmed that graphene can be used as an acceptor material in organic solar cells. Other researchers found that CdS and graphene can lead to a high photo degradation rate under visible light irradiation (Pan and Liu, 2012) and similar results have also been found for CdSe quantum dots with graphene oxide (Lightcap and Kamat, 2012). As such, although graphene and graphene oxide are new materials, they are already becoming of interest for solar cells and related PV devices consideration and study.

We and others focussed recently on new studies towards the synthesis of nanoassemblies porphyrins and carbon nanomaterials. These already showed some great promises as new synthetic scaffolds for functional materials for photovoltaic applications but have not yet been investigated in full (Tong et al., 2008). We reported recently on the lab scale preparation of new functional porphyrins modified in both *meso*- and  $\beta$ -position and metallated to obtain a more tuneable UV-vis absorption. Such functional porphyrins have been deemed challenging to synthesis on a lab scale previously; however, in our recent studies, we isolated these and studied their interactions with carbon nanomaterials (Mao et al., 2016; Tyson et al., 2016a; Mao et al., 2017; Calatayud et al., 2019; Mao et al., 2019; Owen et al., 2020).

The generation of new porphyrin-base complexes incorporating SWNTs as well as graphene oxides was achieved by both applying supramolecular self-assembly (relying on the  $\pi$ -system of the carbon nanomaterials, will remain unaltered) and a more synthetically demanding (and disruptive) covalent approach linking methods. We also reported recently on our investigations regarding the surface modification and functionalisation of SWNTs, synthesis of graphene oxide, and reduction of graphene oxide and performed the characterisation of new porphyrin-carbon nanomaterial blend by TEM, SEM, AFM methods, and Raman spectroscopy. New highly conjugated and soluble porphyrins with tunable UV-vis absorption have been developed by incorporating metal centers. Systematic characterization of their properties has been carried out by UV-vis, fluorescence spectroscopy and single photo confocal microscopy. In addition, the energy levels of the molecular orbitals of the gas-phase porphyrin system have been investigated by DFT calculations. This work will give the possibilities in exploiting porphyrin and carbon nanomaterials complex into real photovoltaic applications.

## SUMMARY TO SUSTAINABLE ENERGY

In summary, solar energy and related sustainable technologies should and could play more important roles in societal daily life in the near future. Organic solar cells exhibit great promise for the future of photovoltaics, due to their high versatility and accessibility among different types of solar cell fabrication techniques. For organic solar cells, small molecules can be employed as the light absorber; this has been demonstrated for both organic bulk heterojunction solar cells and for DSSCs. Although the cells discussed above all differ in structure, the basic operating principle of BHJs and DSSCs is largely the same: the light absorber works as a “donor,” which absorbs light and generates excited electrons; afterwards, the electrons are transferred to “acceptor” and then transferred to an external current.

It can be seen from the above discussions, either in the developments of bulk heterojunction solar cells or due to the recent revolutions leading the photovoltaics development from

DSSCs to perovskite solar cells and from perovskite solar cells to further proposed developing directions, that almost all attempted efforts are based on synthesising and characterising new donor/accepter materials and improving the electron diffusion efficiency within the systems. Thus, this review highlighted current challenges and opportunities highlighted by a small molecule-based donor incorporating a porphyrin motif, which can lead to novel nanodimensional materials-based acceptor systems. These may be of relevance to future application in bulk heterojunction solar cells or DSSC structures.

## AUTHOR CONTRIBUTIONS

All authors contributed to the sections of the manuscript as a part of their PhDs/MChem/MRes theses introductions or personal development plans. The text was then curated, rewritten, and updated by DGC and SIP.

## FUNDING

SIP acknowledges funding from ERC Consolidator Grant O2Sense 617107 (2014–2020), EPSRC (EP/K017160/1 “New manufacturable approaches to the deposition and patterning of graphene materials”), Innovate United Kingdom (previously Technology Strategy Board-CR&D, TS/K001035/1), University of Bath (UoB) Impact fund, and EPSRC Centre for Doctoral Training Centre for Sustainable Chemical Technologies (EP/G03768X/1). BM thanks the UoB for a PhD studentship. DGC also thanks Fundación General CSIC (COMFUTURO Program) for funding.

## ACKNOWLEDGMENTS

The authors thank Professors Paul Raithby and Frank Marken for the co-supervisory support of the PhD and research students involved in this review, and for helpful discussions in supramolecular and sustainable functional materials.

## REFERENCES

- Akamatsu, H., Inokuchi, H., and Matsunaga, Y. (1954). Electrical Conductivity of the Perylene-Bromine Complex. *Nature* 173, 168–169. doi:10.1038/173168a0
- A. K. Soteris (2018). *McEvoy's Handbook of Photovoltaics* (Elsevier). doi:10.1016/C2015-0-01840-8
- Andreoni, W. (2000). *The Physics of Fullerene-Based and Fullerene-Related Materials*. Dordrecht: Springer Science & Business Media.
- Archer, M. D., and Nozik, A. J. (2008). *Nanostructured and Photoelectrochemical Systems for Solar Photon Conversion*. London: IMPERIAL COLLEGE PRESS AND DISTRIBUTED BY WORLD SCIENTIFIC PUBLISHING CO. doi:10.1142/p217
- Armaroli, N., Barigelli, F., Calogero, G., Flamigni, L., Armaroli, N., White, C. M., et al. (1997). Electronic Energy Transfer between Ruthenium(II) and Osmium(II) Polypyridyl Luminophores in a Hydrogen-Bonded Supramolecular Assembly. *Chem. Commun.* 22, 2181–2182. doi:10.1039/a705968j
- Armaroli, N., Diederich, F., Echegoyen, L., Habicher, T., Flamigni, L., Marconi, G., et al. (1999). A New Pyridyl-Substituted Methanofullerene Derivative. Photophysics, Electrochemistry and Self-Assembly with Zinc(II) Meso-Tetraphenylporphyrin (ZnTPP). *New J. Chem.* 23, 77–83. doi:10.1039/a807400c
- Armel, V., Pringle, J. M., Wagner, P., Forsyth, M., Officer, D., and MacFarlane, D. R. (2011). Porphyrin Dye-Sensitized Solar Cells Utilising a Solid-State Electrolyte. *Chem. Commun.* 47, 9327. doi:10.1039/c1cc13205a
- Asif, M., and Muneer, T. (2007). Energy Supply, its Demand and Security Issues for Developed and Emerging Economies. *Renew. Sust. Energ. Rev.* 11, 1388–1413. doi:10.1016/j.rser.2005.12.004
- Babu, V., Fuentes Pineda, R., Ahmad, T., Alvarez, A. O., Castriotta, L. A., Di Carlo, A., et al. (2020). Improved Stability of Inverted and Flexible Perovskite Solar Cells with Carbon Electrode. *ACS Appl. Energ. Mater.* 3, 5126–5134. doi:10.1021/acsaelm.0c00702
- Bach, U., Lupo, D., Comte, P., Moser, J. E., Weissörtel, F., Salbeck, J., et al. (1998). Solid-state Dye-Sensitized Mesoporous TiO<sub>2</sub> Solar Cells with High Photon-To-Electron Conversion Efficiencies. *Nature* 395, 583–585. doi:10.1038/26936
- Badenhorst, H. (2019). A Review of the Application of Carbon Materials in Solar thermal Energy Storage. *Solar Energy* 192, 35–68. doi:10.1016/j.solener.2018.01.062

- Baerends, E. J., Ricciardi, G., Rosa, A., and Van Gisbergen, S. J. A. (2002). A DFT/TDDFT Interpretation of the Ground and Excited States of Porphyrin and Porphyrane Complexes. *Coord. Chem. Rev.* 230, 5–27. doi:10.1016/s0010-8545(02)00093-0
- Bagnall, D. M., and Boreland, M. (2008). Photovoltaic Technologies. *Energy Policy* 36, 4390–4396. doi:10.1016/j.enpol.2008.09.070
- Balch, A. L., and Olmstead, M. M. (1999). Structural Chemistry of Supramolecular Assemblies that Place Flat Molecular Surfaces Around the Curved Exterior of Fullerenes. *Coord. Chem. Rev.* 185–186, 601–617. doi:10.1016/S0010-8545(99)00013-2
- Becerril, H. A., Mao, J., Liu, Z., Stoltenberg, R. M., Bao, Z., and Chen, Y. (2008). Evaluation of Solution-Processed Reduced Graphene Oxide Films as Transparent Conductors. *ACS Nano* 2, 463–470. doi:10.1021/nn700375n
- Beer, P., Gale, P., and Smith, D. (1999). *Supramolecular Chemistry*. Oxford: Oxford University Press. Available at: <https://global.oup.com/academic/product/supramolecular-chemistry-9780198504474?cc=es&lang=en&> (Accessed June 10, 2021).
- Bentsen, N. S., and Møller, I. M. (2017). Solar Energy Conserved in Biomass: Sustainable Bioenergy Use and Reduction of Land Use Change. *Renew. Sust. Energ. Rev.* 71, 954–958. doi:10.1016/j.rser.2016.12.124
- Bessho, T., Zakeeruddin, S. M., Yeh, C.-Y., Diau, E. W.-G., and Grätzel, M. (2010). Highly Efficient Mesoscopic Dye-Sensitized Solar Cells Based on Donor-Acceptor-Substituted Porphyrins. *Angew. Chem. Int. Edition* 49, 6646–6649. doi:10.1002/anie.201002118
- Bhyrappa, P., and Karunanithi, K. (2010). Porphyrin–Fullerene, C60, CocrySTALLates: Influence of C60 on the Porphyrin Ring Conformation. *Inorg. Chem.* 49, 8389–8400. doi:10.1021/ic101030h
- Bolotin, K. I., Sikes, K. J., Jiang, Z., Klima, M., Fudenberg, G., Hone, J., et al. (2008). Ultrahigh Electron Mobility in Suspended Graphene. *Solid State. Commun.* 146, 351–355. doi:10.1016/j.ssc.2008.02.024
- Boyd, P. D. W., Hodgson, M. C., Rickard, C. E. F., Oliver, A. G., Chaker, L., Brothers, P. J., et al. (1999). Selective Supramolecular Porphyrin/Fullerene Interactions. *J. Am. Chem. Soc.* 121, 10487–10495. doi:10.1021/ja992165h
- Boyd, P. D. W., and Reed, C. A. (2005). Fullerene–Porphyrin Constructs. *Acc. Chem. Res.* 38, 235–242. doi:10.1021/ar040168f
- Brabec, C. J., Cravino, A., Meissner, D., Sariciftci, N. S., Fromherz, T., Rispens, M. T., et al. (2001). Origin of the Open Circuit Voltage of Plastic Solar Cells. *Adv. Funct. Mater.* 11, 374–380. doi:10.1002/1616-3028(200110)11:5<374::aid-adfm374>3.0.co;2-w
- Brodie, B. C. (1860). Sur le poids atomique du graphite. *Ann. Chim. Phys.* 59, e472.
- Brown, P., Takechi, K., and Kamat, P. V. (2008). Single-walled Carbon Nanotube Scaffolds for Dye-Sensitized Solar Cells. *J. Phys. Chem. C* 112, 4776–4782. doi:10.1021/jp7107472
- Brunetti, F., Operamolla, A., Castro-Hermosa, S., Lucarelli, G., Manca, V., Farinola, G. M., et al. (2019). Printed Solar Cells and Energy Storage Devices on Paper Substrates. *Adv. Funct. Mater.* 29, 1806798. doi:10.1002/adfm.201806798
- Buchsteiner, A., Lerf, A., and Pieper, J. (2006). Water Dynamics in Graphite Oxide Investigated with Neutron Scattering. *J. Phys. Chem. B* 110, 22328–22338. doi:10.1021/jp0641132
- Calatayud, D. G., Cortezon-Tamarit, F., Mao, B., Mirabello, V., and Pascu, S. I. (2019). “Self- and Directed-Assembly of Metallic and Nonmetallic Fluorophores: Considerations into Graphene and Graphene Oxides for Sensing and Imaging Applications,” in *Handbook of Graphene*. Editors C. Ozkan and U. Ozkan (Wiley), 469–505. doi:10.1002/9781119468455.ch83
- Campbell, W. M., Burrell, A. K., Officer, D. L., and Jolley, K. W. (2004). Porphyrins as Light Harvesters in the Dye-Sensitized TiO<sub>2</sub> Solar Cell. *Coord. Chem. Rev.* 248, 1363–1379. doi:10.1016/j.ccr.2004.01.007
- Campbell, W. M., Jolley, K. W., Wagner, P., Wagner, K., Walsh, P. J., Gordon, K. C., et al. (2007). Highly Efficient Porphyrin Sensitizers for Dye-Sensitized Solar Cells. *J. Phys. Chem. C* 111, 11760–11762. doi:10.1021/jp0750598
- Carella, A., Borbone, F., and Centore, R. (2018). Research Progress on Photosensitizers for DSSC. *Front. Chem.* 481, 1–24. doi:10.3389/fchem.2018.00481
- Cataldo, S., Salice, P., Menna, E., and Pignataro, B. (2012). Carbon Nanotubes and Organic Solar Cells. *Energy Environ. Sci.* 5, 5919–5940. doi:10.1039/c1ee02276h
- Chamberlain, T. W., Champness, N. R., Schröder, M., and Khlobystov, A. N. (2011a). A Piggyback Ride for Transition Metals: Encapsulation of Exohedral Metallofullerenes in Carbon Nanotubes. *Chem. Eur. J.* 17, 668–674. doi:10.1002/chem.201001288
- Chamberlain, T. W., Davies, E. S., Khlobystov, A. N., and Champness, N. R. (2011b). Multi-Electron-Acceptor Dyad and Triad Systems Based on Perylene Bisimides and Fullerenes. *Chem. Eur. J.* 17, 3759–3767. doi:10.1002/chem.201003092
- Chapin, D. M., Fuller, C. S., and Pearson, G. L. (1954). A New Silicon P-n Junction Photocell for Converting Solar Radiation into Electrical Power. *J. Appl. Phys.* 25, 676–677. doi:10.1063/1.1721711
- Charvet, R., Yamamoto, Y., Sasaki, T., Kim, J., Kato, K., Takata, M., et al. (2012). Segregated and Alternately Stacked Donor/Acceptor Nanodomains in Tubular Morphology Tailored with Zinc Porphyrin-C60 Amphiphilic Dyads: Clear Geometrical Effects on Photoconduction. *J. Am. Chem. Soc.* 134, 2524–2527. doi:10.1021/ja211334k
- Chen, R. J., Zhang, Y., Wang, D., and Dai, H. (2001). Noncovalent Sidewall Functionalization of Single-Walled Carbon Nanotubes for Protein Immobilization. *J. Am. Chem. Soc.* 123, 3838–3839. doi:10.1021/ja010172b
- Chen, T., Qiu, L., Yang, Z., and Peng, H. (2013). Novel Solar Cells in a Wire Format. *Chem. Soc. Rev.* 42, 5031–5041. doi:10.1039/c3cs35465b
- Chen, Y.-S., Li, C., Zeng, Z.-H., Wang, W.-B., Wang, X.-S., and Zhang, B.-W. (2005). Efficient Electron Injection Due to a Special Adsorbing Group's Combination of Carboxyl and Hydroxyl: Dye-Sensitized Solar Cells Based on New Hemicyanine Dyes. *J. Mater. Chem.* 15, 1654–1661. doi:10.1039/b418906j
- Chiba, Y., Islam, A., Watanabe, Y., Komiya, R., Koide, N., and Han, L. (2006). Dye-sensitized Solar Cells with Conversion Efficiency of 11.1%. *Jpn. J. Appl. Phys.* 45, L638.
- Chitta, R., Sandanayaka, A. S. D., Schumacher, A. L., D'Souza, L., Araki, Y., Ito, O., et al. (2007). Donor–Acceptor Nanohybrids of Zinc Naphthalocyanine or Zinc Porphyrin Noncovalently Linked to Single-Wall Carbon Nanotubes for Photoinduced Electron Transfer. *J. Phys. Chem. C* 111, 6947–6955. doi:10.1021/jp0704416
- Cho, Y.-J., Ahn, T. K., Song, H., Kim, K. S., Lee, C. Y., Seo, W. S., et al. (2005). Unusually High Performance Photovoltaic Cell Based on a [60]Fullerene Metal Cluster–Porphyrin Dyad SAM on an ITO Electrode. *J. Am. Chem. Soc.* 127, 2380–2381. doi:10.1021/ja044847x
- Chu, S., and Majumdar, A. (2012). Opportunities and Challenges for a Sustainable Energy Future. *Nature* 488, 294–303. doi:10.1038/nature11475
- Chuvilin, A., Bichoutskaia, E., Gimenez-Lopez, M. C., Chamberlain, T. W., Rance, G. A., Kuganathan, N., et al. (2011). Self-assembly of a sulphur-terminated Graphene Nanoribbon within a Single-Walled Carbon Nanotube. *Nat. Mater.* 10, 687–692. doi:10.1038/nmat3082
- Chuvilin, A., Kaiser, U., Bichoutskaia, E., Besley, N. A., and Khlobystov, A. N. (2010a). Direct Transformation of Graphene to Fullerene. *Nat. Chem.* 2, 450–453. doi:10.1038/nchem.644
- Chuvilin, A., Khlobystov, A. N., Obergfell, D., Haluska, M., Yang, S., Roth, S., et al. (2010b). Observations of Chemical Reactions at the Atomic Scale: Dynamics of Metal-Mediated Fullerene Coalescence and Nanotube Rupture. *Angew. Chem. Int. Edition* 49, 193–196. doi:10.1002/anie.200902243
- Cid, J.-J., Yum, J.-H., Jang, S.-R., Nazeeruddin, M. K., Martínez-Ferrero, E., Palomares, E., et al. (2007). Molecular Cosensitization for Efficient Panchromatic Dye-Sensitized Solar Cells. *Angew. Chem.* 119, 8510–8514. doi:10.1002/ange.200703106
- Clifford, J. N., Palomares, E., Nazeeruddin, M. K., Grätzel, M., and Durrant, J. R. (2007). Dye Dependent Regeneration Dynamics in Dye Sensitized Nanocrystalline Solar Cells: Evidence for the Formation of a Ruthenium Bipyridyl Cation/iodide Intermediate. *J. Phys. Chem. C* 111, 6561–6567. doi:10.1021/jp067458t
- Coleman, K. S., Bailey, S. R., Fogden, S., and Green, M. L. H. (2003). Functionalization of Single-Walled Carbon Nanotubes via the Bingel Reaction. *J. Am. Chem. Soc.* 125, 8722–8723. doi:10.1021/ja0355675
- Cooling, N. A., Zhou, X., Sales, T. A., Sauer, S. E., Lind, S. J., Gordon, K. C., et al. (2012). A Study of the Factors Influencing the Performance of Ternary MEH-PPV:porphyrin:PCBM Heterojunction Devices: Electronic Effects in Porphyrinoid Ternary Blend Bulk Heterojunction Photovoltaic Devices. *Solar Energ. Mater. Solar Cell* 98, 308–316. doi:10.1016/j.solmat.2011.10.036
- Corbett, P. T., Leclaire, J., Vial, L., West, K. R., Wietor, J.-L., Sanders, J. K. M., et al. (2006). Dynamic Combinatorial Chemistry. *Chem. Rev.* 106, 3652–3711. doi:10.1021/cr020452p



- Cramer, F. (1956). Einschlußverbindungen. *Angew. Chem.* 68, 115–120. doi:10.1002/ange.19560680306
- Curtis, N. F., and House, D. A. (1961). Structure of Some Aliphatic Schiff Base Complexes of Nickel (II) and Copper (II). *Chem. & Ind.* 42, 1708–1709.
- D'Souza, F., Deviprasad, G. R., El-Khouly, M. E., Fujitsuka, M., and Ito, O. (2001). Probing the Donor–Acceptor Proximity on the Physicochemical Properties of Porphyrin–Fullerene Dyads: “Tail-On” and “Tail-Off” Binding Approach. *J. Am. Chem. Soc.* 123, 5277–5284. doi:10.1021/ja010356q
- Dahash, A., Ochs, F., Janetti, M. B., and Streicher, W. (2019). Advances in Seasonal thermal Energy Storage for Solar District Heating Applications: A Critical Review on Large-Scale Hot-Water Tank and Pit thermal Energy Storage Systems. *Appl. Energ.* 239, 296–315. doi:10.1016/j.apenergy.2019.01.189
- Darcy, R. (2001). Self-Assembly in Supramolecular Systems, L. F. Lindoy and I. M. Atkinson, Monographs in Supramolecular Chemistry, Volume 7 (Ed. J. F. Stoddart). *J. Incl. Phenom. Macrocycl. Chem.* 40, 249. doi:10.1023/A:1011898504925
- Dato, A., Radmilovic, V., Lee, Z., Phillips, J., and Frenklach, M. (2008). Substrate-free Gas-phase Synthesis of Graphene Sheets. *Nano Lett.* 8, 2012. doi:10.1021/nl8011566
- de la Torre, G., Giacalone, F., Segura, J. L., Martín, N., and Guldi, D. M. (2005). Electronic Communication through  $\pi$ -Conjugated Wires in Covalently Linked Porphyrin/C60Ensembles. *Chem. - A Eur. J.* 11, 1267–1280. doi:10.1002/chem.200400604
- De Wolf, S., Descoeurdes, A., Holman, Z. C., and Ballif, C. (2012). High-efficiency Silicon Heterojunction Solar Cells: A Review. *Green* 2, 7–24. doi:10.1515/green-2011-0018
- del Carmen Giménez-López, M., Moro, F., La Torre, A., Gómez-García, C. J., Brown, P. D., van Slageren, J., et al. (2011). Encapsulation of Single-Molecule Magnets in Carbon Nanotubes. *Nat. Commun.* 2, 407. doi:10.1038/ncomms1415
- Dembele, K. T., Selopal, G. S., Soldano, C., Nechache, R., Rimada, J. C., Concina, I., et al. (2013). Hybrid Carbon Nanotubes–TiO<sub>2</sub> Photoanodes for High Efficiency Dye-Sensitized Solar Cells. *J. Phys. Chem. C* 117, 14510–14517. doi:10.1021/jp403553t
- Demoncy, N., Stéphan, O., Brun, N., Colliex, C., Loiseau, A., and Pascard, H. (1998). Filling Carbon Nanotubes with Metals by the Arc-Discharge Method: the Key Role of Sulfur. *Eur. Phys. J. B* 4, 147–157. doi:10.1007/s100510050363
- Department for Business, E. and I. S. (2020). UK Energy Statistics, 2019 & Q4 2019.
- Dibb, G. F. A., Kirchartz, T., Credgington, D., Durrant, J. R., and Nelson, J. (2011). Analysis of the Relationship between Linearity of Corrected Photocurrent and the Order of Recombination in Organic Solar Cells. *J. Phys. Chem. Lett.* 2, 2407–2411. doi:10.1021/jz201104d
- Diskin-Posner, Y., Patra, G. K., and Goldberg, I. (2002). Supramolecular Porphyrin-Based Materials. Assembly Modes of [5,10,15,20-Tetrakis(4-Hydroxyphenyl)porphyrinato]zinc with Bipyridyl Ligands. *CrystEngComm* 4, 296–301. doi:10.1039/B204129B
- Dragonetti, C., and Colombo, A. (2021). Recent Advances in Dye-Sensitized Solar Cells. *Molecules* 26, 2461. doi:10.3390/molecules26092461
- Dreyer, D. R., Park, S., Bielawski, C. W., and Ruoff, R. S. (2010). The Chemistry of Graphene Oxide. *Chem. Soc. Rev.* 39, 228–240. doi:10.1039/b917103g
- Drovetskaya, T., Reed, C. A., and Boyd, P. (1995). A Fullerene Porphyrin Conjugate. *Tetrahedron Lett.* 36, 7971–7974. doi:10.1016/0040-4039(95)01719-x
- D'Souza, F., Gadde, S., Zandler, M. E., Arkady, K., El-Khouly, M. E., Fujitsuka, M., et al. (2002). Studies on Covalently Linked Porphyrin–C60 Dyads: Stabilization of Charge-Separated States by Axial Coordination. *J. Phys. Chem. A* 106, 12393–12404.
- D'Souza, F., and Ito, O. (2009). Supramolecular Donor–Acceptor Hybrids of Porphyrins/phthalocyanines with Fullerenes/carbon Nanotubes: Electron Transfer, Sensing, Switching, and Catalytic Applications. *Chem. Commun.* 33, 4913. doi:10.1039/b905753f
- Dualeh, A., De Angelis, F., Fantacci, S., Moehl, T., Yi, C., Kessler, F., et al. (2011). Influence of Donor Groups of Organic D– $\pi$ -A Dyes on Open-Circuit Voltage in Solid-State Dye-Sensitized Solar Cells. *J. Phys. Chem. C* 116, 1572–1578. doi:10.1021/jp209691e
- Dubin, S., Gilje, S., Wang, K., Tung, V. C., Cha, K., Hall, A. S., et al. (2010). A One-step, Solvothermal Reduction Method for Producing Reduced Graphene Oxide Dispersions in Organic Solvents. *ACS Nano* 4, 3845–3852. doi:10.1021/nn100511a
- Eda, G., Fanchini, G., and Chhowalla, M. (2008). Large-area Ultrathin Films of Reduced Graphene Oxide as a Transparent and Flexible Electronic Material. *Nat. Nanotech* 3, 270–274. doi:10.1038/nnano.2008.83
- Eichhorn, D. M., Yang, S., Jarrell, W., Baumann, T. F., Beall, L. S., White, A. J. P., et al. (1995). [60]Fullerene and TCNQ Donor–Acceptor Crystals of Octakis(dimethylamino) Porphyrazine. *J. Chem. Soc. Chem. Commun.*, 1703–1704. doi:10.1039/C39950001703
- Evans, D. R., Fackler, N. L. P., Xie, Z., Rickard, C. E. F., Boyd, P. D. W., and Reed, C. A. (1999).  $\pi$ -Arene/Cation Structure and Bonding. Solvation versus Ligand Binding in Iron(III) Tetraphenylporphyrin Complexes of Benzene, Toluene, p-Xylene, and [60]Fullerene. *J. Am. Chem. Soc.* 121, 8466–8474. doi:10.1021/ja9910816
- Fathalla, M., Li, S.-C., Diebold, U., Alb, A., and Jayawickramarajah, J. (2009). Water-soluble Nanorods Self-Assembled via Pristine C60 and Porphyrin Moieties. *Chem. Commun.* 28, 4209. doi:10.1039/b908050c
- Flamigni, L., Dixon, I. M., Collin Jean-, J.-P., and Sauvage, P. (2000). A Zn(ii) Porphyrin–Ir(iii) Bis-Terpyridine–Au(iii) Porphyrin Triad with a Charge-Separated State in the Microsecond Range. *Chem. Commun* 24, 2479–2480. doi:10.1039/b007778j
- Ganesamoorthy, R., Sathiyar, G., and Sakthivel, P. (2017). Review: Fullerene Based Acceptors for Efficient Bulk Heterojunction Organic Solar Cell Applications. *Solar Energ. Mater. Solar Cell* 161, 102–148. doi:10.1016/j.solmat.2016.11.024
- Gao, X., Jang, J., and Nagase, S. (2009). Hydrazine and thermal Reduction of Graphene Oxide: Reaction Mechanisms, Product Structures, and Reaction Design. *J. Phys. Chem. C* 114, 832–842. doi:10.1021/jp909284g
- García-Iglesias, M., Yum, J.-H., Humphry-Baker, R., Zakeeruddin, S. M., Péchy, P., Vázquez, P., et al. (2011). Effect of Anchoring Groups in Zinc Phthalocyanine on the Dye-Sensitized Solar Cell Performance and Stability. *Chem. Sci.* 2, 1145. doi:10.1039/c0sc00602e
- Geim, A. K., and Novoselov, K. S. (2007). The Rise of Graphene. *Nat. Mater* 6, 183–191. doi:10.1038/nmat1849
- Gimenez-Lopez, M. d. C., Chuvilin, A., Kaiser, U., and Khlobystov, A. N. (2011). Functionalised Endohedral Fullerenes in Single-Walled Carbon Nanotubes. *Chem. Commun.* 47, 2116–2118. doi:10.1039/c0cc02929g
- Gómez-Navarro, C., Weitz, R. T., Bittner, A. M., Scolari, M., Mews, A., Burghard, M., et al. (2007). Electronic Transport Properties of Individual Chemically Reduced Graphene Oxide Sheets. *Nano Lett.* 7, 3499–3503. doi:10.1021/nl072090c
- Grätzel, M. (2001). Photoelectrochemical Cells. *Nature* 414, 338–344. doi:10.1038/35104607
- Grätzel, M. (2005). Solar Energy Conversion by Dye-Sensitized Photovoltaic Cells. *Inorg. Chem.* 44, 6841–6851. doi:10.1021/ic0508371
- Grimm, B., Isla, H., Pérez, E. M., Martín, N., and Guldi, D. M. (2011). Balancing Binding Strength and Charge Transfer Lifetime in Supramolecular Associates of Fullerenes. *Chem. Commun.* 47, 7449. doi:10.1039/c1cc11693b
- Guo, W., Si, W., Zhang, T., Han, Y., Wang, L., Zhou, Z., et al. (2021). Ultrathin Ni Co-silicate Nanosheets Natively Anchored on CNTs Films for Flexible Lithium Ion Batteries. *J. Energ. Chem.* 54, 746–753. doi:10.1016/j.jechem.2020.06.026
- Green, M. A. (2006). “Third Generation Photovoltaics,” in *Advanced Solar Energy Conversion*. Switzerland, AG: Springer, 160.
- Green, M. A., Emery, K., Hishikawa, Y., Warta, W., and Dunlop, E. D. (2014). Solar Cell Efficiency Tables (Version 44). *Prog. Photovoltaics Res. Appl.* 22, 701–710. doi:10.1002/ppp.2525
- Guo, Z., Du, F., Ren, D., Chen, Y., Zheng, J., Liu, Z., et al. (2006). Covalently Porphyrin-Functionalized Single-Walled Carbon Nanotubes: a Novel Photoactive and Optical Limiting Donor–Acceptor Nanohybrid. *J. Mater. Chem.* 16, 3021–3030. doi:10.1039/b602349e
- Gurung, A., and Qiao, Q. (2018). Solar Charging Batteries: Advances, Challenges, and Opportunities. *Joule* 2, 1217–1230. doi:10.1016/j.joule.2018.04.006
- Gutiérrez-Nava, M., Nierengarten, H., Masson, P., Van Dorselaer, A., and Nierengarten, J.-F. (2003). A Supramolecular Oligophenylenevinylene–C 60 Conjugate. *Tetrahedron Lett.* 44, 3043–3046. doi:10.1016/S0040-4039(03)00561-6
- Hagfeldt, A., Boschloo, G., Sun, L., Kloo, L., and Pettersson, H. (2010). Dye-sensitized Solar Cells. *Chem. Rev.* 110, 6595–6663. doi:10.1021/cr900356p
- Haque, S. A., Tachibana, Y., Klug, D. R., and Durrant, J. R. (1998). Charge Recombination Kinetics in Dye-Sensitized Nanocrystalline Titanium Dioxide Films under Externally Applied Bias. *J. Phys. Chem. B* 102, 1745–1749. doi:10.1021/jp973335k



- Hasobe, T., Imahori, H., Kamat, P. V., Ahn, T. K., Kim, S. K., Kim, D., et al. (2005). Photovoltaic Cells Using Composite Nanoclusters of Porphyrins and Fullerenes with Gold Nanoparticles. *J. Am. Chem. Soc.* 127, 1216–1228. doi:10.1021/ja047768u
- Hasobe, T. (2010). Supramolecular Nanoarchitectures for Light Energy Conversion. *Phys. Chem. Chem. Phys.* 12, 44–57. doi:10.1039/B910564F
- Hassan, H. M. A., Abdelsayed, V., Khder, A. E. R. S., Abouzeid, K. M., Ternier, J., El-Shall, M. S., et al. (2009). Microwave Synthesis of Graphene Sheets Supporting Metal Nanocrystals in Aqueous and Organic media. *J. Mater. Chem.* 19, 3832–3837. doi:10.1039/b906253j
- Hernandez, Y., Nicolosi, V., Lotya, M., Blighe, F. M., Sun, Z., De, S., et al. (2008). High-yield Production of Graphene by Liquid-phase Exfoliation of Graphite. *Nat. Nanotech.* 3, 563–568. doi:10.1038/nnano.2008.215
- Hersam, M. C. (2008). Progress towards Monodisperse Single-Walled Carbon Nanotubes. *Nat. Nanotech.* 3, 387–394. doi:10.1038/nnano.2008.135
- Hiramoto, M., Fujiwara, H., and Yokoyama, M. (1992). p-i-n-like Behavior in Three-layered Organic Solar Cells Having a Co-deposited Interlayer of Pigments. *J. Appl. Phys.* 72, 3781–3787. doi:10.1063/1.352274
- Hoeben, F. J. M., Jonkheijm, P., Meijer, E. W., and Schenning, A. P. H. J. (2005). About Supramolecular Assemblies of  $\pi$ -Conjugated Systems. *Chem. Rev.* 105, 1491–1546. doi:10.1021/cr030070z
- Hoppe, H., and Sariciftci, N. S. (2004). Organic Solar Cells: An Overview. *J. Mater. Res.* 19, 1924–1945.
- Hsin, Y. L., Hwang, K. C., Chen, F., and Kai, J. (2001). Production and In-situ Metal Filling of Carbon Nanotubes in Water. *Adv. Mater.* 13, 830–833.
- Hu, Z., Pantoş, G. D., Kuganathan, N., Arrowsmith, R. L., Jacobs, R. M. J., Kociok-Köhn, G., et al. (2012). Interactions between Amino Acid-Tagged Naphthalenediimide and Single Walled Carbon Nanotubes for the Design and Construction of New Bioimaging Probes. *Adv. Funct. Mater.* 22, 503–518. doi:10.1002/adfm.201101932
- Hummers, W. S., Jr, and Offeman, R. E. (1958). Preparation of Graphitic Oxide. *J. Am. Chem. Soc.* 80, 1339. doi:10.1021/ja01539a017
- Hunter, C. A. (1994). Meldola Lecture. The Role of Aromatic Interactions in Molecular Recognition. *Chem. Soc. Rev.* 23, 101. doi:10.1039/cs9942300101
- Iehl, J., Vartanian, M., Holler, M., Nierengarten, J.-F., Delavaux-Nicot, B., Strub, J.-M., et al. (2011). Photoinduced Electron Transfer in a Clicked Fullerene-Porphyrin Conjugate. *J. Mater. Chem.* 21, 1562–1573. doi:10.1039/C0JM02310H
- Iijima, S. (1991). HELICAL MICROTUBULES OF GRAPHITIC CARBON. *Nature* 354, 56–58. doi:10.1038/354056a0
- Iijima, S., and Ichihashi, T. (1993). Single-shell Carbon Nanotubes of 1-nm Diameter. *Nature* 363, 603–605. doi:10.1038/363603a0
- Imahori, H., and Fukuzumi, S. (2004). Porphyrin- and Fullerene-Based Molecular Photovoltaic Devices. *Adv. Funct. Mater.* 14, 525–536. doi:10.1002/adfm.200305172
- Imahori, H., Hagiwara, K., Aoki, M., Akiyama, T., Taniguchi, S., Okada, T., et al. (1996). Linkage and Solvent Dependence of Photoinduced Electron Transfer in Zincporphyrin-C60Dyads. *J. Am. Chem. Soc.* 118, 11771–11782. doi:10.1021/ja9628415
- Ito, S., Chen, P., Comte, P., Nazeeruddin, M. K., Liska, P., Péchy, P., et al. (2007). Fabrication of Screen-Printing Pastes from TiO<sub>2</sub> Powders for Dye-Sensitized Solar Cells. *Prog. Photovolt: Res. Appl.* 15, 603–612. doi:10.1002/ppv.768
- Ito, S., Murakami, T. N., Comte, P., Liska, P., Grätzel, C., Nazeeruddin, M. K., et al. (2008). Fabrication of Thin Film Dye Sensitized Solar Cells with Solar to Electric Power Conversion Efficiency over 10%. *Thin Solid Films* 516, 4613–4619.
- Ito, S., Zakeeruddin, S. M., Humphry-Baker, R., Liska, P., Charvet, R., Comte, P., et al. (2006). High-Efficiency Organic-Dye-Sensitized Solar Cells Controlled by Nanocrystalline-TiO<sub>2</sub> Electrode Thickness. *Adv. Mater.* 18, 1202–1205. doi:10.1002/adma.200502540
- Itzhak, Y., Niitsoo, O., Page, M., and Hodes, G. (2009). Sb<sub>2</sub>S<sub>3</sub>-sensitized Nanoporous TiO<sub>2</sub> Solar Cells. *J. Phys. Chem. C* 113, 4254–4256. doi:10.1021/jp900302b
- Jeong, J., Kim, M., Seo, J., Lu, H., Ahlawat, P., Mishra, A., et al. (2021). Pseudo-halide Anion Engineering for  $\alpha$ -FAPbI<sub>3</sub> Perovskite Solar Cells. *Nature* 592, 381–385. doi:10.1038/s41586-021-03406-5
- Jose, R., Thavasi, V., and Ramakrishna, S. (2009). Metal Oxides for Dye-Sensitized Solar Cells. *J. Am. Ceram. Soc.* 92, 289–301. doi:10.1111/j.1551-2916.2008.02870.x
- Kadish, K. M., Smith, K. M., and Guillard, R. (1999). *The Porphyrin Handbook*. New York: Elsevier.
- Kahnt, A., Kärnbratt, J., Esdaile, L. J., Hutin, M., Sawada, K., Anderson, H. L., et al. (2011). Temperature Dependence of Charge Separation and Recombination in Porphyrin Oligomer-Fullerene Donor-Acceptor Systems. *J. Am. Chem. Soc.* 133, 9863–9871. doi:10.1021/ja2019367
- Kamat, P. V. (2013). Quantum Dot Solar Cells. The Next Big Thing in Photovoltaics. *J. Phys. Chem. Lett.* 4, 908–918. doi:10.1021/jz400052e
- Karousis, N., Ortiz, J., Ohkubo, K., Hasobe, T., Fukuzumi, S., Sastre-Santos, Á., et al. (2012). Zinc Phthalocyanine-Graphene Hybrid Material for Energy Conversion: Synthesis, Characterization, Photophysics, and Photoelectrochemical Cell Preparation. *J. Phys. Chem. C* 116, 20564–20573. doi:10.1021/jp305783v
- Karousis, N., Sandanayaka, A. S. D., Hasobe, T., Economopoulos, S. P., Sarantopoulou, E., and Tagmatarchis, N. (2011). Graphene Oxide with Covalently Linked Porphyrin Antennae: Synthesis, Characterization and Photophysical Properties. *J. Mater. Chem.* 21, 109–117. doi:10.1039/C0JM00991A
- Katz, H. E., Lovinger, A. J., Johnson, J., Kloc, C., Siegrist, T., Li, W., et al. (2000). A Soluble and Air-Stable Organic Semiconductor with High Electron Mobility. *Nature* 404, 478–481. doi:10.1038/35006603
- Kay, A., and Graetzel, M. (1993). Artificial Photosynthesis. 1. Photosensitization of Tiantia Solar Cells with Chlorophyll Derivatives and Related Natural Porphyrins. *J. Phys. Chem.* 97, 6272–6277. doi:10.1021/j100125a029
- Khlobystov, A. N. (2011). Carbon Nanotubes: from Nano Test Tube to Nano-Reactor. *ACS Nano* 5, 9306–9312. doi:10.1021/nn204596p
- Kieran, A. L., Pascu, S. I., Jarroson, T., and Sanders, J. K. (2005b). Inclusion of C60 into an Adjustable Porphyrin Dimer Generated by Dynamic Disulfide Chemistry. *Chem. Commun. (Camb)* 10, 1276–1278. doi:10.1039/b417951j
- Kieran, A. L., Pascu, S. I., Jarroson, T., Gunter, M. J., and Sanders, J. K. M. (2005a). Dynamic Synthesis of a Macrocyclic Containing a Porphyrin and an Electron Donor. *Chem. Commun.* 14, 1842–1844. doi:10.1039/B418811J
- Kimura, M., Saito, Y., Ohta, K., Hanabusa, K., Shirai, H., and Kobayashi, N. (2002). Self-Organization of Supramolecular Complex Composed of Rigid Dendritic Porphyrin and Fullerene. *J. Am. Chem. Soc.* 124, 5274–5275. doi:10.1021/ja012614p
- Kojima, A., Teshima, K., Shirai, Y., and Miyasaka, T. (2009). Organometal Halide Perovskites as Visible-Light Sensitizers for Photovoltaic Cells. *J. Am. Chem. Soc.* 131, 6050–6051. doi:10.1021/ja809598r
- Komiyama, R., Fukui, A., Murofushi, N., Koide, N., Yamanaka, R., and Katayama, H. (2011). In Technical Digest, 21st International Photovoltaic Science and Engineering Conference, November 2011, Fukuoka.
- Konarev, D. V., Kovalevsky, A. Y., Li, X., Neretin, I. S., Litvinov, A. L., Drichko, N. V., et al. (2002). Synthesis and Structure of Multicomponent Crystals of Fullerenes and Metal Tetraarylporphyrins. *Inorg. Chem.* 41, 3638–3646. doi:10.1021/ic011312l
- Konarev, D. V., Khasanov, S. S., Faraonov, M. A., and Lyubovskaya, R. N. (2012). Coordination of Fullerene C60 and Benzonitrile to Iron(II) Tetraphenylporphyrin in the FeITPP-C60-(C6H4Cl2)<sub>2</sub>-(C6H14)<sub>0.5</sub> and FeITPP-(C6H5CN)<sub>2</sub> Complexes. *CrystEngComm* 14, 4350. doi:10.1039/c2ce25295c
- Konarev, D. V., Khasanov, S. S., Saito, G., and Lyubovskaya, R. N. (2009). Design of Molecular and Ionic Complexes of Fullerene C60 with Metal(II) Octaethylporphyrins, MII OEP (M = Zn, Co, Fe, and Mn) Containing Coordination M–N(ligand) and M–C(C60–) Bonds. *Cryst. Growth Des.* 9, 1170–1181. doi:10.1021/cg8010184
- Kongkanand, A., Domínguez, R. M., and Kamat, P. V. (2007). Single wall Carbon Nanotube Scaffolds for Photoelectrochemical Solar Cells. Capture and Transport of Photogenerated Electrons. *Nano Lett.* 7, 676–680. doi:10.1021/nl0627238
- Krishna, M. B. M., Venkatramiah, N., Venkatesan, R., and Rao, D. N. (2012). Synthesis and Structural, Spectroscopic and Nonlinear Optical Measurements of Graphene Oxide and its Composites with Metal and Metal Free Porphyrins. *J. Mater. Chem.* 22, 3059–3068.
- Kuciauskas, D., Lin, S., Seely, G. R., Moore, A. L., Moore, T. A., Gust, D., et al. (1996). Energy and Photoinduced Electron Transfer in Porphyrin–Fullerene Dyads. *J. Phys. Chem.* 100, 15926–15932. doi:10.1021/jp9612745
- Landi, B. J., Castro, S. L., Ruf, H. J., Evans, C. M., Bailey, S. G., and Raffaele, R. P. (2005). CdSe Quantum Dot-Single wall Carbon Nanotube Complexes for

- Polymeric Solar Cells. *Solar Energ. Mater. Solar Cell* 87, 733–746. doi:10.1016/j.solmat.2004.07.047
- Law, C., Pathirana, S. C., Li, X., Anderson, A. Y., Barnes, P. R. F., Listorti, A., et al. (2010). Water-Based Electrolytes for Dye-Sensitized Solar Cells. *Adv. Mater.* 22, 4505–4509. doi:10.1002/adma.201001703
- Lee, J.-W., Seol, D.-J., Cho, A.-N., and Park, N.-G. (2014). High-Efficiency Perovskite Solar Cells Based on the Black Polymorph of  $\text{HC}(\text{NH}_2)_2\text{PbI}_3$ . *Adv. Mater.* 26, 4991–4998. doi:10.1002/adma.201401137
- Lee, M. M., Teuscher, J., Miyasaka, T., Murakami, T. N., and Snaith, H. J. (2012). Efficient Hybrid Solar Cells Based on Meso-Superstructured Organometal Halide Perovskites. *Science* 338, 643–647. doi:10.1126/science.1228604
- Lehtivuori, H., Lemmetyinen, H., and Tkachenko, N. V. (2006). Exciplex–Exciplex Energy Transfer and Annihilation in Solid Films of Porphyrin–Fullerene Dyads. *J. Am. Chem. Soc.* 128, 16036–16037. doi:10.1021/ja0662366
- Lévy-Clément, C., Tena-Zaera, R., Ryan, M. A., Katty, A., and Hodes, G. (2005). CdSe-Sensitized p-CuSCN/Nanowire n-ZnO Heterojunctions. *Adv. Mater.* 17, 1512–1515. doi:10.1002/adma.200590085
- Li, D., Müller, M. B., Gilje, S., Kaner, R. B., and Wallace, G. G. (2008). Processable Aqueous Dispersions of Graphene Nanosheets. *Nat. Nanotech* 3, 101–105. doi:10.1038/nnano.2007.451
- Li, K., Hu, Z., Ma, J., Chen, S., Mu, D., and Zhang, J. (2019). A 3D and Stable Lithium Anode for High-Performance Lithium-Iodine Batteries. *Adv. Mater.* 31, 1902399. doi:10.1002/adma.201902399
- Li, X., Cai, W., An, J., Kim, S., Nah, J., Yang, D., et al. (2009). Large-area Synthesis of High-Quality and Uniform Graphene Films on Copper Foils. *Science* 324, 1312–1314. doi:10.1126/science.1171245
- Lightcap, I. V., and Kamat, P. V. (2012). Fortification of CdSe Quantum Dots with Graphene Oxide. Excited State Interactions and Light Energy Conversion. *J. Am. Chem. Soc.* 134, 7109–7116. doi:10.1021/ja3012929
- Listorti, A., O'Regan, B., and Durrant, J. R. (2011). Electron Transfer Dynamics in Dye-Sensitized Solar Cells. *Chem. Mater.* 23, 3381–3399. doi:10.1021/cm200651e
- Liu, J., Zubiri, M. R. I., Dossot, M., Vigolo, B., Hauge, R. H., Fort, Y., et al. (2006). Sidewall Functionalization of Single-wall Carbon Nanotubes (SWNTs) through Aryl Free Radical Addition. *Chem. Phys. Lett.* 430, 93–96. doi:10.1016/j.cplett.2006.08.099
- Liu, T., and Schneider, H.-J. (2002). Additivity and Quantification of Dispersive Interactions-From Cyclopropyl to Nitro Groups: Measurements on Porphyrin Derivatives. *Angew. Chem. Int. Edition* 41, 1368–1370. doi:10.1002/1521-3773(20020415)41:8<1368::aid-anie1368>3.0.co;2-n
- Losurdo, M., Giangregorio, M. M., Capezuto, P., and Bruno, G. (2011). Graphene CVD Growth on Copper and Nickel: Role of Hydrogen in Kinetics and Structure. *Phys. Chem. Chem. Phys.* 13, 20836–20843. doi:10.1039/c1cp22347j
- Lotya, M., Hernandez, Y., King, P. J., Smith, R. J., Nicolosi, V., Karlsson, L. S., et al. (2009). Liquid Phase Production of Graphene by Exfoliation of Graphite in Surfactant/water Solutions. *J. Am. Chem. Soc.* 131, 3611–3620. doi:10.1021/ja807449u
- Loutfy, R. O., and Sharp, J. H. (1979). Photovoltaic Properties of Metal-free Phthalocyanines. I. Al/H<sub>2</sub>Pc Schottky Barrier Solar Cells. *J. Chem. Phys.* 71, 1211–1217. doi:10.1063/1.438476
- Lu, L., Xu, T., Chen, W., Lee, J. M., Luo, Z., Jung, I. H., et al. (2013). The Role of N-Doped Multiwall Carbon Nanotubes in Achieving Highly Efficient Polymer Bulk Heterojunction Solar Cells. *Nano Lett.* 13, 2365–2369. doi:10.1021/nl304533j
- Lu, P., Wang, X., Wen, L., Jiang, X., Guo, W., Wang, L., et al. (2019). Silica-Mediated Formation of Nickel Sulfide Nanosheets on CNT Films for Versatile Energy Storage. *Small* 15, 1805064. doi:10.1002/smll.201805064
- Lu, X., Yu, M., Huang, H., and Ruoff, R. S. (1999). Tailoring Graphite with the Goal of Achieving Single Sheets. *Nanotechnology* 10, 269. doi:10.1088/0957-4484/10/3/308
- Lunt, R. R., Giebink, N. C., Belak, A. A., Benziger, J. B., and Forrest, S. R. (2009). Exciton Diffusion Lengths of Organic Semiconductor Thin Films Measured by Spectrally Resolved Photoluminescence Quenching. *J. Appl. Phys.* 105, 53711.
- Luque, A., and Hegedus, S. (2011). Handbook of Photovoltaic Science and Engineering. Available at: www.wiley.com.
- Maggini, L., Füstös, M. E., Chamberlain, T. W., Cebrián, C., Natali, M., Pietraszkiewicz, M., et al. (2014). Fullerene-driven Encapsulation of a Luminescent Eu(III) Complex in Carbon Nanotubes. *Nanoscale* 6, 2887–2894. doi:10.1039/c3nr05876j
- Mann, J. R., Gannon, M. K., Fitzgibbons, T. C., Detty, M. R., and Watson, D. F. (2008). Optimizing the Photocurrent Efficiency of Dye-Sensitized Solar Cells through the Controlled Aggregation of Chalcogenoxanthylum Dyes on Nanocrystalline Titania Films. *J. Phys. Chem. C* 112, 13057–13061. doi:10.1021/jp803990b
- Mao, B., Calatayud, D. G., Mirabello, V., Kuganathan, N., Ge, H., Jacobs, R. M. J., et al. (2017). Fluorescence-Lifetime Imaging and Super-resolution Microscopies Shed Light on the Directed- and Self-Assembly of Functional Porphyrins onto Carbon Nanotubes and Flat Surfaces. *Chemistry* 23, 9772–9789. doi:10.1002/chem.201605232
- Mao, B., Cortezon-Tamarit, F., Ge, H., Kuganathan, N., Mirabello, V., Palomares, F. J., et al. (2019). Directed Molecular Stacking for Engineered Fluorescent Three-Dimensional Reduced Graphene Oxide and Corone Frameworks. *ChemistryOpen* 8, 1383–1398. doi:10.1002/open.201900310
- Mao, B., Calatayud, D. G., Mirabello, V., Hodges, B. J., Martins, J. A. R., Botchway, S. W., et al. (2016). Interactions between an Aryl Thioacetate-Functionalized Zn(II) Porphyrin and Graphene Oxide. *Adv. Funct. Mater.* 26, 687–697. doi:10.1002/adfm.201504147
- Martinson, A. B., Elam, J. W., Hupp, J. T., and Pellin, M. J. (2007). ZnO Nanotube Based Dye-Sensitized Solar Cells. *Nano Lett.* 7, 2183–2187. doi:10.1021/nl070160+
- Mathew, S., Yu, J., Johnston, M. R., Quinton, J. S., and Shapter, J. G. (2008). “Surface Mounted Porphyrin-Nanotube Arrays: Towards Energy-Harvesting Surfaces,” in 2008 International Conference on Nanoscience and Nanotechnology, Melbourne, VIC, Australia, 25–29 Feb. 2008 (IEEE), 206–209. doi:10.1109/ICONN.2008.4639283
- Matsumura, M., Mitsuda, K., Yoshizawa, N., and Tsubomura, H. (1981). Photocurrents in the ZnO and TiO<sub>2</sub> Photoelectrochemical Cells Sensitized by Xanthene Dyes and Tetraphenylporphines. Effect of Substitution on the Electron Injection Processes. *Bcsj* 54, 692–695. doi:10.1246/bcsj.54.692
- Matsumura, M., Nomura, Y., and Tsubomura, H. (1977). Dye-sensitization on the Photocurrent at Zinc Oxide Electrode in Aqueous Electrolyte Solution. *Bcsj* 50, 2533–2537. doi:10.1246/bcsj.50.2533
- Mattevi, C., Eda, G., Agnoli, S., Miller, S., Mkhoyan, K. A., Celik, O., et al. (2009). Evolution of Electrical, Chemical, and Structural Properties of Transparent and Conducting Chemically Derived Graphene Thin Films. *Adv. Funct. Mater.* 19, 2577–2583. doi:10.1002/adfm.200900166
- Meng, H., Pang, S., and Cui, G. (2019). Photo-Supercapacitors Based on Third-Generation Solar Cells. *ChemSusChem* 12, 3431–3447. doi:10.1002/cssc.201900398
- Meng, S., Maragakis, P., Papaloukas, C., and Kaxiras, E. (2007). DNA Nucleoside Interaction and Identification with Carbon Nanotubes. *Nano Lett.* 7, 45–50. doi:10.1021/nl0619103
- Mikhnenko, O. V., Azimi, H., Scharber, M., Morana, M., Blom, P. W. M., and Loi, M. A. (2012). Exciton Diffusion Length in Narrow Bandgap Polymers. *Energ. Environ. Sci.* 5, 6960. doi:10.1039/c2ee03466b
- Mishra, A., and Bäuerle, P. (2012). Small Molecule Organic Semiconductors on the Move: Promises for Future Solar Energy Technology. *Angew. Chem. Int. Ed.* 51, 2020–2067. doi:10.1002/anie.201102326
- Moharam, M. M., El Shazly, A. N., Anand, K. V., Rayan, D. E.-R. A., Mohammed, M. K. A., Rashad, M. M., et al. (2021). Semiconductors as Effective Electrodes for Dye Sensitized Solar Cell Applications. *Top. Curr. Chem. (Z)* 379, 20. doi:10.1007/s41061-021-00334-w
- Murakami, H., Nomura, T., and Nakashima, N. (2003a). Noncovalent Porphyrin-Functionalized Single-Walled Carbon Nanotubes in Solution and the Formation of Porphyrin-Nanotube Nanocomposites. *Chem. Phys. Lett.* 378, 481–485. doi:10.1016/s0009-2614(03)01329-0
- Murakami, T. N., Saito, H., Uegusa, S., Kawashima, N., and Miyasaka, T. (2003b). Water-based Dye-Sensitized Solar Cells: Interfacial Activation of TiO<sub>2</sub> Mesopores in Contact with Aqueous Electrolyte for Efficiency Development. *Chem. Lett.* 32, 1154–1155. doi:10.1246/cl.2003.1154
- Murakoshi, K., Kogure, R., Wada, Y., and Yanagida, S. (1997). Solid State Dye-Sensitized TiO<sub>2</sub> Solar Cell with Polypyrrole as Hole Transport Layer. *Chem. Lett.* 26, 471–472. doi:10.1246/cl.1997.471
- Nakanishi, T., Ohtani, B., and Uosaki, K. (1998). Effect of Immobilized Electron Relay on the Interfacial Photoinduced Electron Transfer at a Layered Inorganic-Organic Composite Film on Gold. *J. Electroanalytical Chem.* 455, 229–234. doi:10.1016/s0022-0728(98)00261-7

- Nazeeruddin, M. K., De Angelis, F., Fantacci, S., Selloni, A., Viscardi, G., Liska, P., et al. (2005). Combined Experimental and DFT-TDDFT Computational Study of Photoelectrochemical Cell Ruthenium Sensitizers. *J. Am. Chem. Soc.* 127, 16835–16847. doi:10.1021/ja052467l
- Nazeeruddin, M. K., Humphry-Baker, R., Officer, D. L., Campbell, W. M., Burrell, A. K., and Grätzel, M. (2004). Application of Metalloporphyrins in Nanocrystalline Dye-Sensitized Solar Cells for Conversion of Sunlight into Electricity. *Langmuir* 20, 6514–6517. doi:10.1021/la0496082
- Nelson, J. (2003). *The Physics of Solar Cells*. London: World Scientific.
- Nobukuni, H., Tani, F., Shimazaki, Y., Naruta, Y., Ohkubo, K., Nakanishi, T., et al. (2009). Anisotropic High Electron Mobility and Photodynamics of a Self-Assembled Porphyrin Nanotube Including C60 Molecules. *J. Phys. Chem. C* 113, 19694–19699. doi:10.1021/jp9076849
- Nojiri, T., Watanabe, A., and Ito, O. (1998). Photoinduced Electron Transfer between C60/C70 and Zinc Tetraphenylporphyrin in Polar Solvents. *J. Phys. Chem. A* 102, 5215–5219. doi:10.1021/jp981446t
- Novoselov, K. S., Jiang, Z., Zhang, Y., Morozov, S. V., Stormer, H. L., Zeitler, U., et al. (2007). Room-temperature Quantum Hall Effect in Graphene. *Science* 315, 1379. doi:10.1126/science.1137201
- NREL <http://www.nrel.gov/ncpv/No Title>. 2015. Available at: <http://www.nrel.gov/ncpv/>
- Nusbaumer, H., Moser, J.-E., Zakeeruddin, S. M., Nazeeruddin, M. K., and Grätzel, M. (2001). CoII(dbbp)22+ Complex Rivals Tri-iodide/Iodide Redox Mediator in Dye-Sensitized Photovoltaic Cells. *J. Phys. Chem. B* 105, 10461. doi:10.1021/jp012075a
- Okada, S., Saito, S., and Oshiyama, A. (2001). Energetics and Electronic Structures of Encapsulated C60 in a Carbon Nanotube. *Phys. Rev. Lett.* 86, 3835–3838. doi:10.1103/physrevlett.86.3835
- Oku, T., Noma, T., Suzuki, A., Kikuchi, K., and Kikuchi, S. (2010). Fabrication and Characterization of Fullerene/porphyrin Bulk Heterojunction Solar Cells. *J. Phys. Chem. Sol.* 71, 551–555. doi:10.1016/j.jpcs.2009.12.034
- O'regan, B., and Grätzel, M. (1991). A Low-Cost, High-Efficiency Solar Cell Based on Dye-Sensitized Colloidal TiO<sub>2</sub> Films. *Nature* 353, 737–740. doi:10.1038/353737a0
- Organic Solar Cell (OSC) | Chihaya Adachi lab Organic Solar Cell (OSC) | Chihaya Adachi Lab. Available at: [http://www.cstf.kyushu-u.ac.jp/~adachilab/lab/?page\\_id=3927](http://www.cstf.kyushu-u.ac.jp/~adachilab/lab/?page_id=3927) (Accessed June 6, 2021).
- Oskam, G., Bergeron, B. V., Meyer, G. J., and Searson, P. C. (2001). Pseudohalogens for Dye-Sensitized TiO<sub>2</sub> Photoelectrochemical Cells. *J. Phys. Chem. B* 105, 6867–6873. doi:10.1021/jp004411d
- Owen, R. E., Cortezon-Tamarit, F., Calatayud, D. G., Evans, E. A., Mitchell, S. I. J., Mao, B., et al. (2020). Shedding Light onto the Nature of Iron Decorated Graphene and Graphite Oxide Nanohybrids for CO<sub>2</sub> Conversion at Atmospheric Pressure. *ChemistryOpen* 9, 242–252. doi:10.1002/open.201900368
- Paetzold, M. (2018). *Lizenz: Creative Commons by-sa-3.0 de, CC BY-SA 3.0 DE*. Wikimedia Commons. Available at: <https://www.nrel.gov/pv/>
- Pan, S., and Liu, X. (2012). CdS-Graphene Nanocomposite: Synthesis, Adsorption Kinetics and High Photocatalytic Performance under Visible Light Irradiation. *New J. Chem.* 36, 1781–1787. doi:10.1039/c2nj40301c
- Parida, B., Iniyen, S., and Goic, R. (2011). A Review of Solar Photovoltaic Technologies. *Renew. Sust. Energ. Rev.* 15, 1625–1636. doi:10.1016/j.rser.2010.11.032
- Park, H. J., Xu, T., Lee, J. Y., Ledbetter, A., and Guo, L. J. (2011). Photonic Color Filters Integrated with Organic Solar Cells for Energy Harvesting. *ACS Nano* 5, 7055–7060. doi:10.1021/nn201767e
- Park, J. K., Lee, H. R., Chen, J., Shinokubo, H., Osuka, A., and Kim, D. (2008). Photoelectrochemical Properties of Doubly  $\beta$ -Functionalized Porphyrin Sensitizers for Dye-Sensitized Nanocrystalline-TiO<sub>2</sub> Solar Cells. *J. Phys. Chem. C* 112, 16691–16699. doi:10.1021/jp804258q
- Pascu, S. I., Kuganathan, N., Tong, L. H., Jacobs, R. M. J., Barnard, P. J., Chu, B. T., et al. (2008). Interactions between Tripodal Porphyrin Hosts and Single Walled Carbon Nanotubes: an Experimental and Theoretical (DFT) Account. *J. Mater. Chem.* 18, 2781. doi:10.1039/b719494c
- Pasquier, A. D., Unalan, H. E., Kanwal, A., Miller, S., and Chhowalla, M. (2005). Conducting and Transparent Single-wall Carbon Nanotube Electrodes for Polymer-Fullerene Solar Cells. *Appl. Phys. Lett.* 87, 203511. doi:10.1063/1.2132065
- Pearce, J. M., Podraza, N., Collins, R. W., Al-Jassim, M. M., Jones, K. M., Deng, J., et al. (2007). Optimization of Open Circuit Voltage in Amorphous Silicon Solar Cells with Mixed-phase (Amorphous+nanocrystalline) P-type Contacts of Low Nanocrystalline Content. *J. Appl. Phys.* 101, 114301–114307. doi:10.1063/1.2714507
- Petermann, J. H., Zielke, D., Schmidt, J., Haase, F., Rojas, E. G., and Brendel, R. (2012). 19%-efficient and 43 Mm-Thick Crystalline Si Solar Cell from Layer Transfer Using Porous Silicon. *Prog. Photovoltaics Res. Appl.* 20, 1–5. doi:10.1002/ppp.1129
- Photovoltaic Research NREL Photovoltaic Research | NREL. Available at: <https://www.nrel.gov/pv/> (Accessed June 6, 2021).
- Qu, X., He, Y., Qu, M., Ruan, T., Chu, F., Zheng, Z., et al. (2021). Identification of Embedded Nanotwins at C-Si/a-Si:H Interface Limiting the Performance of High-Efficiency Silicon Heterojunction Solar Cells. *Nat. Energ.* 6, 194–202. doi:10.1038/s41560-020-00768-4
- Radivojevic, I., Bazzan, G., Burton-Pye, B. P., Ithiuphalap, K., Saleh, R., Durstock, M. F., et al. (2012). Zirconium(IV) and Hafnium(IV) Porphyrin and Phthalocyanine Complexes as New Dyes for Solar Cell Devices. *J. Phys. Chem. C* 116, 15867–15877. doi:10.1021/jp301853d
- Rance, G. A., Marsh, D. H., Bourne, S. J., Reade, T. J., and Khlobystov, A. N. (2010). Van der Waals interactions between nanotubes and nanoparticles for controlled assembly of composite nanostructures. *ACS Nano* 4, 4920–4928. doi:10.1021/nn101287u
- Reina, A., Jia, X., Ho, J., Nezich, D., Son, H., Bulovic, V., et al. (2008). Large Area, Few-Layer Graphene Films on Arbitrary Substrates by Chemical Vapor Deposition. *Nano Lett.* 9, 30–35. doi:10.1021/nl801827v
- Ren, J., Huang, Y., Zhu, H., Zhang, B., Zhu, H., Shen, S., et al. (2020). Recent Progress on MOF-derived Carbon Materials for Energy Storage. *Carbon Energy* 2, 176–202. doi:10.1002/cey2.44
- Renewables – Global Energy Review (2020). Renewables – Global Energy Review 2020 – Analysis - IEA. Available at: <https://www.iea.org/reports/global-energy-review-2020/renewables> (Accessed June 2, 2021).
- Report extract Renewables, Report Extract Renewables (2020).
- Ripolles-Sanchis, T., Guo, B.-C., Wu, H.-P., Pan, T.-Y., Lee, H.-W., Raga, S. R., et al. (2012). Design and Characterization of Alkoxy-Wrapped Push-Pull Porphyrins for Dye-Sensitized Solar Cells. *Chem. Commun.* 48, 4368–4370. doi:10.1039/c2cc31111a
- Rockett, A. A. (2010). The Future of Energy - Photovoltaics. *Curr. Opin. Solid State. Mater. Sci.* 14, 117–122. doi:10.1016/j.cossms.2010.09.003
- Rowell, M. W., Topinka, M. A., McGehee, M. D., Prall, H.-J., Dennler, G., Sariciftci, N. S., et al. (2006). Organic Solar Cells with Carbon Nanotube Network Electrodes. *Appl. Phys. Lett.* 88, 233506. doi:10.1063/1.2209887
- Rundel, K., Maniam, S., Deshmukh, K., Gann, E., Prasad, S. K. K., Hodgkiss, J. M., et al. (2017). Naphthalene Diimide-Based Small Molecule Acceptors for Organic Solar Cells. *J. Mater. Chem. A* 5, 12266–12277. doi:10.1039/C7TA02749D
- Ruoff, R. S., Tse, D. S., Malhotra, R., and Lorents, D. C. (1993). Solubility of Fullerene (C<sub>60</sub>) in a Variety of Solvents. *J. Phys. Chem.* 97, 3379–3383. doi:10.1021/j100115a049
- Sai, N., Gearba, R., Dolocan, A., Tritsch, J. R., Chan, W.-L., Chelikowsky, J. R., et al. (2012). Understanding the Interface Dipole of Copper Phthalocyanine (CuPc)/C60: Theory and Experiment. *J. Phys. Chem. Lett.* 3, 2173–2177. doi:10.1021/jz300744r
- Sariciftci, N. S., Smilowitz, L., Heeger, A. J., and Wudl, F. (1992). Photoinduced Electron Transfer from a Conducting Polymer to Buckminsterfullerene. *Science* 258, 1474–1476. doi:10.1126/science.258.5087.1474
- Sauvé, G., and Fernando, R. (2015). Beyond Fullerenes: Designing Alternative Molecular Electron Acceptors for Solution-Processable Bulk Heterojunction Organic Photovoltaics. *J. Phys. Chem. Lett.* 6, 3770–3780. doi:10.1021/acs.jpclett.5b01471
- Scharber, M. C., and Sariciftci, N. S. (2013). Efficiency of Bulk-Heterojunction Organic Solar Cells. *Prog. Polym. Sci.* 38, 1929–1940. doi:10.1016/j.progpolymsci.2013.05.001
- Schultz, O., Glunz, S. W., and Willeke, G. P. (2004). SHORT COMMUNICATION: ACCELERATED PUBLICATION: Multicrystalline Silicon Solar Cells Exceeding 20% Efficiency. *Prog. Photovoltaics Res. Appl.* 12, 553–558. doi:10.1002/ppp.583



- Schuster, D. I., MacMahon, S., Guldi, D. M., Echegoyen, L., and Braslavsky, S. E. (2006). Synthesis and Photophysics of Porphyrin-Fullerene Donor-Acceptor Dyads with Conformationally Flexible Linkers. *Tetrahedron* 62, 1928–1936. doi:10.1016/j.tet.2005.07.127
- Selopal, G. S., Milan, R., Ortolani, L., Morandi, V., Rizzoli, R., Sberveglieri, G., et al. (2014). Graphene as Transparent Front Contact for Dye Sensitized Solar Cells. *Sol. Energ. Mater. Sol. Cell* 135, 991. doi:10.1016/j.solmat.2014.10.016
- Seo, K. D., Lee, M. J., Song, H. M., Kang, H. S., and Kim, H. K. (2012). Novel D- $\pi$ -A System Based on Zinc Porphyrin Dyes for Dye-Sensitized Solar Cells: Synthesis, Electrochemical, and Photovoltaic Properties. *Dyes Pigm.* 94, 143–149. doi:10.1016/j.dyepig.2011.12.006
- Sessler, J. L., Wang, B., and Harriman, A. (1995). Photoinduced Energy Transfer in Associated, but Noncovalently-Linked Photosynthetic Model Systems. *J. Am. Chem. Soc.* 117, 704–714. doi:10.1021/ja00107a014
- Sharma, K., Sharma, V., and Sharma, S. S. (2018). Dye-Sensitized Solar Cells: Fundamentals and Current Status. *Nanoscale Res. Lett.* 13, 381. doi:10.1186/s11671-018-2760-6
- Shi, Y., Liu, G., Jin, R., Xu, H., Wang, Q., and Gao, S. (2019). Carbon Materials from Melamine Sponges for Supercapacitors and Lithium Battery Electrode Materials: A Review. *Carbon Energy* 1, 253–275. doi:10.1002/cey2.19
- Shin, H. J., Kim, K. K., Benayad, A., Yoon, S. M., Park, H. K., Jung, I. S., et al. (2009). Efficient Reduction of Graphite Oxide by Sodium Borohydride and its Effect on Electrical Conductance. *Adv. Funct. Mater.* 19, 1987–1992. doi:10.1002/adfm.200900167
- Shubina, T. E., Marbach, H., Flechtner, K., Kretschmann, A., Jux, N., Buchner, F., et al. (2007). Principle and Mechanism of Direct Porphyrin Metalation: Joint Experimental and Theoretical Investigation. *J. Am. Chem. Soc.* 129, 9476–9483. doi:10.1021/ja072360t
- Smith, R., Karl, G., and Kevin, K. (2002). *The Porphyrin Handbook*. New York: Academic Press.
- Snaith, H. J. (2013). Perovskites: the Emergence of a new era for Low-Cost, High-Efficiency Solar Cells. *J. Phys. Chem. Lett.* 4, 3623–3630. doi:10.1021/jz4020162
- Solladié, N., Walther, M. E., Gross, M., Figueira Duarte, T. M., Bourgogne, C., and Nierengarten, J.-F. (2003). A Supramolecular Cup-And-ball C60-Porphyrin Conjugate System. *Chem. Commun.* 19, 2412–2413. doi:10.1039/B308631C
- Sommer, J. R., Shelton, A. H., Parthasarathy, A., Ghiviriga, I., Reynolds, J. R., and Schanze, K. S. (2011). Photophysical Properties of Near-Infrared Phosphorescent  $\pi$ -Extended Platinum Porphyrins. *Chem. Mater.* 23, 5296–5304. doi:10.1021/cm202241e
- Sprafke, J. K., Stranks, S. D., Warner, J. H., Nicholas, R. J., and Anderson, H. L. (2011). Noncovalent Binding of Carbon Nanotubes by Porphyrin Oligomers. *Angew. Chem. Int. Ed.* 50, 2313–2316. doi:10.1002/anie.201007295
- Stang, P. J., and Olenyuk, B. (1997). Self-Assembly, Symmetry, and Molecular Architecture: Coordination as the Motif in the Rational Design of Supramolecular Metallocyclic Polygons and Polyhedra. *Acc. Chem. Res.* 30, 502–518. doi:10.1021/ar9602011
- Stankovich, S., Dikin, D. A., Dommett, G. H. B., Kohlhaas, K. M., Zimney, E. J., Stach, E. A., et al. (2006). Graphene-based Composite Materials. *Nature* 442, 282–286. doi:10.1038/nature04969
- Stankovich, S., Dikin, D. A., Piner, R. D., Kohlhaas, K. A., Kleinhammes, A., Jia, Y., et al. (2007). Synthesis of Graphene-Based Nanosheets via Chemical Reduction of Exfoliated Graphite Oxide. *Carbon* 45, 1558–1565. doi:10.1016/j.carbon.2007.02.034
- Staudenmaier, L. (1898). Verfahren zur Darstellung der Graphitsäure. *Ber. Dtsch. Chem. Ges.* 31, 1481–1487. doi:10.1002/cber.18980310237
- Steed, J. W., and Atwood, J. L. (2009). *Supramolecular Chemistry*. 2nd Edition. Wiley.
- Strano, M. S., Dyke, C. A., Usrey, M. L., Barone, P. W., Allen, M. J., Shan, H., et al. (2003). Electronic Structure Control of Single-Walled Carbon Nanotube Functionalization. *Science* 301, 1519–1522. doi:10.1126/science.1087691
- Su, C.-Y., Lu, A.-Y., Xu, Y., Chen, F.-R., Khlobystov, A. N., and Li, L.-J. (2011). High-quality Thin Graphene Films from Fast Electrochemical Exfoliation. *ACS Nano* 5, 2332–2339. doi:10.1021/nn200025p
- Sun, D., Tham, F. S., Reed, C. A., and Boyd, P. D. W. (2002a). Extending Supramolecular Fullerene-Porphyrin Chemistry to Pillared Metal-Organic Frameworks. *Proc. Natl. Acad. Sci.* 99, 5088–5092. doi:10.1073/pnas.072602399
- Sun, D., Tham, F. S., Reed, C. A., Chaker, L., and Boyd, P. D. W. (2002b). Supramolecular Fullerene-Porphyrin Chemistry. Fullerene Complexation by Metalated "Jaws Porphyrin" Hosts. *J. Am. Chem. Soc.* 124, 6604–6612. doi:10.1021/ja017555u
- Sun, D., Tham, F. S., Reed, C. A., Chaker, L., Burgess, M., and Boyd, P. D. W. (2000). Porphyrin-Fullerene Host-Guest Chemistry. *J. Am. Chem. Soc.* 122, 10704–10705. doi:10.1021/ja002214m
- Sun, Y., Drovetskaya, T., Bolskar, R. D., Bau, R., Boyd, P. D. W., and Reed, C. A. (1997). Fullerides of Pyrrolidine-Functionalized C60. *J. Org. Chem.* 62, 3642–3649. doi:10.1021/jo970357u
- Sutton, L. R., Scheloske, M., Pirner, K. S., Hirsch, A., Guldi, D. M., and Gisselbrecht, J.-P. (2004). Unexpected Change in Charge Transfer Behavior in a Cobalt(II) Porphyrin-Fullerene Conjugate that Stabilizes Radical Ion Pair States. *J. Am. Chem. Soc.* 126, 10370–10381. doi:10.1021/ja048983d
- Suzuki, A., Kobayashi, K., Oku, T., and Kikuchi, K. (2011). Fabrication and Characterization of Porphyrin Dye-Sensitized Solar Cells. *Mater. Chem. Phys.* 129, 236–241. doi:10.1016/j.matchemphys.2011.04.010
- Tachibana, Y., Nazeeruddin, M. K., Grätzel, M., Klug, D. R., and Durrant, J. R. (2002). Electron Injection Kinetics for the Nanocrystalline TiO<sub>2</sub> Films Sensitized with the Dye (Bu<sub>4</sub>N)<sub>2</sub>Ru(dcbpyH)<sub>2</sub>(NCS)<sub>2</sub>. *Chem. Phys.* 285, 127–132. doi:10.1016/s0301-0104(02)00695-x
- Tang, C. W. (1986). Two-layer Organic Photovoltaic Cell. *Appl. Phys. Lett.* 48, 183–185. doi:10.1063/1.96937
- Tashiro, K., Aida, T., Zheng, J.-Y., Kinbara, K., Saigo, K., Sakamoto, S., et al. (1999). A Cyclic Dimer of Metalloporphyrin Forms a Highly Stable Inclusion Complex with C60. *J. Am. Chem. Soc.* 121, 9477–9478. doi:10.1021/ja992416m
- Terrones, M. (2003). Science and Technology of the Twenty-First century: Synthesis, Properties, and Applications of Carbon Nanotubes. *Annu. Rev. Mater. Res.* 33, 419–501. doi:10.1146/annurev.matsci.33.012802.100255
- Thomas, S., and Thankappan, A. (2018). Perovskite Photovoltaics. *Perovskite Photovoltaics Basic Adv. Concepts Implement.*, 1–501. doi:10.1016/C2016-0-03790-7
- Tian, Y., and Tatsuma, T. (2005). Mechanisms and Applications of Plasmon-Induced Charge Separation at TiO<sub>2</sub>Films Loaded with Gold Nanoparticles. *J. Am. Chem. Soc.* 127, 7632–7637. doi:10.1021/ja042192u
- Tolkai, A., Kaunisto, K., Efimov, A., Kivistö, H., Storbacka, L., Savikoski, R., et al. (2012). Directed Electron Transfer in Langmuir-Schäfer Layers of Porphyrin-Fullerene and Phthalocyanine-Fullerene Dyads in Inverted Organic Solar Cells. *Phys. Chem. Chem. Phys.* 14, 3498. doi:10.1039/c2cp24022j
- Tong, L. H., Pengo, P., Clegg, W., Lowe, J. P., Raithby, P. R., Sanders, J. K. M., et al. (2011). Complexes of Aryl-Substituted Porphyrins and Naphthalenediimide (NDI): Investigations by Synchrotron X-ray Diffraction and NMR Spectroscopy. *Dalton Trans.* 40, 10833. doi:10.1039/c1dt10880h
- Tong, L. H., Wietor, J.-L., Clegg, W., Raithby, P. R., Pascu, S. I., and Sanders, J. K. M. (2008). Supramolecular Assemblies of Tripodal Porphyrin Hosts and C60. *Chem. Eur. J.* 14, 3035–3044. doi:10.1002/chem.200701686
- Tsao, H. N., Yi, C., Moehl, T., Yum, J.-H., Zakeeruddin, S. M., Nazeeruddin, M. K., et al. (2011). Cyclopentadithiophene Bridged Donor-Acceptor Dyes Achieve High Power Conversion Efficiencies in Dye-Sensitized Solar Cells Based on the Tris-Cobalt Bipyridine Redox Couple. *ChemSusChem* 4, 591–594. doi:10.1002/cssc.201100120
- Tu, X., Manohar, S., Jagota, A., and Zheng, M. (2009). DNA Sequence Motifs for Structure-specific Recognition and Separation of Carbon Nanotubes. *Nature* 460, 250–253. doi:10.1038/nature08116
- Tyson, J. A., Calatayud, D. G., Mirabello, V., Mao, B., and Pascu, S. I. (2016a). "Labeling of Graphene, Graphene Oxides, and of Their Congeners," in *Advances in Inorganic Chemistry*. Editors R. van Eldik and C. D. Hubbard (Elsevier), 397–440. doi:10.1016/bs.adioch.2015.09.007
- Tyson, J. A., Mirabello, V., Calatayud, D. G., Ge, H., Kociok-Köhne, G., Botchway, S. W., et al. (2016b). Thermally Reduced Graphene Oxide Nanohybrids of Chiral Functional Naphthalenediimides for Prostate Cancer Cells Bioimaging. *Adv. Funct. Mater.* 26, 5641–5657. doi:10.1002/adfm.201601123
- Uchida, S., Xue, J., Rand, B. P., and Forrest, S. R. (2004). Organic Small Molecule Solar Cells with a Homogeneously Mixed Copper Phthalocyanine: C60 Active Layer. *Appl. Phys. Lett.* 84, 4218–4220. doi:10.1063/1.1755833



- Umeyama, T., and Imahori, H. (2006). Self-Organization of Porphyrins and Fullerenes for Molecular Photoelectrochemical Devices. *Photosynth. Res.* 87, 63–71. doi:10.1007/s11120-005-4632-z
- Valero, S., Cabrera-Espinoza, A., Collavini, S., Pascual, J., Marinova, N., Kosta, I., et al. (2020). Naphthalene Diimide-Based Molecules for Efficient and Stable Perovskite Solar Cells. *Eur. J. Org. Chem.* 2020, 5329–5339. doi:10.1002/ejoc.202000287
- Vijayaraghavan, S., Ćićija, D., Auwärter, W., Joshi, S., Seufert, K., Seitsonen, A. P., et al. (2012). Selective Supramolecular Fullerene-Porphyrin Interactions and Switching in Surface-Confined C60-Ce(TPP)<sub>2</sub> Dyads. *Nano Lett.* 12, 4077–4083. doi:10.1021/nl301534p
- Vögtle, F., Löhr, H.-G., Franke, J., and Worsch, D. (1985). Host/Guest Chemistry of Organic Onium Compounds-Clathrates, Crystalline Complexes, and Molecular Inclusion Compounds in Aqueous Solution. *Angew. Chem. Int. Ed. Engl.* 24, 727–742. doi:10.1002/anie.198507271
- Walker, B., Tamayo, A. B., Dang, X.-D., Zalar, P., Seo, J. H., Garcia, A., et al. (2009). Nanoscale Phase Separation and High Photovoltaic Efficiency in Solution-Processed, Small-Molecule Bulk Heterojunction Solar Cells. *Adv. Funct. Mater.* 19, 3063–3069. doi:10.1002/adfm.200900832
- Wang, C.-L., Zhang, W.-B., Van Horn, R. M., Tu, Y., Gong, X., Cheng, S. Z. D., et al. (2011). A Porphyrin-Fullerene Dyad with a Supramolecular "Double-Cable" Structure as a Novel Electron Acceptor for Bulk Heterojunction Polymer Solar Cells. *Adv. Mater.* 23, 2951–2956. doi:10.1002/adma.201100399
- Wang, J. T.-W., Ball, J. M., Barea, E. M., Abate, A., Alexander-Webber, J. A., Huang, J., et al. (2013). Low-temperature Processed Electron Collection Layers of graphene/TiO<sub>2</sub> Nanocomposites in Thin Film Perovskite Solar Cells. *Nano Lett.* 14, 724–730. doi:10.1021/nl403997a
- Wang, L., Si, W., Tong, Y., Hou, F., Pergolesi, D., Hou, J., et al. (2020). Graphitic Carbon Nitride (g-C<sub>3</sub>N<sub>4</sub>)-based Nanosized Heteroarrays: Promising Materials for Photoelectrochemical Water Splitting. *Carbon Energy* 2, 223–250. doi:10.1002/cey2.48
- Wang, L., Wen, L., Tong, Y., Wang, S., Hou, X., An, X., et al. (2021a). Photo-rechargeable Batteries and Supercapacitors: Critical Roles of Carbon-based Functional Materials. *Carbon Energy* 3, 225–252. doi:10.1002/cey2.105
- Wang, Q., Campbell, W. M., Bonfantani, E. E., Jolley, K. W., Officer, D. L., Walsh, P. J., et al. (2005a). Efficient Light Harvesting by Using Green Zn-Porphyrin-Sensitized Nanocrystalline TiO<sub>2</sub>Films. *J. Phys. Chem. B* 109, 15397–15409. doi:10.1021/jp052877w
- Wang, X., Wang, L., Zhang, B., Feng, J., Zhang, J., Ou, X., et al. (2021b). A Flexible Carbon nanotube@V<sub>2</sub>O<sub>5</sub> Film as a High-Capacity and Durable Cathode for Zinc Ion Batteries. *J. Energ. Chem.* 59, 126–133. doi:10.1016/j.jechem.2020.10.007
- Wang, X., Zhi, L., and Müllen, K. (2008). Transparent, Conductive Graphene Electrodes for Dye-Sensitized Solar Cells. *Nano Lett.* 8, 323–327. doi:10.1021/nl072838r
- Wang, Y.-B., and Lin, Z. (2003). Supramolecular Interactions between Fullerenes and Porphyrins. *J. Am. Chem. Soc.* 125, 6072–6073. doi:10.1021/ja028998g
- Wang, Z.-S., Cui, Y., Hara, K., Dan-oh, Y., Kasada, C., and Shinpo, A. (2007). A High-Light-Harvesting-Efficiency Coumarin Dye for Stable Dye-Sensitized Solar Cells. *Adv. Mater.* 19, 1138–1141. doi:10.1002/adma.200601020
- Wang, Z.-S., Sayama, K., and Sugihara, H. (2005b). Efficient Eosin Y Dye-Sensitized Solar Cell Containing Br<sup>-</sup>/Br<sub>3</sub>-Electrolyte. *J. Phys. Chem. B* 109, 22449–22455. doi:10.1021/jp053260h
- Watkins, P. K., Walker, A. B., and Verschoor, G. L. B. (2005). Dynamical Monte Carlo Modelling of Organic Solar Cells: The Dependence of Internal Quantum Efficiency on Morphology. *Nano Lett.* 5, 1814–1818. doi:10.1021/nl051098o
- Werner, F., Gnichwitz, J.-F., Marczak, R., Palomares, E., Peukert, W., Hirsch, A., et al. (2010). Grafting Porphyrins (Face-to-Edge/Orthogonal versus Face-to-Face/Parallel) to ZnO en Route toward Dye-Sensitized Solar Cells. *J. Phys. Chem. B* 114, 14671–14678. doi:10.1021/jp102737a
- Wessendorf, F., Grimm, B., Guldi, D. M., and Hirsch, A. (2010). Pairing Fullerenes and Porphyrins: Supramolecular Wires that Exhibit Charge Transfer Activity. *J. Am. Chem. Soc.* 132, 10786–10795. doi:10.1021/ja101937w
- WHO (2018). Climate Change and Health. Available at: <https://www.who.int/news-room/fact-sheets/detail/climate-change-and-health> (Accessed June 3, 2021).
- Williams, G., Seger, B., and Kamat, P. V. (2008). TiO<sub>2</sub>-graphene Nanocomposites. UV-Assisted Photocatalytic Reduction of Graphene Oxide. *ACS Nano* 2, 1487–1491. doi:10.1021/nn800251f
- World Energy Outlook 2020 – Analysis - IEA World Energy Outlook 2020 – Analysis - IEA. Available at: <https://www.iea.org/reports/world-energy-outlook-2020?mode=overview> (Accessed June 3, 2021).
- Xiang, N., Zhou, W., Jiang, S., Deng, L., Liu, Y., Tan, Z., et al. (2011). Synthesis and Characterization of Trivalent Metal Porphyrin with NCS Ligand for Application in Dye-Sensitized Solar Cells. *Solar Energy Mater. Solar Cell* 95, 1174–1181. doi:10.1016/j.solmat.2010.12.051
- Yan, J., Uddin, M. J., Dickens, T. J., and Okoli, O. I. (2013). Carbon Nanotubes (CNTs) Enrich the Solar Cells. *Solar Energy* 96, 239–252. doi:10.1016/j.solener.2013.07.027
- Yella, A., Lee, H.-W., Tsao, H. N., Yi, C., Chandiran, A. K., Nazeeruddin, M. K., et al. (2011). Porphyrin-Sensitized Solar Cells with Cobalt (II/III)-Based Redox Electrolyte Exceed 12 Percent Efficiency. *Science* 334, 629–634. doi:10.1126/science.1209688
- Yu, G., Gao, J., Hummelen, J. C., Wudl, F., and Heeger, A. J. (1995). Polymer Photovoltaic Cells: Enhanced Efficiencies via a Network of Internal Donor-Acceptor Heterojunctions. *Science* 270, 1789–1791. doi:10.1126/science.270.5243.1789
- Yum, J.-H., Walter, P., Huber, S., Rentsch, D., Geiger, T., Nüesch, F., et al. (2007). Efficient Far Red Sensitization of Nanocrystalline TiO<sub>2</sub>Films by an Unsymmetrical Squaraine Dye. *J. Am. Chem. Soc.* 129, 10320–10321. doi:10.1021/ja0731470
- Zeng, W., Cao, Y., Bai, Y., Wang, Y., Shi, Y., Zhang, M., et al. (2010). Efficient Dye-Sensitized Solar Cells with an Organic Photosensitizer Featuring Orderly Conjugated Ethylenedioxythiophene and Dithienosilole Blocks. *Chem. Mater.* 22, 1915–1925. doi:10.1021/cm9036988
- Zhang, J., Zou, H., Qing, Q., Yang, Y., Li, Q., Liu, Z., et al. (2003). Effect of Chemical Oxidation on the Structure of Single-Walled Carbon Nanotubes. *J. Phys. Chem. B* 107, 3712–3718. doi:10.1021/jp027500u
- Zhang, Q., and Cao, G. (2011). Nanostructured Photoelectrodes for Dye-Sensitized Solar Cells. *Nano Today* 6, 91–109. doi:10.1016/j.nantod.2010.12.007
- Zhang, S., Wang, X., Tang, A., Huang, J., Zhan, C., and Yao, J. (2014). Tuning Morphology and Photovoltaic Properties of Diketopyrrolopyrrole-Based Small-Molecule Solar Cells by Tailoring End-Capped Aromatic Groups. *Phys. Chem. Chem. Phys.* 16, 4664–4671. doi:10.1039/c3cp54548b
- Zhang, X.-F., and Xi, Q. (2011). A Graphene Sheet as an Efficient Electron Acceptor and Conductor for Photoinduced Charge Separation. *Carbon* 49, 3842–3850. doi:10.1016/j.carbon.2011.05.019
- Zhang, X., Yin, J., Peng, C., Hu, W., Zhu, Z., Li, W., et al. (2011). Distribution and Biocompatibility Studies of Graphene Oxide in Mice after Intravenous Administration. *Carbon* 49, 986–995. doi:10.1016/j.carbon.2010.11.005
- Zhang, Y.-H., Ruan, W.-J., Li, Z.-Y., Wu, Y., and Zheng, J.-Y. (2005). DFT Study on the Influence of Meso-Phenyl Substitution on the Geometric, Electronic Structure and Vibrational Spectra of Free Base Porphyrin. *Chem. Phys.* 315, 201–213. doi:10.1016/j.chemphys.2005.04.004
- Zhang, Y., Guo, L., Wei, S., He, Y., Xia, H., Chen, Q., et al. (2010). Direct Imprinting of Microcircuits on Graphene Oxides Film by Femtosecond Laser Reduction. *Nano Today* 5, 15–20. doi:10.1016/j.nantod.2009.12.009
- Zhang, Z., Yuan, J., Wei, Q., and Zou, Y. (2018). Small-Molecule Electron Acceptors for Efficient Non-fullerene Organic Solar Cells. *Front. Chem.* 6. doi:10.3389/fchem.2018.00414
- Zheng, J.-Y., Tashiro, K., Hirabayashi, Y., Kinbara, K., Saigo, K., Aida, T., et al. (2001). Cyclic Dimers of Metalloporphyrins as Tunable Hosts for Fullerenes: A Remarkable Effect of Rhodium(III). *Angew. Chem. Int. Ed.* 40, 1857–1861. doi:10.1002/1521-3773(20010518)40:10<1857::aid-anie1857>3.0.co;2-y
- Zhi, J., Cui, H., Chen, A., Xie, Y., and Huang, F. (2015). Efficient Highly Flexible Dye Sensitized Solar Cells of Three Dimensional Graphene Decorated Titanium Dioxide Nanoparticles on Plastic Substrate. *J. Power Sourc.* 281, 404–410. doi:10.1016/j.jpowsour.2015.02.001
- Zhong, S., Zhong, J. Q., Wang, X. Z., Huang, M. Y., Qi, D. C., Chen, Z. K., et al. (2012). Investigation of Interface Properties for ClAlPc/

- C60 Heterojunction-Based Inverted Organic Solar Cell. *J. Phys. Chem. C* 116, 2521–2526. doi:10.1021/jp210533n
- Zhou, M., Wang, Y., Zhai, Y., Zhai, J., Ren, W., Wang, F., et al. (2009a). Controlled Synthesis of Large-Area and Patterned Electrochemically Reduced Graphene Oxide Films. *Chem. Eur. J.* 15, 6116–6120. doi:10.1002/chem.200900596
- Zhou, Y., Bao, Q., Tang, L. A. L., Zhong, Y., and Loh, K. P. (2009b). Hydrothermal Dehydration for the “green” Reduction of Exfoliated Graphene Oxide to Graphene and Demonstration of Tunable Optical Limiting Properties. *Chem. Mater.* 21, 2950–2956. doi:10.1021/cm9006603
- Zhu, H. W., Xu, C. L., Wu, D. H., Wei, B. Q., Vajtai, R., and Ajayan, P. M. (2002). Direct Synthesis of Long Single-Walled Carbon Nanotube Strands. *Science* (80-. ) 296, 884–886. doi:10.1126/science.1066996
- Zhu, Y., Murali, S., Stoller, M. D., Velamakanni, A., Piner, R. D., and Ruoff, R. S. (2010). Microwave Assisted Exfoliation and Reduction of Graphite Oxide for Ultracapacitors. *Carbon* 48, 2118–2122. doi:10.1016/j.carbon.2010.02.001

**Conflict of Interest:** The authors declare that the research was conducted in the absence of any commercial or financial relationships that could be construed as a potential conflict of interest.

**Publisher’s Note:** All claims expressed in this article are solely those of the authors and do not necessarily represent those of their affiliated organizations, or those of the publisher, the editors and the reviewers. Any product that may be evaluated in this article, or claim that may be made by its manufacturer, is not guaranteed or endorsed by the publisher.

Copyright © 2021 Mao, Hodges, Franklin, Calatayud and Pascu. This is an open-access article distributed under the terms of the Creative Commons Attribution License (CC BY). The use, distribution or reproduction in other forums is permitted, provided the original author(s) and the copyright owner(s) are credited and that the original publication in this journal is cited, in accordance with accepted academic practice. No use, distribution or reproduction is permitted which does not comply with these terms.



# Enabling Technology for Supramolecular Chemistry

Katie Ollerton<sup>1</sup>, Rebecca L. Greenaway<sup>2\*</sup> and Anna G. Slater<sup>1\*</sup>

<sup>1</sup>Department of Chemistry and Materials Innovation Factory, University of Liverpool, Liverpool, United Kingdom, <sup>2</sup>Department of Chemistry, Molecular Sciences Research Hub, Imperial College London, London, United Kingdom

Supramolecular materials—materials that exploit non-covalent interactions—are increasing in structural complexity, selectivity, function, stability, and scalability, but their use in applications has been comparatively limited. In this Minireview, we summarize the opportunities presented by enabling technology—flow chemistry, high-throughput screening, and automation—to wield greater control over the processes in supramolecular chemistry and accelerate the discovery and use of self-assembled systems. Finally, we give an outlook for how these tools could transform the future of the field.

**Keywords:** supramolecular chemistry, self-assembly, flow chemistry, high-throughput screening, automation, reaction monitoring

## OPEN ACCESS

### Edited by:

Jennifer Hiscock,  
University of Kent, United Kingdom

### Reviewed by:

Richard J. Hooley,  
University of California, Riverside,  
United States  
Alessandro Scarso,  
Ca' Foscari University of Venice, Italy

### \*Correspondence:

Rebecca L. Greenaway  
r.greenaway@imperial.ac.uk  
Anna G. Slater  
anna.slater@liverpool.ac.uk

### Specialty section:

This article was submitted to  
Supramolecular Chemistry,  
a section of the journal  
Frontiers in Chemistry

**Received:** 13 September 2021

**Accepted:** 21 October 2021

**Published:** 15 November 2021

### Citation:

Ollerton K, Greenaway RL and  
Slater AG (2021) Enabling Technology  
for Supramolecular Chemistry.  
Front. Chem. 9:774987.  
doi: 10.3389/fchem.2021.774987

## INTRODUCTION

Supramolecular chemistry exploits weak, reversible interactions to form complex structures from simpler components (Lehn, 1988; Vantomme and Meijer, 2019). Two key tenets of supramolecular chemistry are host-guest molecular recognition and self-assembly (Davis et al., 2002), which have both become broad disciplines (Albrecht, 2007). Both concepts are ubiquitous in nature: the enzyme-substrate complex, base stacking of DNA and assemblies of virus cages are only a few examples (Whitesides et al., 1991). It is clear to see why chemists want to harness these principles in artificial structures for applications such as artificial enzymes, drug delivery systems, innovative materials, and more.

Huge progress has been made in the function, selectivity, and efficiency of artificial supramolecular systems. The diversity of materials and structures, including those that exploit mechanical bonds [catenanes (Gil-Ramírez et al., 2015), rotaxanes (Yang et al., 2019), knots (Fielden et al., 2017)], host-guest interactions [macrocycle (Liu et al., 2017), cage structures (Hasell and Cooper, 2016)], and framework or soft materials [metal-organic frameworks (MOFs) (Zhou and Kitagawa, 2014; Jiao et al., 2019), hydrogen-bonded organic frameworks (HOFs) (Yusov et al., 2021), supramolecular polymers (Yang et al., 2015) and gels (Weiss, 2014)], is ever-increasing, as is our ability to design and use these structures. As such, promising applications are emerging: porous supramolecular materials have potential in carbon capture (Huck et al., 2014), self-healing polymers could produce materials with enhanced recyclability (Song et al., 2019), and glucose binders could transform how diabetes is managed (Tromans et al., 2019), to name just a few.

However, the formation of supramolecular structures often presents challenges, which in turn limits their wide-spread use. Both non-covalent reversible interactions and reversible covalent reactions can be difficult to control due to their sensitivity to environmental conditions, and often a multitude of possible products are formed as a result (Wu and Isaacs, 2003). Solvent effects (Würthner, 2021) can be unpredictable and lead to unexpected outcomes (Little et al., 2014; Zhang et al., 2015). The use of high-dilution conditions, templating strategies, long reaction times or slow addition of reagents, and/or complex synthetic routes can help overcome these challenges (Martí-Centelles et al., 2015), but in turn limits the scalability of the process. Predictions of which assembly

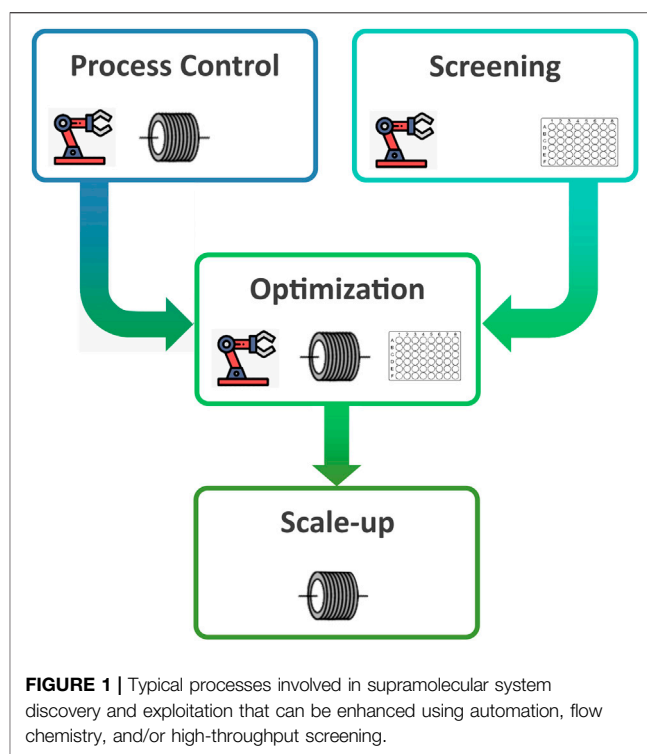
pathway will be followed, or the likely success of the process, can be aided using crystal engineering (Desiraju, 1997) or guided by computation (Greenaway and Jelfs, 2020), but the targeted design of materials with desirable properties can still be a long and restrictive process. Discoveries have generally been made *via* rational and iterative design techniques (Hong et al., 2015), often based on known structures, trial-and-error, or even serendipity (Winpenny, 2002; Saalfrank et al., 2008). However, these approaches limit the scope of possible accessible materials and leave vast areas of chemical space unexplored.

How, then, do supramolecular chemists approach these challenges? Standard tools for the chemist—i.e., round bottomed flasks—do not offer either fine control over environmental parameters (concentration, diffusion and mixing, temperature gradients), particularly on a large scale (Nomura et al., 1996; Kuśmierek and Świątkowski, 2015), or rapid exploration of chemical parameter space. There is therefore a need for tools that enable: 1) greater control over the formation of reversible and/or non-covalent interactions; 2) faster and more extensive exploration of chemical space; and 3) scalable, efficient, and “green” synthesis. This Minireview will explore two complementary approaches to solving these issues: flow chemistry and high-throughput automation, both of which fall under the umbrella of “enabling technology.”

Flow chemistry involves conducting a reaction in a continuous stream in a tube or microreactor (Myers et al., 2014; Plutschack et al., 2017). Flow processes are used extensively in industry; the majority of commodity chemicals are continuously manufactured (Glaser, 2015; Porta et al., 2016; Baumann et al., 2020). Flow chemistry offers benefits such as improved safety and control of reactions, access to a wider range of reaction conditions, easier scale-up, and potential savings in energy use and wastage (Newman and Jensen, 2013). Early adopters of continuous flow chemistry within the supramolecular community used microfluidic chips to influence process outcome (Whitesides, 2006; Zhang et al., 2012; Foster et al., 2015; Parker et al., 2015; Yu et al., 2015; Gong et al., 2016); significant progress in flow technology has since opened a wealth of new opportunities for the field (Arnon et al., 2016; Fang et al., 2018; Cohen-Gerassi et al., 2020; Méndez-Ardoy et al., 2020; Khoeini et al., 2021; Puigmarti-Luis et al., 2021).

High-throughput screening (HTS) enables reactions or processes to be rapidly carried out in parallel, potentially running thousands of samples simultaneously (McNally et al., 2011). Whilst HTS may have been previously affected by a bottleneck in slower dispensing, and analytical or data-processing steps, its growing success has been enabled by the development of automated experimentation platforms and technologies such as liquid and solid handling devices, robotics, autosamplers, and data-analyst software or scripts (Carson, 2020). It has been widely adopted within the pharmaceutical industry (Mennen et al., 2019) and is now finding its use in many other chemical fields.

Although both technologies have had uptake in adjacent fields, there have been fewer reports on the use of flow or HTS in supramolecular chemistry. To showcase the benefits of such enabling technologies, this review will focus on the following four steps of development that are particularly relevant to supramolecular chemistry: enhanced process control, rapid



**FIGURE 1 |** Typical processes involved in supramolecular system discovery and exploitation that can be enhanced using automation, flow chemistry, and/or high-throughput screening.

screening and discovery of new structures, fast and/or automated optimisation, and facilitating scale-up (Figure 1).

## ENABLING TECHNOLOGIES FOR THE STAGES OF DEVELOPMENT IN SUPRAMOLECULAR CHEMISTRY

### Enhanced Process Control

Supramolecular chemists seek to develop materials and systems made of multiple molecular building blocks where the whole is “more than the sum of its parts.” Many have exploited the reversibility of both non-covalent and dynamic covalent systems to form multicomponent structures under thermodynamic equilibrium (Whitesides et al., 1991; Rowan et al., 2002; Otto and Severin, 2007; Han et al., 2010; Okesola and Mata, 2018). Under fully reversible equilibrium conditions, the final outcome of such processes only depends on the molecular building blocks being used and the overall stability of the products: the thermodynamic product is often observed, representing the global energy minimum (Rowan et al., 2002). However, “out-of-equilibrium” structures have recently gained more attention (Ogi et al., 2014). For these systems, the reaction environment has a strong influence on the assembly pathway and the final structures obtained. Under non-equilibrium conditions, or where diffusion is slower than the rate of reaction, the impact of mixing efficiency or local concentration gradients can be substantial (Sevim et al., 2018). Controlling mixing is very difficult to achieve in a standard flask, but can be readily achieved under flow and microfluidic conditions (Nagy et al., 2012; Ward and Fan, 2015).



Microfluidic reactors—where reactions are carried out in channels <1 mm—offer unique control over the mixing of reagents in both space and time (“spatio-temporal control”) (Sevim et al., 2018). The degree of mixing can be much more finely controlled compared to batch, ranging from extremely turbulent flow and thus fast mixing to extremely slow: in the laminar flow regime, streams of fluids flow parallel to each other, creating a defined liquid-liquid interface between them (Brivio et al., 2006). Thus, specific assembly pathways can be deliberately targeted by controlling the flow regime, and obtaining non-equilibrium structures becomes easier in microfluidic environments, facilitating the targeted synthesis of materials with desired properties. Furthermore, in flow, a higher degree of control results in greater reproducibility and a consequent avoidance of off-target reactions due to poor mixing and local concentration gradients.

One recent example where this has been successfully exploited in supramolecular chemistry is the work of Numata et al. (2015b) who were able to synthesise porphyrin microfilms stabilized by an extended two-dimensional hydrogen bonding network. In contrast to batch conditions which formed an amorphous material, the use of microflow conditions enabled the formation of regular hydrogen-bonded networks leading to micron-sized multi-layered porphyrin sheets. This suggested that the microsheets could only be formed following the non-equilibrium kinetic pathway established under microflow conditions. Microfluidic conditions have also been used to access alternative self-assembled structures in a controlled manner in the field of organic conductors (Puigmartí-Luis et al., 2010), co-ordination polymers (Rubio-Martínez et al., 2016b), covalent organic frameworks (COFs) (Rodríguez-San-Miguel et al., 2016; Singh et al., 2018), and MOFs (Ameloot et al., 2011), and to control the hierarchical supramolecular assembly of perylene bisimides (Numata et al., 2015a), nanofibers (Numata and Kozawa, 2013), and amphiphiles (Numata et al., 2015c), with the latter enabling the formation of energetically unfavourable self-assembled structures under kinetic control.

Whilst control over reaction outcomes and the assembly process is a powerful tool, it is made more powerful if it can be rapidly applied to a wide range of systems. One potential drawback of continuous flow is the challenge of parallelising experiments, which currently limits throughput. HTS allows a much faster, and arguably more efficient, exploration of a wider chemical space, and can lead to the accelerated discovery of new structures. Efforts to parallelise or improve the throughput of flow experiments include microdroplet screening (Reizman et al., 2016), continuous variation of variables coupled within inline analysis (Aroh and Jensen, 2018), and multi-channel chip architectures (Headen et al., 2018), and it is likely that these approaches will become increasingly used to combine the benefits of enhanced control with rapid screening.

## Faster, Targeted Screening

Synthetic screening often results in a vast number of structures with only a select few being suitable for the application of interest. Fast and effective screening of the design space thus plays an important role in identifying materials and assemblies with

desirable properties in supramolecular chemistry, and this is where HTS can offer its services.

A typical approach to HTS involves the use of multi-well microtiter plates and is often aided by the use of automated robotic platforms. For example, Greenaway et al. (2018) illustrated the advantages of employing an automated platform for HTS alongside computational analysis in the search for new organic cages. Overall, this led to the streamlined discovery of 33 new organic cages, with two forming bridged-catenane structures upon recrystallization, a new cage topology, highlighting the advantage of HTS in accelerating serendipitous discoveries. Their automated workflow has also been employed in the discovery of other supramolecular assemblies including an unsymmetrical organic cage (Berardo et al., 2018) and socially self-sorted organic pots (Greenaway et al., 2019). More recently, Cui et al. (2019) demonstrated how automated platforms can be used for polymorph screening, resulting in different HOFs being accessed. Additionally, Lin et al. (2021) demonstrated how HTS can screen for supramolecular diversification, resulting in a range of different hierarchical self-assemblies such as thin fibrils, helical ribbons, twisted ribbons, wide and thin ribbons, and macroscopic hydrogels.

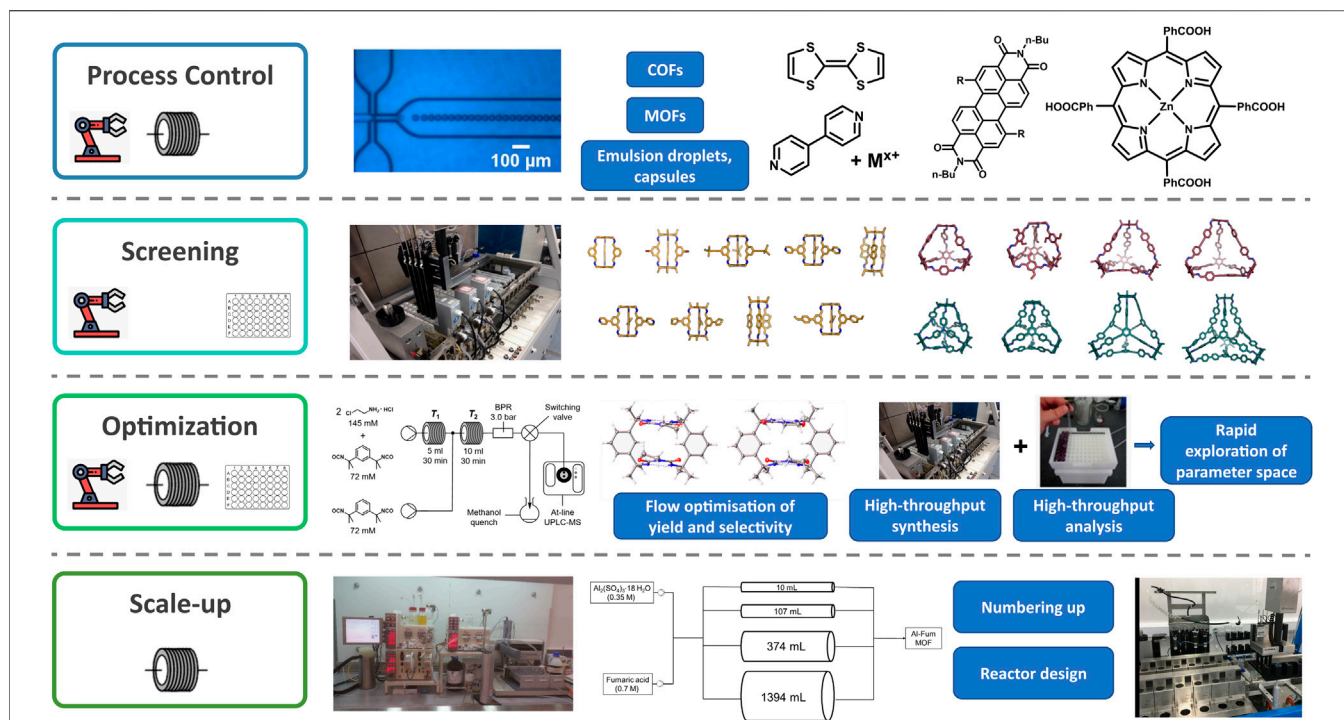
Despite the potential advantages HTS offers, it has still not been widely adopted in the field of supramolecular chemistry. This could be due to factors such as the typically high initial cost of automated platforms, or challenges in finding suitable and equally high-throughput characterisation techniques for the supramolecular assemblies being targeted. However, with the availability of lower cost and open-source automated liquid handling platforms, and with several advances having been made in the HT characterisation of supramolecular materials (Greenaway et al., 2018; White et al., 2020), we expect these techniques to become more widely adopted in the field for screening and discovery of new “hits.”

## Rapid Optimization

Once a “hit” has been found, the next step in the process is to optimize for parameters such as yield, selectivity, performance, throughput, or stability; this process can take as long as the discovery phase. Here, enabling technologies offer the opportunity to shorten this timeline and assist the chemist in making key decisions to ensure the best chance of finding an optimal supramolecular system.

Flow chemistry enables real-time analysis, giving mechanistic insight that can be used to inform optimization. Intermediates can be isolated from the reaction stream and separately analysed to provide a better understanding of the reaction pathway and general self-assembly processes (Sagmeister et al., 2021). For example, recently Jones et al. (2021) exploited this to optimise the synthesis of a macrocyclic molecular hinge using a semi-continuous method informed by at-line analysis. Here, the fast heat transport possible in flow enabled a rapid temperature change mid-synthesis, leading to a threefold increase in yield and simultaneous reduction in reaction times.

HTS can also be used to screen many different parameters in parallel (e.g., reagent stoichiometries, solvents, catalysts, additives, and temperatures), and has been widely used in the pharmaceutical industry to optimise yield and selectivity (Shevlin, 2017; Mennen



**FIGURE 2 |** Examples of supramolecular species and precursors and self-assembly processes that have been examined or enhanced using enabling technology for process control (Puigmartí-Luis et al., 2010; Numata et al., 2015a; Rubio-Martínez et al., 2016b; Gong et al., 2016; Thorne et al., 2019; Puigmartí-Luis et al., 2021, This figure contains an image of Figure 2a from Thorne et al. that has been used to make this composite figure under the terms of a Creative Commons Attribution 4.0 International License <https://creativecommons.org/licenses/by/4.0/>), screening (Greenaway et al., 2018), optimisation (Jones et al., 2021, The flow diagram and crystal structures in the optimization panel have been reused from Figure 2 and 11 from <https://pubs.acs.org/doi/abs/10.1021/jacs.1c02891> respectively with permission from the ACS. Further permission related to the material excerpted should be redirected to the ACS), and scale up (Briggs et al., 2015; Rubio-Martínez et al., 2016a).

et al., 2019). This optimisation process can also be aided by incorporating Design of Experiments (DoE) to narrow down the number of reactions required. In addition, microfluidic platforms can also be employed for HTS which, when compared to automated platforms and microplates, can significantly reduce the quantities of reagents required for both screening and optimisations (Zhou et al., 2020). Whilst there are very few examples of applying flow, microfluidics, or automated platforms for high-throughput screening in supramolecular chemistry, there is no reason why these approaches could not be adopted for the field.

It is worth noting that whilst HTS can enable a large amount of the design space to be investigated, it is not desirable to fully empirically explore all precursor combinations or reaction conditions to ensure the optimal conditions are selected. By combining HTS and flow chemistry with machine learning algorithms and Bayesian optimisations, and *in situ* analysis techniques, this process can be streamlined by using closed-loop autonomous screening to optimise towards a target parameter or property (Zhou et al., 2017; Bédard et al., 2018; Clayton et al., 2019; Clayton et al., 2020). A recent example that highlights this in the area of supramolecular chemistry is the work of Cronin and co-workers who used a closed-loop autonomous “chemical robot” to explore a large combinatorial space for the discovery of coordination architectures (Porwol et al., 2020). The

group calculated that it would take  $4 \times 10^4$  experiments to fully explore the variables chosen, and therefore proposed an autonomous decision-making approach to explore this space as rapidly as possible, discovering four new coordination complexes in the process. This example highlights the importance of decision-making in screening large parameter spaces: the task of deciding “what to explore,” or “what to explore next,” normally taken by the chemist, is a critical point that determines the success or failure of the experiment as well as how fast that point is reached. Emerging research in algorithms for process space exploration, growing from the established science of DoE approaches, are yielding incredible advances in discovery speed in adjacent fields and are likely to make a similar impact in supramolecular chemistry, especially if suitable conditions for scale-up can also be identified.

## Scale-Up

Despite the activity in the field, currently, there are only a few supramolecular materials that are produced for commercial purposes. The many issues surrounding the scale-up process (e.g., large amounts of organic solvents, long reaction times, poor reproducibility) have hindered this transition, preventing structures from being viably used for the many promising applications they present (Rubio-Martínez et al., 2017).

Continuous flow reactors are one of the latest technologies being employed to produce supramolecular structures at scale. Their large surface area-to-volume ratio allows more efficient mass and heat transfer, giving safer and faster reactions. Improvements on the reproducibility and product quality can be obtained due to the higher level of control over the reaction. Flow reactors also generally require less solvent compared to traditional batch reactions, driving down the cost and waste which are all factors that need to be considered for an industrial scale process (Rubio-Martinez et al., 2017).

Recently, flow chemistry has been used to optimize the yield, selectivity, and limited scale-up, of both macrocyclic (Bogdan and James, 2010; Bogdan and James, 2011; Bedard et al., 2013; Bédard et al., 2015; Lucke et al., 2016; Morin et al., 2019; Jones et al., 2021; Seemann et al., 2021) and cage (Briggs et al., 2015; Kitchin et al., 2015) supramolecular structures. For example, Bédard et al. synthesized medicinally relevant (Marsault and Peterson, 2011) macrocyclic lipids under continuous flow, with yields of up to 97% in short reaction times (Bedard et al., 2013). They were also able to increase the reaction to a multigram scale for some macrocycles; high yields were retained without the need for re-optimisation. Similarly, Briggs et al. (2015) translated the synthesis of porous organic cages (POCs) from batch to flow, resulting in greatly reduced reaction times and reduced solvent use, offering a continuous method of scale-up. It should be acknowledged, however, that there is still significant method development required to achieve the multi-kilo or tonne scale needed for many industrial applications, and here collaboration with process chemists and engineers is essential.

Flow has also assisted in the scale-up of MOFs (Munn et al., 2015), which have promising applications in gas storage, gas separation and heterogeneous catalysis, but are typically produced by solvothermal batch synthesis that is challenging on a large scale (Czaja et al., 2009). For example, Rubio-Martinez et al. (2016a) were able to scale-up the synthesis of the aluminium fumate (Al-Fum) MOF from a laboratory to a pilot-plant system by more than 2 orders of magnitude giving an increased space-time-yield (STY) of 97,159 kg m<sup>-3</sup> day<sup>-1</sup>. Since then, significant progress has been made towards the commercial synthesis of MOFs; for example, a continuous hydrothermal synthesis is now being used by Promethean Particles, who commercially produce nine different MOFs and porous structures (Munn et al., 2015).

It is also worth noting that scale-up of supramolecular materials has also been demonstrated under mechanochemical continuous flow, namely using twin-screw extrusion (TSE), which can reduce the solvent requirement for synthesis even further. For example, both MOFs and POCs have been formed on scale with very little to no solvent using TSE (Crawford et al., 2015; Egleston et al., 2020; Casaban et al., 2021). Finally, there have also been promising developments in combining flow reactors and microwave heating for the process intensification of MOF formation (Laybourn et al., 2019). It is clear that the

materials chemist has a number of tools at their disposal to ensure compounds can be made at-scale, and we anticipate this will become more widespread in supramolecular chemistry.

## CONCLUSION AND OUTLOOK

Emerging examples of the use of enabling technology in supramolecular chemistry showcase the potential impact on the field: from faster discovery and screening to efficient optimisation, analysis, and scale-up (Figure 2). Commercial flow reactors, robots and high-throughput work stations are increasingly available alongside low-cost, home-build options (Baas and Saggiomo, 2021), meaning these enabling technologies are becoming more accessible to research laboratories. It is likely that as this availability of technology increases, it will become more integrated in research laboratory procedures and industrial manufacturing. If these technologies are to become mainstream, then training the chemists of the future will become vital. Examples of pre-designed flow chemistry experiments for potential use in undergraduate teaching laboratories (König et al., 2013; Leibfarth et al., 2018; Kuijpers et al., 2021) represent the acknowledgement of a changing skill set required of graduate chemists.

It should also be noted, that whilst this review has focussed on the benefits of enabling technology, it is now frequently coupled with computation to carry out prior predictions and subsequent analysis. Growing examples can already be seen of computational predictions in areas such as organic cages (Berardo et al., 2020), photocatalysts (Singh et al., 2015), and drug molecules (Yu et al., 2020). The likely outlook for the future of chemistry, including supramolecular chemistry, is a hybrid approach of automated experimentation coupled with computation, whether that is using computation to first narrow down the design space, or using HTS to collect large amounts of robust data to feed into data-led computational approaches and machine learning algorithms. It seems certain that the benefits these tools offer will play an increasing role in supramolecular chemistry, from screening to scale-up.

## AUTHOR CONTRIBUTIONS

All authors listed have made a substantial, direct, and intellectual contribution to the work and approved it for publication.

## ACKNOWLEDGMENTS

AS and RG thank the Royal Society for University Research Fellowships that supported this work. KO and AS thank the EPSRC for a Summer Vacation Bursary.

## REFERENCES

- Albrecht, M. (2007). Supramolecular Chemistry-General Principles and Selected Examples from Anion Recognition and Metallosupramolecular Chemistry. *Naturwissenschaften* 94, 951–966. doi:10.1007/s00114-007-0282-7
- Ameloot, R., Vermoortele, F., Vanhove, W., Roelfaers, M. B. J., Sels, B. F., and De Vos, D. E. (2011). Interfacial Synthesis of Hollow Metal-Organic Framework Capsules Demonstrating Selective Permeability. *Nat. Chem.* 3, 382–387. doi:10.1038/nchem.1026
- Arnon, Z. A., Vitalis, A., Levin, A., Michaels, T. C. T., Caflisch, A., Knowles, T. P. J., et al. (2016). Dynamic Microfluidic Control of Supramolecular Peptide Self-Assembly. *Nat. Commun.* 7, 13190. doi:10.1038/ncomms13190
- Aroh, K. C., and Jensen, K. F. (2018). Efficient Kinetic Experiments in Continuous Flow Microreactors. *React. Chem. Eng.* 3, 94–101. doi:10.1039/c7re00163k
- Baas, S., and Saggiomo, V. (2021). Ender3 3D Printer Kit Transformed into Open. *Programmable Syringe Pump Set. HardwareX*. 10, e00219. doi:10.1016/j.hwx.2021.e00219
- Baumann, M., Moody, T. S., Smyth, M., and Wharry, S. (2020). A Perspective on Continuous Flow Chemistry in the Pharmaceutical Industry. *Org. Process. Res. Dev.* 24, 1802–1813. doi:10.1021/acs.oprd.9b00524
- Bédard, A.-C., Adamo, A., Aroh, K. C., Russell, M. G., Bedermann, A. A., Torosian, J., et al. (2018). Reconfigurable System for Automated Optimization of Diverse Chemical Reactions. *Science* 361, 1220–1225. doi:10.1126/science.aat0650
- Bédard, A.-C., Régner, S., and Collins, S. K. (2013). Continuous Flow Macrocyclization at High Concentrations: Synthesis of Macrocyclic Lipids. *Green. Chem.* 15, 1962–1966. doi:10.1039/c3gc40872h
- Bédard, A.-C., Santandrea, J., and Collins, S. K. (2015). Efficient Continuous-Flow Synthesis of Macrocyclic Triazoles. *J. Flow Chem.* 5, 142–144. doi:10.1556/jfc-d-14-00042
- Berardo, E., Greenaway, R. L., Miklitz, M., Cooper, A. I., and Jelfs, K. E. (2020). Computational Screening for Nested Organic Cage Complexes. *Mol. Syst. Des. Eng.* 5, 186–196. doi:10.1039/c9me00085b
- Berardo, E., Greenaway, R. L., Turcani, L., Alston, B. M., Bennison, M. J., Miklitz, M., et al. (2018). Computationally-inspired Discovery of an Unsymmetrical Porous Organic Cage. *Nanoscale* 10, 22381–22388. doi:10.1039/c8nr06868b
- Bogdan, A. R., and James, K. F. (2011). Flow Macrocyclization Using Copper Tubing. *Synfacts* 2011, 0449. doi:10.1055/s-0030-1259736
- Bogdan, A. R., and James, K. (2010). Efficient Access to New Chemical Space through Flow-Construction of Druglike Macrocycles through Copper-Surface-Catalyzed Azide-Alkyne Cycloaddition Reactions. *Chem. Eur. J.* 16, 14506–14512. doi:10.1002/chem.201002215
- Briggs, M. E., Slater, A. G., Lunt, N., Jiang, S., Little, M. A., Greenaway, R. L., et al. (2015). Dynamic Flow Synthesis of Porous Organic Cages. *Chem. Commun.* 51, 17390–17393. doi:10.1039/c5cc07447a
- Brivio, M., Verboom, W., and Reinhoudt, D. N. (2006). Miniaturized Continuous Flow Reaction Vessels: Influence on Chemical Reactions. *Lab. Chip* 6, 329–344. doi:10.1039/b510856j
- Calvo Galve, N., Abrishamkar, A., Sorrenti, A., Di Rienzo, L., Satta, M., D'Abramo, M., et al. (2021). Exploiting Reaction-Diffusion Conditions to Trigger Pathway Complexity in the Growth of a MOF. *Angew. Chem. Int. Ed. Engl.* 60, 15920–15927. doi:10.1002/anie.202101611
- Carson, N. (2020). Rise of the Robots. *Chem. Eur. J.* 26, 3194–3196. doi:10.1002/chem.202000656
- Casaban, J., Zhang, Y., Pacheco, R., Coney, C., Holmes, C., Sutherland, E., et al. (2021). Towards MOF's Mass Market Adoption: MOF Technologie's Efficient and Versatile One-step Extrusion of Shaped MOFs Directly from Raw Materials. *Faraday Discuss.* 231, 312–325. doi:10.1039/D1FD00025J
- Clayton, A. D., Manson, J. A., Taylor, C. J., Chamberlain, T. W., Taylor, B. A., Clemens, G., et al. (2019). Algorithms for the Self-Optimisation of Chemical Reactions. *React. Chem. Eng.* 4, 1545–1554. doi:10.1039/c9re00209j
- Clayton, A. D., Schweidtmann, A. M., Clemens, G., Manson, J. A., Taylor, C. J., Niño, C. G., et al. (2020). Automated Self-Optimisation of Multi-step Reaction and Separation Processes Using Machine Learning. *Chem. Eng. J.* 384, 123340. doi:10.1016/j.cej.2019.123340
- Cohen-Gerassi, D., Arnon, Z. A., Guterman, T., Levin, A., Ghosh, M., Aviv, M., et al. (2020). Phase Transition and Crystallization Kinetics of a Supramolecular System in a Microfluidic Platform. *Chem. Mater.* 32, 8342–8349. doi:10.1021/acs.chemmater.0c02187
- Crawford, D., Casaban, J., Haydon, R., Giri, N., McNally, T., and James, S. L. (2015). Synthesis by Extrusion: Continuous, Large-Scale Preparation of MOFs Using Little or No Solvent. *Chem. Sci.* 6, 1645–1649. doi:10.1039/c4sc03217a
- Cui, P., McMahon, D. P., Spackman, P. R., Alston, B. M., Little, M. A., Day, G. M., et al. (2019). Mining Predicted crystal Structure Landscapes with High Throughput Crystallisation: Old Molecules, New Insights. *Chem. Sci.* 10, 9988–9997. doi:10.1039/c9sc02832c
- Czaja, A. U., Trukhan, N., and Müller, U. (2009). Industrial Applications of Metal-Organic Frameworks. *Chem. Soc. Rev.* 38, 1284–1293. doi:10.1039/b804680h
- Davis, A. V., Yeh, R. M., and Raymond, K. N. (2002). Supramolecular Assembly Dynamics. *Proc. Natl. Acad. Sci.* 99, 4793–4796. doi:10.1073/pnas.052018299
- Desiraju, G. R. (1997). Designer Crystals: Intermolecular Interactions, Network Structures and Supramolecular Synthons. *Chem. Commun.*, 1475–1482. doi:10.1039/a607149j
- Egleston, B. D., Brand, M. C., Greenwell, F., Briggs, M. E., James, S. L., Cooper, A. I., et al. (2020). Continuous and Scalable Synthesis of a Porous Organic Cage by Twin Screw Extrusion (TSE). *Chem. Sci.* 11, 6582–6589. doi:10.1039/d0sc01858a
- Fang, H., Sun, Y., Wang, X., Sharma, M., Chen, Z., Cao, X., et al. (2018). Probing the Kinetics in Supramolecular Chemistry and Molecular Assembly by Microfluidic-NMR Spectroscopy. *Sci. China Chem.* 61, 1460–1464. doi:10.1007/s11426-018-9293-3
- Fielden, S. D. P., Leigh, D. A., and Woltering, S. L. (2017). Molecular Knots. *Angew. Chem. Int. Ed.* 56, 11166–11194. doi:10.1002/anie.201702531
- Foster, J. A., Parker, R. M., Belenguer, A. M., Kishi, N., Sutton, S., Abell, C., et al. (2015). Differentially Addressable Cavities within Metal-Organic Cage-Cross-Linked Polymeric Hydrogels. *J. Am. Chem. Soc.* 137, 9722–9729. doi:10.1021/jacs.5b05507
- Gil-Ramirez, G., Leigh, D. A., and Stephens, A. J. (2015). Catenanes: Fifty Years of Molecular Links. *Angew. Chem. Int. Ed.* 54, 6110–6150. doi:10.1002/anie.201411619
- Glaser, J. A. (2015). Continuous Chemical Production Processes. *Clean. Techn. Environ. Pol.* 17, 309–316. doi:10.1007/s10098-015-0903-3
- Gong, C., Zhang, J., Zeng, X., and Xie, J. (2016). Highly Effective Synthesis of a Cobalt(ii) Metal-Organic Coordination Polymer by Using Continuous Flow Chemistry. *Dalton Trans.* 46, 25–28. doi:10.1039/c6dt04000d
- Greenaway, R. L., and Jelfs, K. E. (2020). High-Throughput Approaches for the Discovery of Supramolecular Organic Cages. *ChemPlusChem* 85, 1813–1823. doi:10.1002/cplu.202000445
- Greenaway, R. L., Santolini, V., Bennison, M. J., Alston, B. M., Pugh, C. J., Little, M. A., et al. (2018). High-throughput Discovery of Organic Cages and Catenanes Using Computational Screening Fused with Robotic Synthesis. *Nat. Commun.* 9, 2849. doi:10.1038/s41467-018-05271-9
- Greenaway, R. L., Santolini, V., Pulido, A., Little, M. A., Alston, B. M., Briggs, M. E., et al. (2019). From Concept to Crystals via Prediction: Multi-Component Organic Cage Pots by Social Self-Sorting. *Angew. Chem. Int. Ed.* 58, 16275–16281. doi:10.1002/anie.201909237
- Han, J.-M., Pan, J.-L., Lei, T., Liu, C., and Pei, J. (2010). Smart Macrocyclic Molecules: Induced Fit and Ultrafast Self-Sorting Inclusion Behavior through Dynamic Covalent Chemistry. *Chem. Eur. J.* 16, 13850–13861. doi:10.1002/chem.201001606
- Hasell, T., and Cooper, A. I. (2016). Porous Organic Cages: Soluble, Modular and Molecular Pores. *Nat. Rev. Mater.* 1, 16053. doi:10.1038/natrevmats.2016.53
- Headen, D. M., Garcia, J. R., and Garcia, A. J. (2018). Parallel Droplet Microfluidics for High Throughput Cell Encapsulation and Synthetic Microgel Generation. *Microsyst. Nanoeng.* 4, 17076. doi:10.1038/micronano.2017.76
- Hong, S., Rohman, M. R., Jia, J., Kim, Y., Moon, D., Kim, Y., et al. (2015). Porphyrin Boxes: Rationally Designed Porous Organic Cages. *Angew. Chem. Int. Ed.* 54, 13241–13244. doi:10.1002/anie.201505531
- Huck, J. M., Lin, L.-C., Berger, A. H., Shahrak, M. N., Martin, R. L., Bhowan, A. S., et al. (2014). Evaluating Different Classes of Porous Materials for Carbon Capture. *Energy Environ. Sci.* 7, 4132–4146. doi:10.1039/c4ee02636e
- Jiao, L., Seow, J. Y. R., Skinner, W. S., Wang, Z. U., and Jiang, H.-L. (2019). Metal-organic Frameworks: Structures and Functional Applications. *Mater. Today* 27, 43–68. doi:10.1016/j.mattod.2018.10.038



- Jones, C. D., Kershaw Cook, L. J., Marquez-Gamez, D., Luzyanin, K. V., Steed, J. W., and Slater, A. G. (2021). High-Yielding Flow Synthesis of a Macrocyclic Molecular Hinge. *J. Am. Chem. Soc.* 143, 7553–7565. doi:10.1021/jacs.1c02891
- Khoeini, D., Scott, T. F., and Neild, A. (2021). Microfluidic Enhancement of Self-Assembly Systems. *Lab. Chip* 21, 1661–1675. doi:10.1039/d1lc00038a
- Kitchin, M., Konstantas, K., Sumby, C. J., Czyz, M. L., Valente, P., Hill, M. R., et al. (2015). Continuous Flow Synthesis of a Carbon-Based Molecular Cage Macrocyclic via a Three-fold Homocoupling Reaction. *Chem. Commun.* 51, 14231–14234. doi:10.1039/c5cc05181a
- König, B., Kreitmeier, P., Hilgers, P., and Wirth, T. (2013). Flow Chemistry in Undergraduate Organic Chemistry Education. *J. Chem. Educ.* 90, 934–936. doi:10.1021/ed3006083
- Kuijpers, K. P. L., Weggemans, W. M. A., Verwijlen, C. J. A., and Noël, T. (2021). Flow Chemistry Experiments in the Undergraduate Teaching Laboratory: Synthesis of Diazo Dyes and Disulfides. *J. Flow Chem.* 11, 7–12. doi:10.1007/s41981-020-00118-1
- Kuśmierz, K., and Świątkowski, A. (2015). The Influence of Different Agitation Techniques on the Adsorption Kinetics of 4-chlorophenol on Granular Activated Carbon. *React. Kinetics, Mech. Catal.* 116, 261–271.
- Laybourn, A., López-Fernández, A. M., Thomas-Hillman, I., Katrib, J., Lewis, W., Dodds, C., et al. (2019). Combining Continuous Flow Oscillatory Baffled Reactors and Microwave Heating: Process Intensification and Accelerated Synthesis of Metal-Organic Frameworks. *Chem. Eng. J.* 356, 170–177. doi:10.1016/j.cej.2018.09.011
- Lehn, J.-M. (1988). Supramolecular Chemistry-Scope and Perspectives Molecules, Supermolecules, and Molecular Devices(Nobel Lecture). *Angew. Chem. Int. Ed. Engl.* 27, 89–112. doi:10.1002/anie.198800891
- Leibfarth, F. A., Russell, M. G., Langley, D. M., Seo, H., Kelly, L. P., Carney, D. W., et al. (2018). Continuous-Flow Chemistry in Undergraduate Education: Sustainable Conversion of Reclaimed Vegetable Oil into Biodiesel. *J. Chem. Educ.* 95, 1371–1375. doi:10.1021/acs.jchemed.7b00719
- Lin, Y., Penna, M., Spicer, C. D., Higgins, S. G., Gelmi, A., Kim, N., et al. (2021). High-Throughput Peptide Derivatization toward Supramolecular Diversification in Microtiter Plates. *ACS Nano* 15, 4034–4044. doi:10.1021/acsnano.0c05423
- Little, M. A., Chong, S. Y., Schmidtman, M., Hasell, T., and Cooper, A. I. (2014). Guest Control of Structure in Porous Organic Cages. *Chem. Commun.* 50, 9465–9468. doi:10.1039/c4cc04158e
- Liu, Z., Nalluri, S. K. M., and Stoddart, J. F. (2017). Surveying Macrocyclic Chemistry: from Flexible crown Ethers to Rigid Cyclophanes. *Chem. Soc. Rev.* 46, 2459–2478. doi:10.1039/c7cs00185a
- Lücke, D., Dalton, T., Ley, S. V., and Wilson, Z. E. (2016). Synthesis of Natural and Unnatural Cyclooligomeric Dipeptides Enabled by Flow Chemistry. *Chem. Eur. J.* 22, 4206–4217. doi:10.1002/chem.201504457
- Marsault, E., and Peterson, M. L. (2011). Macrocycles Are Great Cycles: Applications, Opportunities, and Challenges of Synthetic Macrocycles in Drug Discovery. *J. Med. Chem.* 54, 1961–2004. doi:10.1021/jm1012374
- Martí-Centelles, V., Pandey, M. D., Burguete, M. I., and Luis, S. V. (2015). Macrocyclization Reactions: The Importance of Conformational, Configurational, and Template-Induced Preorganization. *Chem. Rev.* 115, 8736–8834. doi:10.1021/acs.chemrev.5b00056
- McNally, A., Prier, C. K., and Macmillan, D. W. C. (2011). Discovery of an  $\alpha$ -Amino C-H Arylation Reaction Using the Strategy of Accelerated Serendipity. *Science* 334, 1114–1117. doi:10.1126/science.1213920
- Méndez-Ardoy, A., Bayón-Fernández, A., Yu, Z., Abell, C., Granja, J. R., and Montenegro, J. (2020). Spatially Controlled Supramolecular Polymerization of Peptide Nanotubes by Microfluidics. *Angew. Chem. Int. Ed. Engl.* 59, 6902–6908. doi:10.1002/anie.202000103
- Mennen, S. M., Alhambra, C., Allen, C. L., Barberis, M., Berritt, S., Brandt, T. A., et al. (2019). The Evolution of High-Throughput Experimentation in Pharmaceutical Development and Perspectives on the Future. *Org. Process. Res. Dev.* 23, 1213–1242. doi:10.1021/acs.oprd.9b00140
- Morin, É., Sosoe, J., Raymond, M., Amorelli, B., Boden, R. M., and Collins, S. K. (2019). Synthesis of a Renewable Macrocyclic Musk: Evaluation of Batch, Microwave, and Continuous Flow Strategies. *Org. Process. Res. Dev.* 23, 283–287. doi:10.1021/acs.oprd.8b00450
- Munn, A. S., Dunne, P. W., Tang, S. V. Y., and Lester, E. H. (2015). Large-scale Continuous Hydrothermal Production and Activation of ZIF-8. *Chem. Commun.* 51, 12811–12814. doi:10.1039/c5cc04636j
- Myers, R. M., Fitzpatrick, D. E., Turner, R. M., and Ley, S. V. (2014). Flow Chemistry Meets Advanced Functional Materials. *Chem. Eur. J.* 20, 12348–12366. doi:10.1002/chem.201402801
- Nagy, K. D., Shen, B., Jamison, T. F., and Jensen, K. F. (2012). Mixing and Dispersion in Small-Scale Flow Systems. *Org. Process. Res. Dev.* 16, 976–981. doi:10.1021/op200349f
- Newman, S. G., and Jensen, K. F. (2013). The Role of Flow in green Chemistry and Engineering. *Green. Chem.* 15, 1456–1472. doi:10.1039/c3gc40374b
- Nomura, T., He, Y., and Takahashi, K. (1996). Development and Mixing Characteristics of Folded Anchor for Round-Bottomed Flask. *J. Chem. Eng. Jpn.* 29, 134–138. doi:10.1252/jcej.29.134
- Numata, M., Kozawa, T., Nogami, R., Tanaka, K., Sanada, Y., and Sakurai, K. (2015a). Synchronized Activation of  $\pi$ -Conjugated Molecules toward Self-Assembly: Precisely Controlling the Hysteresis of the Metastable State along Microflow. *Bcsj* 88, 471–479. doi:10.1246/bcsj.20140365
- Numata, M., and Kozawa, T. (2013). Supramolecular Polymerization in Microfluidic Channels: Spatial Control over Multiple Intermolecular Interactions. *Chem. Eur. J.* 19, 12629–12634. doi:10.1002/chem.201301810
- Numata, M., Nishino, Y., Sanada, Y., and Sakurai, K. (2015b). Creation of Kinetically Stabilized Porphyrin Microfilms through Synchronized Hydrogen-Bonding Interactions in Microflow. *Chem. Lett.* 44, 861–863. doi:10.1246/cl.150149
- Numata, M., Sato, A., and Nogami, R. (2015c). Energy-dissipative Self-Assembly Driven in Microflow: A Time-Programmed Self-Organization and Decomposition of Metastable Nanofibers. *Chem. Lett.* 44, 995–997. doi:10.1246/cl.150292
- Ogi, S., Fukui, T., Jue, M. L., Takeuchi, M., and Sugiyasu, K. (2014). Kinetic Control over Pathway Complexity in Supramolecular Polymerization through Modulating the Energy Landscape by Rational Molecular Design. *Angew. Chem. Int. Ed.* 53, 14363–14367. doi:10.1002/anie.201407302
- Okesola, B. O., and Mata, A. (2018). Multicomponent Self-Assembly as a Tool to Harness New Properties from Peptides and Proteins in Material Design. *Chem. Soc. Rev.* 47, 3721–3736. doi:10.1039/c8cs00121a
- Otto, S., and Severin, K. (2007). Dynamic Combinatorial Libraries for the Development of Synthetic Receptors and Sensors. *Creat. Chem. Sensor Syst.* 277, 267–288.
- Parker, R. M., Zhang, J., Zheng, Y., Coulston, R. J., Smith, C. A., Salmon, A. R., et al. (2015). Electrostatically Directed Self-Assembly of Ultrathin Supramolecular Polymer Microcapsules. *Adv. Funct. Mater.* 25, 4091–4100. doi:10.1002/adfm.201501079
- Plutschack, M. B., Pieber, B., Gilmore, K., and Seeberger, P. H. (2017). The Hitchhiker's Guide to Flow Chemistry. *Chem. Rev.* 117, 11796–11893. doi:10.1021/acs.chemrev.7b00183
- Porta, R., Benaglia, M., and Puglisi, A. (2016). Flow Chemistry: Recent Developments in the Synthesis of Pharmaceutical Products. *Org. Process. Res. Dev.* 20, 2–25. doi:10.1021/acs.oprd.5b00325
- Porwol, L., Kowalski, D. J., Henson, A., Long, D. L., Bell, N. L., and Cronin, L. (2020). An Autonomous Chemical Robot Discovers the Rules of Inorganic Coordination Chemistry without Prior Knowledge. *Angew. Chem. Int. Ed.* 59, 11256–11261. doi:10.1002/anie.202000329
- Puigmartí-Luis, J., Schaffhauser, D., Burg, B. R., and Ditttrich, P. S. (2010). A Microfluidic Approach for the Formation of Conductive Nanowires and Hollow Hybrid Structures. *Adv. Mater.* 22, 2255–2259. doi:10.1002/adma.200903428
- Reizman, B. J., Wang, Y.-M., Buchwald, S. L., and Jensen, K. F. (2016). Suzuki-Miyaura Cross-Coupling Optimization Enabled by Automated Feedback. *React. Chem. Eng.* 1, 658–666. doi:10.1039/c6re00153j
- Rodríguez-San-Miguel, D., Abrishamkar, A., Navarro, J. A. R., Rodríguez-Trujillo, R., Amabilino, D. B., Mas-Ballesté, R., et al. (2016). Crystalline Fibres of a Covalent Organic Framework through Bottom-Up Microfluidic Synthesis. *Chem. Commun.* 52, 9212–9215. doi:10.1039/c6cc04013f
- Rowan, S. J., Cantrill, S. J., Cousins, G. R. L., Sanders, J. K. M., and Stoddart, J. F. (2002). Dynamic Covalent Chemistry. *Angew. Chem. Int. Ed.* 41, 898–952. doi:10.1002/1521-3773(20020315)41:6<898::aid-anie898>3.0.co;2-e

- Rubio-Martinez, M., Avci-Camur, C., Thornton, A. W., Imaz, I., Maspoch, D., and Hill, M. R. (2017). New Synthetic Routes towards MOF Production at Scale. *Chem. Soc. Rev.* 46, 3453–3480. doi:10.1039/c7cs00109f
- Rubio-Martinez, M., Hadley, T. D., Batten, M. P., Constanti-Carey, K., Barton, T., Marley, D., et al. (2016a). Scalability of Continuous Flow Production of Metal-Organic Frameworks. *ChemSusChem* 9, 938–941. doi:10.1002/cssc.201501684
- Rubio-Martinez, M., Imaz, I., Domingo, N., Abrishamkar, A., Mayor, T. S., Rossi, R. M., et al. (2016b). Freezing the Nonclassical Crystal Growth of a Coordination Polymer Using Controlled Dynamic Gradients. *Adv. Mater.* 28, 8150–8155. doi:10.1002/adma.201506462
- Saalfrank, R. W., Maid, H., and Scheurer, A. (2008). Supramolecular Coordination Chemistry: The Synergistic Effect of Serendipity and Rational Design. *Angew. Chem. Int. Ed.* 47, 8794–8824. doi:10.1002/anie.200702075
- Sagmeister, P., Lebl, R., Castillo, I., Rehrl, J., Krusz, J., Sipek, M., et al. (2021). Advanced Real-Time Process Analytics for Multistep Synthesis in Continuous Flow\*. *Angew. Chem. Int. Ed.* 60, 8139–8148. doi:10.1002/anie.202016007
- Seemann, A., Panten, J., and Kirschning, A. (2021). Flow Chemistry under Extreme Conditions: Synthesis of Macrocycles with Musklike Olfactory Properties. *J. Org. Chem.* 86(20):13924–13933. doi:10.1021/acs.joc.1c00663
- Sevim, S., Sorrenti, A., Franco, C., Furukawa, S., Pané, S., Demello, A. J., et al. (2018). Self-assembled Materials and Supramolecular Chemistry within Microfluidic Environments: from Common Thermodynamic States to Non-equilibrium Structures. *Chem. Soc. Rev.* 47, 3788–3803. doi:10.1039/c8cs00025e
- Shevlin, M. (2017). Practical High-Throughput Experimentation for Chemists. *ACS Med. Chem. Lett.* 8, 601–607. doi:10.1021/acsmchemlett.7b00165
- Singh, A. K., Mathew, K., Zhuang, H. L., and Hennig, R. G. (2015). Computational Screening of 2D Materials for Photocatalysis. *J. Phys. Chem. Lett.* 6, 1087–1098. doi:10.1021/jz502646d
- Singh, V., Jang, S., Vishwakarma, N. K., and Kim, D.-P. (2018). Intensified Synthesis and post-synthetic Modification of Covalent Organic Frameworks Using a Continuous Flow of Microdroplets Technique. *NPG Asia Mater.* 10, e456. doi:10.1038/am.2017.209
- Song, F., Li, Z., Jia, P., Zhang, M., Bo, C., Feng, G., et al. (2019). Tunable "soft and Stiff", Self-Healing, Recyclable, Thermadapt Shape Memory Biomass Polymers Based on Multiple Hydrogen Bonds and Dynamic Imine Bonds. *J. Mater. Chem. A* 7, 13400–13410. doi:10.1039/c9ta03872h
- Thorne, M. F., Simkovic, F., and Slater, A. G. (2019). Production of Monodisperse Polyurea Microcapsules Using Microfluidics. *Sci. Rep.* 9, 17983. doi:10.1038/s41598-019-54512-4
- Tromans, R. A., Carter, T. S., Chabanne, L., Crump, M. P., Li, H., Matlock, J. V., et al. (2019). A Biomimetic Receptor for Glucose. *Nat. Chem* 11, 52–56. doi:10.1038/s41557-018-0155-z
- Vantomme, G., and Meijer, E. W. (2019). The Construction of Supramolecular Systems. *Science* 363, 1396–1397. doi:10.1126/science.aav4677
- Ward, K., and Fan, Z. H. (2015). Mixing in Microfluidic Devices and Enhancement Methods. *J. Micromech. Microeng.* 25, 094001–094017. doi:10.1088/0960-1317/25/9/094001
- Weiss, R. G. (2014). The Past, Present, and Future of Molecular Gels. What Is the Status of the Field, and where Is it Going? *J. Am. Chem. Soc.* 136, 7519–7530. doi:10.1021/ja503363v
- White, L. J., Wark, C., Croucher, L., Draper, E. R., and Hiscock, J. R. (2020). High-throughput Characterisation of Supramolecular Gelation Processes Using a Combination of Optical Density, Fluorescence and UV-Vis Absorption Measurements. *Chem. Commun.* 56, 9557–9560. doi:10.1039/d0cc04033a
- Whitesides, G. M., Mathias, J. P., and Seto, C. T. (1991). Molecular Self-Assembly and Nanochemistry: a Chemical Strategy for the Synthesis of Nanostructures. *Science* 254, 1312–1319. doi:10.1126/science.1962191
- Whitesides, G. M. (2006). The Origins and the Future of Microfluidics. *Nature* 442, 368–373. doi:10.1038/nature05058
- Winpenny, R. E. P. (2002). Serendipitous Assembly of Polynuclear Cage Compounds. *J. Chem. Soc. Dalton Trans.*, 1–10. doi:10.1039/b107118c
- Wu, A., and Isaacs, L. (2003). Self-Sorting: The Exception or the Rule? *J. Am. Chem. Soc.* 125, 4831–4835. doi:10.1021/ja028913b
- Würthner, F. (2021). Solvent Effects in Supramolecular Chemistry: Linear Free Energy Relationships for Common Intermolecular Interactions. *J. Org. Chem.* doi:10.1021/acs.joc.1c00625
- Yang, K., Chao, S., Zhang, F., Pei, Y., and Pei, Z. (2019). Recent Advances in the Development of Rotaxanes and Pseudorotaxanes Based on Pillar[n]arenes: from Construction to Application. *Chem. Commun.* 55, 13198–13210. doi:10.1039/c9cc07373f
- Yang, L., Tan, X., Wang, Z., and Zhang, X. (2015). Supramolecular Polymers: Historical Development, Preparation, Characterization, and Functions. *Chem. Rev.* 115, 7196–7239. doi:10.1021/cr500633b
- Yu, R., Chen, L., Lan, R., Shen, R., and Li, P. (2020). Computational Screening of Antagonists against the SARS-CoV-2 (COVID-19) Coronavirus by Molecular Docking. *Int. J. Antimicrob. Agents* 56, 106012. doi:10.1016/j.ijantimicag.2020.106012
- Yu, Z., Zhang, J., Coulston, R. J., Parker, R. M., Biedermann, F., Liu, X., et al. (2015). Supramolecular Hydrogel Microcapsules via Cucurbit[8]uril Host-Guest Interactions with Triggered and UV-Controlled Molecular Permeability. *Chem. Sci.* 6, 4929–4933. doi:10.1039/c5sc01440a
- Yusov, A., Dillon, A. M., and Ward, M. D. (2021). Hydrogen Bonded Frameworks: Smart Materials Used Smartly. *Mol. Syst. Des. Eng.* 6, 756–778. doi:10.1039/D1ME00055A
- Zhang, B., Zhang, J., Liu, C., Sang, X., Peng, L., Ma, X., et al. (2015). Solvent Determines the Formation and Properties of Metal-Organic Frameworks. *RSC Adv.* 5, 37691–37696. doi:10.1039/c5ra02440d
- Zhang, J., Coulston, R. J., Jones, S. T., Geng, J., Scherman, O. A., and Abell, C. (2012). One-step Fabrication of Supramolecular Microcapsules from Microfluidic Droplets. *Science* 335, 690–694. doi:10.1126/science.1215416
- Zhou, H.-C. J., and Kitagawa, S. (2014). Metal-Organic Frameworks (MOFs). *Chem. Soc. Rev.* 43, 5415–5418. doi:10.1039/c4cs90059f
- Zhou, P., He, J., Huang, L., Yu, Z., Su, Z., Shi, X., et al. (2020). Microfluidic High-Throughput Platforms for Discovery of Novel Materials. *Nanomaterials* 10, 2514. doi:10.3390/nano10122514
- Zhou, Z., Li, X., and Zare, R. N. (2017). Optimizing Chemical Reactions with Deep Reinforcement Learning. *ACS Cent. Sci.* 3, 1337–1344. doi:10.1021/acscentsci.7b00492

**Conflict of Interest:** The authors declare that the research was conducted in the absence of any commercial or financial relationships that could be construed as a potential conflict of interest.

**Publisher's Note:** All claims expressed in this article are solely those of the authors and do not necessarily represent those of their affiliated organizations, or those of the publisher, the editors and the reviewers. Any product that may be evaluated in this article, or claim that may be made by its manufacturer, is not guaranteed or endorsed by the publisher.

Copyright © 2021 Ollerton, Greenaway and Slater. This is an open-access article distributed under the terms of the Creative Commons Attribution License (CC BY). The use, distribution or reproduction in other forums is permitted, provided the original author(s) and the copyright owner(s) are credited and that the original publication in this journal is cited, in accordance with accepted academic practice. No use, distribution or reproduction is permitted which does not comply with these terms.



# Cyclohexanohemicucurbit[8]uril Inclusion Complexes With Heterocycles and Selective Extraction of Sulfur Compounds From Water

Tatsiana Shalima<sup>1</sup>, Kamini A. Mishra<sup>1</sup>, Sandra Kaabel<sup>2</sup>, Lukas Ustrnul<sup>1</sup>, Simona Bartkova<sup>1</sup>, Kaia Tõnsuaadu<sup>3</sup>, Ivo Heinmaa<sup>4</sup> and Riina Aav<sup>1\*</sup>

<sup>1</sup>Department of Chemistry and Biotechnology, School of Science, Tallinn University of Technology, Tallinn, Estonia, <sup>2</sup>Department of Chemistry, McGill University, Montreal, QC, Canada, <sup>3</sup>Laboratory of Inorganic Materials, School of Engineering, Institute of Materials and Environmental Technology, Tallinn University of Technology, Tallinn, Estonia, <sup>4</sup>Laboratory of Chemical Physics, National Institute of Chemical Physics and Biophysics, Tallinn, Estonia

## OPEN ACCESS

### Edited by:

Cally Jo Elizabeth Haynes,  
University College London,  
United Kingdom

### Reviewed by:

Khaleel Assaf,  
Al-Balqa Applied University, Jordan  
Paula M. Marcos,  
University of Lisbon, Portugal

### \*Correspondence:

Riina Aav  
riina.aav@taltech.ee

### Specialty section:

This article was submitted to  
Supramolecular Chemistry,  
a section of the journal  
Frontiers in Chemistry

**Received:** 30 September 2021

**Accepted:** 04 November 2021

**Published:** 03 December 2021

### Citation:

Shalima T, Mishra KA, Kaabel S,  
Ustrnul L, Bartkova S, Tõnsuaadu K,  
Heinmaa I and Aav R (2021)  
Cyclohexanohemicucurbit[8]uril  
Inclusion Complexes With  
Heterocycles and Selective Extraction  
of Sulfur Compounds From Water.  
Front. Chem. 9:786746.  
doi: 10.3389/fchem.2021.786746

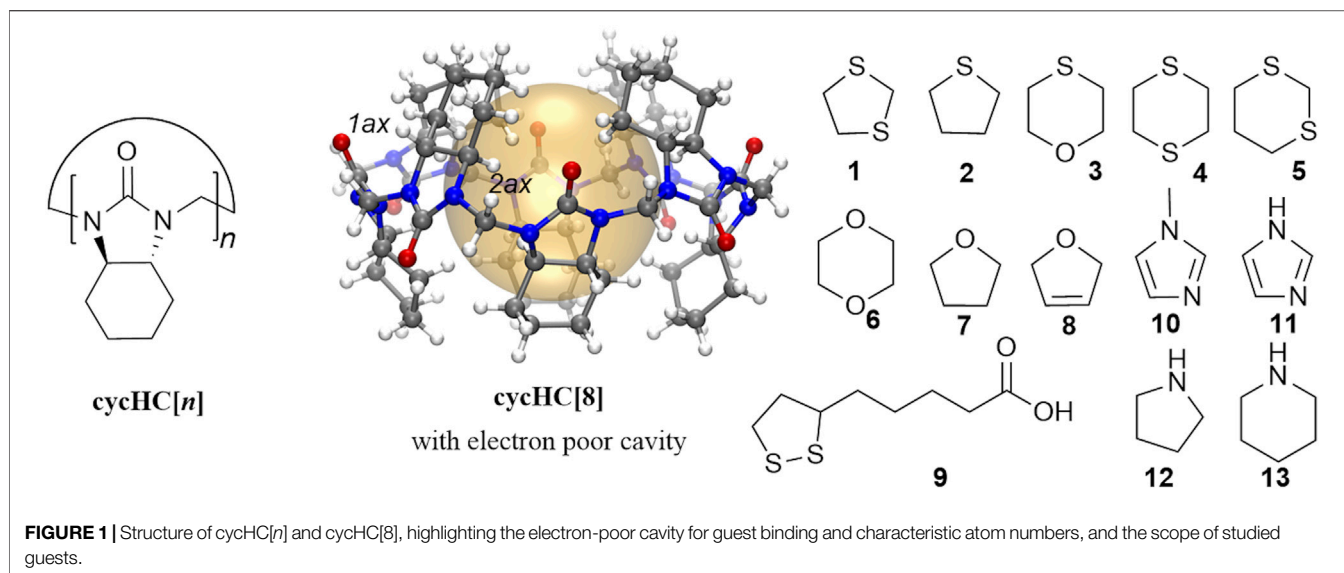
Solid-phase extraction that utilizes selective macrocyclic receptors can serve as a useful tool for removal of chemical wastes. Hemicucurbiturils are known to form inclusion complexes with suitably sized anions; however, their use in selective binding of non-charged species is still very limited. In this study, we found that cyclohexanohemicucurbit [8]uril encapsulates five- and six-membered sulfur- and oxygen-containing unsubstituted heterocycles, which is investigated by single-crystal X-ray diffraction, NMR spectroscopy, isothermal titration calorimetry, and thermogravimetry. The macrocycle acts as a promising selective sorption material for the extraction of sulfur heterocycles, such as 1,3-dithiolane and  $\alpha$ -lipoic acid, from water.

**Keywords:** Hemicucurbituril, solid-phase extraction, heterocycles, inclusion complex, lipoic acid, sorbent recycling, SC-XRD, MAS NMR

## INTRODUCTION

Hemicucurbiturils, formed in templated single-step oligomerization reactions (Kaabel and Aav, 2018), are single-bridged cucurbituril-type macrocycles (Andersen et al., 2018; Lizal and Sindelar, 2018; Xi et al., 2018) that bear an electron-deficient hydrophobic cavity. The latter grants these macrocycles the ability to encapsulate anions (Buschmann et al., 2005; Cucolea et al., 2016; Kaabel et al., 2017; Assaf and Nau, 2018; Reany et al., 2018; Vázquez and Sindelar, 2018; Andersen et al., 2019; Kandrnálová et al., 2019; Valkenier et al., 2019; Maršálek and Šindelář, 2020); in addition, the formation of complexes with acids and some neutral species has been reported in the previous work. In particular, unsubstituted hemicucurbit[*n*]urils (*n* = 6, 12) bind phenol derivatives (Jin et al., 2016a; 2016b) and ferrocene (Jin et al., 2017), and cyclohexanohemicucurbit[*n*]urils cycHC [*n*] (*n* = 6, 8, 12) (Li et al., 2009; Aav et al., 2013; Prigorchenko et al., 2015, 2019; Mishra et al., 2020) form external complexes with both inorganic and organic acids (Öeren et al., 2014; Ustrnul et al., 2019, 2021). We envisioned that heterocycles 1–13 have relatively high electron densities compared to carbocycles and may therefore be able to occupy space within the eight-membered cycHC[8] (Figure 1).

S-heterocycles are compounds of interest as these substances are bioactive (Rezanka et al., 2006; Lamberth et al., 2015) and may contribute to the distinct aromas of food (Mottram and Mottram, 2002; Mahadevan and Farmer, 2006; Schoenauer and Schieberle, 2018), and heterocycle 2 is added as an odorant to the natural gas. Unsubstituted S-containing heterocycles, such as 1,3-dithiolane 1 and



1,4-thioxane **3**, are found in meat (Garbusov et al., 1976) and around chemical warfare dumping sites where they are formed due to the degradation of mustard gas (Røen et al., 2010; Magnusson et al., 2016; Vanninen et al., 2020). Bioactive  $\alpha$ -lipoic acid **9** exhibits antioxidant properties (Rochette et al., 2013; Salehi et al., 2019), and to date, cyclodextrins have been used to enhance its solubility and bioavailability (Lin-Hui et al., 1995; Maeda et al., 2010; Takahashi et al., 2011; Ikuta et al., 2013; Racz et al., 2013; Caira et al., 2017; Celebioglu and Uyar, 2019). Carbon-based materials are used for solid-phase extraction (SPE) of S-heterocycles from water (Lees et al., 2017; Jöul et al., 2018); however, such systems are designed to non-selectively retain all non-polar to moderately polar components.

In this study, we report that cycHC[8] encapsulates neutral electron-rich heterocycles containing sulfur and oxygen atoms and acts as a selective sorbent material for suitably sized S-heterocycles. Complexation was characterized by  $^1\text{H}$  NMR titration and isothermal titration calorimetry (ITC), single-crystal X-ray diffraction (SC-XRD),  $^{13}\text{C}$  solid-state CPMAS NMR (ssNMR), and thermogravimetric analysis (TGA) and applied in SPE.

## MATERIALS AND METHODS

### Materials, Reagents, and Solvents

All reagents and solvents were purchased from commercial suppliers. Ultrapure water for sample preparation in ITC and extraction studies was obtained by means of Milli-Q® IQ 7003/05/10/15. Macrocyclic host compounds (cycHC[n]) were synthesized in our laboratory according to the procedures described in the literature (Aav et al., 2013; Prigorchenko et al., 2015; Kaabel et al., 2019).

### Binding of Heterocycles in Solid State

Single crystals of the host-guest complexes were obtained from saturated cycHC[8] solutions in methanol by adding 20  $\mu\text{L}$  of the

respective guest compound. SC-XRD data were collected at 123 K on a Rigaku Compact HomeLab diffractometer, equipped with a Saturn 944 HG CCD detector and an Oxford Cryostream cooling system using monochromatic Cu-K $\alpha$  radiation (1.54178 Å) from a MicroMax™-003 sealed tube microfocus X-ray source. The crystallographic data are deposited with the Cambridge Crystallographic Data Centre (CCDC 2069875–2069879) and can be obtained free of charge *via* [www.ccdc.cam.ac.uk/data\\_request/cif](http://www.ccdc.cam.ac.uk/data_request/cif).

Complexation between 1,3-dithiolane and cycHC[n] upon SPE was investigated by simultaneous thermogravimetry and differential thermal analysis coupled with evolved gas mass spectrometric analysis (TG-DTA/EGA-MS). The measurements were performed in the apparatus consisting of a Setaram SetSys-Evo 1600 thermal analyzer and a Pfeiffer OmniStar quadrupole mass spectrometer. Additionally, binding of 1,3-dithiolane and  $\alpha$ -lipoic acid by cycHC[n] was characterized with  $^{13}\text{C}$  ssNMR spectroscopy. The solid complexes were obtained *via* ball milling of cycHC[8] with the respective guest in the presence of a small amount of water. The ssNMR spectra were acquired on a Bruker Avance II spectrometer at 14.1 T magnetic field ( $^{13}\text{C}$  resonance frequency 150.91 MHz) using a home-built MAS probe for  $25 \times 4\text{-mm}$   $\text{Si}_3\text{N}_4$  rotors.

### Binding of Heterocycles in Solution

Complexation-induced shifts of cycHC[8] were studied by  $^1\text{H}$  NMR spectroscopy in 3 mM  $\text{CD}_3\text{OD}$  solution upon addition of 60 eq. of the respective guest compound. Association constants for the complexation with 1,3-dithiolane, 1,4-thioxane, and 1,4-dioxane were determined by  $^1\text{H}$  NMR titration.  $^1\text{H}$  NMR (400 MHz) spectra in solution were recorded on a Bruker Avance III spectrometer. Thermodynamic measurements by ITC were performed on a MicroCal PEAQ-ITC calorimeter using a 200- $\mu\text{L}$  calorimetric cell and a 40- $\mu\text{L}$  syringe.



## Characterization of the Sorbents

Prior to analysis and further extraction experiments, cycHC[*n*] were milled in an FTS-1000 shaker mill at 30 Hz frequency by using a 14-ml ZrO<sub>2</sub>-coated grinding jar charged with 3 × 7-mm ZrO<sub>2</sub> milling balls for 30 min. Surface area analysis of the milled cycHC[*n*] was performed on a KELVIN 1040/1042 Sorptometer at 150°C with N<sub>2</sub> as an adsorptive gas and He as a carrier gas. The obtained data were processed by Kelvin 1042 V3.12 software. Microscopic investigation of cycHC[*n*] particle sizes and their distribution was carried out before and after milling. Solid samples were examined by using an Olympus BX61 microscope. The acquired images were further analyzed by CellProfiler (version 4.0.3) software (Carpenter et al., 2006; McQuin et al., 2018).

## Extraction of Heterocycles From Aqueous Solutions

SPE was performed for 0.4–2.7 mM aqueous solutions of heterocyclic guests. A solid sorbent [5 or 20 M excess of cycHC[*n*] or powdered silicarbon TH90 special, Aktivkohle, taken in the equivalent amount by weight/extraction performance to that of the macrocyclic host] was dispersed in the guest solution and rotated for 30–60 min on a Vortex-Genie 2 mixer or Stuart magnetic stirrer. The heterogeneous mixture was further separated by using either a Hettich Universal 32R centrifuge or RC membrane syringe filters, and the liquid phase was analyzed for the guest content by HPLC or UV spectrophotometry. HPLC determination was performed on an Agilent 1200 Series HPLC system equipped with a multiple wavelength detector (MWD), Macherey-Nagel Nucleoshell RP18 column (150 × 3.0 mm, 2.7 μm), or Phenomenex Kinetex XB-C18 column (150 × 4.6 mm, 2.6 μm). UV absorption was measured by using a Jasco V-730 dual beam spectrophotometer and Varian Cary 50 UV-vis spectrophotometer in 10 mm quartz cuvettes. Mettler Toledo AB204-2 analytical balances (precision 0.1 mg) and Radwag MYA 11.4Y microbalances (precision 0.006 mg) were used in sample preparation.

Reusability of cycHC[8] was investigated by comparing its removal efficiency after four sorption–desorption cycles. The sorption step was performed analogously to the extraction procedure. The desorption step included rinsing the material with water, drying for 6 h at 110–120°C in the oven, followed by additional drying for 3 h under vacuum. The dried macrocycle was milled according to the general procedure and utilized in the subsequent cycle.

## RESULTS AND DISCUSSION

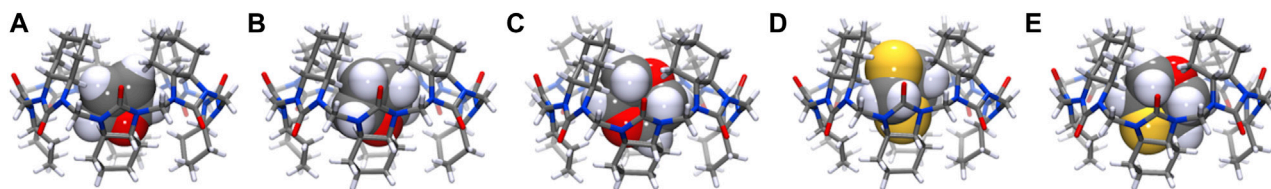
### SC-XRD of Inclusion Complexes

A series of compatibly sized electron-rich S-, O-, and N-heterocyclic compounds were crystallized *via* slow evaporation, and compounds **1**, **3**, **6**, **7**, and **8** formed inclusion complexes with cycHC[8] upon co-crystallization (Figure 2 and Supplementary Materials S4–S13). The N-containing heterocycles, **12** and **13**, and the largest explored guest, **4**, did not yield crystals of inclusion complexes with cycHC[8]. Packing of **1** and **3** inclusion complexes with cycHC[8] gave rise to isomorphous (*Z'* = 4) crystal structures (Supplementary

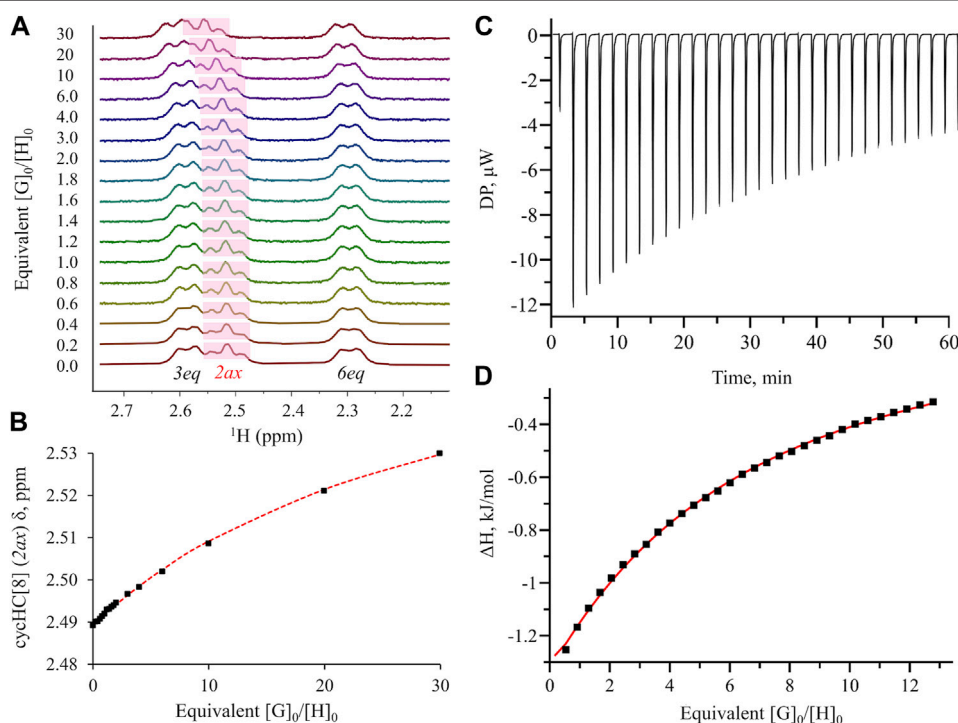
Materials S10,11), in an arrangement previously unrecorded for cycHC[8] inclusion complexes. The packing of complexes involving O-containing smaller heterocycles **6**, **7**, and **8** appears to be mainly directed by hydrogen bonding interactions with methanol such that the resulting crystal structures are isomorphous to each other (Supplementary Materials S6–S8) and the previously published methanol solvate of cycHC[8] (Prigorchenko et al., 2015). The smaller guest molecules **6**, **7**, and **8** had a total site occupancy limited to 50–75% of the resolved disorder components. The remaining electron density map exhibited no clear features, making it impossible to resolve whether the diffuse component of the guest disorder also includes partial substitutional disorder from methanol. In contrast, the position of the larger S-containing guests, **1** and **3**, is more conserved within the respective crystal structures (Supplementary Materials S12,13) with almost no diffuse component observed, indicating that these guests have fewer orientations available within cycHC[8]. Notably, analyzing the disorder models of all inclusion complexes reveals a similarity throughout, namely, where guests are oriented with heteroatoms close to the portals of cycHC[8] (Figure 2 and Supplementary Materials S6–S13). In several structures, heterocycles are located at a suitable distance (2.7–2.8 Å) from a methanol molecule at the portal of cycHC[8] and can therefore potentially accept hydrogen bonds *via* the portals of the macrocycle. This process would explain the observed conservation of this type of guest orientation motif. The guest molecules are tightly enwrapped within cycHC[8], especially the largest S-containing compounds, **1** and **3**, that fill close to 70% of the cavity volume (Figure 2, complexes D and E), indicating that guest binding and release must be accompanied by opening and closing of the host portals. Similar conformational dynamics of cycHC[8] have been previously observed and computationally described in the binding of large anionic guests (Kaabel et al., 2017).

### <sup>1</sup>H NMR and ITC Binding Studies in Solution

Furthermore, we evaluated host-guest complex formation in CD3OD solution. Inclusion complex formation was followed by an observed chemical shift change of cycHC[8] proton H2ax (Figure 1 and Supplementary Materials S14, S15) positioned inside the cavity. Our screening study revealed that S-containing five-membered heterocycles **1** and **2** caused larger chemical shift changes of 0.064 and 0.048 ppm, respectively, compared to the six-membered heterocycles **3**, **4**, **5**, and **6**. A negligible shift was observed for **7**, while no shift was observed for **8** or the N-heterocycles **10** and **11**. Signals of **9** overlapped with the characteristic cycHC[8] signal, and, therefore, its encapsulation could not be evaluated by <sup>1</sup>H NMR. Nevertheless, all chemical shift changes were relatively small compared to those that occurred upon binding of anions (Kaabel et al., 2017). The binding of **1**, **3**, and **6** was further evaluated by <sup>1</sup>H NMR titration (Figures 3A,B). The guest binding in methanol followed the order of log*P* values (Supplementary Materials S48) and agreed with our screening study; the strongest binding was shown for **1**, followed by **3** and **6**, with values of *K* = 7.9 ± 0.2 M<sup>−1</sup>, 2.18 ± 0.04 M<sup>−1</sup>, and 1.77 ± 0.04 M<sup>−1</sup>, respectively (Supplementary Materials S16–S22) for the 1:1 binding model.



**FIGURE 2** | Crystal structures of cycHC[8] inclusion complexes with neutral heterocycles with increasing packing coefficient order: **8@cycHC[8]** (**A**) (PC 0.51), **7@cycHC[8]**; (**B**) (PC 0.54), **6@cycHC[8]**; (**C**) (PC 0.61), **1@cycHC[8]**; (**D**) (PC 0.66), **3@cycHC[8]**; (**E**) (PC 0.69). Their packing coefficient values are the ratios between  $V_{\text{guest}}$  to  $V_{\text{cavity}}$  (host), reflecting the space filled by the encapsulated guest in the host cavity (Mecozzi and Jr, 1998). For more details, see **Supplementary Material S13**.



**FIGURE 3** |  $^1\text{H}$  NMR and ITC titration for cycHC[8] binding with **1** (**A**) spectra for NMR titration in  $\text{CD}_3\text{OD}$ ; (**B**) binding isotherm for NMR titration assuming the 1:1 binding model; (**C**) raw thermogram for ITC measurement in the  $\text{CH}_3\text{OH}:\text{H}_2\text{O}$  (50:50) mixture; (**D**) binding isotherm for ITC measurement using the “one set of sites” model. More details are provided in **Supplementary Material S16–S31**.

**TABLE 1** | Thermodynamic parameters from ITC measurements for complexation of guests **1**, **3**, and **6** with cycHC[8] for the 1:1 binding model. All energy values are given in kJ/mol.

No.	Guest	Solvent	$\Delta H^\circ$	$-T\Delta S^\circ$	$\Delta G^\circ$	$K_a, \text{M}_{-1}$
1	<b>1</b>	$\text{CH}_3\text{OH}$	$-9.8 \pm 0.6$	3.6	-6.2	$13.1 \pm 0.8$
2	<b>1</b>	$\text{CH}_3\text{OH}:\text{H}_2\text{O}$ (50:50)	$-20.4 \pm 0.9$	10.2	-10.2	$65.6 \pm 2.5$
3	<b>3</b>	$\text{CH}_3\text{OH}$	$-13.7 \pm 1.2$	11.4	-2.3	$2.5 \pm 0.2$
4	<b>3</b>	$\text{CH}_3\text{OH}:\text{H}_2\text{O}$ (50:50)	$-42.9 \pm 3.9$	39.6	-3.3	$3.7 \pm 0.3$

The thermodynamic characteristics of binding were collected by ITC (**Figures 3C,D**; **Table 1** and **Supplementary Materials S23–S31**). Binding of **6** with cycHC[8] in methanol was too weak

to be determined by ITC; however,  $K$  values for S-heterocycles **1** and **3** were in agreement with NMR data, showing the strongest binding for guest **1** (**Table 1**, lines 1 and 3). The binding of both guests in

methanol was enthalpically favorable and entropically unfavorable. A similar binding character was observed upon the binding of chaotropic anions to cycHC[8] in protic media (Kaabel et al., 2017). Although chaotropicity is mainly attributed to ionic species, chaotrope-like organic molecules have been reported in studies of crystalline hydrates (Dobrzycki et al., 2019). The chaotropic character (Assaf and Nau, 2018) is most strongly exhibited in aqueous media, and higher solvent polarity can enhance binding to the hydrophobic host. Therefore, we further studied the binding of **1** and **3** in mixtures of CH<sub>3</sub>OH and H<sub>2</sub>O (Supplementary Materials S25–S27, S29). In the presence of water, binding of the guests was indeed stronger, increasing the association constant of **1** from 13 M<sup>-1</sup> in CH<sub>3</sub>OH to a value of 66 M<sup>-1</sup> in the 1:1 CH<sub>3</sub>OH:H<sub>2</sub>O (50:50) mixture (Table 1, lines 1–2). For the bulkier and less hydrophobic guest **3**, the observed increase in the association constant was smaller (Table 1, lines 3–4). Binding enthalpy was strongly increased in the presence of water, accompanied by a rise in the entropic penalty for both guests (Table 1). Any further increase in the proportion of water proved impossible due to the limited solubility of cycHC[8].

## Characterization of Solid cycHC[n] and SPE Experiments

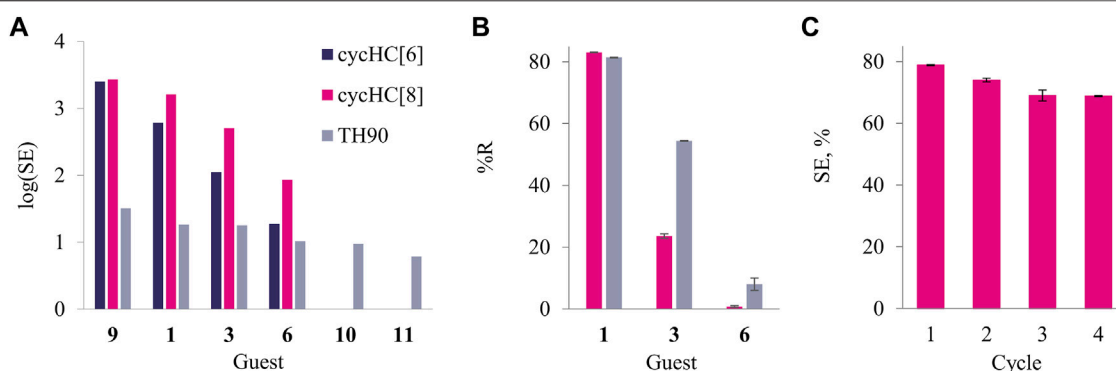
The low water solubility of the hydrophobic cycHC[8] and its ability to form inclusion complexes prompted us to investigate whether cycHC[8] can be used for the sorption of heterocycles from water *via* SPE. In parallel with cycHC[8], powdered silicarbon (TH90) and cycHC[6] were used. The cycHC[6] consists of the same monomers, so the hydrophobic properties of the outer surface are very similar to those of cycHC[8], but its cavity is much smaller (35 Å<sup>3</sup>) (Prigorchenko et al., 2015), and thus, it cannot accommodate the heterocycles studied. Hence, cycHC[6] served as an analog for differentiation between external physisorption and inclusion complex formation during extraction. The commonly used activated carbon-based sorbent TH90 was chosen as a reference to evaluate the efficiency and selectivity of sorption. The cycHC[n] compounds were milled before their use in extraction; microscopy studies and image analysis of the cycHC[n] showed that milling led to a relatively uniform particle size of 5 μm (Supplementary Materials S32–S35). The Brunauer–Emmett–Teller (BET) analysis of cycHC[n] by N<sub>2</sub> adsorption–desorption (Supplementary Materials S36,37) found the available surface area to be relatively similar for both cycHC[6] and cycHC[8] with values of 6.03 m<sup>2</sup>/g and 9.02 m<sup>2</sup>/g, respectively; therefore, the cycHC[n] homologs are expected to have similar extraction efficiencies. In contrast, the surface area of commercially available TH90 is much larger (ca. 1000 m<sup>2</sup>/g), which allows us to predict higher extraction efficiency per weight.

SPE was performed for heterocycles **1**, **3**, **6**, **9**, **10**, and **11** by stirring the dispersed solid sorbent in an aqueous solution of each guest; the change in the guest concentration upon extraction was then determined (Supplementary Materials S47,48). The cycHC[n] demonstrated negligible removal of O-containing **6**, as well as N-containing **10** and **11**. The larger cycHC[8] proved to efficiently extract the S-containing **1** (78%) and moderately remove **3** (25%), while cycHC[6] was considerably less efficient at removing these guests, with a 16% extraction value for **1** and only 3% value for **3**.

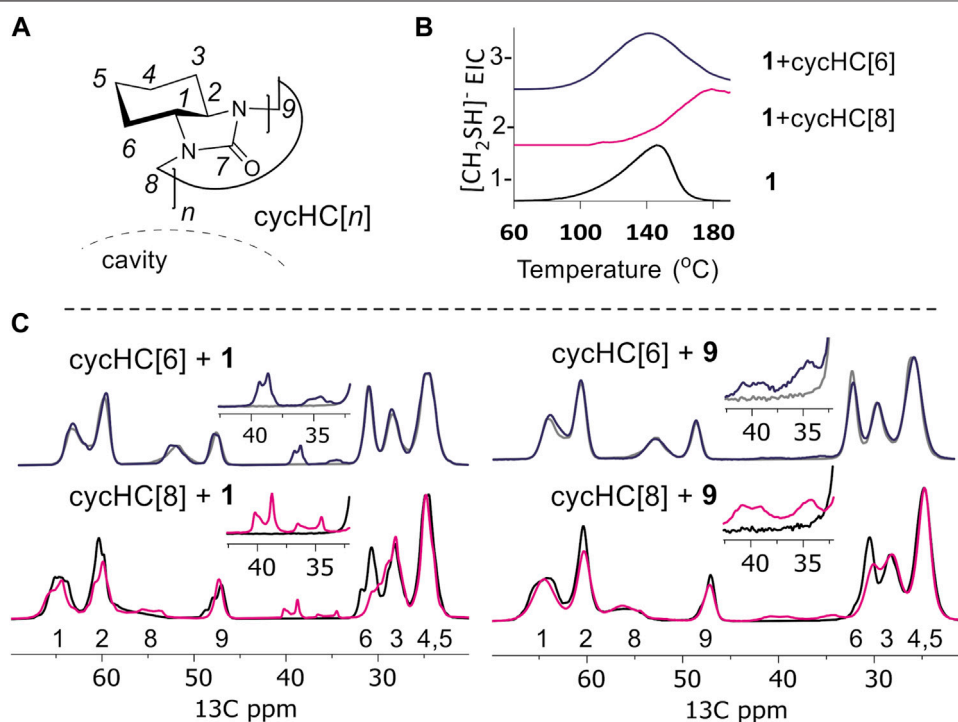
As expected, TH90 acts as a non-selective adsorbent, and taken in the same ratio of guest to sorbent (by weight), it removes over 50% of all of the studied heterocycles from water. Sorption efficiency (SE) was expressed as the mass of the sorbed guest (μg) per cm<sup>2</sup> of the respective sorbent surface area and converted into logarithmic scale. The latter demonstrates that cycHC[n] possess higher affinity toward hydrophobic S-containing heterocycles, while TH90 exhibits roughly the same performance independently of the guest nature (Figure 4A). Furthermore, we evaluated sorption selectivity using a mixture of guests **1**, **3**, and **6**, and the amount of sorbent (cycHC[8] and TH90) providing ca. 80% removal percentage (%R) for guest **1** (Supplementary Materials S49, S50). Both sorbents showed low sorption of the least hydrophobic guest **6**, although TH90 proved to remove ca. 10 times more than cycHC[8]. More importantly, over two times difference was observed between the affinity of two S-heterocycles **1** and **3**; cycHC[8] is 2.3 times more selective than TH90 (Figure 4B and Supplementary Material S50); in addition, cycHC[8] sorbent is reusable after binding of **1**. A simple washing and drying procedure, followed by milling, allows the reactivation of the sorbent's surface for future use without significant loss in binding efficiency for at least four cycles (Figure 4C and Supplementary Materials S57–58).

## TGA and <sup>13</sup>C ssNMR Studies

The formation of inclusion complexes in the cycHC[8] sorbent after SPE of **1** was confirmed by TGA, by identifying the formation of the characteristic fragmentation product [CH<sub>2</sub>SH]<sup>+</sup> (*m/z* 47) of **1** when bound to cycHC[n] sorbents and in pure form (see Supplementary Material S51 for details). The evolution profiles for pure **1** and its complex with cycHC[6] (Figure 5B) occur at similar temperatures of 148°C and 138°C, respectively, indicating that no inclusion complexes form with the smaller macrocycle. Furthermore, the complex with cycHC[8] releases the characteristic degradation product at a significantly higher temperature, 189°C, indicating additional interactions between cycHC[8] and one which impact higher thermal stability to **1** (Figure 5B and Supplementary Material S51). SPE of the largest and most hydrophobic guest in this study, **9**, leads to similar efficiency of extraction by cycHC[6] and cycHC[8], with %R values of 46 and 78%, respectively (Supplementary Materials S47,48), which may indicate a different binding behavior of **9** to cycHC[n] in comparison to **1**. To better understand the interaction of guests **1** and **9** with cycHC[8] and cycHC[6], we investigated complex formation using <sup>13</sup>C ssNMR spectroscopy (Figure 5C and Supplementary Materials S52–56). Recently, complex formation *via* mechanochemical agitation of cucurbit[7]uril was followed by ssNMR (Dračinský et al., 2021). Powders obtained by liquid-assisted grinding of cycHC[n] with the guest in the presence of water served as the model for binding during the extraction process at the solute–solid interphase. Figure 5C illustrates the changes induced upon binding of **1** with cycHC[8] and cycHC[6] (Supplementary Materials S53,54). The most significant change after milling is observed in the <sup>13</sup>C signal of carbons 2 and 6, pointing inside the cavity of cycHC[8] (Figure 5C lower left and Supplementary Material S54). Intensities of these signals are decreased and the chemical shift in position 6 changed from



**FIGURE 4 | (A)** SE of cycHC[6], cycHC[8], and TH90 (dark blue, pink, and gray, respectively) in water, displayed in logarithmic scale; **(B)** selectivity of SPE from the mixture of **1**, **3**, and **6** by cycHC[8] and TH90, at comparable sorbent amount granting %R ca 80% for **1**; **(C)** %R exhibited by cycHC[8] throughout repeated extraction cycles of 1 [Error bars stand for the standard deviation between parallel experiments ( $n \geq 2$ ). For more details, see **Supplementary Material S38–S50,S57**].



**FIGURE 5 | (A)** Structure of cycHC[n] with atom numeration and cavity direction; **(B)** extracted ion current (EIC) of one fragment in TGA: 1 - pure **1**, 2 - cycHC[8] after extraction of **1**, 3 - cycHC[6] after extraction of **1**; **(C)** <sup>13</sup>C ssNMR stacked spectra of cycHC[n] before and after milling with guests: upper left - **1** + cycHC[6] (blue) overlaid with cycHC[6] (gray); lower left - **1** + cycHC[8] (pink) overlaid with cycHC[8] (black); upper right - **9** + cycHC[6] (blue) overlaid with cycHC[6] (gray); lower right - **9** + cycHC[8] (pink) overlaid with cycHC[8] (black).

30.6 to 29.8 ppm, evidencing the formation of inclusion complex **1@cycHC[8]**. In contrast, the spectra of **1** milled with cycHC[6] do not evidence such changes (**Figure 5C** upper left and **Supplementary Material S53**), confirming that physisorption on the surface of cycHC[n] does not have a significant effect on sorbent ssNMR shifts. In an analogous experiment with **9** (**Figure 5C** right and **Supplementary Materials S54–S56**)

similar trends can be observed, that is, a change in the signal intensities of carbons 2 and 6 of cycHC[8], accompanied by a slight chemical shift change at carbon 6 (**Figure 5C** lower right) and no change in the spectrum of cycHC[6] (**Figure 5C** upper right). Thus, the prominent selectivity of cycHC[8] toward binding of five-membered S-heterocycles **1** and **9** is explained by inclusion complex formation during SPE. Unfortunately, no



enantioselectivity was observed during extraction of stereoisomers of **9** (Supplementary Material S48).

## CONCLUSION

Encapsulation of five- and six-membered electron-rich heterocyclic guests by cycHC[8] is mostly related to their size, which must be complementary with the host cavity, and the hydrophobic effect is one of the driving forces of the interaction. From the binding studies of **1** and **3** with cycHC[8] in methanol and a methanol–water mixture, complex formation was found to be even more favorable in the presence of water and the thermodynamic characteristics resembled the binding of chaotropic anions. We showed that cycHC[8] can serve as a selective solid sorbent material for SPE of sulfur heterocycles from aqueous solutions; in addition, cycHC[8] was successfully applied for selective extraction of **1** and **9**. The ssNMR, TGA, and comparative extraction by homologous cycHC[6] and commonly used TH90 revealed that prominent selectivity of cycHC[8] toward binding of five-membered S-heterocycles is driven by inclusion complex formation. Design of advanced material with increased surface area would enhance the extraction performance even further. Crucially, the solid cycHC[8] sorbent material can be reused, which makes it a candidate for applications in selective SPE systems or the removal of pollutants and other target compounds from water, based on molecular recognition properties.

## DATA AVAILABILITY STATEMENT

The datasets presented in this study can be found in Supplementary Material.

## REFERENCES

- Aav, R., Shmatova, E., Reile, I., Borissova, M., Topić, F., and Rissanen, K. (2013). New Chiral Cyclohexylhemicurbit[6]uril. *Org. Lett.* 15, 3786–3789. doi:10.1021/ol401766a
- Andersen, N. N., Eriksen, K., Lisbjerg, M., Ottesen, M. E., Milhøj, B. O., Sauer, S. P. A., et al. (2019). Entropy/Enthalpy Compensation in Anion Binding: Biotin[6]uril and Biotin-L-Sulfoxide[6]uril Reveal Strong Solvent Dependency. *J. Org. Chem.* 84, 2577–2584. doi:10.1021/acs.joc.8b02797
- Andersen, N. N., Lisbjerg, M., Eriksen, K., and Pittelkow, M. (2018). Hemicurbit [n]urils and Their Derivatives - Synthesis and Applications. *Isr. J. Chem.* 58, 435–448. doi:10.1002/ijch.201700129
- Assaf, K. I., and Nau, W. M. (2018). The Chaotropic Effect as an Assembly Motif in Chemistry. *Angew. Chem. Int. Ed.* 57, 13968–13981. doi:10.1002/anie.201804597
- Buschmann, H.-J., Cleve, E., and Schollmeyer, E. (2005). Hemicurbit[6]uril, a Selective Ligand for the Complexation of Anions in Aqueous Solution. *Inorg. Chem. Commun.* 8, 125–127. doi:10.1016/j.inoche.2004.11.020
- Caira, M., Bourne, S., and Mzondo, B. (2017). Encapsulation of the Antioxidant R-(+)- $\alpha$ -Lipoic Acid in Permethylated  $\alpha$ - and  $\beta$ -Cyclodextrins: Thermal and X-ray Structural Characterization of the 1:1 Inclusion Complexes. *Molecules* 22, 866. doi:10.3390/molecules22060866
- Carpenter, A. E., Jones, T. R., Lamprecht, M. R., Clarke, C., Kang, I., Friman, O., et al. (2006). CellProfiler: Image Analysis Software for Identifying and

## AUTHOR CONTRIBUTIONS

RA contributed to conceptualization and idea of the research; TS and KM synthesized cycHC[n]; SK accomplished crystallization and SC-XRD studies; TS, KM, and SK performed  $^1\text{H}$  NMR screening and titrations; KM and LU fulfilled ITC measurements; TS and KM investigated SPE; SB carried out microscopic characterization of cycHC[n]; KT was responsible for TGA; TS and IH conducted  $^{13}\text{C}$  ssNMR experiments. The manuscript was written via contribution of all authors..

## FUNDING

This work was supported by the Estonian Research Council Grants (PRG399, MOBJD556, and MOBJD592), the European Regional Development Fund (CoE 2014-2020.4.01.15-0013 and CoE TK134), and H2020- FETOPEN 828779 (INITIO).

## ACKNOWLEDGMENTS

The authors would like to thank Elina Suut and Jagadeesh Varma Nallaparaju for the synthesis of cycHC[n], Dr. Heidi Lees and Piia Jõul for providing the S-containing heterocyclic compounds used for crystallization and extraction experiments, and Mai Uibu for BET analysis.

## SUPPLEMENTARY MATERIAL

The Supplementary Material for this article can be found online at: <https://www.frontiersin.org/articles/10.3389/fchem.2021.786746/full#supplementary-material>

Quantifying Cell Phenotypes. *Genome Biol.* 7, R100. doi:10.1186/gb-2006-7-10-r100

- Celebioglu, A., and Uyar, T. (2019). Encapsulation and Stabilization of  $\alpha$ -Lipoic Acid in Cyclodextrin Inclusion Complex Electrospun Nanofibers: Antioxidant and Fast-Dissolving  $\alpha$ -Lipoic Acid/Cyclodextrin Nanofibrous Webs. *J. Agric. Food Chem.* 67, 13093–13107. doi:10.1021/acs.jafc.9b05580
- Cuculea, E. I., Buschmann, H.-J., and Mutihac, L. (2016). Hemicurbiturils as Receptors in Extraction and Transport of Some Amino Acids. *Supramolecular Chem.* 28, 727–732. doi:10.1080/10610278.2015.1121267
- Dobrzycki, Ł., Socha, P., Ciesielski, A., Boese, R., and Cyrański, M. K. (2019). Formation of Crystalline Hydrates by Nonionic Chaotropes and Kosmotropes: Case of Piperidine. *Cryst. Growth Des.* 19, 1005–1020. doi:10.1021/acs.cgd.8b01548
- Dračinský, M., Hurtado, C. S., Masson, E., and Kaleta, J. (2021). Stuffed Pumpkins: Mechanochemical Synthesis of Host-Guest Complexes with Cucurbit[7]uril. *Chem. Commun.* 57, 2132–2135. doi:10.1039/D1CC00240F
- Garbusov, V., Rehfeld, G., Wölm, G., Golovnja, R. V., and Rothe, M. (1976). Volatile Sulfur Compounds Contributing to Meat Flavour. Part. I. Components Identified in Boiled Meat. *Nahrung* 20, 235–241. doi:10.1002/food.19760200302
- Ikuta, N., Sugiyama, H., Shimosegawa, H., Nakane, R., Ishida, Y., Uekaji, Y., et al. (2013). Analysis of the Enhanced Stability of R-(+)- $\alpha$ -Lipoic Acid by the Complex Formation with Cyclodextrins. *Ijms* 14, 3639–3655. doi:10.3390/ijms14023639
- Jin, X.-Y., Wang, F., Cong, H., and Tao, Z. (2016a). Host-guest Interactions between Hemicurbiturils and a Hydroxyl-Substituted Schiff Base. *J. Incl. Phenom. Macrocycl. Chem.* 86, 249–254. doi:10.1007/s10847-016-0659-3

- Jin, X.-Y., Wang, F., Cong, H., and Tao, Z. (2016b). Host-guest Interactions of Hemicucurbiturils with Aminophenols. *J. Incl. Phenom. Macrocycl. Chem.* 86, 241–248. doi:10.1007/s10847-016-0653-9
- Jin, X.-Y., Zhao, J.-L., Wang, F., Cong, H., and Tao, Z. (2017). Formation of an Interaction Complex of Hemicucurbit[6]uril and Ferrocene. *J. Organomet. Chem.* 846, 1–5. doi:10.1016/j.jorganchem.2017.05.053
- Joul, P., Vaher, M., and Kuhtinskaja, M. (2018). Evaluation of Carbon Aerogel-Based Solid-phase Extraction Sorbent for the Analysis of Sulfur Mustard Degradation Products in Environmental Water Samples. *Chemosphere* 198, 460–468. doi:10.1016/j.chemosphere.2018.01.157
- Kaabel, S., and Aav, R. (2018). Templating Effects in the Dynamic Chemistry of Cucurbiturils and Hemicucurbiturils. *Isr. J. Chem.* 58, 296–313. doi:10.1002/ijch.201700106
- Kaabel, S., Adamson, J., Topić, F., Kiesilä, A., Kalenius, E., Ören, M., et al. (2017). Chiral Hemicucurbit[8]uril as an Anion Receptor: Selectivity to Size, Shape and Charge Distribution. *Chem. Sci.* 8, 2184–2190. doi:10.1039/c6sc05058a
- Kaabel, S., Stein, R. S., Fomitšenko, M., Järving, I., Friščić, T., and Aav, R. (2019). Size-Control by Anion Templating in Mechanochemical Synthesis of Hemicucurbiturils in the Solid State. *Angew. Chem. Int. Ed.* 58, 6230–6234. doi:10.1002/anie.201813431
- Kandrálová, M., Kokan, Z., Havel, V., Nečas, M., and Šindelář, V. (2019). Hypervalent Iodine Based Reversible Covalent Bond in Rotaxane Synthesis. *Angew. Chem. Int. Ed.* 58, 18182–18185. doi:10.1002/anie.201908953
- Lamberth, C., Walter, H., Kessabi, F. M., Quaranta, L., Beaudegnies, R., Trah, S., et al. (2015). The Significance of Organosulfur Compounds in Crop Protection: Current Examples from Fungicide Research. *Phosphorus, Sulfur, Silicon Relat. Elem.* 190, 1225–1235. doi:10.1080/10426507.2014.984033
- Lees, H., Vaher, M., and Kaljurand, M. (2017). Development and Comparison of HPLC and MEKC Methods for the Analysis of Cyclic Sulfur Mustard Degradation Products. *Electrophoresis* 38, 1075–1082. doi:10.1002/elps.201600418
- Li, Y., Li, L., Zhu, Y., Meng, X., and Wu, A. (2009). Solvent Effect on Pseudopolymorphism of Hemicyclohexylcucurbit[6]uril. *Cryst. Growth Des.* 9, 4255–4257. doi:10.1021/cg9007262
- Lin-Hui, T., Zheng-Zhi, P., and Ying, Y. (1995). Inclusion Complexes of  $\alpha$ - And  $\beta$ -Cyclodextrin with  $\alpha$ -lipoic Acid. *J. Incl. Phenom. Macrocycl. Chem.* 23, 119–126. doi:10.1007/BF00707889
- Lizal, T., and Sindelar, V. (2018). Bambusuril Anion Receptors. *Isr. J. Chem.* 58, 326–333. doi:10.1002/ijch.201700111
- Maeda, H., Onodera, T., and Nakayama, H. (2010). Inclusion Complex of  $\alpha$ -lipoic Acid and Modified Cyclodextrins. *J. Incl. Phenom. Macrocycl. Chem.* 68, 201–206. doi:10.1007/s10847-010-9767-7
- Magnusson, R., Nordlander, T., and Östin, A. (2016). Development of a Dynamic Headspace Gas Chromatography-Mass Spectrometry Method for On-Site Analysis of Sulfur Mustard Degradation Products in Sediments. *J. Chromatogr. A* 1429, 40–52. doi:10.1016/j.chroma.2015.12.009
- Mahadevan, K., and Farmer, L. (2006). Key Odor Impact Compounds in Three Yeast Extract Pastes. *J. Agric. Food Chem.* 54, 7242–7250. doi:10.1021/jf061102x
- Maršálek, K., and Šindelář, V. (2020). Monofunctionalized Bambus[6]urils and Their Conjugates with Crown Ethers for Liquid-Liquid Extraction of Inorganic Salts. *Org. Lett.* 22, 1633–1637. doi:10.1021/acs.orglett.0c00216
- McQuinn, C., Goodman, A., Chernyshev, V., Kamensky, L., Cimini, B. A., Karhohs, K. W., et al. (2018). CellProfiler 3.0: Next-Generation Image Processing for Biology. *Plos Biol.* 16, e2005970. doi:10.1371/journal.pbio.2005970
- Mecozzi, S., and Jr, J. R. (1998). The 55 % Solution: A Formula for Molecular Recognition in the Liquid State. *Chem. Eur. J.* 4, 1016–1022. doi:10.1002/(SICI)1521-3765(19980615)4:6<1016:AID-CHEM1016>3.0.CO;2-B
- Mishra, K. A., Adamson, J., Ören, M., Kaabel, S., Fomitšenko, M., and Aav, R. (2020). Dynamic Chiral Cyclohexanohemicucurbit[12]uril. *Chem. Commun.* 56, 14645–14648. doi:10.1039/D0CC06817A
- Mottram, D. S., and Mottram, H. R. (2002). An Overview of the Contribution of Sulfur-Containing Compounds to the Aroma in Heated Foods. In *ACS Symposium Series, Heteroatomic Aroma Compound*. Editors G. A. Reineccius and T. A. Reineccius 826, 73–92. doi:10.1021/bk-2002-0826.ch004
- Ören, M., Shmatova, E., Tamm, T., and Aav, R. (2014). Computational and Ion Mobility MS Study of (All-S)-Cyclohexylhemicucurbit[6]uril Structure and Complexes. *Phys. Chem. Chem. Phys.* 16, 19198–19205. doi:10.1039/C4CP02202E
- Prigorchenko, E., Kaabel, S., Narva, T., Baškir, A., Fomitšenko, M., Adamson, J., et al. (2019). Formation and Trapping of the Thermodynamically Unfavoured Inverted-Hemicucurbit[6]uril. *Chem. Commun.* 55, 9307–9310. doi:10.1039/C9CC04990H
- Prigorchenko, E., Ören, M., Kaabel, S., Fomitšenko, M., Reile, I., Järving, I., et al. (2015). Template-controlled Synthesis of Chiral Cyclohexylhemicucurbit[8]uril. *Chem. Commun.* 51, 10921–10924. doi:10.1039/c5cc04101e
- Racz, C.-P., Santa, S., Tomoaia-Cotisel, M., Borodi, G., Kacso, I., Pirnau, A., et al. (2013). Inclusion of  $\alpha$ -lipoic Acid in  $\beta$ -cyclodextrin. Physical-Chemical and Structural Characterization. *J. Incl. Phenom. Macrocycl. Chem.* 76, 193–199. doi:10.1007/s10847-012-0191-z
- Reany, O., Mohite, A., and Keinan, E. (2018). Hetero-Bambusurils. *Isr. J. Chem.* 58, 449–460. doi:10.1002/ijch.201700138
- Rezanka, T., Sobotka, M., Spizek, J., and Sigler, K. (2006). Pharmacologically Active Sulfur-Containing Compounds. *Aiamc* 5, 187–224. doi:10.2174/187152106776359002
- Rochette, L., Ghibu, S., Richard, C., Zeller, M., Cottin, Y., and Vergely, C. (2013). Direct and Indirect Antioxidant Properties of  $\alpha$ -lipoic Acid and Therapeutic Potential. *Mol. Nutr. Food Res.* 57, 114–125. doi:10.1002/mnfr.201200608
- Røen, B. T., Unneberg, E., Tørnes, J. A., and Lundanes, E. (2010). Headspace-trap Gas Chromatography-Mass Spectrometry for Determination of sulphur Mustard and Related Compounds in Soil. *J. Chromatogr. A* 1217, 2171–2178. doi:10.1016/j.chroma.2010.01.088
- Salehi, B., Berkay Yilmaz, Y., Antika, G., Boyunegmez Tumer, T., Fawzi Mahomoodally, M., Lobine, D., et al. (2019). Insights on the Use of  $\alpha$ -Lipoic Acid for Therapeutic Purposes. *Biomolecules* 9, 356. doi:10.3390/biom9080356
- Schoenauer, S., and Schieberle, P. (2018). Structure-Odor Correlations in Homologous Series of Mercapto Furans and Mercapto Thiophenes Synthesized by Changing the Structural Motifs of the Key Coffee Odorant Furan-2-Ylmethanethiol. *J. Agric. Food Chem.* 66, 4189–4199. doi:10.1021/acs.jafc.8b00857
- Takahashi, H., Bungo, Y., and Mikuni, K. (2011). The Aqueous Solubility and Thermal Stability of  $\alpha$ -Lipoic Acid Are Enhanced by Cyclodextrin. *Biosci. Biotechnol. Biochem.* 75, 633–637. doi:10.1271/bbb.100596
- Ustrnul, L., Burankova, T., Ören, M., Juhhimenka, K., Ilmarinen, J., Siilak, K., et al. (2021). Binding between Cyclohexanohemicucurbit[n]urils and Polar Organic Guests. *Front. Chem.* 9, 468. doi:10.3389/fchem.2021.701028
- Ustrnul, L., Kaabel, S., Burankova, T., Martõnova, J., Adamson, J., Konrad, N., et al. (2019). Supramolecular Chirogenesis in Zinc Porphyrins by Enantiopure Hemicucurbit[n]urils (N = 6, 8). *Chem. Commun.* 55, 14434–14437. doi:10.1039/c9cc07150d
- Valkenier, H., Akrawi, O., Jurček, P., Sleziaková, K., Lizal, T., Bartik, K., et al. (2019). Fluorinated Bambusurils as Highly Effective and Selective Transmembrane Cl<sup>−</sup>/HCO<sub>3</sub><sup>−</sup> Antiporters. *Chem* 5, 429–444. doi:10.1016/j.chempr.2018.11.008
- Vanninen, P., Östin, A., Beldowski, J., Pedersen, E. A., Söderström, M., Szubska, M., et al. (2020). Exposure Status of Sea-Dumped Chemical Warfare Agents in the Baltic Sea. *Mar. Environ. Res.* 161, 105112. doi:10.1016/j.marenvres.2020.105112
- Vázquez, J., and Sindelar, V. (2018). Supramolecular Binding and Release of Sulfide and Hydrosulfide Anions in Water. *Chem. Commun.* 54, 5859–5862. doi:10.1039/C8CC00470F
- Xi, Y., Man, C., Fang, W., Xian-Yi, J., Hang, C., and Zhu, T. (2018). Development of a Sub-group of the Cucurbituril Family, Hemicucurbiturils: Synthesis and Supramolecular Chemistry. *Mini-rev. Org. Chem.* 15, 274–282.

**Conflict of Interest:** The authors declare that the research was conducted in the absence of any commercial or financial relationships that could be construed as a potential conflict of interest.

**Publisher's Note:** All claims expressed in this article are solely those of the authors and do not necessarily represent those of their affiliated organizations, or those of the publisher, the editors, and the reviewers. Any product that may be evaluated in this article, or claim that may be made by its manufacturer, is not guaranteed or endorsed by the publisher.

Copyright © 2021 Shalima, Mishra, Kaabel, Ustrnul, Bartkova, Tõnsuaadu, Heinmaa and Aav. This is an open-access article distributed under the terms of the Creative Commons Attribution License (CC BY). The use, distribution or reproduction in other forums is permitted, provided the original author(s) and the copyright owner(s) are credited and that the original publication in this journal is cited, in accordance with accepted academic practice. No use, distribution or reproduction is permitted which does not comply with these terms.



# Removal of the Micropollutants Propranolol Hydrochloride and 2-Naphthol From Water by Pyridine-Functionalized Polymers

Qixuan Zheng, Daniel K. Unruh and Kristin M. Hutchins\*

Department of Chemistry and Biochemistry, Texas Tech University, Lubbock, TX, United States

## OPEN ACCESS

### Edited by:

Jennifer Hiscock,  
University of Kent, United Kingdom

### Reviewed by:

Yuanli Liu,  
Guilin University of Technology, China  
Adam Charles Sedgwick,  
University of Texas at Austin,  
United States

### \*Correspondence:

Kristin M. Hutchins  
kristin.hutchins@ttu.edu

### Specialty section:

This article was submitted to  
Supramolecular Chemistry,  
a section of the journal  
Frontiers in Chemistry

**Received:** 12 October 2021

**Accepted:** 31 December 2021

**Published:** 21 January 2022

### Citation:

Zheng Q, Unruh DK and Hutchins KM  
(2022) Removal of the Micropollutants  
Propranolol Hydrochloride and 2-  
Naphthol From Water by Pyridine-  
Functionalized Polymers.  
Front. Chem. 9:793870.  
doi: 10.3389/fchem.2021.793870

The number and concentration of micropollutants in aqueous environments are increasing. Two such micropollutants include the pharmaceutical, propranolol hydrochloride, and dye intermediate, 2-naphthol. Here, we describe the synthesis of both linear and crosslinked pyridine-functionalized copolymers that bind and remove propranolol hydrochloride and 2-naphthol from water solutions. Propranolol hydrochloride and 2-naphthol both contain hydrogen-bond-donor groups, and the pyridine moiety on the polymer acts as a hydrogen-bond acceptor to facilitate removal. Copolymers with different amounts of pyridine comonomer are synthesized, and as the amount of the pyridine comonomer is increased, the ability of the polymer to bind and remove the contaminant also increases. The concentrations of propranolol hydrochloride and 2-naphthol decreased by approximately 20–40% and 60–88%, respectively, depending on the polymer type that is used in the binding experiment. A control polymer was synthesized by using styrene in place of the pyridine monomer. In analogous binding experiments, the styrene polymer decreases the concentration of propranolol hydrochloride by 2% and 2-naphthol by 26%. Thus, the binding effectiveness is significantly reduced when the hydrogen-bond-acceptor group is not present on the polymer. We also show that the best performing crosslinked pyridine-functionalized polymer is reusable. Overall, these polymer adsorbents demonstrate the potential for removal of micropollutants from water.

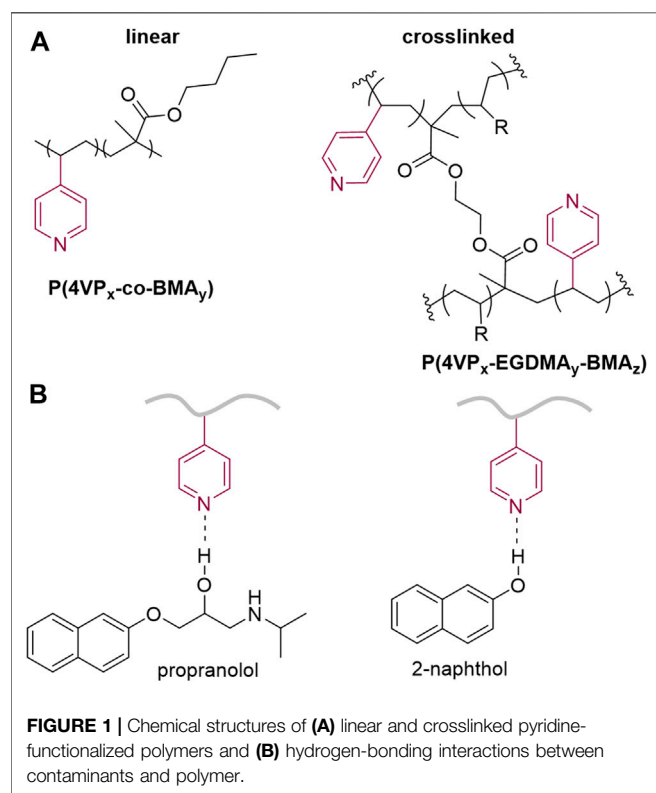
**Keywords:** copolymer, micropollutants, pharmaceuticals, polymeric sorbents, supramolecular

## INTRODUCTION

The fast-growing global consumption of products such as pharmaceuticals, pesticides, and personal-care products has led to the presence of organic micropollutants in the environment, especially in aquatic systems (Schwarzenbach et al., 2006). Although the effects of such micropollutants on human, animal, and plant health remain mostly unknown, there are concerns about negative impacts on aquatic life and human health (Alsaiee et al., 2016; Weber et al., 2016). Most wastewater treatment plants are not equipped to remove micropollutants that enter the water supply (Bui et al., 2016). Activated carbon absorption has attracted significant attention for its effectiveness; however, the material shows poor affinity for polar compounds (Kovalova et al., 2013; Bui et al., 2016). Advanced oxidation processes have also shown promise in reducing micropollutants, but some oxidation products remain toxic (Hollender et al., 2009; Zimmermann et al., 2011; Prasse et al., 2012). Methods and/or materials that target and remove contaminants without generating

**TABLE 1 |** The removal performance of reported materials and polymers in this work for **PPL-HCl** and **2NO**.

Material	Concentration of PPL-HCl water solution (mM)	Concentration decrease for PPL-HCl water solution (%)	Concentration of 2NO water solution (mM)	Concentration decrease for 2NO water solution (%)	Reference
porous $\beta$ -cyclodextrin polymer	0.09	96	0.1	91	Alsaiee et al. (2016)
$\beta$ -cyclodextrin-polyacrylamide hydrogel	0.035–1.0	54	0.035–1.0	60	Song et al. (2021)
porous polycalix [4]arenes	0.1	85	0.1	75	Shetty et al. (2018)
biomass alginate	1.0	50–90	—	—	Coelho et al. (2020)
carbon nanotube-based composite adsorbent	—	—	0.035	60–70	Xu et al. (2018)
pyridine-functionalized copolymers	0.4	40	0.1	88	this work

**FIGURE 1 |** Chemical structures of (A) linear and crosslinked pyridine-functionalized polymers and (B) hydrogen-bonding interactions between contaminants and polymer.

byproducts (Xiao et al., 2019) will aid in addressing contamination problems. Recently, adsorbent materials including macrocycles (Ji et al., 2020; Klemes et al., 2020; Dai et al., 2021), covalent organic frameworks (Skorjanc et al., 2021), assembled molecular rings (Liu et al., 2021), and crosslinked polymers (Wang et al., 2021; Yang L. P et al., 2021) have been designed and synthesized for removal of micropollutants from water.

Propranolol hydrochloride (**PPL-HCl**) is a beta blocker that has been found in aquatic environments, and typical wastewater treatment plant removal is less than 30% (Margot et al., 2015). 2-Naphthol (**2NO**) is an intermediate in the production of dyes and other compounds (e.g., BINOL) and has also been found as a water contaminant (Wang et al., 2006; Zang and Lian, 2009). Both **PPL-**

**HCl** and **2NO** feature aromatic and hydroxyl groups. Polymers and porous materials have been designed and synthesized to remove these two micropollutants from water (Table 1). In 2016, Dichtel et al. reported a porous  $\beta$ -cyclodextrin polymer that can remove 96% of **PPL-HCl** or 91% **2NO** from aqueous solution *via* flow-through adsorption in 30 min (Alsaiee et al., 2016). In 2018, Trabolsi et al. reported porous polycalix [4]arenes that can remove around 85% of **PPL-HCl** or 75% **2NO** from aqueous solutions (Shetty et al., 2018). In 2021, Song et al. reported a  $\beta$ -cyclodextrin-polyacrylamide hydrogel that can remove 54% of **PPL-HCl** or 60% of **2NO** from aqueous solution through host-guest interactions in a period of 8 h (Song et al., 2021). We postulated that polymers functionalized with aromatic groups and hydrogen-bond-acceptor moieties (Diez-Pascual et al., 2016) could form noncovalent interactions with the contaminants to facilitate adsorption. Here, we demonstrate both linear and crosslinked pyridine-functionalized polymers can bind and remove **PPL-HCl** and **2NO** from water solutions. Both the linear and crosslinked polymers contain *n*-butylmethacrylate (**BMA**) and 4-vinylpyridine (**4-VP**) as comonomers, and the crosslinked polymers also include ethylene glycol dimethacrylate (**EGDMA**) as the crosslinker (Figure 1A). The **4-VP**:**BMA** comonomer ratio was systematically increased to afford polymers with different binding abilities. Overall, polymers with higher **4-VP**:**BMA** ratios exhibit greater binding and removal ability. The concentrations of **PPL-HCl** and **2NO** in aqueous solutions decreased by approximately 20–40% and 60–88%, respectively, depending on the type of polymer used. All the polymers contain pyridine rings and carbonyl functional groups, which are both capable of acting as hydrogen-bond acceptor sites (Figure 1B). Small molecule cocrystallization experiments with **2NO** and methyl isonicotinate (**MI**), which contains pyridyl and ester functional groups and mimics the polymer functional groups, demonstrate that hydrogen bonding likely supports binding. Moreover, a control polymer synthesized using styrene in place of the pyridine monomer exhibited significantly reduced binding ability.

## MATERIALS AND METHODS

### Materials

Methyl isonicotinate (**MI**), and propranolol hydrochloride (**PPL-HCl**) were purchased from Oakwood Chemical. 4-vinylpyridine (**4-VP**) and ethylene glycol dimethacrylate (**EGDMA**) were purchased



**TABLE 2 |** Linear polymers: theoretical/synthetic feed ratios of monomers used, obtained ratios, and characterization data.

Linear polymer	Theoretical and synthetic feed ratio 4VP:BMA	Reaction time (h)	Obtained ratio <sup>a</sup>	M <sub>n</sub> (kDa)	M <sub>w</sub> (kDa)	Đ
P(4VP <sub>1</sub> -co-BMA <sub>1</sub> )	1:1 (30:30 mmol)	18	1:0.82	1.2	5.8	4.6
P(4VP <sub>2</sub> -co-BMA <sub>1</sub> )	2:1 (60:30 mmol)	18	2:0.77	13.3	23.4	1.8
P(4VP <sub>3</sub> -co-BMA <sub>1</sub> )	3:1 (90:30 mmol)	18	3:0.84	11.1	18.1	1.6
P(4VP <sub>3</sub> -co-BMA <sub>1</sub> ) <sub>t</sub>	3:1 (90:30 mmol)	36	3:0.88	17.0	28.7	1.7

<sup>a</sup>Based on <sup>1</sup>H NMR, spectroscopy.

from Alfa Aesar. *n*-Butylmethacrylate (BMA) and styrene (STY) were purchased from ACROS Organics. Benzoyl peroxide (BPO) and azobisisobutyronitrile (AIBN) were purchased from Sigma-Aldrich Chemical. 2-Naphthol (2NO) was purchased from Tokyo Chemical Industry Co., LTD. Diethyl ether, methanol, toluene, tetrahydrofuran (THF), and basic alumina were purchased from Fisher Scientific. Inhibitors in commercial 4-VP, EGDMA, BMA, and STY were removed by passage through basic alumina. All other chemicals and solvents were used as received. Full details for all experiments are available in the supporting information.

### General Synthesis of Linear Polymers: Poly(4-Vinyl Pyridine-co-butylmethacrylate) [P(4VP<sub>x</sub>-co-BMA<sub>y</sub>)]

The monomers 4-VP (variable, see Table 2) and BMA (4.2660 g, 30 mmol) were added to a 100 ml round bottom flask containing THF (30 ml) followed by addition of AIBN (0.1641 g, 0.9 mmol) to initiate polymerization. The mixture was heated to 60°C in an oil bath under a nitrogen atmosphere. Polymerization was conducted for 18 h or 36 h. The reaction was cooled to room temperature and approximately two-thirds of the THF was removed using a rotavap. Diethyl ether was added to precipitate the copolymer. The product was then dissolved in methanol and the undissolved compounds were removed by filtration (homopolymer P-BMA is insoluble in methanol). The polymer was re-precipitated with diethyl ether. The precipitate was dissolved in toluene and the undissolved compounds were removed by filtration (homopolymer P-4VP is insoluble in toluene). The polymer was re-precipitated with diethyl ether and isolated. The last two steps (dissolving in methanol and toluene anti-solvents and precipitating) were repeated twice to ensure all unreacted monomers, homopolymers and initiator were removed. The copolymer was dried under vacuum overnight then dried under vacuum with heating at 125°C overnight.

### General Synthesis of Crosslinked Polymers: Poly(4-Vinyl Pyridine-Ethylene Glycol Dimethacrylate-Butylmethacrylate) [P(4VP<sub>x</sub>-EGDMA<sub>y</sub>-BMA<sub>z</sub>)]

Deionized water (110 ml), Mowiol 40–88 (PVA, 0.25 g), BMA (22.041 g, 155 mmol), 4-VP (variable, see Table 3), EGDMA

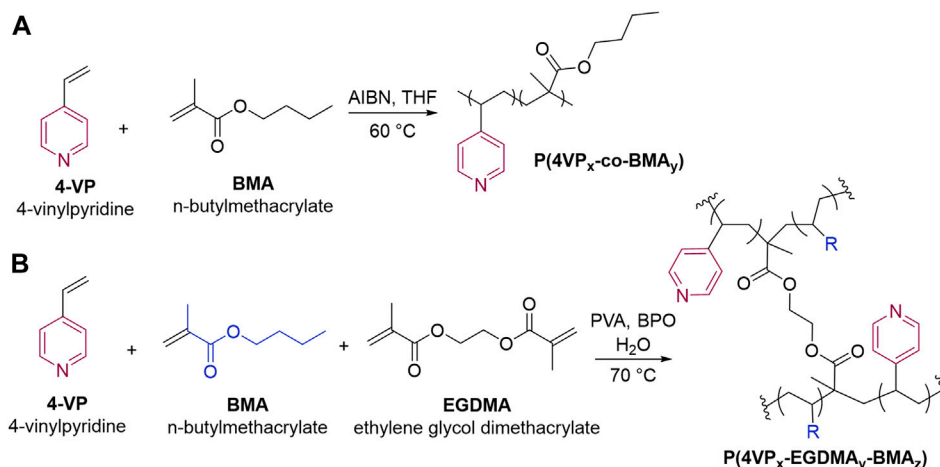
**TABLE 3 |** Synthetic feed of monomers used to synthesize crosslinked polymers.

Crosslinked polymer	4-VP (mmol)	EGDMA (mmol)	BMA (mmol)
P(4VP <sub>1</sub> -EGDMA <sub>0.5</sub> -BMA)	9.8	0.75	155
P(4VP <sub>1</sub> -EGDMA <sub>1.0</sub> -BMA)	9.8	1.5	155
P(4VP <sub>2</sub> -EGDMA <sub>1.0</sub> -BMA)	19.6	1.5	155
P(4VP <sub>3</sub> -EGDMA <sub>1.0</sub> -BMA)	29.4	1.5	155
P(4VP <sub>1</sub> -EGDMA <sub>2.0</sub> -BMA)	9.8	3.0	155

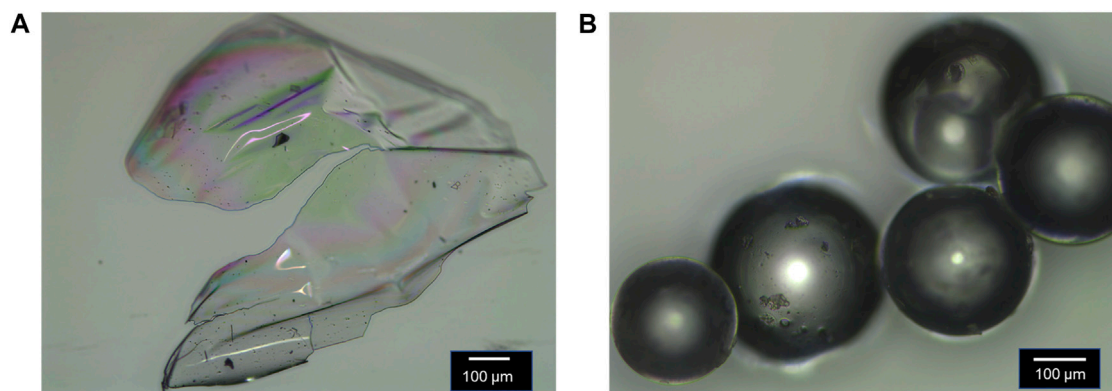
(variable, see Table 3), and BPO (0.50 g, 2.1 mmol) were added to a 300 ml three-neck flask. The mixture was stirred at 240 rpm using an IKA 20 digital mechanical stirrer, purged with nitrogen for 15 min, and heated to 70°C for 12 h. The polymer particles were isolated *via* centrifugation at 3,000 rpm for 3 min. The particles were washed five times using THF (30 ml) and EtOH (70 ml) and centrifuged at 3,000 rpm for 3 min and dried under vacuum to give white solid beads. The polymer beads were purified by Soxhlet extraction using THF at 110°C overnight and subsequently dried under vacuum heating at 120°C overnight. To confirm the crosslinked polymers were dry and free of trapped solvent or synthetic byproducts, a portion of polymer beads was stirred and heated at 95°C in water for 2 h. The solution was filtered to remove the polymer beads and characterized by UV-Vis spectroscopy, which demonstrated minimal signal (Supplementary Figure S18).

### Synthesis of a Control Crosslinked Polymer: Poly(Styrene<sub>3</sub>-Ethylene Glycol Dimethacrylate<sub>1.0</sub>-Butylmethacrylate)

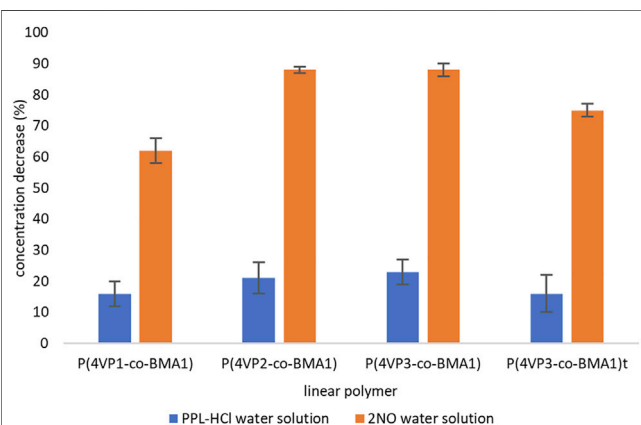
Deionized water (110 ml), Mowiol 40–88 (PVA, 0.25 g), BMA (22.041 g, 155 mmol), STY (3.06 g, 29.4 mmol), EGDMA (0.2973 g, 1.5 mmol), and BPO (0.50 g, 2.1 mmol) were added to a 300 ml three-neck flask. The mixture was stirred at 240 rpm using an IKA 20 digital mechanical stirrer, purged with nitrogen for 15 min, and heated to 70°C for 12 h. The polymer particles were isolated *via* centrifugation at 3,000 rpm for 3 min. The particles were washed five times using THF (30 ml) and EtOH (70 ml) and centrifuged at 3,000 rpm for 3 min and dried under vacuum to give white solid beads. The polymer beads were purified by Soxhlet extraction using THF at 110°C overnight and subsequently dried under vacuum heating at 120°C overnight.



**FIGURE 2 |** Synthetic outline for (A) linear and (B) crosslinked pyridine-functionalized polymers.



**FIGURE 3 |** Morphology of: (A) linear polymer P(4VP<sub>1</sub>-co-BMA<sub>1</sub>) and (B) crosslinked polymer P(4VP<sub>1</sub>-EGDMA<sub>1.0</sub>-BMA). Both images were collected after the polymer was dried under vacuum with heat.

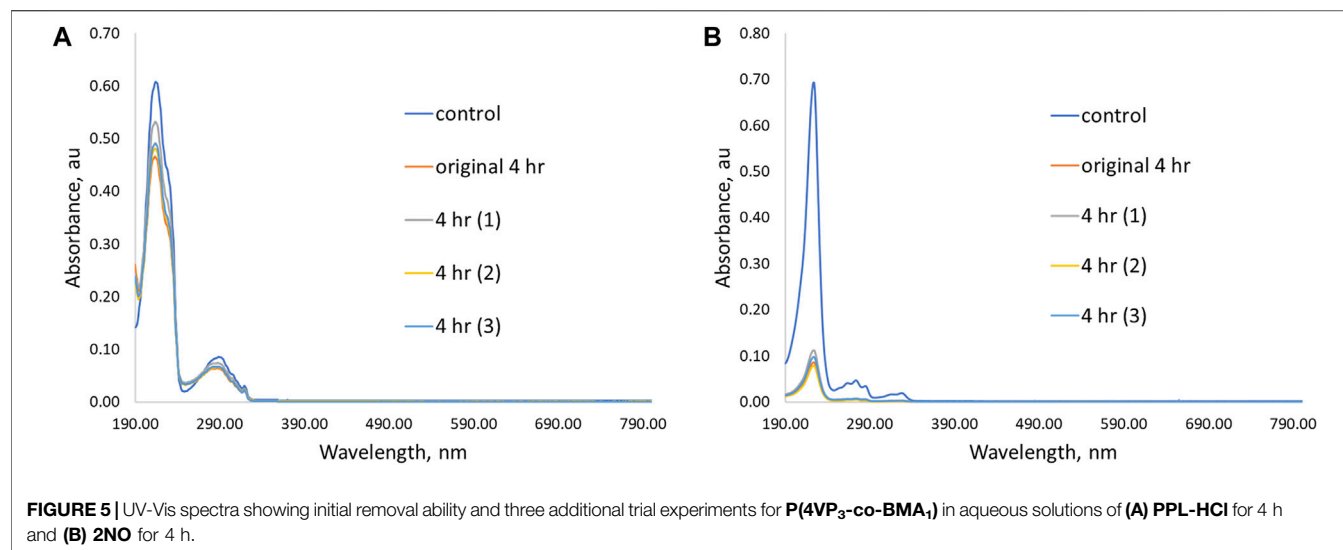


**FIGURE 4 |** Decreases in concentrations of contaminants following binding experiments for linear polymers.

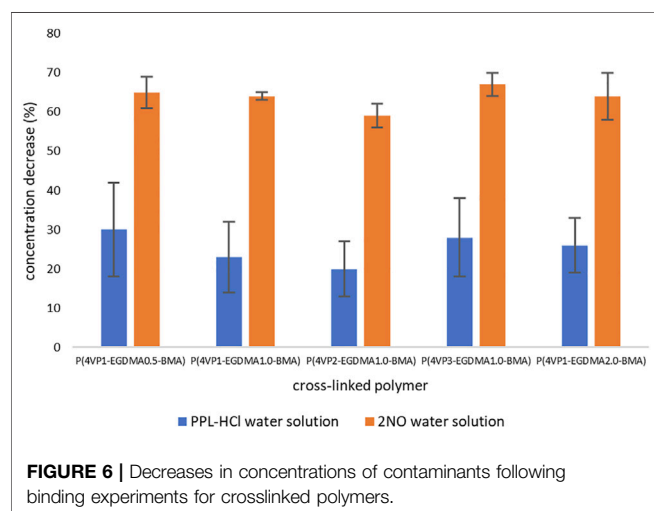
## Solution Binding Experiments

Binding experiments for the linear polymers were conducted by adding 10 mg of the polymer to a vial. Then, 2.5 ml of a PPL-HCl solution in water ( $0.4 \text{ mmol L}^{-1}$ ) or a 2NO solution in water ( $0.1 \text{ mmol L}^{-1}$ ) was added to the same vial. Seven individual samples were prepared, and each mixture was gently stirred for a different period of time at room temperature. The time periods were 15, 30, 45 min, 1, 2, 3, or 4 h. The resulting solution in each vial was filtered through cotton to remove the polymer. The filtrates were diluted with water using a micropipette and volumetric flask, and the concentrations after dilution were measured by UV-Vis (Supplementary Figures S19–S34). Aqueous solutions of PPL-HCl and 2NO were colorless before and after binding experiments.

Binding experiments for the crosslinked polymers were conducted by adding 200 mg of polymer beads to a vial. Then, 2.5 ml of a PPL-HCl solution in water ( $0.4 \text{ mmol L}^{-1}$ )



**FIGURE 5** | UV-Vis spectra showing initial removal ability and three additional trial experiments for **P(4VP<sub>3</sub>-co-BMA<sub>1</sub>)** in aqueous solutions of **(A) PPL-HCl** for 4 h and **(B) 2NO** for 4 h.



**FIGURE 6** | Decreases in concentrations of contaminants following binding experiments for crosslinked polymers.

or a **2NO** solution in water ( $0.1 \text{ mmol L}^{-1}$ ) was added to the same vial. Eight individual samples were prepared, and each mixture was gently stirred for a different period of time at room temperature. The time periods were 15, 30, 45 min, 1, 2, 3, or 4 h, or overnight (17 h). The resulting solution in each vial was filtered through cotton to remove the polymer. The filtrates were diluted with water using a micropipette and volumetric flask, and the concentrations after dilution were measured by UV-Vis (**Supplementary Figures S35–S56**). HPLC also confirmed that the decrease in the signal observed by UV-Vis correlates to a decrease in the signal at retention time corresponding to **2NO** (**Supplementary Table S5**).

Binding experiments for the control polymer **P(STY<sub>3</sub>-EGDMA<sub>1.0</sub>-BMA)** were conducted by adding 200 mg of polymer beads to a vial. Then, 2.5 ml of a **PPL-HCl** solution in water ( $0.4 \text{ mmol L}^{-1}$ ) or a **2NO** solution in water ( $0.1 \text{ mmol L}^{-1}$ ) was added to the same vial. Each mixture was gently stirred at room temperature. The stirring time was 2 h for

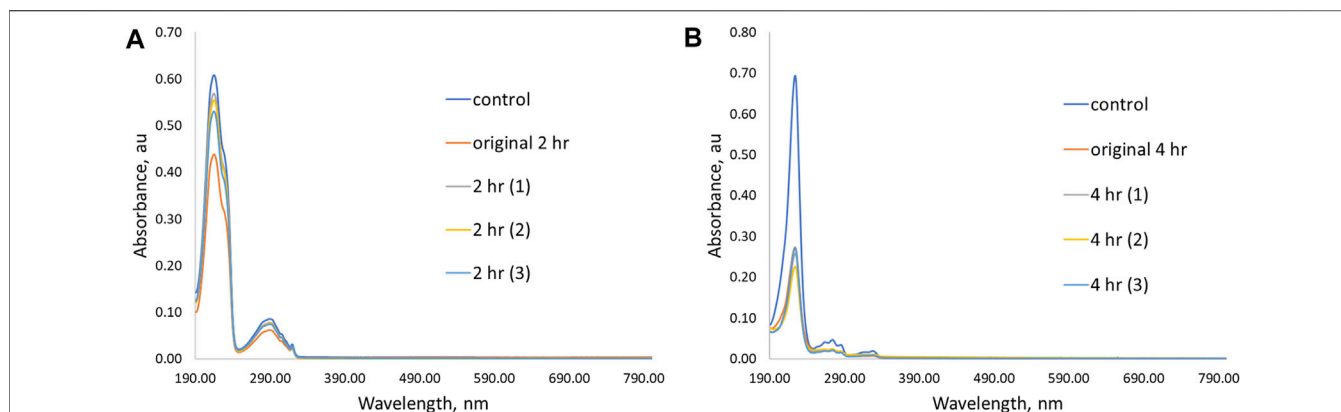
the **PPL-HCl** solution and 4 h for the **2NO** solution, which correlate to the best binding times for the best performing crosslinked pyridine polymer (**P(4VP<sub>3</sub>-EGDMA<sub>1.0</sub>-BMA)**). The resulting solution in each vial was filtered through cotton to remove the polymer. The filtrates were diluted with water using a micropipette and volumetric flask, and the concentrations after dilution were measured by UV-Vis (**Supplementary Figures S57–S58**).

## RESULTS AND DISCUSSION

### Synthesis and Characterization of Pyridine-Functionalized Polymers

We set out to synthesize pyridine-functionalized polymers that could act as adsorbents for micropollutants containing hydroxyl groups. Linear, pyridine-functionalized polymers **P(4VP<sub>x</sub>-co-BMA<sub>y</sub>)** were synthesized by free-radical solution polymerization, and crosslinked pyridine-functionalized polymers **P(4VP<sub>x</sub>-EGDMA<sub>y</sub>-BMA<sub>z</sub>)** were synthesized using suspension polymerization (**Figure 2**). **BMA** was chosen as a comonomer due to its ability to impart hydrophilicity onto the polymer (Ouellette and Rawn, 2014). Copolymers of **4VP** and **BMA** have been synthesized previously (Goswami and Dutta, 2013); however, to our knowledge, they have not been utilized as an adsorbent for removing pollutants.

The number of pyridine functional groups on the polymer backbone could have an impact on the binding ability of the polymers. Therefore, the **4-VP:BMA** comonomer ratio was systematically increased to yield a series of polymers. Four linear polymers were synthesized, namely, **P(4VP<sub>1</sub>-co-BMA<sub>1</sub>)**, **P(4VP<sub>2</sub>-co-BMA<sub>1</sub>)**, **P(4VP<sub>3</sub>-co-BMA<sub>1</sub>)**, and **P(4VP<sub>3</sub>-co-BMA<sub>1</sub>)<sub>t</sub>** (where subscript *t* denotes a doubled reaction time, see **Table 2**). The additional reaction time was used to increase the molecular weight (**Table 2**) and determine if there was any impact on binding ability. Five



**FIGURE 7** | UV-Vis spectra showing initial removal ability and three additional trial experiments for **P(4VP<sub>3</sub>-EGDMA<sub>1.0</sub>-BMA)** in aqueous solutions of **(A) PPL-HCl** for 2 h and **(B) 2NO** for 4 h.

crosslinked polymers were synthesized, namely, **P(4VP<sub>1</sub>-EGDMA<sub>0.5</sub>-BMA)**, **P(4VP<sub>1</sub>-EGDMA<sub>1.0</sub>-BMA)**, **P(4VP<sub>2</sub>-EGDMA<sub>1.0</sub>-BMA)**, **P(4VP<sub>3</sub>-EGDMA<sub>1.0</sub>-BMA)**, and **P(4VP<sub>1</sub>-EGDMA<sub>2.0</sub>-BMA)**. The amount of **BMA** added to the reaction was held constant, while the **4-VP** and **EGDMA** crosslinker amounts were altered systematically (**Table 3**).

The linear polymers exhibit a semitransparent, glassy morphology, and the crosslinked polymers are polydisperse and exhibit a spherical morphology as evidenced by optical microscopy (**Figure 3**). <sup>1</sup>H NMR spectroscopy confirmed the obtained monomer ratios in the polymer are similar to synthetic feed of monomers used (**Supplementary Figures S4–S7**, **Table 2**). Gel permeation chromatography (GPC) confirmed high molecular weight for the linear polymers (**Supplementary Figures S14–S17**, **Table 2**). <sup>13</sup>C NMR spectroscopy confirmed the chemical functionality of the crosslinked polymers (**Supplementary Figures S8–S12**).

### Binding Ability of the Linear Polymers

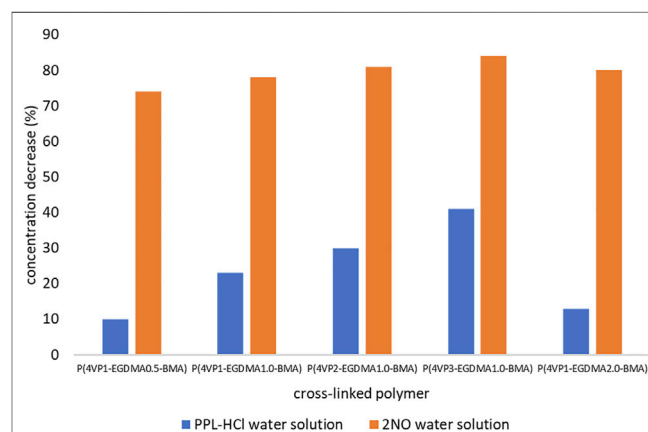
To determine the capability of the pyridine-functionalized polymers for binding **PPL-HCl** or **2NO** from water, binding experiments were conducted, and solutions after binding were characterized by UV-Vis spectroscopy. Binding experiments were conducted for periods of 15, 30, 45 min, 1, 2, 3, or 4 h at room temperature. All four synthesized linear polymers successfully bound **PPL-HCl** and **2NO** from solutions of water. Generally, binding experiments conducted for a period of approximately 4 h afforded the highest removals of **PPL-HCl** and **2NO** (**Supplementary Table S2**, **Figure 4**). However, a decrease in concentration was observed in as little as 15 min for each sample (**Supplementary Figures S19–S34**). After determining the optimal binding time (i.e. the time at which the concentrations of **PPL-HCl** or **2NO** water solution decreased most), three additional trials with the same binding time were conducted to calculate standard deviations (**Figure 4**).

For the **PPL-HCl** experiments, all four linear polymers removed ca. 20% of the drug at their optimal binding time. On the other hand, higher amounts of **4-VP** in the linear polymers resulted in significantly better binding ability for the

**2NO** contaminant. The best performing linear polymer overall was **P(4VP<sub>3</sub>-co-BMA<sub>1</sub>)**, which decreased the concentration of **PPL-HCl** in water by 23% and decreased the concentration of **2NO** in water by 88% (**Figure 5**). The binding performance of these polymers with **PPL-HCl** is lower than reported  $\beta$ -cyclodextrin materials; however binding performance with **2NO** is on par with the reported  $\beta$ -cyclodextrin materials (**Table 1**, Alsbaiee et al., 2016; Song et al., 2021). The polymer **P(4VP<sub>2</sub>-co-BMA<sub>1</sub>)** also bound **2NO** just as effectively as **P(4VP<sub>3</sub>-co-BMA<sub>1</sub>)**. The higher molecular weight polymer **P(4VP<sub>3</sub>-co-BMA<sub>1</sub>)<sub>t</sub>** did not demonstrate enhanced ability to bind either contaminant. The standard deviations for the **PPL-HCl** binding experiments are higher than for the **2NO** experiments. As removal efficiency for **PPL-HCl** is lower than **2NO**, this indicates that binding between the two species is likely not as strong.

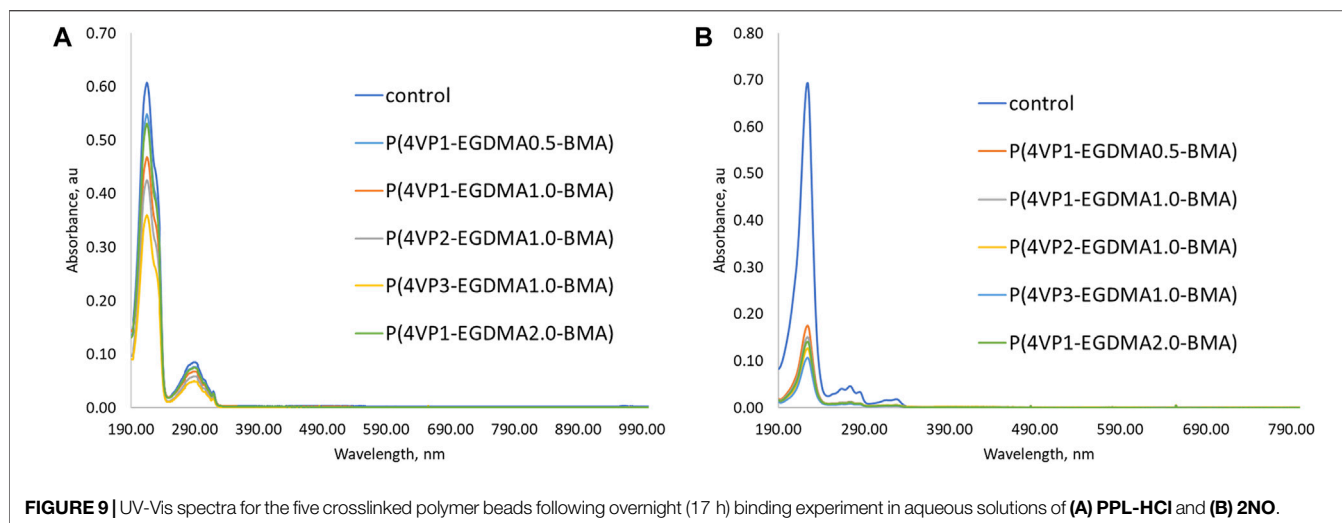
### Binding Ability of the Crosslinked Polymers

Akin to linear polymers, binding experiments with the same **PPL-HCl** or **2NO** solutions in water were conducted using the



**FIGURE 8** | Decreases in concentrations of contaminants following overnight binding experiments (17 h) for crosslinked polymers.



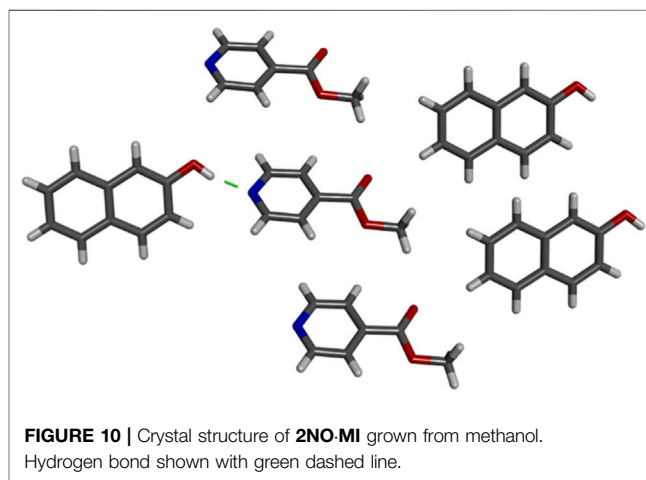


**FIGURE 9** | UV-Vis spectra for the five crosslinked polymer beads following overnight (17 h) binding experiment in aqueous solutions of **(A) PPL-HCl** and **(B) 2NO**.

crosslinked polymers as adsorbents. The same binding experiment times were used as the linear polymers. The UV-Vis spectra demonstrated that all five crosslinked polymers also successfully removed **PPL-HCl** and **2NO** from solutions of water. Generally, a binding period of 1–2 h for **PPL-HCl** or 4 h for **2NO** resulted in the highest removal percentages (**Supplementary Table S3**, **Figure 6**). A decrease in concentration was observed in as little as 15 min for each sample as well (**Supplementary Figures S35–S45**, **S46–S56**). After determining the time at which concentrations of **PPL-HCl** or **2NO** decreased most, three additional trials with the same binding time were conducted to calculate standard deviations (**Figure 6**).

For the **PPL-HCl** experiments, all five crosslinked polymers removed ca. 20–30% of the drug at their optimal binding time. On the other hand, removal of **2NO** was significantly higher at about 65%. The amount of **EGDMA** crosslinker and the amount of **4-VP** in the polymer play an important role in binding ability. When the amount of **EGDMA** is held constant at 1 mol% and the amount of **4-VP** is systematically increased to afford the three polymers **P(4VP<sub>1</sub>-EGDMA<sub>1.0</sub>-BMA)**, **P(4VP<sub>2</sub>-EGDMA<sub>1.0</sub>-BMA)**, and **P(4VP<sub>3</sub>-EGDMA<sub>1.0</sub>-BMA)**, the binding ability is highest for the polymer with the largest amount of pyridine functionalization, namely, **P(4VP<sub>3</sub>-EGDMA<sub>1.0</sub>-BMA)** (**Figure 7**). Interestingly, **P(4VP<sub>2</sub>-EGDMA<sub>1.0</sub>-BMA)** does not exhibit increased binding ability for **PPL-HCl** or **2NO** compared to **P(4VP<sub>1</sub>-EGDMA<sub>1.0</sub>-BMA)**, as was the case for the linear polymers.

When the amount of **EGDMA** is increased from 0.5 to 1 and to 2 mol% while holding **4-VP** constant to afford the three polymers **P(4VP<sub>1</sub>-EGDMA<sub>0.5</sub>-BMA)**, **P(4VP<sub>1</sub>-EGDMA<sub>1.0</sub>-BMA)**, and **P(4VP<sub>1</sub>-EGDMA<sub>2.0</sub>-BMA)**, the average binding ability decreases for **PPL-HCl**, but remains similar for **2NO**. The lower amount of crosslinker allows the polymer bead to swell more readily in solution (Pulko and Krajnc, 2005; Nigmatullin et al., 2014), which results in increased binding ability. Particle swelling has also been demonstrated to influence the effectiveness of solid-phase synthesis, whereby swelling allows nearly all



**FIGURE 10** | Crystal structure of **2NO-MI** grown from methanol. Hydrogen bond shown with green dashed line.

reactive sites within the particle to be chemically accessible (Engström and Helgee, 2006; Nakaie et al., 2011; Mane et al., 2014). As observed for the linear polymers, the standard deviations for the **PPL-HCl** binding experiments with crosslinked polymers are also higher than for the **2NO** experiments, indicating lower binding effectiveness.

In addition to the time experiments ranging from 15 min to 4 h, we also conducted an overnight (17 h) binding experiment for the crosslinked polymer beads (**Figure 8**, **Supplementary Table S4**). The longer time allows the beads to swell in solution and could result in increased removal abilities. Only two polymers exhibited enhanced binding of **PPL-HCl** with increased binding time, namely **P(4VP<sub>2</sub>-EGDMA<sub>1.0</sub>-BMA)** and **P(4VP<sub>3</sub>-EGDMA<sub>1.0</sub>-BMA)**. On the other hand, binding of **2NO** increased to ca. 80% with increased binding time for all the crosslinked polymers. Overall, the best performing polymer was **P(4VP<sub>3</sub>-EGDMA<sub>1.0</sub>-BMA)**, which decreased the concentration of **PPL-HCl** in water by 41% and decreased the concentration of **2NO** in water by 84% (**Figure 9**).

## Reusability of the Highest Performing Crosslinked Polymer

Reusability is an essential performance indicator of a given adsorbent (Yang W. et al., 2021). Thus, after determining binding ability of the synthesized polymers, we were interested in evaluating the reusability. The crosslinked polymers are not soluble in organic solvents, whereas the linear polymers are. Thus, we chose to examine reusability for the best performing crosslinked polymer, **P(4VP<sub>3</sub>-EGDMA<sub>1.0</sub>-BMA)** with **2NO**. After the first 4 h binding experiment, the beads were purified by a Soxhlet extraction using THF at 110°C overnight and subsequently dried under vacuum heating at 120°C overnight. A second 4 h binding experiment was conducted, and the polymer beads remove **2NO** at the same level, demonstrating good reusability (**Supplementary Figure S59**).

## Binding Ability of the Crosslinked Control Polymer

Increasing the amount of pyridine functional groups in the polymers increases binding ability. To support that the binding and removal mechanism is facilitated by hydrogen bonding involving the pyridine groups, a control polymer was synthesized by using **STY** in place of **4VP**. A crosslinked polymer analogous to best performing crosslinked pyridine polymer was synthesized, namely **P(STY<sub>3</sub>-EGDMA<sub>1.0</sub>-BMA)**. The **STY** control polymer removed minimal **PPL-HCl** (2%, **Supplementary Figure S57**) and some **2NO** (26%, **Supplementary Figure S58**). The ability of the **STY** control polymer to bind the contaminants to a lesser extent could be due to favourable hydrophobic interactions. However, the binding ability is significantly reduced when the pyridine groups are absent.

## SMALL MOLECULE COCRYSTALLIZATION

To further understand the recognition between the contaminants and copolymer that leads to effective removal, cocrystallization of the small molecules **2NO** and methyl isonicotinate (**MI**) was conducted. **MI** contains pyridine and ester functional groups and mimics the functional groups in the polymer backbone. Cocrystallization of **2NO** and **MI** in methanol yielded **2NO-MI**, and the two components interact through O-H...N hydrogen bonds between the phenol of **2NO** and pyridine of **MI**. There was no O-H...O (ester) hydrogen bonding observed in the structure. In fact, the carbonyl groups of **MI** are surrounded by either **MI** molecules or the C-H groups of **2NO** (**Figure 10** and **Supplementary Figure S2**). This further supports the idea that hydrogen bonding between the contaminant and pyridine-functionalized polymer is a favorable intermolecular interaction and provides a pathway for increased removal ability. In addition to hydrogen bonding, hydrophobic interactions between the contaminant and polymer backbone could also support binding of these two micropollutants.

## CONCLUSION

Herein, we described the synthesis of pyridine-functionalized linear and crosslinked polymers that bind and remove **PPL-HCl** and **2NO** from water solutions. The amount of pyridine functional groups in the polymer influences binding abilities. Overall, higher synthetic feeds of **4-VP** lead to improved binding abilities for the polymers. Approximately 20–40% of **PPL-HCl** could be removed from water solutions, and binding abilities for **2NO** from water were much higher at 60–88% over a time frame of 1–4 h. For the contaminant **2NO**, the removal ability of the polymers described here is similar to or higher than other polymer-based materials. A control polymer lacking pyridine groups exhibits significantly lower binding ability than the pyridine polymers. Additionally, small-molecule cocrystallization experiments with a polymer backbone mimic, **MI**, demonstrate that O-H...N hydrogen bonding between the phenol of **2NO** and pyridine in **MI** is a favourable intermolecular interaction and supports the high binding ability observed with the pyridine-functionalized polymers. Adsorbents that engage in supramolecular interactions with contaminants have demonstrated promise as micropollutant remediation materials. Rational design of adsorbent materials can help develop design criteria for new adsorbents with high selectivity and rapid removal times.

## DATA AVAILABILITY STATEMENT

The original contributions presented in the study are included in the article/**Supplementary Material**, further inquiries can be directed to the corresponding author.

## AUTHOR CONTRIBUTIONS

KH contributed to conception and design of the study. QZ contributed to the synthesis and characterization of the polymers. QZ and KH wrote the paper. DU contributed to the crystal data collection and solution. All authors contributed to manuscript revision, read, and approved the submitted version.

## FUNDING

Funding from The Welch Foundation D-2068-20210327 and startup funding from Texas Tech University is gratefully acknowledged.

## ACKNOWLEDGMENTS

The authors acknowledge Kaz Surowiec for collecting HPLC data.

## SUPPLEMENTARY MATERIAL

The Supplementary Material for this article can be found online at: <https://www.frontiersin.org/articles/10.3389/fchem.2021.793870/full#supplementary-material>

## REFERENCES

- Alsaiee, A., Smith, B. J., Xiao, L., Ling, Y., Helbling, D. E., and Dichtel, W. R. (2016). Rapid Removal of Organic Micropollutants from Water by a Porous  $\beta$ -cyclodextrin Polymer. *Nature* 529, 190–194. doi:10.1038/nature16185
- Bui, X. T., Vo, T. P. T., Ngo, H. H., Guo, W. S., and Nguyen, T. T. (2016). Multicriteria Assessment of Advanced Treatment Technologies for Micropollutants Removal at Large-Scale Applications. *Sci. Total Environ.* 563–564, 1050–1067. doi:10.1016/j.scitotenv.2016.04.191
- Coelho, C. M., de Andrade, J. R., da Silva, M. G. C., and Vieira, M. G. A. (2020). Removal of Propranolol Hydrochloride by Batch Biosorption Using Remaining Biomass of Alginate Extraction from Sargassum Filipendula Algae. *Environ. Sci. Pollut. Res.* 27, 16599–16611. doi:10.1007/s11356-020-08109-4
- Dai, D., Yang, J., Zou, Y. C., Wu, J. R., Tan, L. L., Wang, Y., et al. (2021). Macrocyclic Arenes-Based Conjugated Macrocyclic Polymers for Highly Selective CO<sub>2</sub> Capture and Iodine Adsorption. *Angew. Chem.* 133, 9049–9057. doi:10.1002/ange.202015162
- Diez-Pascual, A. M., García-García, D., San Andrés, M. P., and Vera, S. (2016). Determination of Riboflavin Based on Fluorescence Quenching by Graphene Dispersions in Polyethylene Glycol. *RSC Adv.* 6, 19686–19699. doi:10.1039/C5RA25547C
- Engström, J. U. A., and Helgee, B. (2006). Hydrophilic Polymer Supports for Solid-phase Synthesis: Hydroxyl-Functional Beads of Poly(vinylpyrrolidone). *J. Comb. Chem.* 8, 355–360. doi:10.1021/cc050148k
- Goswami, S., and Dutta, A. (2013). Conductivity Study of Solid Polyelectrolytes Based on Hydriodide Salt of Poly(4-Vinyl Pyridine-Co-Butylmethacrylate), Poly(4-Vinyl Pyridine-Co-Butylacrylate). *Bull. Mater. Sci.* 36, 635–640. doi:10.1007/s12034-013-0517-5
- Hollender, J., Zimmermann, S. G., Koepke, S., Krauss, M., McArdell, C. S., Ort, C., et al. (2009). Elimination of Organic Micropollutants in a Municipal Wastewater Treatment Plant Upgraded with a Full-Scale post-ozonation Followed by Sand Filtration. *Environ. Sci. Technol.* 43, 7862–7869. doi:10.1021/es9014629
- Ji, X., Wang, H., Wang, H., Zhao, T., Page, Z. A., Khashab, N. M., et al. (2020). Removal of Organic Micropollutants from Water by Macrocyclic-Containing Covalent Polymer Networks. *Angew. Chem. Int. Ed.* 59, 23402–23412. doi:10.1002/anie.202009113
- Klemes, M. J., Skala, L. P., Ateia, M., Trang, B., Helbling, D. E., and Dichtel, W. R. (2020). Polymerized Molecular Receptors as Adsorbents to Remove Micropollutants from Water. *Acc. Chem. Res.* 53, 2314–2324. doi:10.1021/acs.accounts.0c00426
- Kovalova, L., Knappe, D. R. U., Lehnberg, K., Kazner, C., and Hollender, J. (2013). Removal of Highly Polar Micropollutants from Wastewater by Powdered Activated Carbon. *Environ. Sci. Pollut. Res.* 20, 3607–3615. doi:10.1007/s11356-012-1432-9
- Liu, C. H., Fang, W. H., Sun, Y., Yao, S., Wang, S. T., Lu, D., et al. (2021). Designable Assembly of Aluminum Molecular Rings for Sequential Confinement of Iodine Molecules. *Angew. Chem. Int. Ed.* 60, 21426–21433. doi:10.1002/anie.202107227
- Mane, S., Ponrathnam, S., and Chavan, N. (2014). Synthesis and Characterization of Hypercrosslinked Hydroxyl Functionalized Co-polymer Beads. *Eur. Polym. J.* 59, 46–58. doi:10.1016/j.eurpolymj.2014.07.001
- Margot, J., Rossi, L., Barry, D. A., and Holliger, C. (2015). A Review of the Fate of Micropollutants in Wastewater Treatment Plants. *WIREs Water* 2, 457–487. doi:10.1002/wat2.1090
- Nakaie, C. R., Oliveira, E., Vicente, E. F., Jubilit, G. N., Souza, S. E. G., Marchetto, R., et al. (2011). Solid-phase Peptide Synthesis in Highly Loaded Conditions. *Bioorg. Chem.* 39, 101–109. doi:10.1016/j.bioorg.2011.01.001
- Nigmatullin, R., Bencsik, M., and Gao, F. (2014). Influence of Polymerisation Conditions on the Properties of Polymer/clay Nanocomposite Hydrogels. *Soft Matter* 10, 2035–2046. doi:10.1039/C3SM52887A
- Ouellette, R. J., and Rawn, J. D. (2014). *21-Carboxylic Acid Derivatives. Organic Chemistry*. Boston: Elsevier, 699–745. doi:10.1016/B978-0-12-800780-8.00021-8
- Prasse, C., Wagner, M., Schulz, R., and Ternes, T. A. (2012). Oxidation of the Antiviral Drug Acyclovir and its Biodegradation Product Carboxy-Acyclovir with Ozone: Kinetics and Identification of Oxidation Products. *Environ. Sci. Technol.* 46, 2169–2178. doi:10.1021/es203712z
- Pulko, I., and Krajnc, P. (2005). Influence of Crosslinker and Monomer Ratio on Bead Size Distribution, Swelling and Polymer Network Flexibility of 4-nitrophenylacrylate Polymer Supports. *Acta Chim. Slov.* 52 (3), 215–223.
- Schwarzenbach, R. P., Escher, B. I., Fenner, K., Hofstetter, T. B., Johnson, C. A., Von Gunten, U., et al. (2006). The challenge of Micropollutants in Aquatic Systems. *Science* 313, 1072–1077. doi:10.1126/science.1127291
- Shetty, D., Jahovic, I., Raya, J., Asfari, Z., Olsen, J.-C., and Trabolzi, A. (2018). Porous Polycalix[4]arenes for Fast and Efficient Removal of Organic Micropollutants from Water. *ACS Appl. Mater. Inter.* 10, 2976–2981. doi:10.1021/acsami.7b16546
- Skorjanc, T., Shetty, D., and Trabolzi, A. (2021). Pollutant Removal with Organic Macrocyclic-Based Covalent Organic Polymers and Frameworks. *Chem* 7, 882–918. doi:10.1016/j.chempr.2021.01.002
- Song, X., Mensah, N. N., Wen, Y., Zhu, J., Zhang, Z., Tan, W. S., et al. (2021).  $\beta$ -Cyclodextrin-Polyacrylamide Hydrogel for Removal of Organic Micropollutants from Water. *Molecules* 26, 5031. doi:10.3390/molecules26165031
- Wang, X., Xie, L., Lin, K., Ma, W., Zhao, T., Ji, X., et al. (2021). Calix[4]pyrrole-Crosslinked Porous Polymeric Networks for the Removal of Micropollutants from Water. *Angew. Chem.* 133, 7264–7272. doi:10.1002/ange.202016364
- Wang, Y.-P., Wang, L.-J., Peng, P.-Y., and Lu, T.-H. (2006). Treatment of Naphthalene Derivatives with Iron-Carbon Micro-electrolysis. *Trans. Nonferrous Met. Soc. China* 16, 1442–1447. doi:10.1016/S1003-6326(07)60035-1
- Weber, F.-A., aus der Beek, T., Bergmann, A., Carius, A., Grüttnner, G., Hickmann, S., et al. (2016). *Pharmaceuticals in the Environment-The Global Perspective: Occurrence, Effects, and Potential Cooperative Action under SAICM*. Dessau-Roßlau: German Environment Agency.
- Xiao, L., Ching, C., Ling, Y., Nasiri, M., Klemes, M. J., Reineke, T. M., et al. (2019). Cross-linker Chemistry Determines the Uptake Potential of Perfluorinated Alkyl Substances by  $\beta$ -Cyclodextrin Polymers. *Macromolecules* 52, 3747–3752. doi:10.1021/acs.macromol.9b00417
- Xu, L., Wang, S., Zhou, J., Deng, H., and Frost, R. L. (2018). Column Adsorption of 2-naphthol from Aqueous Solution Using Carbon Nanotube-Based Composite Adsorbent. *Chem. Eng. J.* 335, 450–457. doi:10.1016/j.cej.2017.10.176
- Yang, L. P., Ke, H., Yao, H., and Jiang, W. (2021). Effective and Rapid Removal of Polar Organic Micropollutants from Water by Amide Naphthotube-Crosslinked Polymers. *Angew. Chem. Int. Ed.* 60, 21404–21411. doi:10.1002/anie.202106998
- Yang, W., Shi, X., Dong, H., Tang, H., Chen, W., Wu, M., et al. (2021). Fabrication of a Reusable Polymer-Based Cerium Hydroxide Nanocomposite with High Stability for Preferable Phosphate Removal. *Chem. Eng. J.* 405, 126649. doi:10.1016/j.cej.2020.126649
- Zang, S., and Lian, B. (2009). Synergistic Degradation of 2-naphthol by Fusarium Proliferatum and Bacillus Subtilis in Wastewater. *J. Hazard. Mater.* 166, 33–38. doi:10.1016/j.jhazmat.2008.10.117
- Zimmermann, S. G., Wittenwiler, M., Hollender, J., Krauss, M., Ort, C., Siegrist, H., et al. (2011). Kinetic Assessment and Modeling of an Ozonation Step for Full-Scale Municipal Wastewater Treatment: Micropollutant Oxidation, By-Product Formation and Disinfection. *Water Res.* 45, 605–617. doi:10.1016/j.watres.2010.07.080

**Conflict of Interest:** The authors declare that the research was conducted in the absence of any commercial or financial relationships that could be construed as a potential conflict of interest.

**Publisher's Note:** All claims expressed in this article are solely those of the authors and do not necessarily represent those of their affiliated organizations, or those of the publisher, the editors and the reviewers. Any product that may be evaluated in this article, or claim that may be made by its manufacturer, is not guaranteed or endorsed by the publisher.

Copyright © 2022 Zheng, Unruh and Hutchins. This is an open-access article distributed under the terms of the Creative Commons Attribution License (CC BY). The use, distribution or reproduction in other forums is permitted, provided the original author(s) and the copyright owner(s) are credited and that the original publication in this journal is cited, in accordance with accepted academic practice. No use, distribution or reproduction is permitted which does not comply with these terms.

# Advantages of publishing in Frontiers



## OPEN ACCESS

Articles are free to read  
for greatest visibility  
and readership



## FAST PUBLICATION

Around 90 days  
from submission  
to decision



## HIGH QUALITY PEER-REVIEW

Rigorous, collaborative,  
and constructive  
peer-review



## TRANSPARENT PEER-REVIEW

Editors and reviewers  
acknowledged by name  
on published articles

## Frontiers

Avenue du Tribunal-Fédéral 34  
1005 Lausanne | Switzerland

Visit us: [www.frontiersin.org](http://www.frontiersin.org)

Contact us: [frontiersin.org/about/contact](http://frontiersin.org/about/contact)



## REPRODUCIBILITY OF RESEARCH

Support open data  
and methods to enhance  
research reproducibility



## DIGITAL PUBLISHING

Articles designed  
for optimal readership  
across devices



## FOLLOW US

@frontiersin



## IMPACT METRICS

Advanced article metrics  
track visibility across  
digital media



## EXTENSIVE PROMOTION

Marketing  
and promotion  
of impactful research



## LOOP RESEARCH NETWORK

Our network  
increases your  
article's readership